

THE GENESIS OF THE GREY RIVER TUNGSTEN
PROSPECT: A FLUID INCLUSION, GEOCHEMICAL,
AND ISOTOPIC STUDY

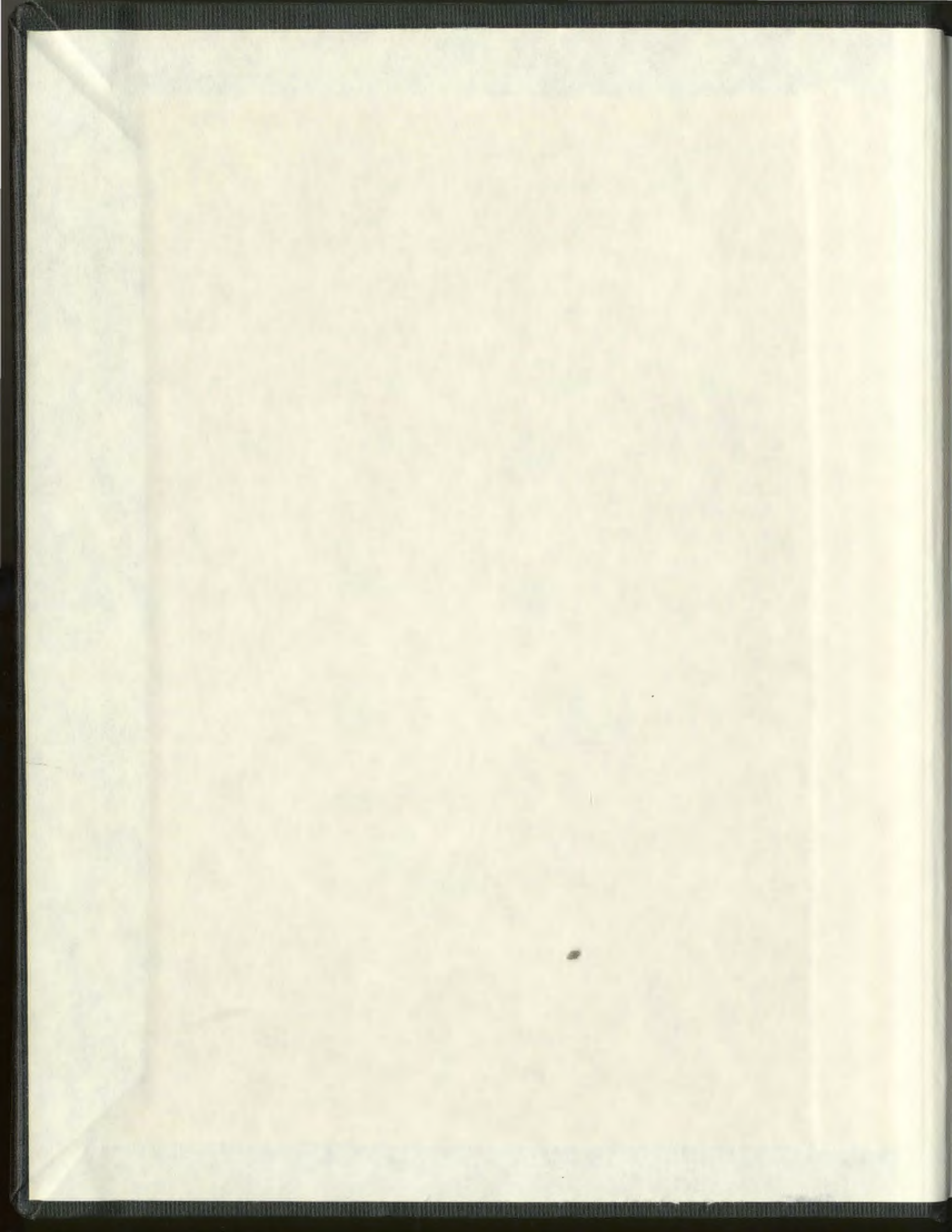
PART 1

CENTRE FOR NEWFOUNDLAND STUDIES

**TOTAL OF 10 PAGES ONLY
MAY BE XEROXED**

(Without Author's Permission)

NEVILLE CHARLES HIGGINS





National Library of Canada
Collections Development Branch

Canadian Theses on
Microfiche Service

Bibliothèque nationale du Canada
Direction du développement des collections

Service des thèses canadiennes
sur microfiche

NOTICE

The quality of this microfiche is heavily dependent upon the quality of the original thesis submitted for microfilming. Every effort has been made to ensure the highest quality of reproduction possible.

If pages are missing, contact the university which granted the degree.

Some pages may have indistinct print especially if the original pages were typed with a poor typewriter ribbon or if the university sent us a poor photocopy.

Previously copyrighted materials (journal articles, published tests, etc.) are not filmed.

Reproduction in full or in part of this film is governed by the Canadian Copyright Act, R.S.C. 1970, c. C-30. Please read the authorization forms which accompany this thesis.

**THIS DISSERTATION
HAS BEEN MICROFILMED
EXACTLY AS RECEIVED**

AVIS

La qualité de cette microfiche dépend grandement de la qualité de la thèse soumise au microfilmage. Nous avons tout fait pour assurer une qualité supérieure de reproduction.

S'il manque des pages, veuillez communiquer avec l'université qui a conféré le grade.

La qualité d'impression de certaines pages peut laisser à désirer, surtout si les pages originales ont été dactylographiées à l'aide d'un ruban usé ou si l'université nous a fait parvenir une photocopie de mauvaise qualité.

Les documents qui font déjà l'objet d'un droit d'auteur (articles de revue, examens publiés, etc.) ne sont pas microfilmés.

La reproduction, même partielle, de ce microfilm est soumise à la Loi canadienne sur le droit d'auteur, SRC 1970, c. C-30. Veuillez prendre connaissance des formules d'autorisation qui accompagnent cette thèse.

**LA THÈSE A ÉTÉ
MICROFILMÉE TELLE QUE
NOUS L'AVONS REÇUE**

THE GENESIS OF THE GREY RIVER TUNGSTEN
PROSPECT: A FLUID INCLUSION, GEOCHEMICAL, AND
ISOTOPIC STUDY

by

© Neville C. Higgins, B.Sc. (Hons)

August, 1980

A Thesis submitted in partial fulfillment
of the requirements for the degree of
Doctor of Philosophy

Department of Geology
Memorial University of Newfoundland

St. John's

Newfoundland

ABSTRACT

Mineralisation in the Grey River Tungsten Prospect, Newfoundland, is contained within a swarm of quartz veins and fractures which traverse the contact between a sheared Devonian (405 ± 10 Ma) K-feldspar megacrystic granite, and metamorphic rocks which are typical of the gneissic terrain of the Gander Zone. The mineralisation is genetically related to a suite of post-tectonic, highly differentiated, alkali-rich leucogranite dykes.

The tungsten-bearing hydrothermal veins, dated at 330 Ma, range from tensional fractures and veinlets to lodes containing several injections of quartz. The mineralisation is divided into four stages; the Early Stage, characterised by quartz-feldspar-molybdenite veins; the Composite Stage, consisting of five vein types (in paragenetic order), quartz-bismuthinite, quartz-wolframite (Fe-rich), greisen, quartz-sulphide, and quartz-wolframite (Mn-rich) veins; the Sulphide Stage, characterised by silver-bearing quartz-galena-sphalerite veins; and the Late Stage, composed of zoned fluorite-calcite-barite veins. A spatial mineral zonation from south to north matches the temporal sequence outlined above, with the exception of the Late Stage veins which crosscut Composite Stage veins.

Fluid inclusion data indicate a complex evolutionary history for the hydrothermal fluid. Initially a homogeneous supercritical fluid ($X_{\text{CO}_2} = 0.4$) with a density of 0.65 g/cc

deposited quartz-feldspar-molybdenite veins at temperatures of 450-500°C and fluid pressures of 1200-1400 bars (120-140 MPa). The simultaneous trapping of CO₂-rich and H₂O-rich fluid inclusions, as well as solid inclusions of calcite in quartz of the quartz-bismuthinite vein type is evidence for the existence of an immiscible heterogeneous fluid during this stage of mineralisation. Fluid phase equilibria indicate immiscibility occurred at temperatures of 390 - 430°C and fluid pressures of 1000-1200 bars (100-120 MPa). Oxygen isotope data indicate that greisen alteration halos of the composite lodes were formed at temperatures between 350-400°C.

In these lodes quartz-sulphide and quartz-wolframite veins were deposited in open spaces created by normal faulting. These movements prompted rapid decreases in fluid pressure and temperature and caused retrograde boiling of the hydrothermal fluid (at 350 bars and 300-390°C) during deposition of quartz-sulphide veins. Deposition of wolframite in quartz-wolframite veins occurred at 270-330°C and fluid pressures less than 350 bars, from an aqueous fluid of low salinity (< 0.5 wt% NaCl) and CO₂ content (< 10 bars P_{CO₂}), and after separation of a CO₂ vapour phase by retrograde boiling.

Calculated $\delta^{18}\text{O}_{\text{H}_2\text{O}}$ values indicate a progressive depletion in ¹⁸O isotopic composition of the hydrothermal fluid with time (7.3 ‰ to 0.5 ‰). The depletion is due to the loss of 40 mol% CO₂ from the hydrothermal fluid by immiscibility and retrograde boiling, and subsequent fractionation

effects. The oxygen isotope data suggest that the hydrothermal fluid was dominantly of magmatic origin.

Heavy REE enrichment and light REE depletion during greisenisation indicate extensive REE mobility, and imply both that CO_3^{2-} was the dominant anionic species in the hydrothermal fluid and that mobilisation of REE occurred by REE carbonate complexing. A positive correlation between heavy REE enrichment and high tungsten concentration suggests that REE mobility is related to tungsten transport. Together with the fluid inclusion evidence these data suggest that the transport of tungsten in hydrothermal fluids might be due to carbonate/bicarbonate complexing.

The fluid inclusion and isotopic data from the Grey River Tungsten Prospect serve to illustrate the previously unrecognised role of CO_2 in the transport and deposition of tungsten in the hydrothermal environment.

7

v

31

This thesis is dedicated to my mother,
the late June Higgins,
who had complete confidence in her children's abilities
and encouraged us to achieve our highest potential.

1

"There is no necessary connection between the size of an object and the value of a fact and ... though the objects I have described are minute, the conclusions to be drawn are great."

H.C. Sorby 1858

ACKNOWLEDGEMENTS

During the course of this study I have been helped by many people whom I wish to acknowledge and thank:

- my supervisors, Dave Strong, John Malpas, and Brian Fryer for guidance, advice, squash games and reviews of the manuscript.

- Richard Henley, for encouragement during early stages of the project and later by courtesy of Canada Post.

- the people of Grey River for hospitality shown during my visits to the community.

- my field assistants, Leslie Lushman, Stan Lushman and Melvin Young.

- R. Kerrich, J. Mitchell, A. Halliday, B. Kronberg, and H. Wagenbaur for analytical data.

- D. Press, G. Andrews, J. Vahtra, P. Davis, H. Longerich, W. Marsh, and M. MacIntyre for sharing their expertise with me.

- the faculty and fellow graduate students of the department for assistance in various ways and for stimulating conversation at coffee breaks.

Financial support was provided by a Memorial University of Newfoundland fellowship, Price-Mineral Resources Division, and research grants to Drs D.F. Strong (NRC-A-7925) and R.W. Henley (NRC-A-3798). The author acknowledges and appreciates these sources of funding.

Finally, I wish to thank my wife, Christine, for typing successive drafts of the thesis and for help and encouragement throughout our stay in Newfoundland.

TABLE OF CONTENTS

	Page
ABSTRACT	ii
ACKNOWLEDGEMENTS	vii
LIST OF TABLES	xvii
LIST OF FIGURES	xxiii
LIST OF PLATES	xxxiii

CHAPTER 1

INTRODUCTION

1.1 LOCATION, TOPOGRAPHY AND ACCESS	1
1.2 HISTORY OF DEVELOPMENT	3
1.3 PREVIOUS WORK	5
1.4 PRESENT STUDY	6

CHAPTER 2

THE GEOLOGICAL AND GEOCHEMICAL FACTORS
CONTROLLING THE DISTRIBUTION OF TUNGSTEN

2.1 TUNGSTEN CHEMISTRY	8
2.2 CRUSTAL ABUNDANCE	10
2.3 GEOLOGICAL OCCURRENCE OF TUNGSTEN DEPOSITS	12
2.3.1 Pegmatites	13
2.3.2 Skarns	13
2.3.3 Quartz Veins	15
2.3.4 Stockwork and Related Deposits	17

	ix
	Page
2.3.5 Stratabound Scheelite Deposits	19
2.3.6 Other Deposits	20
2.4 PLATE TECTONICS AND TUNGSTEN MINERALISATION	21
2.5 PHYSICO-CHEMICAL PARAMETERS OF TUNGSTEN	
DEPOSITION.	22
2.5.1 Paragenesis.	23
2.5.2 Zoning.	24
2.5.3 Temperature and Chemistry of the	
Mineralising Fluid	24
2.6 TRANSPORT OF TUNGSTEN IN HYDROTHERMAL SYSTEMS	28

CHAPTER 3

THE GENERAL GEOLOGY

3.1 INTRODUCTION.	34
3.1.1 The Gander Zone.	34
3.1.2 Igneous Rocks of the Gander Zone	36
3.1.3 Tectonic Models - Gander Zone.	37
3.2 THE GREY RIVER AREA	40
3.2.1 The Metamorphic Suite.	40
3.2.1.1 Unit 1: Tonalitic Gneiss	42
3.2.1.2 Unit 2: Quartz Diorite to Diorite	
Gneiss.	45
3.2.1.3 Unit 3a: Amphibolitic Gneiss	
(Augen Gneiss).	46
3.2.1.4 Unit 3b: Mica Schist (Mylonite).	50
3.2.1.5 Unit 3c: Phyllites (Ultramylonite).	54

	x Page
3.2.1.6 Unit 3d: Metaconglomerate (?)	
Fault Breccia + Cataclasite	55
3.2.1.7 Unit 4: Leucogranite, "Ortho- quartzite" (Mylonite, Ribbon Mylonite)	60
3.2.2 The Igneous Suite.	63
3.2.2.1 Unit 5: Peridotite	63
3.2.2.2 Unit 6: Mafic to Intermediate Dykes	66
3.2.2.3 Unit 7: K-feldspar Megacrystic Granite	67
3.2.2.4 Unit 8: Composite Dyke Suite. Pegmatites, Diorites, Alaskite.	73
3.2.2.5 Unit 9: Leucogranite, Aplite, Pegmatite	74
3.2.2.6 Unit 10: Diabase Dykes	76
3.2.3 Structural and Metamorphic History	79
3.2.3.1 Prograde Metamorphism and Deformation	79
3.2.3.2 Retrograde Metamorphism and Deformation	80
3.2.3.3 Faulting and Jointing	88
3.3 CORRELATION	88
3.4 SUMMARY	92

CHAPTER 4

GEOCHEMISTRY - IGNEOUS ROCKS

	Page
4.1 INTRODUCTION.	95
4.2 CLASSIFICATION OF THE GRANITES.	95
4.3 METASOMATISM.	97
4.3.1 Major and Trace Element Variation.	100
4.3.2 Rare-Earth Elements.	105
4.4 METALLOGENIC ASPECTS.	108
4.5 DIABASE DYKES	115
4.6 CONCLUSIONS	118

CHAPTER 5

THE HYDROTHERMAL VEIN SYSTEM

5.1 INTRODUCTION.	121
5.2 RELATION OF THE VEINS TO THE GRANITOIDS	121
5.3 VEIN FORM AND STRUCTURE	123
5.4 STRESS REGIMES AND STRESS TRAJECTORIES.	127
5.5 RELATIONS BETWEEN STRUCTURE AND MINERALISATION.	131
5.6 EAST-WEST BLOCK FAULTING AND LATE VEINING	135
5.7 VEIN TYPES AND PARAGENESIS.	139
5.8 VEIN MINERALOGY	147
5.8.1 Wolframite	150
5.8.2 Scheelite.	151
5.8.3 Hematite	154
5.8.4 Molybdenite.	154

	xii
	Page
5.8.5 Pyrite	155
5.8.6 Marcasite.	156
5.8.7 Pyrrhotite	156
5.8.8 Chalcopyrite	156
5.8.9 Sphalerite	157
5.9.10 Bismuthinite-Galena	157
5.8.11 Sulphosalts, Tellurides, and Native Elements.	163
5.8.12 Quartz.	164
5.8.13 Feldspar.	165
5.8.14 Beryl	165
5.8.15 White Mica.	165
5.8.16 Fluorite.	166
5.8.17 Carbonates and Sulphates.	167
5.8.18 Chlorite.	168
5.8.19 Supergene Minerals.	168
5.9 F-cb VEINS.	171
5.10 MINERAL CHEMISTRY.	172
5.10.1 Bismuth-, Lead-, Silver-Bearing Minerals.	172
5.10.2 Tungstates.	194
5.11 PHYSICO-CHEMICAL PARAMETERS OF ORE DEPOSITION.	199
5.12 SUMMARY.	204

CHAPTER 6

ALTERATION GEOCHEMISTRY

6.1 INTRODUCTION.	208
6.2 ALTERATION TYPES.	208

	xiii
	Page
6.2.1 Autometasomatism	209
6.2.2 Greisenisation	209
6.2.3 Clay Alteration.	211
6.3 GEOCHEMISTRY.	215
6.3.1 Gain/Loss Diagrams	216
6.3.2 Gresens Composition - Volume Diagram.	222
6.4 RARE-EARTH ELEMENTS	227
6.4.1 REE Behaviour During Autometasomatism.	229
6.4.2 Behaviour During Greisenisation.	229
6.5 IMPLICATIONS OF REE DISTRIBUTION.	235
6.6 COMPARISON OF REE DISTRIBUTION WITH TUNGSTEN CONCENTRATIONS.	239
6.7 SUMMARY	241

CHAPTER 7

FLUID INCLUSIONS

7.1 INTRODUCTION.	243
7.2 DEFINITION OF TERMINOLOGY	245
7.3 ASSUMPTIONS AND PROCEDURES USED IN THIS STUDY	247
7.4 COMPOSITIONAL TYPES OF INCLUSIONS	249
7.5 SECONDARY INCLUSIONS.	258
7.6 THE SIGNIFICANCE OF SOLID MINERAL INCLUSIONS.	266
7.7 MICROTHERMETRIC MEASUREMENTS.	272
7.7.1 Salinity	272
7.7.2 Interpretation of Salinity Measurements.	283
7.7.3 Homogenisation	289

7.8	CRUSHING STAGE EXPERIMENTS.	295
7.9	DENSITY AND COMPOSITION OF CO ₂ -BEARING INCLUSIONS.	296
7.9.1	Purity of Carbon Dioxide	296
7.9.2	Density.	299
7.9.3	Composition.	300
7.10	GEOBAROMETRY	307
7.11	INTERPRETATION OF PRESSURE DETERMINATIONS.	314
7.11.1	Pressure Corrections.	318
7.12	FLUID INCLUSIONS IN FLUORITE-CALCITE-BARITE VEINS.	319
7.12.1	Inclusion Types and Occurrence.	322
7.12.2	Conclusions	325
7.13	SUMMARY.	326

CHAPTER 8

ISOTOPE GEOCHEMISTRY

8.1	INTRODUCTION.	329
8.2	OXYGEN ISOTOPE RELATIONS.	330
8.3	OXYGEN ISOTOPE THERMOMETRY.	332
8.4	CALCULATED $\delta^{18}\text{O}$ FLUID.	334
8.5	DISCUSSION.	338
8.6	SUMMARY	347

CHAPTER 9
RADIOMETRIC DATING

	Page
9.1 INTRODUCTION.	349
9.2 AGE RELATIONS: GRANIDOIDS AND SHEAR ZONE	352
9.3 DISTURBANCE OF THE Rb/Sr SYSTEMATICS.	357
9.4 AGE RELATIONS: MINERALISATION.	363
9.5 REGIONAL SIGNIFICANCE	365
9.6 METALLOGENY	367
9.7 SUMMARY	372

CHAPTER 10
THE GENESIS OF THE GREY RIVER TUNGSTEN PROSPECT
AND IMPLICATIONS FOR THE TRANSPORT OF TUNGSTEN
IN HYDROTHERMAL FLUIDS

10.1 THE GENESIS OF THE GREY RIVER TUNGSTEN PROSPECT. .	374
10.1.1 Source: Ore-forming Elements	374
10.1.2 Source: Hydrothermal Fluids.	378
10.1.3 Structural Controls to Mineralisation	380
10.1.4 Physico-Chemical Controls of Mineral- isation	381
10.2 WOLFRAMITE-SCHEELITE EQUILIBRIA.	384
10.3 CO ₂ -RICH FLUIDS AND TUNGSTEN DEPOSITS.	387
10.4 TUNGSTEN TRANSPORT AS CARBONATE/BICARBONATE COMPLEXES	392

CHAPTER 11
SUMMARY AND CONCLUSIONS

Page

396

REFERENCES 405

APPENDICES

APPENDIX A ANALYTICAL AND DETERMINATIVE

METHODS 442

B GEOCHEMICAL DATA. 452

C POLISHED SECTIONS 485

D CONSTRUCTION OF GRESENS DIAGRAMS. 491

E FLUID INCLUSION ANALYTICAL TECHNIQUES . 493

F FLUID INCLUSION DATA. 510

G P-V-T DATA FOR FLUIDS OF VARIOUS
SALINITIES. 528

H P-V-T DATA FOR CO₂-H₂O MIXTURES 534

REFERENCES 538

LIST OF TABLES

		Page
Table 2.1	Compilation of fluid inclusion and isotopic temperature determinations and chemical data for tin and tungsten deposits.	26
Table 3.1	Rock units of the Grey River area. . . .	41
Table 3.2	Petrographic notes on units of the metamorphic suite.	62
Table 3.3	Petrographic notes on units of the igneous suite.	77
Table 4.1	Comparison of the chemical composition of the Grey River granitoids with granites associated with rare-metal deposits	110
Table 4.2	Tungsten and tin concentrations of the Grey River granitoids.	114
Table 4.3	Major and trace element contents and C.I.P.W. norms of the diabase dykes.	117

Table 5.1	Characteristic features of the Vein Types	143
Table 5.2	Mineralogy of the Grey River Tungsten Prospect.	148
Table 5.3	Composition of bismuthinite.	180
Table 5.4	Composition of galena.	185
Table 5.5	Composition of tellurides, sulpho- salts and native bismuth	186
Table 5.6	Composition of galena and two exsolved Ag-Bi-Pb sulphosalts.	187
Table 5.7	Composition of chalcopyrite associated with silver and bismuth tellurides	188
Table 5.8	Assays of Galena #1 Vein from Bahyrycz (1957).	189
Table 6.1	Mineralogy and distribution of alteration facies.	213

Table 6.2	Mineralogical changes during alteration of amphibolitic gneiss and megacrystic granite.	214
Table 6.3	Tungsten and tin concentrations in metamorphic and hydrothermally altered rocks.	222
Table 6.4	REE contents of altered and unaltered rocks.	228
Table 6.5	Comparison of fluorine concen- trations with La/Yb ratios in the hydrothermally altered rocks	236
Table 7.1	Types of inclusions and distribution among vein types	265
Table 7.2	Types of solid inclusions and their distribution among the vein types.	267
Table 7.3	Calculated composition of Type IIB, IIB* inclusions	303
Table 7.4	Summary of Microthermetric Data.	328

Table 8.1	Oxygen isotope compositions of ore and gangue minerals.	331
Table 8.2	Oxygen isotope fractionation equations.	333
Table 8.3	Calculated isotopic temperatures for $\Delta q-m$ fractionations	333
Table 9.1	Rb, Sr analytical data	350
Table 9.2	Potassium/argon ages, Grey River Tungsten Prospect.	351
Table 10.1	Comparison of fluid inclusion data from deep- and high-level tungsten deposits	388
Table A.2.1.i	Precision and accuracy of replicate determinations	444
Table A.2.1.ii	Precision of A.A.S. analysis	445
Table A.2.2.i	Precision and accuracy XRF: Trace elements	446

Table A.2.3.i	Accuracy of REE determinations	450
Table B.1.i	Geochemical data: Granitoids.	453
Table B.2.i	Wolframite composition	460
Table B.3.i	Scheelite composition.	471
Table B.4.i	X-ray diffraction data - wolframite	474
Table B.5.i	Alteration geochemical data.	476
Table C.1.i	Ore mineral assemblages.	486
Table C.2.i	Reflected light properties	490
Table E.2.i	Melting temperatures - organic standards.	508
Table E.2.ii	Melting points - inorganic and metal standards.	509
Table E.2.iii	Freezing points - organic standards.	509

Table F.1.i	Type I inclusions - microthermo- metric data.	510
Table F.2.i	Type IIA inclusions - micro- thermometric data.	515
Table F.2.ii	Type IIA inclusions - clathrate data	519
Table F.3.i	Type IIB (and IIB*) inclusions - microthermometric data	520
Table F.4.i	Type IIC inclusions - microthermo- metric data.	524
Table F.4.ii	Type IIC - clathrate data.	526
Table F.5.i	Type I, Galena #1 Veins.	527
Table G.i	P-T-density data: Brines.	528
Table H.i	Specific volume of ideal $\text{CO}_2\text{-H}_2\text{O}$ mixtures	532

LIST OF FIGURES

	Page
Figure 1.1 Location map	2
Figure 3.1 Simplified Geology of the Grey River area	39
Figure 3.2 Summary of the structural history of the Grey River area	81
Figure 3.3 Growth history of the metamorphic minerals of the Grey River area	85
Figure 3.4 Inferred P-T conditions for contact metamorphism related to intrusion of the megacrystic granite . . .	87
Figure 4.1 Chemical classification of the Grey River granitoids from mesonorm calculations using Hietanen's (1963) molecular proportion classification. . .	96
Figure 4.2 Triangular ($\text{Na}_2\text{O} + \text{K}_2\text{O}$) -FeO-MgO (AFM) and Al_2O_3 -FeO-MgO (A'FM) plots of Grey River granitoids	98

Figure 4.3	Normative plot of megacrystic granite and leucogranite emphasising the variability of rock chemistry due to metasomatic events which effected each rock type	99
Figure 4.4	Major element variation diagrams for Grey River granitoids	101
Figure 4.5	Trace element variation diagrams for Grey River granitoids	102
Figure 4.6	Rare earth element analysis of Grey River granites	106
Figure 4.7	$\text{Na}_2\text{O}-\text{K}_2\text{O}$ plot of Grey River granites. . .	112
Figure 4.8	Alkali-silica and $\text{K}_2\text{O}-\text{TiO}_2-\text{P}_2\text{O}_5$ plot of diabase dyke geochemical data.	116
Figure 5.1	Location of major lodes in the Grey River Tungsten Prospect	122
Figure 5.2	Stress configuration and trajectories during development of the Grey River hydrothermal vein system.	129

Figure 5.3	The effect of normal faulting on fracture width, after Garnett (1966)	132
Figure 5.4	Vein cross-sections.	133
Figure 5.5	Compilation of assay data (Vein #10, #6).	In Map Holder
Figure 5.6	Correlation between grade, thickness, and dip of Vein #10, adit level.	134
Figure 5.7	Structural development of the Grey River hydrothermal vein system	140
Figure 5.8	Paragenesis.	146
Figure 5.9	Compositional data for bismuthinite, bismuth telluride, silver telluride, galena and Ag-Bi-Pb sulphosalts.	173
Figure 5.10	Summary of the distribution of sulphosalts, tellurides, and native bismuth and their unmixing sequence from Bi, Ag, Pb-rich precursors.	190

Figure 5.11	Phase equilibria and paragenesis in the $\text{PbS-Bi}_2\text{S}_3$ system (after Craig, 1967).	193
Figure 5.12	Variation in wolframite composition. . .	196
Figure 5.13	The effect of T , pH , f_{O_2} , f_{S_2} on wolframite and scheelite compos- ition.	198
Figure 5.14	Inferred pH condition of the Grey River hydrothermal fluid	202
Figure 6.1	Diagrammatic cross-sections of composite lodes showing the zonation of alteration facies developed during greisenisation.	212
Figure 6.2	Isovolume gain/loss diagram for altered amphibolitic gneiss wall rock: Major elements.	217
Figure 6.3	Isovolume gain/loss diagram for altered amphibolitic gneiss wall rock: Trace elements.	219

Figure 6.4	Isovolume gain/loss diagram for altered megacrystic granite: Major and trace elements	220
Figure 6.5	Gresens diagram showing composition- volume relationship for biotitic, calcic, phyllic and silicic alter- ation facies	224
Figure 6.6	Chondrite-normalised REE plot of greisenised and unaltered amphib- olitic gneiss wall rock.	230
Figure 6.7	Chondrite-normalised REE plot of altered (silicic) and unaltered deformed megacrystic granite wall rock	231
Figure 6.8	Depletion and enrichment of REE during greisen alteration and autometasomatism of the leuco- granite dykes.	232
Figure 6.9	Comparison of REE contents with tungsten and fluorine concentrations in greisen alteration facies of the amphibolitic gneiss wall rock.	240

Figure 7.1	Summary of the microthermometric data that can be obtained from a single $\text{CO}_2\text{-H}_2\text{O}$ bearing inclusion.	244
Figure 7.2	Compositional types of fluid inclu- sions found in the Grey River hydrothermal veins	250
Figure 7.3	Products of unmixing of a super- critical $\text{CO}_2\text{-H}_2\text{O}$ fluid	271
Figure 7.4	Salinity determinations for T_m ice of Type I and Type IIA inclusions in quartz, fluorite and scheelite. . . .	273
Figure 7.5	Comparison of salinity determinations from coexisting minerals	274
Figure 7.6	Ice and clathrate microthermometric measurements from Type IIA and IIC inclusions	277
Figure 7.7	Equilibria in the $\text{CO}_2\text{-NaCl-H}_2\text{O}$ system	278
Figure 7.8	Temperature of melting of CO_2 clath- rate for Type IIB inclusions	282

Figure 7.9	Melting point depression of ice for different solutes.	284
Figure 7.10	Effect of P_{CO_2} (dissolved CO_2) on the T_m ice.	288
Figure 7.11	Homogenisation temperature data for Type IIB, IIB* and IIC inclusions	290
Figure 7.12	Homogenisation temperature data for Type I and IIA inclusions.	291
Figure 7.13	Combined salinity/homogenisation temperature plot for Type IIA and Type I inclusions.	293
Figure 7.14	Homogenisation temperature measure- ments of Type I inclusions from coexisting quartz, fluorite and scheelite.	294
Figure 7.15	Temperature of melting of solid CO_2 in Type IIB and IIB* inclusions	297

Figure 7.16	Temperature of transition of liquid and vapour CO ₂ to liquid (Th CO ₂) for Type IIB inclusions.	298
Figure 7.17	A Th-X _{CO₂} plot of Type IIB (and IIB*) inclusions in comparison to the 1 kb solvus in the CO ₂ -H ₂ O system.	306
Figure 7.18	Absolute pressure and temperature determinations from intersection of isochores of immiscible but coexisting fluids.	313
Figure 7.19	The relationship between pressure variation and the structural development of the vein system	316
Figure 7.20	Homogenisation temperature of fluid inclusions in fluorite and apophyllite from F-cb veins.	320
Figure 8.1	Calculated $\delta^{18}\text{O}_{\text{H}_2\text{O}}$ coexisting with quartz, wolframite, and scheelite using trapping temperatures for each vein type derived from fluid inclusion data	335

Figure 8.2	Experimentally determined equilibrium oxygen isotope fractionation curves for various mineral-H ₂ O and mineral-CO ₂ systems.	341
Figure 8.3	$\delta^{18}\text{O}$ fractionation trends caused by immiscibility and retrograde boiling of the Grey River hydrothermal fluid.	342
Figure 8.4	Calculation of the change in $\delta^{18}\text{O}$ fluid due to CO ₂ -H ₂ O fractionation of a residual hydrothermal fluid undergoing progressive CO ₂ loss at 420°C and 300°C	346
Figure 9.1	Radiometric age determinations of metamorphic intrusion and mineralisation from the Grey River Tungsten Prospect	353
Figure 9.2	Rb/Sr whole rock isochron for the Grey River megacrystic granite	356
Figure 9.3	Sr and Rb variation in the Granite Cliff Shear Zone	359

Figure 9.4	Open system behaviour of Sr and Rb during the emplacement of the Grey River megacrystic granite.	360
Figure 9.5	Major W, Sn, Mo deposits in the northern Appalachians.	369
Figure 10.1	Summary of the evolution of the Grey River hydrothermal fluid.	382
Figure E.1.i	The CHAIXMECA system	494
Figure E.1.ii	Freezing mode/heating mode CHAIXMECA stage.	496
Figure E.2.i	Calibration of heating/freezing stage.	500
Figure E.2.ii	Accuracy of heating and freezing runs	501
Figure E.2.iii	Precision of heating and freezing runs	502

LIST OF PLATES

Plate

Plate 3.1	Field relationships of tonalitic and dioritic gneiss units.	43
Plate 3.2	Field relationships of amphibolitic gneiss and mica schist units	47
Plate 3.3	Field and thin section relationships of mica schist and phyllite units.	51
Plate 3.4	Field and thin-section relationships of fault breccia-cataclasite (deformed conglomerate?) unit.	56
Plate 3.5	Field and thin section relationships of fault breccia and leucogranite-orthoquartzite units	58
Plate 3.6	Field relationships of ultramafic, mafic and intermediate dykes, and K-feldspar megacrystic granite	64
Plate 3.7	Progressive deformation of the megacrystic granite in the Granite Cliff Shear Zone; field relationships of the post-tectonic composite dyke suite	68

Plate 3.8	Field relationships of the composite dyke suite and later leucogranites and diabase dykes.	71
Plate 3.9	Petrographic features of the deformation of the K-feldspar megacrystic granite in the Granite Cliff Shear Zone.	83
Plate 5.1	Vein types and structural form of hydrothermal veins	120
Plate 5.2	East-west faulting, F-cb veins and scheelitisation of wolframite.	137
Plate 5.3	Mineralogical aspects: Scheelite, wolframite, molybdenite, muscovite, pyrite, marcasite.	152
Plate 5.4	Mineralogical aspects: Marcasite, siderite, pyrrhotite, chalcopyrite, sphalerite, bismuthinite	158
Plate 5.5	Mineralogical aspects: Galena, Bismuth- inite, tellurides, carbonate, alteration of wolframite.	160

Plate 5.6	Supergene alteration of scheelite and bismuthinite. Apophyllite, F-cb veins, harmotome	169
Plate 5.7	X-ray scan photographs of a galena inclusion in pyrite.	175
Plate 5.8	X-ray scan photographs of galena grains, vein #7.	177
Plate 5.9	X-ray scan photographs of intergrown bismuthinite and galena, and Ag- and Bi- tellurides	179
Plate 7.1	Type I inclusions.	253
Plate 7.2	Type IIA inclusions.	255
Plate 7.3	Type IIB, IIB* inclusions.	259
Plate 7.4	Type IIC inclusions.	261
Plate 7.5	Type IIC and Type IV inclusions.	263
Plate 7.6	Fluid inclusions in apophyllite.	320

CHAPTER 1

INTRODUCTION

1.1 LOCATION, TOPOGRAPHY, AND ACCESS

The Grey River Tungsten Prospect is located at the village of Grey River (Lat. $47^{\circ} 35'$; Long. $57^{\circ} 10'$), one kilometer from the entrance of Grey River fiord on the south coast of Newfoundland (Figure 1.1).

The village of 250 people, established in the 1820's, is built on a small triangular alluvial fan about 150 m by 200 m in dimension. It is bordered on two sides by cliffs, which rise steeply to 250 m above sea level, and on the third side by Grey River. The nearest major settlement, Burgeo, lies about 40 km west along the coast, and Ramea, a minor fishing port, lies 18 km offshore to the southwest, on Ramea Island.

The Grey River area is dominated topographically by two features - the barrens, and the Grey River fiord. The barrens represent an eroded peneplain (Twenhofel and MacClintock, 1940), and has an elevation ranging between 250 m and 350 m above sea level. In detail, the surface of the barrens is rugged, cut by many gullies and dotted with numerous ponds, bogs and depressions. Large lakes occur along glacial valleys and depressions controlled by regional fault systems. Major vegetation is poorly developed except along portions of the Grey River fiord.

The peneplain is dissected by overdeepened glacial valleys - fiords - which now provide egress for Grey River

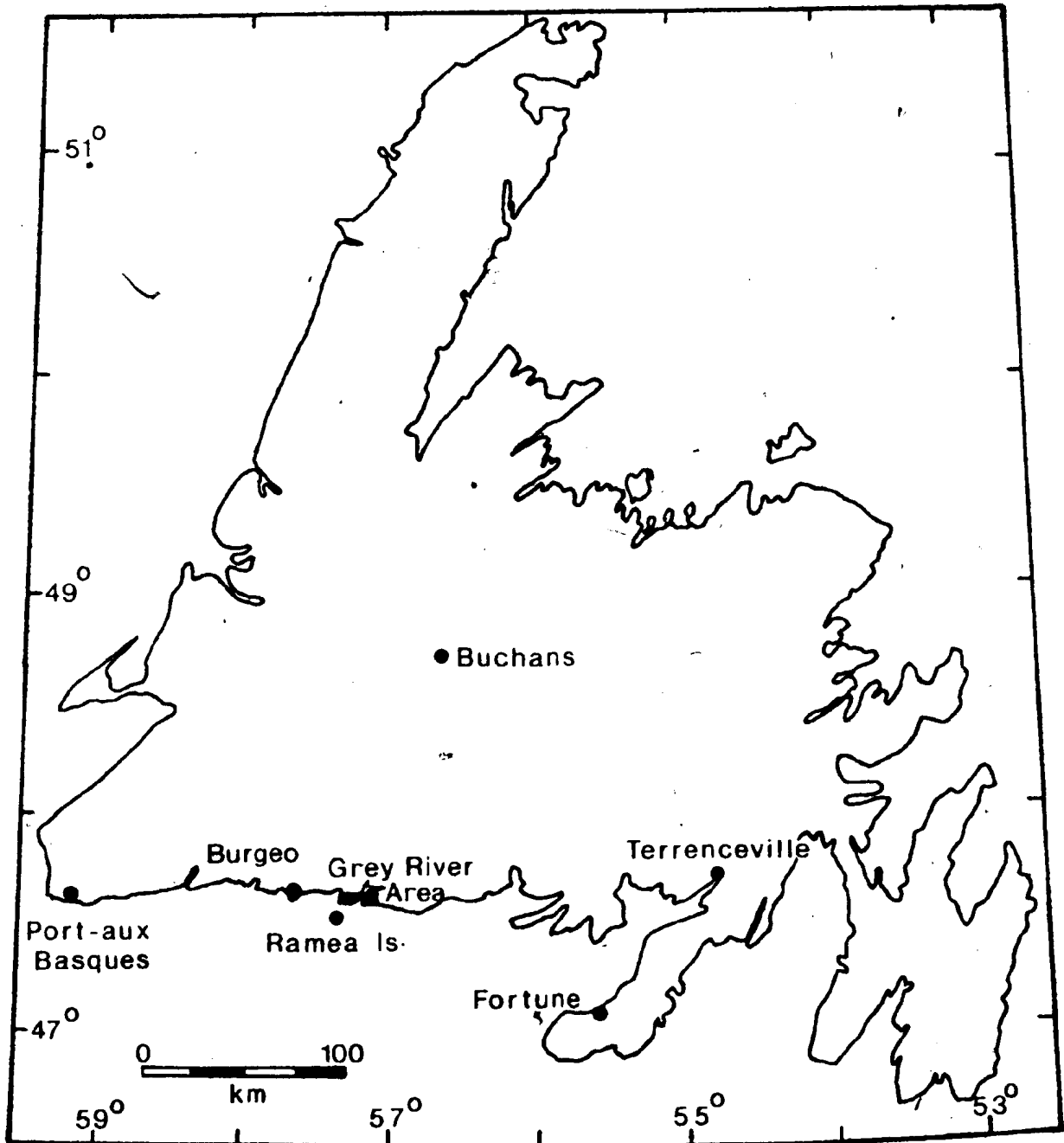


Figure 1.1 Location map .

to the sea coast. The fiord extends 10 km north of the sea coast and branches into three arms - northwest, northeast and southwest.

The area is accessible only by float plane or coastal ferry service from Fortune, Terrenceville, or Port-aux-Basques, but access is hampered by the hostile south coast climate.

1.2. HISTORY OF DEVELOPMENT

Early in the 1950's Mr Henry Rose, a trapper from Grey River, dispatched several "mineral" samples to geologists of Buchans Mining Co. Ltd. One or more of the samples contained cassiterite and silver but the sample locality was unknown. The area was prospected in 1955 by Buchans Mining Co. personnel and several occurrences of economic minerals were reported. The source of the tin and silver eluded the prospectors, however veins containing tungsten minerals were found south of Long Pond near the village of Grey River.

The following years saw extensive development work completed on the prospect and between 1956 and 1958 over 300 veinlets were delineated by trenching and mapping. Soil geochemical prospection was useful in delineating the overall dimensions of the mineralised area but its use in finding individual veins was limited primarily because of poor soil development, the lack of drainage and the occurrence of hundreds of small tungsten-bearing veins in the area. South of Long Pond a mineralised area 1 km by 1 km

trending N 20 E was outlined by this method. Anomalies north of Long Pond indicate an extension of the mineralised area to the North.

The major veins south of Long Pond were trenched and sampled in the 1956-1957 field seasons and only two appeared to contain economic grades (Vein #10, #6). During this time the general geology of the area was compiled on a scale of 1" to 100 feet. In 1957 1400 m of drilling was completed mainly to determine the behaviour of vein #10 at depth. Concentration tests were made on two samples of ore from the prospect by the Mineral Processing Division, Dept. of Mines, Ottawa (Mathieu, 1961).

Numerous scheelite and wolframite occurrences were also found in an area 15 km north of the Grey River Tungsten Prospect. The area was prospected in 1957 using both soil and stream geochemical sampling, but detailed geologic relations are poorly known. Most occurrences in the north-east branch of Grey River occur as float, with in situ veins found sporadically within high grade metamorphic rocks.

The prospect lay dormant till the late 1960's when an adit was excavated to explore the largest of the veins, Vein #10. The portal is situated on the cliffs above Grey River settlement (13 m above sea level), and proceeds horizontally underground northwards for nearly two kilometers. The northern half of the total strike length of Vein #10 exposed on surface (250 m above sea level), was intersected at adit level and channel and chip samples were

taken for assay. Bulk samples (250 tonnes) from 26 raises in the adit were shipped to Ottawa for assay and pilot plant tests (Mathieu and Bruce, 1970; Raicevic and Bruce, 1971).

At that time an overall grade for the prospect of 1.09% WO_3 was calculated from bulk samples, channel samples and drill core intersection assays. Reserves were estimated at 360,000 tonnes assured and probable and 160,000 tonnes possible. In all a total of 68 drill holes were completed (mainly Ex core) for a total length of 4963 m (16,282 feet); 3834 m from surface drilling and 1129 m in the adit.

Excavation ceased on the adit in 1971 and development work on the prospect has been at a standstill since then. Total expenditure on exploration from discovery to present day is estimated to be less than \$1 million. The Grey River Tungsten prospect is presently owned jointly by Abitibi-Price Mineral Resources and ASARCO.

A silica prospect (orthoquartzite) occurs 2 km east of the Grey River Tungsten prospect. Recent drilling and evaluation by the Newfoundland Department of Mines (Butler and Greene, 1976) has delineated 12 million tonnes of 95.5% silica. This yields an 8th quality glass (suitable for making brown bottles!) after a simple beneficiation process.

1.3. PREVIOUS WORK

Two graduate students have presented theses on the Grey River Tungsten prospect. Bahrycz (1957) briefly described the mineralogy and structure of the prospect and elaborated on the metamorphism of the sedimentary and vol-

canic rocks of the area. Gray (1958) dealt mainly with ore mineralogy and the origin of the deposit.

The Grey River area occurs on the boundary of two Geological Survey of Canada maps (Riley, 1959; Williams, 1971). A number of unpublished company reports and maps are available (Bahyrycz, 1956; Higgins and Swanson, 1956; Kadowacki, 1957), and several metallurgical reports (Mathieu, 1961; Mathieu and Bruce, 1970; Raicevic and Bruce, 1971).

1.4. PRESENT STUDY

This thesis is directed towards the formulation of a model for the genesis of the Grey River Tungsten Prospect. Ore formation requires a source, both of the ore-forming elements, and the transporting medium. Also sufficient energy must be available to promote their transfer to a site of deposition which is governed by structural and physico-chemical controls. Any model describing the genesis of an ore deposit must evaluate these parameters.

The excellent underground and surface exposures of the mineralisation in the Grey River prospect facilitate sampling for a detailed study on the transfer and deposition of tungsten in the hydrothermal environment. Furthermore, underground exposures provide evidence of the chemical and structural development of the deposit that was unknown previously. This allows new exploration criteria to be established both on local and more regional scales.

In order to fully evaluate these aspects a multi-directional research approach was sought utilising fluid

inclusion techniques, major and trace element geochemistry (including REE analysis), stable isotopes, and radiometric dating techniques.

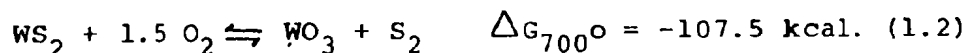
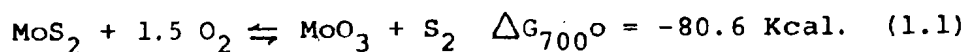
Field and laboratory work was completed during the period September 1976 and August 1980.

CHAPTER 2

THE GEOLOGICAL AND GEOCHEMICAL FACTORS CONTROLLING THE DISTRIBUTION OF TUNGSTEN

2.1 TUNGSTEN CHEMISTRY

Tungsten, a member of the third transition series, belongs to Group VI of the Periodic Table along with chromium and molybdenum. There is considerable chemical coherence between molybdenum and tungsten resulting from the reduction of the 4f shell with progressive addition of electrons in the Lanthanides - the Lanthanide contraction. However, molybdenum and tungsten separate in nature because of the tendency of molybdenum to form MoS_2 and tungsten to form tungstates. The difference is apparent in the free energies of the two reactions.



At concentrations of oxygen and sulphur to be expected in hypogene environments, the first equilibrium would favour the sulphide and the second the oxide (Krauskopf, 1970).

The similarity of energy levels of the 5d and 6s shells allows oxidation states ranging from W^{6+} to W^0 , however the higher oxidation states of tungsten are more stable than lower oxidation states. A characteristic feature of tungsten is its ability to form a wide number of polytungstate acids and their salts, but the naturally occurring compounds of tungsten are limited to the tungstates and hydrated tungstates. An exception is tungstenite, a rare tungsten sulphide. The

complex hydrated tungstates together with russellite, sanmartinite and stolzite are common as alteration products after the hypogene tungstates, wolframite and scheelite.

Limited solid solution exists between wolframite and scheelite (Grubb, 1967; Chang, 1967), although a broad immiscibility gap persists at low temperatures. Solid solution has been demonstrated between scheelite (CaWO_4) and powellite (CaMoO_4) (Hsu and Galli, 1973). However the two differ paragenetically with powellite being formed rarely as an alteration product of molybdenite (Hsu, 1977). Chang (1967) reports a complete solid solution in the synthetic system between scheelite and stolzite (PbWO_4). The chemistry of secondary alteration minerals is rather complex and there is a possibility that a four-way solution may exist of the type $(\text{Pb}, \text{Ca}) (\text{W}, \text{Mo}) \text{O}_4$ (Clark and Sillitoe, 1970). Complete solid solution within wolframite exists between the end members ferberite (FeWO_4) and huebnerite (MnWO_4) and variation of the ratio of Fe/Mn in wolframite has been related to changing thermal conditions (Hosking and Polkinghorne, 1954). The contradictory evidence exposed by Taylor and Hosking (1970) suggests that other mechanisms are responsible for the changing Fe/Mn ratio within deposits. Recently Hsu (1976) has shown experimentally that Fe/Mn variation of the wolframite series cannot be used to evaluate such physico-chemical variables as f_{O_2} , pressure and temperature. Neither f_{O_2} nor f_{S_2} exerts any noticeable influence on the composition of wolframite (Hsu, 1976), and the Fe/Mn ratio is probably controlled by the activities of

Fe^{+2} and Mn^{+2} in the hydrothermal fluids (Clark, 1970).

2.2 CRUSTAL ABUNDANCE

Data pertaining to the crustal abundance of tungsten are scarce due to its relatively low concentration and difficulties with analytical procedures. Krauskopf (1970) lists several tables of tungsten concentrations for differing rock types, and for concentrations in silicate and non-silicate minerals. Generally, felsic rocks exhibit uniform concentrations of tungsten around 1-4 ppm. This has led people to suggest a Clarke concentration of 1.5 ppm (Krauskopf, 1970). Many felsic rocks have tungsten concentrations much greater than the Clarke value even when not associated with ore deposits. This is indicative of the tendency of tungsten (and molybdenum) to remain in a residual crystallising melt (Kosals and Mazurov, 1970) and reflects a slightly higher concentration of the element in mineral phases which crystallise late in the intrusive granite. Such an enrichment is predicted on crystallochemical grounds, particularly the high ionic potential of the W^{6+} ion.

The limited data indicate a possible increase in Clarke values from ultramafic to felsic rocks, and tungsten values are often enhanced in granites with some degree of alteration. This is especially true of greisen alteration where tungsten content increases dramatically with degree of muscovitisation (Ivanova, 1963, 1969; Hall, 1971). Molybdenum does not follow this enrichment and values are

close to those for unaltered rocks (Ivanova, 1963, 1969).

The Clarke value for arenaceous sediments is approximately the same as felsic rocks, and carbonates fall within the narrow limits of 0.2 ppm to 0.7 ppm (Foster, 1973). There is a tendency for carbon-rich sediments to be enriched in tungsten relative to those that are carbon-deficient, and anomalously high concentrations are known from some recent sediments. Up to 130 ppm are recorded from the Black Sea sediments and 16-18 ppm from red clays of the N.E. Pacific (Krauskopf, 1970).

Amongst the silicate minerals, feldspar and quartz contain quite large (0.1 - 1.3 ppm) amounts of tungsten (Ivanova, 1969; Ivanova and Butuzova, 1968; Krauskopf, 1970). This seems unusual in light of the apparent incompatibility of the small, highly charged ion with silicate structures. It is possible that tungsten is present in fluid inclusions within the phases or within crystal defects. The former mechanism might also be applicable to the quartz associated with greisenisation. Biotite and especially muscovite are known to contain very high concentrations (1-70 ppm) of tungsten, even in rocks devoid of mineralisation (Krauskopf, 1970). The high cation-exchange properties of micas are well known, and the high tungsten contents are possibly due to an isomorphous replacement of the octahedrally coordinated aluminium (Foster, 1973).

The W^{6+} ion, having a similar ionic radius to Fe^{3+} and Ti^{4+} readily enters such minerals as magnetite, ilmenite

and sphene. It has been noted that the element is readily leached from these accessory minerals (Lyakhovich and Balanova, 1969), which suggests that isomorphous substitution may not be the dominant mechanism (Foster, 1973).

Extremely high concentrations of tungsten are found in manganese minerals such as psilomelane and pyrolusite. These minerals are known in epithermal deposits (with quartz and carbonate) as supergene alteration products of other primary manganese minerals or as precipitates around hot springs. Concentrations of up to 8.8 wt% WO_3 have been reported in manganiferous clays at Golconda, Nevada (Hewett and Fleischer, 1960).

The mobility of tungsten in natural waters is thought to be slight and although the data are limited, the tungsten contents of waters in the vicinity of ore deposits appear to be somewhat elevated (Kraynov et al., 1965); that is, greater than 1 ppb compared to 0.3 ppb in average river water (Riley and Chester, 1971). It is suggested by Kraynov et al., (1965) that high tungsten concentrations are possible in alkaline carbonate-rich waters with a pH greater than 6.

2.3 GEOLOGICAL OCCURRENCE OF TUNGSTEN DEPOSITS

Both wolframite and scheelite are known to occur in a wide variety of ore deposits. Most of these deposits can be attributed to plutonic activity, with the development of skarns, veins and greisen deposits in close spatial relation to granitic intrusions. Recognition of syngenetic stratabound deposits and deposits of metamorphic origin

are recent developments.

2.3.1 Pegmatites

Pegmatites containing scheelite or wolframite or both have been reported in many parts of the world and are often closely associated with tungsten-bearing quartz veins near the contacts of intrusive rocks. Considerable controversy surrounds deposits that have been termed pegmatitic, mainly as a result of the mis-identification of so-called pegmatites. Most, if not all, tungsten-bearing pegmatitic deposits are probably more correctly described as quartz lodes. Wolframite and scheelite have rarely been described as accessory minerals in igneous rocks (Stemprok and Sulcek, 1969) and then are not magmatic, but the result of hydrothermal alteration (Foster, 1973). However, Hsu and Galli (1973) described a scheelite-bearing pegmatite dyke from the Oreana Mine, Nevada, where the mineral is associated with quartz, oligoclase, potash feldspar, muscovite, beryl, fluorite and minor accessories. For the most part pegmatite deposits are small and have yielded an insignificant portion of world tungsten production in the past.

2.3.2 Skarn

These deposits are a product of high temperature replacement and recrystallisation of pure and impure limestones and dolomites, at or near the contact with intrusive igneous rocks. They are produced basically by two processes - i) a simple thermal metamorphism of impure carbonate strata followed by ii) an additive metasomatic event caused

by the migration of a hydrothermal fluid generated from a magmatic intrusive (Taylor and O'Neil, 1977). Major features of the metasomatic process in skarn bodies involve the removal of carbonate components CaO and CO_2 and addition of considerable quantities of SiO_2 , Al_2O_3 and total iron.

Skarns reported from gneisses of the Bindal area, Norway, are regarded as reaction skarns (metamorphic skarns) which were formed solely by exchange of material between the limestones and bordering supercrustal rocks. The skarns were formed during the peak of metamorphism and migmatization, the granites themselves having no direct influence on their formation (Skaarup, 1974).

Scheelite is essentially restricted to the skarn bodies rather than the calc-silicate hornfels and appears to be deposited during the early formation of the skarn silicate minerals, persisting to lower temperatures in cross-cutting quartz veins (Kerrick, 1977; Taylor and O'Neil, 1977). Scheelite is seldom uniformly distributed in skarn bodies but in many mines is found in fairly well defined shoots or concentrated along certain bands in the skarn. In most places the skarns form sharply bounded bodies whose shape and distribution are controlled mainly by the contact of the associated intrusive rock and the structural orientation and chemical peculiarities of the favourable host rock. Deposits range in size from small isolated pods scattered along an intrusive contact to massive bodies comprising

millions of tons. Typical grades fall in the range 0.5 - 1.5% WO_3 with 1% WO_3 being an average concentration. While they are the principal commercial source of tungsten in North America, skarns place second to quartz veins as a commercial source on a worldwide basis.

2.3.3 Quartz Veins

Tungsten-bearing quartz veins are widely distributed and account for more than three quarters of the world's known reserves of the metal. Like skarn deposits they are generally associated spatially, and in most cases genetically, with plutonic rocks of granitic composition. Deposits, commonly consisting of sheeted systems of veins, occur near the contacts of the granite either in the border zones of the granite or in adjacent country rocks or in both. Being mineralogically simple most tungsten-bearing veins consist of quartz with scheelite and/or wolframite and minor amounts of sphalerite, galena, chalcopryite, pyrite, pyrrhotite, molybdenite, cassiterite, and arsenopyrite. Fluorite, feldspar and calcite may be present as gangue minerals.

The metallogenic district of south-west England provides excellent examples of granite-related vein systems containing tungsten (and tin) mineralisation. Lode mineralisation began in the late stages of the emplacement of a Permian-Carboniferous granite batholith into a lower Paleozoic geosyncline (Rayment et al., 1971). The present erosion level has revealed several of the higher level portions of

this batholith which are associated with numerous sheeted vein complexes (e.g. Cligga Head, Hemerdon Bell) and vein-lode systems (Sth. Crofty and Geevor Mines). The sheeted vein complexes occupy the earliest brittle fractures to form in the cooling intrusion and are thus confined to granite cusps (Moore, 1977; Moore and Jackson, 1977). The vein-lodes occupy fissures in a conjugate system of normal faults, the fissures being produced as a part of a regional stress system imposed by the underlying batholith (Moore, 1975, 1977).

Tungsten-bearing quartz veins often have associated greisen alteration produced by reaction between the hydrothermal fluid and wallrock. Greisen alteration assemblages are dominated by quartz-muscovite-fluorite but a number of accessory minerals may or may not be present, for example, topaz, tourmaline, and wolframite. Greisen alteration can occur as an envelope to a quartz vein (Hall, 1971; Moore and Jackson 1977) or more pervasively (Shepherd *et al.*, 1976). During greisenisation trace elements such as F, Li, Rb, Sn and W are concentrated, while Na is decreased relative to unaltered rocks (Hall, 1971).

Tungsten-bearing quartz veins are typical hydrothermal vein deposits, being tabular bodies that vary greatly in length, width, and depth. Although most sheeted vein systems have quite large dimensions, individual veins tend to be discontinuous and pinch and swell over relatively short distances. Within these component veins, tungsten

minerals have a generally erratic distribution, their deposition from the hydrothermal fluid being controlled by such factors as pressure, temperature, structure, wall rock alteration and chemical composition of the fluid. Such patchy distribution is commonplace and makes exploration and exploitation extremely difficult. While local concentrations of tungsten in veins can be quite high, the average grade from productive veins is close to 1% WO_3 .

Not all vein deposits are genetically associated with igneous rocks and processes, in fact there is considerable evidence for the involvement of metamorphic fluids in hydrothermal ore deposits, especially those of the gold-tungsten association. Many vein deposits previously assigned an igneous-hydrothermal origin have been reclassified as products derived from dehydration reactions during prograde metamorphism (Henley et al., 1976; Kerrich, 1977; Kerrich and Fryer, 1979). Such fluids leach trace metals from the metamorphic rocks and are focussed in zones of dislocation where they migrate to higher crustal levels and deposit ore-bearing lodes when certain physico-chemical conditions are reached.

2.3.4 Stockwork and Related Deposits

There exists a number of tungsten deposits in which the tungsten minerals do not form bodies of skarn nor discrete hydrothermal vein systems but occur as fracture fillings and replacements in stockwork and breccia zones. Two types of deposits are evident; tungsten associated with molybdenite-

bearing porphyries and tungsten associated with multi-metal porphyry (typically breccia pipe) deposits.

Huebnerite occurs in small amounts disseminated through large volumes of the porphyry molybdenite ore body at Climax, Colorado. Although the grade of the tungsten trioxide is only a few hundredths of 1 percent, the huebnerite is recovered as a byproduct of the large scale mining of molybdenite and now constitutes a significant source of the United States supply of the metal.

Wolframite concentrates are produced from several breccia pipe-like deposits in Australia and elsewhere. These contain significant quantities of other metals, including bismuth, tin, molybdenite and copper. The deposits occur in a subvolcanic setting in breccia pipes related to volcanic rocks and in most cases are thought to be genetically related to the host rock.

A W-Mo-Bi stockwork deposit occurs at Mt Pleasant (New Brunswick) and is associated with two subvolcanic plugs of quartz-feldspar porphyry (Dagger, 1972). Mineralisation is intimately related to the volcanic phase since volcanic breccia in part postdates the mineralisation. The W-Mo-Bi mineralisation occurs within the plugs on joint surfaces, and disseminated throughout the rock. Subeconomic tin, copper and zinc mineralisation occur mainly as irregular replacements in the contact zones between volcanic plug and wall rock. A distinct zoning pattern is evident, with a central wolframite core passing outward into a cassiterite zone.

then a sphalerite-chalcopyrite-galena zone. Rock alteration is centered on the two plugs and is a broadly zoned greisen-type alteration passing outwards into chloritisation with silicification (Dagger, 1972).

2.3.5 Stratabound Scheelite Deposits

In recent years a number of stratabound deposits have been found in the early Paleozoic rocks of the European Alps (Maucher, 1965, 1976; Höll et al., 1972; Höll, 1977). Two generations of scheelite-bearing ore occur within lower Paleozoic sediments consisting of graphitic schists alternating with layers of metatuffs and dolomites. The first generation consists of massive to banded streaks and lenses of mostly fine grained stibnite, without gangue minerals, but with irregular, dispersed patches of scheelite. The ore is generally restricted to one bed of either graphitic and sericitic schist or quartzite or dolomite, above a metavolcanic tuff horizon. Locally synsedimentary-diagenetic fabrics are preserved within the ore horizon, e.g. rhythmic bedding, glide folds etc. (Höll et al., 1972).

The second generation consists of short fissure veins which cut the ore horizon of the first generation. These metamorphic veins are mainly filled by quartz or calcite depending on the lithology of the transected rocks. Scheelite and other ore minerals within them are derived by remobilisation of primary ore and the veins are generally spatially associated with the primary ore horizon. Of the ore minerals scheelite, cinnabar, and stibnite, scheelite

is remobilised the least, with increasing mobility in the metamorphic environment being observed for stibnite and cinnabar. In fact later orogenic processes have remobilised many stratabound cinnabar and stibnite occurrences, to form younger epigenetic deposits (Maucher, 1976).

For a variety of reasons, researchers conclude that the primary ore was deposited contemporaneously with its surrounding volcanic-sedimentary host rocks and are related to deep-seated magmatic sources in a volcanic-hydrothermal system. Similar stratabound deposits are now recognised around the world and range in age from Precambrian to Silurian (Skaarup, 1974; Stumpfl, 1976).

2.3.6 Other Deposits

Several unusual occurrences of high concentrations of tungsten are known from hot springs and brines. A small but highly anomalous amount of WO_3 is present in the saline brines of Searles Lake (Carpenter and Garrett, 1959) and to a lesser extent in Owens Lake, both of which are part of the Pleistocene Owens River interior drainage system in eastern California. Searles Lake occurs in a region of many small tungsten deposits from which much of the tungsten in the brines was probably leached. Carpenter and Garrett (1959) note that one of the many springs feeding into Searles Lake contains 240 ppb tungsten and thus may have contributed to the total tungsten that collected in the lakes.

Tungsten in Searles Lake occurs as a solute, probably

as a complex ion in the brines and concentrations vary from 40 to 70 ppm WO_3 . The calculated amount of WO_3 in the brines is thought to be 8.5 million s.t.u. of WO_3 , more than half the known reserves of the United States.

Many manganese- and iron-oxide deposits contain significant amounts of tungsten (Hewett et al., 1963). These deposits, formed at or near the surface, comprise various mixtures of manganese and iron oxide in surficial alluvial material, as hot spring aprons, or as near-surface veins. One of the largest deposits known occurs at Galconda, Nevada, where tungsten-bearing oxides occur within a Pleistocene conglomerate (Kerr, 1940).

Alluvial deposits are relatively rare because of the extreme friability of tungsten minerals in the weathering environment (and during ore beneficiation - a curse for the metallurgist!). Some alluvial deposits are worked especially on the African continent (e.g. Zaire).

2.4 PLATE TECTONICS AND TUNGSTEN MINERALISATION

Many authors have attempted to relate the genesis of mineral deposits to plate tectonics (e.g. Mitchell and Garson, 1976; Pereira and Dixon, 1971). Plate tectonics cannot yet conclusively explain where metals in the ore deposits originated from, but it may explain the origin of rocks hosting the ore in terms of global theory.

Generally speaking, tungsten is known to occur in most tectonic environments. Bolivian, Mexican, Alaskan, Malaysian, Indonesian, E. Australian and Western European

deposits of tungsten are believed to have formed at convergent margins above subduction zones (Sillitoe, 1972, 1976; Mitchell and Garson, 1972; Mitchell, 1973). A model involving a progressive sequence of metallogenic provinces away from a subduction trench was devised from studies of Andean and Western U.S.A. mineral deposits (Sillitoe, 1972). Generally tungsten (and tin) concentrations are believed to arise from the deepest part of the subduction zones. In detail however, the model breaks down and Clark et al. (1976) maintain that the ore deposits are formed as a result of igneous processes operative above subduction zones, reinforcing a persistent anomaly drawn on periodically from the Paleozoic.

Tungsten and tin deposits in intraplate environments where magmatism is largely related to hotspot activity, are well documented. Many tin deposits (and tungsten) are associated with crustal melting during the early stages of hotspot activity and are genetically related to small alkaline and peralkaline granite plutons of anorogenic character.

At mid-ocean ridges anomalous tungsten concentrations are recorded from manganiferous cherts and other chemical sediments formed at, and associated with, constructive plate margins (Krauskopf, 1970).

2.5 PHYSICO-CHEMICAL PARAMETERS OF TUNGSTEN DEPOSITION

Over the last few decades a considerable body of literature has been amassed on the spatial, temporal and chemical parameters that govern the deposition and distri-

bution of tungsten in ore deposits.

2.5.1 Paragenesis

Paragenetic sequences are thought to reflect a gradual decrease in temperature of the ore-forming fluid with time, and studies of vein paragenesis show there is considerable overlap in the relative times of deposition of wolframite and scheelite and associated minerals in any given deposit. Commonly an association of wolframite, cassiterite and arsenopyrite represents an earlier stage of mineralisation succeeded by deposition of base metal sulphides (Kelly and Turneaure, 1970; Dagger, 1972; Groves et al., 1970; Hosking, 1951). Reversals of this sequence can be found, for example, the Ima mine, Idaho (Anderson, 1948), where complex silver-sulphide veins occur as fracture controlled veins at a margin of a granitic body. These veins extend into the quartzitic country rock for over half a kilometer. Beyond this distance the vein mineralogy passes from a complex sulphide assemblage to huebnerite and quartz which persists for another half a kilometer away from the intrusive contact. This paragenesis assumes however that the hydrothermal fluid emanated from this intrusive body and not some unexposed pluton.

Repeated deposition of wolframite occurs in some deposits (Landis and Rye, 1974) and may reflect episodic influx of the hydrothermal fluid into a vein and/or the formation of a composite vein by repeated reopening of the vein system.

2.5.2 Zoning

Zonal relationships are often fairly well developed in vein tungsten deposits and broadly defined tungsten and tin zones give way to base metal sulphides with increasing distance from intrusive centres (Dagger, 1972; Blake and Smith, 1970). Generally tungsten appears to be deposited closer to the emanative centre than tin, and deposits in Cornwall exemplify this with sheeted vein systems containing tungsten confined to margins of granitic cusps while cross-cutting tin-bearing veins transect the granite/killas contact (Moore and Jackson, 1977; Moore, 1977).

Zoning can be on a district-wide scale as is the case for the Herberton tin field, North Queensland (Blake and Smith, 1970). Vertical zoning is noted in some deposits, and matches lateral distribution (Hosking, 1951; Dagger, 1972).

Zonal arrangements appear to match the paragenetic sequence and although the distribution of ore minerals is not unique, the agreement between the paragenetic position of any mineral and its approximate zonal position implies some degree of temperature-controlled deposition in vein tungsten deposits.

2.5.3 Temperature and Chemistry of the Mineralising Fluid

Greisen deposits generally have been accorded a higher temperature origin than lode deposits accompanied by little alteration. However, fluid inclusion data indicate

that there is a variable and wide range of crystallisation temperatures for greisen deposits. Table 2.1 is a compilation of fluid inclusion and isotopic temperature determinations and chemical data for tin and tungsten deposits. Note that greisen deposits can record fairly low temperatures of deposition (Naumov and Ivanova, 1971) even after pressure and salinity corrections have been applied.

Temperatures of deposition for wolframite generally fall within an upper mesothermal to epithermal range (500-200°C). Cassiterite has a close paragenetic relationship to wolframite and thus has a relatively similar depositional temperature range. Scheelite also has a considerable range in depositional temperatures, similar to wolframite. However, several skarn scheelite deposits have quite high homogenisation temperatures of 550-650°C (Kerrick, 1977).

Chemical data obtained from fluid inclusion studies emphasize that solute concentrations may vary during the deposition of tungsten minerals in different deposits. Kelly and Turneare (1970) record solute concentrations ranging from 18.5 to 46 equivalent wt% NaCl. The highest values occur in the high temperature quartz-cassiterite stage and decrease to 1.5 equivalent wt% NaCl at the end of the mineralisation episode. Sawkins (1966) records salinities up to 50 equivalent wt% NaCl from Cornish deposits and Groves et al. (1970) found an average salinity for the Rex Hill Mine, Tasmania, of 5.2 - 10.6 wt% NaCl, although early high temperature quartz also yielded high salinities

Table 2.1
Fluid Inclusion Temperatures and Chemical Data

SOURCE	MINERAL	METHOD	TEMPERATURE	SALINITY (equiv NaCl)	LOCALITY	REFERENCE
Wolf-cass-qtz Volcanic setting	Quartz Cassiterite	H	295-310 PS 390-400 PS	high. 18.5-44 with boiling indicated	Central + Southern Bolivia	Kelly+Turnmore, 1970
Wolframite-cass Plutonic setting	Quartz Cassiterite	H	225-320 PS 330-310 PS	"	"	"
Qtz-wolframite veins	Quartz Wolframite	HD	345 F 260 P	"	South Crofty, Cornwall	Smith, 1949
Qtz-cassiterite Qtz (post-cass)	Quartz Quartz	H	435-440 300-314	Max. 50	Cornwall	Sekine, 1966
Qtz-fluorite- sulphide	Quartz	H	260-410 PS	5.2-10.6	Bux Hill, Tennessee	Groves et al., 1970
Greisam veins	Quartz, beryl, fluorite, cass	H	205-302 PS 350-375 PS	"	Transbaykalia, USSR Karakhatan, USSR	Naumov+Ivanova, 1971
Qtz-wolf veins	Quartz, cass, beryl	H	277-314 PS	"	Chukotka, USSR	"
Greisam veins	Quartz, topaz, cass, fluorite, beryl, wolf	H	205-400 PS	"	Monpolia, USSR	"
Qtz-wolf	Quartz, wolf	HD	200-340 PS	"	Eregebirge	Naumov+Ivanova, 1971
Qtz-feldspar- wolf veins	?	HD	260-390 PS	"	Bulakhtay, USSR	Kozlov+Gubriyeva, 1973
Qtz-hueb-sch veins	?	HD	230-420 PS	"	"	"
Qtz-wolf-sulphide veins	?	HD	260-340 PS	"	"	"
Mo-sil-wolf veins	Fluorite	H	400-250 PS	"	Monpolia	Naumov+Ivanova, 1975
Skarn	Silicates	I	550	"	Nevada	Taylor+O'Sell, 1977
Qtz-wolf-cass (89 localities)	-	H	420-300 320-150	"	Yano-Adyghan, USSR	Smirnov+Vorontsova, 1976
Qtz-wolf veins (78 localities)	Wolframite	HD	400-250	"	World	"
Quartz-cass	Cassiterite	HD	450-300	"	"	"
Quartz-wolf	Quartz	HD	300-270	"	"	"
Qtz-scheelite vein	Scheelite	H	170-130	6-8.5	Japan	Takamachi+Imai, 1971
Qtz-wolf vein	Cassiterite	H	255-350	5.1-10	"	"
Wolf Stage I	Muscovite	H	215-230 PS	15.2	Peru	Landis+Bye, 1974
Wolf Stage II	Forsterite	H	180 PS	"	"	"
Skarn with scheelite	-	H	375-304 600-650 PS	4-8	Sierra Nevada	Kerrick, 1977
Qtz-gold- scheelite lodes	-	I	320 ± 25 230-270	"	New Zealand	Patterson et al., 1975 in prep.
Qtz-wolf-greisen	Quartz	H	227-235	8.3	Carrock Fell, U.K.	Shepherd et al., 1976
Scheelite-wolf veins	Scheelite	H	100-450	"	World	Pogorinov+Naumov, 1972

KEY: H = Homogenization temperatures
D = Dissolution temperatures
I = Isotopic temperature determination
P = Pressure correction applied
S = Salinity correction applied

wolf = wolframite
cass = cassiterite
qtz = quartz
hueb = huebnerite
sch = scheelite
mo = molybdenite

(26-30 equivalent wt% NaCl).

Landis and Rye (1974) in a study of the Pasto-Bueno tungsten-basemetal deposit in Peru, showed that there were three stages of deposition in the evolution of the deposit; initially greisen deposition (60-70% of deposition), then vein deposition (25-35%) followed by vug deposition (5%). Fluid inclusions revealed that greisen and early vein stage fluids were very saline (40 equivalent wt% NaCl), high temperature solutions (400-500°C). In subsequent main vein stages ore fluids attained a temperature range of 175-290°C and a salinity range of 2-17 equivalent wt% NaCl. Boiling was indicated only for early vein stages. Results from stable isotope studies of fluids in primary inclusions indicated mixing of a meteoric or other water component with magmatically derived water. Wolframite deposition was associated with episodes of meteoric water influx; sulphide deposition on the other hand was associated with water of magmatic derivation.

Ivanova et al., (1976), from studies on many cassiterite-tungsten deposits, found that there were two main types of inclusions. Firstly two-phase gas-liquid inclusions and secondly three-phase aqueous solution-liquid CO₂-gas inclusions. CO₂ is a characteristic component of inclusions in minerals for all types of tungsten deposits in Mongolia. Solid phases are less typical but are more common in later stages of mineralisation. Naumov and Ivanova (1971) record a maximum of 26.4 wt% CO₂ from some USSR tungsten deposits

but 38-40 wt% CO_2 is recorded elsewhere (Tugarinov and Naumov, 1972).

It is known that the solute in fluid inclusions is not exclusively NaCl. Ratios of Na^+/K^+ ranging from 0.98 to 7.1 were measured from inclusions from Rex hill, by Groves *et al.*, (1970). Sawkins (1966) records a maximum Na^+/K^+ ratio of 17.9, and in fact Ivanova *et al.*, (1976) maintain that two types of tungsten-bearing solutions can be distinguished from the composition of inclusion solutions,

- 1) high salt contents of Na-F-Cl composition
- and 2) medium salt content of Na-Cl-bicarbonate composition.

2.6 TRANSPORT OF TUNGSTEN IN HYDROTHERMAL SYSTEMS

During upward movement of a crystallising magma the separation of an aqueous phase occurs when P_{total} is less than P_{fluid} . The temperature and pressure at which a vapour phase can be evolved from a granitic melt is dependent on its bulk composition and depth of emplacement (Whitney, 1975, 1977).

The coexistence of magma and aqueous fluid results in partitioning of elements between two phases. It is known that, of the major anions, Cl^- is strongly concentrated into the vapour phase (Holland, 1972; Kilinc and Burnham, 1972), a factor which is likely enhanced by increasing silica activity (Stormer and Carmichael, 1971). Furthermore, because of the "salting-out effect" and lower solubility (Burnham, 1967), CO_2 readily enters a vapour phase, generally before Cl^- . Thus a fluid phase formed at high pressure is

likely to be CO_2 -rich and halogen-poor, while later and/or lower pressure fluids would be halogen-rich and CO_2 -poor (Burnham, 1967). On the other hand F^- appears strongly retained by a simple albite melt in the system $\text{NaAlSi}_3\text{O}_8 - \text{NaF} - \text{H}_2\text{O}$ (Koster Van Gros and Wyllie, 1968).

Foster (1973) experimented with partitioning of tungsten between aqueous $\text{Na}_2\text{WO}_4 - \text{KCl}$ solutions and granitic melts. He found that for an adamellite melt, coefficients of the order of $N \times 10^{-2}$ were indicated, whereas for a melt of composition $\text{Ab}_{30} \text{Or}_{30} \text{Qtz}_{40}$ at $780-870^\circ\text{C}$ and 1000 bars, coefficients of $N \times 10^1$ were obtained. The reason for the difference in partition coefficients is uncertain (Foster, 1976) but the concentration of tungsten in a fluid separating from a granitic melt undoubtedly increases as the final melt approaches the ternary minimum of the system $\text{Ab} - \text{Or} - \text{Qtz}$.

Many transport mechanisms have been proposed for tungsten. These result from consideration of the available partition coefficients as well as studies on paragenesis, and the evidence of the composition of hydrothermal fluids from fluid inclusion studies. The association of fluorite with many tungsten deposits led to the belief that halides and oxyhalides were responsible for the transport of tungsten in hydrothermal fluids (Kogarko and Ryabchikov, 1970) although Ivanova's (1966) thermodynamic evaluation did not support this interpretation.

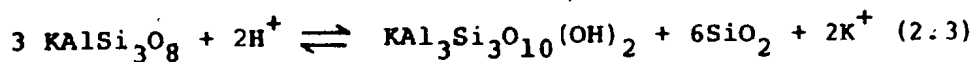
Studenikova et al., (1970) studied the dissociation of tungstic acid (H_2WO_4) in moderately concentrated fluoride-potassium solutions under temperatures and pressures

typical of hydrothermal conditions. In the presence of excess fluoride, tungstic acid is completely dissolved and on cooling precipitates complex oxyfluorotungstates that have low solubility in cold water. The occurrence of complex potassic oxyfluorotungstates in nature is limited because the complex ion $(\text{WO}_2\text{F}_4)^{2-}$ is immediately destroyed as salts of Ca^{2+} , CaF_2 and H_2WO_4 are precipitated. This means that in the presence of calcium ions, fluorite (CaF_2) will be formed before oxyfluorotungstates. Thus for the latter to form there must be an excess of F^- available. It is postulated that this is the reason for the development of wolframite instead of scheelite in greisen, as all available Ca^{2+} is precipitated as fluorite (Studenikova et al., 1970).

In natural silica-bearing solutions, transportation may be provided by tungsten-bearing heteropolyacids. In an acid environment heteropolyacids may be stable up to 300°C . Gundlach and Thormann (1960) showed that pure silicotungstic acid remains completely stable at 200°C and 20 bars and exhibits no dissociation into $(\text{SiO}_4)^{4-}$ and $(\text{WO}_4)^{2-}$ ions in the presence of Fe, Mn and Ca. Titration of the acid with NaOH results in its dissociation, and in the presence of Fe, Mn and Ca, the tungstates of these cations precipitate in order of increasing solubility, FeWO_4 at pH 5.9; MnWO_4 at pH 6.7; CaWO_4 at pH 7.3. Gundlach and Thormann (1960) stress the presence of Si, P and Sb as almost a precondition for the formation of tungsten-bearing heteropolyacids. The

formation of scheelite occurs by the neutralisation of these acids and is accompanied by the formation of quartz, apatite and stibnite if sulphur is present. Transportation of tungsten in this way is postulated by Maucher (1976) and others to explain the existence of the stratabound Sb-Hg-W ores of the eastern European Alps and elsewhere.

In pure water the solubility of tungsten compounds is low, in fact scheelite solubility in water possesses a negative temperature coefficient, decreasing from 13.3 mg/l at 20°C to 2.3 mg/l at 90°C (Bokii and Anikin, 1956). However, scheelite solubility increases with addition of chloride (Bokii and Anikin, 1956) and recently Foster (1977) investigated scheelite solubility in dilute KCl solutions where the molality of the solution was buffered with the solid-phase assemblage quartz - feldspar - muscovite. The solubility of scheelite at 1000 bars increased almost exponentially from approximately 200 ppm at 350°C to more than 1000 ppm at 550°C. The solubility is a function of P_{HCl} which is buffered by the silicate minerals according to the following reaction, which is essentially a greisenisation reaction.



Maximum deposition of tungsten is expected at a temperature interval of 350-450°C provided the solution is saturated with tungsten at these temperatures (which is unlikely). More reasonably, deposition is probably restricted to subcritical temperatures where P_{HCl} is low,

HCl is partially dissociated and ionic tungstates exist (Foster, 1977).

If the fluids responsible for mineral deposition were relatively high density brines during the early stages of mineralisation (Sawkins, 1966; Landis and Rye, 1974) the role of ionic species in transport may be quite important. At temperatures above 400°C and $P_{\text{H}_2\text{O}}$ greater than 1000 bars a dilute chloride solution would be supercritical (Sourirajan and Kennedy, 1962) and molecular species are more likely to persist. Tungstic acid (H_2WO_4) is only slightly dissociated at low temperatures and will persist as a molecular species at high temperatures in dilute chloride solutions (Foster, 1977). For solutions at or near critical temperatures, equilibrium might shift to partially dissociated species such as $\text{H}_4(\text{Si}(\text{W}_3\text{O}_{10}))$ (Barabanov, 1971) and at subcritical temperatures the major tungsten species will likely be ionic. The stability field of ionic species is enlarged with increase in solute concentration and thus high density brines could exhibit subcritical phenomena over a wide range of temperatures and pH would be buffered at values greater than neutral (Barnes and Ernst 1963). Thus the simple tungstate ion WO_4^{2-} may have a considerable range of stability at high temperature (Foster, 1977). However, uncertainty remains as to the identity of the ionic or molecular species that tungsten can be transported as under varying conditions of temperature, pressure and composition.

Deposition of wolframite and scheelite apparently

depends on a number of parameters including temperature, pH, f_{O_2} , f_{S_2} and the activity ratio $a(Ca^{2+})/a(Fe^{2+} + Mn^{2+})$. Temperature, f_{O_2} , f_{S_2} and $a(Ca^{2+})/a(Fe^{2+} + Mn^{2+})$ are most important at super- and near critical temperatures whereas pH is important at lower, subcritical temperatures (Poster et al., 1978).

CHAPTER 3

THE GENERAL GEOLOGY

3.1 INTRODUCTION

The Appalachian structural province has been subdivided into five main zones based on lithological and structural similarities (Williams, 1978, 1979). Four of these zones are represented in Newfoundland (Figure 3.1) and are from west to east; the Humber Zone (the eastern margin of early Paleozoic North America); the Dunnage Zone (the remnant of the early Paleozoic Iapetus ocean); the Gander Zone (the continental rise of the Avalon microcontinent); and the Avalon Zone (the remnant of a late Precambrian and early Paleozoic microcontinent).

The study area (Figure 3.1) lies within the Gander Zone, on the southwest limb of the Hermitage Flexure (Williams et al., 1970).

3.1.1 The Gander Zone

The Gander Zone forms a linear belt of crystalline rocks bounded to the west by the Davidsville Group (Dunnage Zone, Williams, 1979) and to the east along the Hermitage-Dover Fault (Blackwood and Kennedy, 1975) by the Avalon Zone (Williams, 1979).

Most work has been concentrated in the northeastern section of the zone where Twenhofel (1947) named interbedded sedimentary and volcanic rocks in the Gander Lake area the "Gander Lake Series" and assigned them a Silurian age. Jenness (1963) defined these rocks and others as the Gander Lake Group and

subdivided them into three units (lower, middle, and upper). He assigned a Middle Ordovician age to the group based on identification of brachiopods and graptolites in the middle and upper units. He interpreted the units within the group to be conformable and recognised an increase in metamorphism from west to east.

This interpretation was challenged by Kennedy and McGonigal (1972) who redefined the Gander Lake Group to include only the lower unit defined by Jenness and excluded most of the gneissic rocks to the east. Blackwood and Kennedy (1975) renamed these gneissic rocks the Bonavista Bay gneiss complex and presumed them to be a basement terrain of probable Precambrian age. Blackwood (1976, 1977) further subdivided the gneissic complex into a paragneiss unit (Square Pond gneiss) and a migmatite unit (Hare Bay gneiss). Kennedy and McGonigal (1972) renamed the upper and middle units of Jenness (1963) the Davidsville Group, of Middle Ordovician age, and inferred a pre-Middle Ordovician age for their Gander Lake Group.

A presumed tectonic contact between the Gander Lake Group and the Bonavista Bay gneiss complex was regarded as a cover/basement relationship (Blackwood, 1977). In the Gull Pond area, the contact separates low-grade metamorphic rocks from paragneiss and migmatites of the Square Pond gneiss (Blackwood, 1976). Similar interpretations were made in the Hermitage - Bay D'Espoir area (Colman-Sadd, 1974) and Port-aux-Basque region (Brown, 1975). Field relation-

ships near Gambo Pond and elsewhere however, indicate a conformable contact between lower grade rocks of the Gander Group and those within the gneissic terrain, which closely approximates a metamorphic biotite isograd (Blackwood, 1978). Blackwood thus reinterprets the rocks of the Gander Group, Square Pond gneiss, and Hare Bay gneiss as a conformable sequence which underwent prograde metamorphism from west to east, thus confirming the interpretation of Jenness (1963).

3.1.2 Igneous Rocks of the Gander Zone

Intrusive rocks are a dominant component of the Gander Zone lithologies and may be divided into three types; microcline-megacrystic biotite granite, equigranular biotite granite, and two-mica leucogranite (Strong and Dickson, 1978; Strong, 1980). Deformed coarse megacrystic granite and garnetiferous leucogranite are found within the gneissic terrain, the deformation being extremely marked along contacts (Jayasinghe and Berger, 1976; Jayasinghe, 1979). Their emplacement was thought to postdate the gneissic banding of the country rocks (Kennedy and McGonigal, 1972) although recent work suggests that the emplacement and deformation of the granites was contemporaneous with most, if not all, of the deformation in the country rocks (Jayasinghe, 1979).

The foliation within the granites was initially interpreted to have formed during the deformation of the Love Cove Group (Avalon Zone) (Blackwood, 1976). This implied a late Precambrian age for the gneissic and granitic rocks because the Love Cove deformation was presumed to predate

the formation of the late Hadrynian Musgravetown Group (Blackwood, 1976; O'Driscoll and Hussey, 1977). Radiometric dating of the granites in the gneissic terrain has yielded Devonian or younger ages (Bell et al., 1977) suggesting that the deformation in the Gander Zone was dominantly Devonian if the contemporaneous deformation and emplacement model is valid.

According to Kennedy and McGonigal (1972) leucocratic muscovite granites intrude the Gander Group as pre-tectonic, pre-Middle Ordovician intrusions. Data presented by Jayasinghe and Berger (1976) and Currie and Pajari (1977) show that this age connotation and interpretation conflicts with detailed observation of the geology. Radiometric dating of these granites also conflicts with a Precambrian to pre-Middle Ordovician age for these intrusions (Bell et al., 1977; Bell and Blenkinsop, 1977).

Undeformed coarsely crystalline, microcline megacrystic, biotite granites truncate the major structural and lithological units of the Gander Zone. One of these, the Ackley City batholith, appears to truncate the Dover Fault (Strong et al., 1974 a,b), the boundary between the Avalon and Gander Zones. These post-tectonic granites postdate the S_2 schistosity of the metamorphic rocks, and radiometric dating has confirmed their late Devonian - Carboniferous age (Bell et al., 1977; Bell and Blenkinsop, 1977).

3.1.3 Tectonic Models - Gander Zone

Most workers appear to agree that the Gander Zone

sediments represent an accreted continental rise prism or clastic sedimentary wedge (Williams, 1964, 1979; Colman-Sadd, 1974; Kennedy, 1975) although much debate continues on the timing and nature of post-depositional events. Many workers stress the importance of a Precambrian basement, a pre-Middle Ordovician orogeny, and minor Acadian reworking (Kennedy and McGonigal, 1972; Kennedy, 1975, 1976; Blackwood, 1976, 1977) while others propose southeastward obduction of oceanic crust in Lower to Middle Ordovician times (Pajari et al., 1979; Pickerill et al., 1978), mirroring the northwestern continental margin of the Appalachian system during the Taconic Period (Williams and Stevens, 1974).

Subduction-related models explaining the timing and nature of granitoid plutonism (Strong et al., 1974b; Strong, 1974) are constrained by subsequent field and geochronological studies (Bell et al., 1977; Jayasinghe, 1979). Although subduction ceased with the closure of Iapetus in the Middle Ordovician (Strong, 1977; Dean, 1978), compression continued well into the upper Paleozoic and produced significant crustal shortening and thickening (Dean and Strong, 1977). Available geochemical and isotopic data (Bell et al., 1977; Strong, 1980; Jayasinghe, 1979) suggest a crustal origin for the granitoids of the Gander Zone, the most recent synthesis relating their genesis and emplacement to the development of a "megashear" environment (Strong, 1980). This reflects changing patterns of plate behaviour from collision and compression to rotation and oblique interactions, and is

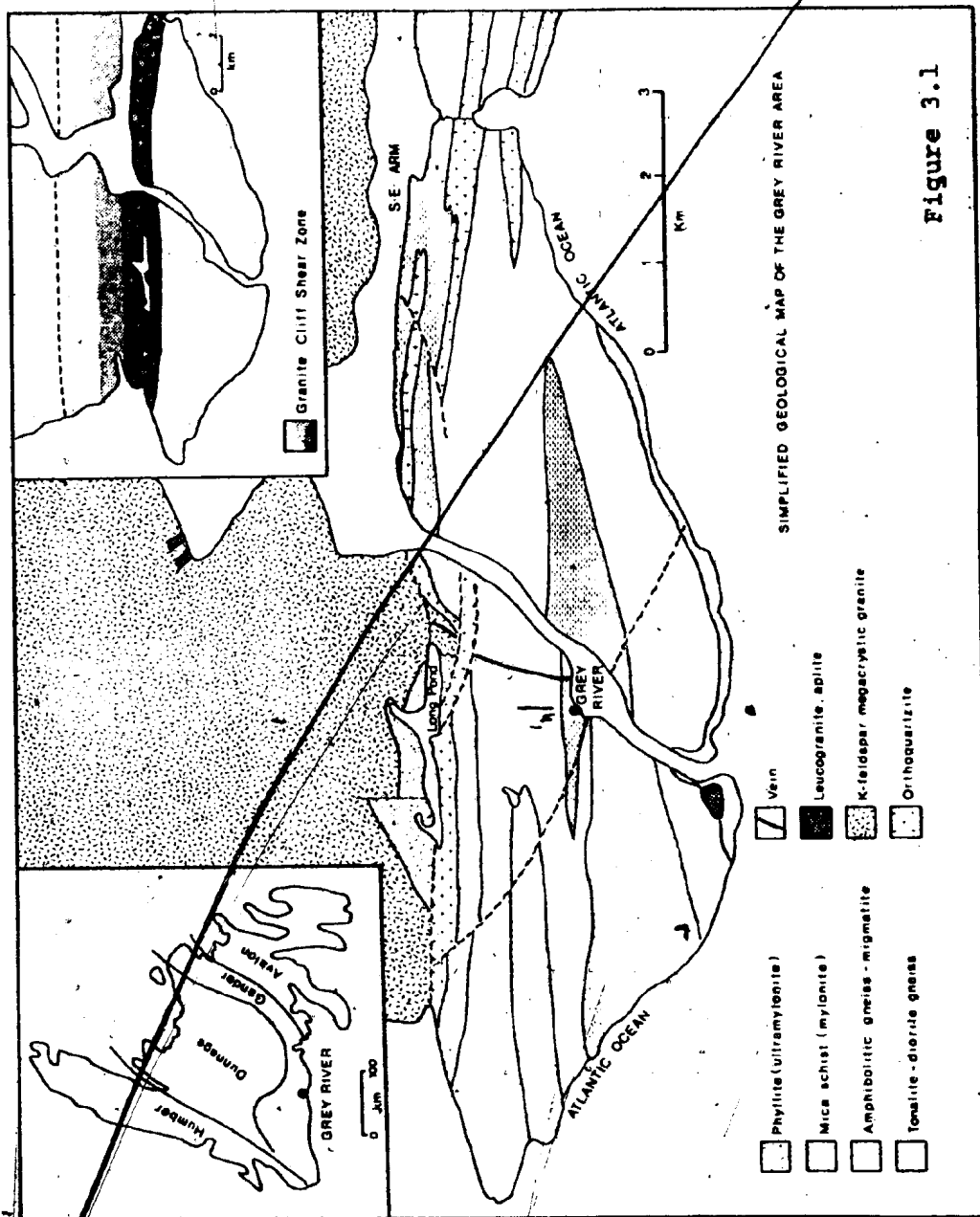


Figure 3.1

supported by available paleomagnetic data for the Phanerozoic (Morel and Irving, 1978) as well as recent structural studies (Jayasinghe, 1979; Hanmer, 1980).

3.2 THE GREY RIVER AREA

The geology of the area is more complex than previously described (Bahyrycz, 1957; Gray, 1958; Mullins, 1958) and is dominated by a number of tectonic and synkinematic intrusive events followed by a complicated post-kinematic history of multiple intrusion. Table 3.1 lists these events in terms of the various mappable units and the order of their inferred sequential development. The various lithologies and their distributions are shown in Maps 1 and 2 (in map folder) which were derived mainly from maps produced by Bahyrycz (1957) and from Buchans Mining Co. files. However, this thesis differs markedly from previous workers in the interpretation of the significance of units.

The geology of the Grey River area is shown in a simplified form in Figure 3.1. There appear to be three main components of the geology of the Grey River area: The metamorphic suite consisting of various lithologies, namely hornblende gneisses and biotite schists; the igneous suite, dominated by K-feldspar megacrystic granite; and the hydrothermal vein system which postdates all the above lithologies.

3.2.1 The Metamorphic Suite

Metamorphic rocks underlie most of the Grey River peninsula, extending from Long Pond to the coast. The belt has a width of 2.5 km and can be traced along strike at least

Table 3.1
Rock Units of the Grey River Area

UNIT	SEDIMENTARY	INTRUSIVE	DEFORMATION
10 9 8		-Diabase dykes -Leucogranite, aplite, pegmatite -Pegmatite, diorite, alaskite Composite dyke suite.	POST TECTONIC
7 6 5		-K-feldspar megacrystic granite -Mafic to intermediate dykes -Peridotite	LATE TECTONIC
4		-Leucogranite-orthoquartzite	SYNTECTONIC
d c b 3a	-Calcareous schist, ? -Phyllites -Mica schist -Amphibolite gneiss		
2 1		-Quartz diorite/diorite gneiss -Tonalitic gneiss	

to La Hune Bay, a distance of 14 km. Striking E-W and dipping at moderate angles to the north, these metamorphosed rocks contain a variety of lithologies which are described below. Detailed petrographic notes are contained in Table 3.2.

3.2.1:1 Unit 1: Tonalitic Gneiss

The tonalitic gneisses occur as rafts or screens within quartz diorite (Unit 2) exposed along sea cliffs west of Grey River point and in coastal sections to the east. The gneisses are light to dark grey, medium grained and variably well banded on a 1-2 cm scale. A discordant contact suggests that the quartz diorite gneisses are intrusive into the tonalitic gneiss unit.

Minor xenoliths of a medium-grained, porphyritic amphibolite occur within the tonalitic gneiss (Plate 3.1A) and either represent an earlier host to the tonalitic gneiss or disrupted dykes. An apparent alignment of these xenoliths in one locality might suggest that they were boudinaged dykes.

As well as being intruded by the quartz-diorite gneiss, the tonalitic gneiss is host to a series of late syntectonic and post-tectonic intrusives dominated by pegmatites, aplites and various basic dykes.

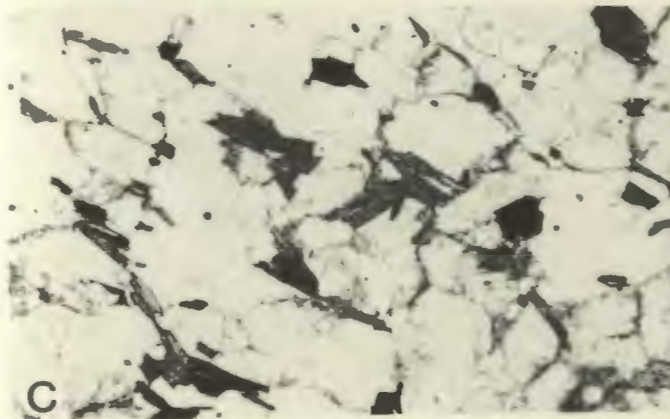
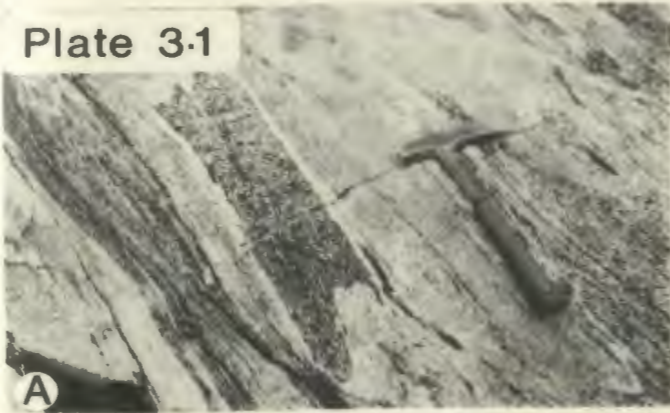
The gneissic banding is inconsistently developed and the dominant fabric is a strong foliation (S_2) which is defined by alignment of mafics. Rare intrafolial folds are found (Plate 3.1B) within the S_2 foliation and represent

Plate 3.1

Field relationships of tonalitic and dioritic gneiss.

- 3.1A Porphyritic amphibolite block in banded tonalitic gneiss (Unit 1). The amphibolite may either be a xenolith or a disrupted dyke. West of Grey River Point.
- 3.1B Intrafolial fold in tonalitic gneiss. West of Grey River Point.
- 3.1C Hornblende foliation transposed by biotite in tonalitic gneiss. Sample 79-5, X 40.
- 3.1D Banded quartz diorite gneiss (Unit 2) with injections of syntectonic granite cut by post-tectonic pegmatite. West of Grey River Point.
- 3.1E Diorite gneiss with injections of syntectonic granite parallel to F_2 , cut by late syhtectonic granite dyke that is folded into D_2 folds. Grev River Point.
- 3.1F Banded amphibolitic gneiss (Unit 3a) cut by leucocratic granite dyke which exhibits a cataclastic texture. Grey River Fiord, location 535.

Plate 3.1



an earlier transposed deformation. A distinct mylonitic fabric (S_m) is also found in zones within the tonalitic gneiss. This strong S_m schistosity is coaxial to the S_2 schistosity.

In thin section the non-sheared tonalitic gneiss shows a typical lepidoblastic texture with alignment of mafic minerals, as well as subparallel arrangement of quartz and feldspar, defining S_2 . Biotite appears to overgrow hornblende and in some sections a transposed cleavage is evident (Plate 3.1C).

The mineralogy of the tonalitic gneiss unit consists of plagioclase (40-60%), quartz (10-30%), biotite (4-10%) and hornblende (1-4%) with accessory amounts of fluorapatite, epidote, chlorite, and opaques.

3.2.1.2 Unit 2: Quartz Diorite to Diorite Gneiss

These rocks have a similar distribution to Unit 1 and are found in seacliffs along the southern shoreline. The tonalitic gneiss is cut by these grey to dark green, medium to coarse grained rocks which were probably originally large sills and dykes. A variability in the amount of mafics (from 10-70%) accounts for the great diversity of rock types in this unit which ranges from quartz dioritic to amphibolitic compositions. The unit is host to a number of post-tectonic intrusives including pegmatites, aplites, diorites and diabase dykes.

These rocks are strongly foliated (Plate 3.1D), the dominant regional schistosity (S_2) being defined by alignment

of mafics. In places the unit is extensively migmatized to produce a banded injection migmatite with individual bands being 1-5 cm thick. Many of the coarse grained amphibole-rich bodies in this unit lack this migmatitic character. Granite dykes cut the migmatitic banding and are themselves folded into tight to open folds (Plate 3.1E) with S_2 as the axial planar fabric. Fabric relationships in the quartz diorite unit are similar to those of the tonalitic gneiss unit.

The mineralogy of the unit is composed of plagioclase (40-50%), quartz (10-30%), hornblende (5-60%), and biotite (5-20%) with minor amounts of chlorite, opaques, epidote, sphene and apatite.

3.2.1.3 Unit 3a: Amphibolitic Gneiss (Augen Gneiss)

Much of the Grey River area is underlain by what has been previously called metasedimentary rock represented presently by amphibolitic gneiss (Unit 3a), mica schist (Unit 3b) and phyllites (Unit 3c).

The greatest proportion of Unit 3 is composed of amphibolitic gneiss (Unit 3a). This medium to coarse grained, dark green to dark grey rock may texturally be called an augen gneiss for it commonly displays coarse augen of feldspar within a dark hornblende-rich matrix. Bands of coarse amphibolite are also common throughout the sequence.

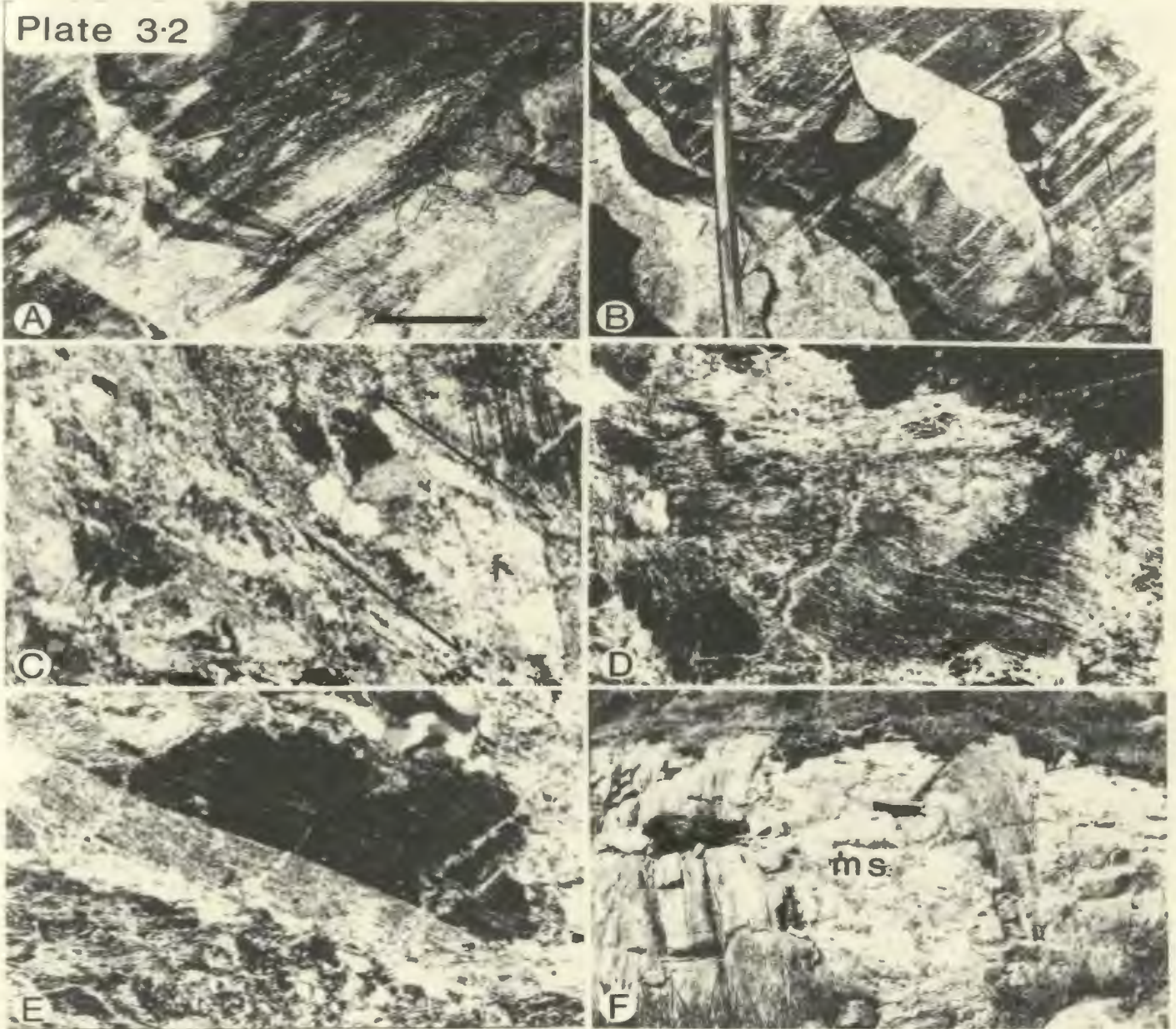
The amphibolitic gneiss is extensively migmatized by injection of granitic material (Plate 3.1F) parallel to the foliation of the rock producing an injection migmatite. Late

Plate 3.2

Field relationships of amphibolitic gneiss and mica schist.

- 3.2A Fold hinges of isoclinally folded granitic material in migmatitic amphibolite gneiss. Adit level, location 93. Bar scale = 30 cm.
- 3.2B Sheared out limbs of isoclinally folded injected granite in migmatitic amphibolitic gneiss. Note fold hinges preserved (arrow). Adit level, location 92..
- 3.2C Conjugate shears developed in feldspar (f) porphyroclast in amphibolitic gneiss. One shear direction strongly developed. Sample 69, x40, X-polars.
- 3.2D Kinked hornblende in amphibolitic gneiss. Brittle deformation in response to faulting. Sample 69, x40, X-polars.
- 3.2E Twinned hornblende crystal in amphibolitic gneiss. Sample 69, x40, X-polars.
- 3.2F Bands of mica schist (m.s.) alternating with migmatitic amphibolitic gneiss. Location 381.

Plate 3.2



Syntectonic granitic dykes cut across the migmatitic banding and retain their igneous texture although a weak mylonitic LS fabric is evident.

The relationships of these amphibolitic gneisses to Unit 2 and Unit 1 are unknown, but equivalents of Unit 2 may be present within the sequence. The gneisses of Unit 3a are cut by a number of post-tectonic intrusives, namely pegmatites, aplites, megacrystic granite and basic dykes.

The fabric of Unit 3a is dominated by the regional S_2 schistosity, striking E-W, dipping at intermediate angles to the north, and axial planar to megascopic tight to isoclinal folds (Plate 3.2A). These folds are emphasised by the leucosome bands, although most fold limbs have been sheared out and transposed to produce the banded gneissic fabric parallel to the axial planar schistosity. In places small fold hinges are preserved between the migmatitic banding (Plate 3.2B).

The regional S_2 foliation is poorly developed, but a relatively strong cataclastic fabric is also evident. This fabric (S_m) is emphasised in thin section by alignment of biotite crystals (which replace hornblende) and by stretched recrystallised aggregates of quartz and in hand specimen, by augen of feldspar.

In rocks that have suffered a later brittle deformation through proximity to faults, a strong conjugate shearing pattern is developed, with one direction more prominent than the other. The shearing direction is emphasised by zones of

recrystallised quartz that displace fractured plagioclase crystals (Plate 3.2C). Large (2-3 mm) hornblende crystals are commonly kinked (Plate 3.2D) and where their orientation is coincident with the shearing direction they show simple twinning (Plate 3.2E). More intensive kinking and fracturing results in the break-up of large hornblende crystals into subgrains, a relatively rarely observed phenomenon (Biermann, 1977; Dollinger and Black, 1975; Allison and Le Tour, 1977). The blue-green hornblendes are often partially altered to muscovite along fractures and grain boundaries (Plate 3.2E).

The essential mineralogy of the amphibolite fraction of the migmatite is hornblende (40-50%), feldspar (30-40%), biotite (3-5%) and quartz (3-5%) with accessory amounts of opaques, chlorite, epidote and muscovite. The leucosome is composed of quartz (20-30%), feldspar (50-60%), and chlorite (1-2%) with minor phases such as epidote, biotite, sericite and opaques.

3.2.1.4 Unit 3b: Mica Schist (Mylonites)

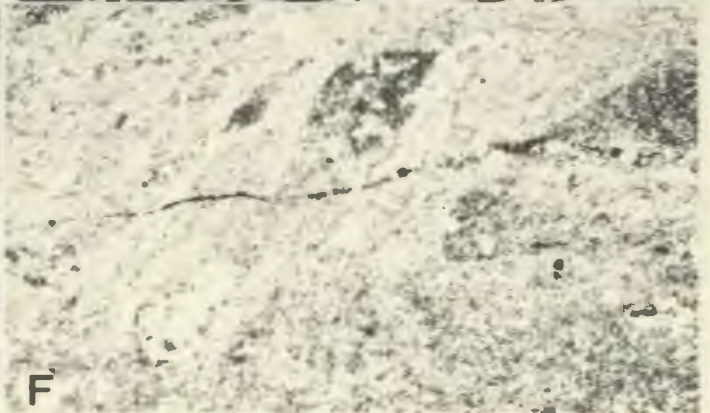
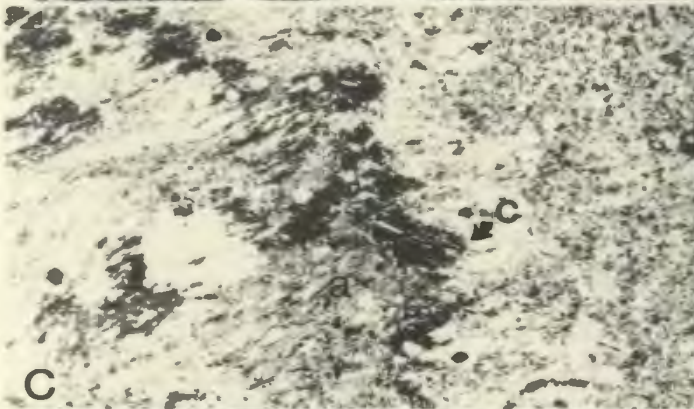
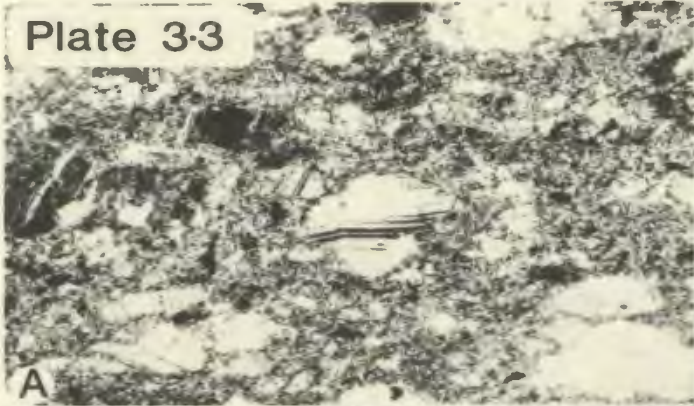
Large bands of mica schist striking east-west can be mapped within the amphibolitic gneiss terrain which underlies much of the Grey River peninsula. There are no sharp contacts between the two units and generally a broad transition zone is marked by increasing amounts of biotite within the amphibolitic gneiss and an increasing cataclastic texture. Sometimes on outcrop scale, bands of mica schist alternate with amphibolite gneiss (Plate 3.2F) and there the contacts are more sharply defined.

Plate 3.3

Field and thin section relationships of mica schist and phyllite units.

- 3.3A Mica schist (Unit 3b) with mylonitic texture. Augen of kinked feldspar and aggregates of quartz in recrystallised matrix. Sample 383, x40, X-polars.
- 3.3B Porphyroblasts of andalusite/cordierite in mica schist. Location 79-2, entrance to S.E. arm, Grey River Fiord.
- 3.3C Crenulated porphyroblast of andalusite (a) rimmed by cordierite (c) overgrowing mylonitic texture in mica schist. Sample 79-2, x15, X-polars.
- 3.3D Mica schist folded into broad open D_3 folds. Location 561, Gulch Cove.
- 3.3E Phyllite (Unit 3c). Location 136, South of Long Pond.
- 3.3F Ultramylonitic texture of phyllite showing ghosts of recrystallised feldspar augen. Sample 142, x40, plane polarised light.

Plate 3.3



The mica schists are cut by a large sill-like body of leucogranite-orthoquartzite (Unit 4) and leucogranite dykes, both of which display variably intense mylonitic fabrics. Contacts with the sill-like body of leucogranite are sharp.

The dominant fabric in the mica schist unit parallels the S_2 foliation in the amphibolitic gneiss but is characteristically a mylonitic fabric with a weak stretching lineation evident in hand specimens.

The mylonitic fabric is confirmed in thin section where a strongly developed mortar texture is evident (Plate 3.3A) and phyllosilicates define a flow structure enclosing porphyroclasts of feldspar and quartz. The strong schistosity is defined by the phyllosilicate orientation, and a weak lineation by the stretching and flattening of quartz aggregates in the plane of the schistosity.

In one locality within the Granite Cliff Shear Zone (Figure 3.1) the mica schist contains porphyroblasts of andalusite rimmed by cordierite (Plate 3.3B and Plate 3.3C). These porphyroblasts overgrow the mylonitic S_m fabric but are crenulated by a later D_3 formation. The porphyroblasts were found very close to the contact with the megacrystic granite and thus may relate to contact metamorphic effects of its intrusion. Mica schist found elsewhere in the Granite Cliff Shear Zone also exhibit a crenulation cleavage which imparts a fish-scale texture to the rock in hand specimen. Near Gulch Cove the mica schists are folded into broad, open, climbing D_3

· folds (Plate 3.3D) with southward vergence.

The essential mineralogy of the mica schist is quartz (20-30%), feldspar (40-50%), biotite (10-20%), muscovite (10-15%), and chlorite (1-2%) with accessory amounts of relict hornblende, opaques and epidote.

3.2.1.5 Unit 3c: Phyllites (Ultramylonites)

This rock type is most commonly found in the northern region of the metamorphic belt close to, or in, the zone of deformation represented by the Granite Cliff Shear Zone. These rocks lie essentially to the immediate south and north of Long Pond. Previous interpretations of these rocks suggested they were low grade metamorphic rocks but a strong mylonitic fabric, evident in hand specimen and thin section, suggests that they are the product of extensive ductile shearing and may be more correctly termed ultramylonites. The phyllites are generally gradational into mica schist and amphibolitic gneiss.

The dominant fabric is a strong but fine mylonitic schistosity (S_m) that parallels the dominant S_2 - S_m schistosity of the amphibolite gneiss (Plate 3.3E) and mica schist. A weak to moderate lineation is evident and defined by stretching and flattening of quartz aggregates and feldspar augen (Plate 3.3F). A D_3 deformation is superimposed on this mylonitic fabric to produce a crenulated cleavage. One limb of the crenulation is more prominent and is emphasised by bands of recrystallised quartz orientated at a moderate angle to the mylonitic fabric.

Accurate determination of the relative proportions of the various minerals present is difficult due to the fine-grained and recrystallised nature of the rock. The essential mineralogy is quartz, feldspar, muscovite, relict biotite, epidote, opaques and chlorite.

3.2.1.6 Unit 3d: Metaconglomerate (?) (Fault Breccia-cataclasite)

Two localities from the area immediately north-west of Long Pond in the middle of the Granite Cliff Shear Zone have vastly different lithology and composition from metamorphic rocks exposed to the south of Long Pond.

What appears to be a deformed conglomerate occurs on northern shores of Long Pond and contains what look like, rhyolitic and granitic pebbles (Plate 3.4A). Thin section evidence (Plate 3.4 and 3.5A, B) reveals however that the rock types and deformed conglomeratic texture may have occurred as a result of ductile shearing, followed by brittle deformation, of an inhomogeneous or very coarse grained rock type. Considering its location the unit may well be a fault breccia (cataclasite) formed by late brittle-ductile deformation along the Granite Cliff Fault (Map 1).

This rock type may have been originally inhomogeneous (i.e. a conglomerate) but extremely coarse grained rocks, such as the leucogranite (Unit 4 or Unit 9) which outcrops on the south-western shore of Long Pond, are possible protoliths. There a less deformed version of the "conglomerate" is found, essentially minus the brittle-ductile conjugate

Plate 3.4

Field and thin section relationships of fault breccia-cataclasite (deformed conglomerate?).

- 3.4A Sample (RS79-4A) of deformed conglomerate (?) (Unit 3d) showing two types of pebbles (?) - rhyolitic, granitic - in a fine-grained matrix. Sample collected from north shore of Long Pond by R. Smyth.
- 3.4B View of recrystallised quartz showing serrated nature of grain boundaries. Section of matrix of the above sample. x40, X-polars.
- 3.4C Porphyroclast of quartz ("granitic pebble") exhibiting deformation bands in a sericite/quartz matrix. Sample RS79-4A, x40, X-polars.
- 3.4D Recovery of deformed quartz grain by polygonisation and subgrain development during ductile shearing. Sample RS74-4A, x40, X-polars.
- 3.4E "Rhyolitic pebble" in sample RS79-4A. The "pebble" contains small quartz grains within a fine-grained sericite matrix. x40, X-polars.
- 3.4F Small quartz grains in "rhyolitic pebble" showing brittle deformation by conjugate shearing. Shears are filled with sericite. Sample RS79-4A, x40, X-polars.

Plate 3.4

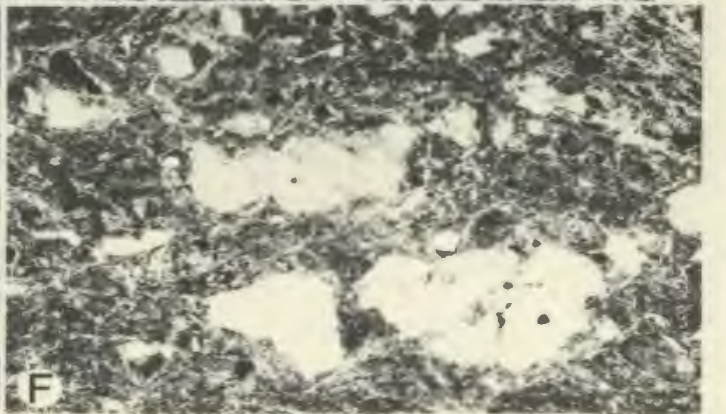
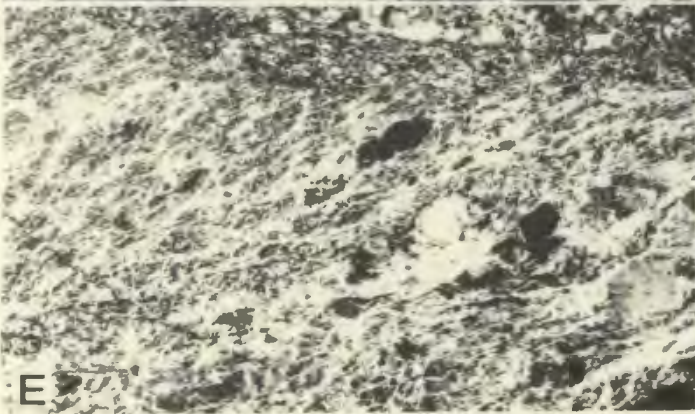
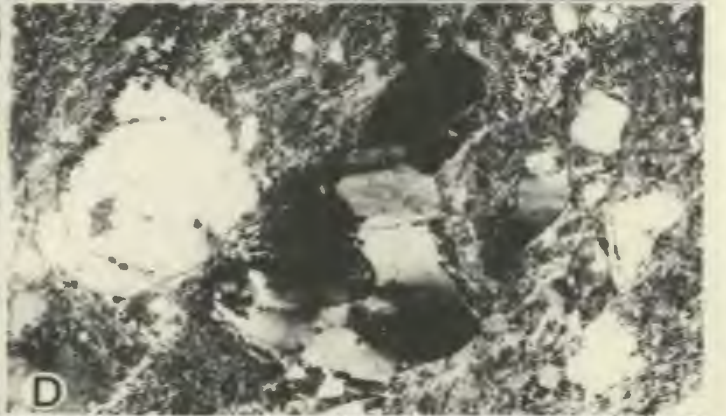
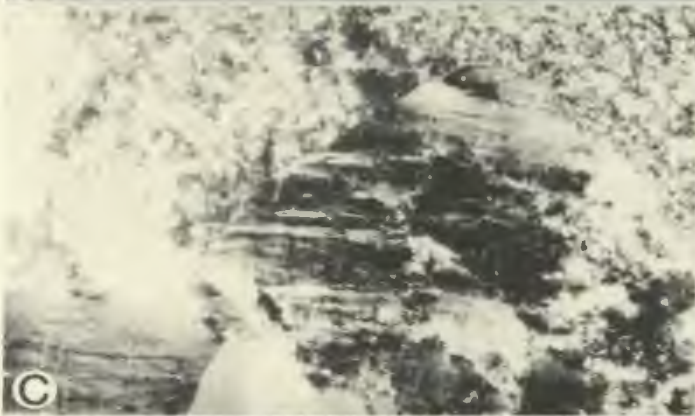
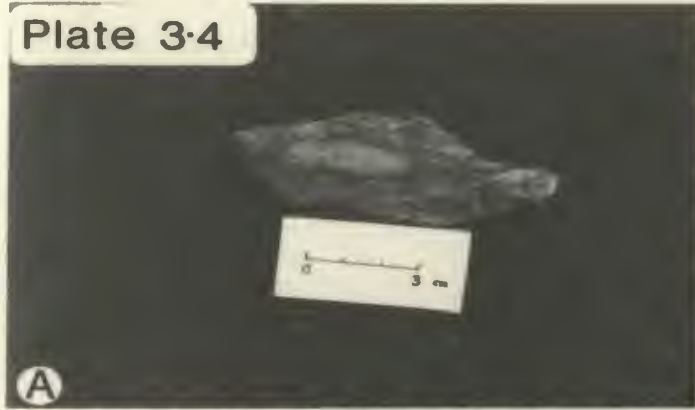
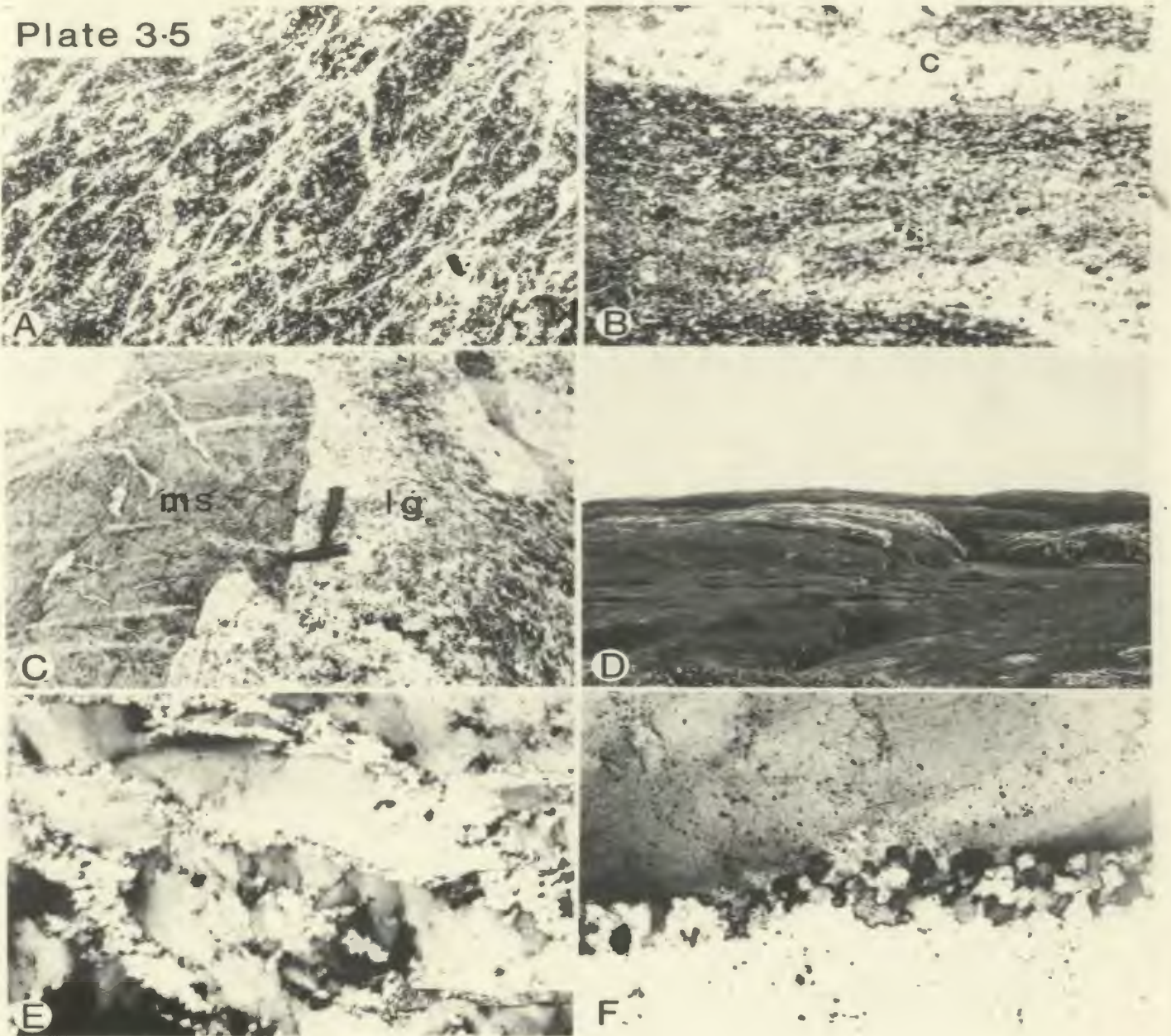


Plate 3.5

Field and thin section relationships of fault breccia and leucogranite-orthoquartzite units.

- 3.5A Matrix of "deformed conglomerate" showing orientation of sericite along conjugate shears. Sample RS79-4A, x40, X-polars.
- 3.5B Thin section of calcareous schist (?) showing lenses of carbonate (c) alternating with fine-grained argillaceous material. Sample RS79-4, x40, X-polars.
- 3.5C Igneous contact between leucogranite - Unit 4 - (lg) and mica schist exposed on shore line of Grey River Fiord near entrance to S.E. arm. Location 79-2.
- 3.5D Orthoquartzite unit cutting amphibolitic gneiss at locality of silica prospect near Gulch Cove, S.E. arm, Grey River Fiord.
- 3.5E Ribbon mylonite texture of orthoquartzite sample 601, x40, X-polars.
- 3.5F Subgrain development at edge of quartz crystal in ribbon mylonite of previous photograph, x160, X-polars.

Plate 3.5



shearing which forms the pseudo-conglomeratic texture.

An outcrop of calcareous schist occurs along the north-west shore of Long Pond in the middle of the Granite Cliff Mylonite Zone and comprises irregular lenticular bands of almost pure white calcite and similarly sized lenses and bands of fine-grained argillaceous material (Plate 3.5B). The latter are composed of well rounded to sub-rounded grains of quartz, less than 1 mm in diameter, set in a fine grained matrix of quartz, feldspar, calcite and sericite. Brittle fractures cutting across the schistosity are common and are filled with calcite and quartz.

The relationship between these two unusual rock types and the other lithologies in Unit 3 are unknown. However, the conglomeratic rock appears to be a fault breccia (cataclasite) developed from a coarse leucogranite protolith during late brittle deformation along the Granite Cliff Fault Zone.

3.2.1.7 Unit 4: Leucogranite, "Orthoquartzite"
(Mylonites, Ribbon Mylonite)

A body of coarse grained leucogranite was emplaced essentially concordant to the foliation of the gneisses and schists in the western part of the area but cuts across the foliation at a shallow angle further east (Map 1). It was formerly interpreted as a metasedimentary rock - quartz-feldspar paragneiss, quartz-sericite schist, metaquartzite (Bahyrycz, 1957; Mullins, 1958; Butler and Greene, 1976), but in places a granitic texture is discernible and good intrusive

contacts preserved (Plate 3.5C).

The part of the unit that outcrops within the Granite Cliff Shear Zone shows extensive mylonitisation, but outcrops along strike to the east have a somewhat less mylonitic fabric. The unit is extremely variable in composition along strike; in the west the unit is more granitic although now a mylonite; in the east it becomes quartz-rich (ortho-quartzite) and in fact areas near Gulch Cove (Plate 3.5D) have been evaluated as a silica prospect. In that area the orthoquartzite body attains a thickness of 183 m and 12 million tons grading 95.5% SiO_2 (1.9% Al_2O_3) have been outlined by diamond drilling (Butler and Green, 1976).

An intense mylonitic texture dominates the fabric of this unit and parallels the S_2 -Sm fabric in the amphibolitic gneiss and mica schist units. Orthoquartzites in the Gulch Cove area show striking development of a quartz ribbon mylonite texture (Plate 3.5E, F) which lack the aggregated quartz texture seen in previous units indicating that they have not been subjected to high temperature deformation, thus suggesting that they were injected after the peak of metamorphism.

In the west much of the original mineralogy has been destroyed by mylonitisation. Feldspar has been altered to muscovite and quartz is thoroughly recrystallised. The present mineralogy of the leucogranite unit is essentially quartz, feldspar (both plagioclase and K-feldspar), muscovite, epidote and opaques. In the east impurities in the ortho-

Table 3.2
Petrographic Notes on Units of the Metamorphic Suite

MINERAL	HABIT/DISTINGUISHING PROPERTIES	FOUND IN UNIT	PETROGRAPHIC NOTES
OLIGOCASE	Subhedral; albite twins	1	Generally fresh. Kinked feldspar grains. porphyroclastic texture in shear zones.
	Anhedral; albite twins	2	Incipient alteration-saussuritisation. In shear zones, feldspar similar to Unit 1.
	Anhedral; kinked twins	3a ₁	Incipient subgrain development. Deformed crystals lack twin planes and are saussuritised.
	Coarse, porphyroclasts	3a ₂	Saussuritised. Some kinked feldspars. Polygonisation and subgrain development common.
	Augen	3b	Deformation kinks common. Subgrain development on rims of porphyroclasts.
	Fine grained	3c	Porphyroclasts recrystallised. Serrated grain boundaries.
	Fine grained Porphyroclasts	3d 4	Untwinned recrystallised grains, serrated edges. Feldspar sericitised and recrystallised. Some K-feldspar present.
QUARTZ	Anhedral, undulose	1	Elongate parallel to foliation. Minor subgrain development. In shear zones quartz recrystallised and forms aggregates.
		2	Recrystallised granoblastic texture.
		3a ₁	Aggregates of fine-grained crystals.
		3a ₂	Recrystallised. Much subgrain development. Preferred orientation defines weak cataclastic texture.
		3b	Aggregates with stretched-flattened aspect, crenulated by D ₃ deformation.
		3c	Aggregates. Recrystallised quartz in matrix.
	Porphyroclasts	3d 4	Polygonisation and subgrain development, "floating" grains in feldspar/sericite matrix. Recrystallised quartz; ribbon quartz - subgrain development.
HORNBLANDS	Blue-green, polygonal	1	Partially overgrown by biotite.
	Poikiloblastic, blue-green	2	Overgrown by biotite.
	Blue-green	3a ₁	Rarely recrystallised to green hornblende. Biotite transposes hornblende foliation.
		3b	Relict grains incompletely replaced by biotite.
BIOTITE	Brownish-green	1	Replaces hornblende. Partially altered to chlorite. Transposes cleavage.
	Brownish-green	2	Overgrows hornblende. Transposes cleavage.
	Brownish-green	3a ₁	Overgrows hornblende. Parallel to weak S ₂ fabric.
	Brown	3a ₂	Cloes of crystals replaced by chlorite.
	Brown	3b	Replaces hornblende nearly completely. Crenulated by D ₃ . Altered to muscovite.
MUSCOVITE	Subhedral	3c	Replaces biotite-crenulated by D ₃ deformation.
SERICITE	Pink-grained	3d	Fill conjugate microshears.
		4	Crenulated in ribbon mylonite.
		1, 2, 3a ₁ , 3a ₂	Accessory; after feldspar
CHLORITE		1, 2, 3a ₁ , 3a ₂	Minor component after hornblende or biotite.
		3b	
ANDALUSITE	Porphyroblast-oid	3c	Rims preserved. Overgrows mylonite fabric (S ₂), slight crenulated itself. Rimmed by cordierite.
CORDIERITE	Yellow	3c	Rims andalusite porphyroblasts.
CALCITE		3d	Occurs in lenses and as fracture-filling.
APATITE	Stubby, equant	1, 3a ₁ , 3a ₂	Accessory.
EPIDOTE		all units	Accessory. Saussuritisation of feldspar.
OPAKES		all units	Accessory. Associated with hornblende and sphene.
SPHENE		2, 3a ₁	Accessory. Associated with hornblende and opakes.

3a₁ = Melasosome of migmatitic Unit 3a; 3a₂ = Leucosome of migmatitic Unit 3a.

quartzite include muscovite, feldspar and magnetite.

3.2.2 The Igneous Suite

Late-tectonic and post-tectonic times were marked by the intrusion of a variety of igneous bodies into the Metamorphic Suite. These igneous rocks are represented by Units 5 to 10 which are described below. Petrographic details of the Igneous Suite are found in Table 3.3.

3.2.2.1 Unit 5: Peridotite

Late in the deformational episode a series of small oval (100-200 m wide) plugs or dykes of ultramafic material were intruded into the migmatized gneisses of Unit 3a and 3b. A number of these outcrops mapped by Bahrycz (1957) were found by this writer to be coarse hornblendites, a variant of Unit 3a. However at least one dyke, that outcrops above the Grey River community, has ultramafic affinities.

The body has a roughly circular outline and contacts with the amphibolitic gneiss and mica schist are sharp and cross-cutting. It has a finer grained (chilled ?) margin which becomes coarser towards the central zone of the dyke. The rock weathers greenish-grey with various shades of brown and has a characteristic fracture pattern (Plate 3.6A) that is a result of differential weathering of the serpentinised fractures that criss-cross the body. Fibrous serpentine (chrysotile) was found in a few fractures.

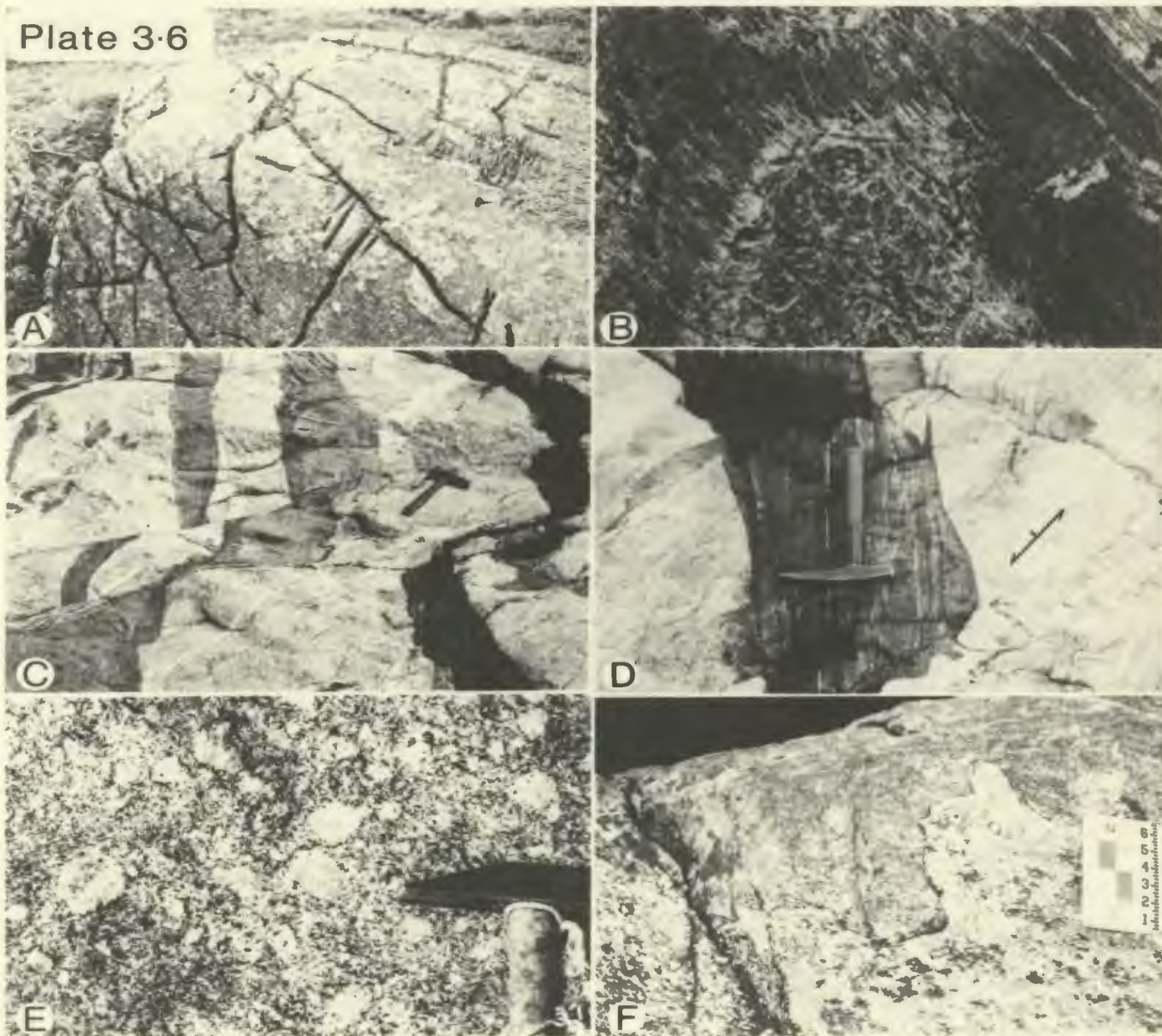
There is a pronounced fabric in the margin of the plug which parallels the S_2 foliation in the amphibolitic gneiss country rock. However, this foliation dies out

Plate 3.6

Field relationships of ultramafic, mafic and intermediate dykes, and K-feldspar megacrystic granite.

- 3.6A Characteristic weathering feature of ultramafic dykes (Unit 5) resulting from differential erosion of serpentinised fractures. Location 404.
- 3.6B Cumulate texture of peridotite dyke showing cumulate olivine and intercumulate augite phases. Sample 404, x40, X-polars.
- 3.6C Foliated mafic to intermediate dykes (Unit 6) intruding into shear zones which cut the tonalitic gneiss. Dykes later offset by E-W faulting. The foliation in the tonalitic gneiss is emphasised by orientation of the hammer. Shoreline west of Grey River Point.
- 3.6D Close up of mafic dyke of previous photograph. Foliation in the dyke is divergent to dyke wall and foliation in the tonalitic gneiss. Shoreline west of Grey River Point.
- 3.6E K-feldspar megacrystic granite (Unit 7). Location 556, Grey River Fiord.
- 3.6F Northern contact of K-feldspar megacrystic granite with a biotite-hornblende tonalite. Mouth of river feeding into northwest arm, Grey River Fiord.

Plate 3.6



towards the centre of the body.

The peridotite is composed of olivine, hypersthene, and augite but alteration and metamorphic effects have resulted in the introduction of serpentine, talc, chlorite and muscovite to the assemblage. In thin section a cumulate texture is preserved, with orthopyroxene and clinopyroxene phases intercumulus to olivine grains (Plate 3.6B).

Colourless, non-pleochroic olivine originally comprised 60-70% of the rock. The olivine grains were 2-3 mm long but are now 70% serpentised leaving only small grains (0.2 - 0.4 mm) as islands within a serpentine mesh. Pleochroic green to colourless augite makes up 10-15% of the peridotite and is much altered along cleavages to chlorite and muscovite. The augite generally contains abundant small opaque grains. Hypersthene comprises 10-15% of the peridotite but is nearly completely altered to fine grained talc. Some coarse (1-2 mm) talc crystals are also present as an alteration of the orthopyroxene, clinopyroxene and serpentine. They sometimes show kinked undulose extinction possibly as a result of the late deformational episode - D₃. Alignment of these coarse talc grains defines a weak foliation in the rock.

3.2.2.2 Unit 6: Mafic to Intermediate Dykes

A series of dioritic to quartz diorite dykes were injected into cross-cutting shear zones in the tonalitic gneiss (Unit 1) and quartz diorite gneiss (Unit 2). They are intruded by post-tectonic pegmatites and diorites of

Unit 8 and offset by later E-W faulting (Plate 3.6C).

The dykes are strongly foliated (Plate 3.6D), the foliation being slightly divergent to the orientation of the dyke walls and to the foliation of the enclosing gneisses. This divergence argues against the dyke foliation being developed by a flow mechanism but suggests that one of two situations prevailed. Firstly, that the deformation in the dykes was synchronous with the deformation in the gneiss, the divergence resulting from local modifications of the stress field by an anisotropy i.e. the dyke wall; or secondly that the dykes were intruded late in the deformation cycle along fractures that had some component of shearing.

The latter view is supported by textural evidence, where hornblende and biotite do not have the retrogressive relationship typically found in the gneisses (i.e. biotite after hornblende), and quartz and feldspar grains occur in an equigranular almost mosaic texture indicative of deformation under high temperature - low strain conditions.

The essential mineralogy is hornblende (30-90%), biotite (0-20%), plagioclase (5-40%), quartz (0-10%), and sphene (1-3%) with opaques, apatite, sericite and epidote as accessories.

3.2.2.3 Unit 7: K-feldspar Megacrystic Granite

A batholith of K-feldspar megacrystic, biotite granite forms the northern boundary of the metamorphic rocks (Map 1). This lithology dominates the igneous rocks in the area occupying an estimated 70 square km's in areal extent.

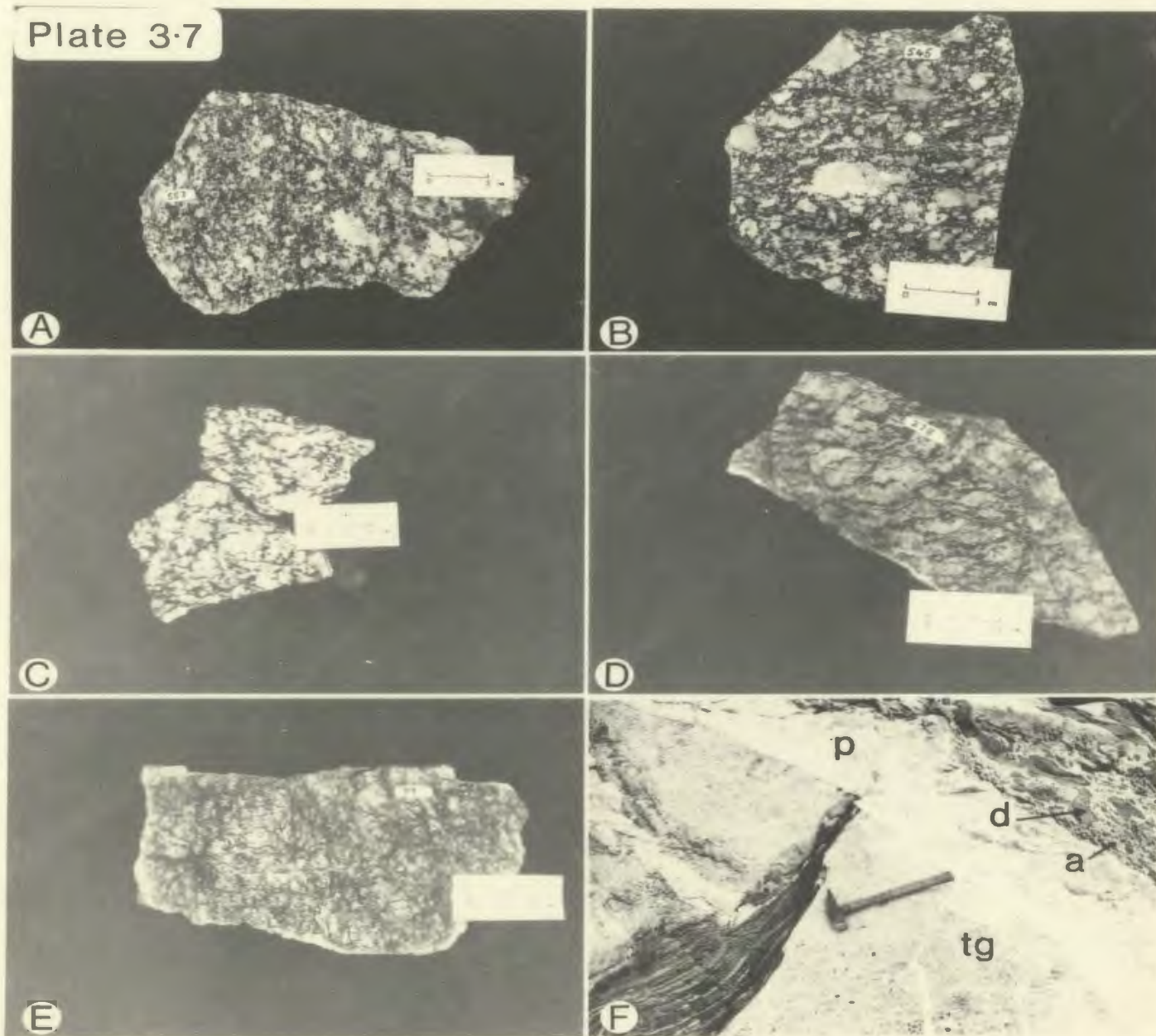
Plate 3.7

Progressive deformation of the megacrystic granite in the Granite Cliff Shear Zone; field relationships of the post-tectonic composite dyke suite.

3.7A - 3.7E Sequence of rock slab photographs showing progressive deformation of the K-feldspar megacrystic granite, from north to south in the Granite Cliff Shear Zone. With progressive deformation the feldspar megacrysts are aligned (3.7B) then form augen (3.7D) and are finally completely obliterated in the most intensely deformed sample (3.7E).

3.7F Field relationships of the composite dyke suite (Unit 8). In this photograph tonalitic gneiss (tg) is cut by a foliated mafic dyke which in turn is cut by a pegmatite (p), the margin of the composite dyke. The pegmatite is intruded up its centre (the other margin of dyke not visible) by a diorite (d) which is brecciated by intrusion of alaskite (a).

Plate 3.7



The rock is more correctly described as a quartz monzonite and is characterised by white orthoclase megacrysts up to 3 cm long (Plate 3.6E) locally with plagioclase mantles. The euhedral megacrysts comprise 10-25% of the rock and are set in a groundmass composed of K-feldspar, plagioclase and biotite. Additionally hornblende occurs in specimens associated with the deformed southern contact of the pluton.

The northern contact is exposed in the river outlet at the head of Northwest Arm. There the megacrystic granite intrudes a massive biotite, hornblende tonalite with a sharp contact (Plate 3.6F) around which megacrysts are weakly aligned. Away from the contacts the megacrysts are randomly distributed. Xenolithic blocks of tonalite occur in the megacrystic granite and pegmatites orientated perpendicular to the contact are found in the tonalite. The southern contact with metamorphic rocks of Unit 3 (a,b,c,d) is broadly defined by the Granite Cliff Fault (centred on Long Pond). The eastern and western contacts are unknown but the Francois granite pluton appears to truncate it in the east (Williams, 1971).

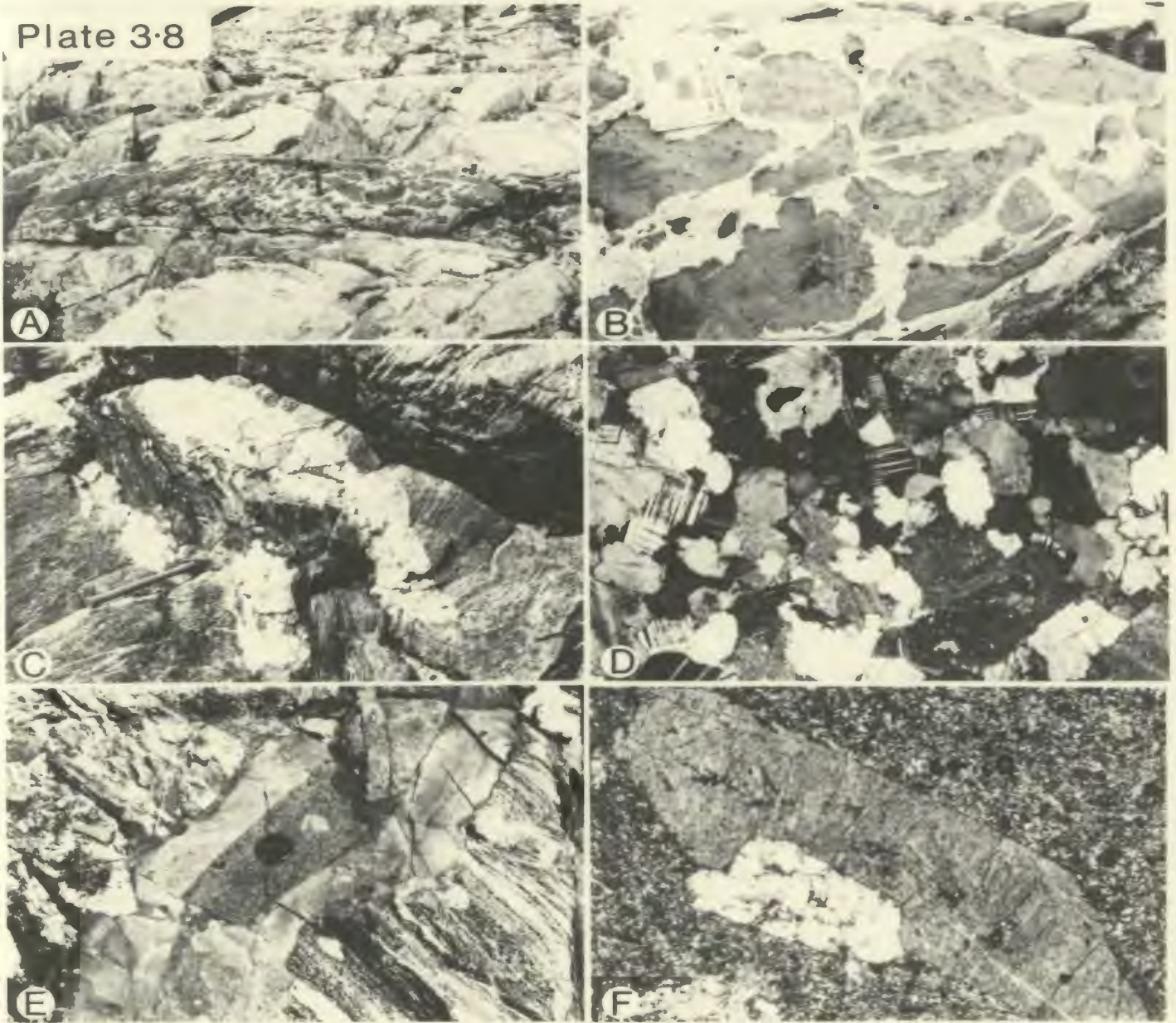
The megacrystic granite contains bands of equigranular medium grained granite that are essentially non-megacrystic equivalents of the main body and have a similar deformational fabric. Also the megacrystic granite is intruded by equigranular medium grained pink to white granite aplite dykes and pegmatites (Unit 9) and fine-grained diabase dykes of Unit 10. East-west striking faults dissect the granite and

Plate 3.8

Field relationships of the composite dyke suite and later leucogranites and diabase dykes.

- 3.8A Igneous breccia. Diorite intruded by alaskite granite. Note lack of pegmatite rim to composite dyke as in Plate 3.7F. Coast west of Grey River Point.
- 3.8B Close-up of igneous breccia shown in Plate 3.8A.
- 3.8C Diorite dyke intruding up center of pegmatite. Note that in this locality the diorite has not been injected later by alaskite. Coast north of Grey River Point.
- 3.8D Leucogranite (Unit 9) with aplitic texture also showing saussuritisation of plagioclase. Sample 424, x40, X-polars.
- 3.8E Diabase dyke (Unit 10) with chilled margin cutting quartz diorite gneiss. Grey River Point.
- 3.8F Thin section of porphyritic diabase dyke showing euhedral crystals of augite and plagioclase. The plagioclase is extremely altered to sericite, sample 79-11, x40, X-polars.

Plate 3.8



fault zones are usually epidotised.

The granite is essentially undeformed in the north but an increase in deformation is evident towards the southern contact. The deformation is marked by the gradual alignment and rotation of the K-feldspar megacrysts into a foliation plane which parallels the southern contact, and by an increase in mafics, notably hornblende, biotite and chlorite. The white, euhedral orthoclase megacrysts found in undeformed granite become increasingly ovoid (augen) and pink-coloured with increasing deformation. Simple twinning of the megacrysts is evident in hand specimens. Plate 3.7 illustrates the increase in deformation seen in hand specimen from north to south.

The mineralogy of the undeformed megacrystic granite is composed of quartz (10-20%), plagioclase (30-40%), K-feldspar (30-40%) and mica (10-15%) with minor accessories of sericite, opaques, chlorite, apatite and epidote. The opaque phases consist of magnetite, hematite and ilmenite.

3.2.2.4 Unit 8: Composite Dyke Suite. Pegmatites, Diorites, Alaskite.

Igneous units postdating the megacrystic granite (Unit 7) are strongly discordant, show no evidence of deformation and are clearly post-tectonic. The first of these units, a composite dyke suite is found in southern coastal exposures cutting tonalitic and quartz dioritic gneisses of Units 1 and 2, and are mappable only on outcrop scale.

The composite dyke suite consists of zoned dykes with

margins of pegmatite and cores of diorite, variably veined by alaskite (Plate 3.7F). These dioritic cores can be so veined by alaskite that spectacular igneous breccias are developed (Plate 3.8A and B). Dykes of the brecciated diorite, containing rare xenoliths of gneiss, are found without the pegmatitic rim, while in others the diorite is not brecciated but veined by anastomosing small veinlets of the alaskite. Still others show no veining but are intruded along centres of pegmatites (Plate 3.8C) and show a strong flow foliation parallel to the dyke margin.

There is an obvious close spatial and temporal relationship between the three compositionally distinct phases of the composite dyke suite. There is always a sharp contact between pegmatite margins and dyke cores. Also rare xenoliths of pegmatite occur in some diorite dykes. This suggests that the pegmatite was solidified before intrusion of the diorite but very probably still hot, thus providing a zone of thermal weakness for later intrusion of the diorite dykes. In thin section brecciated diorite blocks show reaction rims with the alaskite suggesting the diorite was cooled prior to the intrusion of the latter. However, no reaction rims were seen in net veined dykes implying that some diorite dykes were still hot and plastic.

3.2.2.5 Unit 9: Leucogranite, Aplite, Pegmatite.

Postdating the composite dyke suite of Unit 8 are a series of granitic dykes and sills that occur throughout the map area. Concentrations of these granitic dykes occur in the south especially along the seacoast of the Grey River

peninsula. A small granitic stock of 250 x 400 m areal extent is exposed in the 250 m high hill immediately west of the entrance to Grey River fiord. The frequency of granitic dykes is observed to increase towards this body, much of which is dyke material. Elsewhere similar dykes cut the megacrystic granite and all metamorphic units, including parts of the Granite Cliff Shear Zone. The stock and related granitic dykes are cut by diabase dykes (Unit 10) and the hydrothermal vein system.

Unit 9 exhibits a variety of rock types ranging from pink-red, coarse pegmatite to white two-mica leucogranite and aplite that are locally garnetiferous. The fine grained dykes have an allotriomorphic granular-aplitic texture (Plate 3.8D) defined by interlocking anhedral grains of quartz, microcline, orthoclase and albite, and are typically mafic poor. In these dykes, grain size is variable and ranges from 1-3 mm.

Coarser leucogranite dykes contain anhedral porphyritic microcline (up to 10 mm grainsize) set in a medium to coarse grained matrix of quartz, microcline, perthitic orthoclase and oligoclase. The porphyritic microcline crystals enclose quartz and plagioclase as inclusions. Pegmatites are the coarsest rock type observed with feldspars up to 5 cm long. Dykes that are texturally gradational between the pegmatite and aplites are common. In hand specimen many show a graphic texture with cuneiform intergrowths of quartz and feldspar, and a micrographic texture

is widespread in thin section.

The leucogranites are chiefly composed of quartz (15-30%), K-feldspar (50-40%), plagioclase (25-35%), chlorite (1%) and muscovite (1%) with relict biotite, fluorapatite, magnetite and garnet as accessories.

Much of the present mineralogy of the leucogranite dykes is a result of extensive hydrothermal alteration which appears to be characteristic of the suite. With regard to feldspar minerals, oligoclase is extensively altered to albite, while perthitic orthoclase is inverted to microcline. Furthermore saussuritisation of plagioclase is common. The minor amounts of biotite present in the leucogranite dykes are nearly completely altered to chlorite; where present garnets are also partially altered to chlorite. Primary minerals, apparently stable during the alteration episode, include muscovite and quartz.

3.2.2.6 Unit 10: Diabase Dykes

Diabase dykes with a common approximate southwest-northeast strike occur throughout the area, but are more prevalent in southern coastal sections. They are typically fine to medium grained and grey-green in colour and attain thicknesses ranging from 15 cm to 5 m. Chilled margins are common (Plate 3.8E) as are porphyritic textures. In the latter case phenocrysts make up 3 - 10% of the dyke and include euhedral crystals of plagioclase and augite (Plate 3.8F). Rare glomeroporphyritic textures are found.

The phenocrysts occur in a fine-medium grained ground-

Table 1.3
Petrographic Notes on the Units of The Igneous Suite

MINERAL	HABIT/DISTINGUISHING PROPERTIES	FOUND IN UNIT	PETROGRAPHIC NOTES
PLAGIOCLASE	Equigranular	6	In matrix with quartz. Oligoclase composition.
	Subhedral-anhedral	7	Oligoclase, mainly as groundmass constituent. Rarely as megacrysts. Occurs as inclusions in orthoclase megacrysts. Inclusions commonly have albite rims.
	Anhedral, untrinned	8 ₁	Matrix constituent with quartz. Granoblastic texture.
	Subhedral-euhedral	8 ₂	Oligoclase. Porphyritic crystals (1-2 mm) commonly zoned. Contain quartz and biotite inclusions.
		9	Oligoclase. Variably altered to sericite and epidote. Myrmekitic intergrowths with K-feldspar. Oligoclase partially albited (untrinned).
	Phenocrysts	10	Generally altered to muscovite and epidote.
QUARTZ	Equigranular	6	Mosaic with feldspar. Grain size 0.3 - 1.0 mm. Strongly undulose.
	Anhedral	7	Undulose. Variable grain size 0.4 - 1.0 mm.
	Anhedral	8 ₁	In groundmass with feldspar. Granoblastic texture. Weakly undulose.
	Anhedral	8 ₂	Variable grain size (0.2 - 1.5 mm). Undulose.
	Anhedral.	9	Smaller grain size than feldspar. Often micrographic-graphic texture with K-feldspar.
K-FELDSPAR	Megacrysts	7	Perthitic orthoclase. Twinning common. Rarely rimmed by plagioclase. Megacrysts contain quartz, plagioclase and rarely biotite as inclusions. Inverted to microcline in shear zone where they form augen.
		9	Both microcline and perthitic orthoclase. Orthoclase partially replaced by microcline (cross-hatched twinning). Porphyritic crystals contain quartz intergrowths - micrographic texture.
AMPHIBOLE	Blue-green, subhedral	6	Hornblende, preferred orientation defines fabric. Grain size (0.5 - 1.5 mm). Minor alteration to chlorite.
		7	Hornblende, constituent of megacrystic granite in shear zone.
	Euhedral, green	8 ₁	Hornblende, major mafic mineral. Intergrown with biotite. Grain size 0.1 - 0.8 mm.
		10	Actinolite, after clinopyroxene.
MICA	Anhedral, ragged	6	Biotite. Pleochroic brown to yellow brown. Grain size up to 1.5 mm. Orientation parallel hornblende.
	Subhedral-euhedral	7	Biotite. Only mafic undeformed granite. Minor alteration to chlorite. Grain size 0.5 - 2 mm. Biotite greenish-brown in deformed megacrystic granite. Formed after hornblende.
	Euhedral	8 ₁	Brown biotite intergrown with hornblende. Similar grain size.
	Anhedral-subhedral	8 ₂	Biotite rare. Pleochroic brown-yellow brown.
	Euhedral	9	Pleochroic brown to colourless biotite. Mainly altered to chlorite.
	Euhedral	9	Coarse primary muscovite. Also found as secondary mineral formed during saussuritisation of plagioclase.
		10	Plagioclase phenocrysts altered almost completely to muscovite.

Table 3.3 continued.

MINERAL	HABIT/DISTINGUISHING PROPERTIES	FOUND IN UNIT	PETROGRAPHIC NOTES
OLIVINE	Cumulate	5	Colourless crystals up to 3 mm long. 70% serpentinised.
HYPERSTHENE	Intercumulate	5	Almost completely altered to muscovite.
AUGITE	Intercumulate	5	Pleochroic green to colourless. Much altered to chlorite, muscovite and talc.
	Phenocrysts	10	Fresh to weakly altered (to actinolite). Rare glomerophyritic textures. Clinopyroxene in groundmass altered to actinolite.
SERPENTINE	Mass	5	After Olivine.
TALC		5	Alteration of orthopyroxene, clinopyroxene, and serpentine. Alignment defines weak foliation. Exhibits linked undulose extinction.
GARNET	Euhedral, red	9	Commonly zoned; red-brown core - colourless rim. Others extremely fractured and altered to chlorite.
CHLORITE		7, 8 ₁ , 9	Accessory after biotite or hornblende.
APATITE	Elongate, prismatic	6, 7, 8 ₁ , 8 ₂ , 9	Accessory.
EPIDOTE		9, 10	Accessory. After feldspar occurs with sericite/muscovite.
OPAQUES		5, 6, 7, 10	Accessory. Associated with sphene in deformed megacrystic granites.
SPHENE	Euhedral	6	Diamond shape - orientation parallel to foliation. No associated opaques.
		7	Rare in undeformed megacrystic granites. Increases at expense of opaques with increasing deformation.

8₁ - diorite - composite dyke suite; 8₂ - alkali - composite dyke suite.

mass, composed of clinopyroxene, feldspar, epidote and actinolite, with minor quartz, displaying a subophitic texture. Plagioclase phenocrysts are typically altered almost completely to coarse sericite while clinopyroxene is weakly altered to actinolite, both implying some degree of hydrothermal alteration. Similar dykes found in the adit are cut by the hydrothermal vein system.

3.2.3. Structural and Metamorphic History

The metamorphic rocks of the area have undergone a complex geologic history involving migmatization, folding, intrusion and shearing. Four deformational episodes are resolved, however only the first two have regional significance. The last two episodes are intimately associated with the Granite Cliff Shear Zone (Figure 3.1).

3.2.3.1 Prograde Metamorphism and Deformation

The oldest rock unit, the tonalitic gneiss (Unit 1) appears to have undergone an earlier phase of deformation prior to the emplacement and deformation of the quartz dioritic gneiss (Unit 2) and amphibolitic gneiss (Unit 3a) protoliths. Fold hinges of this earlier phase are preserved as rare intrafolial folds between the gneissic banding of the second deformation, D_2 .

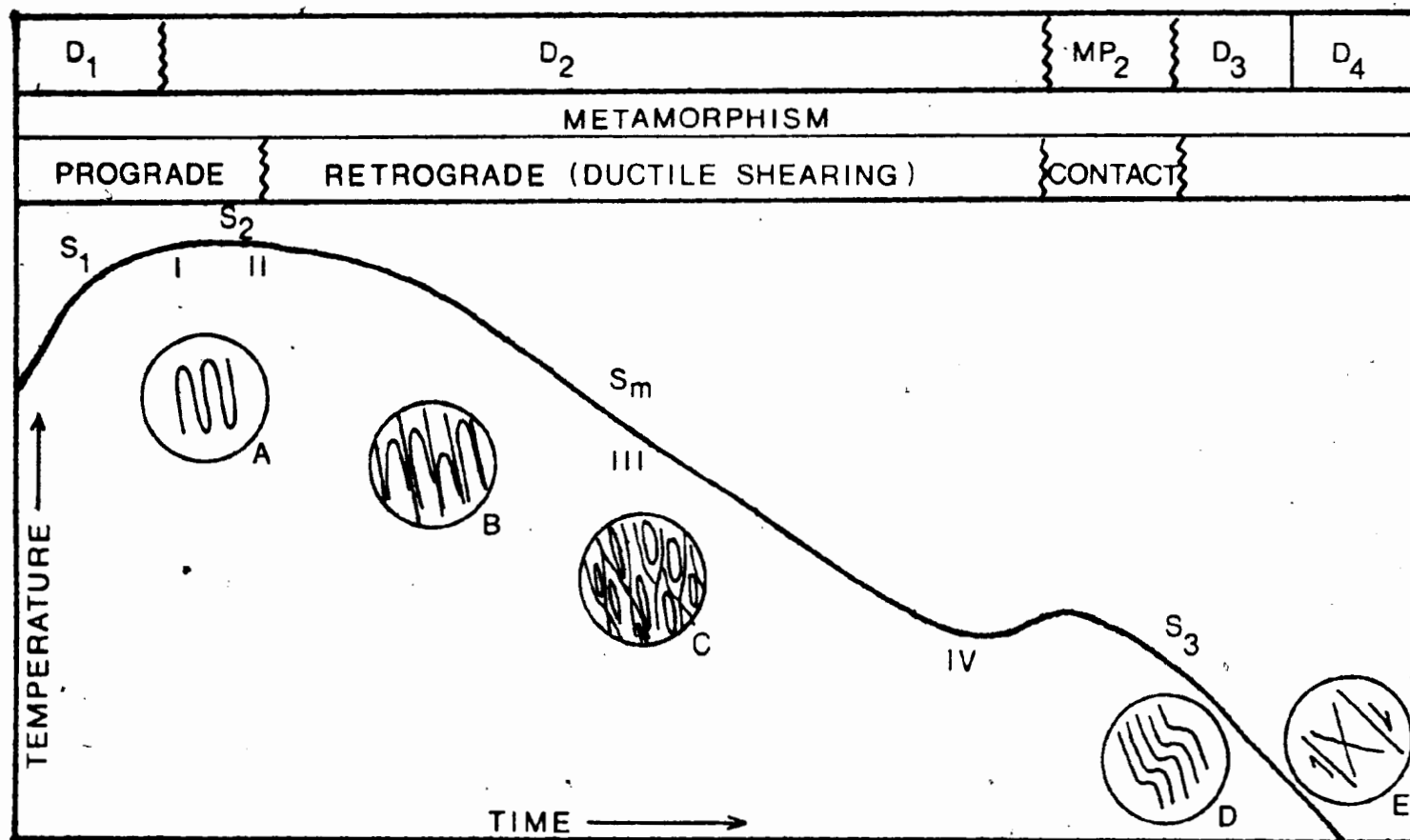
Extensive migmatization of the quartz diorite and amphibolitic gneisses during D_2 , preceded, or was concomitant with, the major folding phase which cumulated in tight to isoclinal folds within these units. Macroscopic isoclinal folds are rarely observed but mesoscopically folded

leucosome bands with sheared out limbs are common in the amphibolitic gneiss (Unit 3a). The dominant schistosity (S_2) of the area, which strikes approximately east-west, is axial planar to those isoclinal folds. Late granitic dykes intruded into these units during D_2 deformation, cut the migmatitic banding but are folded into more open folds or are boudinaged.

On the basis of textural evidence from the tonalitic, quartz dioritic, and amphibolitic gneisses, the peak of regional metamorphism was reached between the first and second deformations (Figures 3.2, 3.3). These units lack the diagnostic metamorphic minerals found in rocks of pelitic composition but their mineral assemblages are dominated by hornblende, plagioclase and quartz. The hornblende is characteristically strongly pleochroic blue-green and occurs as coarse poikiloblastic crystals crowded with inclusions of quartz. Plagioclases are typically of oligoclase composition and quartz occurs in coarse aggregates that have annealed textures indicative of high temperature/low strain conditions. Such an assemblage is typical of amphibolite facies metamorphism and suggests that the metamorphic rocks may have attained temperatures of 550° - 750°C and pressures of 4-8 kb (Turner, 1968; Hyndman, 1972).

3.2.3.2 Retrograde Metamorphism and Deformation

In its waning stages the second deformation is characterised by inhomogeneous strain. Areas of low strain are preserved by zones of amphibolitic gneiss, tonalitic gneiss



I-migmatisation, II-injection of granitic dykes, III-intrusion of leucogranite-orthoquartzite sill, IV-intrusion of megacrystic granite. A-isoclinal folds, B-sheared isoclinal folds, C-mylonitisation, D-crenulation, E-brittle-ductile deformation.

Figure 3.2 Summary of the structural history of the Grey River area.

and quartz diorite gneiss showing a mildly cataclastic texture (protomylonites) and are gradational with mylonitic areas of high strain (shear zones). In such zones a strong mylonitic fabric (S_m) is developed, with a similar orientation to S_2 , and amphibolite metamorphic assemblages have been retrogressed to greenschist facies or lower grades. Mineralogical changes and the grain size reduction by ductile and diffusional processes in these shear zones (Beach, 1979) resulted in the formation of mica schists and phyllites with increasing amounts of shearing (Bell and Etheridge, 1973; Roy, 1977).

The megacrystic granite (Unit 7) was intruded during the final stages of the retrogressive ductile shearing episode (Figure 3.2) and was intensely deformed at its southern contact where it intrudes the Granite Cliff Shear Zone, the major shear zone of the area. The deformation in the granite parallels the mylonitic (and S_2) fabric of the Metamorphic Suite but dies out towards the north. Petrographic features of the deformation in the granite are illustrated in Plate 3.9.

Within the Granite Cliff Shear Zone the mylonitic fabric is commonly crenulated (D_3 deformation) and megascopically folded into broad, open, southward climbing folds. Close to the contact with the megacrystic granite, andalusite porphyroblasts rimmed by cordierite overgrow the mylonitic fabric but are also affected by the D_3 crenulation cleavage (Figure 3.3). The porphyroblastic growth relates to the

Plate 3.9

Petrographic features of the deformation of the K-feldspar megacrystic granite in the Granite Cliff Shear Zone.

- 3.9A Low degree of deformation: Partial rotation of megacryst into foliation plane defined by weakly aligned biotite crystal. Megacryst slightly rounded twinned, perthitic orthoclase. Perthitic lamellae become noticeably coarser with increasing deformation. Sample 571, x14, X-polars.
- 3.9B Conjugate fractures developed within megacrysts with increasing deformation. Fractures are filled with chlorite and muscovite. Plagioclase crystals (upper right) become nearly completely saussuritised. Sample 526, x40, X-polars.
- 3.9C Increasing deformation results in complete alignment of the megacrysts with the foliation wrapping around the crystals to produce an augen texture. Megacrysts become quite ovoid-shaped by recrystallisation around the edge of the crystal resulting in a zone of fine-grained recrystallised K-feldspar as a halo to the megacrysts. Sample 544, x14, X-polars.
- 3.9D Chessboard texture (microcline) developed in areas of low strain at tips of augen. Sample 542, x40, X-polars.
- 3.9E Twinned megacryst showing development of chessboard texture in one (lower) twin only. Note that edges of fractures in the other twin are similarly effected. Sample 546, x40, X-polars.
- 3.9F Highly deformed granite. Crystals of K-feldspar barely recognisable as a megacryst. Grain size reduction by dislocation along conjugate shears. Sample 128 x14, X-polars.

Plate 3.9

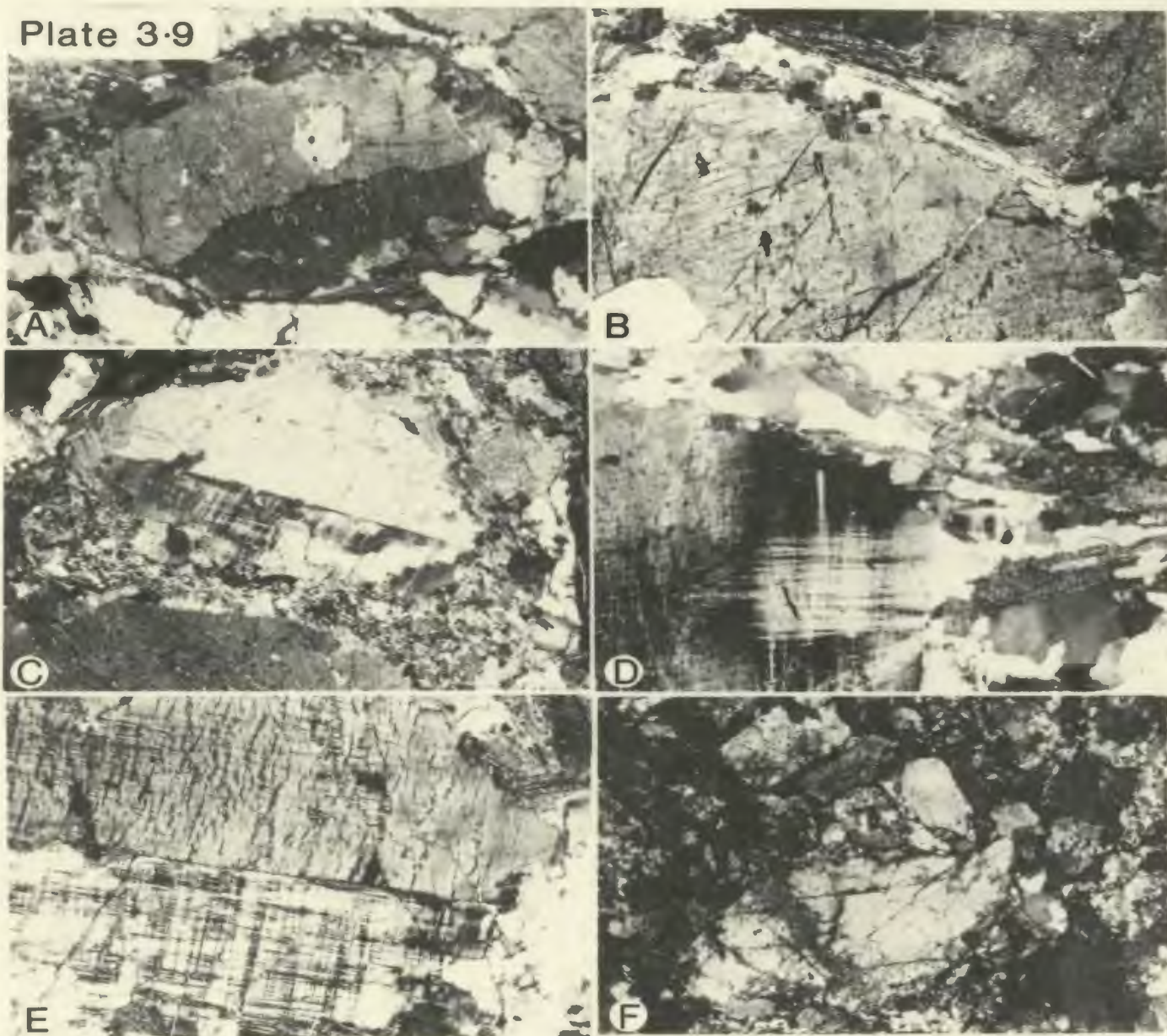


Figure 3.3

Growth history of the metamorphic minerals
in the Grey River Area

MINERALS	D ₁	D ₂	MP ₂	D ₃	D ₄
HORNBLende	_____	_____		•	
PLAGIOCLASE	_____	_____			
QUARTZ	_____	-----			
BIOTITE		-----			
CHLORITE		-----			
MUSCOVITE		-----		-----	
ANDALUSITE			-----		
CORDIERITE			-----		
SERICITE		-----		-----	-----

intrusion of the megacrystic granite and the crenulation to continued deformation in the Granite Cliff Shear Zone.

The assemblage quartz-muscovite-andalusite-cordierite in these rocks may be related to experimentally produced P-T equilibria for these metamorphic minerals. The relevant curves are given in Figure 3.4 from which an estimate of the pressure and temperature prevailing during the intrusion of the megacrystic granite is possible. However, the diagram is not strictly an accurate petrogenetic grid since the experimental curves are plotted as recorded, with no allowance for phases not present in the original study.

In the rocks affected by the contact metamorphism, muscovite and quartz appears to be stable during the growth of andalusite and cordierite, and sillimanite and K-feldspar were not formed. This indicates that the rock equilibrated at temperatures lower than 650°C and at pressures of 2.5 kb (point A, Figure 3.4). If Holdaway's (1971) Al_2SiO_5 equilibria data are used (curve d, Figure 3.4) then the stability field for andalusite is decreased and inferred pressure and temperature conditions are lower (approximate 2 kb and 600°C). The maximum possible range of P-T conditions over which the assemblage muscovite-quartz-andalusite-cordierite is stable are shown in the shaded portions of Figure 3.4.

Crenulation of the mylonitic fabric during D₃ resulted in little growth of new metamorphic minerals although pre-existing muscovite may have been coarsened. However, most

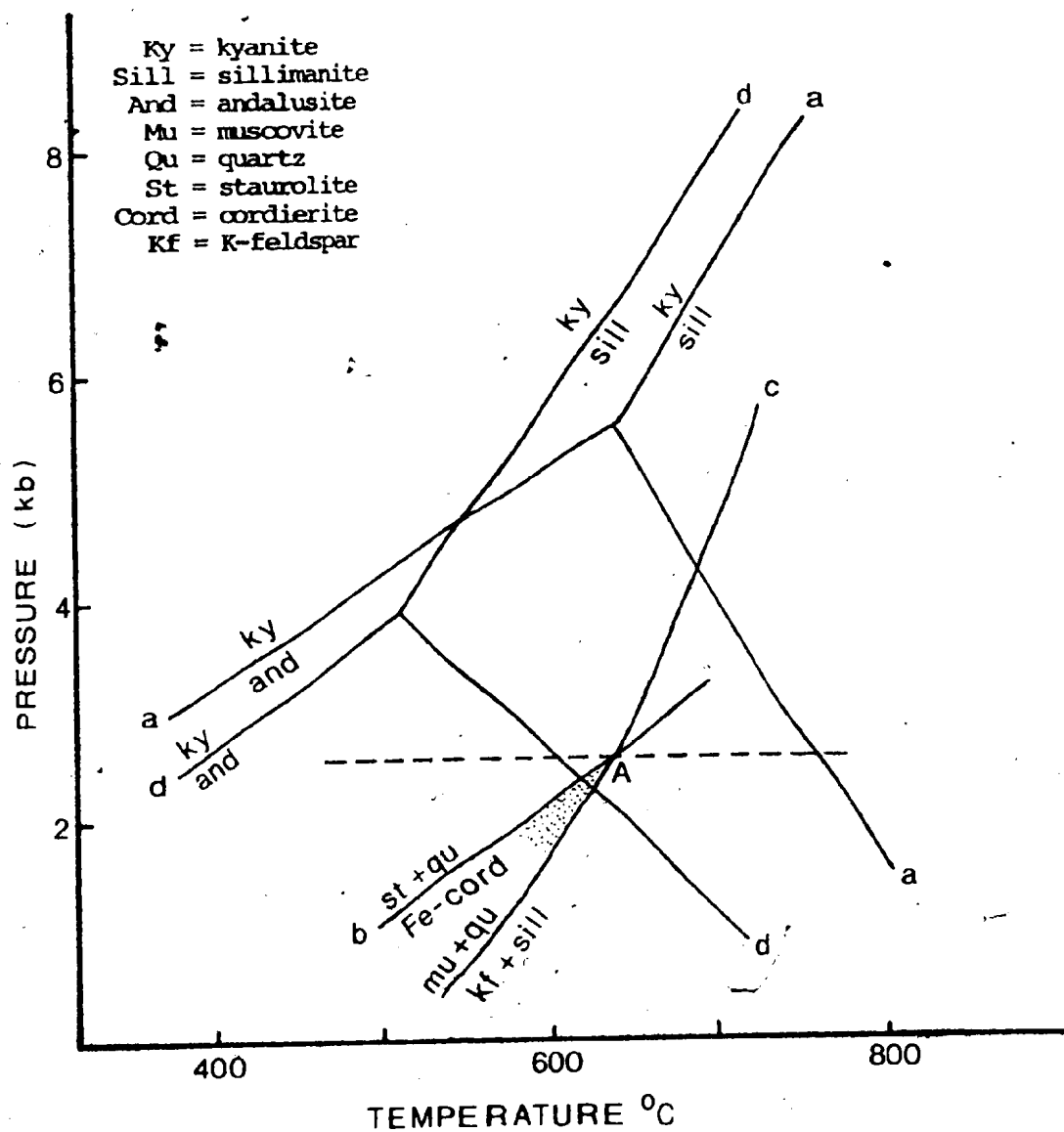


Figure 3.4 Inferred P-T conditions for contact metamorphism related to intrusion of the megacrystic granite. Mineral equilibria a-Richardson et al., 1969; b-Richardson, 1968; c-Evans, 1965; d-Holdaway, 1971.

thin sections show that the coarse muscovite is crenulated as well and fine grained sericite may be the only metamorphic mineral formed during the D_3 deformation.

3.2.3.3 Faulting and Jointing

The map area is well dissected by faults which are dominantly steeply dipping normal faults. In the subdued topography of the barrens, these faults are generally represented by large depressions and as such are readily discernible from air photos. The principal set of faults strike E-W and dip steeply to the North. Several faults of this generation offset the hydrothermal vein system and thus postdate the mineralisation episode.

A late, very localised brittle deformation (D_4) is related to fault movements along the Granite Cliff Fault and produces conjugate shearing in post tectonic leucogranite dykes which are cut by the fault, as well as other rocks.

Jointing is well developed in most rock types, and appears uniform over the whole area in both igneous and metamorphic rocks. The most prominent set strikes $N30^{\circ}E$ with an essentially vertical dip. A less well defined set strikes E-W and dips to the north.

3.3 CORRELATION

The tonalitic, quartz dioritic, and amphibolitic gneisses (Units 1, 2, 3a) in the Grey River area are similar to lithologies mapped as a basement gneiss complex in Baie D'Espoir (Colman-Sadd, 1978); specifically the Little Passage Gneiss and unnamed equivalents exposed in the

Gaultois map area. The Hare Bay gneiss and Square Pond gneiss, defined in the NE Gander Area (Blackwood, 1978), also correlate closely with the gneissic rocks at Grey River and although they are decidedly more psammitic in composition, they have undergone a similar deformational and metamorphic history (Blackwood, 1976). Intensely schistose rocks that are found locally within the Square Pond gneiss may represent zones of shearing and retrogression similar to zones developed in the amphibolitic gneiss at Grey River (i.e. mica schists, and phyllites (Unit 3b, 3c)). Furthermore a regional cataclastic texture is recognised (Blackwood, 1976; Jayasinghe, 1976).

Gneisses of the Port-aux-Basques area are texturally and lithologically similar to parts of the Grey River area. The Port-aux-Basques gneiss as defined by Brown (1976), is composed of banded injection migmatites of which 40% are amphibolites. Schistose bands are common and again probably represent retrograde ductile shear zones. The Harbour Le Cou Group (Brown, 1976) was interpreted as cover to the Port-aux-Basques gneiss "basement" but in the type area is found to be in tectonic contact with reworked Port-aux-Basques gneiss (D. Wilton pers. comm., 1980), which from descriptions given by Brown, (1976) is mylonitised-sheared Port-aux-Basque granite. It is possible that the reworked Port-aux-Basques gneiss and the Harbour Le Cou Group are products of a regional ductile shear zone. The relationship of the concordant (sheeted) Port-aux-Basques granite (after Brown, 1975) to the

Port-aux-Basques gneiss is not well understood at present, but may be similar to the leucogranite-orthoquartzite unit (4) in the Grey River area. Correlatives in the La Poile-Grand Bruit region may include the Keeping gneiss (possible extension of the Port-aux-Basques gneiss) and the Cinq Cerf Complex (Chorlton, 1978), both of which appear to have undergone a similar structural and plutonic history to the gneisses at Grey River.

Equivalents to the metasedimentary terrain, i.e. the Gander Group (Blackwood, 1978) and Baie D'Espoir Group (Colman-Sadd, 1978), do not outcrop in the Grey River area. Detailed mapping by mining companies throughout the Gander Zone indicate that these units may be correlative and continuous (N. Briggs pers. comm., 1979) with metasedimentary and metavolcanic rocks in the La Poile-Grand Bruit area (Chorlton, 1978). Equivalents to these rocks crop out 25 km north of the Grey River area (Williams, 1979) and their continuity with the La Poile area is confirmed by reconnaissance mapping by Smyth (1979, 1980) in the Burgeo map area.

Deformed megacrystic granites are a common component of the gneissic terrain throughout the Gander Zone. The Grey River megacrystic granite has obvious similarities with the Cape Freels granite, N.E. Gander (Jayasinghe, 1976) and the Gaultois granite (Colman-Sadd, 1978) in the Baie D'Espoir area. Furthermore, like the Grey River megacrystic granite, the deformed margin of the Cape Freels granite is intimately

associated with a shear zone of regional magnitude (Jayasinghe, 1976, 1979). The closest correlatives in S.W. Newfoundland are the variably deformed Cape Ray granite (D. Wilton, pers. comm., 1980) and the Otter Point and La Poile batholiths (Chorlton, 1978) which intrude the Cinq Cerf Complex.

Volumetrically large batholiths of garnetiferous leucogranites may not be present or are not exposed in the immediate vicinity of Grey River. The Francois (megacrystic) granite which truncates the eastern portion of the Grey River metamorphic rocks may represent the late undeformed megacrystic granites typical of other parts of the Gander Zone. Correlatives with the Francois granite may include the Deadmans Bay granite, N.E. Gander (Jayasinghe, 1976; Blackwood, 1978), the Piccaire Granite, Baie D'Espoir (Colman-Sadd, 1978) and the Chetwynd Complex and Isle aux Morts Brook granite (Chorlton, 1978; Brown, 1976) in S.W. Newfoundland.

In summary, the Grey River metamorphic rocks are most closely allied with the gneissic terrain that occurs on the eastern margin of the Gander Zone. Based on concepts developed elsewhere in the Gander Zone (Kennedy and McGonigal, 1972; Colman-Sadd, 1974; Kennedy, 1976) these gneisses may represent pre-Appalachian basement rocks although these interpretations have been recently challenged (Blackwood, 1978; Jayasinghe, 1979; Strong, 1980; Hanmer, 1980). The controversial basement/cover relationship cannot be resolved

in the Grey River area because of the lack of rocks typical of the metasedimentary terrain (cover). Discussion of the significance of the timing of deformation and intrusive events at Grey River will be postponed until the section dealing with radiometric dating (Chapter 9).

3.4 SUMMARY

The Grey River metamorphic belt has undergone a complex history involving a number of tectonic and synkinematic events followed by a complicated post-kinematic history of multiple intrusion.

The oldest rock unit is a tonalitic gneiss which occurs as screens within younger intrusives. Sills and dykes of quartz diorite to diorite which intrude the tonalitic gneiss have been extensively injected with migmatitic granite that has been transposed by, and parallel, the axial planar fabric of the D_1 deformation.

Much of the Grey River peninsula is underlain by coarse to medium grained amphibolitic gneiss that have suffered a similar deformation history to the quartz diorite gneiss unit. Their interrelationship however, is unknown. The amphibolite gneiss is folded into tight isoclinal folds during D_2 deformation and the axial plane cleavage associated with this folding phase is the dominant fabric in the region. The peak of metamorphism coincided with this folding phase and reached the amphibolite facies.

During the waning stages of the D_2 deformation, extensive shear zones were developed, probably in response to migration

of metamorphic fluids produced during prograde metamorphism at the greenschist/amphibolite facies boundary. All previously mentioned units were in part affected by this episode and retrograde assemblages were produced in these ductile shear zones now represented by mica schists and phyllites (mylonite and ultramylonite).

Several igneous bodies including a leucogranite-orthogneiss unit, were intruded during the early stages of the retrogressive deformation episode. These were followed by the intrusion of a batholith of K-feldspar megacrystic granite, the southern contact of which intrudes a zone of intense ductile shearing represented by the Granite Cliff Shear Zone. Along this contact the megacrystic granite exhibits a strongly sheared fabric which disappears towards the north. Porphyroblasts of andalusite rimmed by cordierite overgrow the mylonite fabric of the Granite Cliff Shear Zone and relate to intrusion of the megacrystic granite batholith. These porphyroblasts are crenulated by the D_3 deformation which probably represents continued deformation in the shear zone. Mineral equilibria indicate that the porphyroblasts were formed at approximately 600°C and 2 kb.

Following retrogressive deformation and intrusion of the megacrystic granite the area was subjected to a series of intrusive events which culminated in the emplacement of a suite of leucogranite dykes. All of these units were later intruded by diabase dykes and cut by a hydrothermal vein system, which contains tungsten and basemetal mineral-

isation, the genesis of which is the principal subject of this thesis.

CHAPTER 4

GEOCHEMISTRY - IGNEOUS ROCKS

4.1 INTRODUCTION

The igneous rocks of the Grey River area were analysed for major and trace elements to investigate:- 1) possible genetic relationship between the megacrystic granite and the late stage granite-leucogranite dykes; 2) possible sources of the ore-forming elements; 3) geochemical peculiarities (if any) of the igneous rocks associated with the ore deposit; 4) geological conditions under which the ore-bearing intrusions were able to produce concentrations of ore; and 5) comparisons of these geochemical and geological parameters with similar igneous-hydrothermal environments elsewhere.

Thirty-two samples (11 of megacrystic granite and 21 of leucogranite) were analysed for the normal major element oxides as well as Zr, Rb, Sr, Zn, Cu, Ba, Sn, Nb, W, Pb, Ni, Li, Cr, Y, V, F, Ga and rare earth elements (2 samples). Sample preparation and analytical techniques are given in Appendix A and individual analyses are listed in Appendix B.1.

4.2 CLASSIFICATION OF THE GRANITES

Unfortunately, from the classification point of view, primary igneous chemistry is rarely preserved and evidence presented below shows that most of the granitic rocks have undergone extensive metasomatism. Thus in this thesis nomenclature will follow that of other studies on the

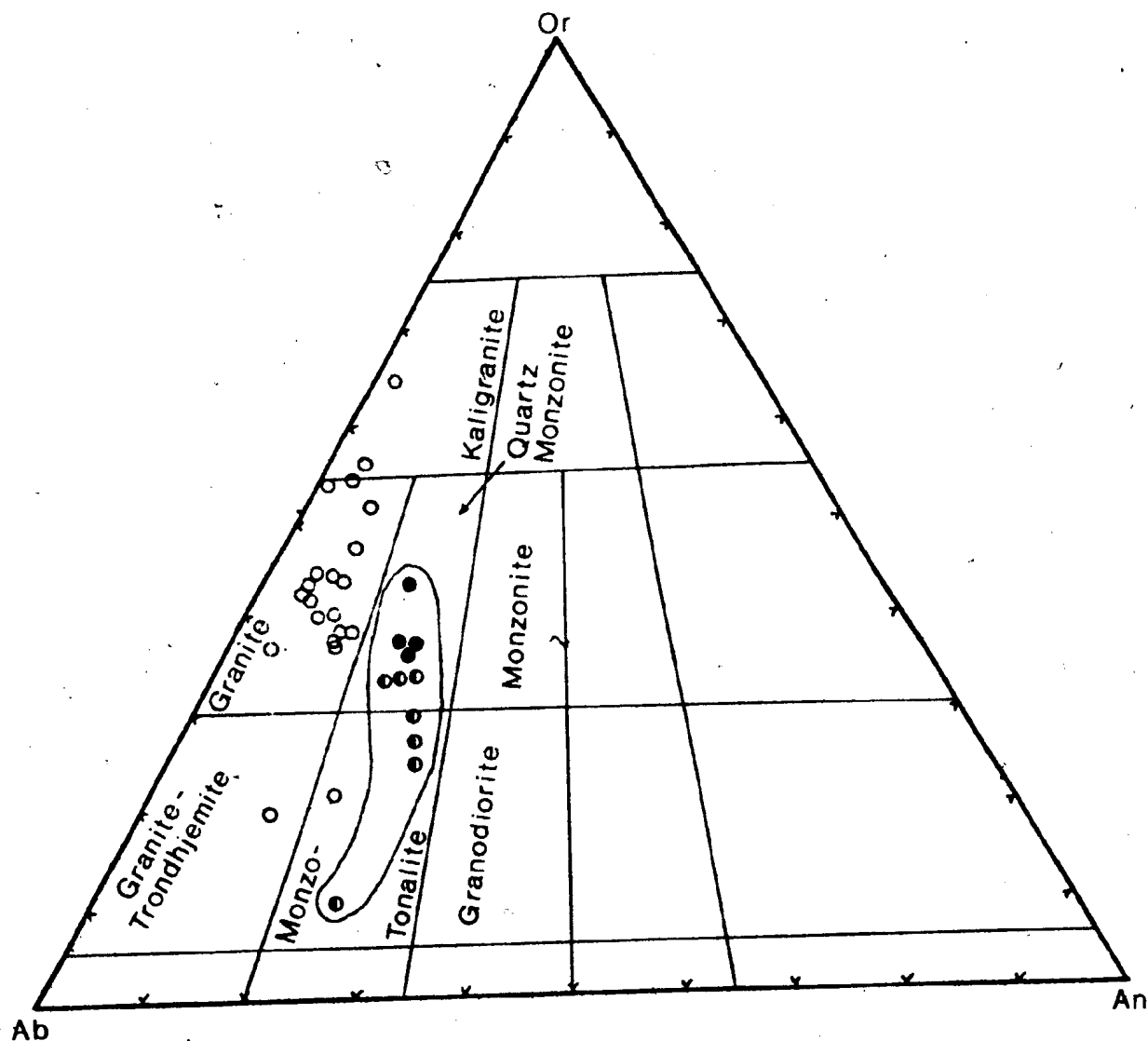


Figure 4.1 Chemical classification of the Grey River granitoids from mesonorm calculations, using Hietanen's (1963) molecular proportion classification. Solid circle represents undeformed megacrystic granite; half-filled circle-sheared megacrystic granite; open circle-leucogranite.

granitoids of the Gander Zone (Blackwood, 1978; Jayasinghe, 1979; Strong, 1980). That is, although Unit 7 is chemically a quartz monzonite, it will be termed megacrystic granite, while the aplite, pegmatite, and leucogranite dykes (Unit 9) will collectively be termed leucogranite.

Most samples of the megacrystic granite plot chemically as quartz monzonites, especially the relative undeformed samples (separated in Figure 4.1). Those samples from the deformed margin range from quartz monzonite to monzotonalite, reflecting the appearance of hornblende as a mineral phase. The more basic nature of the southern deformed margin may be due to ingestion of country rock xenoliths or metasomatic-metamorphic processes operative in shear zones (Beach, 1979). The latter mechanism is favoured in view of the sharp, relatively xenolith-free northern margin of the pluton.

The post-tectonic leucogranite dykes (Unit 9) plot predominantly in the granite field although a few occur in the kaligranite and trondhjemitic to tonalitic fields. This variability is due to the extreme alkali metasomatism evident in these rocks.

4.3 METASOMATISM

There is no conclusive geochemical evidence for a differentiation sequence between the megacrystic granite and the leucogranite, and field evidence is equivocal. Triangular $(\text{Na}_2\text{O} + \text{K}_2\text{O})\text{-FeO-MgO}$ (AFM) and $\text{Al}_2\text{O}_3\text{-FeO-MgO}$ (A'FM) plots of data from the two rock types (Figure 4.2) indicate a linear trend that approximates, but does not follow, the calc-alkaline

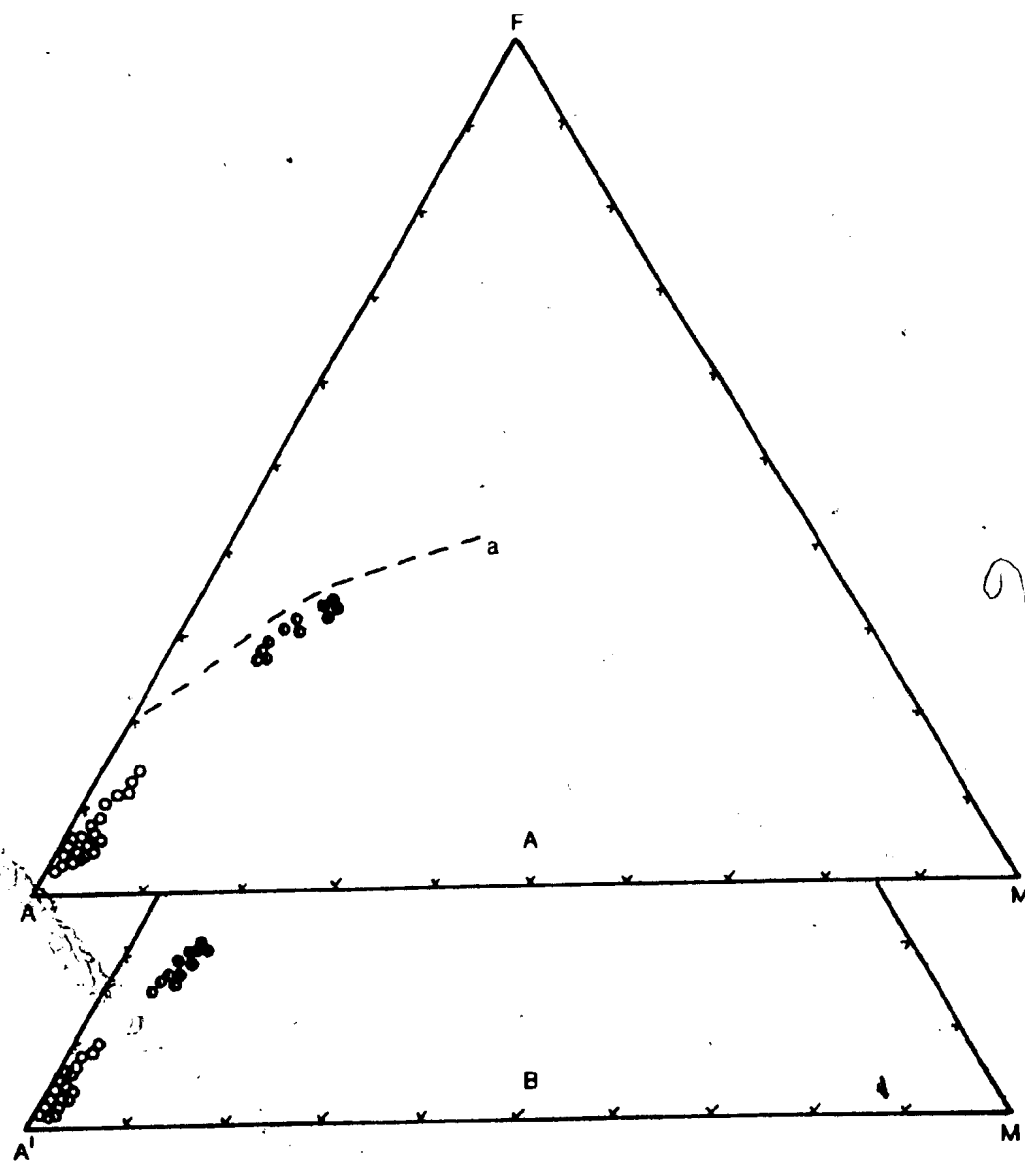


Figure 4.2 Triangular $(\text{Na}_2\text{O}+\text{K}_2\text{O})$ -FeO-MgO (AFM) and Al_2O_3 -FeO-MgO (A'FM) plots of Grey River granitoids. Line a represents the calc-alkaline trend of Irvine and Baragar (1971). Symbols as for Fig. 4-1.

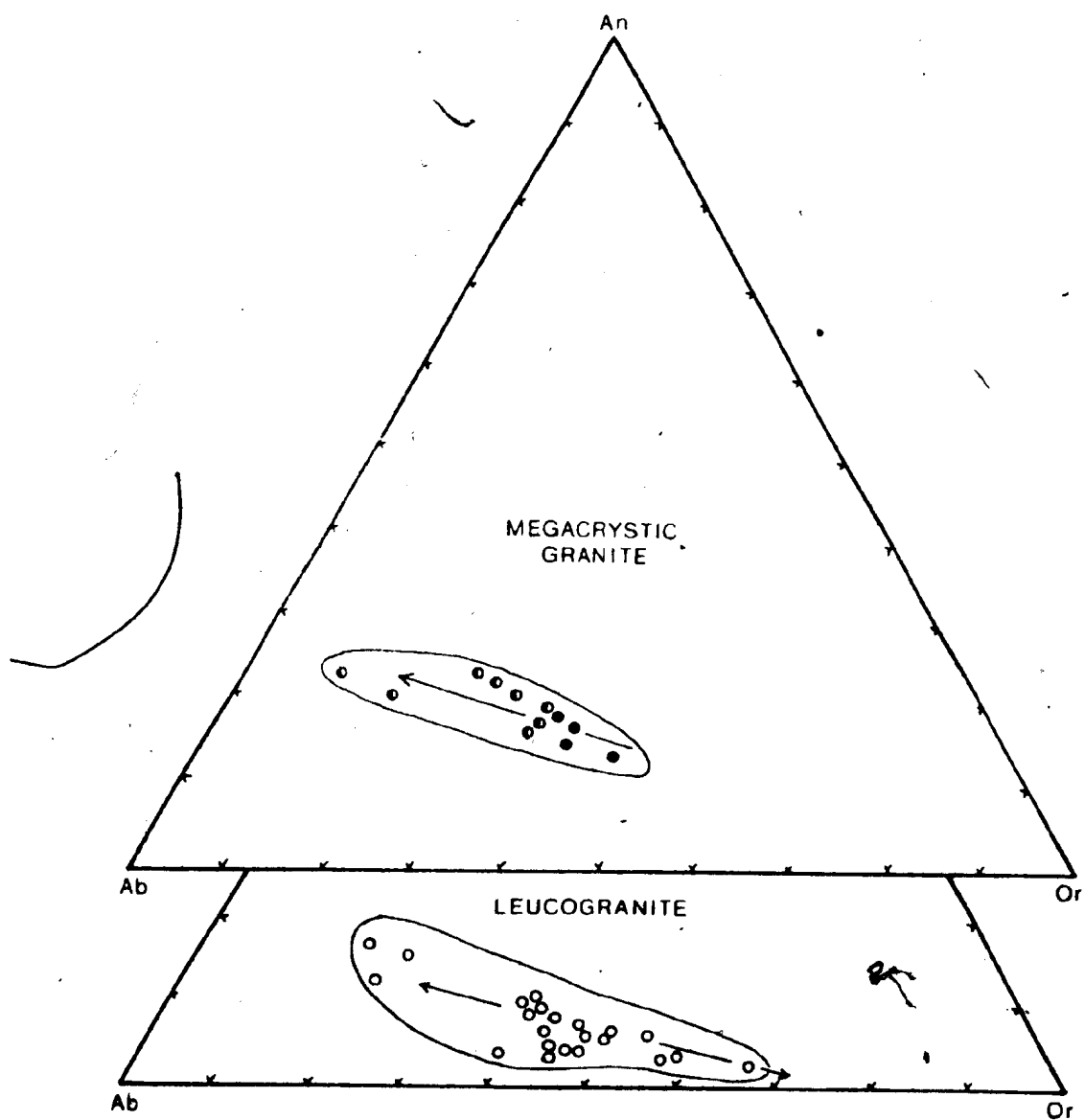


Figure 4.3 Normative plot of megacrystic granite and leucogranite emphasising the variability of rock chemistry due to metasomatic events which affected each rock type. Symbols as for Fig.4.1.

differentiation trend of Irvine and Baragar (1971). Furthermore there is a compositional gap between the two rock types which might argue against a continuous differentiation sequence.

Metasomatism accounts for the wide variability in rock chemistry in both the megacrystic granite pluton and the post-tectonic leucogranite dykes. Alteration in the leucogranite dykes appears to be related to the evolution of a volatile phase, while the megacrystic granite was altered by metasomatism in the shear zone. From the variation between undeformed and deformed megacrystic granite (Figure 4.3A) potash depletion appears to be dominant in the shear zone, certainly in relation to the feldspar minerals.

The leucogranites exhibit a much wider range in Ab/Or and Ab/An ratios than the megacrystic granite (Figure 4.3B), which suggests that these rocks were affected by sodium and potassium metasomatism. This agrees with the petrographic evidence which indicates the development of secondary microcline and albite in these rocks. The metasomatism is similar to the characteristic albitisation and microclinisation found in altered European leucogranites associated with tungsten and tin deposits (Shcherba, 1970).

4.3.1 Major and Trace Element Variation

Major and trace element data from the megacrystic granite pluton generally plot as linear trends with respect to SiO_2 (Figure 4.4, 4.5). If the southern contact zone

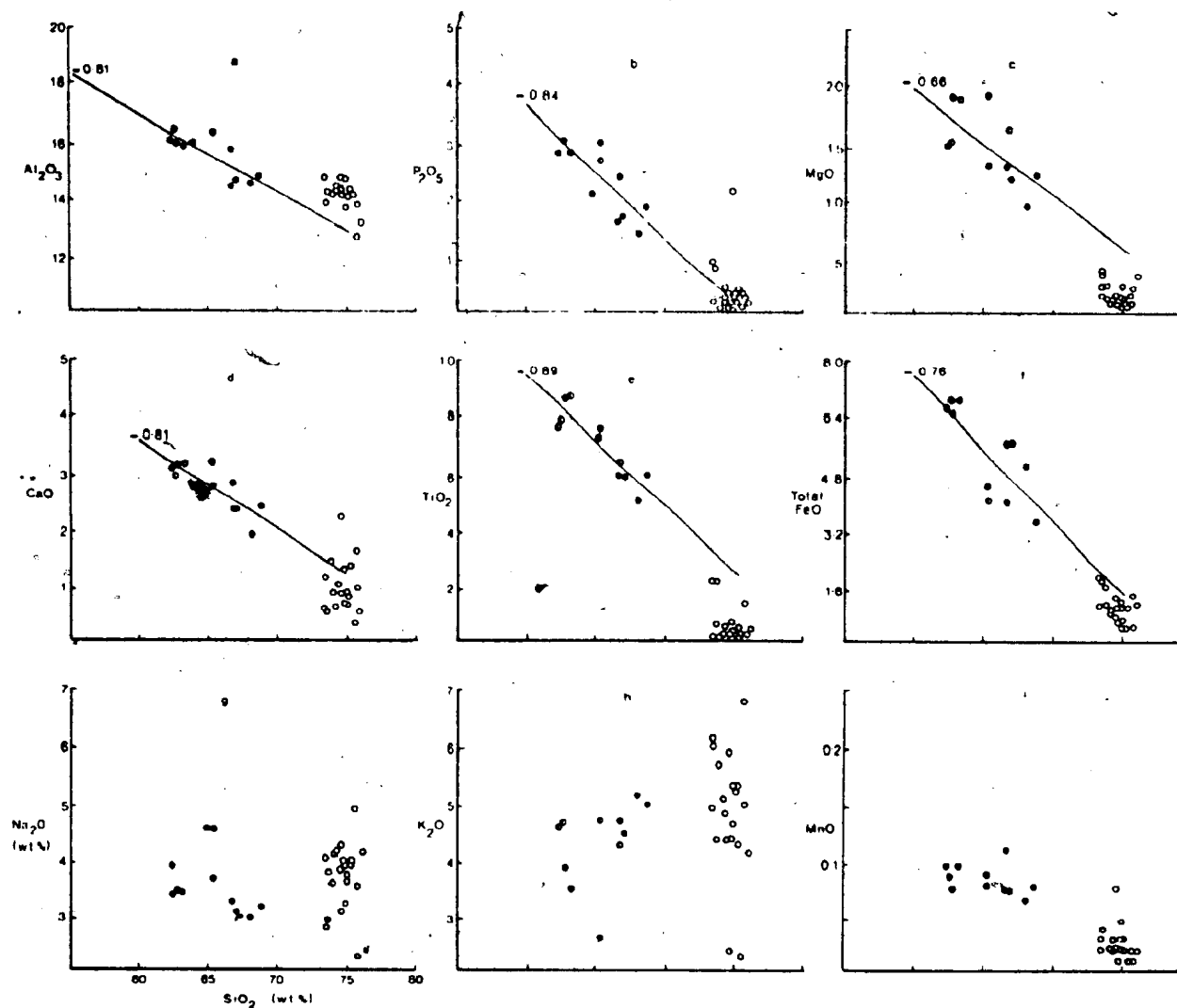


Figure 4.4 Major element variation diagram for Grey River granitoids. Symbols as for Figure 4.1. Where applicable correlation coefficients are shown.

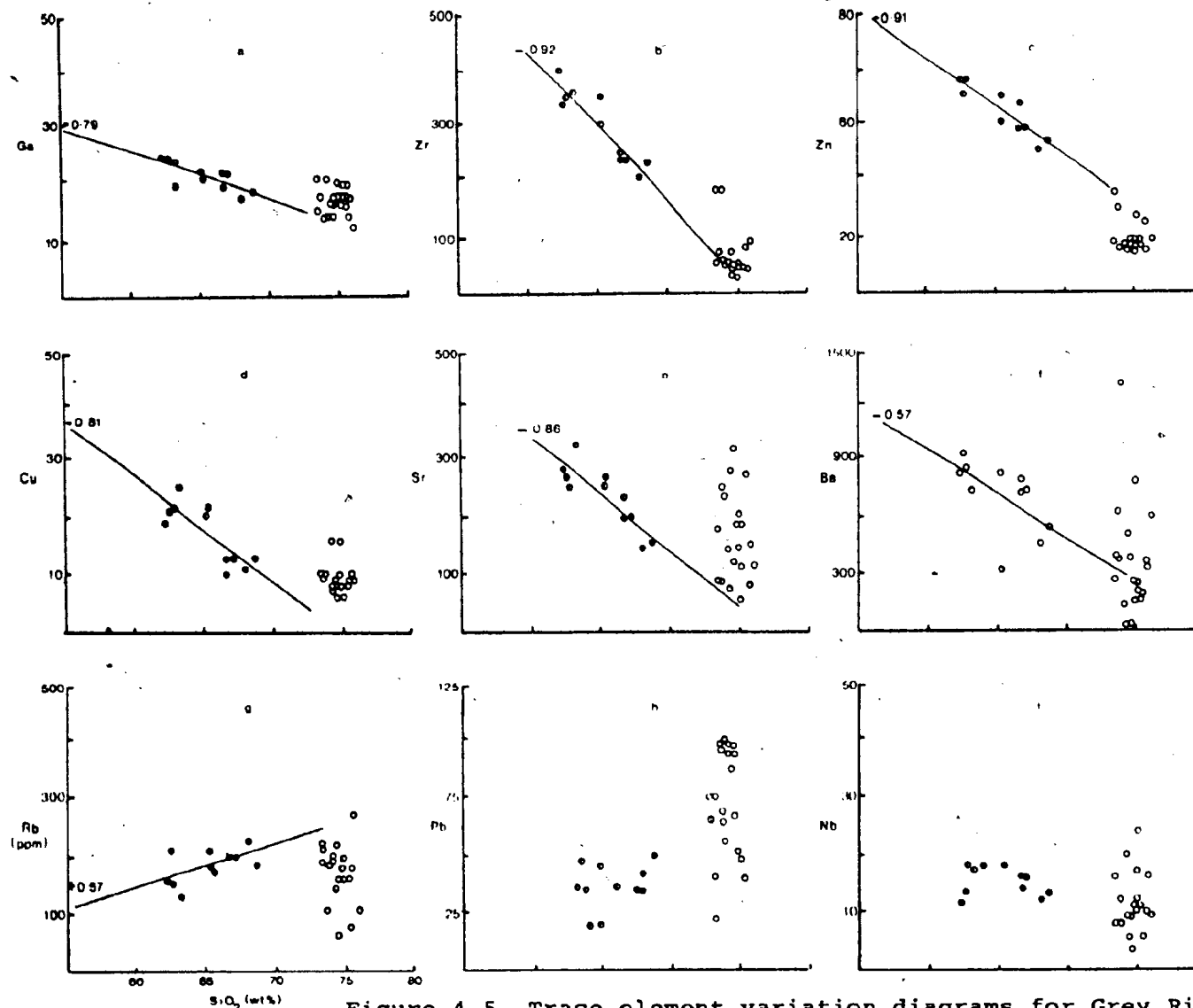


Figure 4.5 Trace element variation diagrams for Grey River granitoids. Symbols as for Figure 4.1. Where applicable correlation coefficient is shown.

of the megacrystic granite pluton were to represent a more basic border phase of a zoned pluton, then one would expect the central portions of the pluton to be enriched in elements that are concentrated during differentiation. Measured abundances of Zr and Cu (Figure 4.5B and D) argue against such a differentiation trend within the pluton, since these elements would be expected to increase with differentiation (Chao and Fleischer, 1960; Taylor, 1965). On the other hand assimilation of country rock in the contact zone might account for such trends, except that vast amounts of assimilation would be required (Stevens and Halliday, 1979), the evidence of which is not observed in the field.

If a distinction is made between undeformed and deformed megacrystic granite (Figures 4.4, 4.5) it is apparent that the linear trends reflect increased deformation and metasomatism in the shear zone. Regression lines through the data suggest an increase in Al_2O_3 , P_2O_5 , MgO, TiO_2 , CaO, total FeO, Ga, Zn, Zr, Cu, and Ba occurs with increasing deformation in the granite and is matched by a decrease in SiO_2 contents. These changes reflect mineral transformations during metasomatism and deformation which show an increase in mafics, especially hornblende, biotite and chlorite, over quartz and feldspar. Increased TiO_2 contents likely reflect the appearance of sphene after opaques during deformation and metasomatism.

Rb exhibits the opposite trend with deformation in comparison to other elements and has a positive correlation

with SiO_2 (Figure 4.5g), although poorly defined (i.e. low correlation coefficient). K_2O and Na_2O are quite variable in the megacrystic granite samples while MnO , Pb and Nb remain relatively constant during the deformation and associated metasomatic event.

In contrast to the megacrystic granite suite, the leucogranite dykes exhibit different major and trace element variation patterns. Emplaced in post-tectonic conditions, the leucogranite escaped the shearing episode but appears to have been variably altered by the development of a vapour phase after consolidation. The textural differences in the leucogranite suite indicate the dykes were emplaced under water-saturated conditions (Fournier, 1968; Jahns and Burnham, 1969). After disappearance of the silicate melt, the crystals and volatile phase reacted, resulting in metasomatism of the dykes (autometasomatism).

Many elements have been extremely mobile during this hydrothermal alteration stage and large variations are found within the alkaline and alkaline-earth elements. These variations reflect the alteration of feldspar minerals within the leucogranite, which includes the development of secondary albite and microcline after oligoclase and orthoclase. The mobility of alkalis in supercritical fluids is thought to be a common process in nature (Orville, 1963; Burnham, 1979).

In summary, major and trace element variation trends within the megacrystic granite and leucogranite reflect the effect of metasomatic events during their geologic history.

In the case of the megacrystic granite this involved shearing and mylonitisation along the southern margin of the pluton and resulted in increases in almost every element with a concomitant decrease in SiO_2 . The leucogranite dykes were variably altered by reaction with a fluid phase after consolidation which resulted in redistribution and addition by alkalis and alkaline earths, primarily due to feldspathisation.

4.3.2 Rare-Earth Elements

Two samples (MG 556 and LSG 424) were analysed for ten rare-earth elements (REE) by a thin film X-ray fluorescence method developed by Fryer (1977) and described in Appendix A.2.3. The megacrystic granite sample (MG) is from the undeformed portion of the pluton, while the leucogranite (LSG) is typical of the altered leucogranite dykes (two-mica aplite).

The megacrystic granite shows a pattern of relative fractionation (Figure 4.6A) that is markedly depleted in heavy REE. Furthermore it has a higher total REE abundance than the leucogranite and a smaller europium anomaly. In contrast the leucogranite displays a negative europium anomaly and a concave up pattern from light to heavy REE.

The REE abundance and fractionation pattern for the megacrystic granite are similar to those of granitic rocks of Nova Scotia (Albuquerque, 1977) and granites from other orogenic belts (Emmertmann *et al.*, 1975; Albuquerque, 1978). These granites are interpreted through REE modelling as having been derived by partial melting of a greywacke-argillite

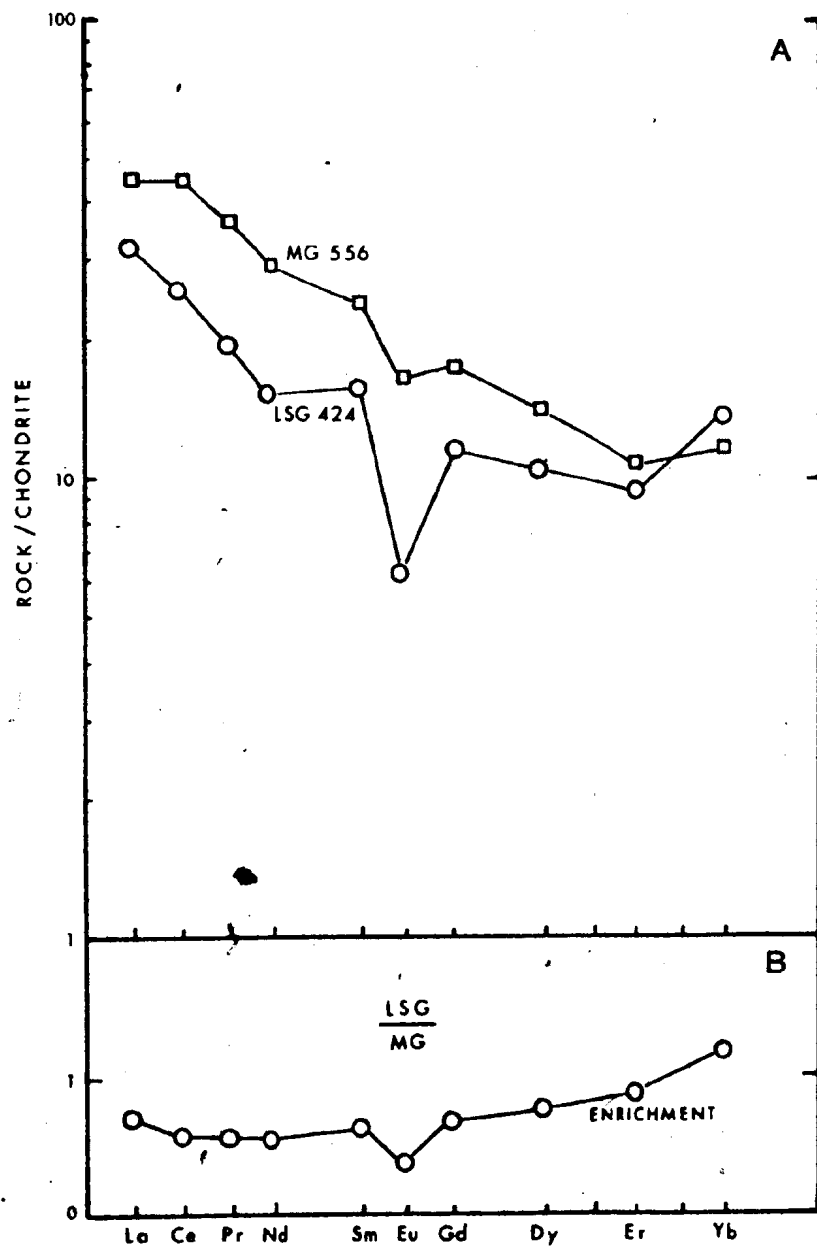


Figure 4.6 Rare-earth element analyses of Grey River granites.

metamorphic sequence (Albuquerque, 1977, 1978). The granites of the Gander Zone are also interpreted to have formed from melting of crustal rocks (Strong and Dickson, 1978; Strong, 1980), and Jayasinghe (1979) deduced this origin from modelling of trace element distributions. Thus it seems reasonable to assume a similar origin for the Grey River megacrystic granite.

If the REE pattern for the leucogranite is compared to that of the megacrystic granite (Figure 4.6B), it is apparent that the former is relatively depleted in light REE and enriched in heavy REE. Such a fractionation pattern could not be produced by any fractional crystallisation process between the two rock types, nor by any cumulate process, except perhaps through accumulation of garnet (Hanson, 1978). Garnets are known to occur as an accessory in some of the leucogranite dykes but were not observed in thin sections of the analysed sample. The only other explanation for such a heavy REE enrichment involves redistribution of REE by a hydrothermal fluid (Collerson and Fryer, 1978; Kerrich and Fryer, 1979). Such a process is possible for the Grey River leucogranites since there is abundant evidence for a hydrothermal-autometasomatic alteration episode during their cooling history.

Kosterin (1959) showed that the principal means of REE transport in hydrothermal fluids is in the form of REE carbonate, fluoride, or sulphate complexes. The heavy REE enrichment pattern of the leucogranite is therefore thought

to reflect the interaction of a CO₂-rich or F-rich hydrothermal fluid with the leucogranite (Taylor and Fryer 1980 a, b).

4.4 METALLOGENIC ASPECTS

An ore deposit is the end product of a number of geochemical and physical processes which occur infrequently in nature. With regard to granitoid deposits there is a specific relationship between deposit type and granitoid composition. This is illustrated by the association of porphyry copper deposits with intermediate alkaline to calc-alkaline plutons (e.g. Sutherland-Brown, 1976), and rare metal deposits (U, Nb, Sn, W, Be, etc.) with high silica plutons (Tischendorf, 1977; Taylor, 1979). This separation is due to a variety of geochemical parameters, including; the timing of the evolution of a fluid phase; the amount of differentiation and fractional crystallisation processes; fluid-melt partition coefficients; and emplacement level (Strong, 1980).

Tauson and Kozlov (1973) suggest that trace element concentrations in granites indicate the source of the rock and its mode of origin and they divided granites into five main types; plagiogranites, ultra-metamorphic granites, agpaitic leucogranites, palingenic granite and plumasitic leucogranites. The last two are genetically related, the plumasitic leucogranite being the late stage differentiate of normal palingenic granite magmas.

Plumasitic leucogranites are often associated with rare metal concentrations of W, Sn, Mo, Be and B while Sn- and

Li-bearing ore deposits are most commonly related to palinogenic granites. Concentrations of certain major and trace elements of these granite types are presented in Table 4.1.

In comparison, the granitoids of the Grey River area are chemically closer to the palinogenic and plumbitic granites than any other type listed by Tauson and Kozlov (1973). Certainly the undeformed samples of the megacrystic granite have the closest correlation with the palinogenic granite suite, while the Grey River leucogranites differ from the average plumbitic leucogranite, probably reflecting their metasomatic nature and the mobility of elements such as K, Na, Ba, Rb, and Sr during autometasomatism.

It is commonly stated that granites associated with rare metal deposits have a distinct chemistry in comparison to normal (unmineralised) granites. Extensive surveys of available data (Tischendorf, 1977; Taylor, 1979) reveal that such "specialised" granites are enriched in SiO_2 and have high $\text{K}_2\text{O}/\text{Na}_2\text{O}$ ratios. Hesp (1971) considers a SiO_2 content of 75% - 77% is common for leucogranites associated with Sn (and W) deposits while Flinter *et al.*, (1972) maintain that Sn and Mo occur in two distinct environments:- 1) in lodes and veins (with W) associated with high- SiO_2 ($> 72\% \text{SiO}_2$) granitoids, and 2) disseminated in low- SiO_2 ($< 72\%$) meso-granitoids.

The excess in SiO_2 reflects the significant number of leucogranites and aplites associated with Sn and W ores, and Taylor (1979) cautions that the leucocratic and potash-

Table 4.1

Comparison of the Chemical Composition
of the Grey River Granitoids
with Granites Associated with Rare-metal Deposits

ELEMENT	A	B	C	D	E
SiO ₂	-	-	68.3	74.65	73.38 \pm 1.39
Na ₂ O	2.9	2.8	3.22	3.71	3.20 \pm 0.61
K ₂ O	3.3	4.0	4.93	4.98	4.69 \pm 0.68
Al ₂ O ₃	-	-	14.80	16.04	13.97 \pm 1.07
CaO	-	-	2.30	1.00	0.75 \pm 0.41
Zr	200	260	218	55	-
Sr	300	100	167	182	-
Rb	140	400	208	164	580 \pm 200
Zn	45	57	54	19	-
Ba	750	200	567	488	-
Sn	5.3	6.3	42*	9*	40 \pm 20
W	2	4.1	<4-8*	<4-4*	7 \pm 3
Nb	20	22.6	14	11	-
Pb	25	30	33	53	-
Li	36	93	35	6	400 \pm 200
F	600	3000	907	45	3700 \pm 1500
K/Na	1.1	1.4	1.53	1.34	-
K/Rb	240	100	240	304	-
Ba/Rb	5.3	0.5	2.8	3.0	-
Li x 1000/K	1.1	2.4	0.74	0.14	-
F/Li	16	31	36.3	7.9	-
Ba/Pb	30	6.7	17.5	9.2	-
Li/Zn	0.8	1.7	0.62	0.26	-

A = Palingenic granite; B = Plumasitic leucogranite (A and B from Tauson and Kozlov (1973)); C = Grey River megacrystic granite (average 4 analyses); D = Grey River leucogranite (average 21 analyses); E = Specialised granite associated with Sn, W deposits (Tischendorf, 1974); * Analyses are considered accurate to within a factor of 3. Detection limit for W = 4 ppm.

rich tendency may be enhanced by autometasomatic or secondary processes involving silicification and greisenisation.

Na_2O and K_2O contents of the Grey River leucogranites are varied but significantly higher than both specialised granites (Table 4.1 and Figure 4.7) and leucogranites associated with mineralisation in Brittany (Strong and Hanmer, 1980). Furthermore average K_2O and Na_2O contents of leucogranites (Jayasinghe, 1979) of the N.E. Gander Zone (Figure 4.7) are lower than the Grey River leucogranites, as are others in the Gander Zone (Strong, 1980). The autometasomatic alteration of the Grey River leucogranites probably accounts for the varied $\text{K}_2\text{O}/\text{Na}_2\text{O}$ ratios.

Trace elements are thought to be more reliable than major elements as a guide to the ore-bearing potential of a granite (Taylor, 1979; Tauson and Kozlov, 1973; Tischendorf, 1977). Ore deposits of Sn and W are predominantly associated with alaskite, aplite, two-mica granite and leucogranite which have anomalous concentrations of Sn, F, Li, Be, and B (Tischendorf, 1977). Li-rich granites are typically associated with Sn-bearing ore deposits and average Li values for such granites are 220 ± 100 ppm (Table 4.1). It is considered an important indicator element (average granite has 40 ppm) and enrichments of 5-10 times are observed (Tischendorf, 1977). Similarly fluorine is an extremely enriched element in specialised granites (especially those associated with tin deposits) with values averaging 3700 ± 1500 ppm compared to the Clarke value of 880 ppm for normal

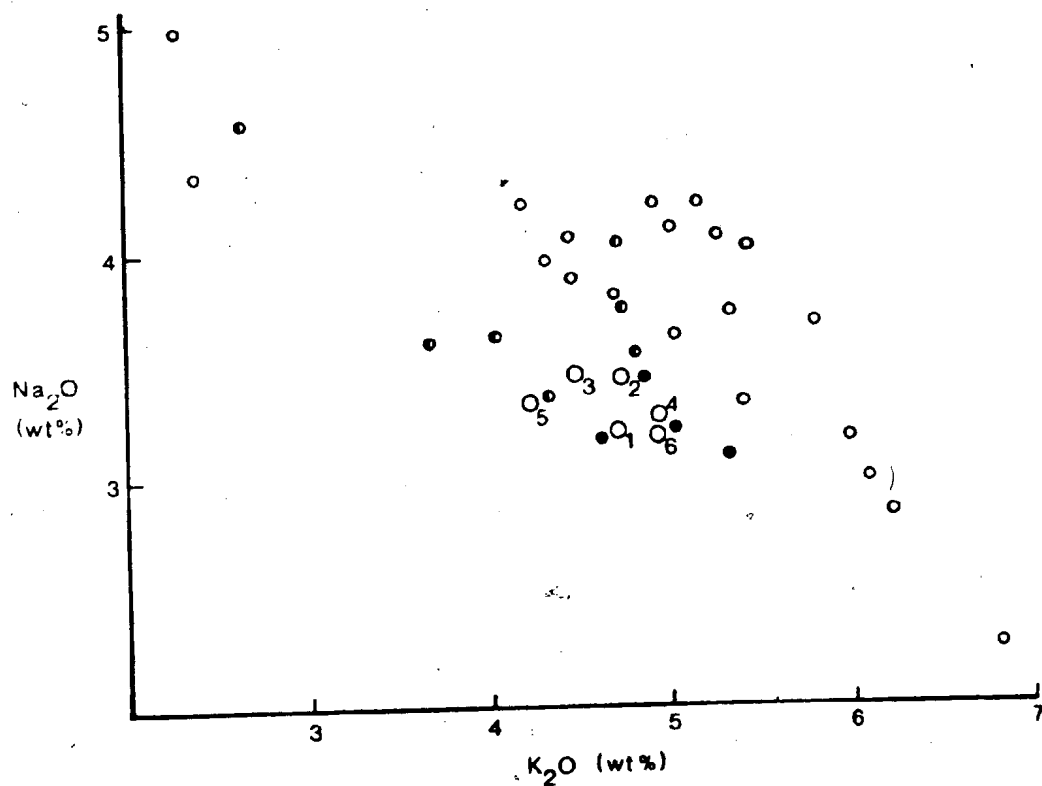


Figure 4.7 Na₂O-K₂O plot of Grey River granites. Symbols as for Figure 4.1. Analysis 1=average specialised granite (Tischendorf, 1977); 2=alaskite, Ackley granite (Whalen, 1976); 3=average Brittany leucogranite (Strong and Hanmer, 1980); 4, 5, 6=leucogranites from the Gander Zone (Jayasinghe, 1979).

granites (Vinogradov, 1962).

The Grey River granitoids are not markedly enriched in either of these elements although the fluorine content of the megacrystic granite (Table 4.1) exceeds the Clarke value. Tauson and Kozlov (1973) consider the F/Li ratio to be important in the understanding of the processes involved in the migration of a fluid phase. Fluorine and lithium behave similarly in magmatic processes (Burnham, 1979) as is illustrated by the stability of the F/Li ratio in successive intrusive phases of palingenic granites (Table 9 of Tauson and Kozlov, 1973). However, it should be noted that aplites associated with these palingenic granite suites have a lower F/Li ratio than their precursors, as do the aplite-leucogranite dykes of the Grey River area (Table 4.1). Furthermore, granites that are associated with tungsten deposits sometimes have specialised Sn contents but are not markedly enriched in fluorine (Tischendorf, 1970; Kozlov *et al.*, 1974). An analogous situation exists for the Grey River megacrystic granite which is Sn-specialised (average 42 ppm Sn compared to average granite, 3.0 ppm) but has moderate to low fluorine contents (average 907 ppm).

A number of authors have expressed their belief that granites enclosing tungsten deposits are not enriched in tungsten (Ivanova, 1963; Sotnikov and Izyumova, 1965; Odikadze, 1968) while others present the opposing view (Jeffrey, 1959; Dekate, 1967; Reedman, 1967). Compared to tin, the relationships are far less clear, however

Table 4.2
Tungsten and Tin Concentrations
for the Grey River Granitoids

	W (ppm)	Sn (ppm)
MG 555	4	25
556	4	50
557	4	50
550	4	25
288	8	25
LSG 414	4	5
423	4	5
424	4	10
501	4	25
508	4	10
511	4	5
513	4	5
517	4	5

KEY: MG = megacrystic granite
LSG = leucogranite

Analysed by B. Kronberg using spark source
mass spectrometry methods. Analyses are
considered accurate to a factor of 3.

Tischendorf's (1977) review of chemical data suggests that the average W value for granites associated with tungsten deposits is 7 ± 3 ppm.

Tungsten contents for the Grey River granites (Table 4.2) exceed the Clarke value of 1.5 ppm and fall in the range $< 4^*-8$ ppm for the megacrystic (and non megacrystic granite, sample 288) and 4 ppm or less for the leucogranites. These concentrations would indicate the granites are W-specialised as well as Sn-specialised.

4.5 DIABASE DYKES

Ten post-tectonic diabase dykes (Unit 10) were analysed for major and trace elements and the data are presented in Table 4.3 with their C.I.P.W. normative proportions. All are hypersthene-normative but standard chemical plots such as alkalis versus SiO_2 (MacDonald and Katsura, 1964) and potash versus SiO_2 (Engel et al., 1965) show that the dykes are chemically alkali basalts (Figure 4.8A and B). One alkali-poor sample (516) however plots in the tholeiitic field and its uniqueness cannot be related to any alteration process. A $\text{TiO}_2 - \text{K}_2\text{O} - \text{P}_2\text{O}_5$ plot (Pearce et al., 1975) indicates (Figure 4.8C) that they are continental alkali basalts which agrees with a trace element classification of "within plate basalts" from Nb/Y ratios (Pearce and Cann, 1973).

* detection limit for W.

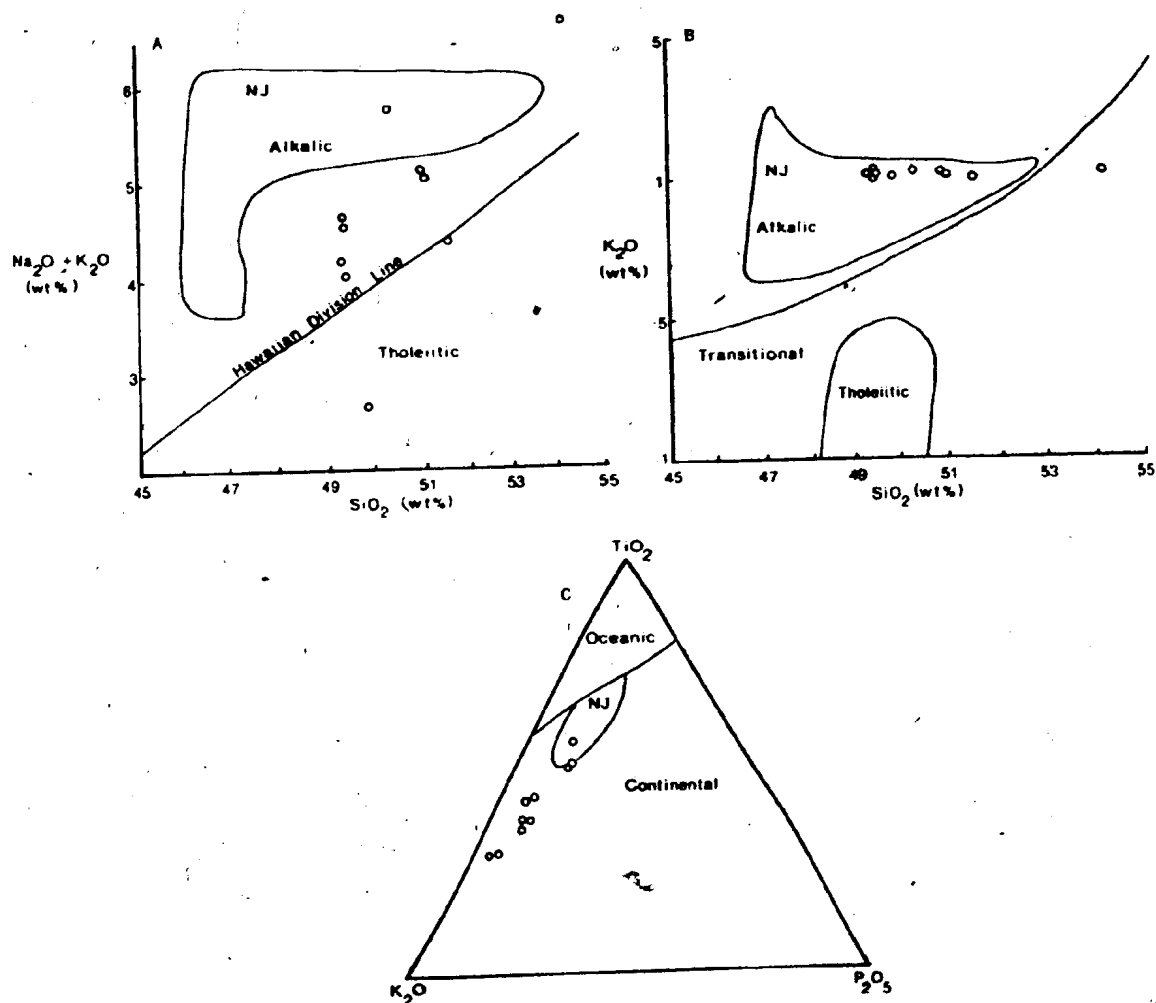


Figure 4.8 Alkali-silica and K_2O - TiO_2 - P_2O_5 plot of diabase dyke suite. Composition of diabase dykes from N.E. Gander Zone are shown as fields labelled N.J. (Jayasinghe, 1978).

Table 4.3
Major and Trace Element Contents
and the C.I.P.W. Norms of the Diabase Dykes

SAMPLE	DB 469	DB 491	* DB 310	DB 499	DB 516	DB 469A	DB 469B	DB 474	DB 490	DB 498
SiO ₂ (wt%)	50.19	51.30	49.47	51.04	48.70	48.30	49.50	47.90	48.70	48.00
TiO ₂	1.40	0.98	1.35	1.12	1.23	1.20	1.38	1.32	0.98	0.82
Al ₂ O ₃	17.74	18.10	17.76	20.42	18.14	15.80	17.40	15.80	16.40	14.90
Fe ₂ O ₃ *	8.61	8.83	9.39	6.08	9.99	9.01	8.43	9.52	9.29	9.09
MnO	0.12	0.15	0.21	0.09	0.16	0.16	0.12	0.17	0.21	0.17
MgO	7.47	5.79	5.82	4.65	10.02	9.44	7.49	8.89	9.11	11.19
CaO	7.46	9.86	7.88	5.31	9.66	9.10	7.45	8.62	9.79	8.90
Na ₂ O	3.94	2.93	2.54	5.04	1.86	2.74	3.91	3.02	2.77	2.28
K ₂ O	1.00	1.43	3.12	1.79	0.73	1.72	1.06	1.48	1.20	1.79
P ₂ O ₅	0.35	0.20	0.21	0.29	0.22	0.32	0.35	0.25	0.15	0.17
L.O.I.	2.46	1.38	1.86	1.88	2.25	1.70	2.46	3.50	1.69	2.50
TOTAL	100.74	100.95	100.11	99.49	99.96	99.69	99.55	100.47	100.29	99.81
zr (ppm)	140	104	137	185	125	144	159	138	88	77
Sr	499	411	446	483	331	383	359	306	265	268
Rb	26	67	632	264	37	86	50	73	52	218
Zn	83	81	143	59	77	77	77	87	97	97
Ba	238	304	391	281	88	259	230	248	272	372
Nb	8	3	11	11	7	8	7	9	5	7
Ga	25	21	23	26	21	20	21	21	21	21
Pb	16	11	4	-	7	4	-	-	5	4
W	57	33	59	84	257	201	130	182	100	25
Cr	78	108	52	84	393	312	187	271	295	45
V	236	237	276	163	206	195	221	231	242	196
Cu	15	13	87	11	68	19	12	33	14	14
Qz (wt%)	-	2.92	-	-	3.51	-	-	-	-	-
Or	6.01	8.48	18.76	10.81	4.41	10.38	6.45	9.01	7.19	10.87
Ab	33.90	24.88	21.86	43.58	16.09	23.69	34.05	26.33	23.75	19.83
An	28.23	32.13	28.05	25.22	31.50	26.29	27.58	25.95	29.16	25.82
Di	2.12	10.11	5.13	-	9.59	11.03	2.93	9.70	12.85	12.67
Hy	2.92	-	0.17	1.81	-	7.63	4.29	7.09	5.00	8.54
Il	0.23	0.30	0.44	0.18	0.28	0.30	0.23	0.33	0.41	0.36
Hm	8.75	8.86	10.16	6.21	10.21	9.21	8.68	9.81	9.41	9.34
Sp	3.20	2.03	2.80	-	2.72	2.62	3.19	2.91	1.91	1.60
Ap	0.83	0.47	0.50	0.69	0.52	0.76	0.84	0.60	0.35	0.41

Similar dykes are noted in the northeastern part of the Gander Zone (Jayasinghe, 1978, 1979) and in the Grand Bruit area (Chorlton pers. comm., 1980). The chemical data presented by Jayasinghe (1978) are included in Figure 4.8 as compositional fields for comparison with the Grey River diabase dyke suite.

Continental alkali basalts are generally found in extensional environments that often herald the start of continental rifting (Bailey, 1974; Scrutton, 1973; Strong, 1975). Jayasinghe (1979) cites the occurrence of continental alkali basalts in the northeast Gander region as evidence for a period of extension in Devonian-Carboniferous times, which could be the early signs of a major continental break up. On the other hand localised extensional environments are found within a shearing environment (Koide and Bhattacharji, 1978), thus the occurrence of the alkali basalt dykes in the Gander Zone may relate to extensional features in the Devonian-Carboniferous "megashear" (Strong, 1980) environment.

4.6 CONCLUSIONS

Geochemical analyses of the Grey River granitoids reveal that they are extensively altered by metasomatic events; the megacrystic granite by a shear zone along its margin; the leucogranites by reaction with a coexisting fluid phase (autometasomatism). Because of these factors no conclusive evidence is found for a differentiation trend between the two.

During the mylonitisation-metasomatism that affected the southern margin of the megacrystic granite pluton, nearly all major and trace elements were affected, and show negative correlation with SiO_2 with progressive deformation. Major and trace element trends are compatible with the greenschist facies metamorphic assemblage that is developed in the shear zone.

On the other hand metasomatism in the leucogranites appears to affect only the alkalis (Na, K, Ca) and alkaline earths (Rb, Sr, Ba,) and possibly some base metals. Textural evidence and alteration features imply the existence of a fluid phase during emplacement of the leucogranite suite (aprites and pegmatites), i.e. water-saturated conditions existed prior to the consolidation of the aprite and pegmatite. The alaskitic component of the composite dyke suite (Unit 8) may represent the under-saturated precursor to the aprite and pegmatite dykes (Unit 9).

Evidence for the nature of this fluid phase is provided by REE data from the leucogranite suite. Heavy REE are enriched in the leucogranite dykes and suggest deposition of heavy REE during autometasomatism of those dykes. The principal means of REE transport in hydrothermal solutions is in the form of REE carbonate and fluoride complexes (especially heavy REE), suggesting that the fluid phase evolved from the melt, and later involved in the autometasomatism of the dykes, was CO_2 - or F-rich.

Metallogenically the megacrystic granite is Sn- and W-specialised with values of 42 ppm (average) and 4-8 ppm respectively. Concentrations of these elements in the leucogranite suite are much lower, which may reflect either the lack of mafics or leaching or partitioning into the fluid phase associated with the emplacement of these dykes. Noteworthy also is the fact that Li and F concentrations are not enriched relative to average granite values, as is the case for many granites associated with rare-metal deposits (especially tin). Other major and trace element contents of the leucogranite suite are compatible with leucogranites associated with W and Sn deposits in Western Europe and elsewhere, reflecting the consanguinity between silica- and potash-rich granitoids and rare metal deposits.

CHAPTER 5

THE HYDROTHERMAL VEIN SYSTEM

5.1 INTRODUCTION

The hydrothermal vein system postdates all geologic units in the Grey River area and is composed of a complex swarm of quartz veins occupying tensional fractures within megacrystic granite and amphibolitic gneiss. The veins strike approximately north-south (010° average), almost perpendicular to the general strike of the metamorphic rocks. The distribution of the thickest and most persistent veins (and the most likely to be exploited) is shown in Figure 5.1, although hundreds of smaller veins are known (Bahyrycz, 1956) within the 1600 x 2000 m area outlined in that figure. The aim of this chapter is to establish the structural development of the vein system, the distribution and mineralogy of the veins, and the major structural controls of ore deposition.

5.2 RELATION OF THE VEINS TO THE GRANITOIDS

The hydrothermal mineralisation formed after the emplacement and deformation of the megacrystic granite, as the vein system cuts the deformed megacrystic granite within the Granite Cliff Shear Zone. Zoning relationships, discussed in detail below, indicate that higher temperature mineralisation occurs away from the megacrystic granite contact, into the metamorphic rocks. This would suggest that the megacrystic granite has no direct link with the

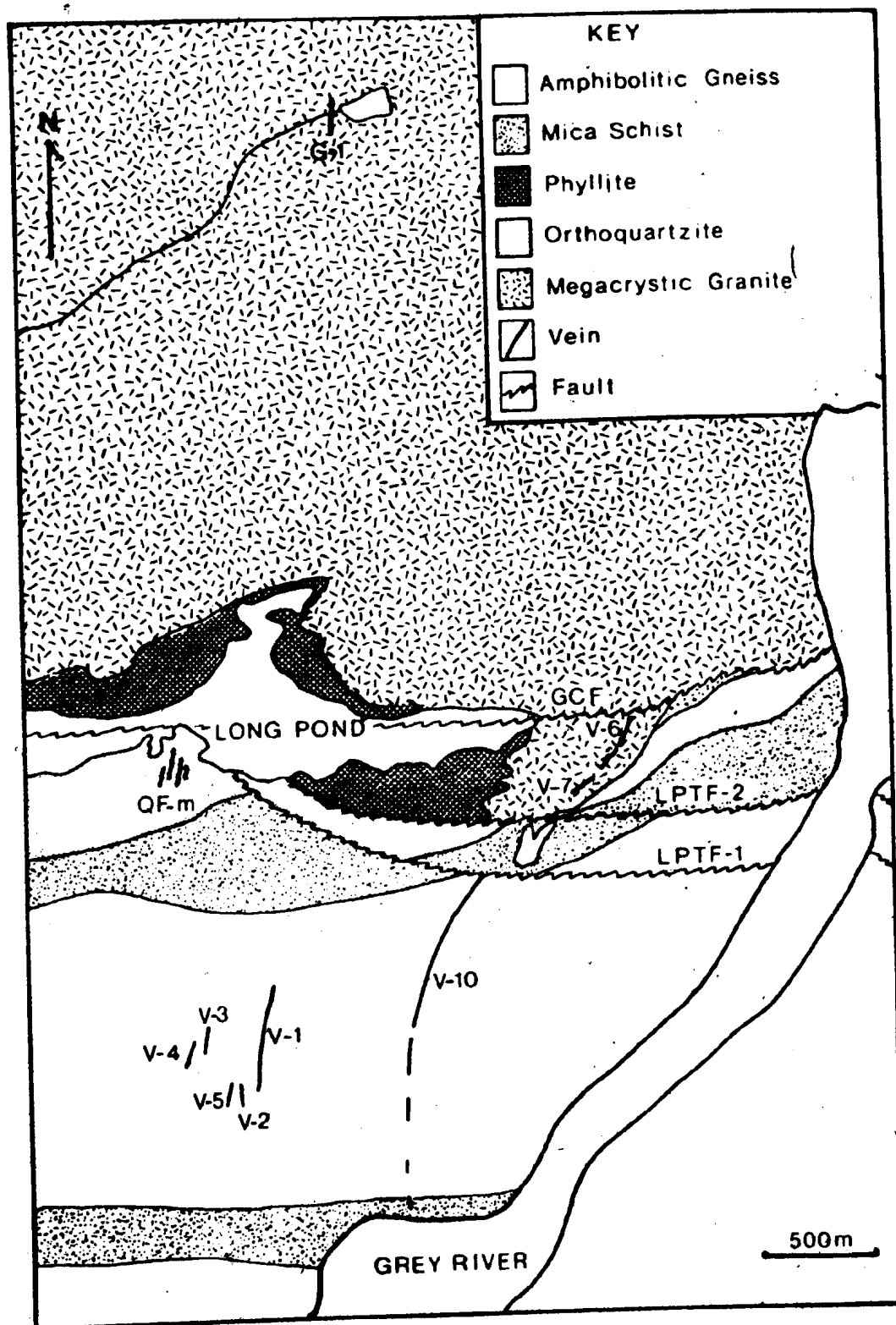


Figure 5.1 Location of major lodes in the Grey River Tungsten Prospect.

mineralisation, although an indirect link is inferred from geochemical studies outlined previously.

A closer relationship between the mineralisation and the post-tectonic aplite, pegmatite and leucogranite is indicated by the characteristic hydrothermal alteration of these rock types in areas where little or no mineralisation is found. From evidence of crosscutting relationships seen in adit level exposures, the veins at least in part postdate the aplite and pegmatite dykes. However, many altered leucogranite dykes contain coarse quartz-rich centers, and Bahyrycz (1957) reports evidence of a pegmatite grading along strike into a quartz vein containing mineralisation.

It is implied from this evidence and from the geochemical specialisation outlined above, that the hydrothermal vein system is intimately related to the leucogranite, which probably was the source of the hydrothermal fluid and the metals concentrated in the mineralisation. Thus a body of alaskite-leucogranite is inferred to exist at some as yet unexposed level below the mineralisation.

5.3 VEIN FORM AND STRUCTURE

Mineralisation occurs in three forms:- 1) as fractures coated with pyrite and scheelite (and minor quartz); 2) as tensional quartz veins with no displacement of wall rock; and 3) as quartz lodes showing much displacement of wall rock.

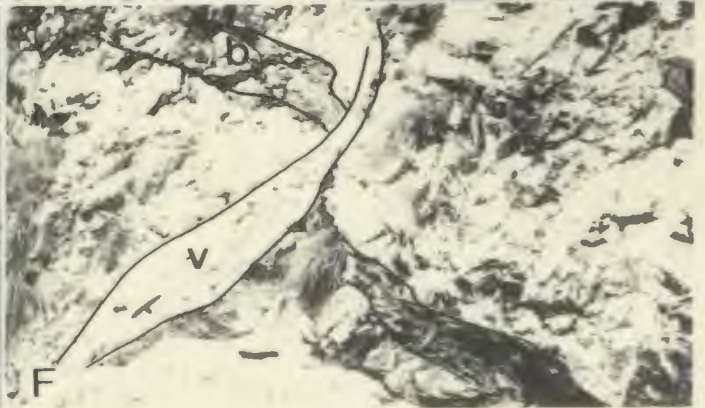
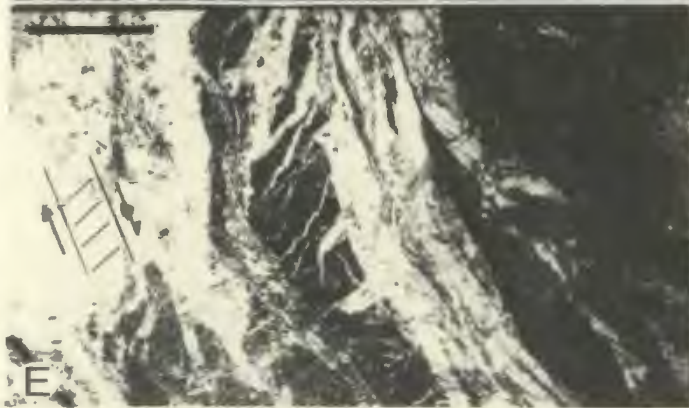
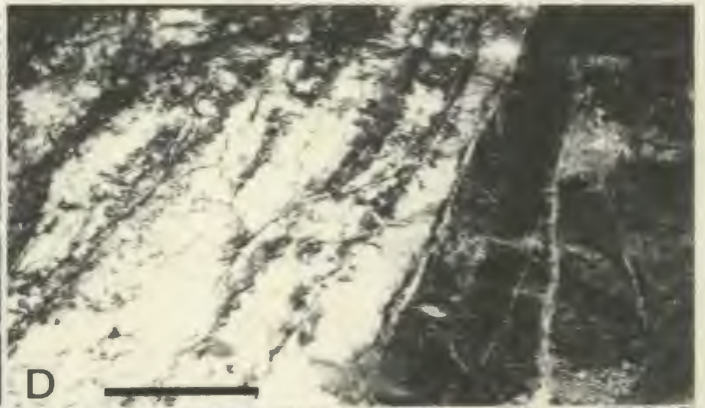
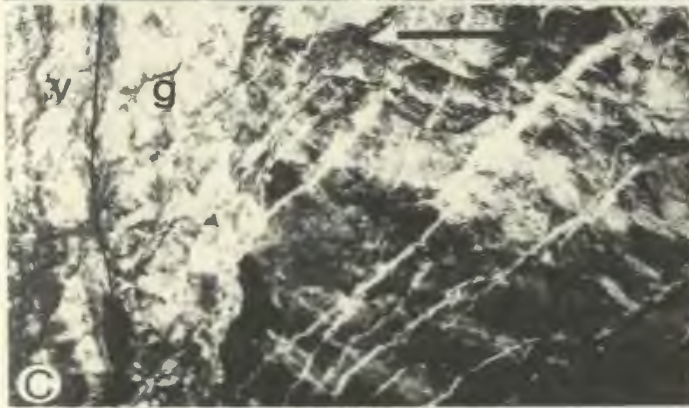
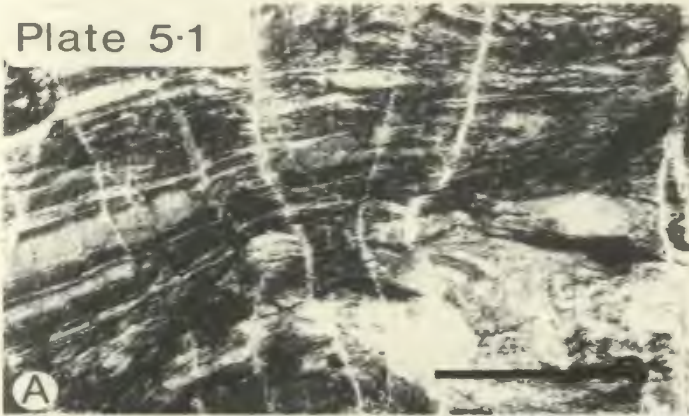
1) Wall rock surrounding the largest veins (#10, #1, #6, etc.) is intensely fractured (Plate 5.1A) by 1 mm to

Plate 5.1

Vein types and structural form of hydrothermal veins. Where applicable bar scale = 30 cm (approx 1 foot).

- 5.1A Fracture-style mineralisation ranging from hairline fracture to veinlets containing quartz-pyrite-muscovite and scheelite. Location 87 adit level.
- 5.1B Close up of tensional veinlet with muscovite selvage. Sample contains bismuthinite and pyrite as sulphide phases. Sample 82, adit level.
- 5.1C Muscovite selvaged tensional veinlets apparently cut off by greisen (g) alteration halo of composite Vein #10 (v). Location 267, adit level.
- 5.1D Sheeted nature of vein-lode indicative of multiple injection of vein material. Note also sharp contact of vein with wall rock and lack of alteration. This is typical of thick, steeply-dipping sections of the lode. Location 359, adit level.
- 5.1E Tensional fractures in wall rock xenolith induced by normal faulting movements within the lode. Location 286, adit level.
- 5.1F Displacement of wall rock by normal faulting within the vein (v) emphasised by offset of basic dyke (b) which cuts the amphibolitic gneiss. Cliff face above Portal.

Plate 5.1



1 cm wide tension veinlets. These are orientated approximately north-south and appear to dip into the major veins. The mineralisation occurs as a coating on the fracture surfaces and is composed of pyrite and scheelite (pyrite > scheelite). Muscovite and calcite are minor components in these fractures but are locally concentrated. The frequency of fracturing is variable, but appears most intense in southern portions of the adit where there are fractures on average every 15 cm. Vein #10 is not exposed at this point in the adit but is projected to be 150 m to the east, suggesting that the fracturing may not be localised on the main vein but has a more "regional" aspect. Unpublished assays from fractured sections of wall rock in the adit indicate grades of 0.1% WO_3 , but locally higher values are found.

2) The fracture-filled mineralisation grades into small tensional quartz veins which show no displacement of wall rock. These veins vary from 1 to 40 cm in thickness and are composed of milky quartz with fluorite, scheelite, pyrite, bismuthinite, and calcite. These veins are characterised by selvages of coarse platy muscovite up to 1 cm thick (Plate 5.1B). Other evidence of a tensional environment includes vugs, branching of veins, the variation in strike along individual veins, and the common overlapping of subparallel veins ("eel tail" structures).

The tensional veinlets are often oriented in a complimentary or conjugate fashion to the major veins, i.e. they strike parallel to the major veins but dip into

them with a 45-60° angle between the two. However, their formation in part predates much of the movement and emplacement of quartz in the main veins, since greisen alteration, a result of increased wall rock interaction in the latter, overprints the tensional veinlets (Plate 5.1C).

3) Veins or lodes which show much displacement of the wall rock effectively comprise the major veins in the area (Vein #10, #6, #1, etc.). They vary from 15 cm to 4 meters in thickness and characteristically display a sheeted form indicative of a multiple injection history (Plate 5.1D). Sheeting may occur on either, or both, margins of the vein.

The surfaces of individual sheets show slickensides which indicate movement of the hanging wall down-dip with respect to the footwall, i.e. a normal fault mechanism. Some of these surfaces are coated with calcite or sericite; the latter appears to be derived from alteration of wall rock fragments. Normal fault movements are indicated as well from tension gashes created in wall rock xenoliths (vein horses) within the vein (Plate 5.1E) and displacement of matching wall rock (Plate 5.1F).

The large lodes are therefore characterised by repeated reopening and injection of new quartz (with mineralisation) into open spaces created by differential movements of wall rock during normal faulting.

5.4 STRESS REGIMES AND STRESS TRAJECTORIES

Stress trajectory analysis has been applied to vein systems to investigate the regional factors responsible for

their formation (Moore, 1975). Stress trajectories are lines which represent the orientation of principal compressive or extensional stresses (σ_1 , σ_2 , σ_3) throughout an area. Two out of three principal stresses can be represented as trajectory lines on a geological plan or section corresponding to a principal plane (Figure 5.2A).

In a fracture regime dominated by normal faulting and extension (e.g. Grey River) the surface plan corresponds approximately to the principal plane containing the σ_2 and σ_3 axes (Figure 5.2A). Thus at Grey River σ_2 stress trajectories can be drawn parallel to the surface outcrop traces of veins irrespective of whether they occupy normal faults or tensional fractures.

The maximum principal stress can be located by bisecting the acute angle between intersecting planes of complementary faults or extension fractures. Thus a model for the stress regime operative during formation of the veins at Grey River may be illustrated by Figure 5.2B and C.

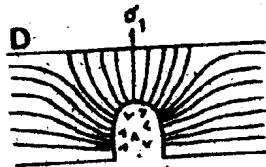
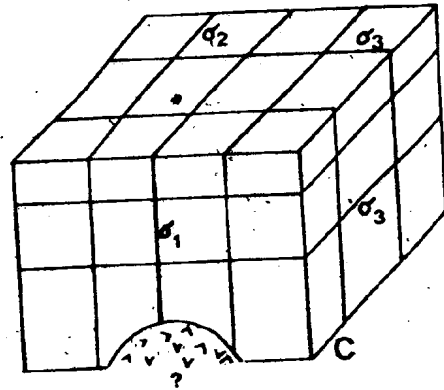
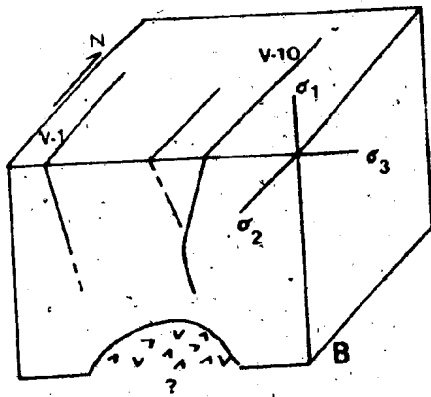
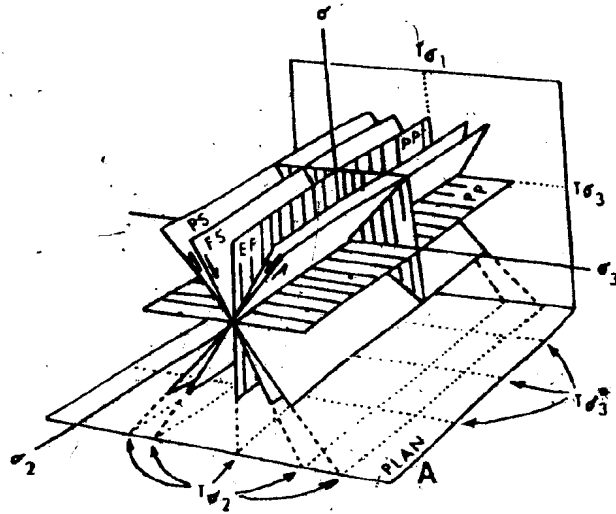
A fracture system created by stresses induced by intrusion of a cupola has been modelled by Roberts (1970) and is shown in Figure 5.2D and E. The stress regime may result from an expansional or contractional phase of the cupola intrusion. Above a cupola the maximum principal stress (σ_1) is parallel to the orientation of potential extension fractures (Figure 5.2A and D) and matches the orientation of extensional veins at Grey River. The trajectories of maximum shearing stress (Figure 5.2E) in the cupola model

Figure 5.2 Stress configuration and trajectories during the development of the Grey River hydrothermal vein system.

5.2A Stress configuration in normal faulting (from Moore, 1975). PP = principal plane; PS = plane of maximum shearing stress; FS = failure surface (normal fault); EF = plane of extension fissures; T_{σ_1} = trajectory of principal stress in plan or section.

5.2B,C Orientation of stresses during the development of the Grey River hydrothermal vein system.

5.2D,E Approximate form of stress trajectories around a (semi) circular cavity near the free edge of a semi-infinite plate (after Roberts, 1970). This models the stress pattern induced by the intrusion of a cupola.



represent fault traces (normal faults) and may mimic the situation for the major veins at Grey River. The model of the fracture pattern induced by the intrusion of a cupola is thus quite similar to the fracture pattern found in the Grey River Tungsten Prospect and reinforces the suggestion of a hidden cupola beneath the tungsten mineralisation.

5.5 RELATIONS BETWEEN STRUCTURE AND MINERALISATION

It has long been recognised that sudden changes in vein attitude often accompany the loss or appearance of ore and hence a comparison of lode structure to assay data is important. Appraisal of these data for the Grey River Prospect reveals that there is a correlation between grade, vein width, vein attitude, and alteration.

If a fracture, which has a curved and irregular surface, is subjected to movements it is obvious that in some parts of the fracture the wall rock will still be touching while in others they will be separated by open spaces. The size and shape of the open spaces depends, of course, on the original shape and attitude of the fracture. During normal faulting (Figure 5.3) thick open spaces will develop where the vein is steepest, while cavities developed in more shallow dipping portions of the vein will be thinner. Such features are obvious in vein cross-sections (Figure 5.4) and are further evidence for development of the lodes by normal faulting.

Assay data from channel and bulk sampling are presented in Figure 5.5 (in map folder), which serves to illustrate firstly, that grades are not affected to any great extent by

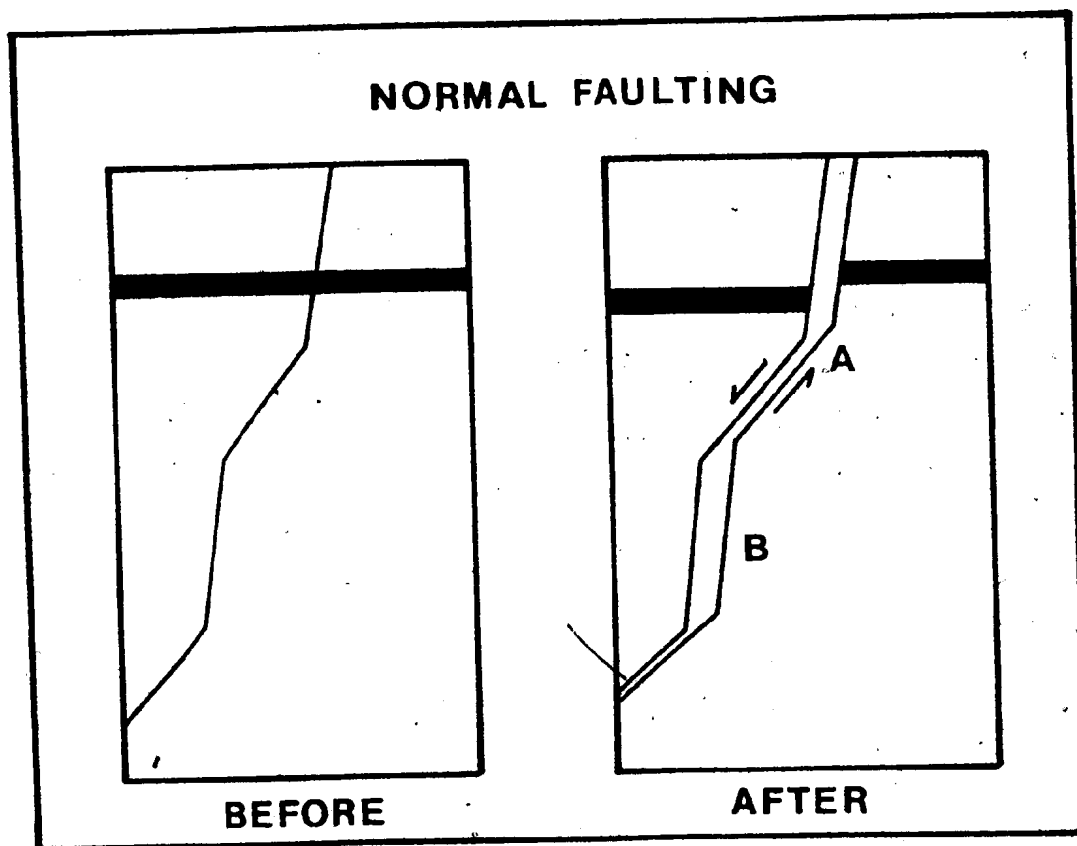


Figure 5.3 The effect of normal faulting on fracture width, after Garnett (1966).

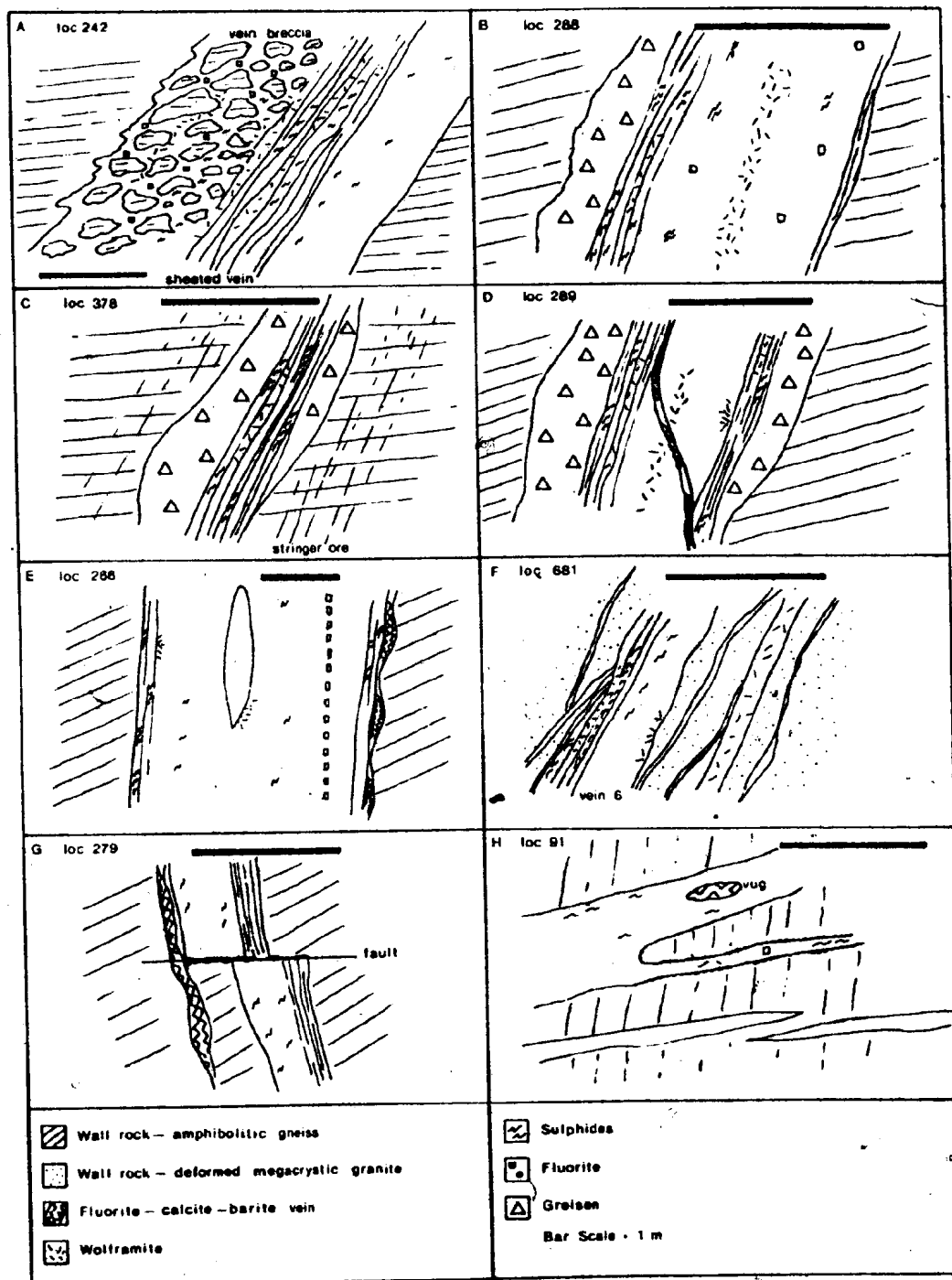


Figure 5.4 Vein cross-sections.

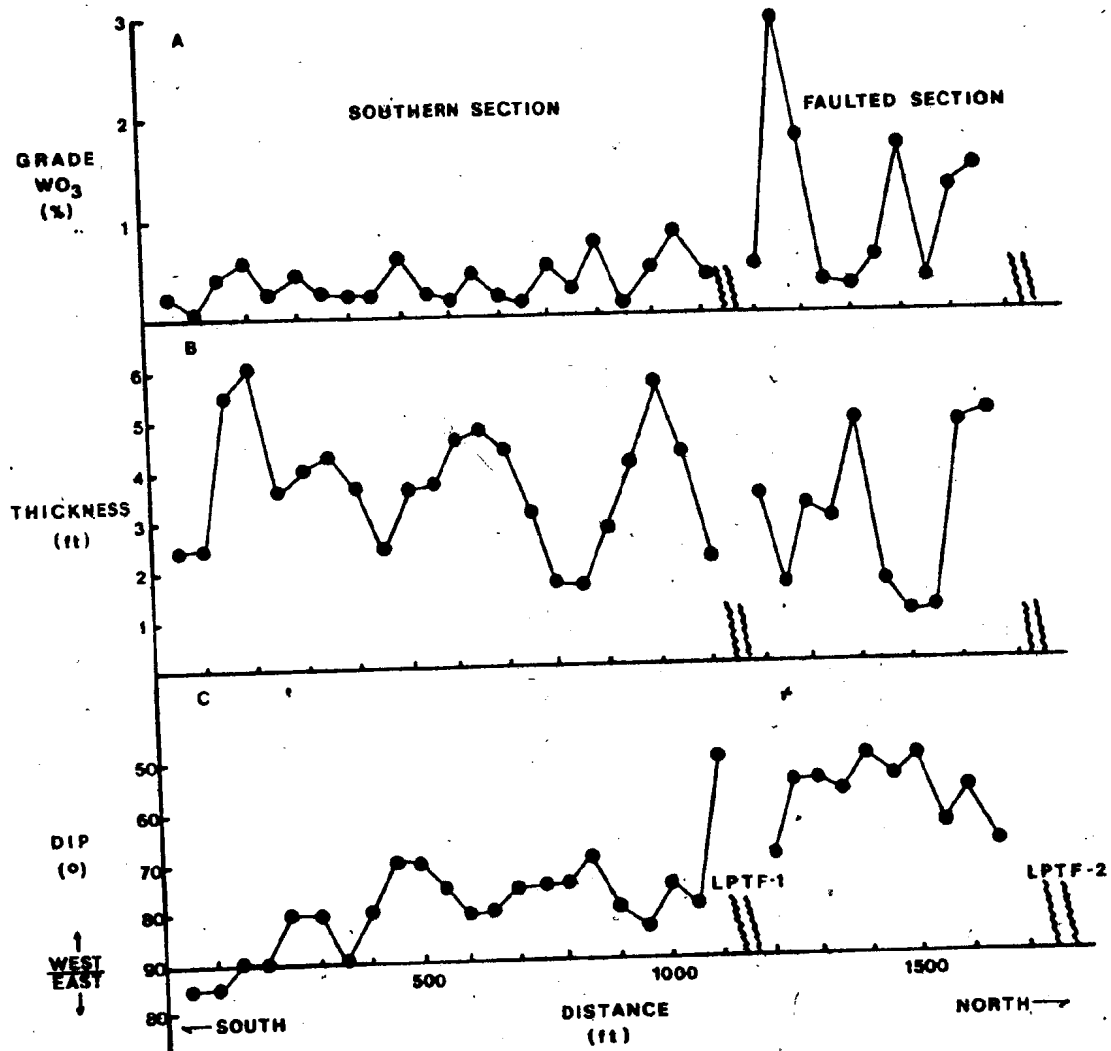


Figure 5.6 Correlation between grade, thickness and dip of vein #10, adit level.

rock type (c.f. granite section Vein #6, and northern part Vein #10) and secondly, that the shallower dipping portions of the vein system have the higher grades. More detailed data from adit level of Vein #10 have been compared in Figure 5.6 to thickness and attitude of the vein. In the faulted section there is an inverse correlation between grade and thickness; the highest grade being associated with the thinnest portions of the vein. This is similar to the more general comparison between the faulted section and the southern section, where the latter has a lower grade and is thicker on average than the faulted section.

Note also that the richest section of the adit is also the most shallow dipping. The portions of the vein closest to the first Long Pond Twin Fault (points Y,Z, Figure 5.6C), appear to have been reorientated by drag movement along that fault and this suggests that the attitudes displayed in the rest of the faulted section are "primary", i.e. indicative of a pre-faulting orientation and not rotation in the fault block.

An important consequence of the normal faulting mechanism is that the greatest shearing stress will be concentrated along the shallowest portions of the vein, thus one might expect more brecciation or fracturing of the wall rock and more fluid-rock interaction and alteration along such sections. Steep open spaces will represent areas of lower stress and hence sharper contacts and less wall rock alteration is expected. Vein cross-sections (Figure 5.4)

illustrate this feature. Furthermore the distribution of the wall rock alteration (map 3, in folder) matches the grade distribution, the faulted section having the most intense greisen alteration halos while the southern section is marked by sporadic greisen development. The mineralogical and geochemical features of the alteration halos are discussed in detail in Chapter 6.

The above observations suggest that the mineralisation is structurally controlled. Lodes were formed by differential movement of wall rock during normal faulting of tensional fractures, and resulted in portions of the veins being thicker and steeply dipping while other sections are thinner and more shallow dipping. The tungsten mineralisation appears to be concentrated in these latter sections, where wall rock alteration is also most intense.

5.6 EAST-WEST BLOCK FAULTING AND LATE VEINING

After the formation of the tungsten-bearing quartz veins the area was subjected to extensive east-west block faulting which offset a number of the major veins. The three major faults are shown in Figure 5.1 and are labelled Long Pond Twin Faults (LPTF, 1 and 2) and Granite Cliff Fault (GCF).

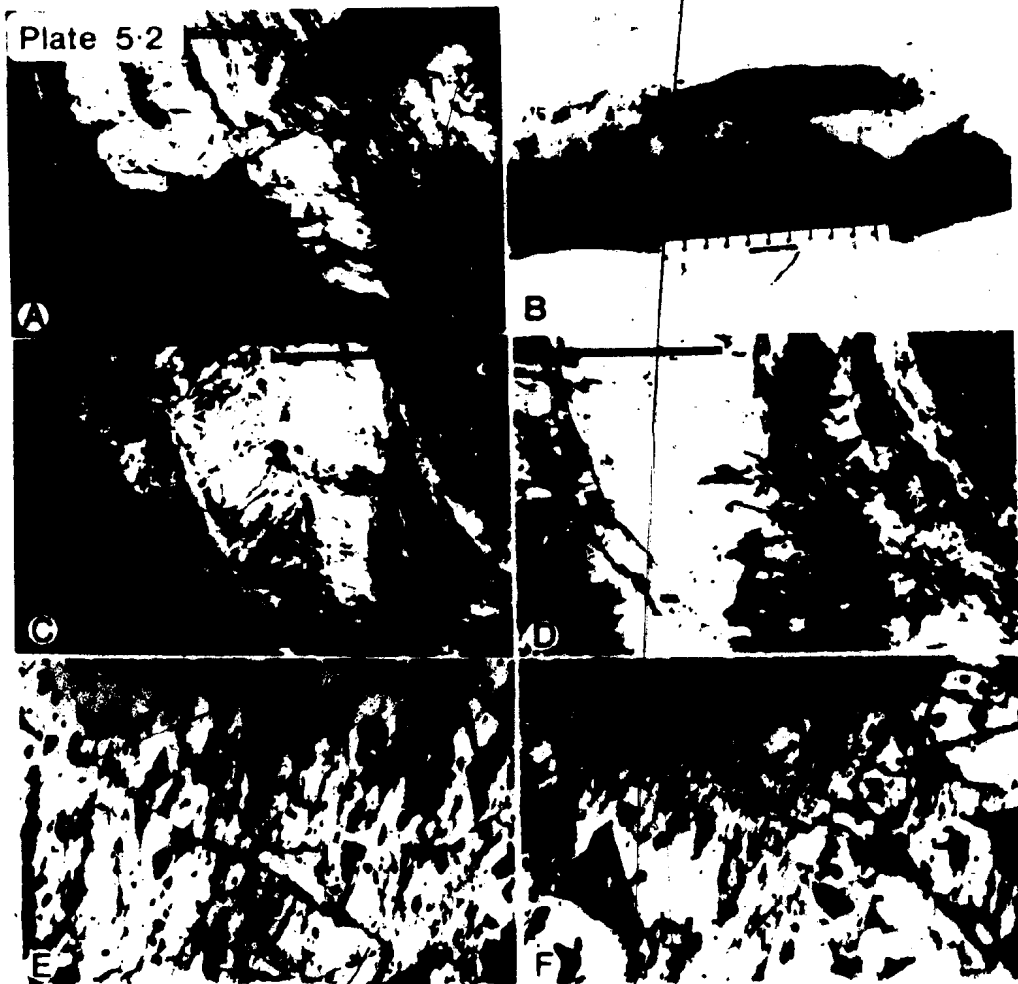
Offset relationships in the adit (Plate 5.2A and map 2) suggest that the Long Pond Twin Faults are normal faults, but if the geochemical anomaly that occurs north of Long Pond represents a continuation of Vein #10 and #6 north of the Granite Cliff Fault, movements on that fault may well have been in the

Plate 5.2

East-west faulting, F-cb veins and scheelitisation of wolframite. Where appropriate bar scale = 30 cm.

- 5.2A Vein offset by E-W normal faulting, location 279, adit level.
- 5.2B Example of fluorite-calcite-barite veins which cut the main tungsten-bearing lodes and E-W faults. Note finely laminated crustiform habit of the fluorite margin of the vein. Sample 153.
- 5.2C En echelon ladder-work of fluorite-calcite-barite veins which fill tensional fractures created by normal faulting within the main lode, location 273 adit level.
- 5.2D Coarse wolframite crystal partially altered to scheelite in high grade section of vein, location 378, adit level.
- 5.2E Polished section of wolframite (wf) crystal partially altered to scheelite (sc) along cleavage and fractures. Sample 377, x62.
- 5.2F More advanced scheelite alteration of wolframite. Typical shredded texture. Sample 377c, x62.

Plate 5-2



opposite direction to the Long Pond Twin Faults (i.e. reverse faulting).

A period of tensional fracturing followed the E-W block faulting, and veinlets containing primarily zoned fluorite-calcite-barite (F-cb veins) were emplaced during that time (Plate 5.2B). Fissures or depressions, seen in aerial photographs, which cut across the E-W fault depressions are probably the surface expression of these tensional veins. These veins cut both the tungsten-bearing quartz vein and the E-W faults (Figure 5.4G). The F-cb veins have also been intruded along some of the E-W fault zones (Figure 5.4G). An en echelon "ladder-work" of F-cb veins (Plate 5.2C) suggests some shearing occurred during their emplacement.

A summary of the structural development of the Grey River hydrothermal vein system is given in Figure 5.7.

5.7 VEIN TYPES AND PARAGENESIS

The parallelism in strike of the major veins does not allow relative time sequences of veins to be established by simple cross-cutting relationships alone.

No one vein contains the entire mineral assemblage but spatially associated veins have overlapping and telescoping segments of the paragenetic sequence. The paragenesis is complicated by the multiple injection history of the major veins. Individual cross-sections of such composite veins generally contain two (or more) vein types that were repeatedly injected so that time relationships are

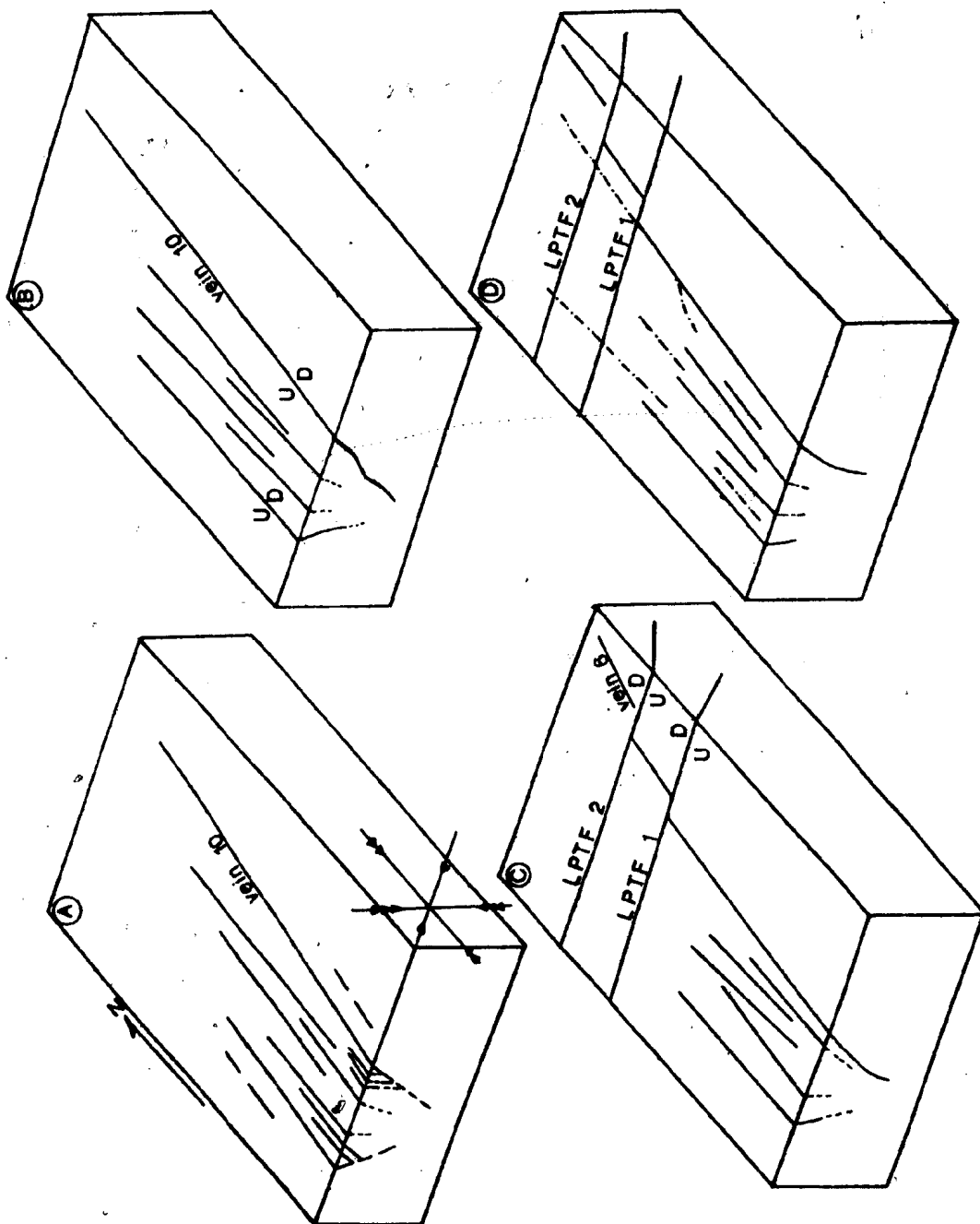
Figure 5.7 Structural development of the Grey River hydrothermal vein system.

5.7A Initial extensional fractures filled with quartz.

5.7B Repeated opening and injection of vein material into several of these early fractures to form the large composite lodes. Internal vein movements due to normal faulting.

5.7C Faulting and offset of veins by E-W normal faults.

5.7D Development of extensional fractures (dashed line) filled by fluorite, calcite, and barite.



nearly impossible to ascertain (see Figure 5.4). Furthermore one vein type may be deposited at one location while at the same time, but at another location, another vein type is being precipitated. Data presented later indicated that these two locations are connected at that instant in time and that structural and physico-chemical parameters govern their spatially separate deposition. Furthermore mineral paragenesis in hydrothermal vein systems is generally temperature and time-dependent (Landis and Rye, 1974). Thus the paragenetic sequence in the Grey River Tungsten Prospect is based on internal vein and polished section relationships, mineral telescoping between veins, and in part by fluid inclusion studies.

Four stages of mineralisation can be resolved; Early Stage; Composite Stage; Sulphide Stage; and Late Stage (Table 5.1).

The Early Stage is characterised by quartz, feldspar and molybdenite-bearing veins (QF-m) that are more common in western and southern portions of the mineralised area (Figure 5.1). The negative sign in the abbreviation signifies that molybdenite may or may not be contemporaneous with quartz and feldspar deposition. The feldspar component is minor (1%) but is characteristic of the vein type and is the basis for the subdivision. Other characteristics are listed in Table 5.1.

The Composite Vein stage quantitatively dominates the mineralisation and is subdivided into five vein types.

Table 5.1
Characteristic Features of the Vein Types

STAGE	ASSEMBLAGE	DIAGNOSTIC VEIN CHARACTERISTICS	VEIN EXAMPLE OR SAMPLE
EARLY	QF-m	- Pink K-feldspar - Muscovite selvage - Molybdenite	S #385
	Q-b	- Coarse vuggy quartz - Needle-like crystals bismuthinite - Pyrite cubes - Blue fluorite (I) - Muscovite selvage	1
	Q ^a + v	- Fe-rich wolframite (I)	1,5,4
COMPOSITE	Greisen	- Muscovite, quartz, fluorite assemblage - sulphides - Purple-red fluorite (II) - Fe-rich wolframite (I)	10
	Q-s	- Coarse vuggy quartz - Sulphides in vugs - esp. chalcopyrite - Blue to colourless fluorite (III)	10
	Q + v	- Mixed Fe-Mn wolframite (II) to Mn-rich wolframite (III) - Chalcopyrite, pyrite dominant sulphide	10,6
	SULPHIDE Q + g	- Abundant galena, sphalerite and pyrite - Needle crystals of quartz in vein centres	G #1
LATE	F-ob	- Crosscutting relation- ship with other assemblages - Green fluorite (IV) - vugs	S #164

Q = quartz; F = K-feldspar; m = molybdenite; b = bismuthinite;
v = wolframite; g = galena; s = sulphides (chalcopyrite,
pyrite, sphalerite, etc.); G = greisen.
Roman numerals refer to compositional differences.

Although temporal relationships are difficult to establish for the veins of this stage, they occur in distinct groups in individual composite veins, i.e., quartz-sulphide (Q-s) and quartz-wolframite (Q + w) veins are found in Vein #10 and #6 along with greisen alteration halos. Progressive changes in chemistry of the wolframite (detailed below) indicate that the composite (Q-b) (Q* + w) veins were deposited earlier (and possibly at higher temperatures) than the greisen enveloped (Q-s) (Q + w) composite veins. Fluid inclusion studies also support this interpretation of the sequential development of the veins.

The positive sign in the Q* + w and Q + w notation indicates that deposition of the wolframite occurred with deposition of the quartz, while the negative sign of Q-b and Q-s veins signifies that the sulphides were not deposited contemporaneously with quartz. In detail bismuthinite is recorded as a microscopic accessory in some portions of the composite (Q-b) (Q + w) veins and is therefore not wholly restricted to veins containing a Q-b assemblage. However, in the latter situation, the bismuthinite is a macroscopic feature and is therefore useful as a discriminating characteristic. Similarly other sulphides common to the Q-s veins occur within the Q-b veins.

Deposition of galena (as well as sphalerite and pyrite) occurred at the same time as quartz in veins associated with the Sulphide Stage. The quartz-galena (Q + g) vein type is characteristic of the Galena #1 Vein which crops

out 1½ km north of Long Pond. Although not seen to be continuous with the tungsten-bearing veins to the south, other features indicate a possible continuity, and this vein type probably represents lower-temperature deposition after the composite mineralisation stage. Evidence pointing to this relationship is presented below.

The Late Stage is represented by deposition of fluorite-calcite-barite veins (F-cb) in tensional fractures which have cross-cutting relationships with the preceding mineralisation. The minerals common to this vein type also fill vugs in the composite veins.

The complete paragenesis for the Grey River Tungsten Prospect is given in Figure 5.8. The complex inter-relationships between minerals will be explained in more detail in the mineralogy section (5.8).

Major features of the paragenesis include:-

- 1) Minerals with pegmatitic affinities such as feldspar and beryl are recorded only from early-formed veinlets (QF-m, Q-b veins).
- 2) In all vein types, except QF-m and F-cb, the sulphides are precipitated after quartz (and wolframite), generally in vugs within the quartz.
- 3) Bismuth-bearing minerals are common almost throughout the vein types, bismuthinite being the Bi-bearing phase in early-formed veinlets while later veinlets are characterised by Ag- and Bi-bearing galena, Ag- and Bi-tellurides and native bismuth.

PARAGENESIS

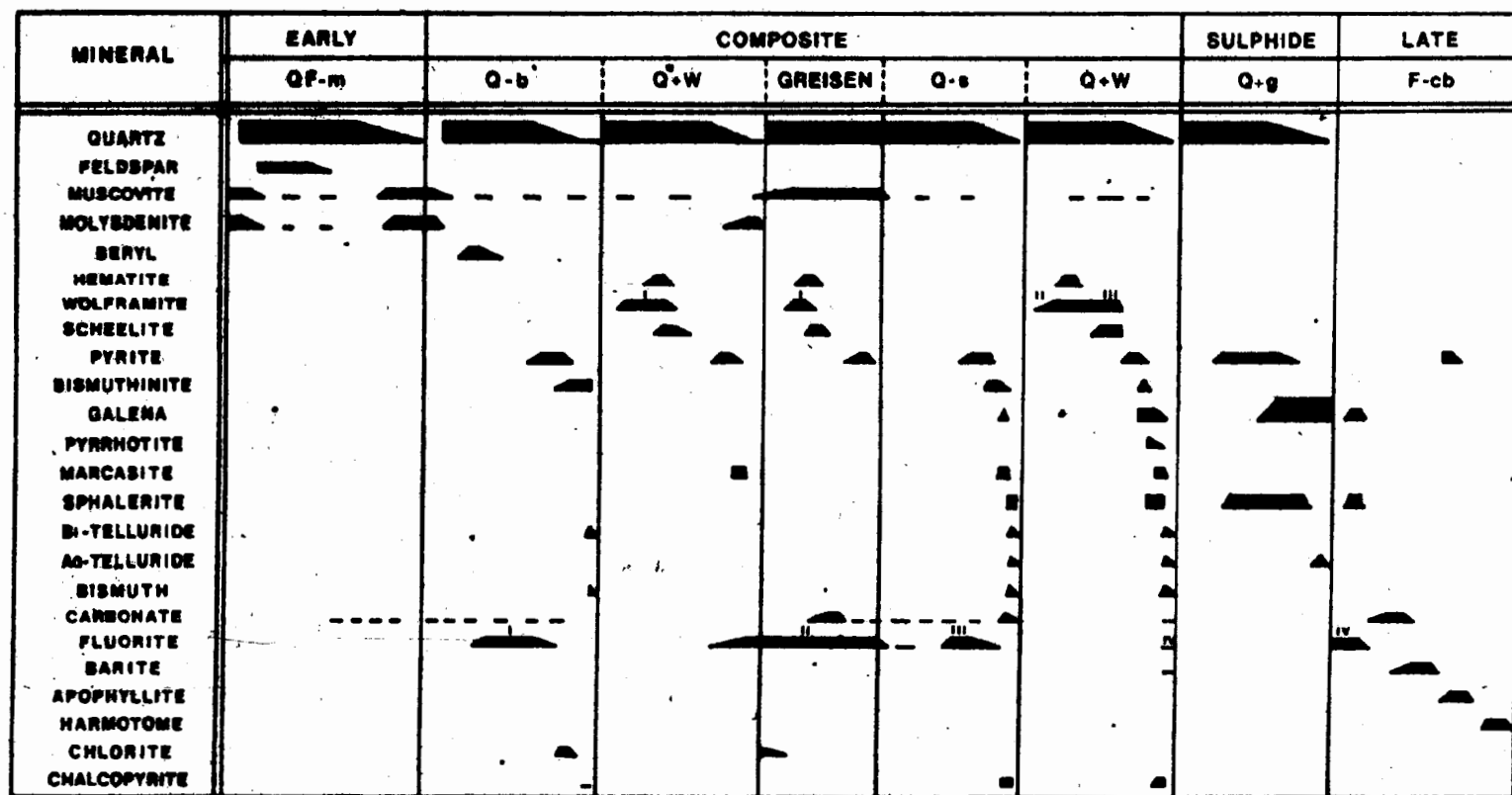


Figure 5.8

4) The paragenesis reflects a spatial distribution as well as temperature and time relationships. Early formed, higher temperature vein types occur in southern or southwestern parts of the mineralised area, while the locus of successively younger and lower temperature veins moved towards the north.

5.8 VEIN MINERALOGY

Gray. (1958) and Bahrycz (1957) described the mineralogy of the deposit from material collected by surface trenching and drilling. Bulk samples from the adit level were studied by Raicevic and Bruce (1971) by microscopic, X-ray, and infrared spectral analysis. In the present study, a much more comprehensive description of the mineralogy was possible through sampling of surface and adit exposures, the latter being unavailable for earlier workers. Some new mineral species, namely bismuth and silver tellurides, and sulphosalts and carbonates and sulphates, previously unreported from this deposit, are described. The mineralogy of the Grey River Tungsten Prospect is listed in Table 5.2.

No quantitative data on mineral abundances are available but obviously quartz predominates and comprises more than 90-95% of the vein. Available assays suggest that wolframite/scheelite occupies less than 1% (by volume) of the vein, with sulphides, fluorite, muscovite and carbonate being the principal accessories. An indication of the relative abundances of the mineral species is given in Table 5.2.

Table 5.2

Mineralogy of the Grey River Tungsten Prospect

HYPOGENE

Tungstates

Wolframite (Fe, MnWO_4)

● C

Scheelite (CaWO_4)

● C

Sulphides

Molybdenite (MoS_2)

● C

Pyrite (FeS_2)

● C

Pyrrhotite (Fe_{1-x}S)

● R

Marcasite (FeS_2)

● C

Chalcopyrite (CuFeS_2)

● C

Bismuthinite (Bi_2S_3)

● S

Galena (PbS)

● S-C

Sphalerite (ZnS)

● S-C

Covellite (CuS)

● R

Stibnite (Sb_2S_3)

○ -

Arsenopyrite (FeAsS)

○ -

Tellurides and Sulphosalts

Tetradymite ($\text{Bi}_2\text{Te}_2\text{S}$)

○ R

Pilsenite (Bi_3Te_2)

○ R

Hedleyite ($\text{Bi}_{14}\text{Te}_6$)

○ R-S

Hessite (Ag_2Te)

○ R-S

Pb, Bi, Ag sulphosalts

○ R

Native Elements

Bismuth (Bi)

● S

Copper (Cu)

○ -

Gangue

Quartz (SiO_2)

● C

Muscovite ($\text{KAl}_2(\text{Si}_3\text{AlO}_{10})(\text{OH})_2$)

● C

Fluorite (CaF_2)

● C

Feldspar ($\text{K, Na(AlSi}_3\text{O}_8)$)

● S

Harmotome ($(\text{K, Ba})(\text{Al}_2\text{Si}_5\text{O}_{14} \cdot 5\text{H}_2\text{O})$)

○ R

Apophyllite ($\text{KFCa}_4(\text{Si}_8\text{O}_{20}) \cdot 8\text{H}_2\text{O}$)

○ R

Table 5.2 (continued)

HYPOGENE

Gangue (continued)

Chlorite ((Mg,Fe)₅Al(AlSi₃)₁₀(OH)₈)

● S

Beryl (Be₃Al₂(Si₆O₁₈))

● S-R

Zircon (ZrSiO₄)

○ -

Calcite (CaCO₃)

● S-C

Siderite (FeCO₃)

○ S-C

Dawsonite (NaAlCO₃(OH)₂)

○ S

Gypsum (CaSO₄)

○ S-C

Oxides

Hematite (Fe₂O₃)

● R

Magnetite (Fe₃O₄)

○ -

Bismuth oxide?

○ R

SUPERGENE

Ferrimolybdate (Fe₂O₃·3MoO₃·8H₂O)

● S

Tungstate (WO₃·H₂O)

● C

Anglesite (PbSO₄)

○ -

-
- - previously reported : confirmed in present study
 - - previously reported : unconfirmed in present study
 - - newly reported in this study
 - C = Common
 - S = Sparse
 - R = Rare

5.8.1 Wolframite ((Fe,Mn)WO₄)

Macroscopically wolframite appears to be the dominant tungsten-bearing phase but ultraviolet lamping and polished section studies reveal that scheelite is volumetrically equally important, mainly as a pseudomorphic replacement of wolframite. This pseudomorphic replacement results in wolframite crystals that appear to fluoresce under ultraviolet light, a feature that is helpful in evaluating grade and mineral distribution.

The wolframite occurs as isolated to stubby prismatic crystals which vary in size from less than 1 cm to 10 cm long. The crystal size is generally smaller in early sheeted portions of the composite veins, possibly in part due to mild brecciation, but later injections of quartz contain spectacularly large crystals of wolframite. (Plate 5.2D). In hand specimen the wolframite varies in colour from a black Fe-rich variety (ferberite) to a reddish-brown, Mn-rich (huebnerite) variety. Ferberite appears to be restricted to Veins #1, #4 and #5 while reddish brown wolframite is common to Vein #6. X-ray diffraction and electron microprobe analyses (Appendix B.2 - B.4) show the chemical variation in the wolframite throughout the vein system, and its significance is discussed in detail below.

Within tungsten-bearing veins, wolframite is an early deposited vein mineral along with quartz and is frequently found in radiating clusters attached or rooted to one wall of a veinlet. Quartz is generally molded around wolframite

and occasionally occupies cavities in corroded or mildly brecciated wolframite. However, wolframite does sporadically occur as veinlets within quartz. Although quartz deposition occurs through nearly the complete paragenesis, where associated with wolframite both are generally coprecipitational.

The characteristic feature of the wolframite is its extensive replacement by scheelite. On average wolframite crystals are 40% altered to scheelite but a few crystals are almost completely altered and contain only small inclusions of wolframite which indicate its former presence. Replacement progresses along fractures and cleavages in the wolframite (Plate 5.2E) and a characteristic shredded texture results (Plate 5.2F).

5.8.2 Scheelite (CaWO_4)

Scheelite occurs as a pseudomorphic replacement of wolframite. It is coloured orange to yellow-brown, and fluoresces blue-white, indicating low molybdenum contents. Approximately 98% of the scheelite in the deposit has this characteristic colour which implies, but does not prove, that most if not all the scheelite is secondary after wolframite. Very few scheelite crystals do not show evidence of a wolframite precursor.

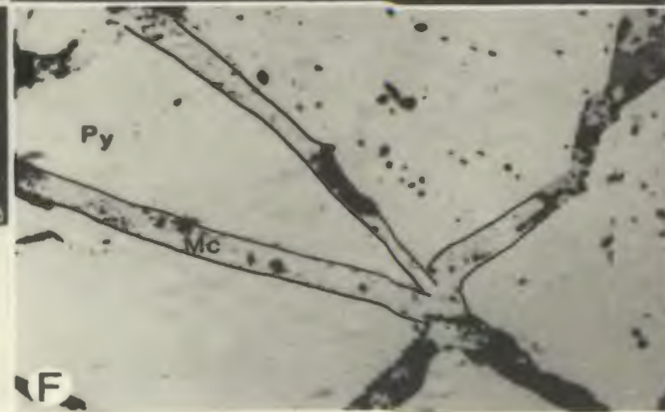
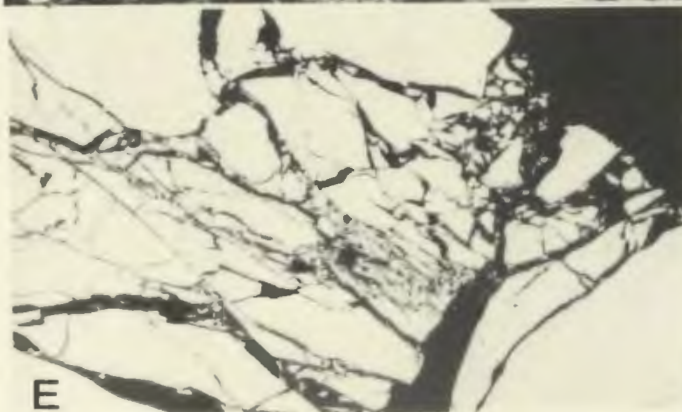
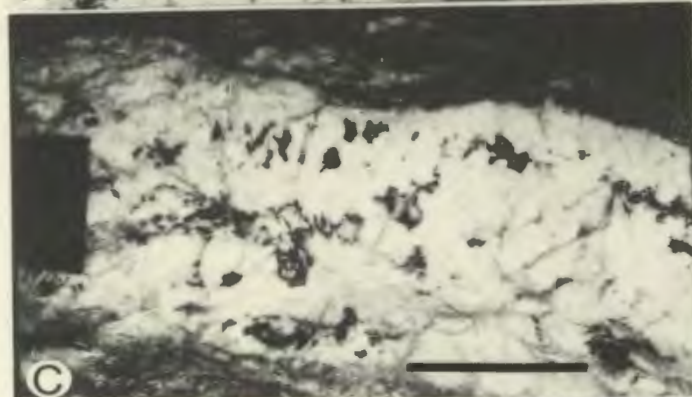
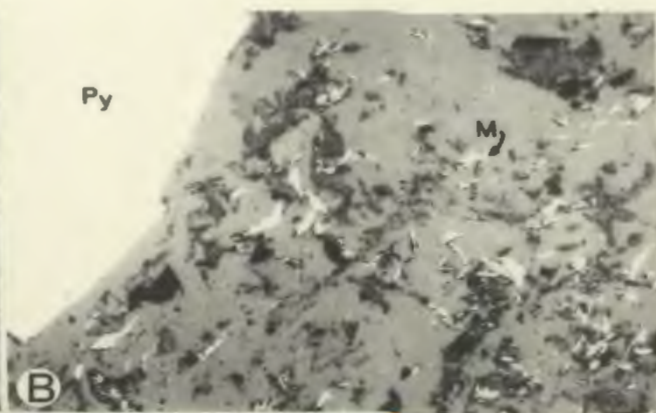
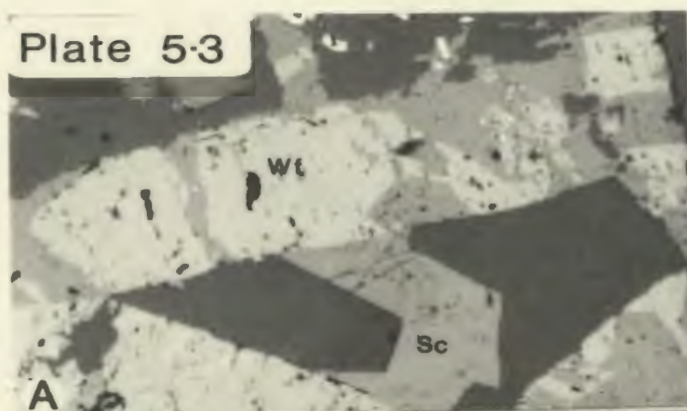
Sporadically however, scheelite overgrowths are evident (Plate 5.3A) and some rare euhedral scheelite crystals appear zoned. This zoning is emphasized by colour variation; from white in the core to orange and yellow-brown

Plate 5.3

Mineralogical aspects: scheelite, wolframite, molybdenite, muscovite, pyrite, marcasite.

- 5.3A Passive overgrowth of scheelite (sc) on partially altered wolframite crystal (wf). Sample 631, x62.
- 5.3B Association of molybdenite (m) and muscovite in quartz gangue - Py = pyrite crystal. Sample 152, x62.
- 5.3C Quartz-sulphide veinlet of composite lode (Vein #10). Note sulphides fill vugs in early precipitated quartz. Location 392, adit level. Bar scale = 30 cm.
- 5.3D Crystal of pyrite (py) lining vug in quartz later filled by chalcopyrite (cp). Sample 391, x62.
- 5.3E Brecciated pyrite crystal with fractures filled by gangue quartz. Sample 206, x62.
- 5.3F Replacement of pyrite by marcasite along incipient fractures. Sample 214, x62.

Plate 5-3



on the rim of the crystals. The white core is softer than the rim and has a poor polish in polished section. Electron microprobe data (Appendix B.3) of these zoned (?) crystals indicate that there is no significant chemical difference between the core and the rims.

The exact paragenetic position of scheelite is difficult to ascertain. Available textures (Plate 5.2E, F, and 5.3A) however suggest that this scheelitisation process occurs relatively soon after the deposition of the wolframite, sometimes before quartz deposition, and prior to the deposition of sulphide phases such as pyrite and chalcopyrite.

5.8.3 Hematite (Fe_2O_3)

Euhedral crystals of hematite occur as a minor component of veins containing wolframite mineralisation. The hematite appears to be precipitated with wolframite and quartz but in one section occurs as an intergrowth with muscovite which was deposited slightly later than the wolframite.

5.8.4 Molybdenite (MoS_2)

Molybdenite is the first sulphide phase to appear, but it also occurs sporadically throughout the mineralising sequence. It is primarily associated with QF-m veins where it occurs intergrown with muscovite and in vugs within the quartz. It is found also in vein types from the composite stage, intergrown with muscovite (Plate 5.3B), along late fractures in the quartz (with muscovite), and in muscovite selvages.

Molybdenite-bearing veins are restricted to southern

and south-western portions of the mineralised area. They are especially common in the vicinity of Vein #1 and in southern sections of the adit level (Vein #10).

5.8.5 Pyrite (FeS_2)

Pyrite is a ubiquitous component in all veins except QF-m veins and is disseminated also in wall rock as a result of alteration. In veins not subjected to reopening, pyrite forms euhedral crystals up to 2 cm long and is commonly found in vugs (Plate 5.3C). The vuggy nature of their occurrence is emphasized by a distinct "molar" texture (Plate 5.3D) in which crystals of pyrite (and some marcasite) crystals appear to have grown in cavities in quartz which were later filled with chalcopyrite. Pyrite in veinlets subjected to reopening is typically brecciated (Plate 5.3F), the fractures filled rarely by quartz and more commonly by later sulphides.

Rarely pyrite crystals partially overgrow wolframite/scheelite crystals but are not observed to replace them. Pyrite itself is typically replaced and resorbed by later deposited sulphides such as bismuthinite, galena and chalcopyrite. Much of the pyrite is partially altered to marcasite especially around the rims of pyrite crystals and along incipient fractures (Plate 5.3F). The marcasite rims do not take up a good polish and thus have a spongy appearance in contrast to pyrite. Many pyrite grains have a weak anisotropy under reflected light which may be due to stress, especially during brecciation.

Pyrite deposition was evidently long-lived but at any point in a vein type it was precipitated after wolframite (and scheelite) and prior to the deposition of bismuthinite, galena and later sulphides.

5.8.6 Marcasite (FeS_2)

As well as occurring as alteration rims on pyrite, marcasite is found as fine grained porous aggregates of crystals lining vugs (Plate 5.4A) later infilled by chalcopryite. Furthermore, a lamellar texture is common (Plate 5.4B) possibly resulting from coprecipitation of carbonate (siderite?) and marcasite.

5.8.7 Pyrrhotite (FeS_{1+x})

Pyrrhotite occurs rarely as small isolated blebs in chalcopryite and is apparently an uncommon mineral in the deposit. In one sample it was seen to envelope pyrite in a cavity within a wolframite crystal (Plate 5.4C). Gray (1958) maintains that pyrrhotite was formerly a much more common phase and that it has been extensively altered to marcasite or replaced by chalcopryite. Marcasite alteration of pyrrhotite is commonly recorded from other tungsten deposits (Kelly and Turneure, 1970; Kelly and Rye, 1979) but the usual gradations from unaltered to altered are apparently absent at Grey River.

5.8.8 Chalcopryite (CuFeS_2)

In northern parts of Vein #10 and in Vein #6 chalcopryite is an important constituent of the sulphide component of the vein. In fact in those areas the amount of chalcopryite is

pyrite may exceed that of pyrite and it is likely to be an economically recoverable mineral in any future mining operation. Typically, chalcopyrite fills vugs in quartz but also occurs as veinlets in fractured wolframite and pyrite (Plate 5.4D).

Exsolution stars of sphalerite are common in chalcopyrite (Plate 5.4E) but larger grains of sphalerite as well as muscovite occur as vug fillings with chalcopyrite. Chalcopyrite is absent as a major phase in the Galena #1 Vein north of Long Pond but there occurs as exsolution blebs and lamellae in sphalerite.

Sulphides which precipitated early are partially replaced by injection of chalcopyrite into vugs and fractures; this appears to cause local unmixing of bismuth- and silver-tellurides and sulphosalts plus native bismuth from bismuthinite and galena (detailed below).

5.8.9 Sphalerite (ZnS)

Paragenetically sphalerite deposition overlaps that of chalcopyrite to which it is spatially related. Rarely sphalerite partially overgrows wolframite but more commonly it occurs in vugs with chalcopyrite in which it also occurs as exsolution lamellae. Sphalerite also appears as myrmekitic intergrowths in pyrite but some sections suggest that this texture results from incipient replacement along fractures. Covellite occurs as a supergene replacement mineral of sphalerite and galena in Vein #6.

5.8.10 Bismuthinite (Bi_2S_3) - Galena (PbS)

Acicular crystals of bismuthinite up to 7 cm long are

Plate 5.4

Mineralogical aspects: Marcasite, siderite, pyrrhotite, chalcopyrite, sphalerite, bismuthinite.

- 5.4A Marcasite (mc) lining a vug in quartz later filled by chalcopyrite (cp). Sample 23, x62.
- 5.4B Siderite (black) and marcasite (white) in lamellar (intergrowth?) texture. Crystal lining vug in quartz later filled by chalcopyrite. Sample 21, x100.
- 5.4C Pyrrhotite (Po) coating pyrite (Py) crystal in vug within wolframite crystal. Sample 649, x80.
- 5.4D Brecciated wolframite with fractures filled by chalcopyrite. Sample 217A, x80.
- 5.4E Exsolution stars of sphalerite in chalcopyrite. Sample 610, x100.
- 5.4F Bismuthinite (Bt) replacing pyrite. Sample 314B, x62.

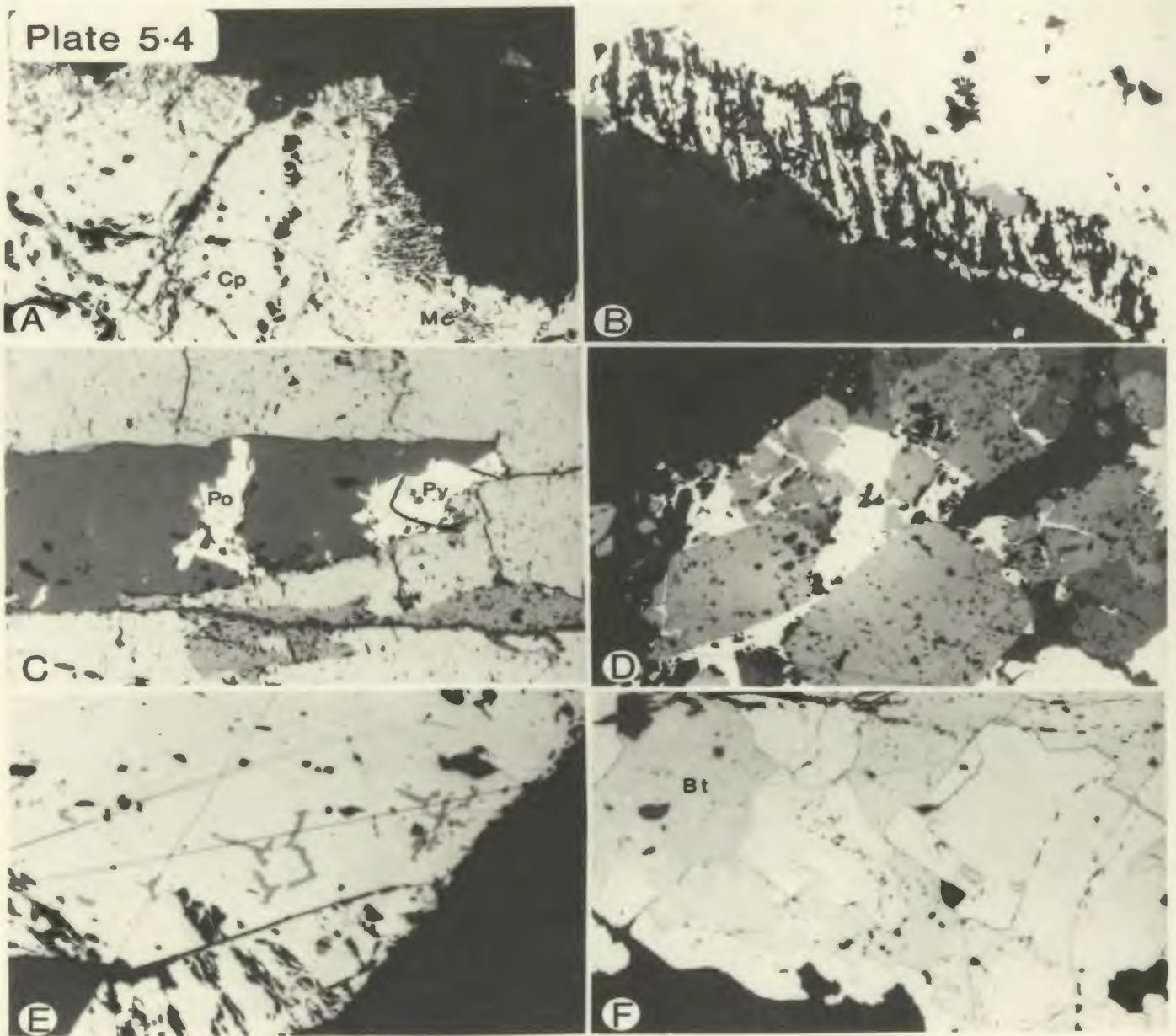
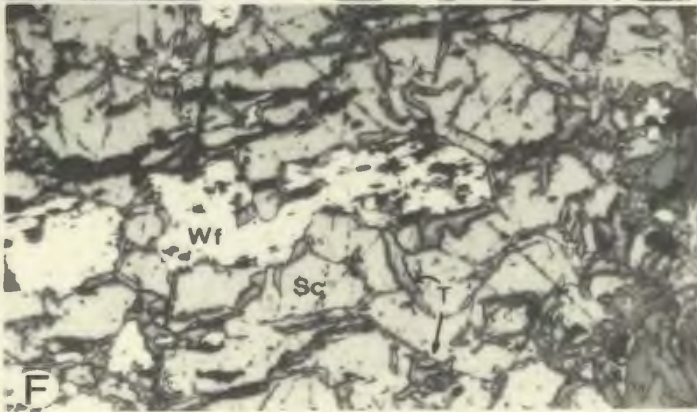
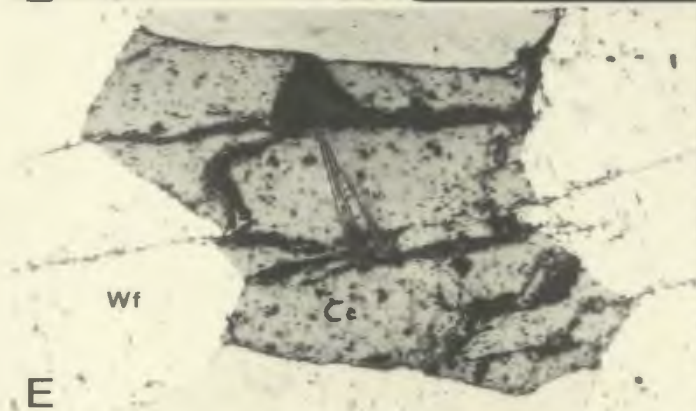
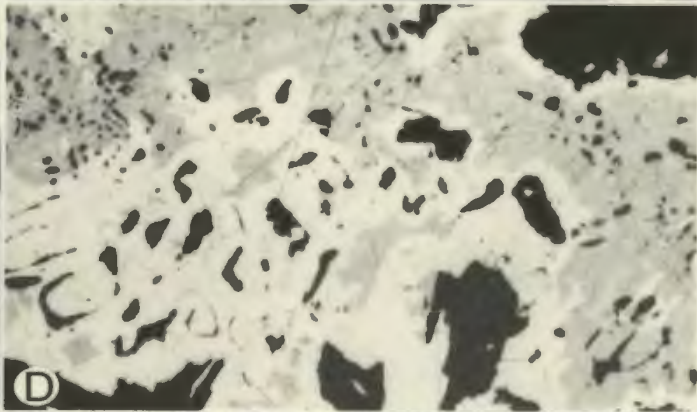
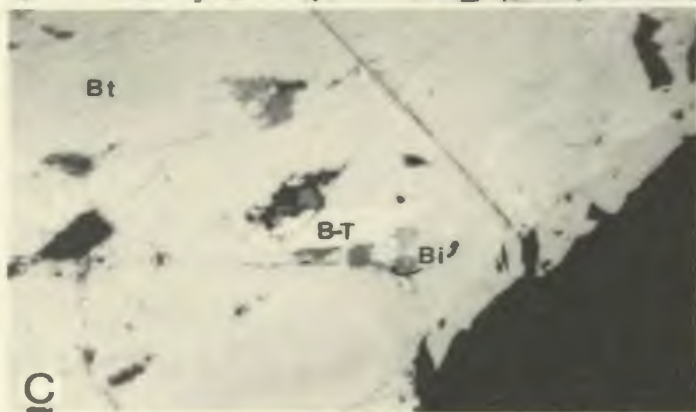
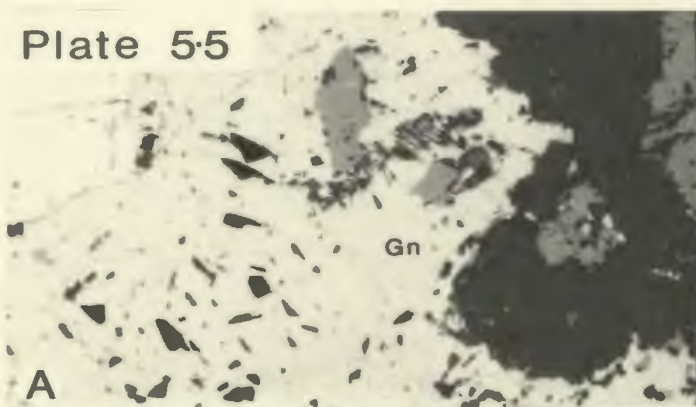


Plate 5.5

Mineralogical aspects: Galena, bismuthinite, tellurides, carbonate, supergene alteration of wolframite.

- 5.5A Galena (Gn) replacing pyrite, Vein #7, sample 675, x80.
- 5.5B Bismuthinite and galena intergrowths (unmixing products) in sample 644B, adit level, x100, X-polars.
- 5.5C Bismuthinite (Bt) with Bi-telluride (B-T) and native bismuth (Bi) inclusions. Sample 207, x62.
- 5.5D Myrmekite-like intergrowths (unmixing products) of hessite (Ag_2Te - grey mineral) and hedleyite ($\text{Bi}_{14}\text{Te}_6$ - white mineral). Sample 23, x200.
- 5.5E Unaltered wolframite crystal (wf) in contact with carbonate mineral (cc), probably calcite, within a quartz crystal, Vein #10, sample 217A, x200.
- 5.5F Wolframite (wf) crystal altered to scheelite (Sc) during hypogene alteration. Scheelite is altered to tungstite (T) during supergene alteration. Sample 671, x100.

Plate 55



common in Q-b vein types found in southern and southwestern portions of the mineralised area. They are generally attached to coarse euhedral crystals of quartz and are orientated at right angles to the vein walls. Bismuthinite occurs also as a minor component of the Q-s and Q + w veinlets found in southern sections of the composite Vein #10. There it replaces pyrite (Plate 5.4F) in which it occurs as inclusions and as partial overgrowths. Both are partially replaced by chalcopyrite.

Greisen alteration associated with the formation of the composite Vein #10 disrupts Q-b veinlets and thus the bismuthinite associated with the latter is paragenetically earlier than bismuthinite deposited in composite Vein #10.

In Vein #6 bismuthinite is absent but galena appears in a similar paragenetic position occurring as inclusions within pyrite as well as partially enclosing and replacing pyrite grains (Plate 5.5A). Electron microprobe analyses of these galenas reveal unusually high contents of silver and bismuth ranging from 0.18 to 1.5 wt% and 0 - 3.16 wt% respectively.

Strongly anisotropic bluish-white grains mantling pyrite (Plate 5.5B) occur in samples from the faulted section of Vein #10 (adit level). X-ray photos reveal that they are myrmekite-like intergrowths of galena and bismuthinite (Plate 5.9) suggesting that they result from unmixing of an initially homogeneous Pb-Bi sulphosalt with falling temperature (Ramdohr, 1969).

These data suggest that the mineral that replaces pyrite paragenetically in the sequence changes in composition depending on location within the vein system (i.e. from south to north). In samples from veins exposed in the south the mineral is bismuthinite; in the north galena predominates. A zone of what was probably a lead-bismuth sulphide (solid solution) occurs in an intermediate position to the two extremes.

Stibnite previously reported from this deposit (Gray, 1958) was not detected in this study. From the description of its occurrence it appears that bismuthinite was misidentified as stibnite by Gray.

5.8.11 Sulphosalts, Tellurides, and Native Elements

Bismuthinite, galena and the myrmekitic intergrowths of the two were affected by a later annealing or reheating event probably related to their partial replacement or resorption by chalcopyrite. The annealing caused unmixing of bismuth sulphosalts (tetradyte, $\text{Bi}_2\text{Te}_2\text{S}$), bismuth telluride (pilsenite, Bi_3Te_2), and bismuth from bismuthinite, and bismuth and silver-tellurides (hedleyite, $\text{Bi}_{14}\text{Te}_6$; hessite Ag_2Te), Pb-Bi-Ag, sulphosalts plus bismuth from galena (Plate 5.5C and D). Native bismuth and bismuth- and silver-telluride occur as exsolution blebs in the galena-bismuthinite intergrowths.

Identification of these phases by polished section methods is very difficult and most phases were resolved by electron microscopy. However, observed polish section

characteristics of the phases are given in Appendix C2. The mineral chemistry and significance of these unusual phases is discussed in section 5.10.

5.8.12 Quartz

Quartz comprises by far the largest portion of the gangue mineralogy. Its deposition continued almost throughout the entire vein paragenesis and in $Q^* + w$ and $Q + w$ veins, is generally coprecipitational with wolframite. In such veins the quartz is poorly crystalline and white and the veins contain few vugs. The whiteness is due to a greater abundance of small fluid inclusions than the more transparent-glassy quartz from Q-b and Q-s veins.

Quartz from the latter type is generally coarser and shows more well developed crystal forms, the veins being typically vuggy. These contrasts in physical properties may imply slightly different environments of deposition between Q-b, Q-s and $Q^* + w$, $Q + w$ veins. Vugs and euhedral crystal forms imply slower, open-spaced deposition for the Q-b and Q-s vein quartz while lack of well defined crystals and vugs suggests an environment of rapid deposition for the tungsten-bearing veins ($Q^* + w$, $Q + w$). This agrees with the evidence for the structural control of mineralisation which indicates, that in lodes reopened by normal faulting, tungsten mineralisation ($Q^* + w$, $Q + w$) is concentrated in shallow-dipping, more intensely sheared portions of the vein while Q-b and Q-s vein types are found in steeply dipping sections that allow for more open-spaced deposition.

Quartz from QF-m veins is commonly white and poorly crystalline while Q + g vein quartz is white but often occurs as a mesh of interfingering needle-like crystals in central portions of the vein.

5.8.13 Feldspar

Coarse pink orthoclase crystals occur in, and are restricted to, veins of the QF-m type which are common in the south-western portions of the mineralised area. No feldspar was observed in the major composite veins although Raicevic and Bruce (1971) recorded possible feldspar from infra red spectral studies of assay samples.

5.8.14 Beryl

A rare mineral in this deposit, beryl has only been recorded from the southern end of Vein #1 and in a muscovite-selvedged tensional veinlet exposed in the extreme southern end of the adit. It is associated with glassy quartz and minor amounts of white mica. The beryl is typically pale green in colour and occurs as prismatic crystals up to 5 cm long and 1 cm wide.

5.8.15 White Mica

Mica deposition occurred throughout the paragenesis in a variety of forms:-

- 1) It occurs as muscovite selvedges up to 5 mm thick around QF-m and Q-b veins. Within selvedges, books of mica are orientated with 001 planes perpendicular to the vein edge.

- 2) White mica occurs as a result of hydrothermal

alteration of the wall rock in greisen halos around major composite (Q-s, Q + w) veins. Whole rock trace element geochemistry of the greisen indicates high concentrations of Li which suggests that the mica associated with the alteration is Li-rich (lepidolite). Mica also occurs within the vein as an alteration of wall rock xenoliths and is also found on slickenside surfaces.

3) Coarse white mica occurs in vugs in QF-m and Q-b veins and rarely as rosettes attached to wolframite crystals in Q* + w and Q + w veinlets in composite veins.

5.8.16 Fluorite (CaF₂)

After quartz, fluorite is the most abundant gangue mineral of the veins, and it is also found as disseminations in alteration halos in wall rock. A variety of colours are evident and characteristic of various vein types.

Q-b veins contain a blue coloured fluorite (I - Figure 5.8) which occurs mainly as a vug filling in a similar paragenetic position to bismuthinite. Greisen stage deposition is marked by a deep-purple coloured fluorite (II - Figure 5.8) which is intimately related to quartz and muscovite as products of hydrothermal alteration of wall rock. Colourless to bluish fluorite (III - Figure 5.8) occurs as vug fillings in Q-s veinlets of composite veins and to a lesser extent in Q + w veins.

Fluorite appears after quartz in any vein type, filling vugs in quartz. It should therefore occur after wolframite in Q + w veins, but its scarcity in those veins

precludes an exact definition of the time relationships, although in one or two cases it appears to fill small vugs.

Light to dark green, crustiform fluorite (IV - Figure 5.8) occurs in F-cb veins which postdate the composite vein formation and probably the Sulphide Stage of the mineralisation.

5.8.17 Carbonates and Sulphates

Carbonate deposition occurred throughout the paragenesis but is more marked in some stages than others. Calcite (plus anhydrite-gypsum) and dawsonite occur as accidentally trapped minerals in fluid inclusions, as well as solid inclusions, in quartz from QF-m, Q-b and Q-s vein types. Their distribution and occurrence is discussed in Chapter 7, but in general their deposition resulted from immiscible separation of CO_2 and H_2O from an originally homogeneous fluid and by later retrograde boiling of the H_2O -rich fluid.

Carbonate, probably siderite, occurs as lamellar intergrowths with marcasite (Plate 5.4B) which are deposited as vug linings later filled by chalcopyrite. Greisenised wall rock contains sparse amounts of carbonate along with disseminated wolframite and the ubiquitous quartz, mica and fluorite. One sample from a Q + w vein shows the coexistence of wolframite and calcite (enclosed in quartz) (Plate 5.5E) and suggests that carbonate was precipitated during or immediately after deposition in those veins.

A large amount of calcite occurs as vug fillings in composite veins and is associated with light green fluorite

and barite in the F-cb-veins which postdate the formation of tungsten-bearing composite veins.

5.8.18 Chlorite

Small amounts of dark green massive and radiating-fibrous aggregates of chlorite are found as fracture and vug fillings in several vein types (Q-b, Q-s) and are thought to be of an Fe-rich composition (Gray, 1958).

5.8.19 Supergene Minerals

Yellow to yellow-green microcrystalline masses and earthy crusts are formed on wolframite crystals in surface exposures of all tungsten-bearing veins. X-ray diffraction analysis of this yellow alteration mineral was inconclusive, primarily as a result of the large amount of scheelite in the sample. Polished sections indicated that the alteration was not after wolframite but occurred in cracks and as veinlets in scheelite (Plate 5.5F). Rarely the alteration mineral occurred as a coarse strongly anisotropic grain (Plate 5.6A) which qualitative electron microprobe analysis showed to be tungstite ($\text{WO}_3 \cdot \text{H}_2\text{O}$) a common weathering product of scheelite.

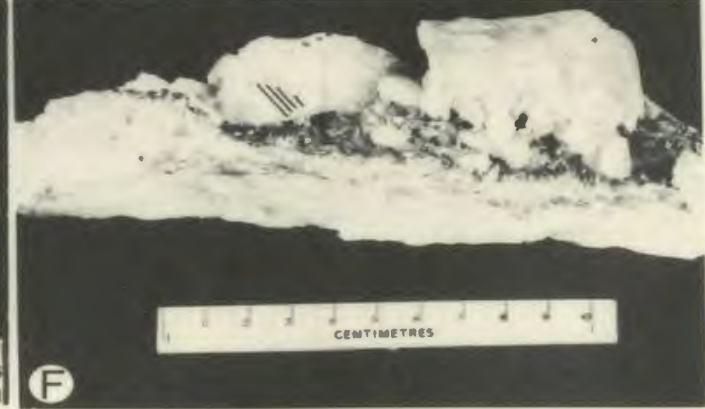
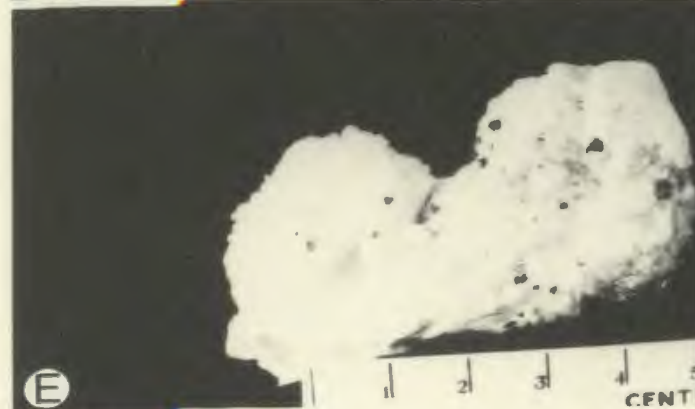
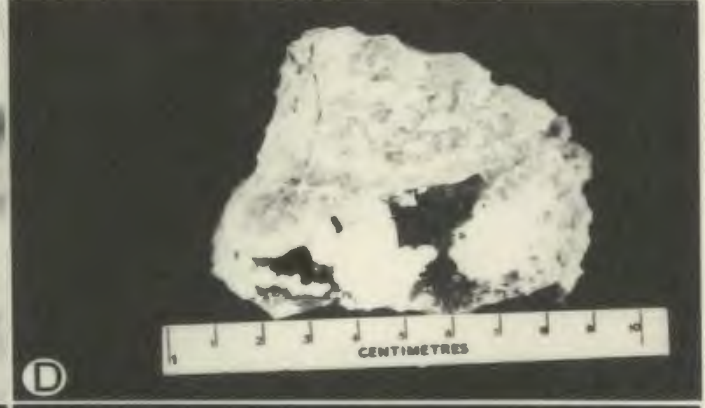
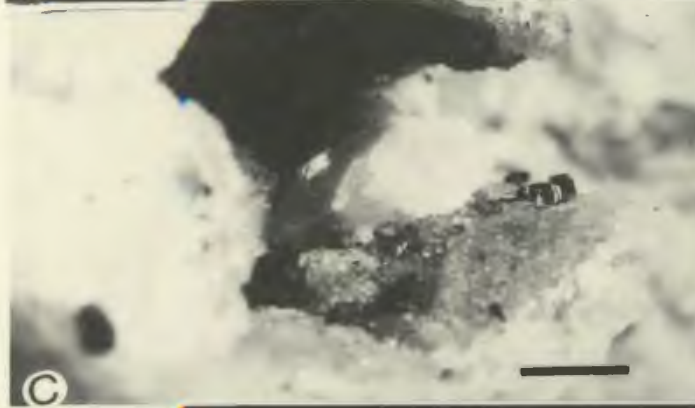
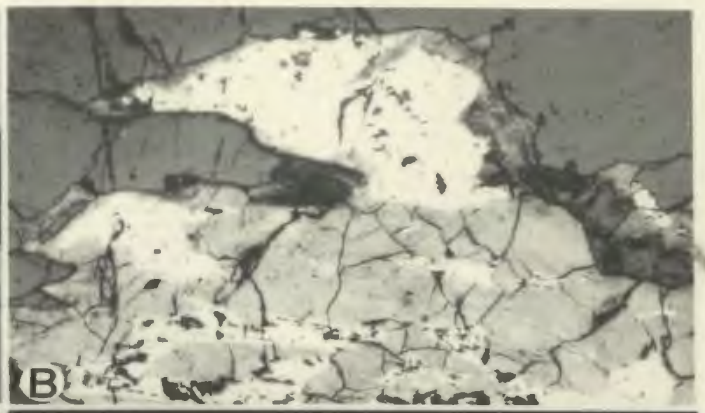
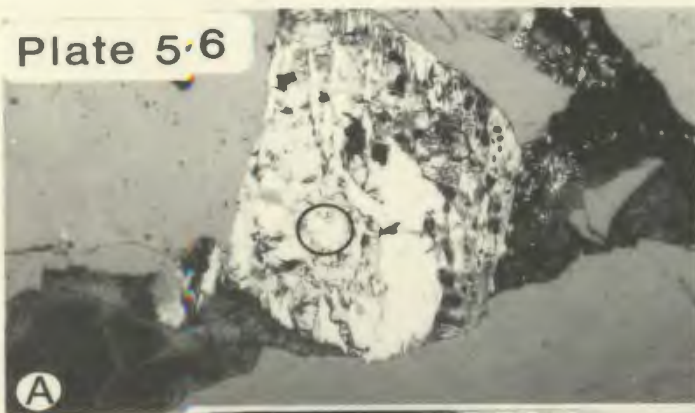
A yellow (sulphur-coloured) alteration mineral of molybdenite was found by X-ray diffraction to be ferri-molybdate. As well, in surface exposures, bismuthinite is often coated with a soft white-grey mineral (Plate 5.6B). A multi-element electron microprobe scan showed no elements apart from bismuth and minor sulphur were present and the white-grey mineral is inferred to be a bismuth oxide.

Plate 5.6

Mineralogical aspects. Supergene alteration of scheelite and bismuthinite, apophyllite, F-cb veins, harmotome.

- 5.6A Anisotropic tungstite grain (circled) formed during supergene alteration of scheelite (after wolframite). Sample 699, x100.
- 5.6B Bismuthinite (white mineral) altered to bismuth oxide (light grey mineral) during supergene alteration. Sample 249, Vein #1, x62.
- 5.6C Apophyllite ($\text{KF Ca}_4(\text{Si}_8\text{O}_{20}) \cdot 8\text{H}_2\text{O}$) crystal in vug within fluorite-calcite-barite (F-cb) vein, sample 212, adit level, Bar scale = 1cm.
- 5.6D Vug in fluorite-calcite-barite vein lined with apophyllite crystal and calcite. Adit level, sample 603.
- 5.6E Etched calcite crystal coated with small prismatic harmotome crystals. Fluorite-calcite-barite vein, sample 603.
- 5.6P Vug surface coated with etched calcite crystals that provide evidence for a period of dissolution prior to the precipitation of harmotome crystals. Sample 111, adit level.

Plate 5.6



5.9 F-cb VEINS

Open-spaced fissures partially filled by fluorite, calcite, and barite were formed after the deposition of the composite veins and probably after the sulphide stage of mineralisation. Light to dark green crustiform fluorite lines surfaces of these fissures (Plate 5.2B), the crustiform habit being emphasised by colour banding on a millimetre scale. Galena and sphalerite occur sporadically within the fluorite.

White calcite and reddish barite, in cockscomb habit, partially fill the central portions of the veins while chalcopryite, apophyllite and harmotome occur in vugs. The apophyllite occurs as colourless (rarely yellow) crystals of prismatic habit (Plate 5.6C) showing a well developed basal cleavage. Some apophyllite crystals have been altered to a white microcrystalline material which occurs in sheets parallel to the basal cleavage and on crystal surfaces (Plate 5.6D). An X-ray diffraction pattern suggests that no new mineral is formed implying that the apophyllite has been leached by reaction with a fluid (acid?) that penetrated along cleavage planes.

Harmotome crystals generally occur in vugs that do not contain apophyllite and are attached to calcite (Plate 5.6E) and rarely fluorite. The calcite overgrown by harmotome crystals display etched dissolution pits on crystal surfaces (Plate 5.6F) indicating that a mild acid leaching episode occurred prior to the deposition of the

harmotome. This event probably coincided with the leaching that affected the apophyllite.

5.10 MINERAL CHEMISTRY

5.10.1 Bismuth-, Lead-, Silver-bearing Minerals

Bismuth-, lead-, silver-bearing minerals are characteristic of the sulphides associated with the quartz-wolframite-scheelite mineralisation at Grey River. Such an association is common in other tungsten deposits especially those of the magmatic-hydrothermal affiliation (Chang and Bever, 1973; Czamanske and Hall, 1975; Malakhov, 1969; Ontoev *et al.*, 1960; Mintser, 1979). The association of silver with galena is also common in ore deposits and may be subdivided further into two groups characterised by Ag-Sb (Hall and Czamanske, 1972) and Ag-Bi associations (Malakhov, 1969), representing low and high temperature origins respectively. At Grey River the Bi-Pb-Ag mineralisation postdates deposition of pyrite, however, the present mineralogy of the Bi-Pb-Ag minerals is a function of annealing and unmixing at temperatures lower than their initial formation temperature.

Electron microprobe analyses indicate that there is a regular change in composition of Bi-Pb-Ag minerals with time and space within the vein system. The paragenetically earlier bismuthinite from Q-b veins is chemically richer in copper and lead than the later deposited bismuthinite of Q-s and Q + w veins (Table 5.3 and Figure 5.7A). Bismuthinites are generally pure (Ramdohr, 1969) but at high temperature a solid solution exists between aikinite (PbCuBiS_3) and

Figure 5.9 Compositional data for bismuthinite, bismuth telluride, silver telluride and Ag-Bi-Pb sulphosalts.

5.9A 1 = pure bismuthinite composition.

5.9B 1 = tetradymite ($\text{Bi}_2\text{Te}_2\text{S}$); 2 = wehrlite (BiTe);
3 = joseite ($\text{Bi}_4(\text{Te},\text{S})_3$); 4 = pilsenite (Bi_3Te_2);
5 = hedleyite ($\text{Bi}_{14}\text{Te}_6$). Arrow shows change
in composition of bismuth telluride with time.

5.9C 1 = hessite (Ag_2Te).

5.9D 1 = phase X ($\text{Ag}_2\text{Pb}_7\text{Bi}_{10}\text{S}_{23}$);
2 = "schirmerite" ($\text{AgPb}_2\text{Bi}_3\text{S}_7$);
3 = " " "
4 = heyrovskyite ($\text{Pb}_{4.6}\text{Bi}_2\text{S}_{7.6}$);
5 = lillianite ($\text{Pb}_3\text{Bi}_2\text{S}_6$);
6 = cosalite ($\text{Pb}_2\text{Bi}_2\text{S}_5$);
7 = galenobismutite (PbBi_2S_4);
8 = pavonite (AgBi_3S_5);
9 = matildite (AgBiS_2);

Composition of phases after Czamanske and Hall (1975). Solid circles represent composition of galena and associated Ag-Bi-Pb sulphosalt inclusions. Open circle represents composition of galena associated with unmixed Ag-telluride, Bi-telluride and native bismuth.

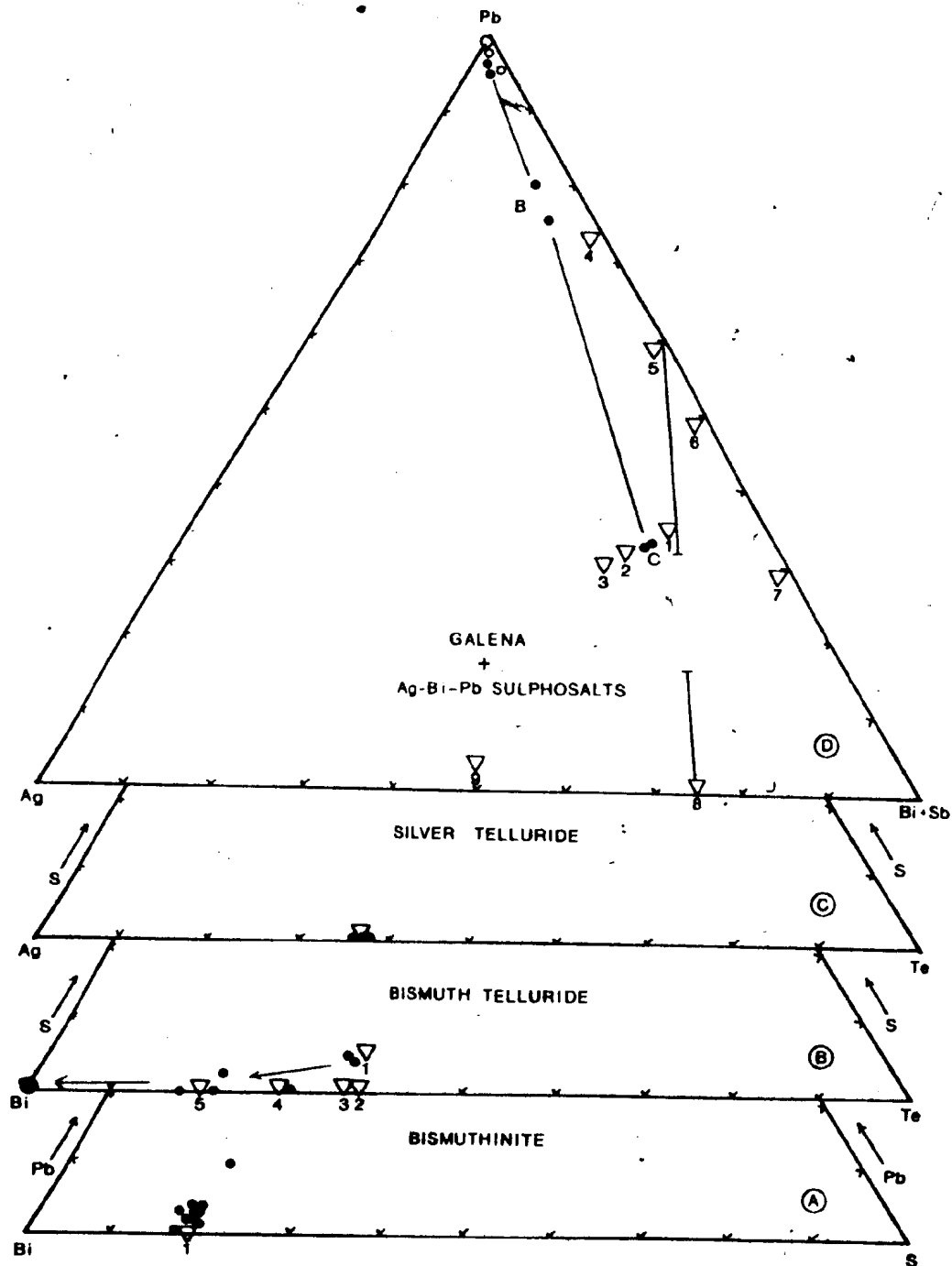
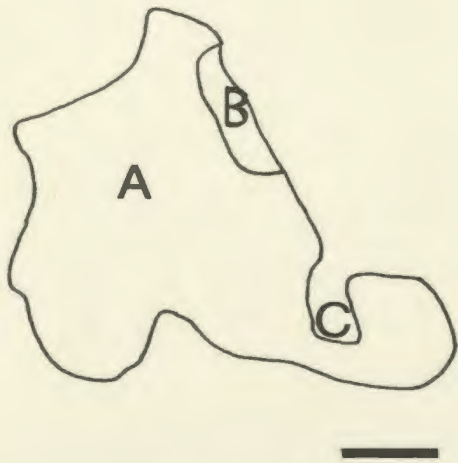


Plate 5.7

X-ray scan photographs of a galena inclusion in pyrite.
Sample 222, Vein #6.

- 5.7A For discussion of phases A,B,C refer to text. Bar
scale = 1 mm.
- 5.7B X-ray scan for Pb ($M\alpha$, PET crystal).
- 5.7C X-ray scan for Ag ($L\alpha$, PET crystal).
- 5.7D X-ray scan for Bi ($M\alpha$, PET crystal).

Plate 5.7



A



Plate 5.8

X-ray scan photographs of galena grains, sample 675, Vein #7.

- 5.8A Polished section photograph of galena grain showing whitish patches of unmixed native bismuth. Bar scale = 1 mm.
- 5.8B X-ray scan for Pb ($M\alpha$, PET crystal).
- 5.8C X-ray scan for Ag ($L\alpha$, PET crystal) reveals unmixed AgTe blebs within the galena grain.
- 5.8D X-ray scan for Bi ($M\alpha$, PET crystal) showing exsolution blebs of native bismuth in galena.

Plate 5·8

A



B



C



D



Plate 5.9

X-ray scan photographs (A-B) of a grain of intergrown bismuthinite and galena, sample 644B, Vein #10. Bar scale = 1 mm.

5.9 X-ray scan for Bi ($M\alpha$, PET crystal) revealing distribution of bismuthinite.

5.9B X-ray scan for Pb ($M\alpha$, PET crystal) revealing distribution of galena.

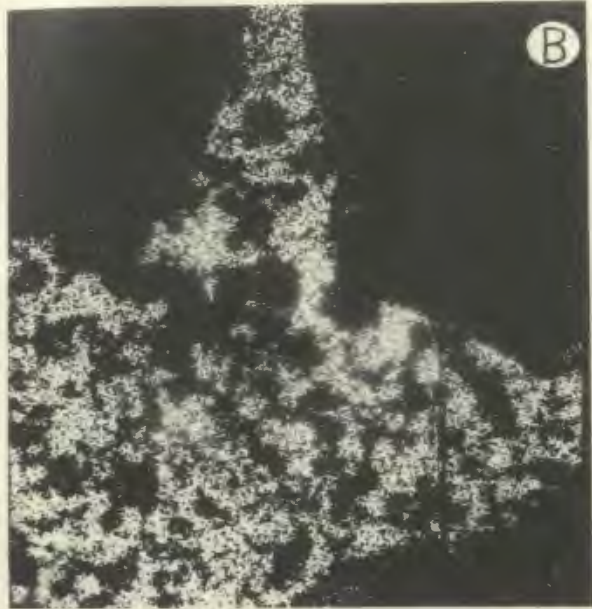
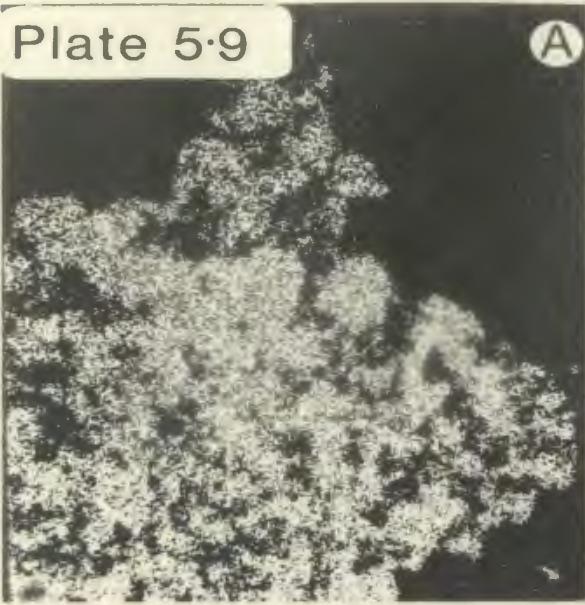
X-ray scan photographs (C-E) of a grain of intergrown Ag- and Bi-telluride. Sample 21. Bar scale = 1 mm.

5.9C X-ray scan for Te ($L\alpha$, PET crystal).

5.9D X-ray scan for Bi ($M\alpha$, PET crystal) showing the distribution of bismuth telluride, Hedleyite ($Bi_{14}Te_6$).

5.9E X-ray scan for Ag ($L\alpha$, PET crystal) showing distribution of silver telluride, hessite (Ag_2Te).

Plate 5.9



bismuthinite (Bi_2S_3). The structures of the end members are similar and Pb and Cu readily substitute for Bi in bismuthinite (Springer, 1971). The higher concentrations of Pb and Cu in bismuthinites from Q-b veins probably indicate a higher temperature of formation than the bismuthinite from Vein #10 (c.f. Chang and Bever, 1972).

Galena is restricted to northern sections of Vein #10, Vein #6 and Galena #1 Vein and is characterised by high silver and occasionally high bismuth contents (Table 5.4). Both galena and bismuthinite have been variably affected by an annealing event resulting from deposition of chalcopyrite. This annealing episode caused unmixing of Bi-, Ag- and Pb-sulphosalts as well as tellurides and native bismuth from these minerals. Because chalcopyrite is more common in northern sections of the vein system, galena appears to have been annealed to a greater extent than bismuthinite. Analyses (Table 5.5; Figure 5.9B) indicate that increasing degrees of annealing promote unmixing of sulphosalts and tellurides with increasing Bi/Te ratios (i.e. $\text{Bi}_2\text{Te}_2\text{S} \rightarrow \text{Bi}_3\text{Te}_2 \rightarrow \text{Bi}_{14}\text{Te}_6 \rightarrow \text{Bi}$).

Galena inclusions in pyrite from Vein #6 which appear to have been isolated from much of the annealing, have characteristically higher Ag and Bi contents than those in contact with chalcopyrite in the same vein (c.f. Table 5.6 with Table 5.4). X-ray scan photographs reveal that these silver- and bismuth-rich galenas contain Ag-Bi-Pb sulphosalts as inclusions whose orientation suggests that they are

unmixed lamellae (Plate 5.7). Their compositions are shown in Table 5.6 and plotted in Figure 5.9D. They do not correspond to any known minerals although heyrovskyite ($\text{Pb}_{4.6}\text{Bi}_2\text{S}_{7.6}$) is close in composition to sulphosalt B while the phase X and "schirmerite" of Karup-Moller (1972, 1973) are chemically comparable to sulphosalt C.

The silver and bismuth contents of the galena associated with the sulphosalts appear to be evenly distributed within the grains (Plate 5.8 C,D) and do not appear to occur as submicroscopic lamellae of silver and bismuth sulphosalts. Mineralogical studies suggest that high bismuth contents are correlatable with high temperatures of formation (Malakhov, 1969; Craig, 1967). Galenas that are partially replaced by chalcopyrite have low or negligible bismuth contents (Table 5.4) a result of unmixing of this component by annealing. In fact native bismuth (and hessite) occur as exsolution blebs in these grains (Plate 5.8). Associated chalcopyrite (Table 5.7) have unusually high values of lead, bismuth and silver (and occasionally gold). This might suggest that the chalcopyrite is incorporating these elements in its structure during replacement of galena and bismuthinite.

Galena from Galena #1 Vein does not contain any bismuth or silver in solid solution (Table 5.4) but unpublished assays of the vein and altered wall rock indicate high (3.0 - 4.0 oz/ton) silver contents (Table 5.8). The silver assays appear to correlate with lead assays in all but one case, suggesting that the galena hosts the silver mineral-

isation. Only one analysis (anal. 12, Table 5.4) showed any indication of silver (and gold) but Gray (1958) reported that minute laths of a grey anisotropic mineral were present in the galena. Etching with dilute HNO_3 revealed only that the coarse galena crystals were aggregates of small polygonal grains (i.e. annealed) but no silver-bearing inclusions were observed. Available data and the photographic evidence presented by Gray (1958) suggests, however, that the silver component of the Galena #1 Vein is attributable to small laths of a Ag-rich sulphosalt exsolved from galena and probably preserved along grain boundaries. It is interesting to note that a concentration of 0.22 wt% Ag in galena will give an assay of 0.6 oz/ton for each 1% Pb in the ore. Using these figures the first three assays from the Galena #1 Vein could be attributed to concentrations as low as 0.04 - 0.08 wt% Ag in galena.

The original high temperature mineralogy of the Bi-Pb-Ag mineralisation may be inferred from their present composition which is a result of unmixing during annealing. Given that the deposition of Q-b veins preceded formation of Q-s and Q + w vein types (Vein #10, #6), and the Q + g vein (Galena #1 Vein), then there is a regular change in the composition of individual Bi-Pb-Ag minerals with time and space in the vein system. This may be related to a progressive change in the chemistry of the hydrothermal fluid depositing these minerals.

An early Bi-rich fluid deposited bismuthinite (1, Figure

Table 5.3

Composition of Bismuthinite (Weight Percentages and Atomic Proportions)

Analysis	1	2	3	4	5	6	7	8	9	10	11	12
Sample	314	314	314	82	82	82	82B	707	707	353	214	644B
Fe	.02	-	.03	.07	.04	-	.06	.22	.08	-	-	-
Cu	.92	2.22	.89	1.11	.65	1.05	.52	.59	.45	.58	.29	-
S	18.38	18.36	18.15	17.08	18.16	18.01	16.4	18.75	17.57	18.50	18.23	17.35
Pb	3.91	9.02	3.16	3.93	2.30	3.04	3.07	1.52	2.08	1.89	1.38	.51
Bi	75.27	69.41	76.77	76.28	76.67	77.92	79.31	78.1	78.54	77.86	80.30	80.81
Ag	-	-	-	.18	-	-	.03	-	-	-	.05	-
Sb	.13	.16	.17	.07	.09	.07	.06	.08	.11	-	-	.05
Zn	.09	-	.02	.07	.05	-	.04	.08	.05	-	.06	.06
Se	.11	.11	.07	.12	.13	.06	.06	.08	.14	.13	.04	-
Te	n.d.	n.d.	-	-	-	-	.03	n.d.	n.d.	-	-	-
Au	-	-	-	-	-	-	-	.09	-	-	-	.07
Total	98.83	99.26	99.31	98.90	98.90	100.16	99.61	99.52	99.02	99.03	100.48	98.87
Fe	-	-	.004	.007	.004	-	.004	.02	.008	-	-	-
Cu	.074	.176	.074	.098	.054	.086	.043	.048	.039	.047	.024	-
S	2.950	2.902	2.930	2.995	2.991	2.900	2.789	2.994	2.990	2.970	2.997	2.997
Pb	.098	.223	.078	.083	.059	.074	.082	.038	.055	.05	.035	.014
Bi	1.860	1.684	1.902	2.065	1.937	1.926	2.066	1.914	2.051	1.920	2.025	2.141
Ag	-	-	-	-	-	-	-	-	-	-	.002	-
Sb	.008	.008	.008	.008	.004	.004	.004	.003	.005	-	-	.002
Zn	.008	-	-	.002	.004	-	.004	.006	.004	-	.005	.005
Se	.008	.008	.004	.005	.004	.004	.004	.005	.010	.004	.026	-
Te	n.d.	-	-	-	-	-	.004	-	-	-	-	-
Au	-	-	-	-	-	-	-	.002	0	0	0	.005
Total	5.000	5.000	5.004	5.263	5.062	4.996	4.996	5.030	5.162	5.000	5.114	4.838

Table 5.4

Composition of Galena (Weight Percentages and Atomic Proportions)

Analysis Sample	1 392	2 644B	3 675	4 675	5 675	6 V6C	7 V6C	8 V6C	9 528	10 529	11 529	12 528
Fe	.04	.14	.02	-	.02	.05	.14	.12	.06	.34	-	.03
Cu	-	-	-	0.01	.04	-	.05	-	-	.03	-	-
S	13.13	13.02	12.55	13.62	13.57	13.45	12.96	13.16	13.50	13.42	13.04	13.33
Pb	85.34	85.87	86.10	85.68	83.25	85.07	85.01	82.34	85.38	85.10	87.04	84.00
Bi	-	-	-	-	.79	-	-	3.16	-	-	-	-
Ag	.18	.02	.61	.34	1.09	.38	.41	.9	-	-	-	.06
Sb	-	-	.02	.01	.01	-	-	.05	.05	.07	.05	.01
Zn	.04	.08	-	-	.05	-	-	.04	.04	.12	-	.02
Se	.04	.32	.03	-	-	.02	-	.04	-	.05	.02	-
Te	-	-	n.d.	n.d.	n.d.	.07	.04	.02	-	-	-	n.d.
Au	-	-	-	-	.10	-	-	.17	-	-	-	.39
Total	99.10	99.46	99.32	99.80	98.91	99.04	98.59	100.00	99.04	99.13	100.75	97.84
Fe	-	.008	-	-	-	-	.008	.004	.004	.016	-	-
Cu	-	-	-	-	-	-	-	-	-	-	-	-
S	.988	.980	1.000	1.012	1.008	1.004	.984	.980	1.008	.996	.980	1.008
Pb	.992	1.000	.984	.977	.957	.984	1.000	.949	.988	.980	1.020	.984
Bi	-	-	-	-	.008	-	-	.035	-	-	-	-
Ag	.004	-	.012	.008	.023	.008	.008	.02	-	-	-	-
Sb	-	-	-	-	-	-	-	-	-	-	-	-
Zn	-	.004	-	-	.004	-	-	-	-	.004	-	-
Se	.012	.012	-	-	-	-	-	-	-	-	-	-
Te	-	-	-	-	-	-	-	-	-	-	-	-
Au	-	-	-	-	-	-	-	.004	-	-	-	.004
Total	1.996	2.004	2.000	1.996	2.000	1.996	2.000	1.990	2.000	1.996	2.000	1.996

Table 5.5

Composition of Tellurides, Sulphosalts and Native Bismuth (Weight Percentages)

	1 314	2 314	3 151B	4 644B	5 21	6 V6C	7 151B	8 21	9 23	10 214	11 392
Fe	-	-	-	.02	.04	.24	.03	.07	.01	-	.09
Cu	.05	-	-	-	.08	-	-	-	.11	-	-
S	4.80	4.78	-	.02	2.73	.03	.09	.13	.10	-	.43
Pb	.08	.15	.39	.11	.17	-	-	-	.06	.31	1.86
Bi	59.22	59.16	68.24	76.15	74.90	80.04	.13	-	.16	99.72	96.71
Ag	.57	.45	.03	-	-	.09	63.63	63.34	62.99	-	-
Sb	.23	.27	.22	.14	.18	.13	.17	.25	.27	-	-
Zn	.05	.01	-	.07	.07	.02	.06	-	.04	-	.06
Se	.17	.18	.02	.23	.2	.02	.04	-	-	-	-
Te	33.91	34.19	30.13	21.41	21.28	17.98	37.06	36.44	37.01	-	-
Au	-	-	-	-	.13	-	-	-	.14	-	-
Total	00.26	99.21	99.07	98.16	99.79	98.55	101.23	100.23	100.89	100.03	99.16

- 1-2 Tetradymite, Muscovite selvedged vein (Q-b).
 3 Pilsenite, Adit level Vein #10, southern section.
 4-5 Hedleyite, Adit level Vein #10, faulted section.
 6 Hedleyite, Vein #6.
 7-9 Hessite, Adit level Vein #10, southern section.
 10-11 Native bismuth, Vein #10, Adit level.

Table 5.6

Composition of Galena
and Two Exsolved Ag-Bi-Pb Sulphosalts
(Weight Percentages and Atomic Proportions)

	A	A	B	B	C	C
Fe	.20	.18	.55	1.25	1.08	2.03
Cu	-	-	-	.02	-	-
S	13.21	13.34	14.96	14.07	15.99	17.06
Pb	82.47	83.12	64.09	66.55	27.68	25.63
Bi	1.63	1.59	16.38	12.89	43.92	40.88
Ag	1.36	1.48	4.22	3.41	12.00	11.61
Sb	.05	.05	-	-	.07	.07
Zn	-	.04	.09	-	.07	.10
Se	.07	.05	.02	-	.06	-
Te	n.d.	n.d.	n.d.	n.d.	n.d.	-
Au	.19	-	.26	-	-	-
Total	99.18	99.85	100.58	98.28	100.87	97.37

Fe	.008	.008	.023	.051	.039	.074
Cu	-	-	-	-	-	-
S	.984	.988	1.031	1.000	1.023	1.066
Pb	.953	.953	.684	.734	.273	.246
Bi	.02	.020	.172	.141	.430	.391
Ag	.031	.031	.086	.070	.227	.215
Sb	-	-	-	-	-	-
Zn	-	-	.004	-	.004	.004
Se	.004	-	-	-	-	-
Te	-	-	-	-	-	-
Au	.004	-	.004	-	-	-
Total	2.004	2.000	2.004	1.996	1.996	1.996

Analyses from sample 222, Vein #6. ♦

Table 5.7
Composition of Chalcopyrite Associated With
Silver and Bismuth Tellurides

Analysis Sample	1 222	2 222	3 21	4 98A	5 23
Fe	30.93	28.89	30.43	30.77	30.66
Cu	31.87	27.42	39.94	32.69	33.50
S	34.21	31.43	34.36	34.63	34.11
Pb	.23	8.29	.05	.08	.09
Bi	.11	1.93	.29	.32	.20
Ag	.07	.46	.27	.04	.10
Sb	-	.05	.02	.03	-
Zn	.07	-	.13	-	-
Se	-	.03	-	-	.01
Te	n.d.	n.d.	n.d.	n.d.	.06
Au	.13	.05	-	-	.11
Total	97.61	98.51	98.50	98.55	98.84

Fe	1.043	1.043	1.020	1.024	1.023
Cu	.945	.871	.969	.960	.984
S	2.008	1.977	2.000	2.008	1.984
Pb	.004	.082	-	-	-
Bi	-	.020	.004	-	-
Ag	-	.008	.004	-	-
Sb	-	-	-	-	-
Zn	-	-	.004	-	-
Se	-	-	-	-	-
Te	-	-	-	-	-
Au	-	-	-	-	-
Total	4.000	4.000	4.000	3.992	3.992

Table 5.8
Assays of Galena #1 Vein from Bahyrycz (1957)

		Gold oz/ton	Silver oz/ton	Pb%	Cu%	Zn%	Fe%
S #1	WR	2.90	1.30	12.3	.2	3.9	7.4
S #2	Vein	.04	4.2	18.5	.3	3.7	10.8
S #3	Vein	.04	2.6	13.9	Tr	1.4	6.5
S #4	Vein	.04	3.0	4.0	.1	2.4	6.9

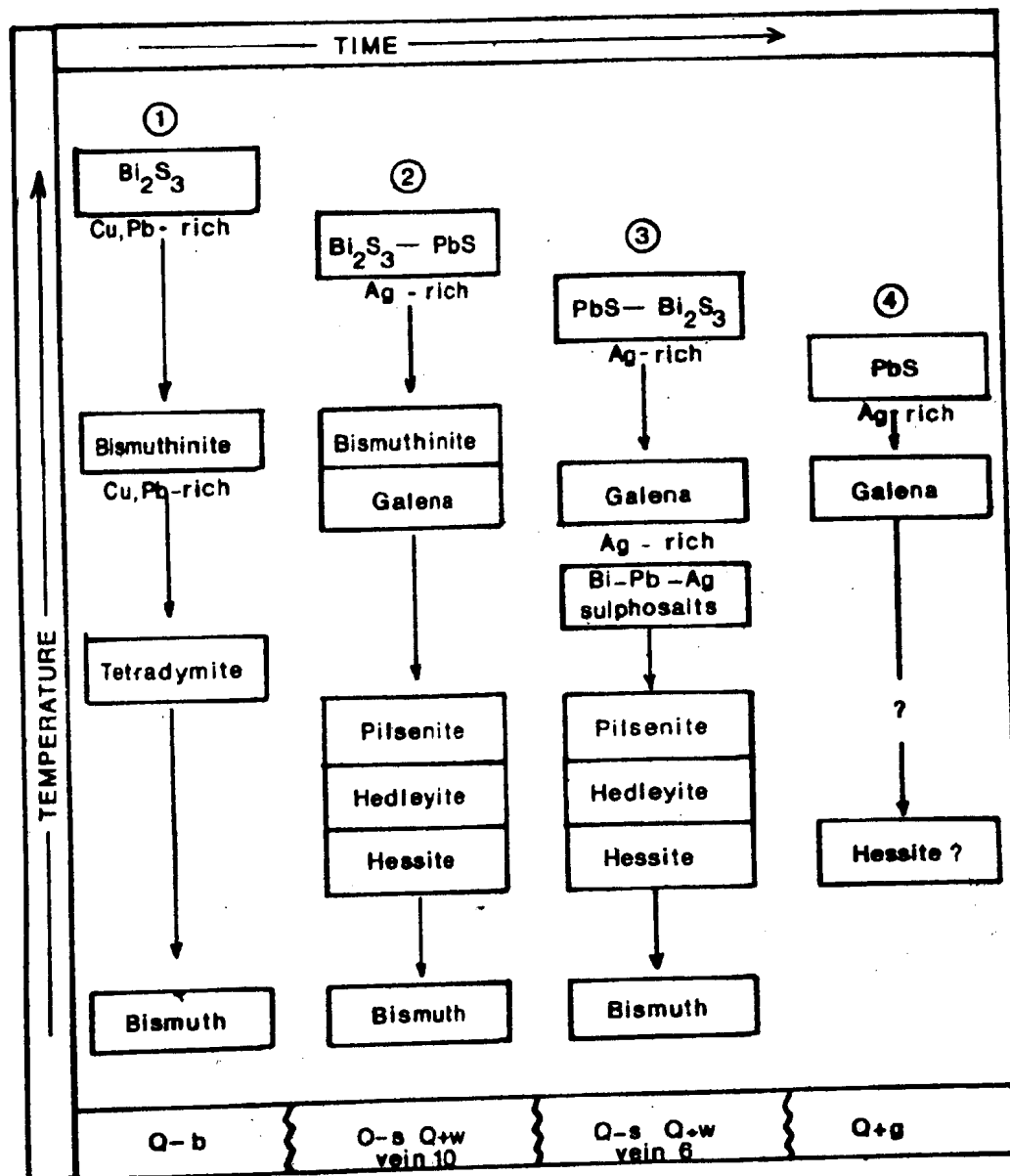


Figure 5.10 Summary of the distribution of sulphosalts, tellurides and native bismuth, and their unmixing sequence from Bi, Ag, Pb-rich precursors.

5.10) rich in Cu and Pb and was followed by the deposition of bismuthinite with progressively lower concentrations of Cu and Pb. A later (and lower temperature) Bi- and Pb-rich fluid (2, Figure 5.10) deposited a complex Bi-Pb sulphosalt (perhaps cosalite, $Pb_2Bi_2S_5$) which broke down at temperatures below that of its formation to a myrmekitic intergrowth of galena and bismuthinite. Finally a Pb-rich fluid (3, Figure 5.10), containing Bi and Ag, deposited galena rich in these elements. However, with falling temperature this fluid deposited galena with progressively lower concentrations of Bi and Ag (4, Figure 5.10). All these minerals were subjected to annealing which modified their composition by unmixing phases rich in Bi, Ag and Te.

The stability of the Pb-Bi sulphosalts has been studied by Van Hook (1960) and Craig (1967). There are three main Pb-Bi sulphosalts in the $PbS-Bi_2S_3$ system (Figure 5.11A): phase II with composition $Pb_{4.6}Bi_2S_{7.6}$; phase III - $Pb_{2.7}Bi_2S_{5.7}$; phase IV - $Pb_{0.95}Bi_2S_{3.95}$, which have been shown to correspond to the natural minerals heyrovskyite (Klominsky *et al.*, 1971), lillianite (Salanci and Moh, 1969), and galeno-bismutite (Craig, 1967) respectively. A fourth phase (labelled V, Figure 5.11C) is a high temperature Pb-Bi sulphosalt with a narrow range of stability and is not recorded in nature.

The $PbS-Bi_2S_2$ phase equilibria predict that galena would be followed paragenetically by phase II, phase III etc., and finally by bismuthinite (Craig, 1967; Chang and

Bever, 1973). Chang and Bever (1973) present evidence from a few ore deposits (Klominsky *et al.*, 1971) to illustrate this sequence (Figure 5.11C) which is opposite to that shown at Grey River (Figure 5.11B). The theoretical paragenesis also contravenes the general paragenetic schemes proposed by Lindgren (1933).

There are several possible reasons for the deviation from the idealised sequence produced from the pure binary $\text{PbS-Bi}_2\text{S}_3$ system. These include 1) the complex overlapping of deposition of mineral species primarily as a consequence of essentially simultaneous crystallisation; 2) fluctuations in temperature and/or chemical compositions of the fluid; 3) misinterpretation of ore textures. The second reason is favoured for the Grey River situation from fluid inclusion evidence (presented below) that shows a decrease in temperature between Q-b, Q-s, and Q + w vein types.

On the basis of thermodynamic and experimental data Mintser (1979) has suggested that the presence of bismuthinite in a mineral assemblage indicates a weak acid to neutral nature of the hydrothermal fluid. This is well illustrated by the predominance of this mineral in high temperature ores, especially greisens, where bismuth enrichment is characteristic (Popova *et al.*, 1966). An increase in alkalinity leads to a progressive change in the composition of bismuth minerals deposited from a hydrothermal fluid. This is expressed by a change in the nature of ore mineralisation with time, the general sequence being bismuthinite →

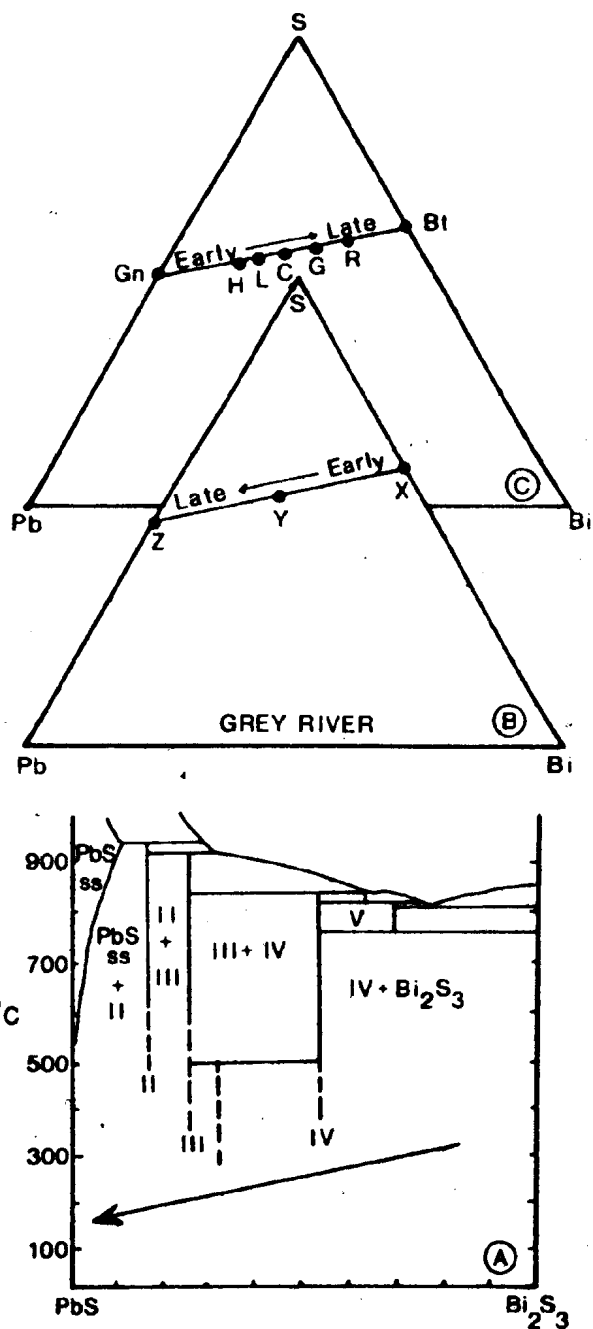


Figure 5.11 Phase equilibria and paragenesis in the $\text{PbS-Bi}_2\text{S}_3$ system (after Craig, 1967). See text for explanation of compositional relationships. Figure 5.11C after Chang and Bever (1973).

bismuth \rightarrow Bi-Pb complex sulphide \rightarrow Cu-Pb-Bi complex sulphide \rightarrow Pb-Cu-Ag-Bi complex sulphide with increased alkalinity (Mintser, 1979).

Such a sequence is observed in the quartz-wolframite Kara-Oba deposit (Popova *et al.*, 1966; Mintser, 1979) where successively deposited bismuth-lead sulphides and sulphosalts have progressively higher $\text{PbS}/\text{Bi}_2\text{S}_3$ ratios both within each separate stage of the mineralisation and throughout the entire hydrothermal process. The paragenetic sequence bismuthinite \rightarrow Bi-Pb complex sulphide \rightarrow Pb (Ag-Bi) sulphide observed at Grey River might also suggest that the hydrothermal fluid became more alkaline with time.

5.10.2 Tungstates

Variations in colour of wolframite crystals from black, in Veins #1, #4, #5 and greisen, to brown in Veins #10 and #6 suggest that there may be a change in composition from ferberite to huebnerite within the vein system at Grey River. Twenty-seven wolframites were analysed for Mn/Fe ratio by an X-ray diffraction method described by Sasaki (1959) and Foster (1973) which is outlined in Appendix A.2.6. Results indicate a range in composition from 40-78% MnWO_4 between Vein #1 and Vein #6 i.e. from south to north in the vein system (Appendix B.4). More extensive data were obtained by electron microprobe analysis (Appendix B.2) and confirm the compositional variation shown by X-ray diffraction methods.

Wolframite from Veins #1, #4 and #5 and from the greisen

envelopes of Vein #10 (Figure 5.12) contain more Fe than Mn with the Mn/Fe ratio (huebnerite/ferberite ratio) falling in the range 0.6 - 1.23 but clustered dominantly around 0.8. Sample 79-25 (Figure 5.12A) is from a wolframite-bearing vein on strike with Vein #1 but outcropping just south of Long Pond (see inset Figure 5.12). The wolframite from this vein has a substantially higher Mn/Fe ratio than wolframite from Vein #1 and might suggest that the Mn concentration of wolframite is increasing from south to north. This is substantiated by analyses from Vein #10 wolframite whose Mn/Fe ratios vary from 1.0 - 2.3 (Figure 5.12).

The Mn/Fe ratio increases from the southern exposures of Vein #10 (sample 707, Mn/Fe = 1) to the most northerly section of the vein (faulted section, adit level) where sample 651 has a Mn/Fe ratio of 2.19. There is no substantial difference in Mn/Fe ratio of wolframites between adit level (approximately sea level) and surface (250 m) exposures of Vein #10. Vein #6 wolframites have a much wider range of Mn/Fe ratio from 2.0 to 9.0, the highest value being close to the pure huebnerite composition (Figure 5.12).

Compositional variations in wolframite have been recorded on a regional scale (Groves and Baker, 1972), within single ore deposits (Ganeev and Sechina, 1960), and even within single crystals (Churikov, 1959). Many workers have suggested that such compositional variations indicate changes in the temperature of formation. However, the data are contradictory and the Mn/Fe ratio may not be used reliably

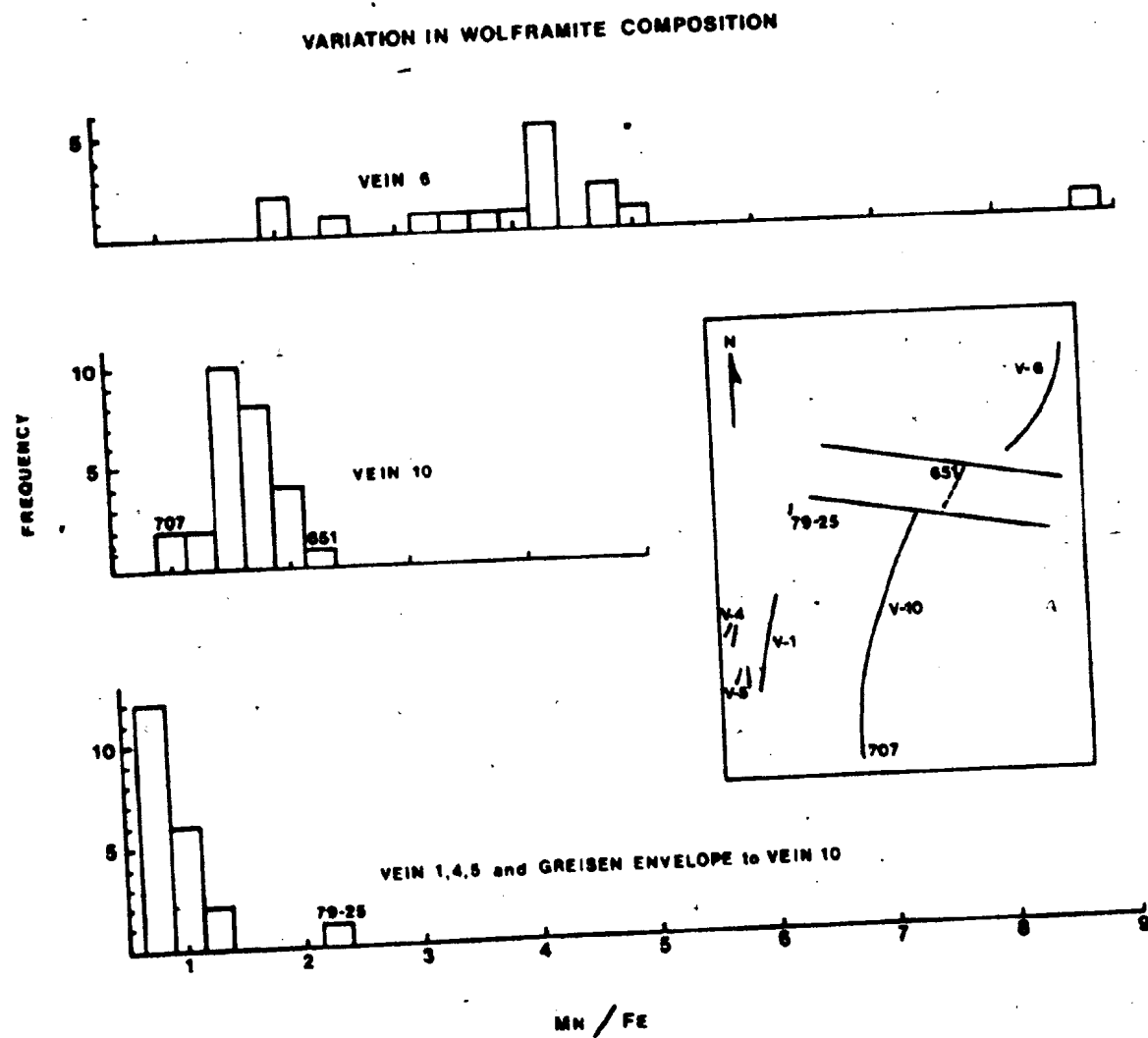


Figure 5.12 Variation in wolframite composition.

as a geothermometer (Taylor and Hosking, 1970; Clark, 1970; Groves and Baker, 1972). Hsu (1976) showed that neither $\{O_2\}$ nor $\{S_2\}$ exert any noticable influence on wolframite composition and suggested that experimental work on silicotungstic acid (Gundlach, 1967) indicated that pH is the most important factor.

Recently Horner (1979) provided experimental data (Figure 5.13A, B) on the solubility and hydrolysis of wolframite which showed that pH and temperature are the main controls of wolframite composition. Under isothermal conditions a change in wolframite composition is promoted by a change in pH. Horner showed that Fe-rich wolframite is deposited from acid solutions while Mn-rich wolframite forms under neutral to alkaline conditions. In a fluid of constant cation concentration wolframite compositions become more ferruginous with falling temperature.

At Grey River, wolframite crystallised at much the same temperature (approximately 280°C) throughout the vein system (see fluid inclusion evidence), which suggests that pH was the dominant control with regard to their composition. This implies that the pH of the hydrothermal fluid changed from acid to alkaline between Veins #1, #4, #5 and Vein #10, and Vein #6, and thus with time.

In hydrothermal vein systems, pH is commonly buffered by wall rock reactions (Helgeson, 1979) and thermodynamic calculations (Horner, 1979) show that pH conditions suited for muscovite deposition in hydrothermal solutions are

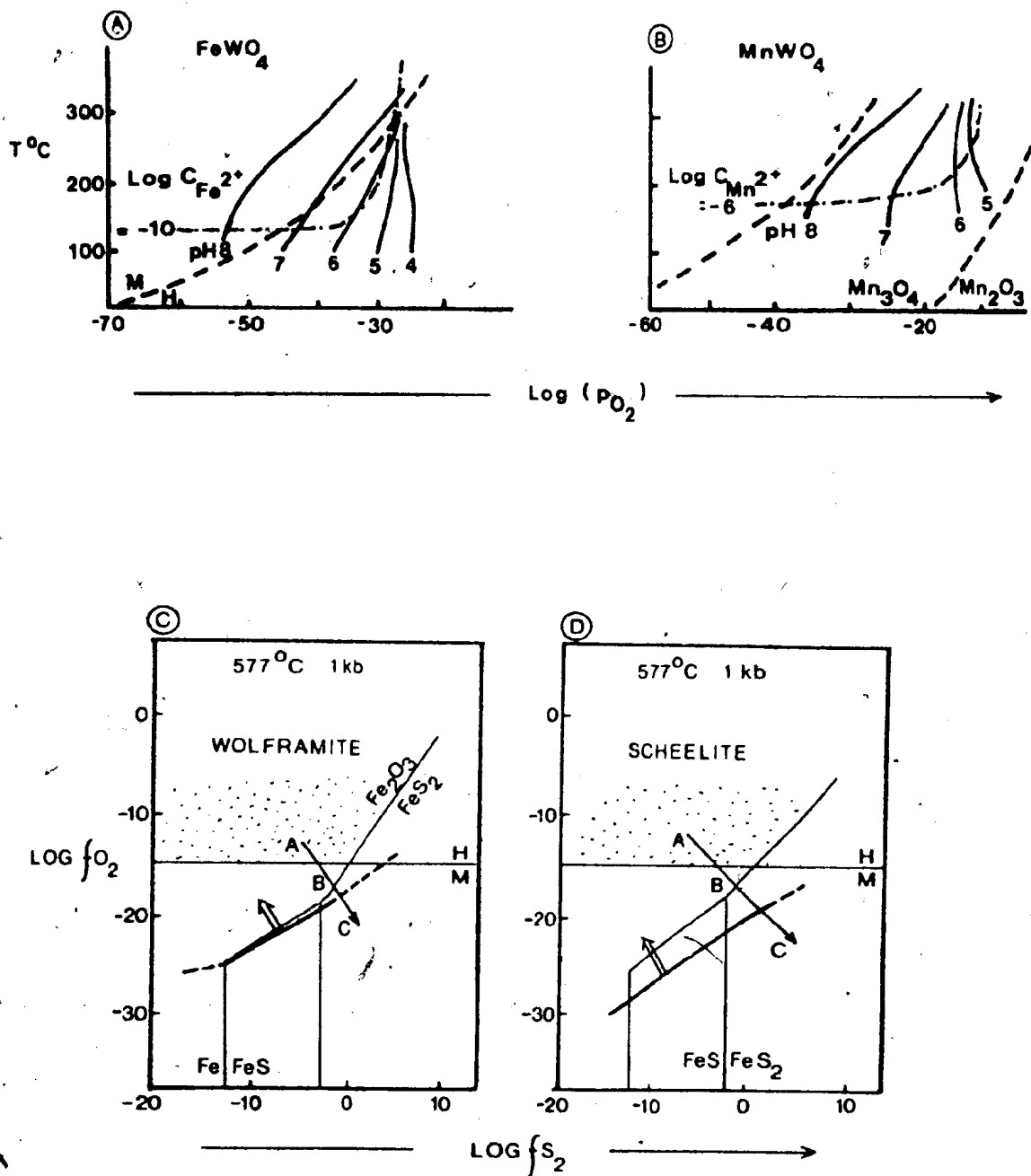


Figure 5.13 The effect of T , pH , O_2 , S_2 on wolframite and scheelite composition. Figure 5.13A,B from Horner (1979); Figure 5.13C,D from Hsu (1976, 1977).

identical with conditions promoting deposition of Fe-rich wolframite. Wolframite from the greisen (muscovite-rich) envelope of Vein #10 is ferruginous, and this supports Horner's thermodynamic calculations. It is interesting that wolframite from central vein portions of Vein #10 are richer in Mn than wolframite from the greisen surrounding the vein. This might suggest that the pH of hydrothermal fluids injected earliest into the vein fracture was buffered by wall rock reactions but with repeated reopening of the vein fracture subsequent injections were isolated from the wall rock by pre-existing (unreactive) vein material.

Fluid inclusion evidence (Chapter 7) shows firstly that sudden decreases in the content of CO_2 in the hydrothermal fluid (and temperature) promoted deposition of wolframite, and secondly that CO_2 concentrations in the fluid were gradually decreased with time. Loss of dissolved CO_2 from a hydrothermal fluid would have a marked effect on the pH of the fluid and would result in changes from acid to alkaline conditions. Thus in the Grey River hydrothermal system pH may have been dominantly controlled by progressive CO_2 loss rather than wall rock alteration, especially in veins characterised by multiple injection of hydrothermal fluid.

5.11 PHYSICO-CHEMICAL PARAMETERS OF ORE DEPOSITION

Temperature:

Ore minerals are generally poor geothermometers (Kelly and Turneaure, 1970) because of their relative ease of

equilibration at lower temperatures. Even relative indications of temperature from compositional data are misleading or contradictory (e.g. Mn/Fe ratio of wolframite, Hsu, 1976), however sulphide invariant points occasionally yield useful temperature information (Barton and Skinner, 1979).

The Bi-Pb-Ag mineralogy of the Grey River Prospect is a function of subsolidus reactions which are not experimentally determined for low temperatures. Higher temperature liquidus and subsolidus relationships are better understood and can often provide upper limits on the temperature of formation. Liquidus relationships for native bismuth and tetradymite suggest a maximum temperature range of 266° - 581°C (Abrikosov and Bankina, 1957; Glatz, 1967). Comparison of fluid inclusion data and paragenesis suggests, however, that the sulphide and telluride minerals were formed at temperatures below 300°C .

Pressure:

The Grey River prospect does not provide suitable sulphide mineralogy for evaluation of pressure conditions. Sphalerite geobarometry is negated by obvious disequilibrium relations between pyrrhotite-pyrite-sphalerite and the compositional effect of chalcopyrite associated with sphalerite (Scott, 1976).

pH:

The pH conditions of the hydrothermal fluid may be inferred from compositional and stability data for tungstates

and sulphides (Figure 5.14). Chemical variation in wolframite imply that the pH of the hydrothermal fluid increased with time and is supported by bismuthinite-galena relationships.

Fluctuations in pH occurred in each vein type after deposition of early vein minerals such as quartz, wolframite and the early sulphides. This is suggested by the common occurrence of pyrite altered to marcasite. Pyrite is formed under a variety of conditions while marcasite formation is subjected to stricter limitations (Blain and Andrews, 1977). Hydrothermal laboratory experiments have shown that the formation of pyrite is favoured at elevated temperatures in neutral and slightly alkaline solutions while marcasite forms in colder more acidic solutions (Berner, 1964).

Carbonate minerals have retrograde solubility and in general precipitate under low P_{CO_2} (high pH) conditions (Holland, 1979). The occurrence then of siderite as lamellar intergrowths with marcasite is equivocal and suggests that either marcasite (primary) and siderite precipitated under similar conditions (high pH) or that the marcasite formed by alteration of pyrrhotite under low pH conditions, with the carbonates a later feature. The latter mechanism might be favoured, for during alteration of pyrrhotite shrinkage cracks are developed (Blain and Andrews, 1977) which might be filled with siderite with increasing alkalinity of the solution.

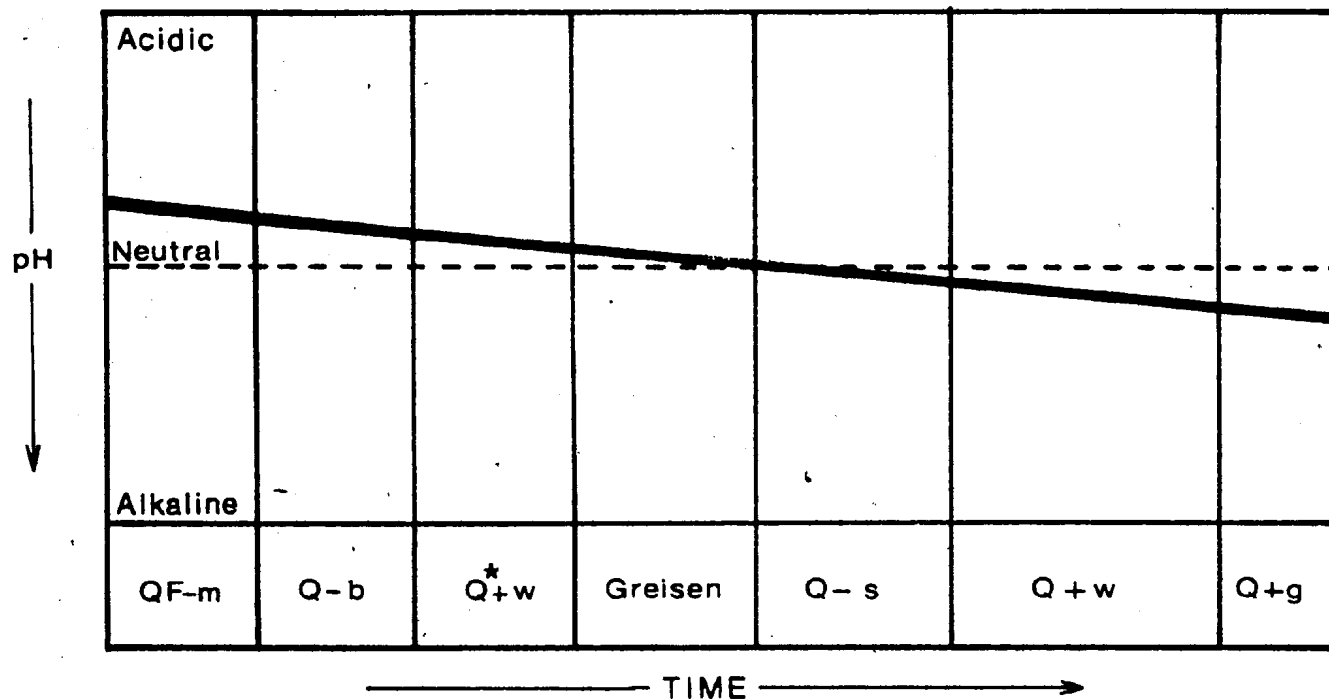


Figure 5.14 Inferred pH conditions of the Grey River hydrothermal fluid during deposition of early vein minerals from composition and stability relationships of tungstates and sulphides.

Oxygen and sulphur fugacities:

The stability fields of ferberite and huebnerite do not differ appreciably in the presence of both oxygen and sulphur (Hsu, 1976) and wolframite of any composition will be stable under $f_{O_2} - f_{S_2}$ conditions common in hydrothermal environments (Figure 5.13C). The fact that hematite is deposited with wolframite at Grey River indicates that the $f_{O_2} - f_{S_2}$ conditions that prevailed during deposition of the latter fall in the shaded region of Figure 5.13C. Those values are not absolute however, as the equilibrium curves were produced from experimental pressure-temperature conditions not directly applicable to the Grey River situation. With decreasing temperature, the position of the equilibrium curves will shift but their relationship to solid buffer assemblages will not be greatly affected (Hsu, 1976). The effect of pressure is negligible due to the low ΔV 's of the reactions involved, but with decreasing temperature wolframite and hematite will probably be stable to lower oxygen fugacities.

A characteristic feature at Grey River is the universal partial alteration of wolframite to scheelite. The $f_{O_2} - f_{S_2}$ stability field of scheelite is much wider than that of wolframite (Figure 5.13D) and is stable to lower f_{O_2} and higher f_{S_2} than the latter (Hsu, 1977). This is consistent with the common association of molybdenite with scheelite in skarn deposits. The deposition of sulphides after tungstates at Grey River suggests that during the evolution of the hydrothermal fluid f_{O_2} decreased while f_{S_2} increased

possibly along some path such as A-C (Figure 5.13C, D).

Available textural evidence suggests that scheelite replacement occurred prior to the deposition of sulphides and thus must have formed under changing $\{O_2 - \{S_2$ conditions outside the stability field of wolframite and hematite but before conditions suitable for pyrite precipitation, that is position B on path A-C (Figure 5.13C,D). After deposition of wolframite the $Ca^{2+}/Fe^{2+} + Mn^{2+}$ ratio of the hydrothermal fluid would probably be high, which could promote the scheelitisation process.

5.12 SUMMARY

The tungsten mineralisation is contained within a hydrothermal vein system which postdates both the metamorphic rocks and the two phases of granitoid intrusion. A genetic link between the mineralisation and the Grey River granitoids is suggested by the characteristic autometasomatic alteration, quartz-rich segregations, and geochemical specialisation of the latter.

The hydrothermal veins range from tensional fractures and veinlets to quartz lodes showing much displacement of wall rock. This latter type is characteristic of the major veins of the area which display a multiple injection history as evidenced by their sheeted nature. Wall rock displacements, tension gashes in wall rock xenoliths, and slickensides on sheeted surfaces indicate that the lodes were formed by repeated opening and injection of mineralisation into open spaces created by differential movements of wall rock

during normal faulting. A stress analysis of the vein fracture system is similar to stress patterns induced by intrusion of a cupola and reinforces the suggestion of a hidden granitic body beneath the mineralisation.

Assay and structural data from the major lodes indicate that the tungsten mineralisation is structurally controlled by internal vein movements due to normal faulting, and is concentrated in portions of the veins that are thin and shallow dipping. Furthermore, the wall rock alteration is most intense in high grade areas of the lode and results from the greater shearing in shallow-dipping sections during vein movements.

The mineralisation may be divided into four main stages; the Early Stage characterised by deposition of quartz, feldspar, and molybdenite-bearing veins; the Composite Stage which is characterised by multiple injection of several vein types, two or more of which occur together as components of the major lodes; the Sulphide Stage which represents lower temperature deposition after the composite mineralisation; and the Late Stage represented by deposition of fluorite-calcite-barite veins in tensional fractures which have cross-cutting relationships with the preceding mineralisation.

Minerals with pegmatitic affinities (feldspar, beryl) occur in early formed veins that are concentrated in southern and south-western parts of the mineralised area. Higher temperature minerals such as molybdenite and bismuthinite

are also concentrated in southern exposures and give way to the north to lower temperature assemblages. Bismuth-bearing minerals are common almost throughout the vein types, bismuthinite being the Bi-bearing phase in early formed veins while later veins are characterised by Ag- and Bi-bearing galena, Ag- and Bi-tellurides and native bismuth. Wolframite composition varies spatially and temporally within the vein system being more Fe-rich in early formed veins while later and more northerly generations are characterised by Mn-rich wolframite.

During the composite vein stage in tungsten-bearing veins, quartz is generally precipitated at the same time as wolframite while sulphides are deposited after in vugs within the quartz. This is also true of non tungsten-bearing veins where sulphides are deposited later than quartz.

These and other features of the paragenesis indicate that early-formed higher temperature vein types occur in southern or southwestern parts of the mineralised area while the locus of successively younger and lower temperature veins moved towards the north (from metamorphic rocks to the megacrystic granite).

Physico-chemical parameters of ore deposition can be inferred from sulphide and tungstate phase equilibria. Chemical variation in the wolframite and bismuthinite-galena relations imply that the pH of the hydrothermal fluid increased with time although pH fluctuated after deposition of quartz (and wolframite) in each vein type during

deposition of later sulphide phases. Hematite-wolframite relationships restrict oxygen and sulphur fugacities to high f_{O_2} - low f_{S_2} condition during deposition of wolframite, while a falling f_{O_2}/f_{S_2} ratio and an increasing Ca^{+2} concentration possibly prompted replacement of wolframite by scheelite prior to the deposition of sulphide phases under low f_{O_2} - high f_{S_2} conditions.

CHAPTER 6

ALTERATION GEOCHEMISTRY

6.1 INTRODUCTION

Studies of hydrothermal alteration in mineral deposits are useful as both a guide to ore and as an indication of the character of the ore fluid. In North America conventional alteration terms such as propylitic, sericitic, etc. grew out of studies of porphyry copper deposits (Meyer and Hemley, 1967; Rose, 1970; Creasey, 1959) and essentially describe pervasive alteration although they may have a more local application. In the Grey River tungsten deposit wall rock alteration is localised around the vein system and is dominantly a greisenisation phenomenon.

Greisen is defined as a high temperature post-magmatic alteration of rocks by a residual magmatic fluid evolved from cooling alkali-rich granite intrusives (Shcherba, 1970 a,b). It is characterised by enrichment in Li, B, Be, F, rare-earths and rare-metals such as tungsten and tin (Hall, 1971; Boyle 1970). Greisen is a general term and includes many alteration types depending on original rock composition and intensity of alteration, although, phyllic (sericitic) alteration is dominant.

6.2 ALTERATION TYPES

At Grey River the hydrothermal alteration occurs in three principal stages (with subdivisions): 1) autometamorphism of the leucogranite; 2) greisenisation related to

hydrothermal vein formation; 3) clay alteration associated with fluorite-calcite-barite veins.

6.2.1 Autometasomatism

Alkaline Alteration: Alkali metasomatism affects the leucogranite dykes of the Grey River area. The geochemical features of the autometasomatism have been described above (Chapter 4) and essentially they involve the redistribution of alkalis and alkaline earths. This is evident as a development of secondary feldspar, i.e. microcline after orthoclase, and albite after calcic plagioclase. Also sericite and epidote are produced by alteration of plagioclase, and chlorite replaces biotite.

6.2.2 Greisenisation

Potassic Alteration: An essentially monomineralic zone, dominantly composed of muscovite, occurs as thin (<1 cm) selvages to quartz-bismuthinite (Q-b) and quartz-feldspar-molybdenite veins (QF-m) which are commonly tensional and show no displacement of wall rock. Strictly speaking these selvages may not have formed by alteration of wall rock, rather textural evidence suggests that they are the first products of deposition from the hydrothermal fluid. They are included here as an alteration type because of their position and their mineralogy which is characteristic of the more widely dispersed alteration zones. As well as muscovite, these selvages contain minor pyrite and scheelite (the latter considered to be secondary after wolframite).

Phyllic Alteration: Phyllic alteration is the most conspicuous alteration type of the greisen and is characterised by a sericite-quartz-pyrite-fluorite-scheelite-wolframite assemblage (sericite much more dominant than other phases). The alteration occurs as an envelope to the composite veins (#10 and #6 especially) and is most commonly developed in portions of the lodes that are shallow dipping and that contain high tungsten grades. The thickness of this alteration varies from a few centimeters up to 1.5 meters. Phyllic alteration is best developed in amphibolite wall rock but it occurs in deformed megacrystic granite, although in the latter quartz is dominant and the alteration might more correctly be termed silicic.

Biotitic Alteration: This alteration type sporadically developed in the amphibolitic wall rock of vein #10, is gradational with the phyllic alteration. It forms an outer halo to the phyllic alteration, which is closest to the vein, and is characterised by the development of hydrothermal biotite (pleochroic brown to light brown) after hornblende. Minor accessories include sericite, fluorite and pyrite with veinlets of epidote and chlorite. This hydrothermal biotite is itself replaced by sericite in zones of more intense phyllic alteration. Scheelite or wolframite have not been observed. The biotitic alteration may attain a thickness of up to 0.5 m although it is generally much thinner.

Calcic Alteration: A soft, greenish-white altered wall rock composed of carbonate and sericite is sporadically

developed as an outer alteration halo to the phyllic alteration from which it grades. Away from the vein it is gradational with biotitic or unaltered wall rock. Minor amounts of fluorite and pyrite are also present in this alteration type which can be up to 0.5 m wide.

Silicic Alteration: Silicic alteration is found as a halo to the composite Vein #6 and it affects deformed megacrystic granite wall rock. The altered granite is a bleached white to greenish-white colour in outcrop and much of the silicification is due to development of a network of quartz veinlets. As well as quartz, the altered wall rock contains sericite and pyrite with minor fluorite and chlorite. Fluorite is noticeably less abundant than in the phyllic altered amphibolitic wall rock of Vein #10.

Silicic alteration is quite pervasive in the deformed megacrystic granite wall rock occurring up to 10 m away from the composite Vein #6. Zones of silicification not associated with quartz veins are also observed in drill core. Small tensional fractures in these zones appear to have provided channelways for the hydrothermal fluid.

A diagrammatic representation of the types and association of the alteration halos formed during greisenisation is shown in Figure 6.1.

6.2.3 Clay Alteration

Argillic Alteration: The wall rock around the fluorite-calcite-barite veins (F-cb) is commonly altered to a soft clay-rich rock type. These veins postdate the formation of

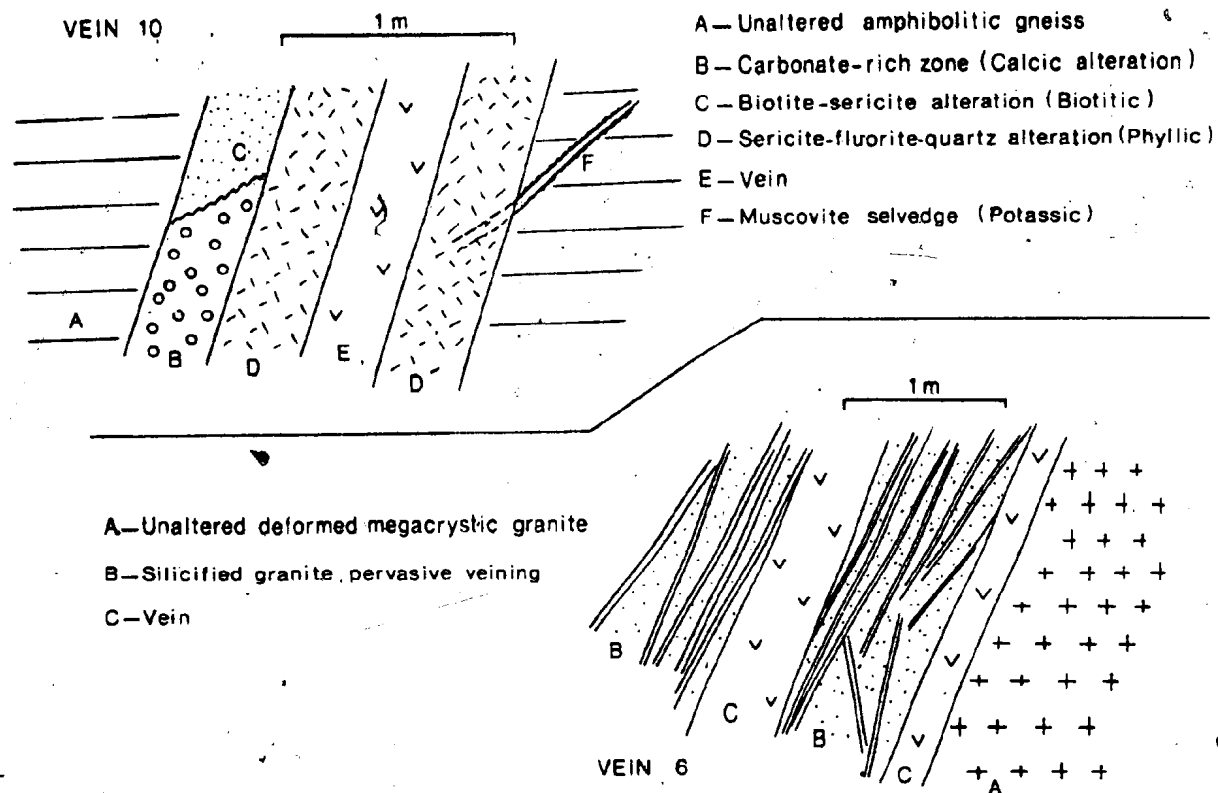


Figure 6.1 Diagrammatic cross-section of composite lodes showing the zonation of alteration facies developed during greisenisation.

Table 6.1

Mineralogy and Distribution of Alteration Facies

ALTERATION TYPE		PRINCIPAL MINERALOGY	DISTRIBUTION AND ROCK TYPE AFFECTED
ALKALIC		-micro., alb., chl., epid., musc.*	Pervasive in leucogranite dykes.
GREISENISATION	POTASSIC	-musc., py., sch. (wolf.).	Selvages to Q-b, QF-m veins - tensional veins showing no displacement of wall rock.
	PHYLIC	-Ser., py., fluo., musc., qtz., sch. (wolf.).	Alteration envelope to composite veins (esp. #10) containing Q + w vein types. Affects amphibolite wall rock. Alteration localised on shallow dipping sections of the composite veins.
	BIOTITIC	-biot., ser., fluo., py., chl., epid.	Outer alteration zone gradational to phyllic alteration (above). Affects amphibolite. Variably developed Epidote and chlorite occur in veinlets.
	CALCIC	-calc., ser., fluo.	Variably developed outer alteration zone gradational with phyllic alteration. Affects amphibolite.
	SILICIC	-qtz., ser., py., fluo., chl. + calc.	Ramifying network of quartz veinlets that occur as an alteration envelope to composite Vein #6. Affects deformed megacrystic granite (DMG). Pervasive in zones in fractured DMG. Also occurs as the outermost alteration halo in amphibolitic wall rock to Vein #10.
ARGILLIC		-kaol., biot., qtz., chl.	Associated with F-cb veins. Postdates previous alteration events.

micro. = microcline, alb. = albite, chl. = chlorite, epid. = epidote, musc. = muscovite, py. = pyrite, sch. = scheelite, wolf. = wolframite, ser. = sericite, fluo. = fluorite, qtz. = quartz, calc. = calcite, kaol. = kaolinite, biot. = biotite.

* stable mineral - not alteration product.

Table 6.2
Mineralogical Changes during Alteration
of Amphibolitic Gneiss and Megacrystic Granite

UNALTERED*		ORTHOCLASE	PLAGIOCLASE	HORNBLende	BIOTITE	MUSCOVITE	CHLORITE	QUARTZ	ADDITIONS
ALKALIC		microcline	albite, ⁺ sericite, ⁺ epidote		chlorite	unaffected		unaffected	
GREISENISATION	POTASSIC								-muscovite -pyrite -scheelite (wolframite)
	PHYLIC	sericite	sericite					decreased	-fluorite -pyrite -scheelite (wolframite)
	BIOTITIC		sericite	biotite	chlorite			decreased	-pyrite -fluorite -epidote
	CALCIC		sericite					decreased	-carbonate -fluorite -pyrite
	SILICIC	sericite	sericite	chlorite			unaffected	increased	-pyrite -fluorite - ⁺ calcite
ARGILLIC			kaolinite	biotite	⁺ chlorite ⁺ muscovite		unaffected	unaffected	

* composite mineralogy - amphibolite and deformed megacrystic granite.

the composite lodes. The alteration is patchy and appears to be enhanced where the veins cut wall rock displaying an increased permeability due to shearing or faulting. Kaolinite is the dominant component of the mineralogy and is formed by alteration of plagioclase. Biotite, formed after hornblende during shear zone metasomatism, is stable under these conditions and has undergone only minor alteration to chlorite and muscovite.

Table 6.1 summarises the principal mineralogy of each alteration type and its distribution, while Table 6.2 details the mineralogical changes which occur during the various alteration stages.

6.3 GEOCHEMISTRY

The alteration types were analysed for the normal major and trace elements by XRF and A.A.S. techniques (Appendix A.2), and the data are listed in Appendix B.5. Tungsten and tin concentrations were determined by Dr B. Kronberg (Univ. of Western Ontario) by Spark Source Mass Spectrometry (Appendix A.2). The variation in major and trace element chemistry in the alkalic alteration, characteristic of the leucogranites, is discussed in Chapter 4. No geochemical data are available for the argillic alteration associated with the late fluorite-calcite-barite veins.

The subdivision of alteration types on petrographic grounds is substantiated by their major and trace element chemistry. Normal variation diagrams are unsuitable for evaluating metasomatic processes, since the data are normal-

ised to 100% and a change in one element results in a compensating change in another. Chemical transfer data can be calculated using equations (Appendix D) that quantify metasomatic reactions (Gresens, 1967; Babcock, 1973). This is possible assuming either the volume of the rock remains constant during the metasomatism or the magnitude of transfer of any single component is known (e.g. constant Al_2O_3 or TiO_2 etc).

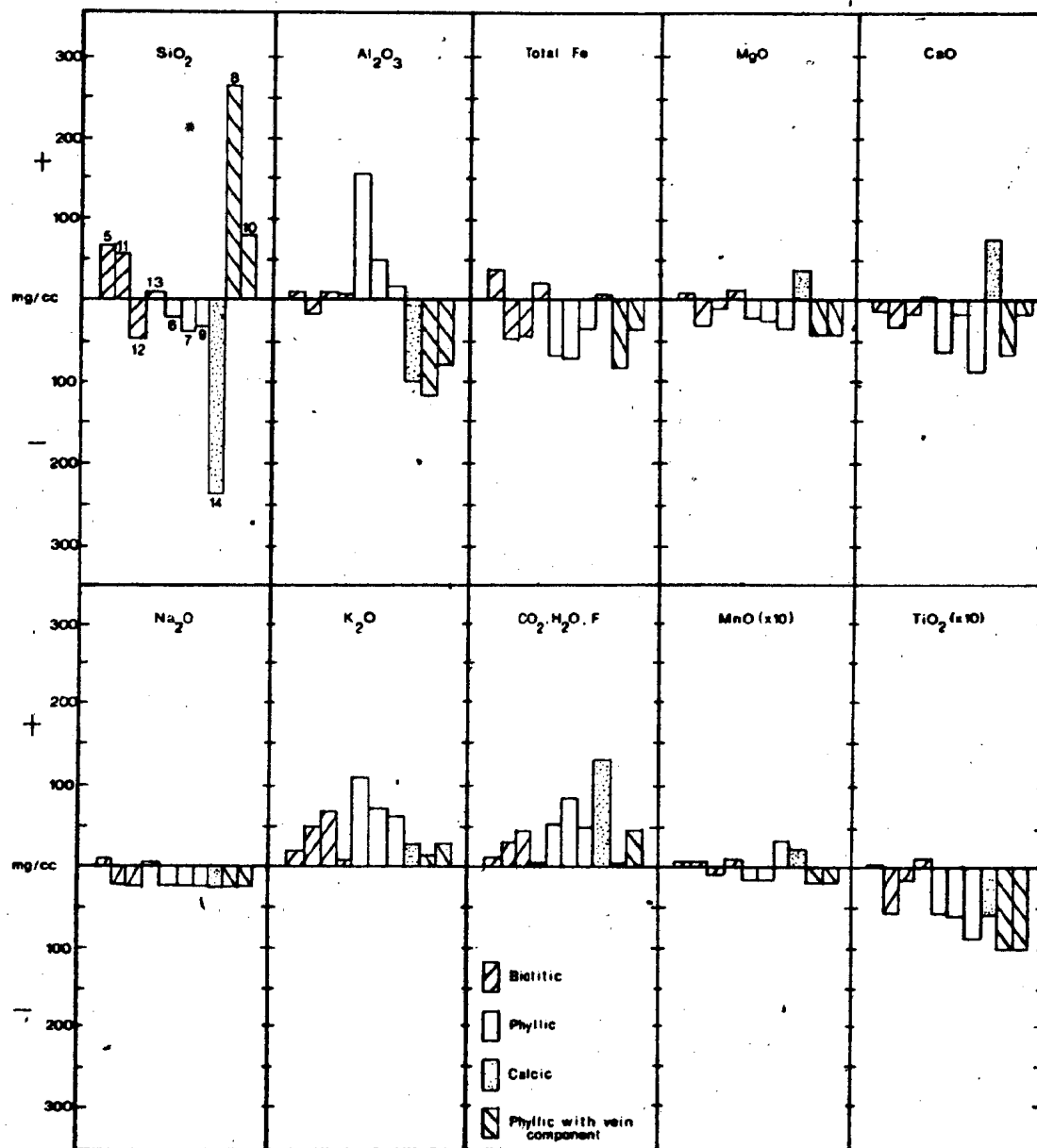
6.3.1 Gain/Loss Diagrams

Assuming an isovolumetric relationship between the unaltered and altered rocks, one can construct a gain/loss diagram (Camus, 1975; Ford, 1978) that quantitatively reflects changes in chemical composition during metasomatism (Figures 6.2, 6.3, 6.4).

In the amphibolite wall rock greisenisation appears to have resulted in decreases in SiO_2 , total Fe, CaO, MgO, Na_2O and CaO and increase in Al_2O_3 and K_2O . Increase in the volatile component is reflected in the increased proportions of mica and fluorite in the altered rocks. Note that sample 14 (Figure 6.2) representative of the calcic alteration shows high concentrations of CaO and volatiles reflecting its carbonate dominated mineralogy.

Slightly different trends are obvious for the major element variation in altered deformed megacrystic granite samples (Figure 6.3). SiO_2 is markedly enriched and Al_2O_3 depleted relative to the deformed megacrystic granite as well as the unaltered amphibolite. K_2O and volatile

Figure 6.2 Isovolume gain/loss diagram for altered amphibolitic gneiss wall rock: Major elements. Derived from equations of Gresens (1967) and Babcock (1973). For Figures 6.2 to 6.4 average unaltered wall rock represented by horizontal base line. Numbers above gain/loss bar scale represent analysis numbers listed in Appendix B5.



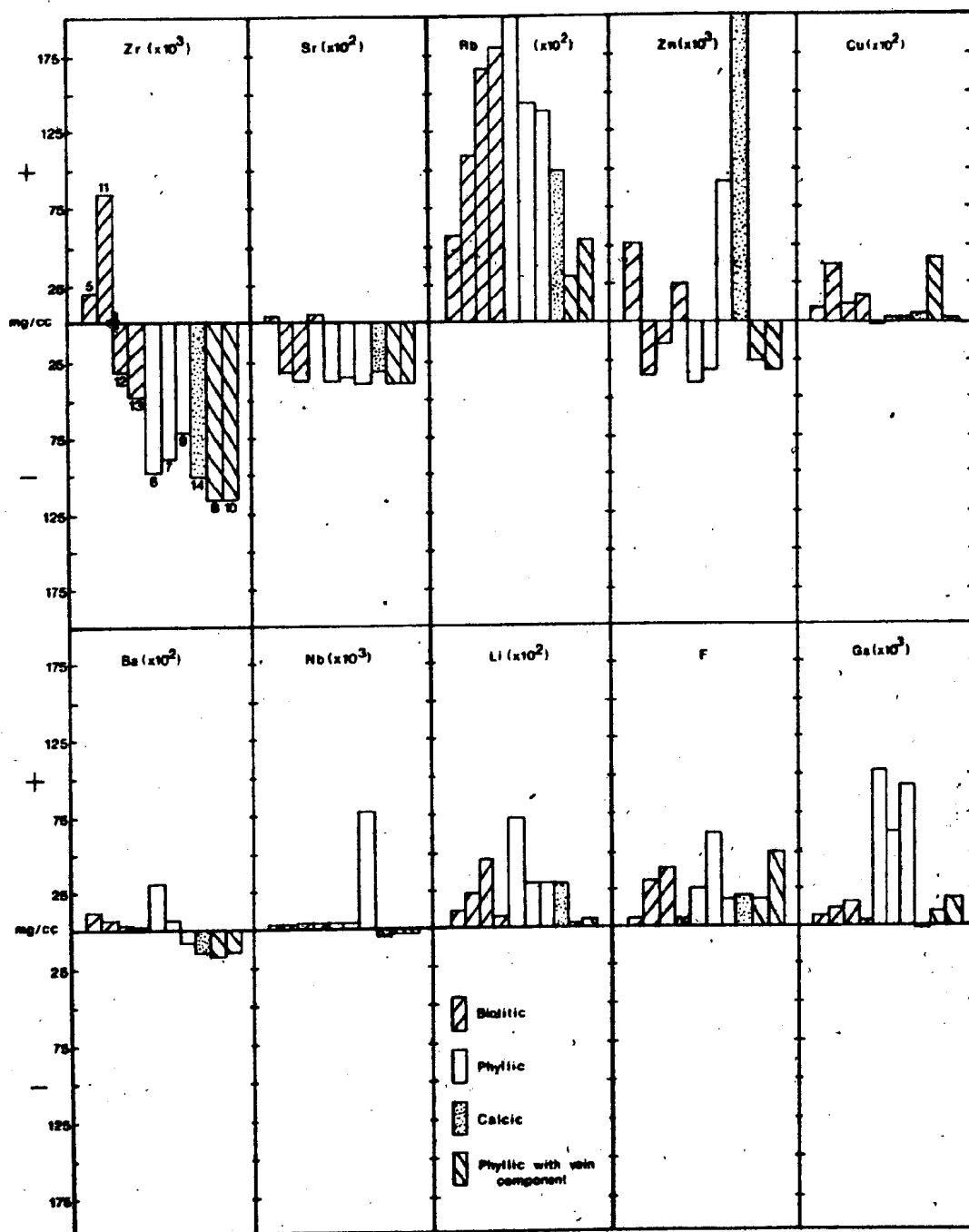


Figure 6.3 Isovolume gain/loss diagram for altered amphibolitic gneiss wall rock : Trace elements.

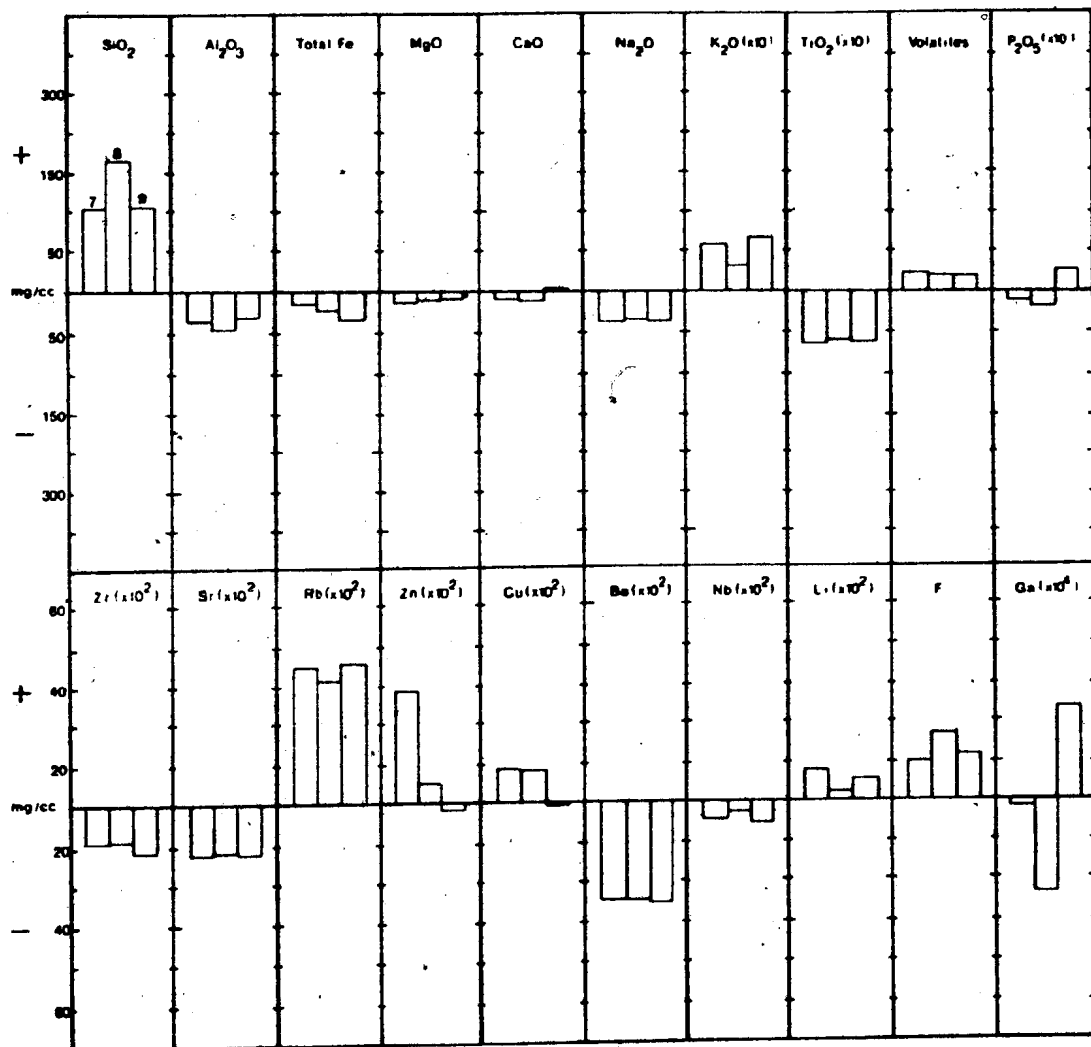


Figure 6.4 Isovolume gain/loss diagram for altered megacrystic granite wall rock: Major and trace elements.

increases, and decreases in other elements, are similar to those found in the amphibolite section. Net veining by quartz may account for the high SiO_2 content of silicic altered rocks (suggesting the alteration was not isovolumetric).

Trace element distribution between alteration types reflects mineralogical changes as well (Figure 6.3). Altered amphibolitic rocks are enriched in Rb, Li, and Ga relative to unaltered amphibolite and reflect increased amounts of micaceous minerals in the altered rocks. Gallium can occur in both feldspars and mica but tends to be more abundant in the latter because the relatively large Ga ion substitutes more readily for Al in octahedral sites in mica than in tetrahedral sites in feldspar (Hall, 1971),

Strontium is depleted in altered amphibolitic rocks. It usually occurs in feldspars which are altered and replaced in the greisenisation process. Zinc and copper vary substantially in each alteration type and might reflect variation in fluid conditions (pH etc.) or sample bias due to inhomogeneous distribution of these elements (as ore minerals) in each alteration zone.

In the granite wall rock (Figure 6.4) Rb, Li and F gains are all reflected in the dominant mineral components of the alteration, namely quartz, sericite and fluorite. Ba and Sr are depleted by breakdown of feldspar while Ga appears to be only slightly enriched in the most altered sample, possibly due to lower amounts of mica in the silicic

Table 6.3

Tungsten and Tin Concentrations
in Metamorphic and Hydrothermally Altered Rocks

SAMPLE	W(ppm)	Sn(ppm)	Rock Type
64	< 4*	25	Amphibolite
383	< 4	75	Mica Schist
142	< 4	10	Phyllite
495	44	75	Tonalitic gneiss
			Alteration Type
362	70	5	Biotitic
363	40	25	Calcic
360	6000	40	Phyllic

Analyst: Dr B. Kronberg (University of Western Ontario)

* detection limit 4 ppm.

alteration.

Tungsten and tin analyses of unaltered and altered rocks (Table 6.3) indicate that tungsten is concentrated (70-6000 ppm) by the process of greisenisation at Grey River. Tin appears to be slightly enriched (40 ppm) in the most altered rock sample (360 - Table 6.3) but some supposedly unaltered samples (e.g. 495 - tonalitic gneiss) have exceptionally high values of Sn and W (75 ppm and 44 ppm respectively). This may be due to contamination during crushing procedures (Appendix A.1) but care was taken to avoid such problems.

The tin, tungsten enrichment might suggest that the metamorphic rocks of the Grey River area have anomalous concentrations of these elements. This inference is probably premature, based on only a few samples and needs to be verified by a statistical sampling program.

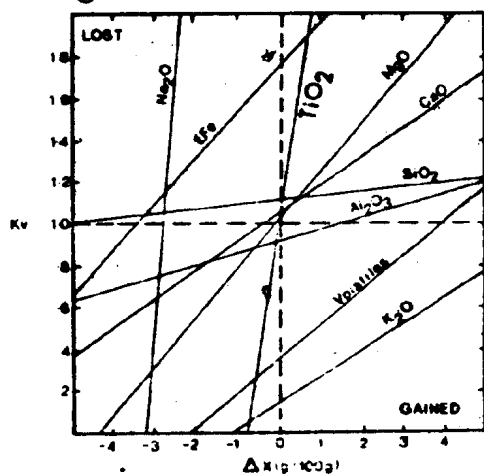
No distinct tungsten-bearing phase was observed in biotitic or calcic alteration types so that the 40-70 ppm W concentrated in these rocks may be contained in the mica phase (Ivanova, 1969). Wolframite and scheelite are however observed in the phyllic alteration zones and account for their exceedingly high tungsten concentrations. Unpublished assays indicate concentrations of 1000 to 10000 ppm in the greisenised wall rock of Vein #10.

6.3.2 Gresens Composition - Volume Diagrams

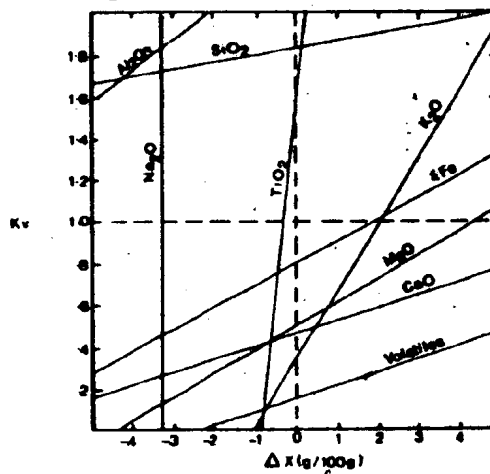
Although the gain/loss diagrams of Figures 6.2 to 6.4 mimic the change in mineralogy during the alteration, the underlying assumption that there has been no volume change

Figure 6.5 Gresens diagram showing composition-volume relationship for biotitic, calcic, phyllic, and silicic alteration facies. Dashed lines indicate isovolumetric ($K_v=1$) and isochemical ($\Delta X=0$) relations. The quadrant in which the lines cross these axes indicate whether the elements are gained or lost in the reaction.

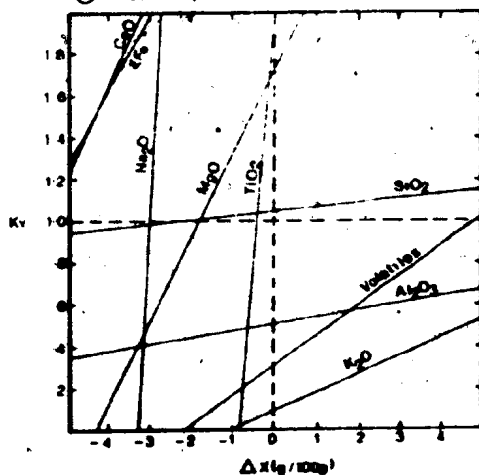
Ⓐ Biotitic alteration (434-8-66)



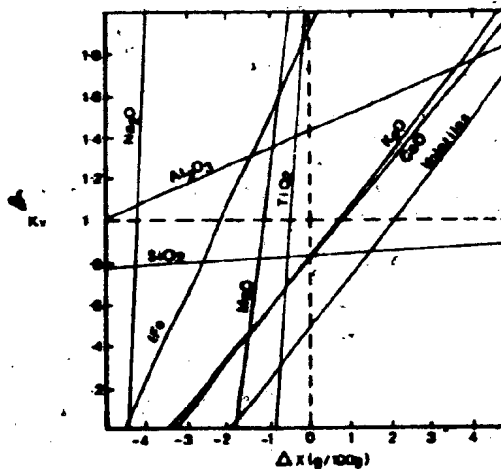
Ⓑ Calcic alteration (363-8-66)



Ⓒ Phyllic alteration (2-64-66)



Ⓓ Silicic alteration (20-108 - 20-108)



appears to be invalid when Gresens composition-volume diagrams are constructed (Gresens, 1967; Babcock, 1973). These diagrams (Figure 6.5) show that chemical variations are linearly related to volume change during metasomatism.

Elements added to the rock are represented by lines that pass through the lower right-hand quadrant, while those lost from the rock are represented by lines which pass through the upper left-hand quadrant. The points at which these lines cross the isochemical line ($\Delta x = 0$) are important, since they indicate the magnitude of the volume change and the direction of chemical transfer during metasomatism.

The clustering of intercepts in the Gresens diagrams for the biotitic alteration (Figure 6.5A) suggests that the metasomatism was isovolumetric at this relatively weak alteration stage, or very nearly so. However, intercepts for intensely altered rocks (e.g. calcic, phyllic, silicic - Figure 6.5B,C,D,) are more widely scattered, but overall suggest a decrease in volume during the hydrothermal alteration (i.e. K_v less than 1.0).

The above data indicate that the hydrothermal alteration at Grey River involved a change in volume of the rock as well as changes in the concentrations of all chemical components. Even Al and Ti, two elements commonly assumed to be constant in hydrothermal environments (Gresens, 1967; Carmichael, 1969; Beswick and Soucie, 1978; Beach, 1976), appear to be mobile during greisenisation. Since no element remains constant in amount during the hydrothermal

alteration (except perhaps during the biotitic alteration facies) a unique solution for the sign and magnitude of the chemical transfer cannot be obtained.

6.4 RARE-EARTH ELEMENTS

The coherent geochemical behaviour of the Rare-Earth Elements* have allowed them to be used as a petrogenetic indicator in igneous, metamorphic and sedimentary processes (Haskin, 1966; Frey *et al.*, 1978; Fryer, 1977). Recently measurements of REE's have been successfully applied to hydrothermal ore deposits to evaluate the role of various fluid phases involved in their formation (Graf, 1977; Kerrich and Fryer, 1979; McLennan and Taylor, 1979; Taylor and Fryer, 1980 a,b). Taylor and Fryer (1980b) suggest that the behaviour of REE in hydrothermal systems can effectively monitor changing fluid conditions and identify the nature of the anionic species responsible for REE complexing and associated metal transport.

With this objective, samples of the alteration zones were analysed for REE by a thin film X-ray Fluorescence technique (Fryer, 1977, see Appendix A.2.3 for description of method). Precision and accuracy for all elements are ± 5 to 10% or 0.1 ppm whichever is the greater. The data are plotted normalised to the chondritic values of Taylor and Gorton (1977).

* Throughout this discussion the abbreviations REE, LREE and HREE will be used for rare-earth elements, light rare-earth elements (La to Sm), and heavy rare-earth elements (Gd to Yb) respectively.

Table 6.4

REE Contents of Altered and Unaltered Rocks

SAMPLE	64	9-68	9-62	362	431	434	363	453	166	9-64	436
La (ppm)	9.7	18.8	45.8	2.9	8.9	5.7	2.9	2.9	1.9	0.7	0.3
Ce	23.5	39.8	88.3	8.1	22.0	14.8	8.0	8.6	6.4	1.1	0.6
Pr	2.9	4.7	10.1	1.2	2.8	1.8	0.9	0.9	0.6	0.3	0.1
Nd	12.7	19.0	35.4	5.3	12.6	8.3	6.4	4.6	3.8	1.2	0.4
Sm	2.9	4.0	7.0	1.4	2.7	1.7	2.3	1.3	2.6	0.4	0.5
Eu	1.1	1.3	1.9	0.6	0.8	0.4	0.9	0.4	1.2	0.6	0.2
Gd	2.9	3.5	4.8	1.5	2.6	2.0	2.5	1.1	4.6	0.7	0.8
Dy	2.9	3.5	3.9	2.0	4.2	3.5	2.7	3.3	7.9	4.1	1.7
Er	1.3	1.8	2.1	0.9	1.1	1.2	0.9	3.2	1.6	0.9	1.1
Yb	1.1	1.4	1.6	0.9	0.9	1.6	0.8	12.3	3.7	2.3	1.7
Σ REE ^a	102	123	591	29	52	48	35	36	68	14	7
Eu/Eu ^b	1.19	1.16	1.02	1.30	0.99	0.64	1.08	1.08	1.05	2.93	0.88
Description	U/A	U/A	SHZ	BIOT	BIOT	BIOT	CALC	PHY	PHY	PHY	PHY

SAMPLE	20-192	20-198	20-194	20-198	20-199	556	424
La	119.3	55.1	58.0	33.1	16.5	14.1	9.9
Ce	245.5	125.5	104.6	68.6	32.7	35.9	20.5
Pr	28.2	15.4	10.6	6.9	3.7	4.3	2.3
Nd	97.2	55.6	32.4	23.5	12.5	17.3	9.1
Sm	20.1	11.2	5.6	4.0	2.5	4.7	3.0
Eu	3.3	1.9	.9	1.8	0.7	1.2	0.5
Gd	14.7	8.8	3.8	2.8	2.0	4.5	3.1
Dy	11.5	7.8	2.9	2.8	2.0	4.5	3.4
Er	4.9	3.8	1.3	1.5	1.3	2.3	2.0
Yb	3.3	24.8	1.1	1.5	1.0	2.5	2.9
Σ REE ^a	1442	361	351	199	93	107	78
Eu/Eu ^b	0.60	0.58	0.64	1.68	0.90	0.82	0.48
Description	U/DMG	U/DMG	SIL	SIL	SIL	MG	LSG

U/A = Unaltered amphibolitic gneiss; BIOT = Biotitic alteration; CALC = Calcic alteration; PHY = Phyllic alteration;
 U/DMG = Unaltered deformed megacrystic granite; SIL = Silicic alteration; MG = Megacrystic granite; LSG = Leucogranite;
 SHZ = Shear zone mica schist.
 a = calculated from chemical yields.
 b = Eu^a abundance by extrapolation between Sm and Gd.

6.4.1 REE Behaviour During Autometasomatism

By nature of its origin the autometasomatic alkalic alteration does not allow for a comparison between unaltered and altered leucogranite. The REE content of one leucogranite dyke (Sample 424) is shown in Table 6.4 and plotted chondrite-normalised in Figure 6.7. In comparison to the megacrystic granite (Figure 6.7 and 6.8A) the leucogranites are depleted in LREE while HREE are enriched.

The enrichment in HREE is best explained by redistribution of REE by a hydrothermal fluid phase (Collerson and Fryer, 1978; Kerrich and Fryer, 1979). The alkalic alteration is characterised by K, Na, Ba, Sr and Rb addition during development of secondary feldspars. This is accompanied by chloritisation of biotite and development of epidote and sericite by alteration of plagioclase. Under these conditions the HREE (Gd-Yb) appear to be deposited, possibly due to the appearance of octahedral sites with the development of epidote as an alteration mineral (Taylor and Fryer, 1980a).

6.4.2 Behaviour During Greisenisation

Large variations in REE abundances and distribution are found in rock types affected by greisenisation. Unaltered amphibolitic gneiss (migmatite) have a straight REE pattern that is enriched in LREE relative to chondrite values (Figure 6.6A). In contrast unaltered mica schist from a shear zone within the amphibolitic gneiss (sample 9-62 Figure 6.6A) has much higher total REE concentration (Table 6.4). Also LREE are more enriched than HREE in these shear zones but an

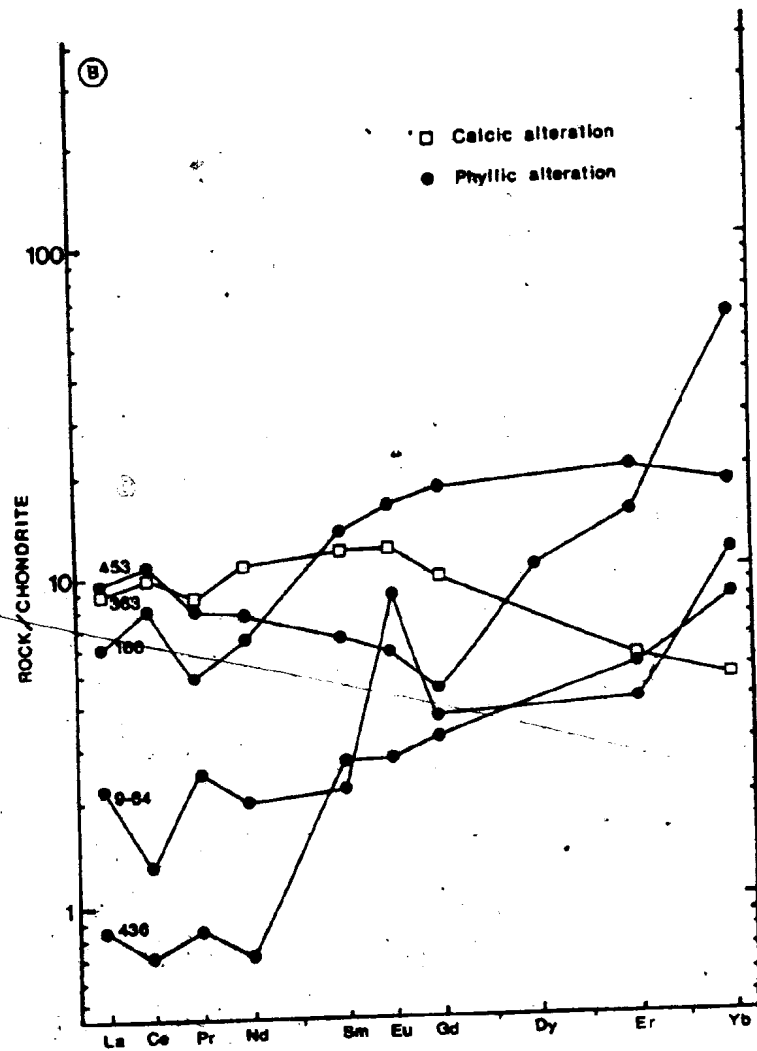
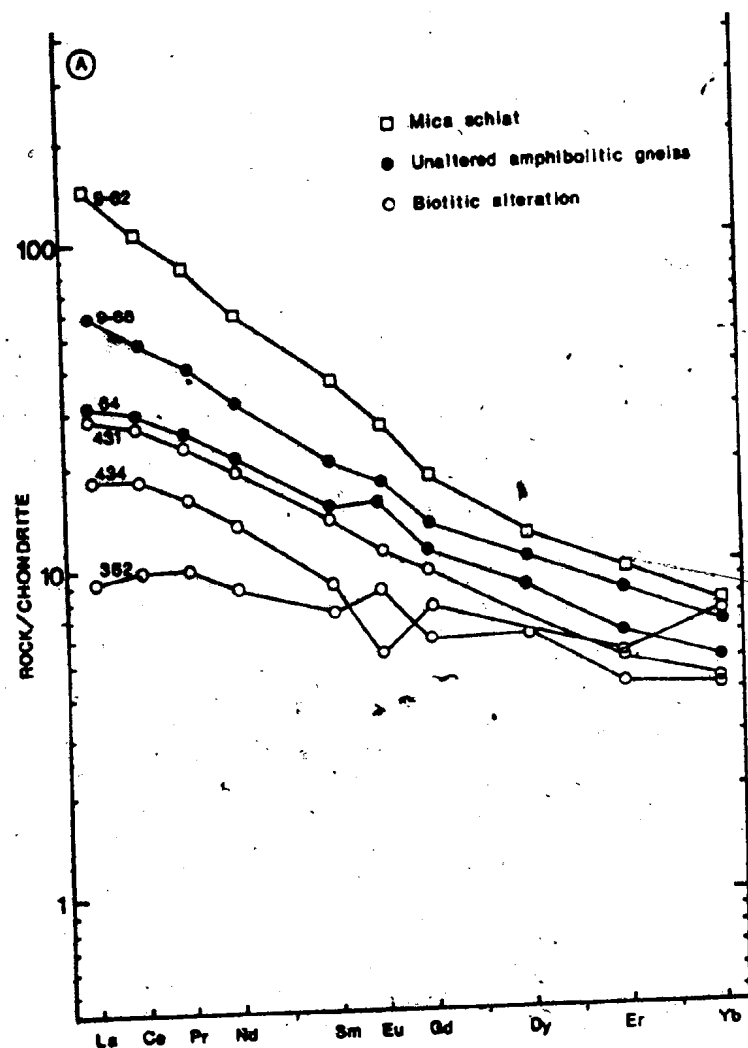


Figure 6.6 Chondrite-normalised REE plots of greisen and unaltered amphibolitic wall rock. A shear zone sample (9-62) of mica schist is also shown.

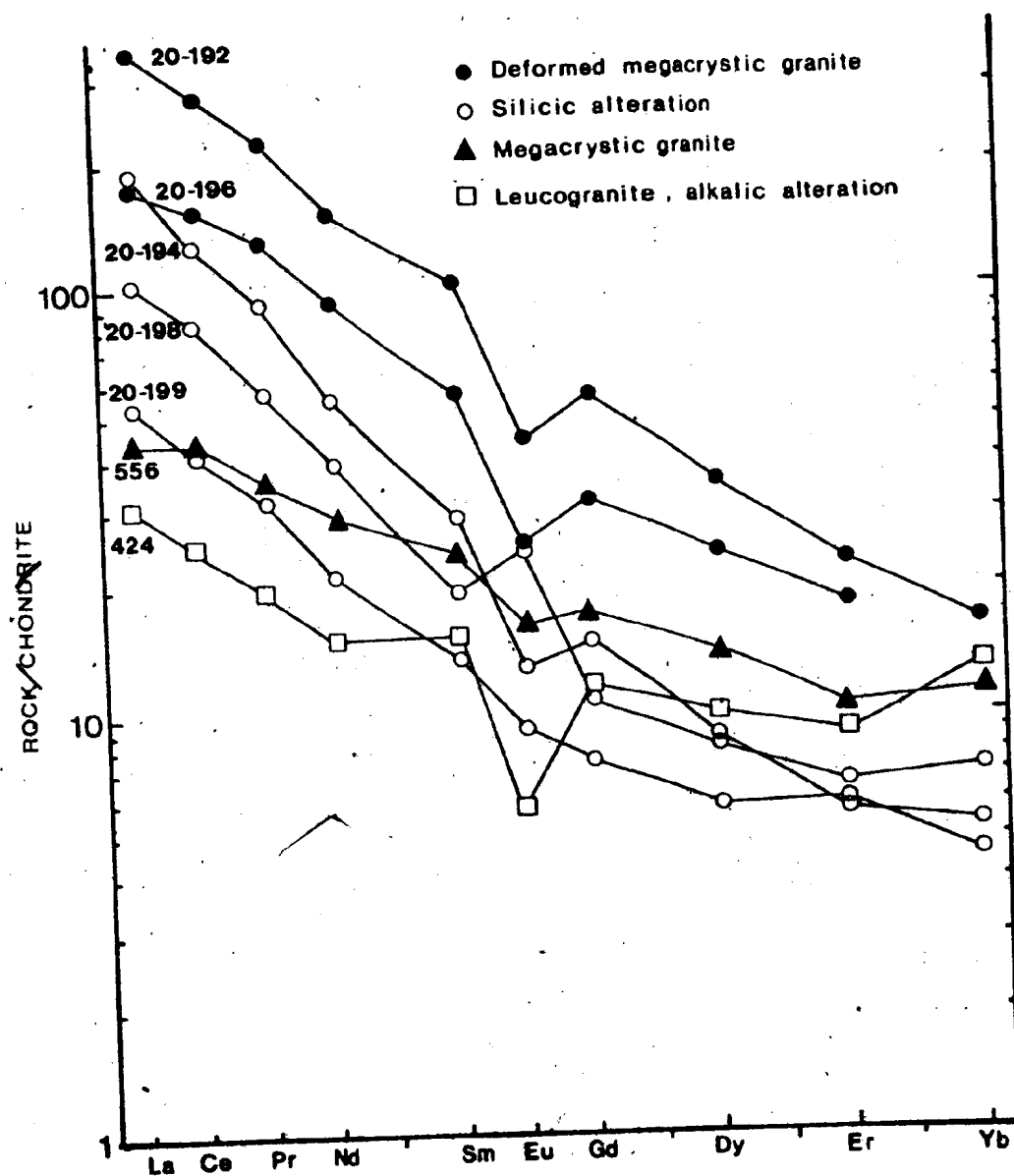
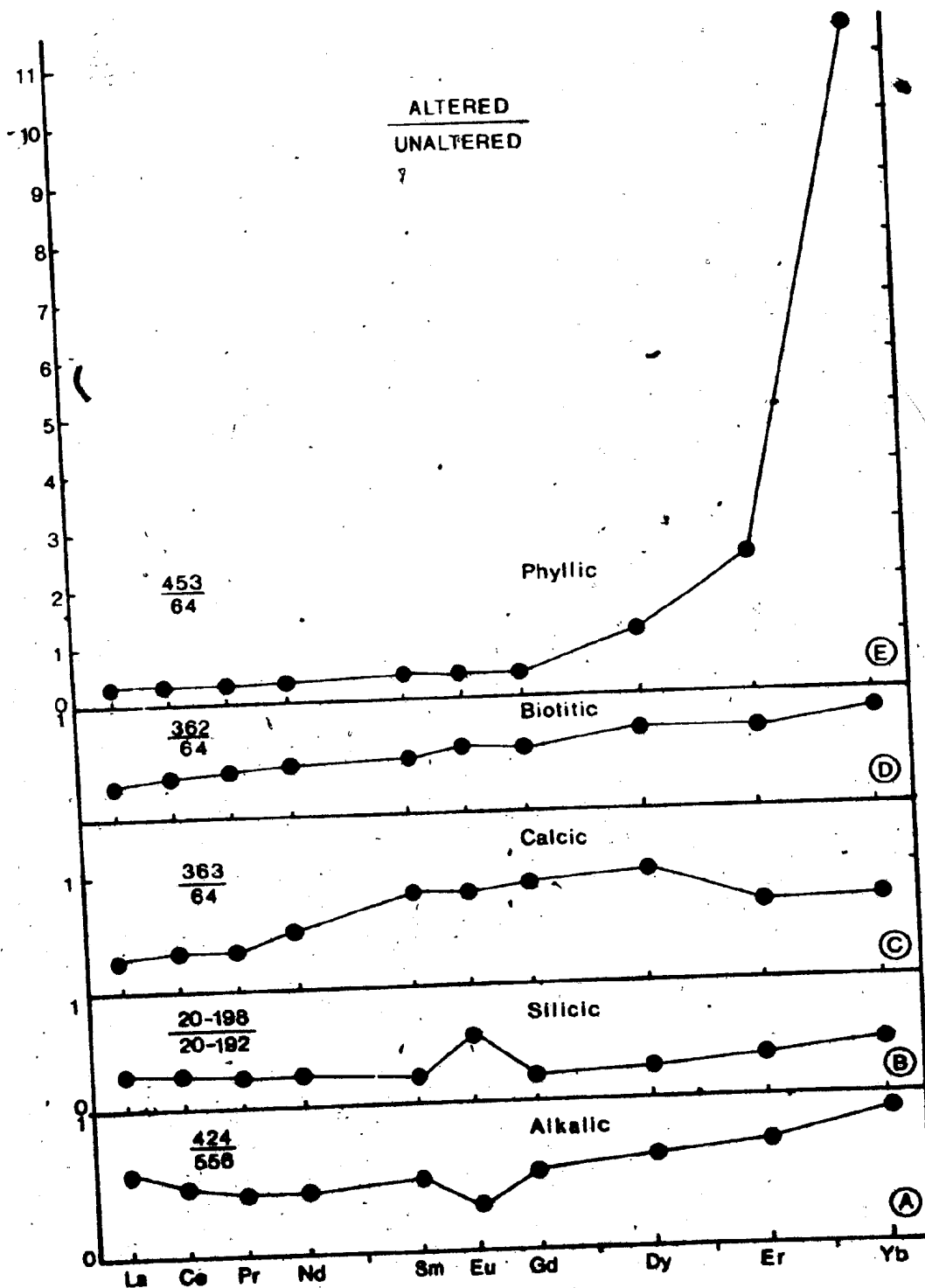


Figure 6.7 Chondrite-normalised REE plot of altered (silicic) and unaltered deformed megacrystic granite wall rock. An unaltered undeformed megacrystic granite sample (556) and an altered (alkalic) leucogranite (424) are also shown.

Figure 6.8 Depletion and enrichment of REE during greisen alteration and autometasomatism of the leucogranite dykes. A ratio of altered:unaltered below 1 indicates a depletion; above 1 an enrichment.



increase in all REE has occurred during metasomatism that accompanied ductile shearing under retrograde metamorphic conditions.

Later hydrothermal alteration results in a marked reduction in REE, the magnitude of which increases with increasing intensity of alteration. Weakly altered rocks exhibiting a biotitic alteration, have depleted REE patterns relative to unaltered rock (Samples 431, 434, 362, Figure 6.6A) indicating leaching of REE during initial greisen alteration. LREE appear to be leached to a greater extent than HREE (Figure 6.7D), in fact one sample (434 - Figure 6.6A) shows a slight enrichment in Yb.

A sample from the calcic alteration zone (363 - Figure 6.6B) has a similar total REE content (Table 6.4) as those of the biotitic alteration but exhibits a concave downward REE pattern. Light REE are depleted relative to unaltered rocks, as are the HREE, but a maximum exists in the intermediate REE range (Sm-Gd). REE distribution in carbonate minerals is poorly understood. Generally they have low REE concentrations (Haskin et al., 1966) but acid leaching experiments of calcareous rocks (Haskin et al., 1966; Javis et al., 1975; McLennan et al., 1979) documented high proportions of the REE in the soluble fraction. McLennan et al., (1979) note that a marked depletion in HREE relative to normal crustal abundances is common for calcareous rocks. Furthermore, Moller et al., (1979) showed that REE patterns of hydrothermal calcites from Pb-Zn veins of Western Harz

(Germany) are characterised by maxima at Sm through Eu. A similar pattern for the calcareous alteration at Grey River likely reflects the dominance of calcite in the mineralogy.

Intense phyllic alteration results in the most marked redistribution of REE during the greisenisation process (Figure 6.6B). The LREE are leached while HREE appear to be strongly enriched relative to unaltered rocks (Figure 6.8). Several samples from the phyllic alteration have low total REE contents (e.g. 436, 9-64, Table 6.4) due to the dilutant affect of a high quartz (vein) component. Although the most characteristic feature of this alteration is the HREE enrichment it should also be noted that most samples show no europium anomaly (Figure 6.8, 6.6B). This appears to be a characteristic of the calcic and biotitic alterations also.

Hydrothermal alteration in the granite wall rock similarly results in changes in REE abundances and distribution. The deformed megacrystic granite wall rock (samples 20-192, 20-196) has much higher total REE contents (Table 6.4) than that of unaltered amphibolitic wall rock. Furthermore the deformed megacrystic granite is enriched in all REE (LREE especially) compared to undeformed megacrystic granite (sample 556, Figure 6.7). The REE enrichment pattern is likely a result of metasomatism in the ductile shear zone that affected both the megacrystic granite and the amphibolite gneiss. The magnitude of the enrichments is

similar to enrichments seen in ductile shear zones within the amphibolitic gneiss (sample 9-62, Figure 6.6A).

Greisenisation of the deformed megacrystic granite (dominantly silicic alteration) results in a progressive decrease in total REE content with increasing intensity of alteration (Figure 6.7, sample 20-194 → 20-198 → 20-199). The depletion in total REE results from leaching of light and heavy REE in approximately equal proportions (Figure 6.8B). Note that the most intensely altered samples (20-198, 20-199) are enriched in europium relative to unaltered samples (Figure 6.8B).

No REE data are available for rocks affected by the argillic alteration that is associated with late fluorite-calcite-barite veins.

6.5 IMPLICATIONS OF REE DISTRIBUTION

The progressive leaching of the REE can be related to decreasing pH of the hydrothermal fluid in equilibrium with the altered rock. This is suggested by the increasing phyllic character of the alteration (a dominant mineralogy of sericite and pyrite), which would suggest low pH (Field et al., 1971; Sheppard et al., 1971). Under low pH conditions the LREE are more soluble than the HREE and in a simple chloride solution the intermediate to heavy REE are progressively less soluble (Flynn and Burnham, 1977).

However, Kosterin (1959) showed that the principal means of REE transport in hydrothermal solutions is in the form of a $(\text{REE}(\text{CO}_3)_3)^{3-}$ complex, the stability of which

Table 6.5

Comparison of Fluorine Concentration
with La/Yb Ratios
in the Hydrothermally Altered Rocks.

Amphibolitic Gneiss Wall Rock									
SAMPLE	9-68	9-62	431*	434*	363*	453*	166*	9-64*	436*
La/Yb	13.4	28.6	9.9	3.6	3.6	0.2	0.5	0.3	0.2
F (%)	0.11	0.60	3.30	5.64	2.34	1.92	6.00	2.34	5.34

Deformed Megacrystic Granite Wall Rock				
SAMPLE	20-192	20-194*	20-198*	20-199*
La/Yb	36.2	52.7	22.1	16.5
F %	0.26	1.84	3.14	2.27

* Hydrothermally altered, contain fluorite.

increases with increasing REE atomic number. Similarly REE may be transported in fluoride or sulphate complexes. The strong HREE leaching accompanying removal of the LREE in silicic, biotitic, and calcic alteration, indicates that F^- or CO_3^{2-} is present in the hydrothermal fluid (Taylor and Fryer, 1980b). Similarly the evidence of a strong HREE enrichment in the phyllic zone accompanying LREE depletion restricts the dominant anionic species in the hydrothermal fluid to CO_3^{2-} (McLennan and Taylor, 1979) or F^- .

Although there are no data available on the fractionation of REE in fluorite, preliminary investigations suggest that fluorites are preferentially enriched in HREE over LREE (B. Fryer, personal communication, 1980). The association of fluorite with greisen alteration at Grey River might suggest that the observed HREE enrichment in highly altered rocks is a function of their fluorite content. However, assuming fluorine concentrations are proportional to the amount of fluorite in the altered rocks, there does not appear to be any positive correlation between fluorine and La/Yb ratio (Table 6.5). This implies that the dominant anionic species in the hydrothermal fluid is CO_3^{2-} .

The REE distribution in zones of retrogression (amphibolite facies to greenschist facies) at Grey River is noteworthy. Both amphibolitic gneiss and megacrystic granite show marked enrichment in total REE concentrations in these zones. The LREE are enriched to a greater extent than HREE which would suggest that the fluid phase present

during retrogression was chloride-bearing (Taylor and Fryer, 1980a). This is consistent with available experimental data for chloride-bearing fluids and silicate melts (Flynn and Burnham, 1977) which shows that the partition coefficients decrease in the order

$$k_d^{Ce^{3+}} > k_d^{Gd^{3+}} > k_d^{Yb^{3+}}$$

This would result in LREE enrichment and HREE depletion in a rock showing evidence of interaction with a chloride-bearing fluid phase (Taylor and Fryer, 1980a).

The HREE enrichment accompanying LREE enrichment in the shear zones suggests the presence of another anionic species in the metasomatic fluid, namely CO_3^{2-} or F^- . CO_2 is compatible with available evidence on the composition of metamorphic fluid associated with amphibolite facies metamorphism (Henley and Sheppard, 1977; Poty et al., 1974; Johns and Huang, 1967; Pecher, 1979; Crawford et al., 1979) which indicates chloride contents of less than 4 wt% and CO_2 concentrations of up to 27 wt%.

Evidence for HREE transport in CO_2 -rich fluids has been shown in the granulite terrane of Bahia, Brazil (Collerson and Fryer, 1978). Bahia migmatites with depleted HREE patterns are retrogressed in K-metasomatic zones by a CO_2 -rich fluid derived from the granulite metamorphism (Touret, 1971, 1977; Bilal and Touret, 1976). Within these zones strong leaching and redeposition of HREE is shown by depleted and enriched HREE patterns respectively. The leaching and redeposition process is

interpreted as reflecting a change of stability conditions of the HREE complex in the fluid (Collerson and Fryer, 1978; Kerrich and Fryer, 1979).

The behaviour of europium in hydrothermal situations is complex, but it has been used to characterise the fO_2 conditions of the hydrothermal fluid (Kerrich and Fryer, 1979; Bowden *et al.*, 1979). At Grey River europium abundances vary between alteration types. Alkalic alteration exhibits a strong europium depletion ($Eu/Eu^* = 0.48$) while nearly all the greisen alteration types show a relatively flat distribution curve between Sm and Gd (Eu/Eu^* approximately equal to 1; Table 6.4).

If soluble carbonate complexes control REE distribution then Eu^{2+} would be expected to behave differently than REE^{3+} . Since most greisen-altered rocks are not anomalous with respect to Eu, then it would appear reasonable to assume, that Eu occurred in its oxidised +3 form, although the transport of Eu^{2+} due to a different complexing agent is possible (McLennan and Taylor, 1979). High fO_2 conditions for the hydrothermal fluid are also inferred from wolframite-hematite relationships discussed in Chapter 5.

6.6 COMPARISON OF REE DISTRIBUTION WITH TUNGSTEN CONCENTRATION.

The previous data have shown that extreme REE mobility occurred during tungsten mineralisation at Grey River. Overall, heavy REE were enriched and light REE depleted during greisenisation indicating that the REE were mobilised

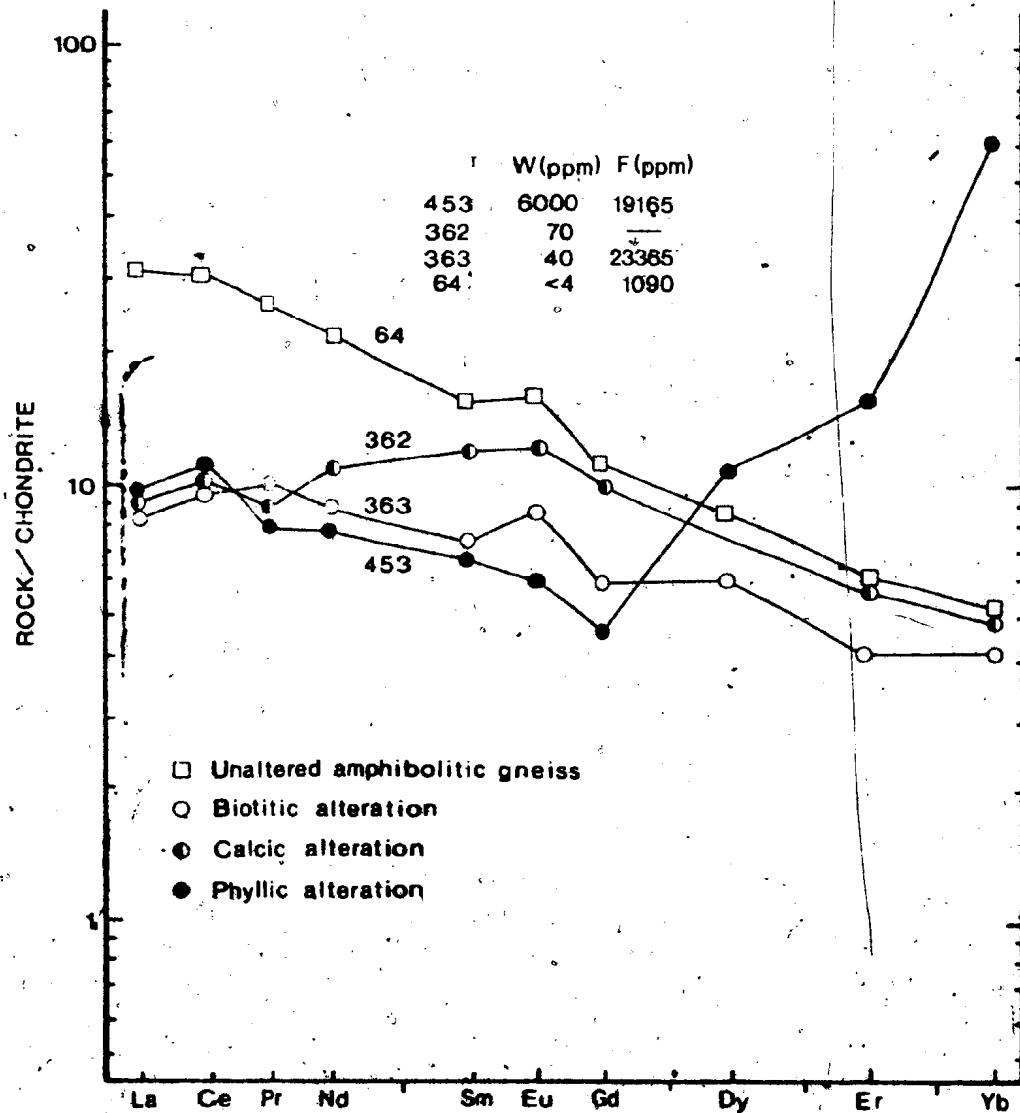


Figure 6.9 Comparison of REE contents with tungsten and fluorine concentrations in greisen alteration facies of the amphibolitic gneiss wall rock.

generally as carbonate complexes.

Tungsten analyses for the alteration zones (Table 6.3) show a remarkable correlation with REE distribution. Wall rocks exhibiting a phyllic alteration are known to contain wolframite and scheelite and unpublished assays indicate concentrations between 1000 and 10000 ppm tungsten. Such wall rocks also show enrichment of HREE relative to LREE while alteration zones containing low tungsten contents (biotitic, calcic) have correspondingly low HREE concentrations (Figure 6.9). No correlation exists however between HREE enrichment and fluorine concentration of the altered rocks (Figure 6.9).

The correlation between W and REE suggests that REE transport is related to tungsten movement and would also imply that tungsten was transported as a carbonate complex in the Grey River hydrothermal fluid. Deposition mechanisms for the tungsten and REE are speculative but possibly relate to destabilising of the carbonate complex by changes in pH and the activity of CO_2 .

6.9 SUMMARY

Alteration associated with the Grey River Tungsten Prospect occurred in three principal stages; 1 - autometallisation associated with alkalic alteration of leucogranite dykes; 2 - greisenisation related to hydrothermal vein formation; 3 - clay alteration associated with late fluorite-calcite-barite veins.

Greisen alteration can be divided mineralogically into

several alteration types depending on intensity of alteration and the composition of the rock affected. Gresens composition-volume diagrams indicate that all elements were mobile during greisenisation and that the volume of the altered rock decreased relative to unaltered rock. Major and trace element variation between the rock types reflects the change in mineralogy. During greisenisation, most element changes can be related to the replacement of feldspar by white mica. Furthermore, additions of F, W, and Sn are evident.

Rare-earth elements effectively monitor changing fluid conditions and identify the nature of the anionic species responsible for REE complexing and associated metal transport. These data indicate that extreme REE mobility occurred during greisenisation and tungsten mineralisation. This mobility is characterised by initial leaching of all REE with increasing intensity of alteration but culminates in a strong enrichment by HREE in the most intensely altered wall rock.

The HREE enrichment and LREE depletion suggest that CO_3^{2-} was the dominant anionic species in the Grey River hydrothermal fluid and implies that transport of REE occurred by carbonate complexing. There is a strong positive correlation between HREE enrichment and tungsten concentration suggesting that REE and tungsten transport are related and thus implies that tungsten was transported as a carbonate complex.

CHAPTER 7

FLUID INCLUSIONS

7.1 INTRODUCTION

A priority in research on ore deposits has been the determination of physical and chemical parameters of ore deposition. Researchers have used a variety of techniques to evaluate such parameters, and for several decades fluid inclusion studies have proved to be informative and reliable in this regard (Roedder, 1976). For adequate interpretation of microthermometric data an accurate knowledge of appropriate fluid phase equilibria is essential. There is a wide variation possible in fluid inclusion compositions (Roedder, 1972) but most are dominated by Na^+ , Cl^- , CO_2 and H_2O , although K^+ , Mg^{2+} , Ca^{2+} and CH_4 are important components of fluids in some situations (Konnerup-Madsen, 1979; Touret, 1977).

Detailed reviews of the $\text{NaCl-H}_2\text{O}$ and $\text{CO}_2\text{-H}_2\text{O}$ systems and their application to fluid inclusion research are given by Sourirajan and Kennedy (1962) and Hollister and Burruss, (1976). Melting and homogenisation phenomena observed in fluid inclusions can be related to experimentally determined equilibria in the $\text{CO}_2\text{-H}_2\text{O}$ and $\text{NaCl-H}_2\text{O}$ systems. In reality, fluid inclusions are more correctly related to the $\text{CO}_2\text{-CH}_4\text{-NaCl-KCl-H}_2\text{O}$ system, of which our present knowledge is limited. Notwithstanding this liability, the measurement of melting and homogenisation phenomena allow an estimation of

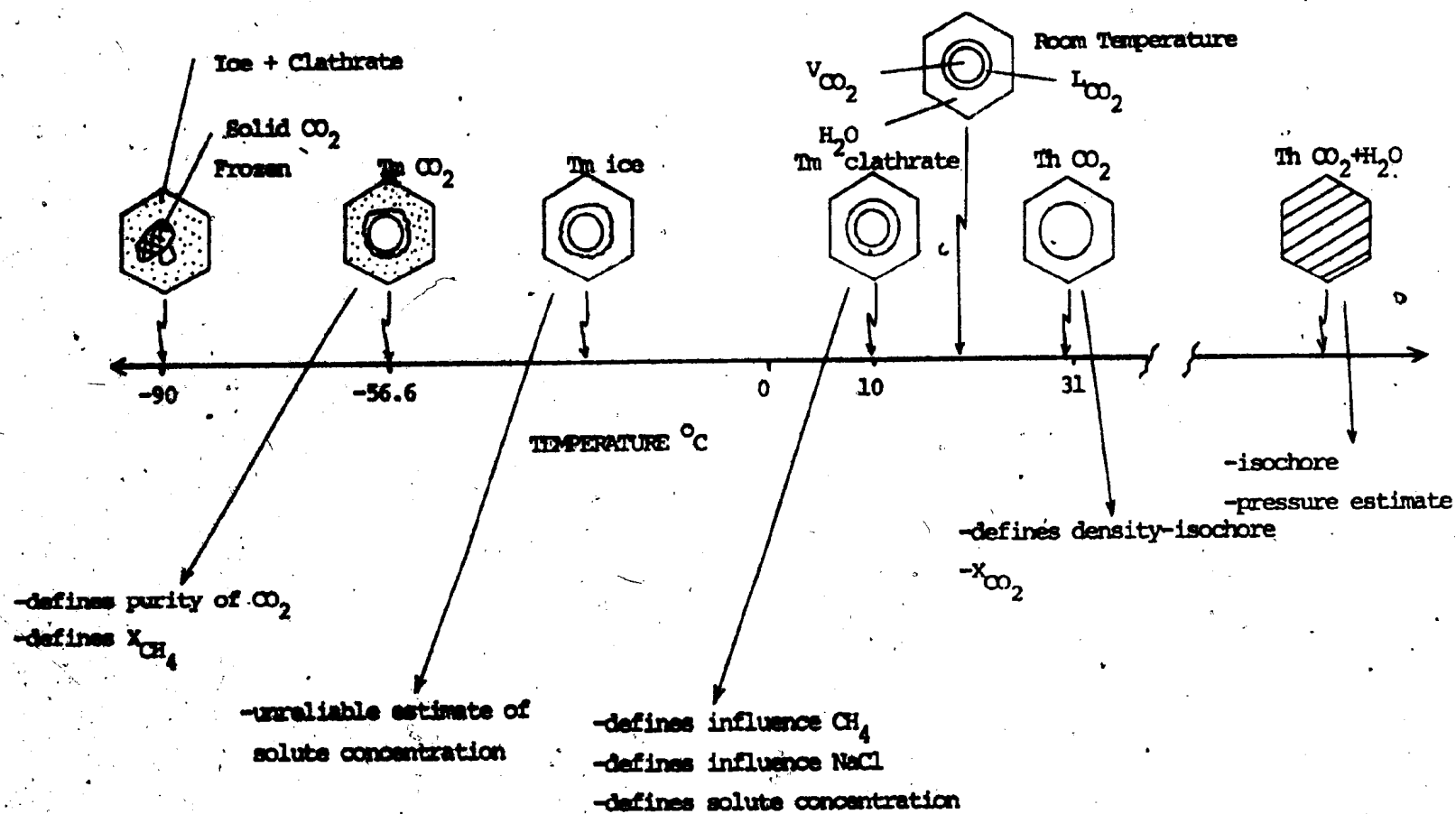


Figure 7.1 Summary of microthermometric data that can be obtained from a single $\text{CO}_2\text{-H}_2\text{O}$ bearing inclusion.

a wide-range of physico-chemical parameters. Figure 7.1 summarises the information that can be obtained from a single $\text{CO}_2\text{-H}_2\text{O}$ bearing fluid inclusion.

7.2 DEFINITION OF TERMINOLOGY

A wide variety of terms and abbreviations are found in the literature for temperatures at which specific phase changes occur within inclusions. In an attempt to standardise the terminology, Roedder (pers. comm., 1979) has recommended the use of the following terms and abbreviations and these will be used throughout this thesis.

- Th: Temperature of total homogenisation of phases. This will be taken to mean the temperature at which two phases become one, disregarding the independent behaviour of possible daughter minerals. The phase into which homogenisation occurs can be stated as Th L or Th V. If critical phenomena are observed then Th CP is used.
- Th CO_2 : Temperature of homogenisation of two CO_2 phases to one phase. The phase which persists beyond the homogenisation point will be added as a suffix e.g. Th $\text{CO}_2\text{-L}$, Th $\text{CO}_2\text{-V}$, Th $\text{CO}_2\text{-CP}$.
- Tt: Temperature of trapping. Equivalent to Th corrected for pressure and salinity.
- Td: Temperature of decrepitation.
- Tn: Temperature of nucleation. Equivalent to the temperature at which a phase first freezes on

lowering the temperature of the inclusion. Nucleation in an inclusion generally occurs only after considerable supercooling and depends on many factors (e.g. foreign nuclei, cooling rate, size of inclusion) unrelated to the chemistry of the fluid. This term covers any nucleation event and is suffixed by the specific phase to which it refers e.g. T_n ice, T_n clathrate etc.

T_e : Eutectic Temperature. The temperature at which liquid first appears on heating a formerly all-crystalline inclusion. This represents the lowest temperatures at which a melt can exist within a specific chemical system.

T_m : Temperature of melting of specific solid phases and is equivalent to a dissolution temperature. The phase to which it refers is appended to the abbreviation e.g. T_m ice, T_m clathrate etc.

Immiscibility: The term immiscibility is used in its most general sense (Roedder and Coombs, 1967) to refer to the existence at equilibrium of two or more non-crystalline polycomponent solutions (in this case two fluid phases), differing in physical properties and generally in composition. Gas and liquid on the boiling curve in a one component system thus becomes a special limiting case of immiscibility in which

the composition variable is eliminated.

- QF-m = Quartz-feldspar-molybdenite veins.
- Q-b = Quartz-bismuthinite veins.
- Q-s = Quartz-sulphide veins (pyrite, chalcopryite, galena).
- Q* + w = Quartz-wolframite (Fe-rich) veins.
- Q + w = Quartz-wolframite (mixed Fe-Mn and Mn-rich) veins.
- Q + g = Quartz-galena veins.
- F-ch = Fluorite-calcite-barite veins.

7.3 ASSUMPTIONS AND PROCEDURES USED IN THIS STUDY

Scheelite and gangue mineral from the Grey River veins provide excellent samples for fluid inclusion analysis because of their crystal size and optical clarity. Descriptions of the veins and their paragenesis are given in Chapter 5. Because of the paragenetic overlap of wolframite and quartz, fluid inclusions from quartz coexisting with wolframite are assumed to be similar and representative of fluids trapped during the deposition of the wolframite.

Fluid inclusions are gross defects in crystals and result from a number of complex processes. Those formed as the crystal is growing are called primary (P). Any process interfering with the growth of perfect crystals may cause the trapping of primary inclusions, Secondary (S) inclusions originate from reheating of cracks within crystals and trap fluids that bathed the crystal at some later time. Generally, such inclusions occur within planes containing similar

inclusions. A third group called pseudosecondaries (PS) are formed by fracturing and reheating during the growth of the host crystal (Roedder, 1976).

Reliable distinction of primary, pseudosecondary and secondary inclusions is a prerequisite for meaningful fluid inclusion microthermometry. Criteria for recognition of inclusion origin are given by Roedder (1976, p 74-75). In the absence of growth phenomena in the majority of the minerals studied the following criteria were used to establish a primary (P) or pseudosecondary (PS) origin.

- 1) Large size of inclusion relative to others.
- 2) Isolated occurrence away from other inclusions.
- 3) Random 3-D distribution throughout the crystal.
- 4) Occurrence in isolated non-planar groups.
- 5) Occurrence in discontinuous intersecting planar arrays.

A secondary origin for some inclusions was established by their occurrence in planar groups outlining healed fractures.

More than 100 polished plates of representative samples of quartz, fluorite, scheelite and apophyllite were studied under the microscope. Of these approximately 35 were found suitable for microthermometric use and over 700 heating and freezing measurements were made.

The fluid inclusions display a wide variety of morphologies. Some are regularly-shaped (evold, multifaceted, negative crystals, spherical, tabular etc.) while others are

highly irregular (ameoboid, branching etc.). The majority of fluid inclusions observed were in the 5-40 μ m size range with smaller inclusions visible only under 1200-2000 X magnification using an oil immersion lens. Inclusions used for heating/freezing stage work were generally greater than 5 μ m in length and width, although the condensing lens incorporated in the design of the Chaixmeca Stage allowed some smaller inclusions to be used. Typically, however, melting of ice was difficult to observe in inclusions less than 5 μ m in dimensions. Appendices E.1, E.2 and E.3 outline the design and specifications of the Chaixmeca Stage and procedures used in this microthermometric study. Data are presented in Appendix F.

In selecting inclusions for analysis care was taken to avoid those which showed features indicative of modification after trapping. These include, trails of minute inclusions between two large inclusions, variable vapour-liquid ratios between spatially associated inclusions, and obvious signs of leakage such as cracks or anomalous gas-rich inclusions.

7.4 COMPOSITIONAL TYPES OF INCLUSIONS

Inclusions may exhibit a wide range of composition depending on the physical and chemical parameters of the fluid at the time of trapping. Three main compositional types are found in nature (gas-rich, fluid-rich, solid) but a continuum exists between these end members. At Grey River the range of inclusion compositional types may be displayed

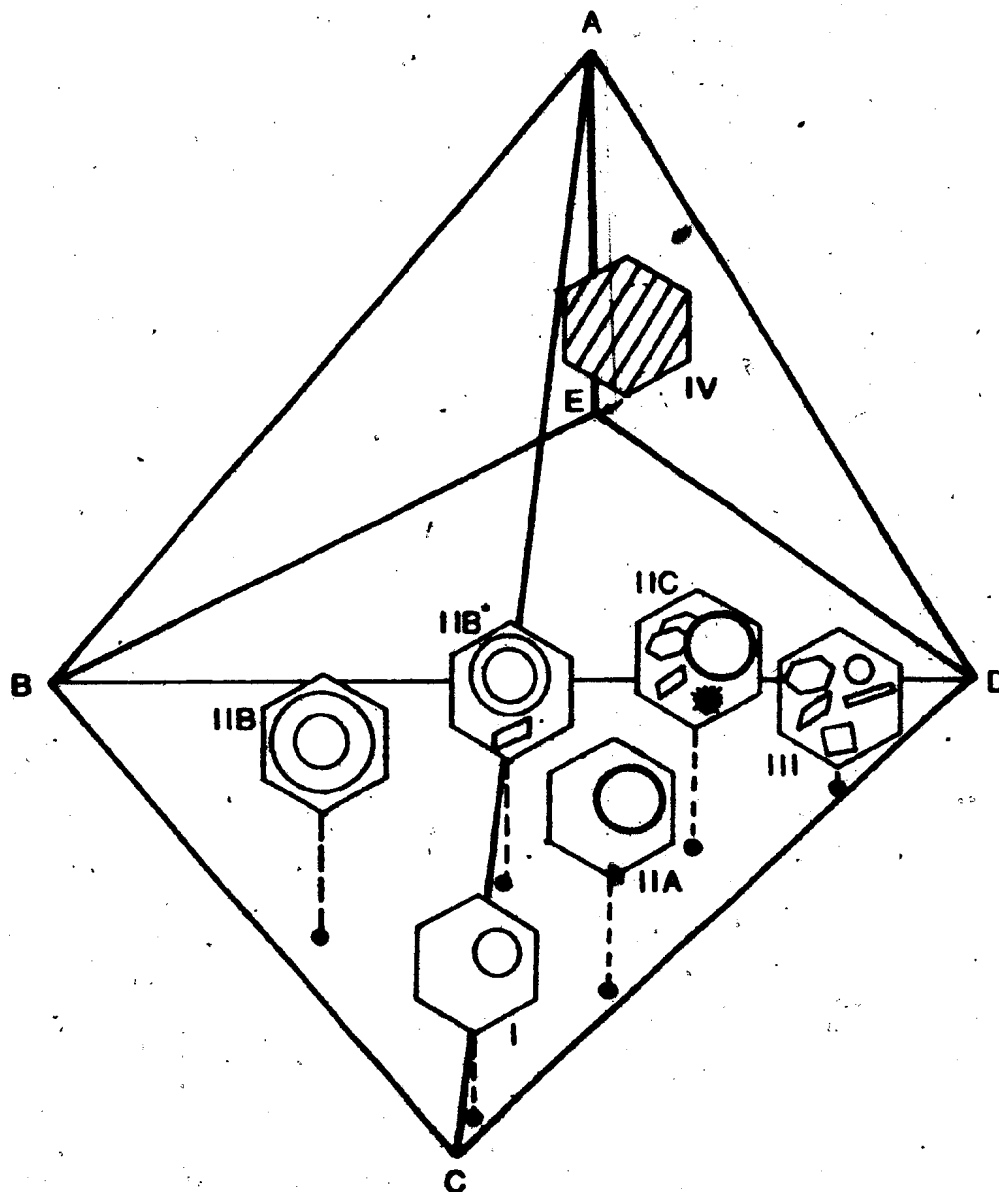


Figure 7.2 Compositional types of fluid inclusions found in the Grey River hydrothermal veins. A = Gas-rich inclusions; B = CO₂-rich inclusions; C = low salinity aqueous inclusion; D = high salinity aqueous inclusion; E = crystalline inclusion; Solid circle represent projections to the BCD plane.

in a polyhedral diagram (Figure 7.2) where the end-members are solid inclusion, high and low salinity aqueous inclusion, CO₂ inclusion, and gas inclusion.

Six main types of inclusions were observed in the Grey River samples.

Type I: Two-phase (L-V) inclusions containing a liquid and gas bubble (volume percent gas varying from 10-60%).

Type II: Carbon dioxide-bearing inclusions which can be classified as several subtypes.

Type IIA: Two-phase (L-V_{CO₂}) inclusions occasionally containing an opaque mineral. Vapour bubbles generally occupy 10-50% by volume, of the inclusions.

Type IIB: Complex three-phase inclusions consisting of liquid CO₂, CO₂ gas, and aqueous solution. Rarely these inclusions contain solid minerals, predominantly carbonates (Type IIB*).

Type IIC: Polyphase inclusions consisting of aqueous solution, CO₂ vapour, and a variable number of solid minerals (carbonates, sulphates?, unknowns).

Type III: Polyphase secondary inclusions consisting of aqueous solution, vapour and a large number of solid minerals.

Type IV: Solid inclusions of carbonate and sulphate.

Table 7.1 illustrates the relative distribution of these inclusion types between the vein types outlined previously (Chapter 5).

Type I

Liquid-vapour inclusions of primary or pseudosecondary

origin are largely restricted to veinlets containing tungsten mineralisation in quartz associated with wolframite. They also occur as secondary inclusions with small gas bubbles in most other veins. Some inclusions contain a small opaque mineral that was either incorporated during growth of the host crystal or as a result of precipitation during cooling of the fluid. Freezing experiments show no sign of clathrate formation at low temperatures indicating low amounts of CO_2 in the vapour phase in Type I inclusions. Plate 7.1 illustrates the typical occurrence of Type I inclusions.

Type IIA

The presence of CO_2 in the gas phase of these inclusions is evidenced by the growth of liquid CO_2 around the gas bubble on cooling and the formation of the clathrate hydrate ($\text{CO}_2 \cdot 5.75 \text{H}_2\text{O}$). At room temperature these inclusions have an abnormally thick dark rim at the interface between gas and aqueous phases, which may be due to a thin skin of liquid CO_2 . P-PS Type IIA inclusions are restricted to veins containing no tungsten mineralisation but occur also as secondaries in quartz-feldspar (QF-m) and quartz-wolframite (Q + w, Q* + w) veins. Plate 7.2 illustrates the typical form and occurrence of Type IIA inclusions.

Type IIB

Complex liquid CO_2 -bearing inclusions are common as P-PS inclusions within quartz-feldspar veins (QF-m) and quartz-bismuthinite (Q-b) veins. They occur rarely within

Plate 7.1

Type I inclusions. Bar scale = 10 μ m.

- 7.1a Primary liquid-vapour inclusion in quartz from wolframite-bearing vein. Sample 377C, adit level.
- 7.1b Primary Type I inclusion in quartz from wolframite-bearing vein. Sample 377C, adit level.
- 7.1c P-PS liquid-vapour inclusion in quartz from wolframite-bearing vein. Planes of secondary liquid-vapour inclusions also visible. Sample 377C, adit level.
- 7.1d P-PS Type I inclusion in quartz from wolframite-bearing vein showing variable morphology.
- 7.1e P-PS Type I inclusion in quartz from Fe-rich wolframite-bearing quartz vein. Sample 344.
- 7.1f Primary liquid-vapour inclusion from wolframite-bearing quartz vein. Sample 377C, adit level.

Plate 71

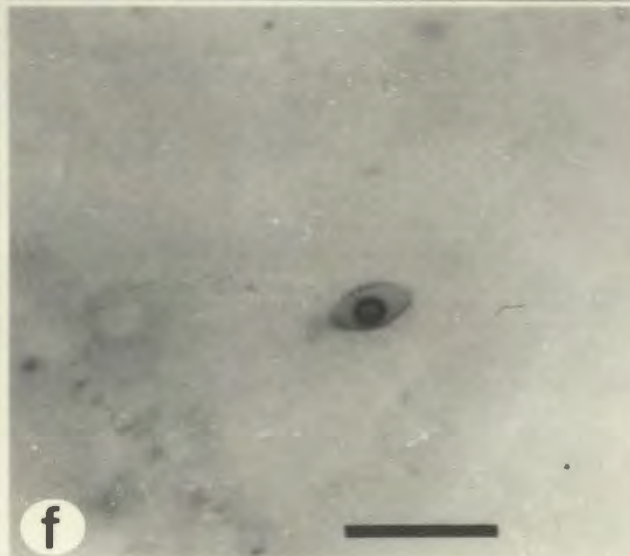
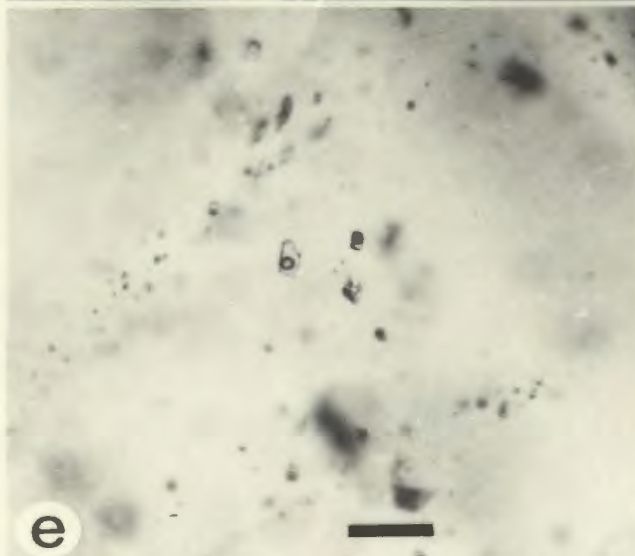
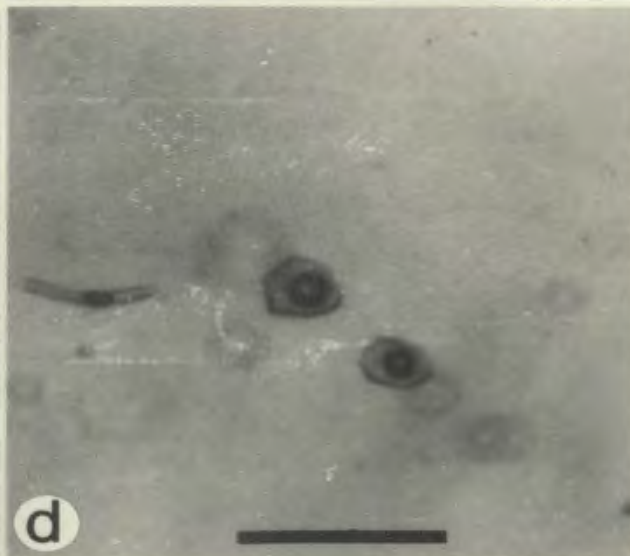
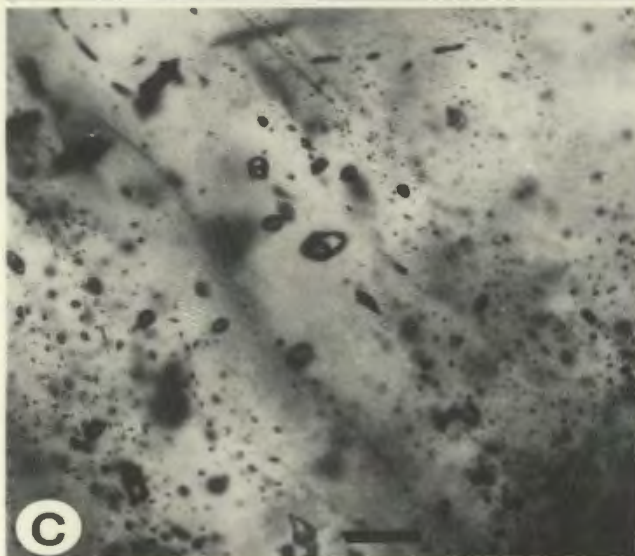
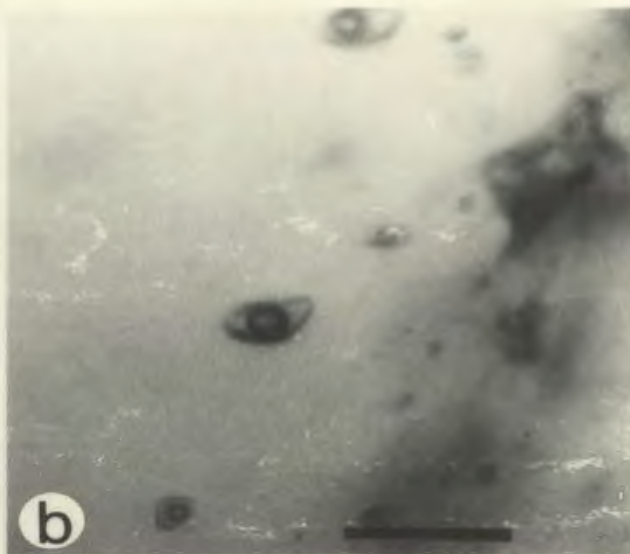
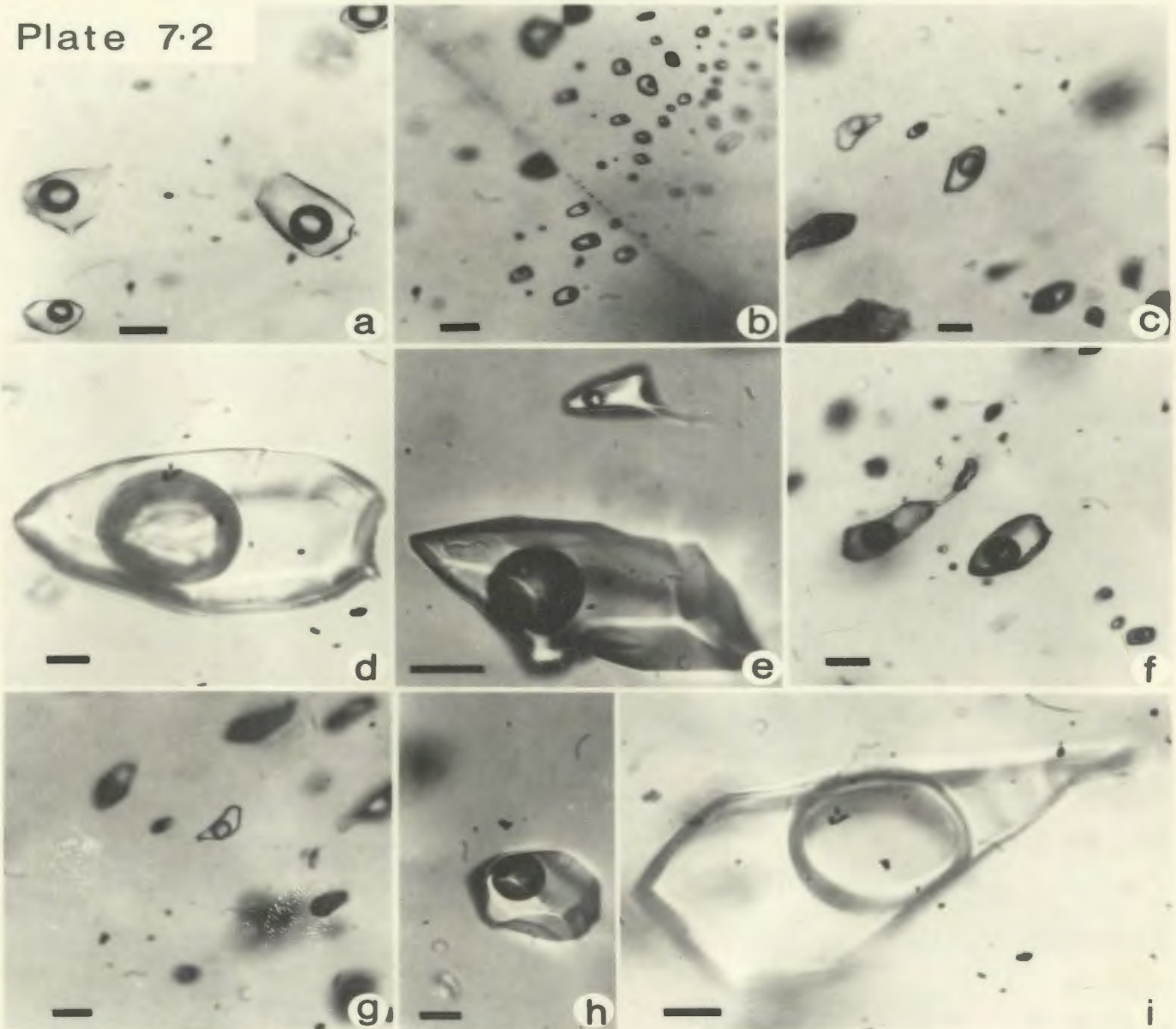


Plate 7.2

Type IIA inclusions. Bar scale = 10mm.

- 7.2a Primary Type IIA liquid-vapour (CO_2) inclusions in quartz from quartz-sulphide vein. Sample 709, adit level.
- 7.2b Plane of secondary Type IIA inclusions in quartz of quartz-sulphide veinlet. Sample 450, adit level.
- 7.2c Pseudosecondary liquid-vapour (CO_2) in quartz from quartz-sulphide vein. Sample 709, adit level.
- 7.2d Primary Type IIA inclusions. Black spots not opaque daughter but photographic artifact. Sample 709, adit level.
- 7.2e P-PS Type IIA inclusion. Sample 709, adit level.
- 7.2f Type IIA inclusion in quartz from a quartz-sulphide vein showing modification by necking down after trapping. Sample 450, adit level.
- 7.2g Pseudosecondary liquid-vapour (CO_2) inclusion in quartz from a quartz-sulphide veinlet. Sample 709, adit level.
- 7.2h,i Primary Type IIA liquid-vapour (CO_2) inclusions in quartz from a quartz-sulphide veinlet. Black spots are photographic artifacts not opaque daughter minerals. Sample 709, adit level.

Plate 7.2



quartz-sulphide (Q-s) veinlets of composite Vein #10.

Solid minerals within the inclusion occur uncommonly and are more prevalent in veins containing bismuthinite; the most common mineral being carbonate, possibly calcite.

Relative proportions of CO_2 (L+V) : aqueous solution vary and fall in within the range 1:9 to 6:4. Typically inclusions with the greatest proportion of CO_2 appear to be primary and occur mainly within quartz from QF-m veins. Those with lower proportions occur in isolated discontinuous planes (i.e. pseudosecondaries) associated with polyphase inclusions of Type IIC (described below) and IIA. Rare Type IIB inclusions (designated IIB*) containing a rhombohedral solid mineral and small amounts of liquid CO_2 are also associated with these inclusions in discontinuous rehealed fractures. Type IIB inclusions are illustrated in Plate 7.3.

Type IIC

Primary-pseudosecondary L-V inclusions containing a variable number of solid minerals are found in all veins excluding those containing wolframite and scheelite ($\text{Q} + \text{w}$, $\text{Q}^* + \text{w}$). These inclusions nucleate a clathrate on cooling indicating the presence of a CO_2 component in the vapour phase. Carbonates are universal as solid minerals in the inclusions although hexagonal platelets of probable gypsum-anhydrite are often present. A carbonate mineral, dawsonite is restricted to the non tungsten-bearing Q-s veins of the composite lode, Vein #10.

These polyphase inclusions are also found in discontin-

uous healed fractures with liquid CO₂-bearing inclusions (Type IIB, and IIB*) and Type IIA inclusions. Plates 7.4 and 7.5 contain representative examples of Type IIC inclusions.

Type III

Extremely rare, very irregular-shaped, secondary inclusions are found in Q + w veins. These polyphase (L-V-S) inclusions contain a great diversity of solid minerals; one inclusion within a partially rehealed fracture contained eight daughter mineral phases of unknown composition. Vapour bubbles are generally very small (1-5 vol.%) indicating a low temperature of homogenisation and hence formation.

Type IV

Small 1-10 μ m crystals of rhombohedral, platy and acicular habit occur as solid inclusions in several of the vein types. Carbonates, probably calcite, occur in quartz of QF-m veins but the greatest concentration of solid inclusions occurs in quartz of the Q-b and Q-s veins. In the latter a greater variety of solid inclusions are found with calcite, sulphates - probably anhydrite, and dawsonite being the principal types. No solid inclusions were found in quartz of the Q* + w or Q + w veins. Representative examples of Type IV inclusions are shown in Plate 7.5.

7.5 SECONDARY INCLUSIONS

Type I, IIA, IIB, and III inclusions also occur as secondary inclusions (Table 7.1) and their distribution between veins confirms the proposed sequential trapping of

Plate 7.3

Type IIB, IIB* inclusions. Bar scale = 10 μ m.

- 7.3a P-PS Type IIB inclusion containing three-phases, liquid CO₂ (L₁), Vapour CO₂ (V) and aqueous solution (L₂), in quartz from a quartz-feldspar-molybdenite vein. Sample 385.
- 7.3b,c, Primary Type IIB three-phase inclusions in quartz
d from a quartz-feldspar-molybdenite vein. Sample 385.
- 7.3e Primary three-phase Type IIB inclusion from a quartz-feldspar-molybdenite vein. Plane of secondary Type IIA or I inclusions also visible. Sample 385.
- 7.3f Pseudosecondary three-phase Type IIB inclusion in quartz from a quartz-feldspar molybdenite vein. Sample 385.
- 7.3g,i Primary Type IIB three-phase inclusion in quartz from a quartz-bismuthinite vein. Note significant drop in proportion of liquid and vapour CO₂: aqueous solution compared to those in quartz-feldspar-molybdenite veins. Sample 253.
- 7.3h Type IIB* inclusion containing liquid and vapour CO₂, aqueous solution, and an accidentally trapped solid mineral, probably calcite in quartz from a quartz-bismuthinite veinlet. Sample 253.
- 7.3j Association of low density Type IIB and IIA inclusions in quartz from a quartz-sulphide vein. Sample 687.
- 7.3k Close up of box area in Plate 7.3j. The CO₂ phases in the Type IIB inclusions homogenise to the vapour phase indicating that they contain highly compressed, low density CO₂. The association of IIB and IIA inclusions and solid inclusions (Type IV) such as calcite in quartz of the quartz-sulphide vein type represents a boiling environment.
- 7.3l Low density Type IIB inclusion (arrow) associated with Type IIA inclusions in quartz from a quartz-sulphide vein.

Plate 7.3

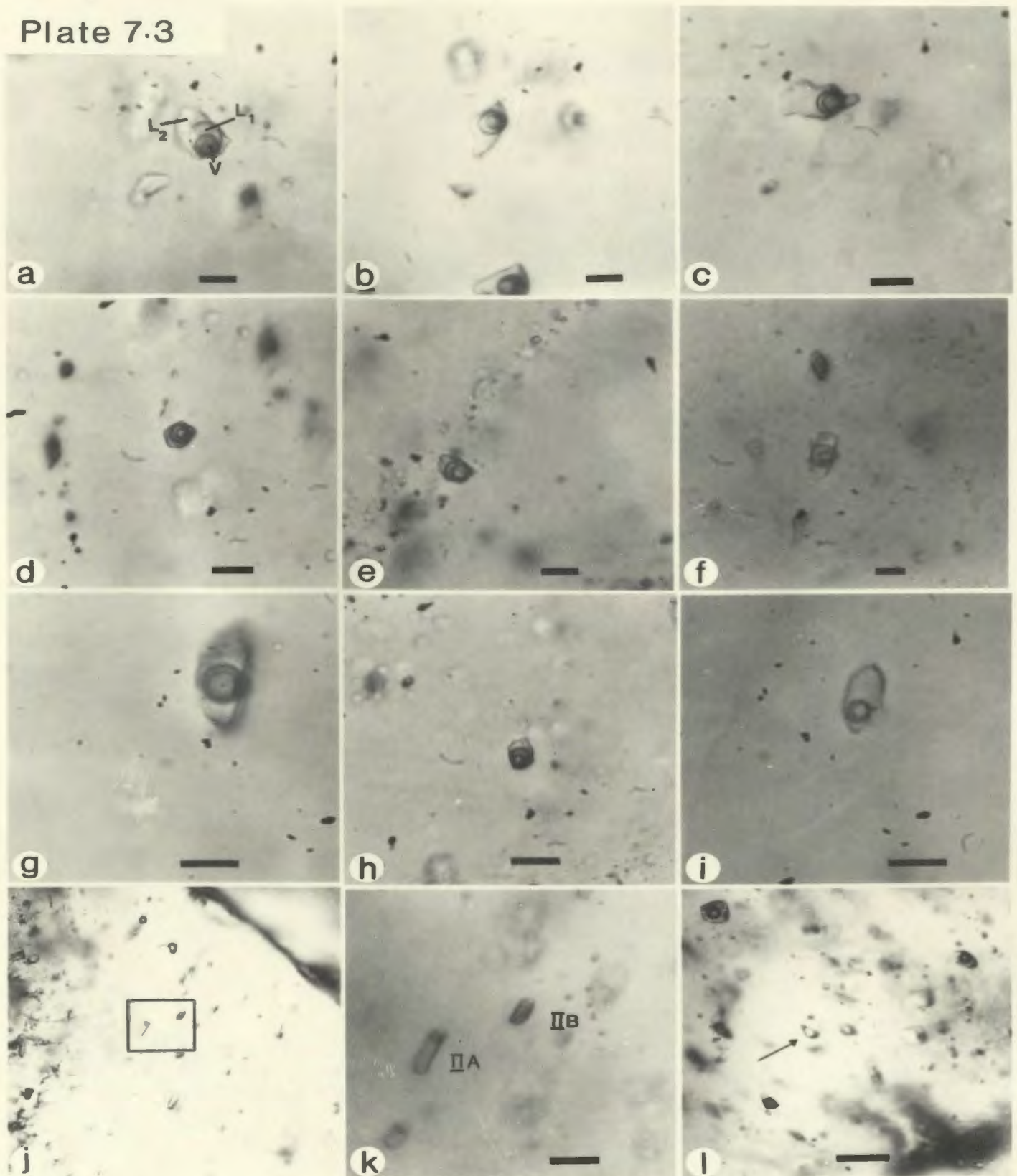


Plate 7.4

Type IIC inclusions. Bar scale = 10mm.

- 7.4a Type IIC inclusion containing two solid mineral phases; a carbonate rhomb, probably calcite, and a birefringent platy mineral, probably gypsum. These inclusions are associated with high density Type IIB (CO₂-rich) and IIA (H₂O-rich) inclusions as well as small inclusions of carbonate (Type IV), representing the trapping of immiscible fluids. Lack of regular phase ratios and the presence of solid carbonate minerals as inclusions suggest that the solid phases in Type IIC inclusions were accidentally trapped. Sample 246, Vein #1, quartz-bismuthinite veinlet.
- 7.4b Type IIC inclusion containing carbonate mineral associated with Type IIA and IIB inclusions in quartz from sample 253, Vein #3. Black specks are photographic artifacts, not opaque minerals.
- 7.4c Type IIC inclusion containing three birefringent minerals. Rhomb-shape mineral probably calcite, others unknown. The inclusion is associated with Type IIA, IV and rare low density Type IIB inclusions indicative of retrograde boiling conditions. Sample 709 from quartz-sulphide veinlet, Vein #10.
- 7.4d P-PS Type IIC inclusion associated with water-rich Type IIA inclusion (shown) and CO₂-rich Type IIB inclusion in quartz of quartz-feldspar-molybdenite vein. Sample 385.
- 7.4e Type IIB inclusion containing two birefringent minerals as well as a platy opaque mineral, possibly hematite. Vapour bubble is out of focus in lower portion of the inclusion. Sample 253, Vein #3.
- 7.4f Type IIC inclusion associated with Type IIA inclusion and rare low density Type IIB inclusion in quartz of a quartz-sulphide veinlet, Vein #10. Inclusion contains three or four birefringent minerals. Sample 709.
- 7.4g, h, Dawsonite-bearing Type IIC inclusions in quartz from a quartz-sulphide veinlet, Vein #10. Dawsonite occurs in its typical habit; birefringent, needle-like crystals in radial aggregates. Sample 709.

Plate 7.4

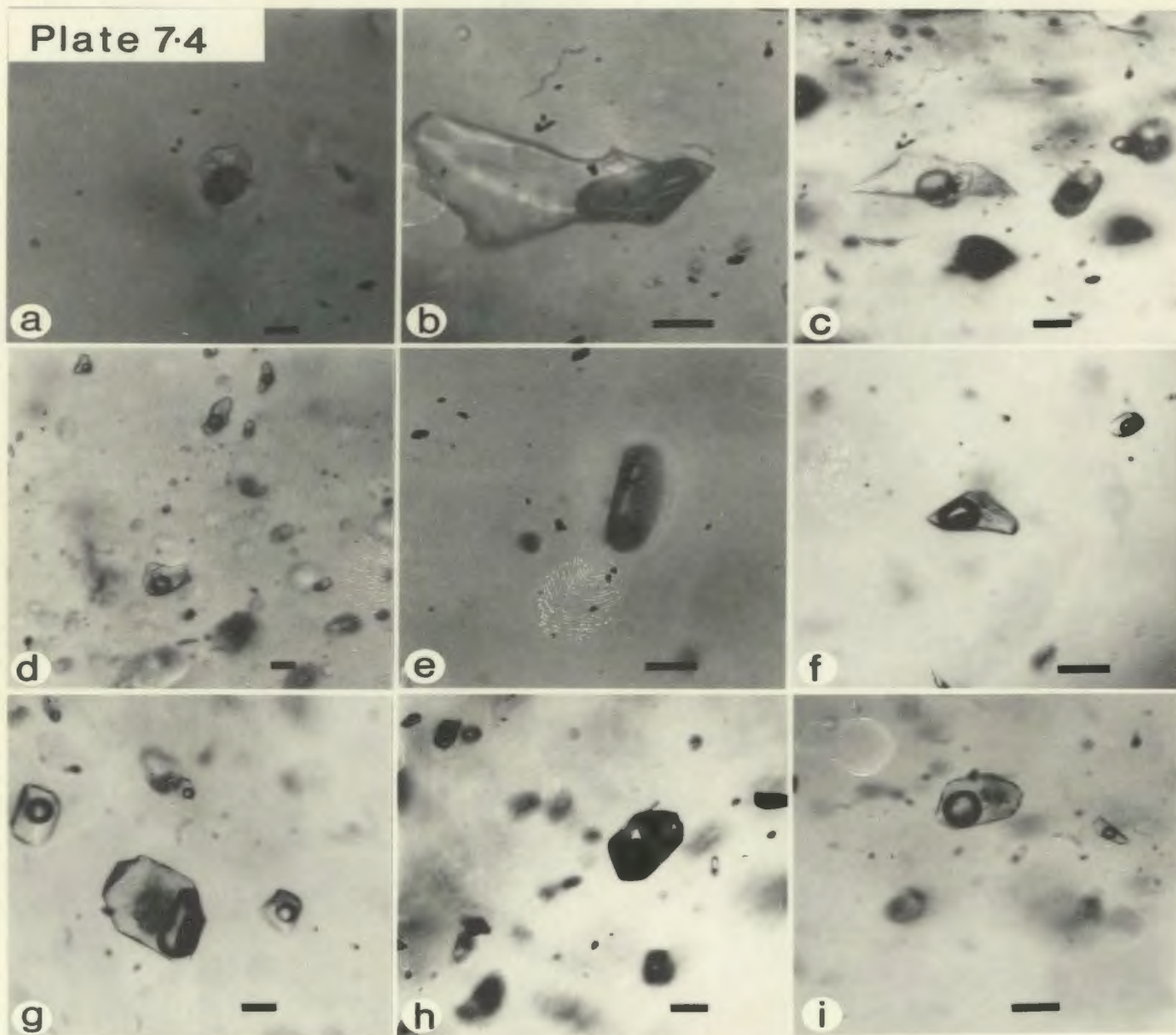


Plate 7.5

Type IIC and Type IV inclusions. Bar scale = 10mm.

- 7.5a Type IIC inclusions containing two unknown birefringent minerals, possibly gypsum and anhydrite, in quartz from quartz-sulphide veinlet, Vein #10, sample 709.
- 7.5b Type IIC inclusion containing an acicular birefringent mineral of unknown composition. Sample 709, quartz-sulphide veinlet. X-polars.
- 7.5c Crystal of calcite in a P-PS Type IIC inclusion which is associated with Type IIA and low density Type IIB inclusions in quartz from a quartz-sulphide veinlet, Vein #10, sample 709.
- 7.5d PS Type IIC inclusion containing fibrous crystals which exhibit a moderate birefringence and are similar to the dawsonite crystals shown above (Plate 7.4 g-i) except for their radial habit. Sample 709.
- 7.5e PS inclusion containing a number of birefringent mineral phases; one, possibly two, having rhombohedral habit, while the rest are platy. They are assumed to be carbonate and sulphate minerals.
- 7.5f Primary Type IIC inclusion containing a birefringent rhombohedral crystal, probably calcite, and a thin platy opaque (hematite?). Sample 709, X-polars.
- 7.5g Solid inclusion (Type IV) exhibiting a moderate birefringence. May have caused the trapping of a liquid-vapour inclusion spatially associated with it (bubble not quite in focus). Sample 709, quartz-sulphide vein.
- 7.5h,i Type IV inclusion (arrow) in quartz of quartz-sulphide veinlet of Vein #10 (sample 709). In Plate 7.5i the crystal appears to have caused the trapping of a small amount of liquid.

Plate 7.5

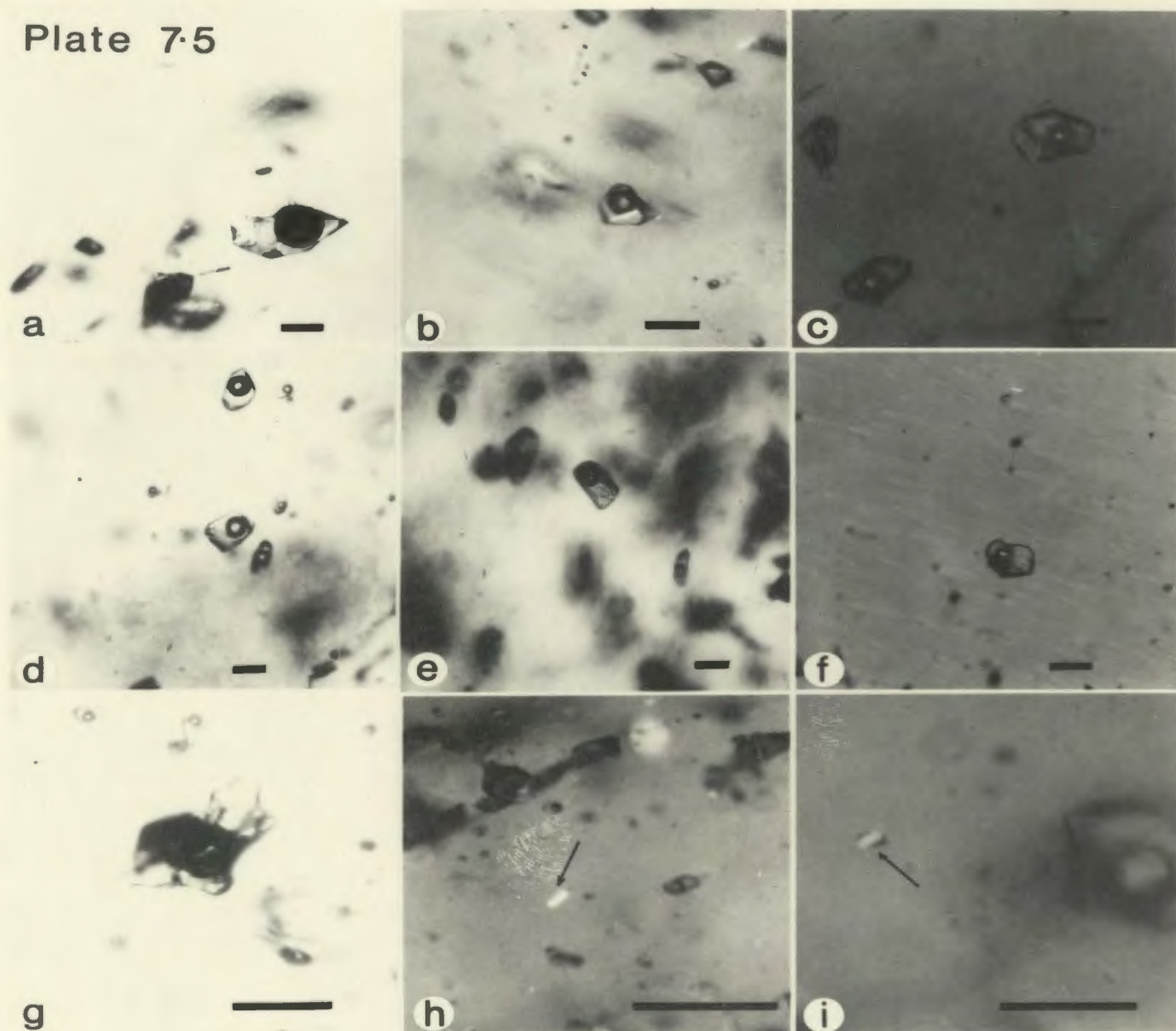

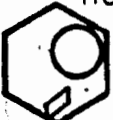












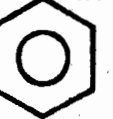





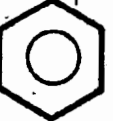


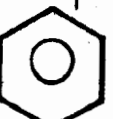




Table 7.1 Types of Inclusions and Distribution Among Vein Types

VEIN TYPE	PRIMARY-PSEUDOSECONDARY					SECONDARY		
QF-m	 IIB	 IIC	 IIA	 IIB'	 IV	 I	 IIA	 IIB
Q-b	 IIA	 IIB	 IIB'	 IIC	 IV	 I	 IIA	 IIB
Q-s	 IIA	 IIB	 IIC	 IV		 I	 IIA	
Q+W, Q+W	 I					 I	 IIA	 III

the P-PS inclusions and the vein types. Secondary CO₂-rich inclusions do not occur in vein types associated with Vein #10 which suggests that deposition in the latter postdated the deposition of the quartz-feldspar-molybdenite (QF-m) and quartz-bismuthinite (Q-b) veins. Type I and IIA inclusions occur as secondary inclusions in both wolframite-bearing (Q + w) and wolframite-free (Q-s) veinlets of Vein #10 reflecting the multiple injection history of that vein.

7.6 THE SIGNIFICANCE OF SOLID MINERAL INCLUSIONS











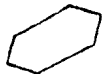




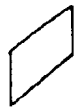



Daughter minerals in fluid inclusions, solid phases that crystallise out of the fluid during cooling, indicate saturation of the fluid with respect to those phases at room temperature. Their identification provides information on the composition of the fluid although there is a problem in distinguishing between daughter minerals formed by cooling of the inclusion fluid and accidental solid minerals trapped along with the liquid. Regularity of phase ratios among similar inclusions would suggest precipitation from a cooling fluid (Roedder, 1972).

With the exception of opaque minerals, solid minerals in fluid inclusions are restricted to Type IIB*, IIC and III inclusions. Table 7.2 illustrates the types of solid minerals and their distribution between vein types. Within the range of temperatures reached during homogenisation studies (0-400°C) none of the mineral phases were observed to dissolve. This is to be expected since carbonates and sulphates have retrograde solubility with increasing

Table 7.2

Types of Solid Inclusions
and their Distribution Among the Vein Types

1. Carbonates: Rhombohedral morphology and high birefringence. Probably calcite. One twinned crystal observed.
2. Dawsonite ($\text{NaAlCO}_3(\text{OH})_2$): Clusters of fiber-radial aggregates. Moderate birefringence and a positive relief against enclosing fluid. Associated with CO_2 -bearing inclusions.
3. Gypsum ? ($\text{CaSO}_4 \cdot 2\text{H}_2\text{O}$)
Bassanite ? : Hexagonal platelet with moderate optical relief. Colourless, clear.
4. Anhydrite ? (CaSO_4): Platey to prismatic, moderate to high relief, high birefringence.
5. Halite (NaCl): Cubic, isotropic with moderate to high optical relief.
6. Unknown A: Poor morphology - partially rectangular. Medium to high optical relief.
7. Unknown B: Thin single acicular crystal. Medium to low relief. Birefringence low.
8. Unknown C: Several octohedral platelets of varying overall shape. Low-medium relief and birefringence low.
9. Opaque minerals - irregular minute grains, rarely platey.

	PRIMARY-PSEUDOSECONDARY				SECONDARY ¹
QF-m	1 	7 	6 	9 	
Q-b	1 	9 	4 		
Q-s	1?  	2 	3 	9 	
Q+w				5  4  9  1 	
Q+w				6  8  8 	

¹-In rare Type III only

temperatures (Holland, 1967).

Solid minerals occur both in quartz (as Type IV inclusions) and within inclusions in quartz (Type IIB*, Type IIC) which strongly suggests that they were trapped accidentally. Furthermore minerals in Type IIC inclusions often have variable L:V:S ratios which is indicative of accidental trapping rather than precipitation from a cooling fluid. Volume percent salts range from 0.4 to 18% although some individual groups of inclusions have similar L:V:S ratios. This is especially true of inclusions containing dawsonite which have no other daughter minerals present. However, the overall irregularity in phase ratios of Type IIC inclusions is emphasised by the common absence of one or more of the daughter minerals between similar inclusions. This may represent only a nucleation difficulty (Roedder, 1972) or perhaps dissolution with falling temperature, although it is probably more indicative of accidental trapping of the crystals.

Carbonate deposition primarily depends on pH and P_{CO_2} although calcite solubility increases with increasing NaCl content of the fluid (Ellis, 1959). In most situations calcite cannot be precipitated from a cooling hydrothermal fluid but may be deposited by release of CO_2 from the system (Holland, 1967). The solubility of sulphates, like carbonates, decreases rapidly with increasing temperature but available data (Blount and Dickson, 1969) indicates increased solubility with increasing solute concentration (NaCl) and

increasing pressure. However, for the salinities and pressures indicated for the Grey River hydrothermal fluid, sulphates cannot be precipitated by falling temperature. Loss of SO_2 from the systems however may cause anhydrite to precipitate (Holland, 1967).

Loss of CO_2 and SO_2 from a hydrothermal system is possible when immiscibility or boiling occurs. If a supercritical CO_2 - H_2O fluid containing dissolved carbonate, bicarbonate, and sulphate unmixes, two fluids will result, one rich in CO_2 , the other in H_2O . Because of the loss of CO_2 and SO_2 from the H_2O -rich fluid, the solubility of the dissolved carbonate and sulphate will be sharply reduced and precipitation of these phases could occur. If such fluids were trapped at this point the resulting inclusions should have the following forms:- CO_2 -rich inclusions, H_2O -rich inclusions, solid inclusions of carbonates and sulphates, and mixtures of these types. This is illustrated in Figure 7.3.

A similar association of inclusions occur in all vein types except $\text{Q}^* + \text{w}$ and $\text{Q} + \text{w}$ veins. Density measurements on the CO_2 -bearing inclusions (discussed below) show that the association of these five inclusion types in QF-m veins (as PS inclusions) and Q-b veins (as P inclusions) is a result of the trapping of immiscible CO_2 - and H_2O -rich fluids. Low density CO_2 -bearing inclusions in Q-s veins indicate that the association of the five inclusion types resulted from boiling of the H_2O -rich fluid during deposition of these veins.

PRODUCTS OF UNMIXING OF A SUPERCRITICAL
CO₂-H₂O FLUID

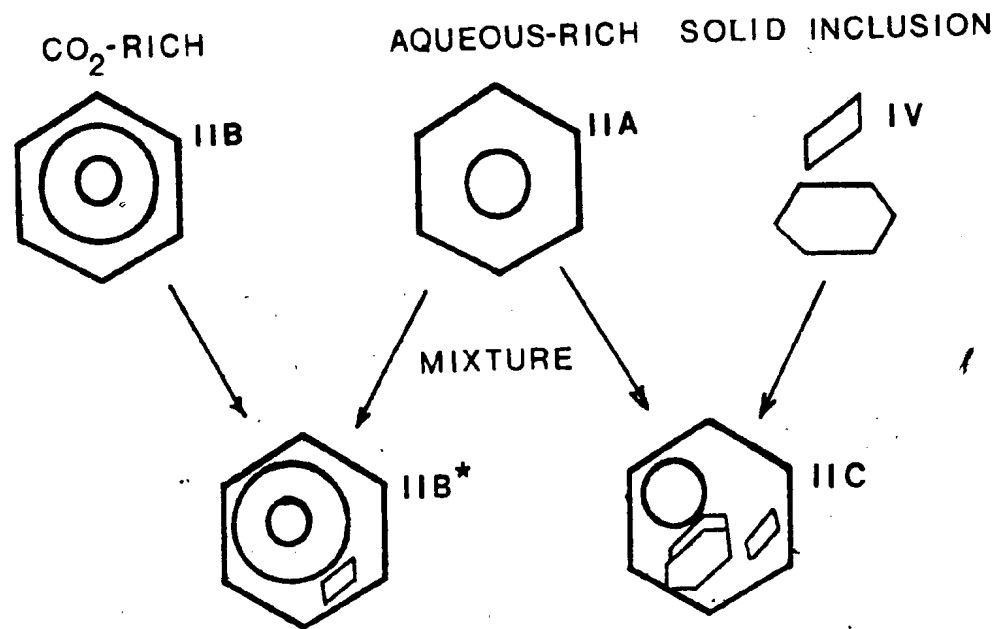


Figure 7.3

7.7 MICROTHERMETRIC MEASUREMENTS

While considerable information is evident from observation of fluid inclusions, use of the heating and freezing stage allows measurements of the homogenisation temperature and composition of the fluid and indicates temporal and spatial variations of these parameters throughout the vein system.

7.7.1 Salinity

Standard techniques (Appendix E.1) were used to determine salinity on approximately 200 inclusions by the depression of T_m ice method. In the range of operating temperature, measurements are accurate to within $\pm 0.2^\circ\text{C}$ (2σ). The freezing point determination is expressed in terms of NaCl content which would produce an equivalent depression, thus the error in measurement is ± 0.4 equivalent wt% NaCl. However, the predominance of CO_2 in many of the inclusions would indicate that NaCl is perhaps not a major constituent of the ore fluid (salting out effect, Ellis, 1959). Hence although expressed in NaCl contents the salinities are a measure of the total dissolved solute concentration whether it be HCO_3^- , CO_3^{2-} , NaCl, KCl or some other species.

Figure 7.4A shows the salinity determinations (Appendix F.1) for P-PS Type I inclusions in quartz, fluorite and scheelite from veins containing tungsten mineralisation (Q + w, Q* + w). No data are available for Type I inclusions from Vein #6 nor Galena #1 Vein, as their small size and other factors (necking down etc.) precluded their measurement.

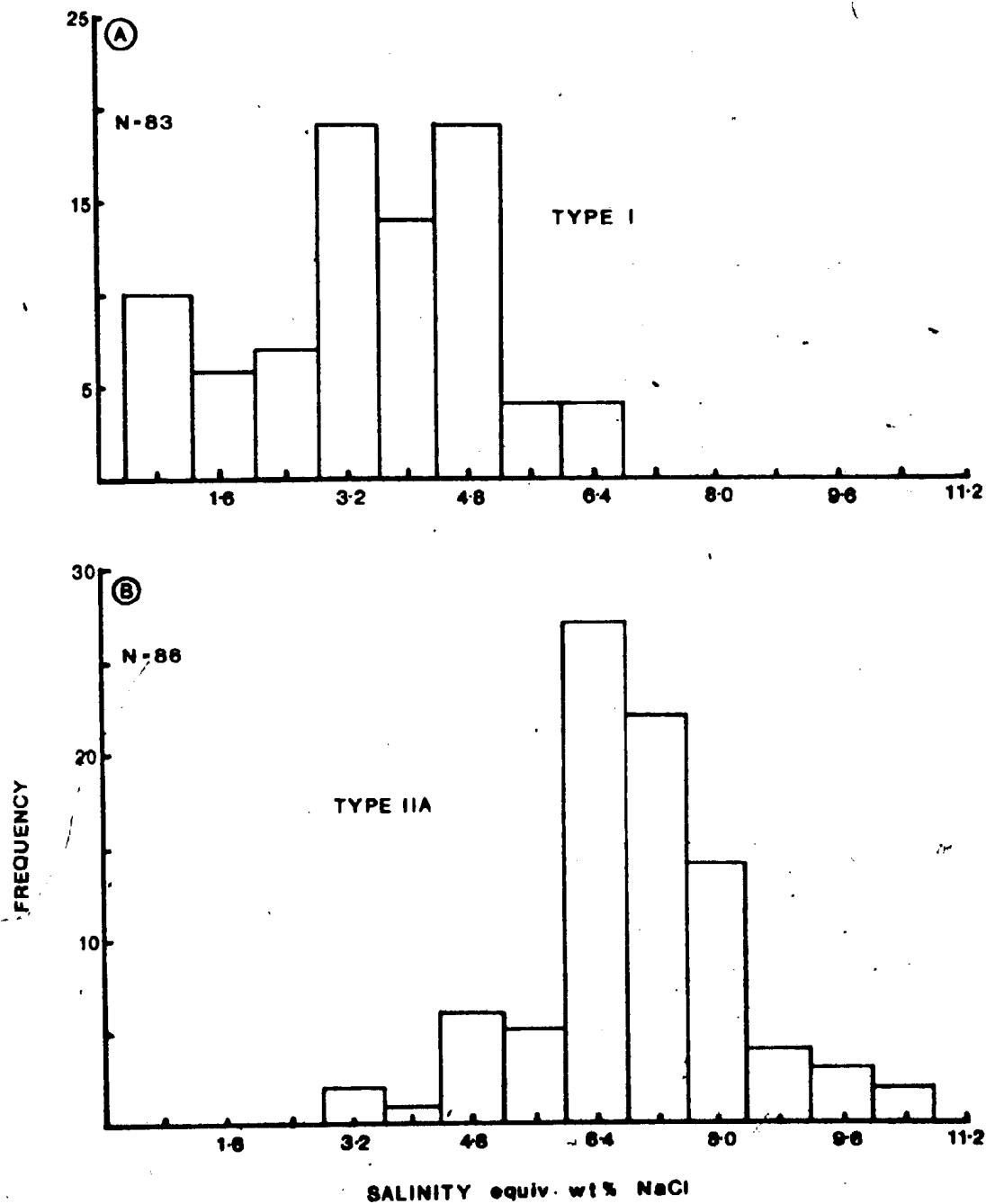


Figure 7.4 Salinity determinations from Tm ice of Type I and Type IIA inclusions in quartz, fluorite and scheelite.

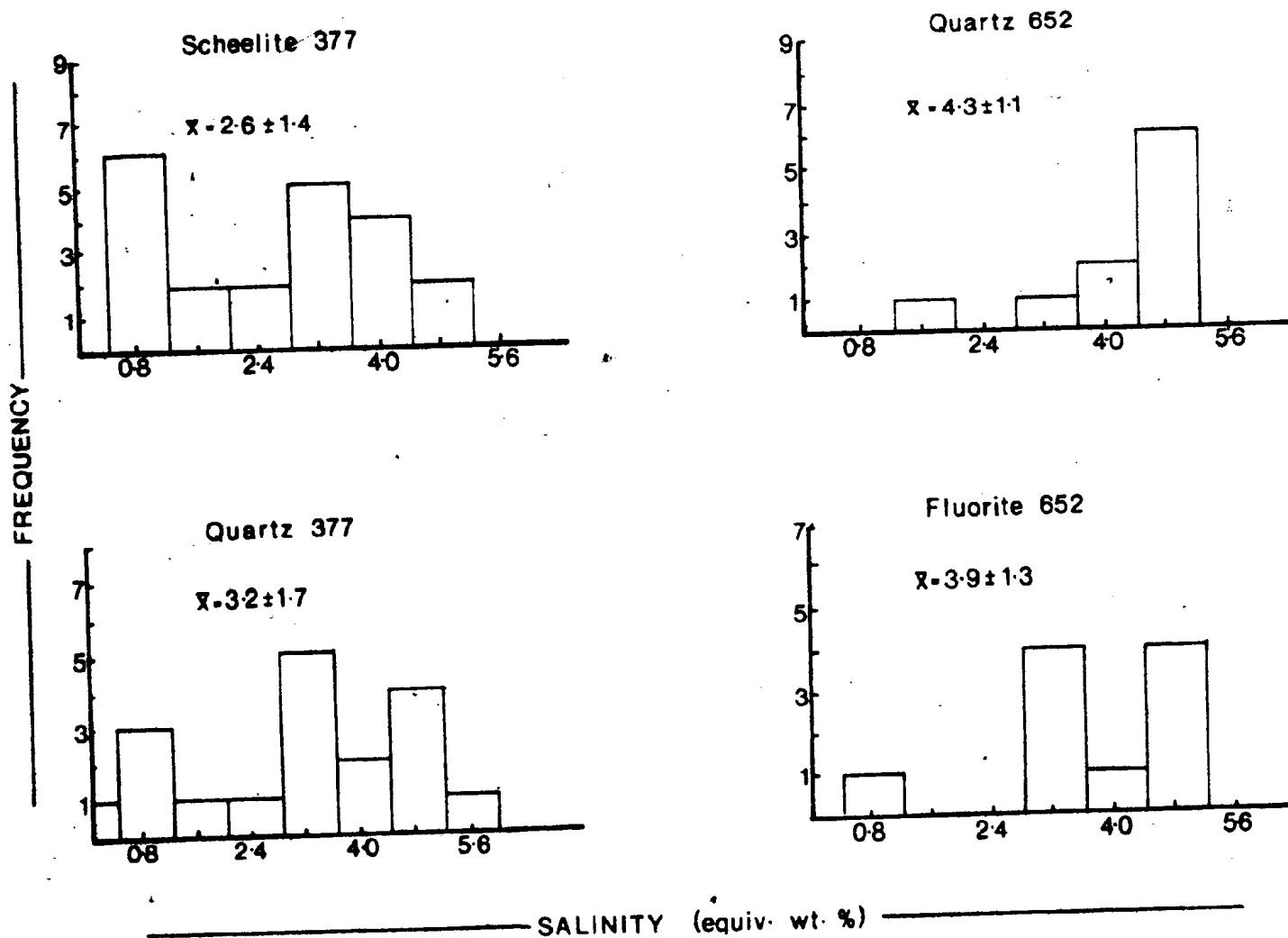


Figure 7.5 Comparison of salinity determinations from coexisting minerals.

All inclusions exhibited metastable phenomena (Roedder, 1963) requiring considerable supercooling to nucleate ice. Most nucleated ice in the range -40°C to -50°C , substantially below their ice melting temperature range of -5° to 0°C . This metastable feature, although a result of many factors, is said to indicate a relatively slow rate of flow of the hydrothermal fluid in the vein system (Kerrick et al., 1978).

Inclusions in quartz from Q + w and Q* + w veins have a mean salinity of 3.5 ± 1.6 equivalent wt% NaCl with a mean depression of melting point of ice of -1.1°C . Salinities of fluids were measured from inclusions in quartz, fluorite and scheelite to ascertain any variation between phases from the same mineral assemblage (Figure 7.5). For both samples (377 and 652) the salinities for the quartz-scheelite and quartz-fluorite pairs matched within 1 σ limits. Both of these samples were from late injections in Vein #10 but the data are similar to values obtained from earlier tungsten-bearing quartz injections (see Appendix F.1, e.g. sample Q-611-10), which suggests that salinities for tungsten-bearing quartz injections were constant regardless of relative age. Most, if not all, the scheelite in the veins is pseudomorphic after wolframite, and the salinity of inclusions in the scheelite are similar to inclusions from quartz which coexists with unaltered wolframite. Similarly homogenisation temperature measurements on inclusions in scheelite (discussed below) are identical to those from quartz associated with unaltered wolframite.

This might suggest that scheelitisation of the wolframite occurred quite soon after the initial deposition of the wolframite.

Two phase (L-V) Type IIA inclusions exhibited melting of ice at substantially lower temperatures than those of Type I inclusions. Salinities determined from depression of melting point of ice for these inclusions (Figure 7.4B) give an average of 6.9 ± 1.3 equivalent wt% NaCl (average $T_m \text{ ice} = -4.5 \pm 0.7^\circ\text{C}$). However, in freezing runs the clathrate hydrate ($\text{CO}_2 \cdot 5.75 \text{ H}_2\text{O}$) typically nucleated in Type II inclusions. Though difficult to observe, the formation of clathrate provides a sensitive test for the occurrence of CO_2 in an inclusion (Hollister and Burruss, 1976). Furthermore, the formation of clathrate in an inclusion has a considerable effect on the salinity of the residual fluid (Collins, 1979). Gas hydrates are very pure compounds involving only dissolved gases and water, with all other dissolved species (e.g. salts) excluded from the lattice. This exclusion causes considerable salinity increase in the residual solutions after clathration, with salinity increases up to 50% recorded by Collins (1979).

Supercooling is required to nucleate clathrate in Type IIA and IIC inclusions and occurs predominantly in the temperature range -30°C to -40°C , or about 10°C above the nucleation temperature of ice. A few inclusions, however, nucleated clathrate and ice simultaneously at low temperatures. Clathrate formation resulted in a radial crystalline texture which appears to emanate from the vapour bubble surface into

Figure 7.6 Ice and clathrate microthermometric measurements from Type IIA and IIC inclusions.

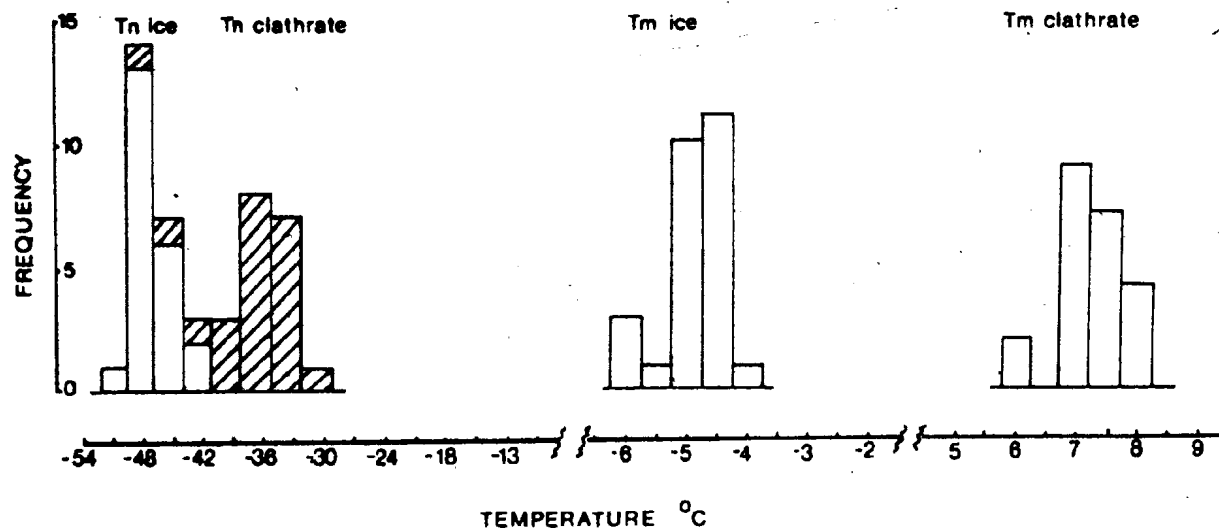
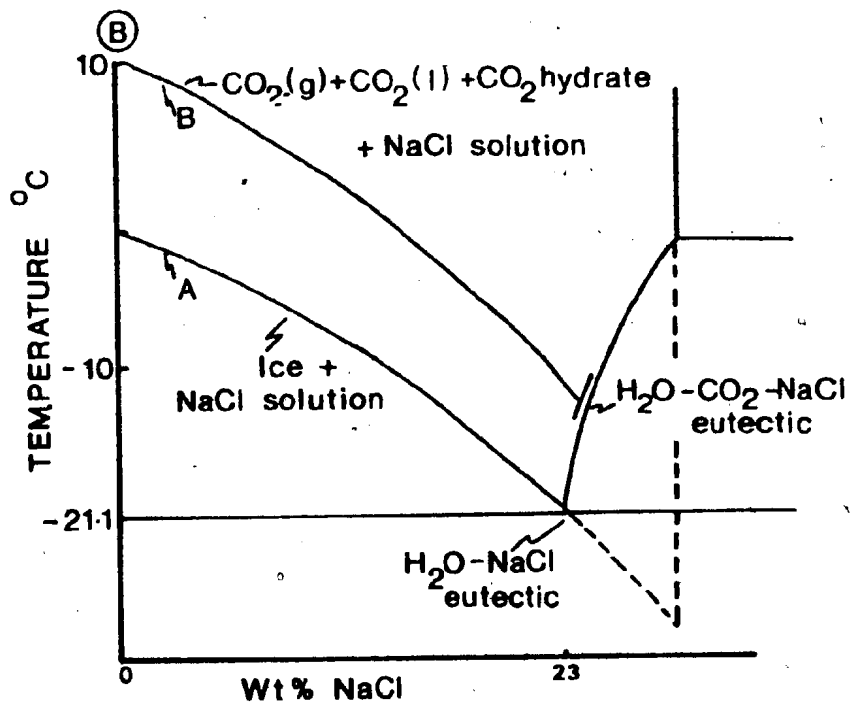
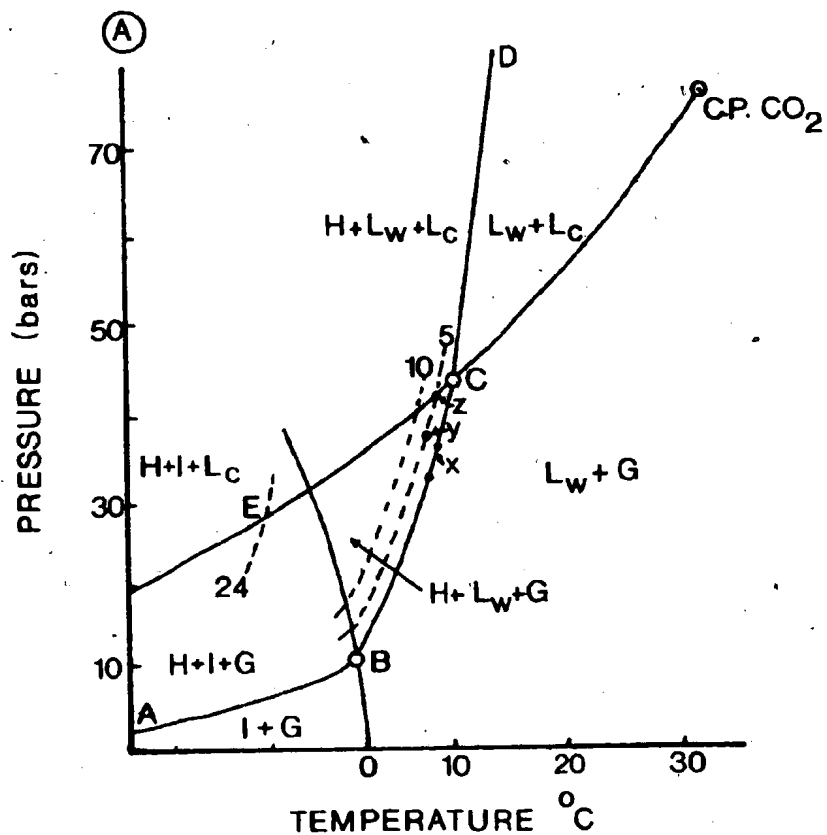


Figure 7.7 Equilibria in the $\text{CO}_2\text{-H}_2\text{O-NaCl}$ system.

- 7.7A Phase diagram for the system $\text{H}_2\text{O-CO}_2$ (after Collins, 1979) compiled from data of Larson (1955), Takenouchi and Kennedy (1965) and Chen (1972). The dashed lines indicate the shift to lower temperatures of the decomposition of CO_2 hydrate in equilibrium with 5 wt%, 10 wt%, and saturated NaCl solutions (from Chen, 1972; Bozzo et al., 1975).
- 7.7B Depression of the melting temperature of CO_2 hydrate by NaCl in the presence of CO_2 liquid and CO_2 gas (from Chen, 1972; Bozzo et al., 1975). The melting temperature depression of ice by NaCl is included for comparison. Diagram from Collins (1979).

Abbreviations used in diagram:

H = hydrate, L_w = liquid water, L_c = liquid CO_2 , G = gas, I = ice. See text for further explanation.



the aqueous fluid. This texture was transformed to a fine-grained translucent aggregate upon nucleation of ice.

Measurement of the T_m ice, T_m clathrate, T_m ice and T_m clathrate are shown in Figure 7.6 for several Type IIA and IIC inclusions (assuming solid minerals of Type IIC inclusions were accidentally trapped). The average T_m ice is -4.9°C (7.0 equiv. wt% NaCl) which agrees closely with the T_m ice for other Type IIA inclusions from quartz in Q-s and Q-b veins (Figure 7.4B). The average clathrate melting temperature is $+7.2^{\circ}\text{C}$ indicating a depression of 2.8°C from the clathrate melting temperature in the pure $\text{CO}_2\text{-H}_2\text{O}$ systems ($+10^{\circ}\text{C}$).

CO_2 -hydrate melting temperatures can be used to measure salinities of the aqueous fluid in inclusions, provided no other gas phase is present (Hollister and Burruss, 1976; Collins, 1979). The temperature of decomposition of the CO_2 hydrate in the presence of CO_2 liquid and CO_2 gas is depressed by salts in solution in a manner similar to the effect of NaCl on the melting temperature of ice (line A, Figure 7.7B). In the pure $\text{CO}_2\text{-H}_2\text{O}$ system the T_m clathrate would occur at the invariant point C (Figure 7.7A). With increased concentration of dissolved salts in solution the invariant point is depressed along the line CE (Figure 7.7A) and line B (Figure 7.7B). Inclusions in which a liquid CO_2 phase is not present cannot be used for salinity determinations, as the melting of clathrate in that case occurs along line BC (Figure 7.7A) or a lower temperature

analogue with increasing NaCl concentrations. Thus salinities for Type IIA and Type IIC inclusions cannot be determined by clathrate melting but must be less than 5 equivalent wt% NaCl (i.e. lie at some point between X and Z (Figure 7.7A)). Also the partial pressure of CO₂ present at room temperature in Type IIA and IIC inclusions must be between 25 and 40 bars (Figure 7.7A).

If the estimate of Collins (1979) that salinities measured by T_m ice are increased by 25-50% in the presence of clathrate, then the salinities measured in Type IIA inclusions by that method (Figure 7.4B) are too high by a factor of 2. Thus an average salinity for Type IIA (and IIC) inclusions is 3.5 equivalent wt% NaCl (depression T_m ice = -1.2°C).

Type IIB inclusions contain liquid CO₂ at room temperature hence the T_m clathrate from these inclusions may be used to estimate salinity as the decomposition of the clathrate takes place along curve EC (Figure 7.7A) and line B (Figure 7.7B). Figure 7.8 shows the clathrate melting temperature recorded for Type IIB inclusions in quartz from QF-m and Q-b veins. The melting temperature averages +7.3°C and indicates a depression of 2.7°C from the T_m clathrate in the pure CO₂-H₂O system. This is equivalent to 5 equivalent wt% NaCl in the aqueous phase (Figure 7.7B) and a depression of -3.0 for the melting point of ice. The small size of the inclusions as well as the small volume of H₂O available precluded the accurate determination of T_m ice.

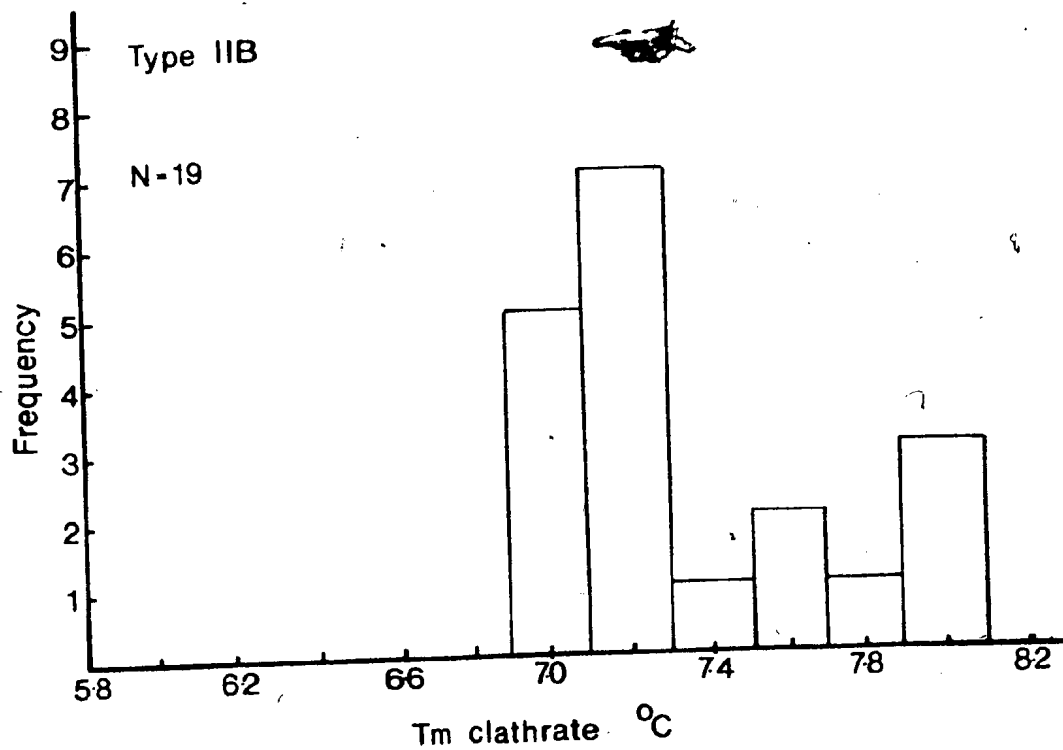


Figure 7.8 Temperature of melting of CO₂ clathrate for Type IIB inclusions.

Rare Type IIB inclusions in Q-s assemblages of Vein #10 had Tm clathrate in the range +8.7°C to +10.0°C (average 5 samples = +9.2°C Appendix F.2) indicating quite low salinities of 1.0 equivalent wt% NaCl or Tm ice of -0.5°C. Measurement of Tm ice from one of these inclusions shows a surprisingly high depression of -4.9°C and indicates the erroneous salinities such measurements can give in the presence of clathrate.

7.7.2 Interpretation of Salinity Measurements

Gross observational features of the fluid inclusions suggest that CO₂, H₂O, CO₃²⁻, HCO₃⁻, Ca²⁺, and Na⁺ are the dominant species involved in the hydrothermal fluid. It is worthwhile to consider the effect of these species on the Tm ice since freezing experiments indicate relatively low salinities.

Different solutes will effect the depression of melting temperature of ice by different magnitudes and it is possible to predict the depression by the following equation:

$$- T_m = K_f \cdot M. \quad (7.1)$$

Where Kf is the constant of proportionality for freezing point depression (Kf water = 1.86) and M = molality of solute. A plot of melting point depression for different concentrations of dissolved CO₂ is shown in Figure 7.9, and is compared to values for other solutes (NaCl, KCl, CaCl₂, KHCO₃, and MgSO₄) given by Roedder (1971). The effect of dissolved CO₂ is considerable; 3 mol% CO₂ (7.6 wt%) will

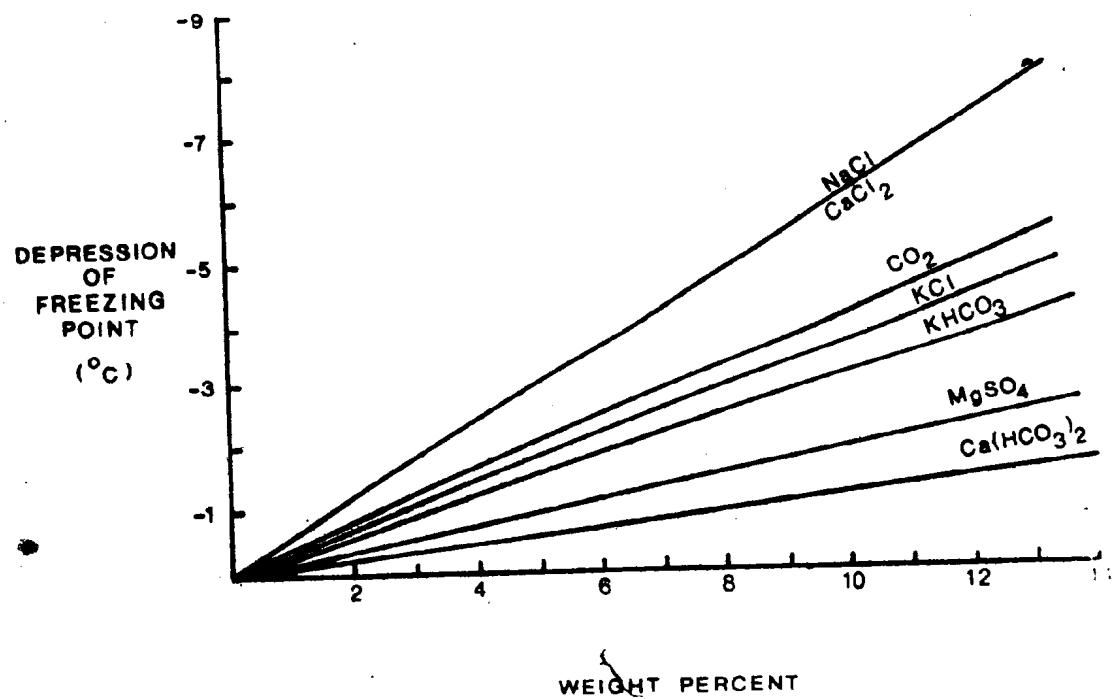


Figure 7.9 Melting point depression of ice for different solutes.

depress the T_m ice by nearly -3.2°C . Even 2 wt% dissolved CO_2 (0.8 mol%) will depress the T_m ice by approximately -1.0°C .

Due to formation of CO_2 hydrate in experimental runs, little data are available on the solubility of CO_2 in H_2O at low temperatures and pressures, although the data of Wiebe and Gaddy (1939, 1940), Malinin and Savelyeva (1973), Malinin and Kurovskaya (1975) and Rosasco *et al.*, (1975) indicate that 2-3 mol% CO_2 is soluble in H_2O at room temperature.

An inclusion with a vapour phase containing CO_2 at less than or equal to 10 bars pressure will nucleate ice on freezing before clathrate (Figure 7.7A). In that situation clathrate will not form, since after ice has nucleated there will be no H_2O to form the CO_2 hydrate. Type I inclusions did not nucleate clathrate on freezing and, assuming that the vapour phase contained CO_2 under 10 bars pressure (see crushing stage experiments, section 7.8), then a maximum of 1.0 wt% CO_2 could be dissolved in the aqueous solution at room temperature (Roedder, 1971; Takenouchi and Kennedy, 1965). Also it was noted that during supercooling, the vapour bubbles in Type I (and IIA and IIC) inclusions became smaller, perhaps indicating an increase in solubility with lower temperatures in the aqueous phase, similar to the observation of Collins (1979).

A solute concentration of 1.0 wt% CO_2 will depress the T_m ice by approximately 0.6°C and if solubility is increased

to 1.5 wt% by supercooling then a depression of -1.0°C is possible. The average depression of T_m ice for Type I inclusions is -1.2°C (3.5 equivalent wt% NaCl) indicating that a $0.5 - 0.6^{\circ}\text{C}$ depression may be due to a solute other than dissolved CO_2 , as depressions due to several solutes are roughly additive (Roedder, 1971).

Dissolved bicarbonate ions can also significantly depress the T_m ice (Figure 7.9) and up to 16 wt% of dissolved $\text{Ca}(\text{HCO}_3)_2$ is possible at room temperature (Clark, 1966). Even 2 to 3 wt% $\text{Ca}(\text{HCO}_3)_2$ would depress the T_m ice by -0.2 to -0.4°C . If the only solutes are NaCl and CO_2 then the maximum concentration of NaCl in the Type I inclusion is 0.5 wt% assuming a P_{CO_2} of 10 bars in the vapour phase. If dissolved bicarbonates are present then this concentration might be greatly reduced.

A similar situation is reported in fluid inclusions from the Broadlands geothermal field (Browne *et al.*, 1974) where measurements of the depression of T_m ice indicate salinities of 0.5 to 1.5 wt% NaCl although the present day geothermal field fluid has a NaCl content of 0.25 wt% NaCl. It also contains 4 wt% CO_2 (Sutton and McNabb, 1977). The T_m ice were measured on inclusions that did not nucleate the CO_2 clathrate.

Clathrate decomposition is affected by solute concentration and Larson (1955) established that this solute effect is nearly independent of the nature of the solute. 1 N HCl, 1 N NaOH and 1 M NaCl all result in a similar

depression in clathrate melting. In the $\text{CO}_2\text{-H}_2\text{O-NaCl}$ system clathrate melting begins at the eutectic point of -10°C (Collins, 1979) and as melting progresses CO_2 will be redissolved in H_2O and may have an effect on the decomposition of the clathrate (E. Roedder pers. comm., 1979).

Type IIB inclusions show clathrate melting at temperatures indicative of a 5 wt% solute concentration. These inclusions contain liquid CO_2 at room temperatures, indicating a P_{CO_2} of 45 bars, and thus should have the maximum dissolved CO_2 content of 2 to 3 mol% in the aqueous phase. This is equivalent to approximately 5 wt% dissolved CO_2 and may account for most of the solute concentration indicated by clathrate melting. Type IIA and IIC inclusions have salinities of less than 5 wt%, which is matched by the correspondingly lower P_{CO_2} and hence concentration of dissolved CO_2 .

In summary, dissolved CO_2 appears to have a profound effect on the depression of T_m ice in the Grey River inclusions. The partial pressure of CO_2 is highest in Type IIB inclusions and is progressively lower in Type IIA, IIC and Type I inclusions (Figure 7.10). This CO_2 depletion is matched by a decrease in salinities recorded from freezing experiments and can be related to a correspondingly lower concentration of dissolved CO_2 and hence depression of T_m ice. Comparison of measured depressions with relative depressions for CO_2 suggest that NaCl contents in the hydrothermal fluids were very low (less than 0.5 wt% NaCl),

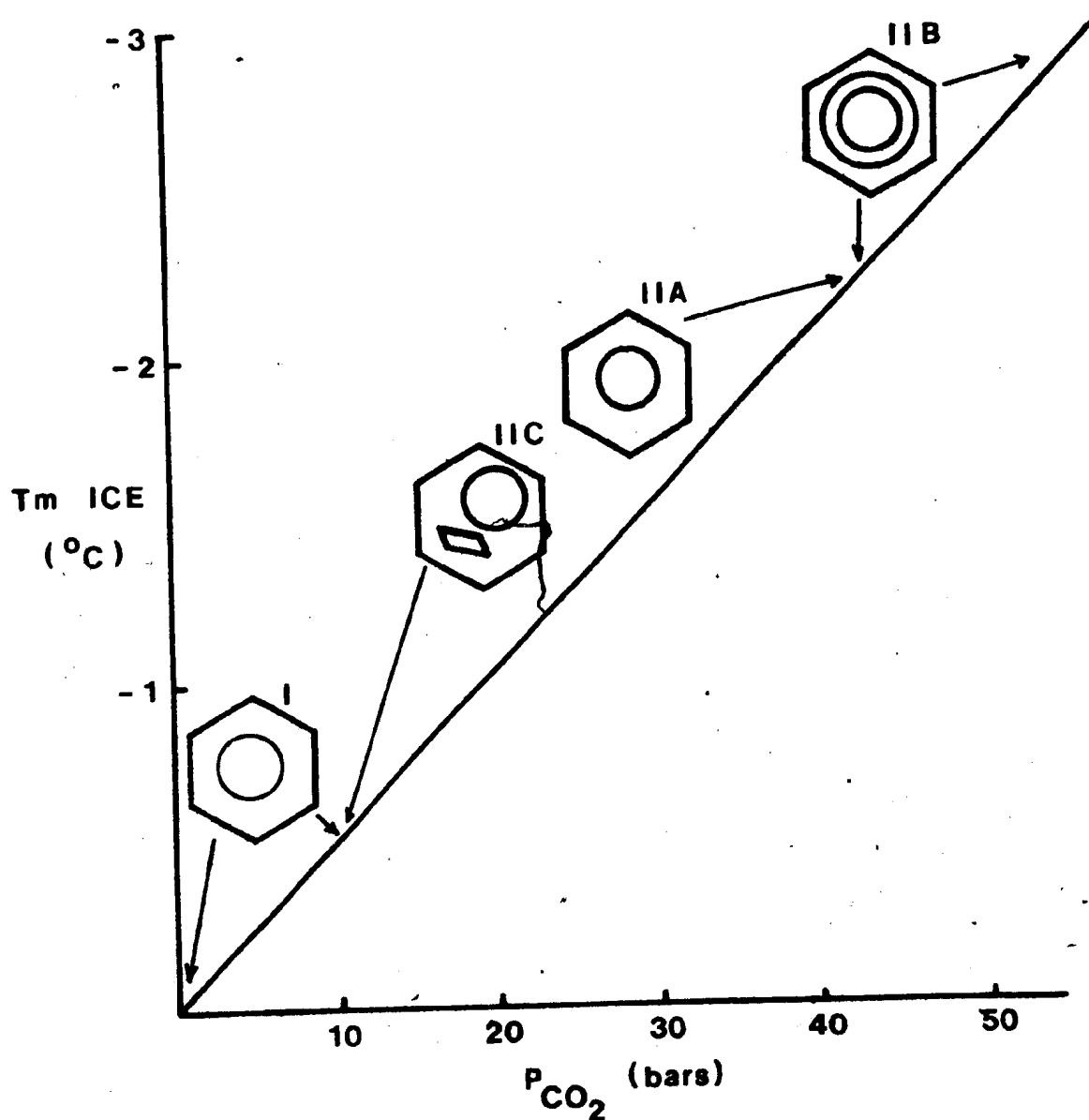


Figure 7.10 Effect of P_{CO_2} (dissolved CO_2) on the T_m ice. Grey River inclusions show a progressive depletion in CO_2 which is matched by a decrease in the T_m ice for such inclusions.

especially if there is any other dissolved species present as well (e.g. $\text{Ca}(\text{HCO}_3)_2$, KHCO_3 etc.).

7.7.3 Homogenisation Temperature

Standard techniques were used in the measurement of homogenisation temperatures on the heating stage (Appendix E.1). Approximately 400 heating measurements were made and these data are presented in Appendix F. Measurements made on specimens from the late fluorite-calcite-barite veins which postdate the tungsten mineralisation (are discussed in a separate section below. No data are available from Vein #6 because the size of the inclusions precluded their measurement. Inclusions from Galena #1 Vein showed evidence of extensive necking down and leakage which resulted in a wide spread of data points (Appendix F.5).

For all the heating data above 200°C , errors were approximately 0.5% of the measurement. Possible leakage of inclusions during heating was checked by remeasuring the size of the vapour bubble at room temperature and at times a second heating run was performed.

Figure 7.11A displays Th data (Appendix F.3) from liquid CO_2 -bearing Type IIB (and IIB*) inclusions in quartz from QF-m veins. While most of these P-PS inclusions decrepitated on heating due to the build up of high internal pressures, some homogenised either to the CO_2 -rich phase, the H_2O -rich phase, or by exhibiting critical phenomena. Those that did not decrepitate homogenised at a temperature greater than 280° , the bulk falling in the range $300\text{--}361^\circ\text{C}$.

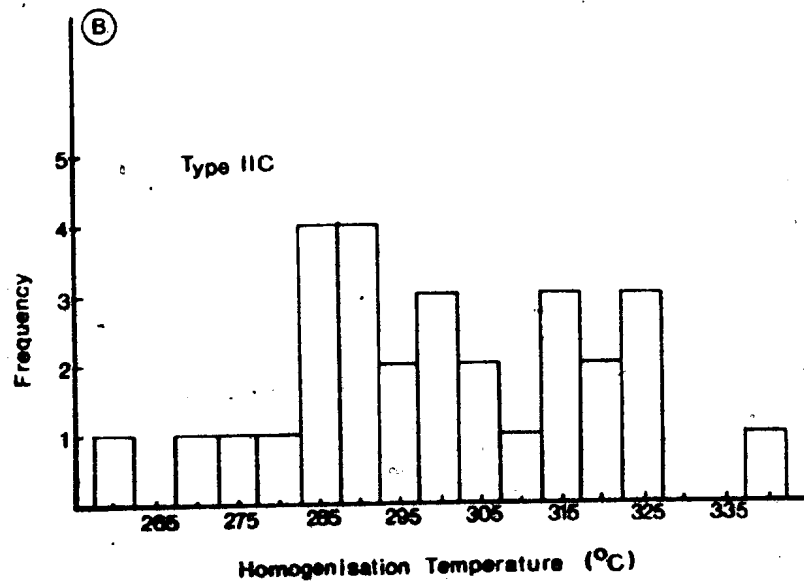
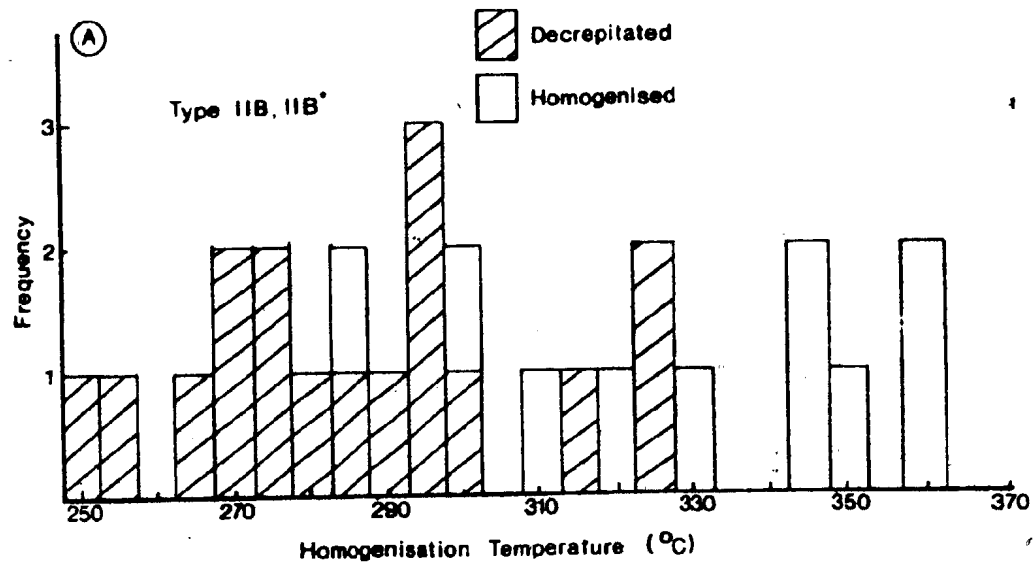


Figure 7.11 Homogenisation temperature data for Type IIB, IIB* and IIC inclusions.

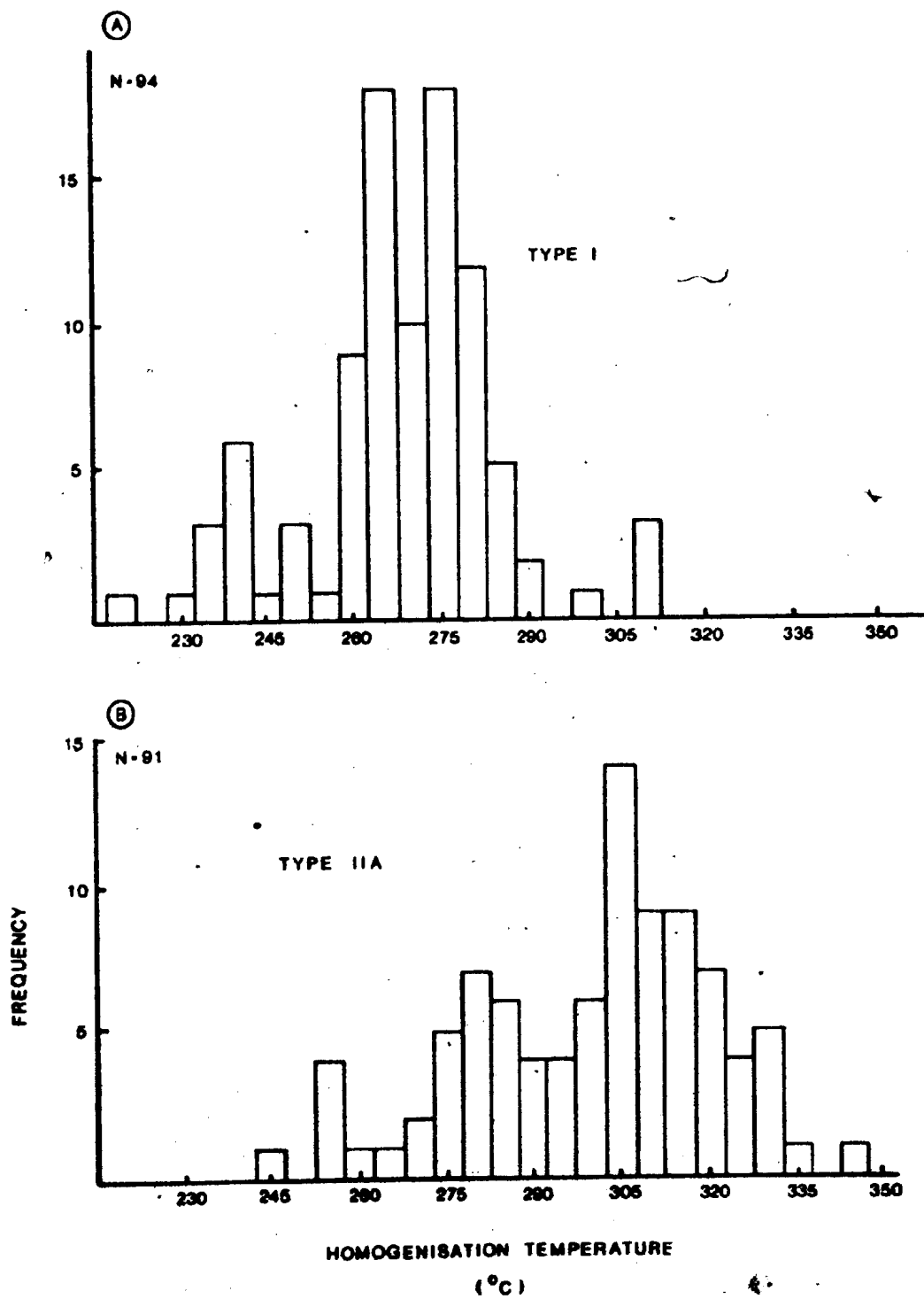


Figure 7.12 Homogenisation temperature data for Type I and IIA inclusions.

Type IIA inclusions are associated with Type IIB inclusions (and Type IV inclusions), pseudosecondaries in the QF-m veins, and as P-PS inclusions in the Q-b and Q-s vein types. Their homogenisation temperatures generally fall below 340°C (Figure 7.12B) and average $300^{\circ} \pm 21^{\circ}\text{C}$. Type IIC inclusions with the same distribution as Type IIA inclusions, show a similar range (Figure 7.11B) in homogenisation temperature.

Type I inclusions associated with tungsten-bearing veins ($\text{Q}^* + \text{w}$ and $\text{Q} + \text{w}$) have a substantially lower T_h than other types, the average T_h being $268^{\circ} \pm 17^{\circ}\text{C}$ (Figure 7.12). A combined salinity and homogenisation plot for Type I and IIA inclusions demonstrate this temperature difference (Figure 7.13) between Type IIA and Type I inclusions. Generally Type IIA inclusions plot above the line X-Y, Type I below it. However salinity measurements on Type IIA inclusions were shown (above) to be too high because of clathrate formation and a more correct distribution in a salinity/ T_h plot is illustrated in the inset of Figure 7.13.

T_h measurements on Type I inclusions in coexisting quartz, fluorite and scheelite in samples 652 and 377 are essentially identical except that the average fluorite T_h in sample 652 is approximately 10°C lower than inclusions in the quartz (Figure 7.14). This may mean that the fluorite postdates quartz deposition although the errors are large on the T_h measurements.

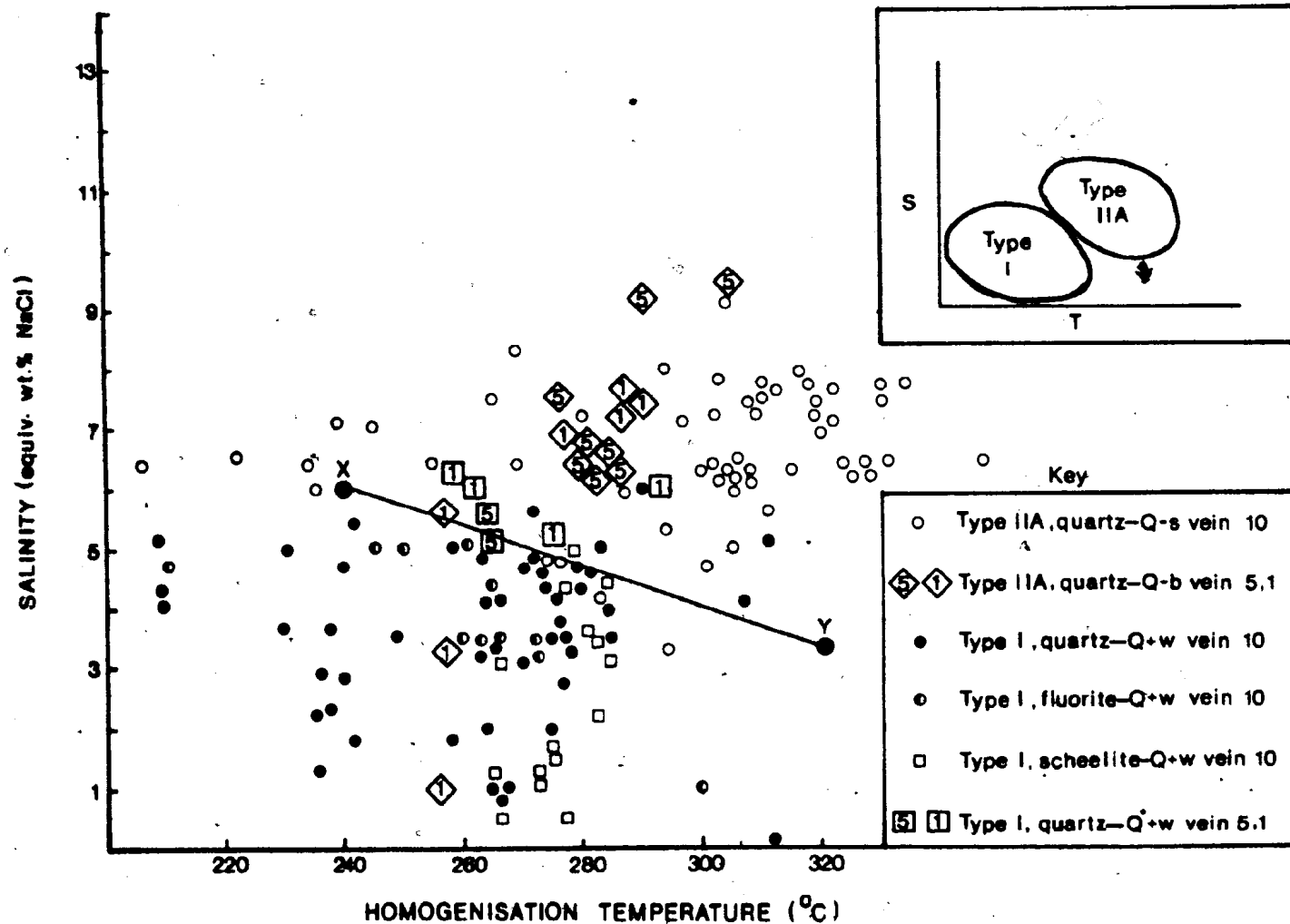
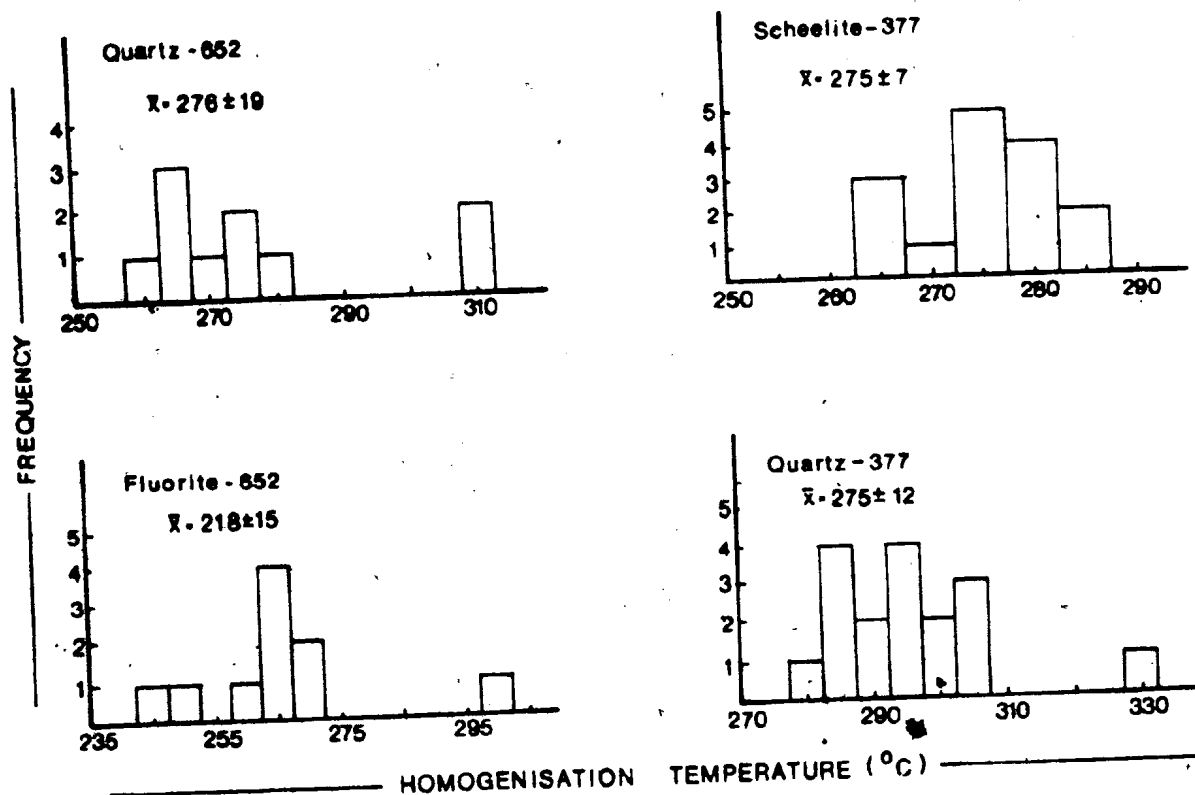


Figure 7.13 Combined salinity/homogenisation temperature plot for Type IIA and Type I inclusions.

Figure 7.14 Homogenisation temperature measurements of Type I inclusions from coexisting quartz, fluorite, and scheelite.



7.8 CRUSHING STAGE EXPERIMENTS

Crushing stage techniques have been used as an extremely sensitive test for the presence of gases under pressure in inclusions (Deicha, 1950; Roedder, 1970). These techniques, while essentially qualitative, permit the recognition of as little as 10^{-14} grams of noncondensable gases (Roedder, 1970). During the crushing of a grain, the presence of gas under pressure in an inclusion is detected by the sudden expansion of the gas to form bubbles in the oil medium surrounding the grain.

Representative samples from each of the vein types were studied using a crushing stage designed by the author from a suggestion by E. Roedder. A clear relationship was evident, between the amount of gas released (size of bubble) and vein type within the Grey River Tungsten Prospect. The intensity of gas released is highest for the QF-m vein type and is progressively lower for Q-b, Q-s and Q* + w, Q + w vein types, in that order.

While inclusions from quartz coexisting with wolframite display the smallest released gas bubbles, the expansion nevertheless implies the presence of a significant amount of CO₂ or other noncondensable gases during the deposition of wolframite. These qualitative crushing tests suggest that the CO₂ content of the hydrothermal fluid decreased with time, and confirms observational evidence and data from freezing studies.

7.9 DENSITY AND COMPOSITION OF CO₂-BEARING INCLUSIONS

Some CO₂-bearing inclusions occur in all vein assemblages except those containing wolframite, in which the inclusions appear to contain less than 10 bars P_{CO₂} in the vapour phase at room temperature. Liquid CO₂-bearing (Type IIB) inclusions occur as P-PS inclusions in the QF-m veins and their regularity of phase ratio indicates they were trapped from a homogeneous CO₂-H₂O fluid. The occurrence of Types IIA, IIB, IIC and IV inclusions as pseudosecondaries in the QF-m veins and as P-PS inclusions in all others except the tungsten-bearing veins indicates the contemporaneous trapping of a heterogeneous fluid derived by unmixing or immiscibility of a homogeneous CO₂-H₂O fluid. This unmixing was most pronounced during deposition of the Q-b veins but occurred also by boiling during the deposition of Q-s veins of composite Vein #10.

7.9.1 Purity of Carbon Dioxide

The occurrence of liquid CO₂ in the inclusion permits the measurement of the purity of the CO₂ and the density and composition of the fluid. Figure 7.15 presents the available data for the melting point of solid CO₂ in Type IIB inclusions.

Due to metastability most liquid CO₂ did not freeze till temperatures reached -100°C. The phase transition of solid CO₂ to liquid CO₂ occurs quite suddenly and is generally easy to observe provided there is no condensation problem. The formation of ice on the lens and sample at these very low temperatures (-90°C to -56.6°C) made determination

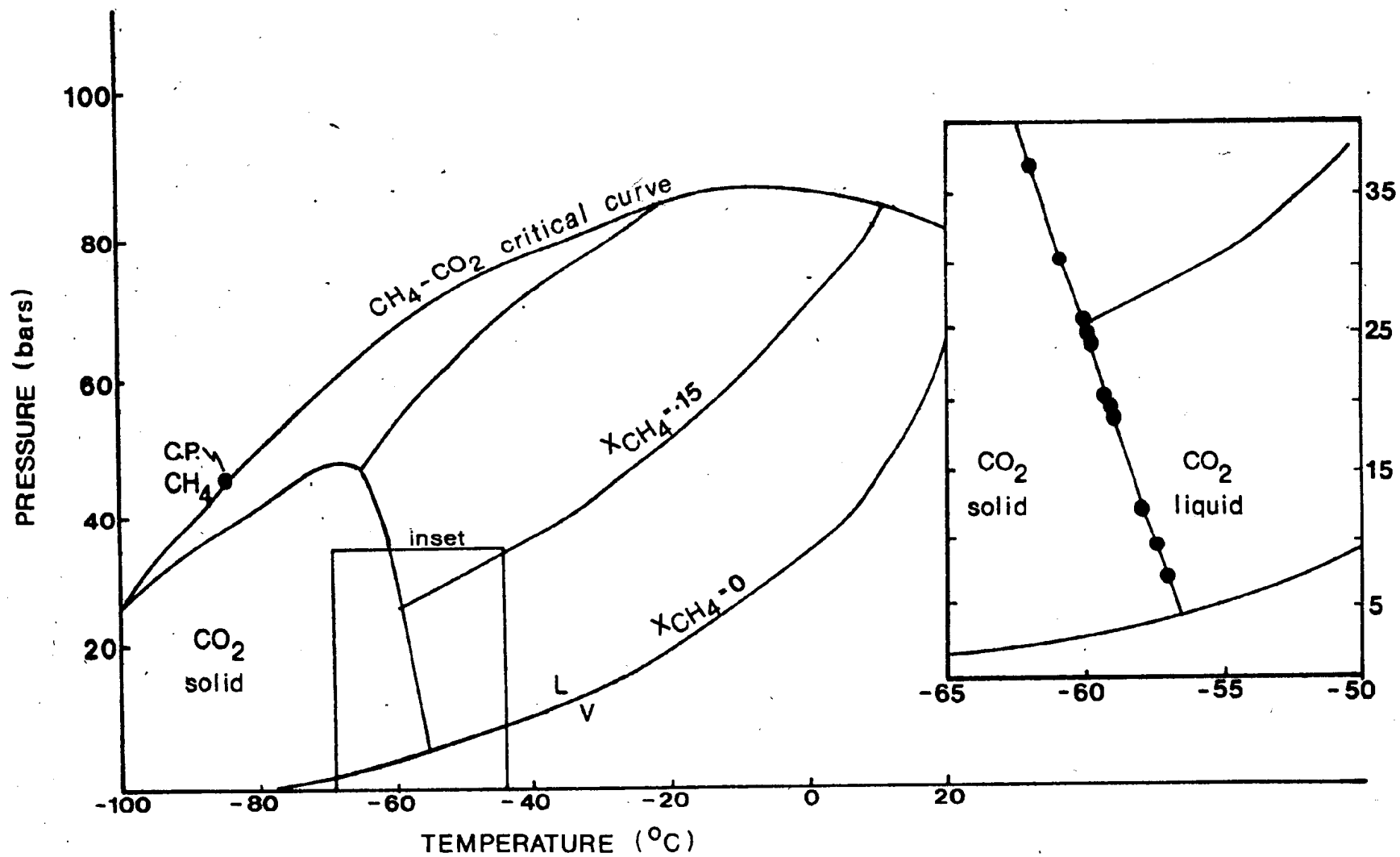


Figure 7.15 Temperature of melting of solid CO_2 in Type IIB and IIB* inclusions.

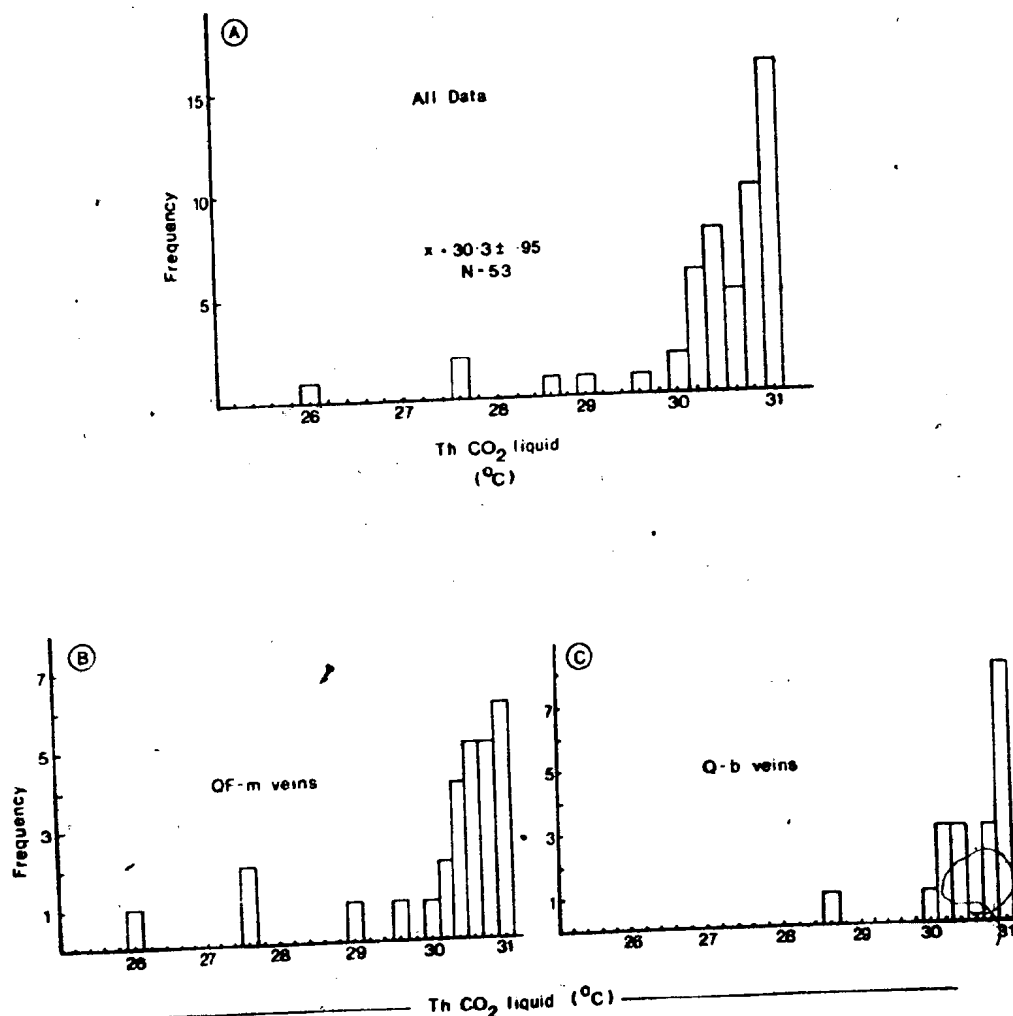


Figure 7.16 Temperature of transition of liquid and vapour CO₂ to liquid CO₂ (Th CO₂) for Type IIB inclusions.

of this melting temperature extremely difficult. The apparatus designed to overcome this condensation problem (see Appendix E.1) increases the vertical thermal gradient within the stage and hence the errors in measurement. The polarity of the thermal gradient results in the sample being warmer than the temperature sensor located beneath the sample. Thus the melting temperature of solid CO_2 would appear to occur at temperatures lower than the true melting point.

Measured $T_m \text{CO}_2$ in Type IIB and IIB* inclusions (Figure 7.15) predominantly lie above -60°C and, considering the operating gradient, the error in measurement is at least $+1.5^\circ\text{C}$. Considering errors, the closeness of the measurements to the melting point of pure CO_2 indicates a relatively pure CO_2 -rich phase in Type IIB inclusions, since a CH_4 component, miscible with CO_2 , lowers the $T_m \text{CO}_2$ considerably.

7.9.2 Density

The density of a fluid inclusion containing vapour and liquid CO_2 is defined when, on heating, one of these phases disappears at the homogenisation temperature ($T_h \text{CO}_2$). Figure 7.16A records the $T_h \text{CO}_2$ for the Type IIB inclusions from data in Appendix F.3. Nearly all the inclusions homogenised to the liquid phase but some exhibited "critical phenomena", that is, the fading and eventual disappearance of the boundary between the liquid and gas phases. The available data on the two phase field (liquid and vapour CO_2) show it to be quite flat on top (Kobe and Lynn, 1953;

Lowrey and Erickson, 1927), thus CO_2 inclusions with a wide range of densities will exhibit "pseudo-critical phenomena". True critical phenomena occur when the inclusion has a density of 0.468 g/cm^3 (Lowrey and Erickson, 1927); those with a density above this figure homogenise to the liquid phase; those below, to the gas phase.

Most of the 53 Th CO_2 measurements of Figure 7.16A lie within the temperature range $30^\circ - 31^\circ\text{C}$ and are therefore very close to the critical point of pure CO_2 . The average Th CO_2 for these data is 30.3 ± 0.95 (1 σ) giving a density of $0.62 - 0.65 \text{ g/cm}^3$. Within the range of error the density varies from 0.58 to 0.70 g/cm^3 (Kennedy and Holser, 1966). A histogram plot of Th CO_2 data from QF-m veins (Figure 7.16B) show them to be more variable than those obtained from Q-b vein types (Figure 7.16C).

Homogenisation of CO_2 phases in Type IIB inclusions from Q-s veins (Appendix F.3, sample Q-709-10) indicates relatively low densities. All five determinations homogenised to the vapour phase with Th CO_2 in the range $+17^\circ\text{C}$ to $+23^\circ\text{C}$. This implies a density of approximately 0.2 to 0.25 g/cm^3 (Lowrey and Erickson, 1927) for these inclusions.

7.9.3 Composition

The homogenisation of CO_2 phases defines the density of the fluid and, combined with an estimate of the volume of CO_2 and H_2O in an inclusion, permits the calculation of the concentration of each phase (Touret, 1977). Table 7.3 lists the densities of individual inclusions of Type IIB obtained from their Th CO_2 . Volumetric proportions shown in column

3 and 4 of Table 7.3 were obtained by accurately sketching each inclusion on cardboard and cutting out and weighing the various "phases". These areal proportions were adjusted to volume proportions assuming the inclusions to be spherical.

The composition of the fluid may be determined if the following parameters are known:-

V_1 = volume CO_2 (liquid and gas)

V_2 = volume H_2O

salinity (T_m ice, from microthermometry)

density (T_h CO_2 , from microthermometry)

If the temperature of melting of solid $\text{CO}_2 = -56.6^\circ\text{C}$ then the fluid in the inclusion approximates the three component system $\text{CO}_2\text{-H}_2\text{O-NaCl}$. Assuming that the mutual solubilities of CO_2 and H_2O are low at room temperature (2.3 moles CO_2 in H_2O (Touret, 1977)), and the vapour pressure of H_2O at room temperature is negligible then:

$$x_{\text{CO}_2} = \frac{N_1}{N_1 + N_2 + N_3} \dots\dots\dots (7.2)$$

where N_1 = number of moles CO_2

N_2 = number of moles H_2O

N_3 = number of moles NaCl

$$\text{and } N_1 = \frac{V_1 \cdot d_{\text{CO}_2}}{\text{MW } \text{CO}_2} + \frac{2.3 \cdot V_2 \cdot d_{\text{H}_2\text{O}}}{100 \text{ MW } \text{H}_2\text{O}} \dots\dots (7.3)$$

$$N_2 = \frac{V_2 \cdot d_{\text{H}_2\text{O}}}{\text{MW } \text{H}_2\text{O}} \dots\dots\dots (7.4)$$

$$N_3 = N_2 \cdot x \quad \dots\dots\dots (7.5)$$

Where x = equivalent mole% NaCl derived from Tm ice.

d = density (d_{H_2O} , d_{CO_2}).

MW = molecular weight.

The molar composition of individual inclusions is listed in column 5 to 7 of Table 7.3. These were derived from equations 7.2 to 7.5 (above) assuming 2 mole% NaCl is present in the aqueous solution (estimated from clathrate melting measurements). Note however that the solute in most inclusions is probably mainly dissolved in CO_2 , therefore increasing the concentration of CO_2 in the inclusion from that calculated.

Although errors in the determination of the volume ratios can be large, potentially this method obtains a precision far superior to that obtained from destructive methods, for example mass spectrometry, where problems of contamination by mixing of primary and secondary inclusions occur (Piperov *et al.*, 1979).

The molar compositions of CO_2 in Type IIB inclusions varies from 5.6 to 40 mol% CO_2 (Table 7.3). Noticeably the P-PS inclusions from quartz in the QF-m veins (samples 385A to E) have higher X_{CO_2} than inclusions from the Q-b vein assemblage (253A, B, 249A, B). Those with highest X_{CO_2} also homogenise in the upper range of Th which probably reflect the changing character of the hydrothermal fluid

Table 7.3

Calculated Composition
of Type IIB, IIB* Inclusions

SAMPLE	d(g/cc)	$V_1 = \text{Vol CO}_2 : V_2 = \text{Vol H}_2\text{O}$		$X_{\text{CO}_2}^{*1}$	$X_{\text{H}_2\text{O}}$	X_{NaCl}	Th °C
253B	0.65	0.20	0.80	8.1	90.2	1.7	
	0.62	0.25	0.75	9.5	88.7	1.8	
	0.65	0.15	0.85	6.4	91.8	1.8	> 270 D*
	0.65	0.18	0.82	7.4	90.1	2.5	
	0.65	0.73	0.27	42.1	56.8	1.1	> 275 D
	0.62	0.27	0.73	10.3	88.0	1.7	
	0.62	0.17	0.83	6.9	91.3	1.8	
	0.62	0.53	0.47	23.3	75.2	1.5	
	0.62	0.13	0.87	5.6	92.4	2.0	
	0.62	0.43	0.57	17.4	81.0	1.6	
249A	0.62	0.29	0.71	11.0	87.2	1.8	
	0.65	0.14	0.86	6.1	92.1	1.8	
	0.62	0.18	0.82	7.2	91.0	1.8	
	0.62	0.30	0.70	11.4	86.8	1.8	
	0.62	0.35	0.65	14.0	84.4	1.6	
249B	0.65	0.35	0.65	14.0	84.4	1.6	
	0.62	0.18	0.82	7.2	91.1	1.7	290 (H ₂ O)**
	0.65	0.22	0.78	8.8	89.4	1.8	> 263 D
	0.62	0.10	0.90	4.8	93.4	1.8	> 262 D

Table 7.3 continued.

SAMPLE	d(g/cc)	V ₁ =Vol CO ₂ :V ₂ =Vol H ₂ O	X _{CO₂} ^{*1}	X _{H₂O}	X _{NaCl}	Th °C
385A	0.65	0.20	0.80	8.1	90.1	1.8
	0.62	0.25	0.75	9.5	88.7	1.8
	0.62	0.42	0.58	16.9	81.5	1.6
	0.66	0.29	0.71	11.6	86.6	1.8
	0.62	0.33	0.67	12.7	85.6	1.7
	0.65	0.42	0.58	17.5	80.4	1.6
	0.62	0.40	0.60	15.8	82.5	1.7
	0.62	0.41	0.59	11.2	86.9	1.9
	0.65	0.45	0.54	19.3	79.1	1.6
	0.62	0.45	0.54	18.7	79.7	1.6
	0.62	0.40	0.60	15.9	82.5	1.6
	0.62	0.35	0.65	13.5	84.8	1.7
	0.62	0.38	0.62	14.9	83.4	1.7
	0.65	0.45	0.55	19.1	79.3	1.6
	0.70	0.47	0.53	21.4	77.1	1.5
	0.65	0.48	0.52	20.8	77.7	1.5
	0.70	0.54	0.46	26.0	72.5	1.5
	0.66	0.60	0.40	29.5	69.1	1.4
	0.62	0.72	0.28	39.8	58.9	1.3
	0.65	0.41	0.59	16.9	81.4	1.7
						311 (Crit.)
						>296 D
						>296 D
						361 (CO ₂)
						>276 D
						359 (CO ₂)
						>298 D
						>284 D
						>274 D
						345 (CO ₂)
						346 (Crit.)
						>313 D

Table 7.3 continued.

SAMPLE	d(g/cc)	$V_1 = \text{Vol CO}_2 : V_2 \text{Vol H}_2\text{O}$	$x_{\text{CO}_2}^{*1}$	$x_{\text{H}_2\text{O}}$	x_{NaCl}	Th °C	
385B	0.75	0.65	0.35	36.8	62.0	1.2	284 (CO ₂)
385C	0.66	0.54	0.46	25.0	73.5	1.5	298 (CO ₂)
	0.66	0.48	0.52	21.1	77.4	1.5	>250 D
	0.66	0.45	0.55	19.3	79.1	1.6	>325 D
	0.66	0.40	0.60	16.6	81.8	1.6	320 (CO ₂)
385D	0.62	.35	.65	13.5	84.8	1.7	>282 D
	0.62	.52	.48	22.6	75.9	1.5	>263 D
	0.65	.24	.76	9.5	88.7	1.8	>240 D
	0.62	.54	.46	23.9	74.6	1.5	352 (H ₂ O)
253A	0.69	.40	.60	17.2	81.2	1.6	>230 D
385E	0.65	.33	.67	13.1	85.2	1.6	>253 D
	0.65	.20	.80	8.1	90.1	1.8	330 (H ₂ O)
	0.62	.21	.79	8.1	90.1	1.8	>323 D
	0.62	.25	.75	9.5	88.7	1.8	>289 D
	0.62	.19	.81	7.5	90.7	1.8	>295 D

Crit. = critical phenomena

*1 = Mole

* D = Decrepitated

** = composition of homogenised phase

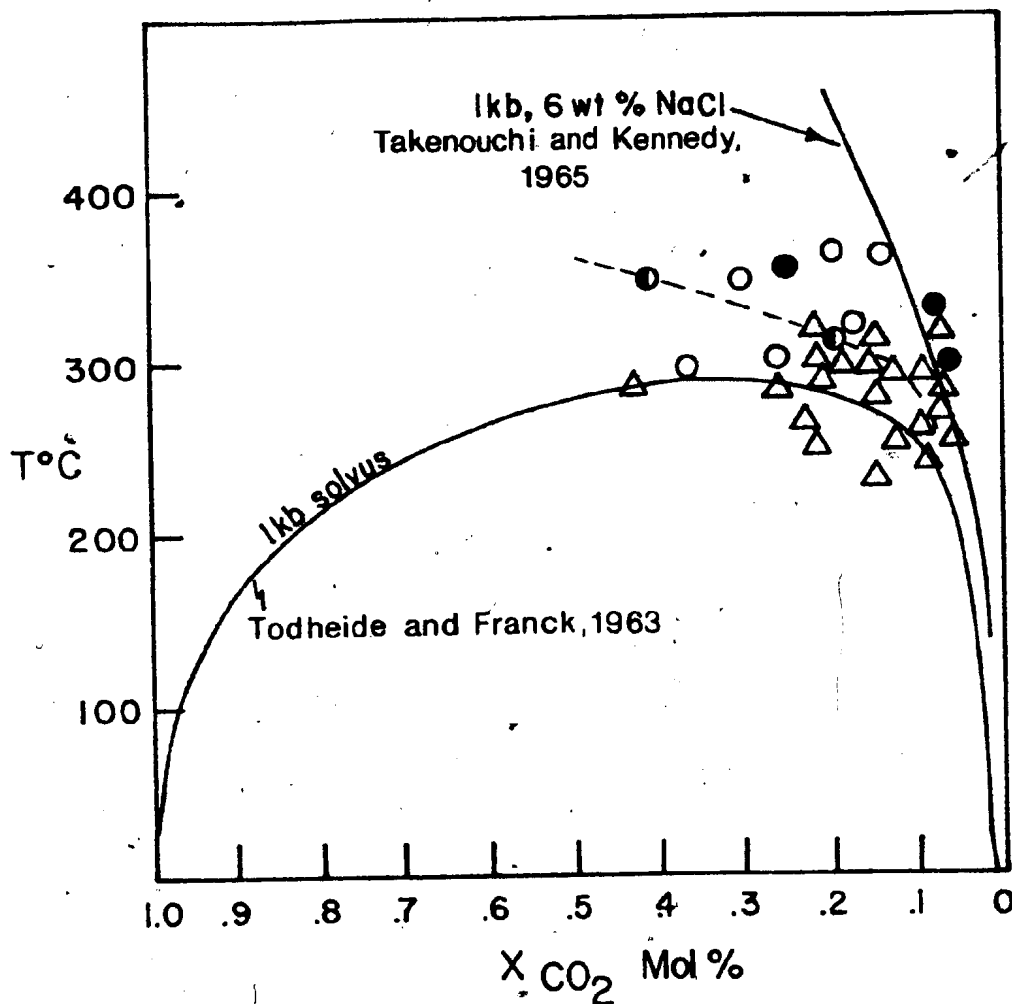


Figure 7.17 A Th-X_{CO₂} plot of Type IIB (and IIB*) in comparison to the 1 kb solvus in the CO₂-H₂O system. Open circle = homogenised to CO₂ phase; solid circle = homogenised to H₂O phase; half-filled circle = critical phenomenon; triangle = decrepitated before homogenisation.

with time, from a homogeneous (supercritical) fluid to a heterogeneous fluid.

Figure 7.17 plots concentration of CO_2 in individual inclusions with homogenisation temperature. Although many decrepitated, two inclusions exhibited critical phenomena; the others either homogenised to the CO_2 -rich or H_2O -rich phase. Most of the data points in Figure 7.17 are inclusions from QF-m veins and fall above the 1 kb solvus in the pure CO_2 - H_2O system (Todheide and Franck, 1963); this pressure being close to that estimated from CO_2 - H_2O equilibria discussed in a later section. The solvus is affected by other components, for example, Takenouchi and Kennedy (1965) showed that it expands with addition of 6 wt% NaCl (Figure 7.17).

Since the inclusions from QF-m veins were trapped from a supercritical fluid then they should plot above the solvus for their specific composition. The position of the solvus for such a fluid might be estimated from inclusions exhibiting critical phenomenon and is represented by the dashed line in Figure 7.17. This suggests a substantial rise in the solvus from that of the pure system and is likely a result of the dissolved constituents in the fluid. From its position, a solute concentration of substantially less than 6 wt% NaCl is indicated.

7.10 GEOBAROMETRY

Homogenisation temperatures may be corrected to trapping temperatures provided an independent estimate of the pressure

can be made. Pressure estimates are possible from

1) reconstruction of the lithostatic load from geological evidence or 2) by determining the density and composition of the inclusion fluids and applying the appropriate equilibria data for the systems $\text{NaCl-H}_2\text{O}$ and $\text{CO}_2\text{-H}_2\text{O}$.

Unfortunately an estimate of the lithostatic load prevailing during mineralisation at Grey River is impossible to ascertain from geological reconstruction. However, CO_2 -rich inclusions are suited for barometry as they commonly separate into two immiscible fluids under common hydrothermal temperatures and pressures. Approximations of pressure are possible by construction of isochores from CO_2 -rich inclusions (Touret, 1977) but to be useful under normal geological conditions such isochores have to be extrapolated assuming them to be straight lines. This extrapolation is based on ideal mixing of the two phases at higher temperature and pressure, although deviation from ideality is known to occur (Ypma, 1963; Greenwood, 1973). Touret (1977) maintains that extrapolation of isochores is valid for most one component systems in the supercritical region, as is evidenced by comparison of P-T estimates of metamorphic rocks from fluid inclusions and those from independent sources (Bilal and Touret, 1976).

Using data from a $\text{CO}_2\text{-H}_2\text{O}$ bearing inclusion a crude estimate of pressure is possible by adding the partial pressures of H_2O and CO_2 . One estimates the partial density of H_2O and CO_2 by assuming that each component

occupies the whole cavity at room temperature. Thus if the average density of the Grey River CO_2 -rich fluid is 0.65 and the visual estimates of the volume ratio $V_{\text{CO}_2}(\text{L+G}):V_{\text{H}_2\text{O}}$ are 4:6 and 3:7 for QF-m and Q-b veins respectively, then the apparent density (d^*) of the components assuming each occupies the cavity alone are:

QF-m veins

$$d^* \text{H}_2\text{O} = 1 \times 0.6 = 0.60$$

$$d^* \text{CO}_2 = 0.65 \times 0.40 = 0.26$$

Q-b veins

$$d^* \text{H}_2\text{O} = 1 \times 0.7 = 0.70$$

$$d^* \text{CO}_2 = 0.65 \times 0.3 = 0.20$$

If a typical homogenisation temperature for the P-PS type IIB inclusion of the QF-m assemblage is 350°C then the partial pressures of H_2O and CO_2 at 350°C are: $P_{\text{H}_2\text{O}} = 300$ bars (Burnham et al., 1969); $P_{\text{CO}_2} = 300$ bars (Kennedy and Holser, 1966). Thus a minimum estimate of the pressure prevailing during deposition of the quartz-feldspar-molybdenite veins is 600 bars.

For P-PS Type IIB inclusions from the Q-b veins with, a typical homogenisation temperature of 330° , the partial pressures of H_2O and CO_2 are: $P_{\text{H}_2\text{O}} = 520$ bars; $P_{\text{CO}_2} = 230$ bars. This gives a total of 750 bars for the pressure during deposition of the quartz-bismuthinite veins, however, as this mixture is not ideal (Greenwood, 1973) the obtained pressure is lower than the real pressure.

Another approximation, also based on the ideal mixing

model assuming that H_2O-CO_2 isochores are straight lines, utilises the measurements of partial homogenisation of the CO_2 , and hence the density, and extrapolates along the isochore to the total homogenisation temperature. The point of intersection of the total homogenisation temperature and the isochore also defines the "critical" curve for a given X_{CO_2} (Touret, 1977). For the QF-m veins with an average partial homogenisation temperature defining a density of 0.65 (Figure 7.16), and a total homogenisation temperature of $350^{\circ}C$, the pressure is 1080 bars (Kennedy and Holser, 1966). For the Q-b veins with a similar density and a total homogenisation temperature of $330^{\circ}C$, the pressure is 1020 bars. These pressure determinations again reflect a minimum pressure only due to non ideal mixing.

A unique solution for pressure and temperature can be obtained from the intersection of the isochores derived from the homogenisation behaviour of pairs of inclusions which were trapped from separate, but coexisting, immiscible fluids. Such a condition will occur when fluids are trapped below or on the solvus in the CO_2-H_2O system. The barometry is based on the recognition of contemporaneity of the immiscible fluids, one rich in CO_2 and the other in H_2O . Once this has been determined and the composition of the two fluids has been derived from inclusion data then the pressure of trapping is easily deduced.

In practice, one determines the homogenisation temperature of the H_2O -rich fraction which defines the isochore

of that fluid if the salinity is known (Appendix G). Next, one determines the density of the coexisting CO_2 -rich fluid thus establishing the isochore of that fluid. The intersection of these isochores gives a unique determination of the pressure and temperature (Koltun, 1965; Groves and Solomon, 1969).

The contemporaneous trapping of Types IIB, IIA and IV inclusions as well as mixtures of these types (IIB*, IIC), indicates the existence of two immiscible fluids during the evolution of the hydrothermal system at Grey River. These immiscible fluids, one rich in CO_2 , the other in H_2O , were trapped on or below the solvus in the CO_2 - H_2O system. These conditions prevailed during deposition of the Q-b assemblage and during the deposition of the Q-s vein type of composite Vein #10.

A typical homogenisation temperature for Type IIA and IIC inclusions associated with Type IIB inclusions is 325°C . An average salinity of 5 wt% is indicated by clathrate melting temperatures and the solute is considered to be mainly dissolved CO_2 and HCO_3^- . Although inclusions do not contain a simple NaCl - H_2O solution, Potter and Clynne (1978) showed that the P-V-T-X properties of solutes of various compositions can be estimated quite accurately by comparison with properties of a NaCl - H_2O fluid of a similar salinity. Therefore the volumetric data for the system NaCl - H_2O (Appendix G) can be used as a good approximation of the P-V-T properties of the inclusion fluids.

Thus from Type IIA (and IIC) inclusions a density of 0.75 - 0.7 g/cm³ is indicated for the H₂O-rich fluid trapped simultaneously with a CO₂-rich fluid of 0.65 g/cm³.

A plot of the isochores of these coexisting immiscible fluids gives an intersection at 1.55 kb and 475° (point A, Figure 7.18). If the range in densities of the two fluids are considered then the field of possible P-T conditions is indicated by the shaded portion in Figure 7.18. The CO₂ isochores are based on P-V-T data for the pure CO₂ system (Kennedy, 1954), however the CO₂-rich fluids trapped in Type IIB inclusions are a mixture of CO₂ and H₂O with maximum CO₂ content of 40 mol%.

The experimental isochores for such a fluid are not available but may be derived by assuming ideal mixing of the two non-ideal gases. Using this assumption Rich (1975) tabulated the P-V-T data for CO₂-H₂O mixtures (Appendix H), from data on the pure substances (Burnham *et al.*, 1969; Kennedy and Holser, 1966; Juza *et al.*, 1965; Kennedy, 1954). The isochore for a fluid containing $X_{\text{CO}_2} = 0.4$ is shown in Figure 7.18 and intersects the H₂O-rich isochore at approximately 1.2 kb and 430°C (point B).

An accurate determination of pressure is limited by the availability of good experimentally derived fluid phase equilibria of appropriate compositions over geologically useful pressure and temperature conditions. Notwithstanding this, a fluid pressure of greater than 1.1 kb is indicated for mineralisation during the QF-m and Q-b vein stages.

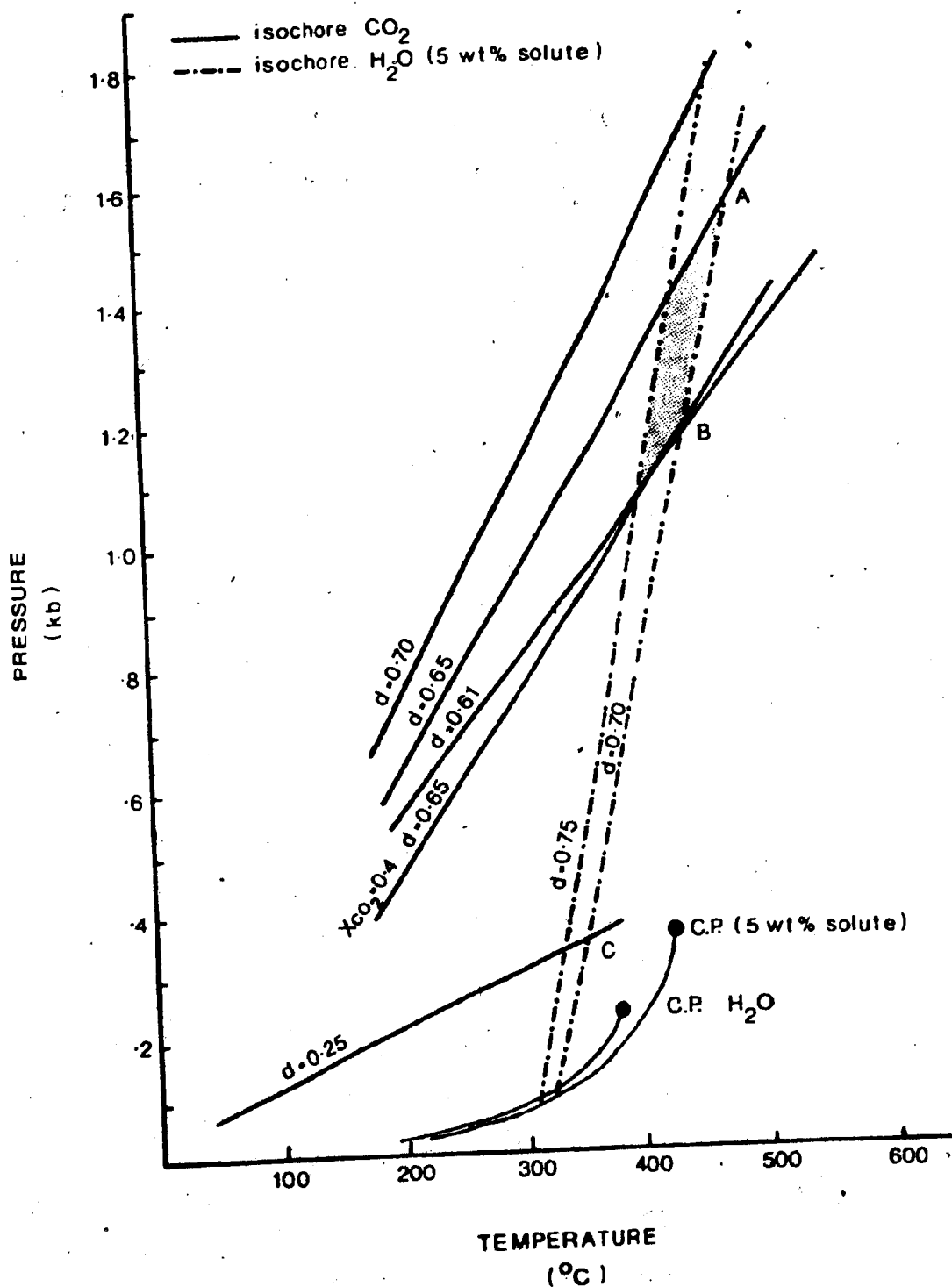


Figure 7.18 Absolute pressure and temperature determinations from intersection of isochores of immiscible but coexisting fluids. Density (d) in g/cc.

Rare Type IIB inclusions, trapped contemporaneously with Type IIA and IIC inclusions in the Q-s veins of composite Vein #10, have very low densities (0.25 g/cm^3) indicated by their homogenisation to the vapour phase. Intersections of isochores for these inclusions suggest a fluid pressure prior to deposition of tungsten mineralisation of 300-350 bars (point C, Figure 7.18).

Type I inclusions from tungsten-bearing veins ($Q + w$, $Q^* + w$) have low solute concentrations (less than 3 equivalent wt% NaCl) much of which appears to be dissolved CO_2 and HCO_3^- . If such fluids can be modelled after the NaCl- H_2O system (Potter and Clynne, 1978), and since there is no evidence for boiling during the trapping of these inclusions, the minimum pressure needed to prevent boiling of a fluid of 3-5 wt% salinity at 270°C is 155 bars (600 m depth, Haas, 1971). This calculation together with the estimate of pressure conditions during deposition of Q-s veins, suggests that the tungsten-bearing veins were deposited at fluid pressures between 155 and 350 bars.

7.11 INTERPRETATION OF PRESSURE DETERMINATIONS

Most pressures determined from fluid inclusions are said to represent lithostatic or hydrostatic pressure or some intermediate value. However, the pressure at the site of trapping of an inclusion represents a hydrostatic pressure because it is a fluid pressure (Roedder and Bodnar, 1980). Many factors such as boiling, vein choking or throttling, and hydraulic fracturing affect pressures locally and can

result in considerable variation in fluid pressure within a vein system.

Variation in fluid pressure is indicated between vein types in the Grey River Tungsten Prospect. Pressure determinations from fluid inclusions suggest a fluid pressure of greater than 1000 bars during deposition of the QF-m and Q-b veins and only 350 bars in Q-s veinlets of composite Vein #10. Such variation likely reflects the structural development of the vein system, particularly that of the composite veins. Structural evidence suggests that the composite veins were reopened and resealed by repeated episodes of hydraulic fracturing. Slickensides on these fracture planes indicate internal vein displacements resulting from a normal faulting mechanism.

The relationship between pressure variation and structural development of the vein system is illustrated in Figure 7.19A where fluid pressure is plotted against trapping temperature (T_h corrected for pressure and salinity). Inclusion types and regularity of phase ratios in QF-m veins suggest the presence of a supercritical CO_2 - H_2O fluid at pressures greater than 1200 bars and 450°C . During the deposition of Q-b veins this supercritical fluid unmixes, resulting in the separation of CO_2 -rich and H_2O -rich fluids. The intersection of isochores derived from these coexisting immiscible fluids defines the pressure and temperature of trapping at 1000-1200 bars and 430 - 450°C . This unmixing episode occurs at point B on Figure 7.19 and is similarly

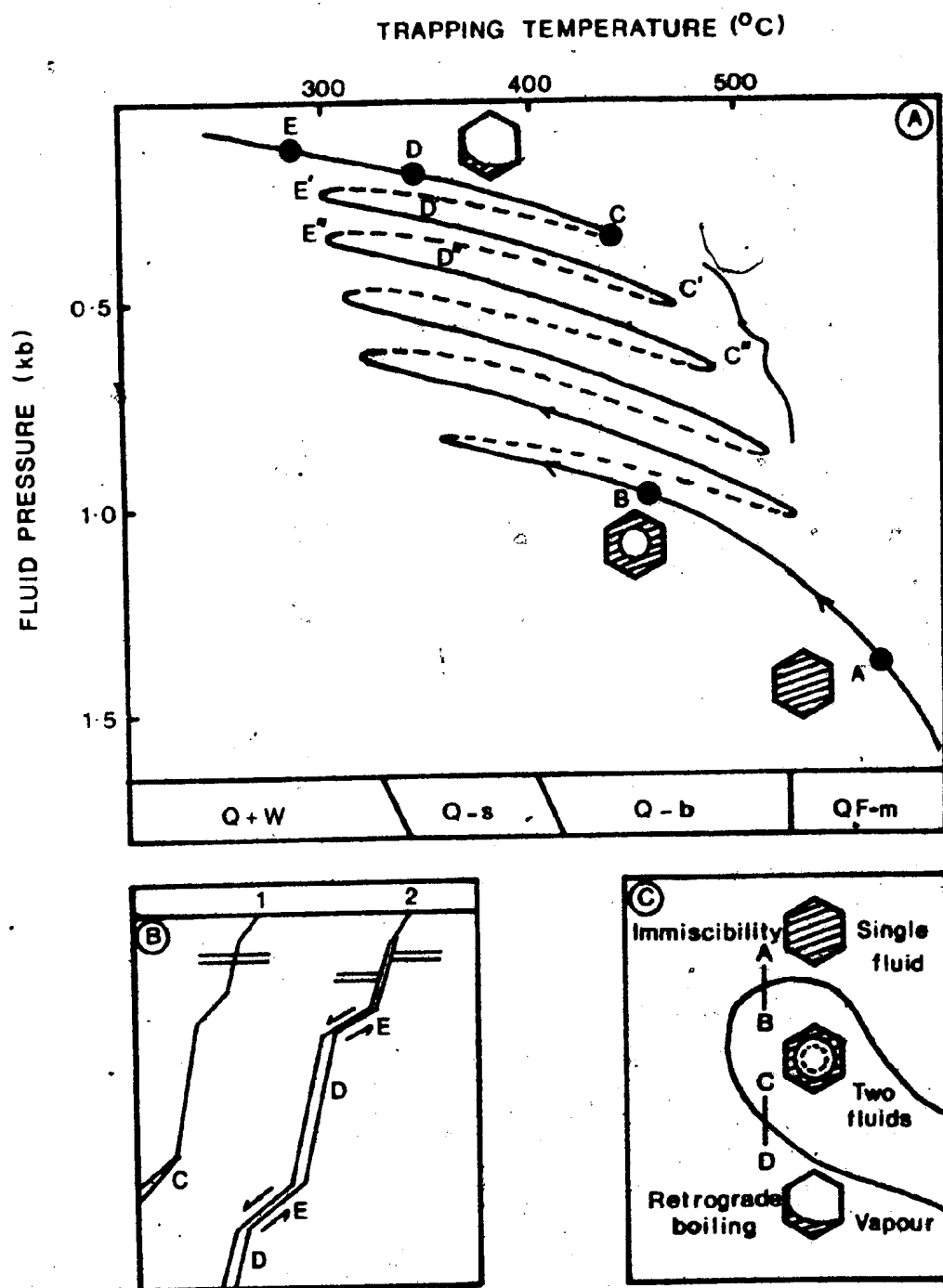


Figure 7.19 The relationship between pressure variation and the structural development of the vein system. See text for explanation of the symbols.

represented in Figure 7.19C where the fluid intersects the solvus with decreasing pressure.

Deposition of later vein types in composite veins (Vein #10, Vein #6) is accompanied by extensive hydraulic fracturing. This occurs when fluid pressure exceeds the value of the minimum principal stress and the tensile strength of the rock (Price, 1975). The pre-fracture situation is portrayed at point C (or C^1 , C^{11} etc.) in Figure 7.19 A and B where the pressure of a flowing fluid at an inclusion site equals the hydrostatic head and some unknown overpressure (Roedder and Bodnar, 1980).

Hydraulic fracturing of the vein results in a rapid decrease in fluid pressure and temperature and the hydrothermal fluid follows the path C-D-E (Figure 7.19A). If fault movements have increased the volume occupied by a momentarily fixed volume of fluid then retrograde boiling occurs when the vapour pressure exceeds the load pressure. This situation occurs in Vein #10 and other veins where steeply dipping portions are offset by normal faulting (Figure 7.19 B-2). The pressure of an inclusion trapped in this environment would be equal to the vapour pressure at that temperature even though the vein might be at some considerable depth in the upper crust (Roedder and Bodnar, 1980).

Retrograde boiling of a H_2O fluid containing dissolved CO_2 would result in the separation of a vapour phase rich in CO_2 (Touret, 1977). Rare Type IIB inclusions occur in

the Q-s assemblages of Vein #10 and coexist with inclusions of Type IIA and IIC. Liquid CO_2 in these inclusions homogenises to the vapour phase at quite low temperatures indicating that these inclusions contain highly compressed CO_2 vapour of low density. The rarity of preservation or trapping of these low density Type IIB inclusions might be expected when the bulk of the growth of the host crystal occurs from the continuous fluid phase in a heterogeneous mixture, for example - water and steam (Roedder, 1971; Roedder and Bodnar, 1980).

This retrograde boiling situation is illustrated by the path C-D-E in Figure 7.19C where the CO_2 vapour evolves at point D and subsequent lowering of pressure (P_{CO_2}) and temperature results in the deposition of wolframite at point E (and E^1 , E^{11} , E^{111} , etc.) in Figure 7.19A. This loss of P_{CO_2} and lowering of temperature between Q-s and Q + w, Q* + w veins is substantiated by measurements of salinity and homogenisation temperature discussed previously.

7.11.1 Pressure Corrections

Inclusions trapped from non-boiling hydrothermal fluids do not nucleate a vapour bubble until the internal pressure of the inclusion drops below the total vapour pressure of the fluid. Hence homogenisation temperatures do not represent trapping temperatures but may be corrected to that value provided pressure is known.

Fluid pressure fluctuated widely during the evolution of the Grey River hydrothermal fluid so that a common pressure

correction cannot be applied to all the veins. QF-m and Q-b veins were deposited under fluid pressures greater than 1000 bars. Assuming a salinity of 5 wt% for the fluid a pressure correction of 90-140°C is warranted (Potter, 1977). Trapping temperatures for the QF-m veins are thus in the region 450° - 490°C; for Q-b veins trapping temperatures of 390 - 430° are indicated.

As discussed above these pressure determinations represent fluid pressures, and during the deposition of the QF-m and Q-b veins the hydrothermal fluid was also subjected to some unknown overpressure. This means that the trapping temperatures derived above represent minimum values for these assemblages and would need to be corrected for this overpressure.

Hydraulic fracturing accompanied the deposition of Q-s and Q + w veins, and fluid pressures varied from 1000 to 350 bars prior to the deposition of these assemblages in Vein #10. Boiling of the hydrothermal fluid is indicated during deposition of Q-s veins and hence no pressure correction is needed. Since fluids associated with Q + w (and Q* + w) veins were apparently not boiling (i.e. above the L-V curve for their specific fluid composition) then estimated fluid pressures of 150-350 bars necessitate a pressure correction of +10 to +25°C to the homogenisation temperatures.

7.12 FLUID INCLUSIONS IN FLUORITE-CALCITE-BARITE VEINS

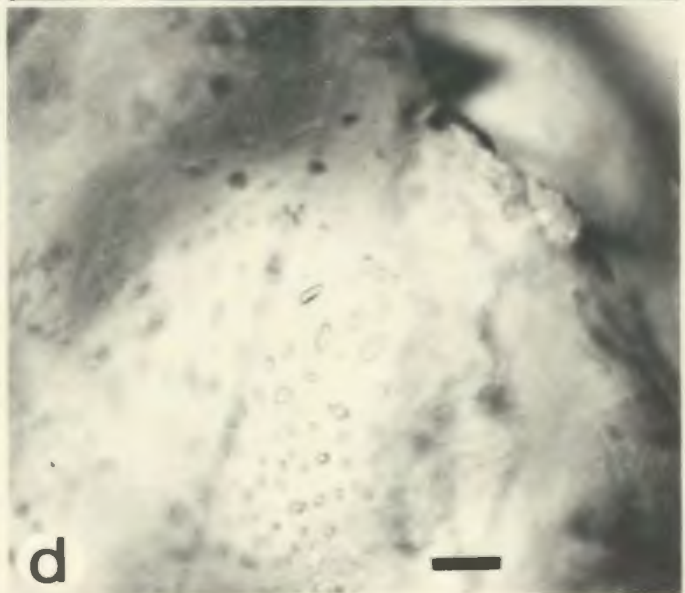
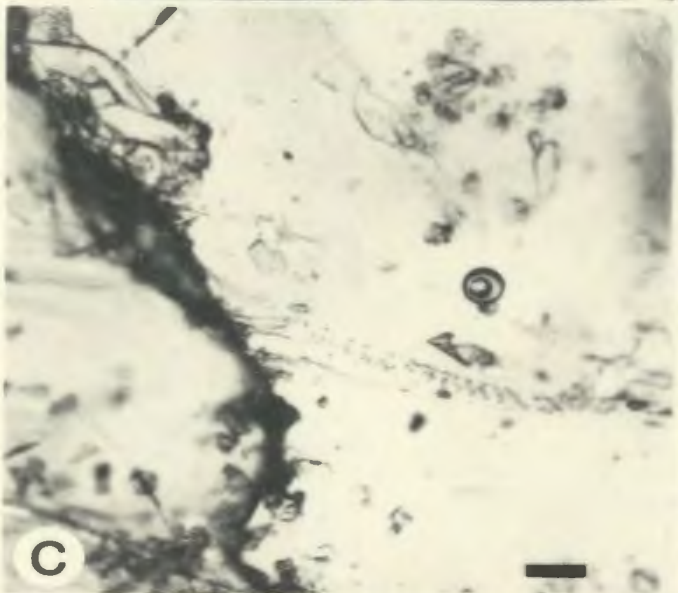
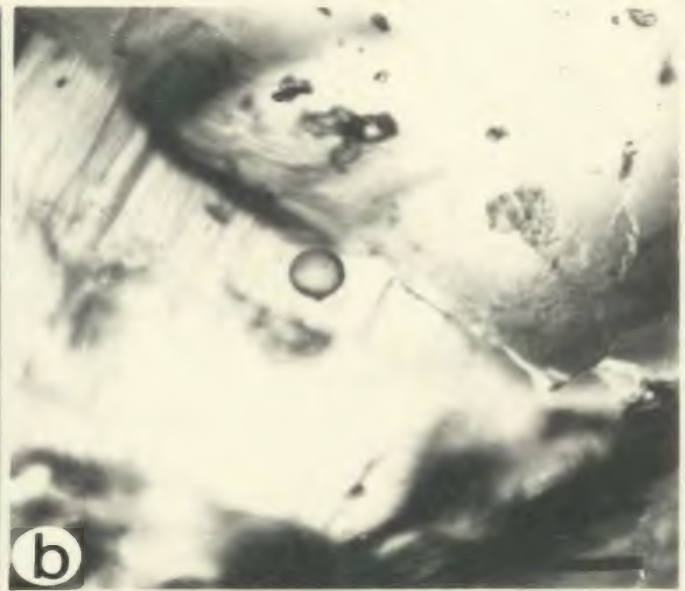
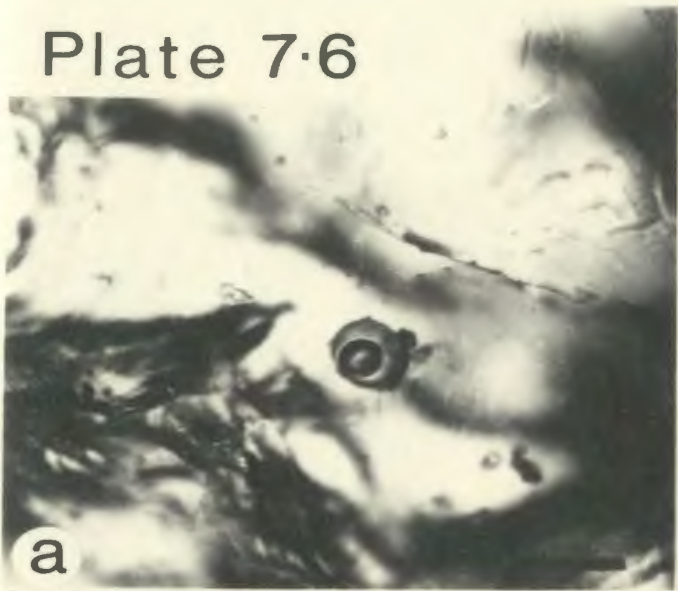
Fluorite veins containing a variety of minerals occur in extensional fractures which postdate all other mineral-

Plate 7.6

Fluid inclusions in apophyllite. Bar scale = 10 μ m.

- 7.6a Flat, circular liquid-vapour inclusion in apophyllite from fluorite-calcite-barite vein, adit level.
- 7.6b Flat, circular liquid only inclusion in apophyllite from fluorite-calcite-barite vein, adit level.
- 7.6c Flat, circular liquid-vapour inclusion in apophyllite.
- 7.6d Plane of pseudosecondary liquid-vapour inclusions in apophyllite. Photograph taken after homogenisation run. Bubble did not nucleate on cooling.
- 7.6e Flat circular liquid-vapour inclusion in apophyllite illustrating the trapping of these inclusions along the basal cleavage of apophyllite crystals.

Plate 7.6



isation in the area. The veins are zoned, with light green fluorite at the edge of the fracture succeeded by calcite-barite, apophyllite and harmotome towards the centre. Galena and sphalerite occur within fluorite, barite and calcite, and pyrite is found coating cavities within the vein. See Chapter 5 for a detailed description of the vein occurrence and mineralogy.

7.12.1 Inclusion Types and Occurrence

Due to its crustiform nature the fluorite contains relatively few fluid inclusions. All those found occurred as isolated inclusions and do not seem to be associated with any healed fractures. The inclusions were of two types, L-V and L-V-S; this latter group containing a variety of solid daughter minerals too small to be resolved under operating conditions.

None of these inclusions nucleated ice on cooling runs even with repeated freezing to -180°C . This metastability implies a slow moving fluid was involved in the deposition of the fluorite which may also be suggested by the laminar, crustiform habit of the mineral.

The inclusions show a wide range of homogenisation temperatures (Figure 7.20A) from 270°C to 90°C with L-V-S inclusions typically at the top end of the range. These data fall into two groups (A,B) which possibly reflect their P-PS (A) or secondary (B) origin.

Inclusions from calcite and barite were not used for fluid inclusion work because of the many problems associated

with geothermometry of soft, well cleaved minerals (Roedder, 1972b).

Large crystals of apophyllite were split along their basal cleavage and the resulting thin cleavage chips were used directly on the freezing stage without polishing. At no time in the preparation were the specimens handled directly nor were they immersed in any fluid medium (e.g. oils).

Three types of inclusions occur in the apophyllite. These are:-

- a) Perfectly circular liquid-vapour inclusions (Plate 7.6 a,c) with varying L-V ratios (5-60 vol% vapour).
- b) Perfectly circular liquid only inclusions (Plate 7.6b).
- c) A discontinuous plane (PS) of negative faceted liquid-vapour inclusions with a constant 1-3 vol% vapour (Plate 7.6d).

All three types failed to nucleate ice on cooling, similar to inclusions within fluorite.

Figure 7.20B shows the homogenisation temperature data for the circular L-V inclusions and for one isolated irregular-shaped L-V inclusion which homogenised at 194°C. The circular L-V inclusions all homogenised in the range 60°C - 115°C and did not nucleate bubbles on cooling. At 10°C - 20°C above the homogenisation temperature the inclusions expanded their volume and in most cases migrated. Liquid-only inclusions exhibited this phenomenon at similar

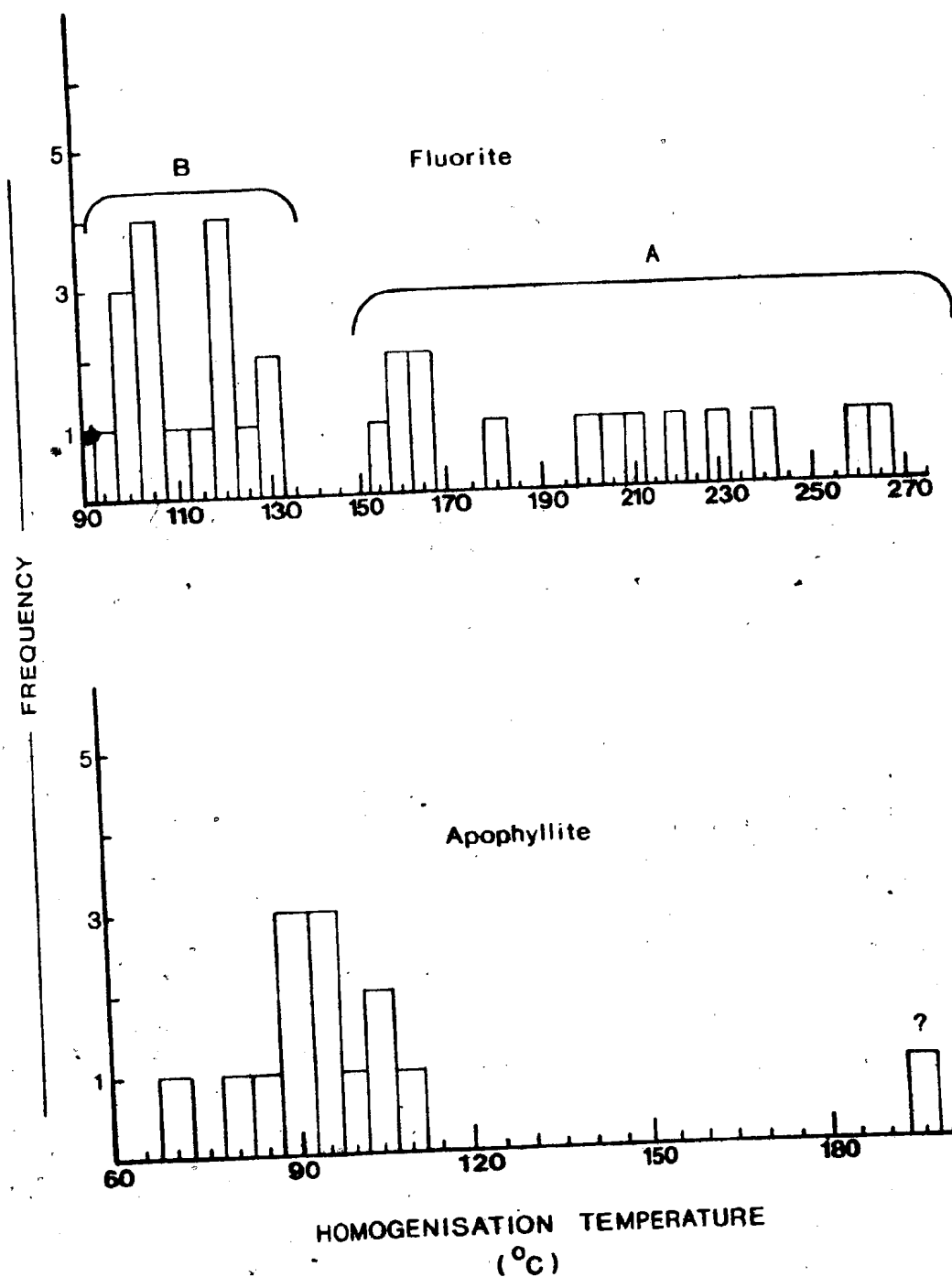


Figure 7.20 Homogenisation temperature of fluid inclusions in fluorite and apophyllite from F-cb veins.

temperatures (120-130°C). The flat and perfectly circular aspect of the inclusions, as well as their migratory property suggest that these inclusions are secondaries trapped along the basal cleavage of apophyllite (see Plate 7.6e).

The third group, a plane of pseudosecondary inclusions (approximately 40 inclusions) with low volume % vapour, homogenised in the temperature range 90-115°C and failed to renucleate a vapour bubble on cooling.

7.12.2 Conclusions

Fluorite, calcite and barite appear to have been deposited in the range 270°C to 150°C. Pseudosecondary inclusions in apophyllite suggest a temperature of deposition of approximately 100°C although one possibly primary inclusion would indicate a temperature of 194°C.

The secondary circular inclusions trapped along cleavages in apophyllite represent a fluid that bathed the crystal at some time after its deposition. Evidence from vugs of partial dissolution of calcite and hydration of apophyllite (see Chapter 5) seems to indicate that these minerals have been subjected to acid attack after their deposition. It seems reasonable to suggest that this acid fluid is represented by the secondary circular inclusions found in apophyllite and possibly the lower temperature inclusions within the fluorite. Alteration effects in the apophyllite are concentrated along basal cleavage fractures, precisely the position in which the circular inclusions are

found. Furthermore, the consistency of the microthermometric results and their relatively elevated temperature (90°C) would suggest that these inclusions have an origin related to the vein mineralogy and not a result of accidentally trapped immersion oils or groundwater.

Harmotome crystals are found mantling partially resorbed calcite and thus are later or concomitant with the dissolution and hydration event. Hence the fluid trapped as circular inclusions within the apophyllite may represent the fluid from which the zeolite precipitated. If so, then the harmotome crystallised at temperatures of approximately 90 to 100°C from a weakly acid solution. The acid nature of the fluid may have resulted from an influx of CO_2 , a common constituent of the fluid associated with the preceding tungsten mineralisation.




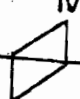




7.13 SUMMARY

The distribution and types of inclusions in gangue and ore minerals indicate a complex evolutionary history for the hydrothermal fluid which is summarised in Table 7.4. An initial homogeneous CO_2 - H_2O fluid with a solute concentration of 5 wt% deposited veins containing quartz, feldspar and molybdenite at temperatures of 450 - 490°C and fluid pressures of 1.0 to 1.4 kb. With falling pressure and temperature this supercritical fluid became immiscible, separating into CO_2 -rich and H_2O -rich fluids. This unmixing episode severely reduced the P_{CO_2} in the aqueous fluid promoting precipitation of carbonates.

The simultaneous trapping of CO_2 -rich and H_2O -rich fluid inclusions, as well as solid inclusions of calcite in quartz from the quartz-bismuthinite veins is evidence for the existence of a heterogeneous fluid during this phase of mineralisation. Evaluation of fluid phase equilibria data for these inclusions suggest that immiscibility occurred at temperatures of $390\text{--}430^\circ\text{C}$ and pressures of $1.0 - 1.2 \text{ kb}$.

A period of repeated hydraulic fracturing resulted in the deposition of quartz-sulphide and quartz-wolframite veinlets in composite veins. During hydraulic fracturing rapid temperature and pressure fluctuations initiated retrograde boiling of the aqueous hydrothermal fluid further depleting the solution in CO_2 by evolving a low density CO_2 vapour phase. This loss of CO_2 (decrease in P_{CO_2}) promoted the deposition of wolframite in the temperature range $270^\circ - 330^\circ$.

Table 7.4 Summary of Microthermetric Data

VEIN	CHARACTERISTIC INCLUSION TYPE	Salinity ¹ (wt%)	Th (°C)	Fluid Pressure (kb)	Tt (°C)	X _{CO₂} (mol%)	COMMENTS
QF-m	 IIB	5	350	1.0—1.4	450-490	20-40	Homogeneous Supercritical CO ₂ -H ₂ O Fluid
Q-b	 IIB  IIA  IV	5	300-325	1.0—1.2	390-430	10-40	Immiscibility Heterogeneous CO ₂ -H ₂ O Fluid
Q-s	 IIA  IIB  IV	<5	300-325	0.3—1.0	300-390	2-10	Retrograde Boiling Of Aqueous Fluid
Q+w Q'+w	 I	<3	270-300	0.3-0.15	270-330	<1	Deposition Of Wolframite

¹ total dissolved CO₂ and salts (NaCl, HCO₃⁻ etc)

CHAPTER 8

ISOTOPE GEOCHEMISTRY

8.1 INTRODUCTION

Stable isotope geochemistry has been applied widely to the investigation of ore genesis and the evolution of hydrothermal fluids (e.g. Taylor, 1979). The major types of waters found in the earth's crust (magmatic, metamorphic, seawater, formation brines and meteoric) have characteristic isotopic ranges of $\delta^{18}\text{O}$ and δD (Taylor, 1974, 1979; Sheppard, 1977) and hence the origin of hydrothermal fluids associated with ore deposition may be identified from isotopic analysis of the ore and gangue minerals (Sheppard *et al.*, 1971; Landis and Rye, 1974; Bethke and Rye, 1979).

Samples of oxygen-bearing minerals deposited from, or in equilibrium with, the hydrothermal fluid(s) were analysed to define the temperature of mineralisation, as well as the oxygen isotopic composition of the fluid and hence its origin. The samples selected by the author were analysed by R. Kerrich, University of Western Ontario. Conventional techniques were employed for the extraction of oxygen from minerals using bromine pentafluoride, with quantitative conversion to carbon dioxide prior to mass spectrometric analysis (Clayton and Mayeda, 1963).

Isotopic data are reported as $\delta^{18}\text{O}$ values in per mille (‰) relative to standard mean ocean water (SMOW).

That is:-

$$\delta = \left(\frac{R_{\text{sample}}}{R_{\text{standard}}} - 1 \right) \times 1000 \quad (8.1)$$

Where R sample is the $^{18}\text{O}/^{16}\text{O}$ ratio in the sample while R standard is the corresponding ratio in the standard (SMOW). The fractionation factor (α) or isotopic partition coefficient between two minerals (A,B) is equal to

$$\alpha_{AB} = \left(\frac{R_A}{R_B} \right) \quad (8.2)$$

which can be closely approximated by the equation

$$\Delta_{AB} = 1000 \log \alpha_{AB} = \delta A - \delta B \quad (8.3)$$

when α values are less than 10.

8.2 OXYGEN ISOTOPE RELATIONS

The $\delta^{18}\text{O}$ values of selected quartz, muscovite, wolframite and scheelite samples are shown in Table 8.1. The $\delta^{18}\text{O}_{\text{quartz}}$ values do not vary substantially between each vein type and range from 9.74 to 11.13 ‰. The analytical error on these measurements is ± 0.18 ‰ (2 σ). The most marked change in $\delta^{18}\text{O}$ mineral between vein types occurs for wolframite which is highest (3.54 ‰) for the Q* + w vein type (composite Vein #1) and lowest (1.15 ‰) in the Q + w vein component of composite Vein #10.

A solid solution control might account for the difference in $\delta^{18}\text{O}_{\text{wolframite}}$ between the Q* + w and Q + w vein types (Casaderall and Rye, 1980), as wolframite from the former is Fe-rich compared to wolframite from the latter.

On the other hand, the higher $\delta^{18}\text{O}_{\text{wolframite}}$ from Q* + w veins could also reflect a slightly higher temperature of deposition (smaller $\Delta q - wf$) than wolframite from Q + w veins.

$\delta^{18}\text{O}_{\text{scheelite}}$ values are very similar to $\delta^{18}\text{O}_{\text{wolframite}}$.

Table 8.1

Oxygen Isotope Compositions of Ore and Gangue Minerals

Vein Type	Sample	$\delta^{18}O$ quartz	$\delta^{18}O$ muscovite	$\delta^{18}O$ wolframite	$\delta^{18}O$ scheelite	$\Delta q-m$	$\Delta q-wf$	$\Delta q-sch$
QP-m	385	11.08	6.51 (7.74)			4.57 (3.34)		
Q-b	685	11.00						
	687	10.79					6.51	
Q+w	684	10.05		3.54				
Greisen	166	10.01	5.81			4.20		
			6.03					
Greisen	436	9.96	5.73			4.23		
			5.66					
Q-b	720	10.25						
	626	10.78						
Q+w	377	10.54		1.15	1.31		9.39	9.23
					2.29			
	652	9.74			1.07			8.67
	651	10.28		1.77			8.51	
	671	10.31		2.21			8.10	
	165	11.13		2.38			8.75	
	627	10.21						
	648	10.59						
	623	10.69						
	661	10.99						
	670	10.27						
	610	10.21						
	678	11.11						

Analytical error ± 0.18 ‰

as are the respective $\Delta q\text{-wf}$ and $\Delta q\text{-sch}$ fractionations. If the scheelite-water fractionation mechanism is similar to that of wolframite-water, then this similarity in $\delta^{18}\text{O}$ strengthens the evidence that reaction of wolframite to scheelite occurred immediately after deposition of wolframite, at high temperature, and in equilibrium with fluids of similar $\delta^{18}\text{O}$.

8.3 OXYGEN ISOTOPE THERMOMETRY

Oxygen isotope fractionation between coexisting pairs may be used to calculate the temperature at which the mineral attained isotopic equilibrium, the fractionation factor being a function of temperature only (Javoy, 1977). Isotopic temperatures can be calculated from equations derived from theoretical and experimental data describing quartz-muscovite fractionation. Several equations are available for mineral-water fractionations as a function of temperature (Table 8.2).

Three separate fractionation equations for quartz-muscovite have been used (equations 1 to 3, Table 8.2) to calculate the isotopic temperature of greisen mineralisation. Coexisting quartz and muscovite pairs from the greisen mineralisation give similar fractionations (Table 8.1) of approximately $4.20 - 4.23 \text{ ‰} \pm 0.18 \text{ ‰}$. Isotopic temperatures calculated from the three equations yield temperatures in the range $404^{\circ} - 350^{\circ}\text{C} \pm 30^{\circ}\text{C}$ (Table 8.3).

Errors in the calculated isotopic temperatures arising from the analytical uncertainty of $\pm 0.18 \text{ ‰}$ are about $\pm 30^{\circ}\text{C}$.

Table 8.2

Oxygen Isotope Fractionation Equations

- 1) $\Delta q-m = -0.6 + 2.2 \times 10^6 \cdot T^{-2}$: Bottinga and Javoy, (1973)
- 2) $\Delta q-m = +1.3 + 1.27 \times 10^6 \cdot T^{-2}$: Blattner, (1975)
- 3) $\Delta q-m = +1.16 + 1.19 \times 10^6 \cdot T^{-2}$: Clayton et al., (1972)
- 4) $\Delta q-w = -2.73 + 3.57 \times 10^6 \cdot T^{-2}$: Clayton et al., (1972)
- 5) $\Delta wf-w = -9.9 + 3.0 \times 10^6 \cdot T^{-2}$: Landis and Rye, (1974)

q = quartz, m = muscovite, w = water, wf = wolframite

Table 8.3

Calculated Isotopic Temperatures (°C)
for $\Delta q-m$ Fractionations

Sample	q-m	Equations*		
		(1)	(2)	(3)
166	4.20	405°	390°	355°
436	4.23	400°	385°	350°

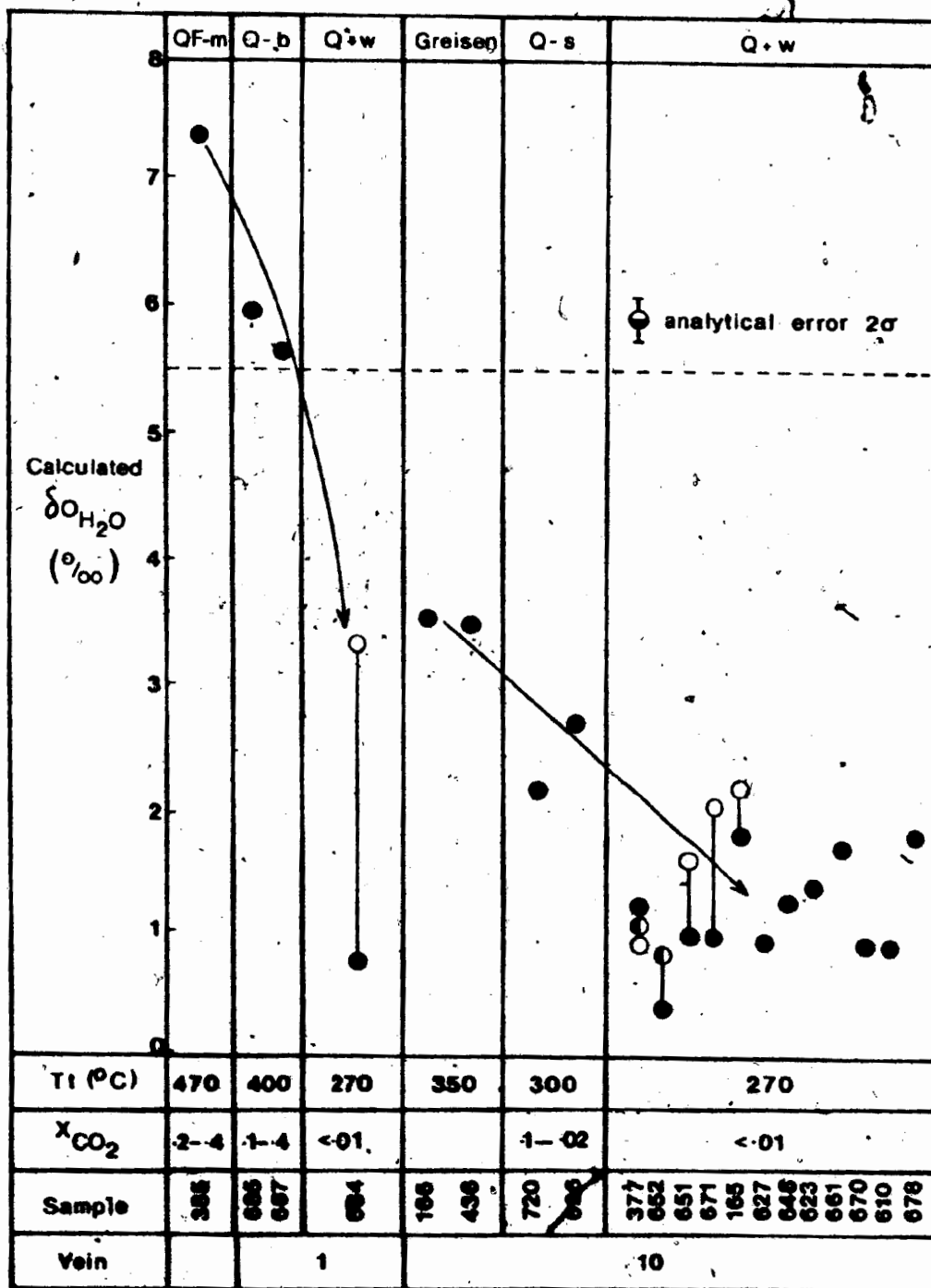
* see Table 8.2

Fluid inclusion temperatures for greisen mineralisation are not available for comparison with the calculated isotopic temperatures, but the calculated range of 350°C - 404°C for the three $\Delta q-m$ fractionations fits into the observed trend of fluid inclusion trapping temperatures for the various vein types in the deposit. The lower end of that calculated isotopic temperature range is favoured (350°C), because wolframite coexists with muscovite and quartz in the greisen. From fluid inclusion evidence, wolframite deposition in the veins ($Q + w$) occurs at temperatures below 300°C (average 270°C). However, greisen wolframite is Fe-rich similar to the wolframite from $Q^* + w$ veins, and as noted above, the quartz-wolframite fractionation for the latter is lower than $\Delta q-w$ from $Q + w$ veins, possibly suggesting a higher temperature of deposition for the Fe-rich wolframite. Unfortunately, no reliable quartz-wolframite fractionation equations are available to allow an isotopic temperature to be calculated (Casadevall and Rye, 1980).

8.4 CALCULATED $\delta^{18}\text{O}$ FLUID

The oxygen isotopic composition of the hydrothermal fluid coexisting with specific minerals may be calculated using trapping temperatures deduced from fluid inclusion studies combined with isotopic compositions of coexisting mineral phases and their relevant mineral-water fractionations. The quartz-water fractionation (Table 8.2, equation 4) of Clayton et al., (1972) was used to derive the isotopic composition of the hydrothermal fluid coexisting

Figure 8.1 Calculated $^{18}\text{O}_{\text{H}_2\text{O}}$ coexisting with quartz, wolframite and scheelite using trapping temperatures for each vein type derived from fluid inclusion data. Dashed line is lower limit of normal magmatic $^{18}\text{O}_{\text{H}_2\text{O}}$ values (Faure, 1977). Lines link coexisting minerals from the same sample. Solid circle = quartz; half-solid circle = scheelite; open circle = wolframite.



with quartz, while the empirical wolframite-water fractionation (Table 8.2, equation 5) of Landis and Rye (1974) was utilised for wolframite. Assuming a similar isotopic fractionation, the isotopic composition of the hydrothermal fluid coexisting with scheelite was also calculated from the Landis and Rye (1974) wolframite-water fractionation.

Figure 8.1 displays the calculated $\delta^{18}\text{O}$ composition of the hydrothermal fluid coexisting with quartz, wolframite and scheelite. Several features are evident. Firstly the $\delta^{18}\text{O}_{\text{H}_2\text{O}}$ isotopic composition becomes depleted with time showing a maximum range from 7.3 ‰ to 0.5 ‰ between QF-m and Q + w vein types. Secondly the isotopic compositions of the fluids calculated for coexisting quartz and wolframite (and scheelite) in Q + w veins are very similar (although derived from different fractionation equations), strengthening the suggestion that they were coprecipitated from the same fluid and at the same time. However, hydrothermal fluids coexisting with quartz and wolframite from Q* + w veins are quite different implying that they precipitated from different fluids or that the wolframite crystallised prior to the quartz at a different (higher) temperature.

Note that the fluid coexisting with the Fe-rich wolframite of the Q* + w vein is similar to that calculated for quartz from the greisen mineralisation which also contains wolframite of a similar composition. This might also suggest that the Fe-rich wolframite was deposited at slightly higher temperature, and before quartz, in the

Q* + w veins. Individual trends within composite veins (#1 and #10) are also suggested (Figure 8.1) with a regular depletion in $\delta^{18}\text{O}_{\text{H}_2\text{O}}$ culminating in the deposition of wolframite from a hydrothermal fluid of low $\delta^{18}\text{O}$ composition.

8.5 DISCUSSION

The isotopic evolution of the Grey River hydrothermal fluid is characterised by a depletion in $\delta^{18}\text{O}$ with time. Such a variation is normally interpreted as indicating the mixing of isotopically distinct fluids (Taylor, 1979; Sheppard, 1977). Magmatic waters have isotopic compositions that are controlled by equilibration with magmas at high temperature. Most volcanic and plutonic rocks have relatively uniform $\delta^{18}\text{O}$ (and δD) values, so that their associated fluid phases have a relatively restricted $\delta^{18}\text{O}$ range of +5.5 to +10.0 ‰ (Faure, 1977; Taylor, 1974).

The calculated $\delta^{18}\text{O}_{\text{H}_2\text{O}}$ of the hydrothermal fluid coexisting with quartz from the QF-m and Q-b vein types falls within this magmatic field which is shown in Figure 8.1. Furthermore, minerals with pegmatitic affinities (beryl, alkali feldspar) are restricted to those vein types, suggesting that the hydrothermal fluid involved the mineralisation to this point, was dominantly of magmatic origin.

Taylor (1978) however stresses that the extreme lower limit of magmatic $\delta^{18}\text{O}$ values could be +3 ‰, which might result if magmatically derived fluids re-equilibrate with

an isotopically normal felsic intrusive at 300°C. Thus any fluid with $\delta^{18}\text{O}$ values lower than 3 ‰ must have involved some other water component, the contemporary consensus favouring isotopically light meteoric water. Although $\delta^{18}\text{O}$ values less than 3 ‰ might indicate a source other than magmatic fluids, values greater than that limit cannot absolutely prove the presence of magmatic waters because meteoric waters might attain high $\delta^{18}\text{O}$ values by equilibration with metamorphic rocks (Kelly and Rye, 1979). Thus the 7.4 to 5.6 ‰ range in $\delta^{18}\text{O}_{\text{H}_2\text{O}}$ for the hydrothermal fluid during deposition of QF-m and Q-b veins does not unequivocally prove, but strongly suggests that a dominant magmatic fluid component was present.

Subsequent mineralisation stages exhibit much more depleted $\delta^{18}\text{O}_{\text{H}_2\text{O}}$ compared to magmatic values, being below 3 ‰ for Q-s, Q* + w, and Q + w vein types. Such values might suggest the involvement of an isotopically light fluid such as meteoric waters for the later stages of mineralisation (Sheppard, 1977; Taylor, 1979).

For the Pasto Bueno Tungsten deposit (Peru), Landis and Rye (1974) presented isotopic evidence that a magmatic-hydrothermal fluid was dominant in certain stages of mineralisation but that major fluctuations in isotopic composition of the fluid reflected incursion of meteoric and/or connate-metamorphic waters into the vein system. Moreover, these fluctuations (depletions) in $\delta^{18}\text{O}_{\text{H}_2\text{O}}$ (and $\delta \text{D}_{\text{H}_2\text{O}}$) accompanied major episodes of wolframite depo-

sition. Oxygen isotope data from the Carrock Fell tungsten deposit (Shepherd et al., 1976) suggested an interaction of isotopically light non-magmatic water with the granite during greisenisation and vein mineralisation (ore fluid $\delta^{18}O = +3.85$ ‰). Isotopic data from the Grey River Tungsten Prospect could be similarly interpreted; however fluid inclusion evidence suggests other controls govern the fluctuations in $\delta^{18}O_{H_2O}$.

The $\delta^{18}O_{H_2O}$ (and $\delta^{D}_{H_2O}$) of hydrothermal fluids reflect the original isotopic composition of the source fluid modified by the degree of isotopic exchange between the fluid and the wall rocks they encounter. The isotopic signature of the hydrothermal fluid may further be modified by mixing of fluids, by boiling, or by chemical change of the fluid. Fluid inclusion evidence (Chapter 7) indicates that the evolution of the Grey River hydrothermal fluid was characterised firstly by immiscible separation of CO_2 - and H_2O -rich fluids and later by retrograde boiling of the H_2O -rich fluid with concomitant evolution of a CO_2 vapour phase. This progressive loss in CO_2 is also traced by a marked lowering of the salinity of fluid inclusions; dissolved CO_2 lowering the temperature of freezing of the inclusion fluid like any other solute. The changes in X_{CO_2} of the hydrothermal fluid with time are indicated on Figure 8.1.

Since most minerals would be deposited from the H_2O -rich fluid, isotope fractionation between "boiled off" phases and

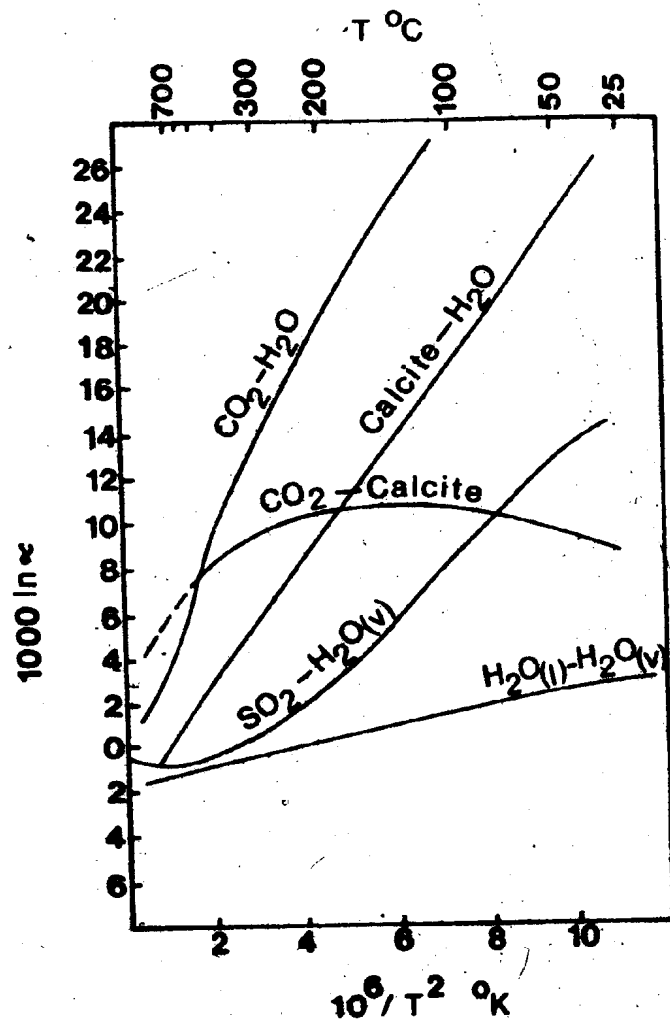


Figure 8.2 Experimentally determined equilibrium oxygen isotope curves for various mineral-H₂O and mineral-CO₂ systems. CO₂-H₂O curve (Bottinga, 1968); CO₂-CaCO₃ (Bottinga, 1968); calcite-H₂O (O'Neill et al., 1969); SO₂-H₂O (Urey, 1947); H₂O_l-H₂O_v (Friedman and O'Neill, 1977).

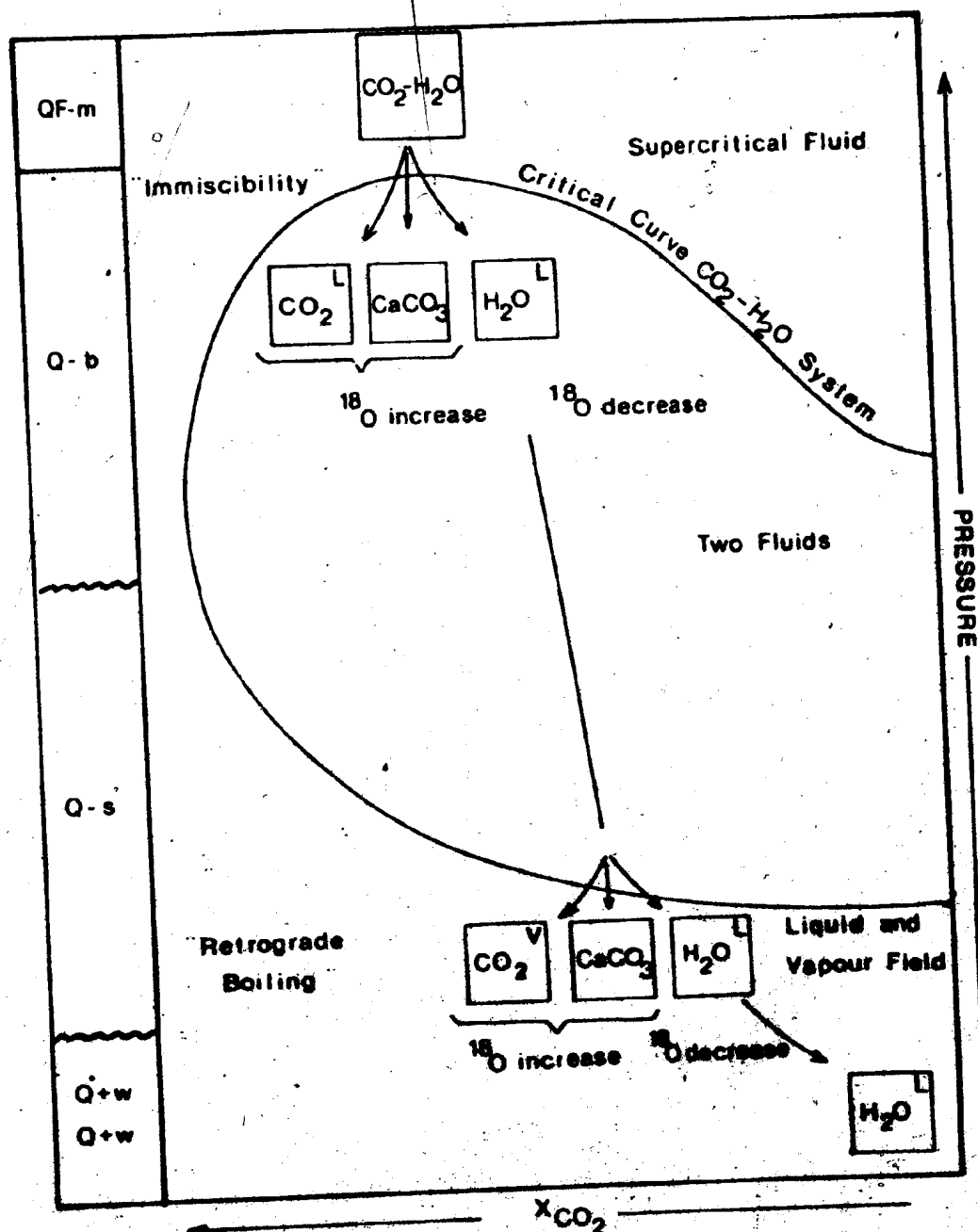
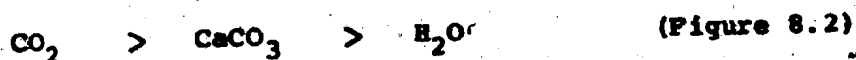


Figure 8.3 ¹⁸O fractionation trends caused by immiscibility and retrograde boiling of the Grey River hydrothermal fluid.

the H₂O-rich fluid could have considerable effect on the isotopic composition of the precipitated minerals.

The theoretical calculation of the fractionation for ¹⁸O exchange between carbon dioxide and water vapour has been described by Urey (1947). From these data Bottinga (1968) and Bottinga and Craig (1969) calculated the fractionation for CO₂-liquid water and showed that CO₂ is markedly enriched in ¹⁸O (Figure 8.2).

Fluid inclusion evidence from Grey River also suggests that during immiscibility and retrograde boiling stages, carbonates (and sulphates) were precipitated due to the sudden loss of CO₂ (and SO₂?) in the H₂O-rich fluid, and were subsequently trapped as solid inclusions in the quartz. Available isotopic fractionation data between CO₂-calcite-H₂O (Bottinga, 1968; O'Neil *et al.*, 1969) suggest that fractionation at hydrothermal temperatures decreases in the following order:-



Thus the formation of solid carbonates during immiscibility and retrograde boiling would further enhance the depletion in $\delta^{18}\text{O}$ in the residual H₂O-rich fluid (Figure 8.3).

Calculated fractionation factors for isotopic exchange in the CO₂-CaCO₃-H₂O system (Bottinga, 1968, 1969; O'Neil *et al.*, 1969) are substantiated by a variety of studies. Metamorphic decarbonation reactions result in ¹³C and ¹⁸O-depleted carbonates (Hoeft and Frey, 1976) with low ratios of ¹³C/¹²C and ¹⁸O/¹⁶O usually correlated with the

presence of newly-formed calc-silicate minerals. The gaseous CO_2 phase released during decarbonation must therefore be enriched in ^{18}O (and ^{13}C).

Well documented evidence exists from contact aureole-skarn deposits (Shieh and Taylor, 1969; Deines and Gold, 1969) which shows that the isotopic composition of the CO_2 liberated during decarbonation is about 5 ‰ richer in $\delta^{18}\text{O}$ than the carbonate in equilibrium with it at high temperature. In a study of skarn formation, Taylor and O'Neil (1977) recorded evidence of a C-O-H fluid formed by mixing of magmatic water and a ^{18}O -enriched CO_2 fluid, the latter produced by decarbonation reactions in the contact aureole. In all such studies the $\delta^{18}\text{O}_{\text{Carb.}}$ shift produced during decarbonation ranges from 2-6 ‰.

In the few studies available from high grade granulite terranes (Sheih and Schwarcz, 1974; Fourcade and Javoy, 1972; Baker et al., 1976), ortho- and paragneisses exhibit $^{18}\text{O}/^{16}\text{O}$ ratios which are very uniform and abnormally low ($\delta^{18}\text{O}$, 5-8 ‰). Fluid inclusion studies show that CO_2 is a dominant component of granulite metamorphic fluids (Touret, 1971, 1977; Hollister and Burruss, 1976) and the low $\delta^{18}\text{O}$ values for the gneisses may result from a loss of a CO_2 -rich metamorphic fluid. All the above studies show the affinity of ^{18}O for CO_2 -rich fluids, the loss or gain of which, in many geologic situations, can result in significant variation in isotopic composition of the associated fluids, minerals, or bulk rock.

The magnitude of the variation in $\delta^{18}\text{O}_{\text{H}_2\text{O}}$ with x_{CO_2} decrease can be calculated assuming an initial isotopic composition of the fluid and applying calculated fractionation factors (Bottinga, 1968) at appropriate temperatures. The variation in $\delta^{18}\text{O}_{\text{H}_2\text{O}}$ as a function of CO_2 loss at 420°C and 300°C is shown in Figure 8.4.

At 420°C CO_2 in equilibrium with H_2O will be approximately 10 ‰ enriched in $\delta^{18}\text{O}$; at 300°C, approximately 14 ‰ enriched (Figure 8.2). Assuming that the initial isotopic composition of the Grey River hydrothermal fluid was the same as that calculated for the QF-m veins ($\delta^{18}\text{O} = 7.5$ ‰; point A, Figure 8.4), then a 30 mol% CO_2 loss due to immiscibility at 420°C (as recorded by fluid inclusions) would result in a depletion of the isotopic composition of the residual fluid by 3 ‰. A subsequent loss of 10 mol% CO_2 due to retrograde boiling at 300°C would further deplete the residual fluid by 1.4 ‰.

In total, a 40 mol% CO_2 loss from the hydrothermal fluid could result in a shift in oxygen isotopic composition in the residual fluid on the order of 4.5 ‰. Fractionations of 2-4 ‰ are possible between carbonates and water at temperatures between 420°C and 300°C (Figure 8.2). Thus precipitation of carbonates during immiscibility and retrograde boiling would enhance the depletion.

These calculations show that changes in the chemical composition of the Grey River hydrothermal fluid could account for the shift (depletion) in the $\delta^{18}\text{O}$ of the fluid

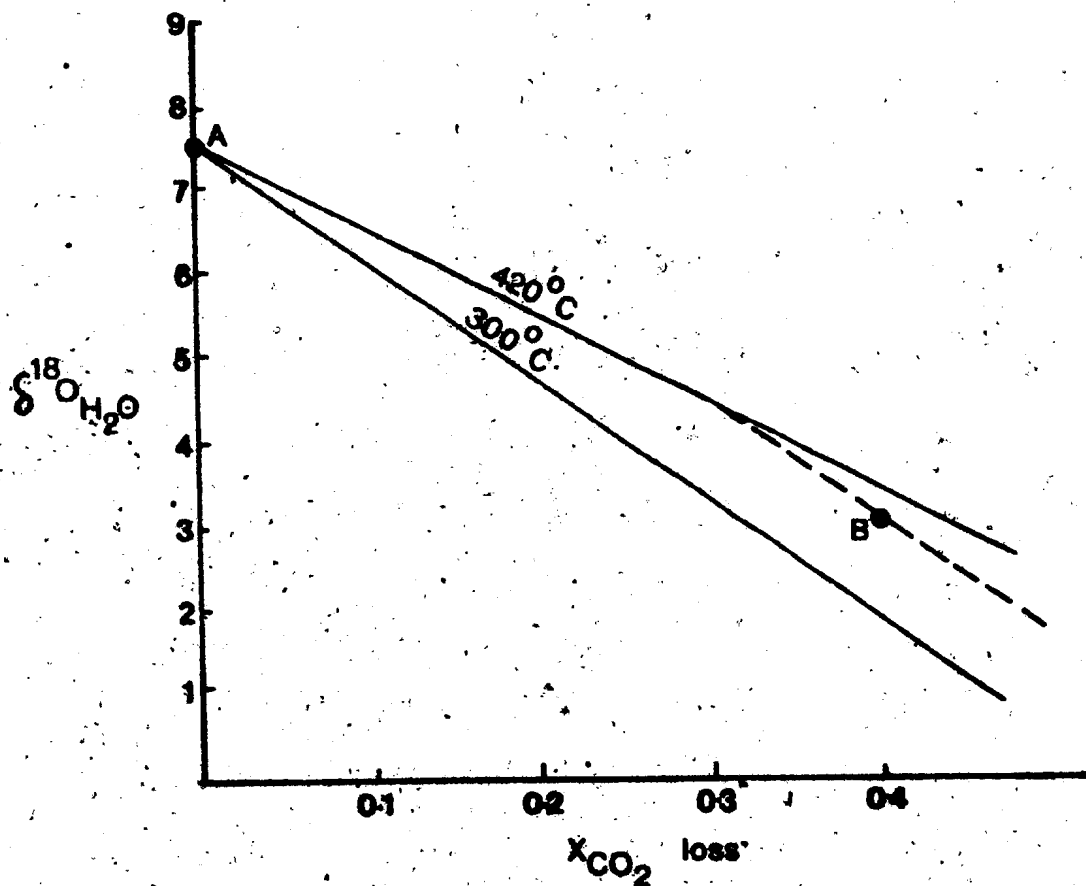


Figure 8.4 Calculation of the change in $\delta^{18}\text{O}$ fluid due to CO_2 - H_2O fractionations of a residual hydrothermal fluid undergoing progressive CO_2 loss at 420°C and 300°C.

with time. Previous studies on tungsten deposits such as Panasqueira (Kelly and Rye, 1979), Tungsten Queen (Casadevall and Rye, 1979) and Carrock Fell (Shepherd et al., 1976) have not evaluated this possibility although the evidence for substantial loss of CO_2 during the evolution of their respective hydrothermal fluids is suggested in the data these authors present.

8.6 SUMMARY

The isotopic composition of the Grey River hydrothermal fluid varied during successive stages of the mineralisation. Early deposited veins with pegmatitic affinity appear to have been deposited from magmatic fluids with a $\delta^{18}\text{O}_{\text{H}_2\text{O}}$ composition in the range 5.6‰ to 7.4 ‰. Later stages show a marked depletion in $\delta^{18}\text{O}_{\text{H}_2\text{O}}$ (3.2 ‰ to 0.5 ‰) which would normally be interpreted as interaction with an isotopically light fluid (e.g. meteoric water).

However, fluid inclusion evidence suggests that CO_2 loss occurred during immiscibility and retrograde boiling episodes which would have significantly changed the isotopic composition of the hydrothermal fluid. Available fractionation factors between CO_2 and H_2O indicate that CO_2 is preferentially enriched in ^{18}O , implying that significant CO_2 separation from a hydrothermal fluid would result in a marked lowering of $\delta^{18}\text{O}$ composition of the residual fluid and the minerals precipitated from it. Calculations of the magnitude of $\delta^{18}\text{O}$ depletion with decrease in X_{CO_2} of the hydrothermal fluid match the

recorded variation in isotopic composition of the Grey River hydrothermal fluid and thus support the fractionation model suggested above.

Available quartz-muscovite oxygen isotope fractionations indicate a range in temperature of 350-400°C for greisen alteration that accompanies the formation of the major veins.

CHAPTER 9

RADIOMETRIC DATING

9.1 INTRODUCTION

Geochemical evidence (presented above) suggests a genetic link between the tungsten mineralisation and the granitoids of the Grey River area. In an attempt to further assess this relationship, radiometric dating techniques were utilised to determine the time of emplacement of the megacrystic granite and the onset of mineralisation. Whole-rock and mineral separates selected by the author were analysed by Dr A.N. Halliday (Scottish Universities Research and Reactor Centre) and Dr J.G. Mitchell (University of Newcastle-upon-Tyne) for Rb-Sr and K-Ar isotopes respectively. Analytical techniques are summarised by Halliday et al., (1980) and Ineson and Mitchell (1975).

The field evidence indicates that the megacrystic granite was intruded into the metamorphic complex while the area was undergoing retrogressive metamorphism in shear zones. As a result, an extensive portion of the southern margin of the pluton was deformed by ductile shearing. Both the megacrystic granite and the metamorphic complex were intruded post-tectonically by leucogranites and diabase dykes (in that order), and later cut by a hydrothermal vein system containing tungsten mineralisation.

No previous age determinations are available from the area.

Table 9.1
Rb, Sr, Analytical Data

SAMPLE NUMBER	Rb (ppm)	Sr (ppm)	$^{87}\text{Rb}/^{86}\text{Sr}$ (atomic)	$^{87}\text{Sr}/^{86}\text{Sr}$ (atomic)
556	228.5	142.0	4.667	0.73610 ± 0.00005
555	188.7	158.6	3.449	0.72912 ± 0.00004
557	199.8	195.0	2.970	0.72630 ± 0.00004
550	210.0	257.8	2.360	0.72217 ± 0.00005
545	174.2	251.7	2.005	0.71849 ± 0.00003
571	147.5	264.9	1.614	0.71475 ± 0.00007

$\pm 0.7\%$ (2 σ)

$\pm 2\sigma$,
(mean run
precision)

Table 9.2

Potassium/Argon Ages*, Grey River Tungsten Prospect

SAMPLE NUMBER	ROCK TYPE	MINERAL ANALYSED	K (%)	$^{40}\text{Ar}_g$ (rad) (nm ³ m ⁻¹)	^{40}Ar (atm)	Age $\pm 1\sigma$ (Ma)
550	Megacrystic Gran.	Biotite	4.62 \pm 0.25	(7.93 \pm 0.07)10 ⁻²	4.9	466 \pm 25
557	"	Biotite	6.30 \pm 0.25	(1.07 \pm 0.01)10 ⁻¹	4.3	462 \pm 18
415	Leucogranite	Muscovite	10.30 \pm 0.27	(1.67 \pm 0.01)10 ⁻¹	7.5	444 \pm 11
64	Amphibolitic gneiss	Hornblende	0.56 \pm 0.01	(8.48 \pm 0.10)10 ⁻³	16.1	418 \pm 9
71	Mica Schist	Biotite	3.32 \pm 0.06	(4.73 \pm 0.05)10 ⁻²	7.5	395 \pm 8
495	Gneiss	Hornblende	1.65 \pm 0.02	(2.67 \pm 0.03)10 ⁻²	7.2	434 \pm 7
432	Greisen	Muscovite	10.60 \pm 0.08	(1.47 \pm 0.02)10 ⁻¹	5.8	386 \pm 6
453	Greisen	Muscovite	9.52 \pm 0.15	(1.30 \pm 0.15)10 ⁻¹	4.8	381 \pm 8
166	Greisen	Muscovite	10.40 \pm 0.10	(1.41 \pm 0.02)10 ⁻¹	5.3	378 \pm 6
390	Greisen	Muscovite	9.89 \pm 0.18	(1.29 \pm 0.02)10 ⁻¹	5.2	365 \pm 8
444	Greisen	Muscovite	9.85 \pm 0.04	(1.28 \pm 0.02)10 ⁻¹	3.5	364 \pm 6
206	Muscovite Selvedge	Muscovite	10.52 \pm 0.10	(1.39 \pm 0.01)10 ⁻¹	4.5	369 \pm 4
603	Muscovite Selvedge	Muscovite	9.66 \pm 0.26	(1.26 \pm 0.01)10 ⁻¹	11.7	365 \pm 10
568	Muscovite Selvedge	Muscovite	10.38 \pm 0.18	(1.33 \pm 0.01)10 ⁻¹	5.4	360 \pm 7
301	Muscovite Selvedge	Muscovite	10.86 \pm 0.28	(1.36 \pm 0.01)10 ⁻¹	5.2	352 \pm 9
518	Vein	Muscovite	4.06 \pm 0.01	(4.73 \pm 0.05)10 ⁻²	9.8	329 \pm 4

* Constants used: $^{40}\text{K}/\text{K} = 1.167 \times 10^{-4}$ mol/mol; $\lambda_\beta = 4.962 \times 10^{-10} \text{ A}^{-1}$, $\lambda_e = 0.581 \times 10^{-10} \text{ A}^{-1}$.

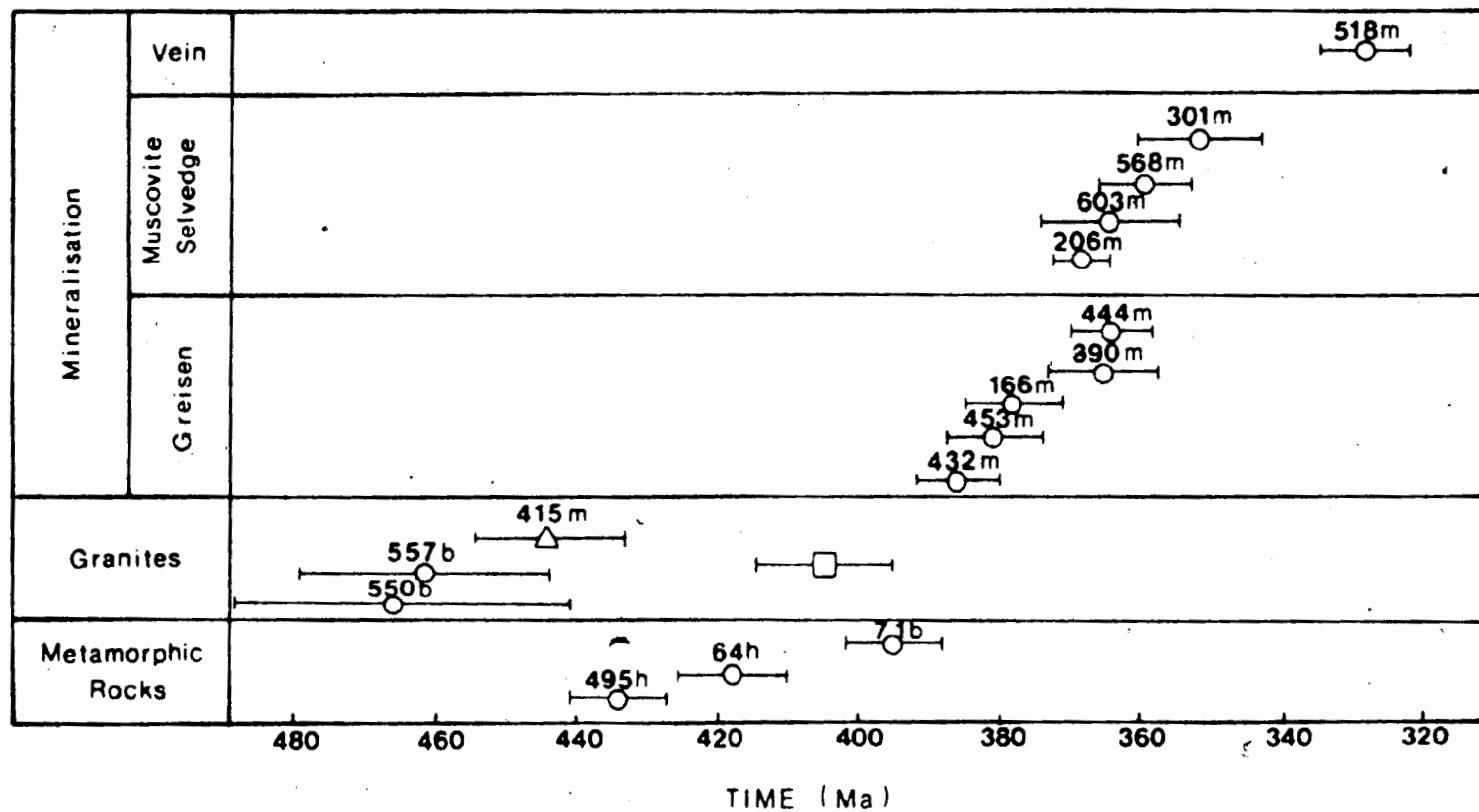
9.2 AGE RELATIONS: GRANITOIDS AND SHEAR ZONE

Radiometric dating techniques confirm (with minor exceptions) the chronology developed by field relationships, although interpretations are hampered by the obvious disturbance of Rb-Sr systematics during shear zone deformation, and apparently by excess argon in K/Ar age determinations.

Rb/Sr and K/Ar isotope measurement are presented in Tables 9.1 and 9.2 respectively. K/Ar mineral dates from the granitoids conflict with field and geochemical evidence in that they suggest that the granitoids are older than the metamorphic complex (Figure 9.1), and much older than the hydrothermal mineralisation. Although there is a minor overlap in age between the metamorphic rocks (Samples 495 and 64, Figure 9.1) and the granitoids, a K/Ar biotite date from a shear zone sample (71), is significantly younger at 395 ± 8 Ma.

Since the isotopic blocking temperature of hornblende is higher than for biotite (Hart, 1964), the K/Ar hornblende age of the metamorphic rocks presumably represents the time at which the last major high temperature phase of the metamorphism took place, while the biotite age for the shear zone probably represents the metamorphic age reset by the retrogressive metamorphic episode (hornblende is altered to biotite in the shear zones). Thus, the K/Ar age for the megacrystic granites is clearly discordant with known field relationships which indicate that the granite was intruded during the shearing episode.

Figure 9.1. Radiometric age determinations of metamorphism, intrusion, and mineralisation from the Grey River Tungsten Prospect. Open circles represent K/Ar mineral ages; open square = Rb/Sr whole rock isochron; triangle = leucogranite (K/Ar mineral age). Error bar equals 1σ error. 557b represents sample number and mineral analysed; h = hornblende, b = biotite, m = muscovite.



In an attempt to reconcile this problem, a Rb/Sr whole-rock isochron (Figure 9.2) was obtained from a north-south sample profile collected along the shores of Grey River fiord. A least squares fit (York, 1969) of all data points gives an "errorchron age" of 523 Ma; however, given the high analytical precision, the data do not fit a straight line, in fact they essentially plot on a curve.

Petrographic studies show that samples 556, 555 and 557 are undeformed while the rest exhibit intense deformation due to ductile shearing. The line joining the three undeformed samples gives an isochron age of 405 ± 10 Ma and an initial ratio (R_i) of 0.7092 ± 0.0005 . A line joining the three deformed samples has a slope corresponding to an "age" of 670 Ma with an initial ratio of 0.6993. Since this initial ratio is essentially impossible (similar to a value for the solar system at 4.6 Ga), then the curvature of the isochron does not represent a progressive resetting of the Rb/Sr system at 405 Ma. Rather, some phenomenon related to the deformation in the shear zone appears to have disturbed the Rb/Sr systematics.

The undeformed samples apparently record the age of intrusion (405 ± 10 Ma), which is in agreement with the age set by the K/Ar mineral data for the deformation in the shear zone. Both the megacrystic granite and the metamorphic rocks are post-tectonically intruded by leucogranite dykes and stocks, which are closely related to the mineralisation. Hence the 405 ± 10 Ma age for the megacrystic granite is

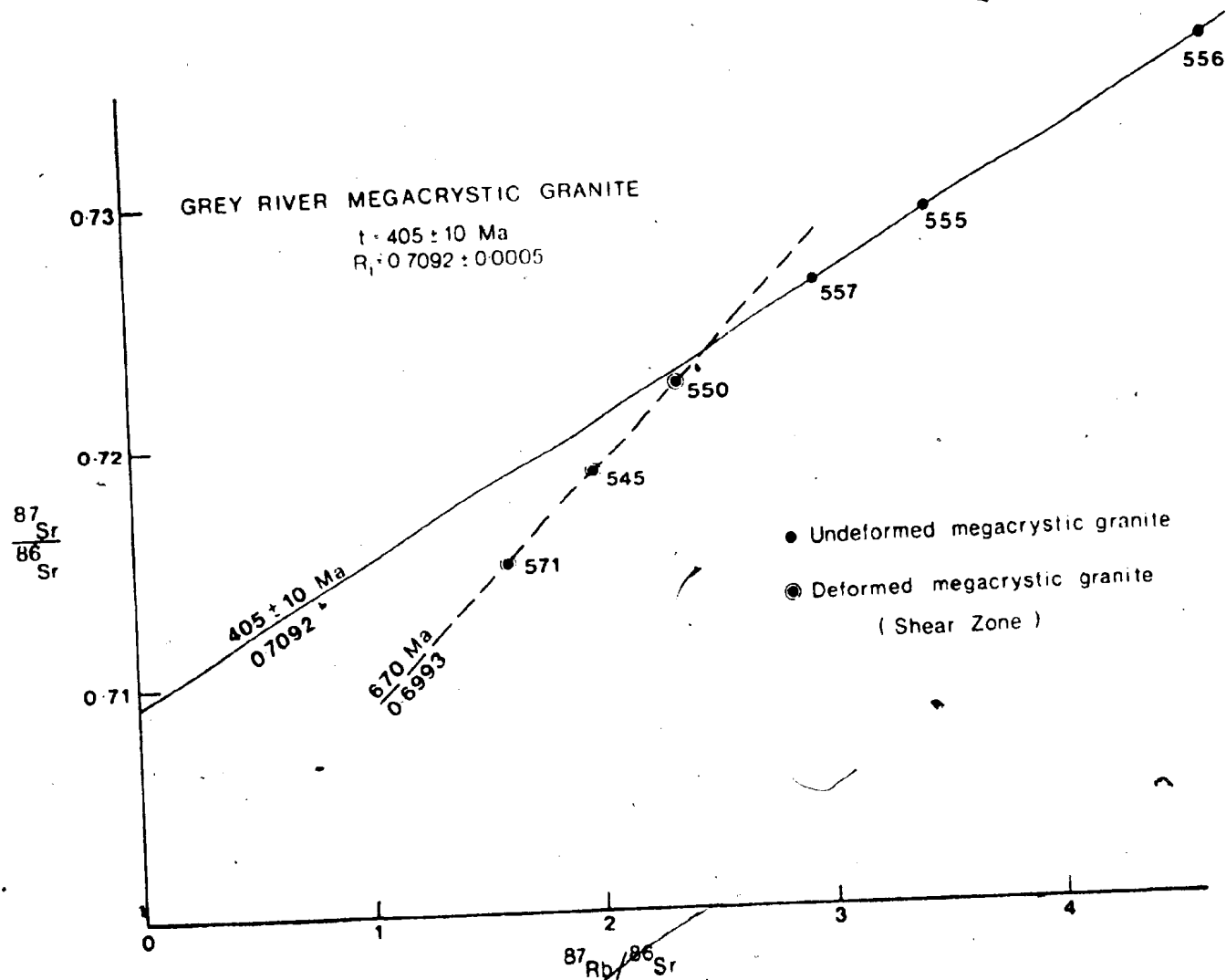


Figure 9.2 Rb/Sr whole rock isochron for the Grey River megacrystic granite.

the maximum age possible for the leucogranite dykes which were thus probably intruded in the time range 330-390 Ma, that is, after the deformation in the shear zone and prior to the mineralisation (see below)

9.3 DISTURBANCE OF THE Rb/Sr SYSTEMATICS

The curvature in the Rb-Sr data might be explained in one of two ways.

1) Firstly, that we are looking at variations in the initial $^{87}\text{Sr}/^{86}\text{Sr}$ ratio of the granite, the southern margin of the pluton being more basic than the rest of the pluton. This might be caused by crustal assimilation and contamination, zoning by fractional crystallisation, or, as shown by Stevens and Halliday (1979) for the Galloway plutons, by incomplete mixing of magmas derived from a complex or composite source region.

The first two reasons may be dismissed on the grounds that they require on the one hand, vast amounts of assimilation, and on the other hand, extremely slow fractional crystallisation; both of which are not indicated from field evidence. With respect to the third mechanism, if the age of intrusion of the granite is 405 ± 10 Ma ($R_i = 0.7092 \pm 0.00045$) then calculated initial ratios for the remaining samples (550, 545 and 571) are 0.70856 ± 0.00045 , 0.70693 ± 0.00038 , 0.70544 ± 0.00032 respectively. The errors account for the error in the age as well as the analytical error. These calculated initial ratios display a rather large range, especially when compared to the zoned plutons of Galloway (Stevens and Halliday, 1979), which show a variation on the order of 0.7042 to 0.7058 between

diorite, granodiorite, and biotite granite zones. By this comparison, the data for the Grey River megacrystic granite would probably argue against an initial ratio variation caused by incomplete mixing of magmas from different sources.

2) Large scale mobilisation of Sr and Rb may account for the disturbance of the Rb-Sr system in the Grey River megacrystic granite. Many workers have shown that isotopic homogenisation during a thermal event is limited with isotopic equilibrium or exchange between minerals being probable, but unlikely between samples spread over great distances (Gray and Compston, 1978). However, mobilisation of Sr is enhanced by fluids (Margaritz and Hofmann, 1978), and retrogressive effects involving hydrothermal alteration will affect whole rock ages (Hickman, 1980).

Shear zones are characterised by a hydrothermal metasomatism (Beach, 1979; Beach and Fyfe, 1972) which is broadly coeval with the strong deformation. All the mineral reactions are hydration reactions, and the large amounts of water required for them imply much fluid/rock interaction. In view of the strong ductile shearing that affects both the southern margin of the megacrystic granite pluton and the metamorphic complex, large scale diffusion of Sr and Rb is possible, and in fact indicated from trace element analyses (Figure 9.3).

The megacrystic granite becomes enriched in Sr and depleted in Rb with increasing intensity of shearing, while the metamorphic complex shows opposite trends. These data indicate that large scale redistribution or re-equilibration

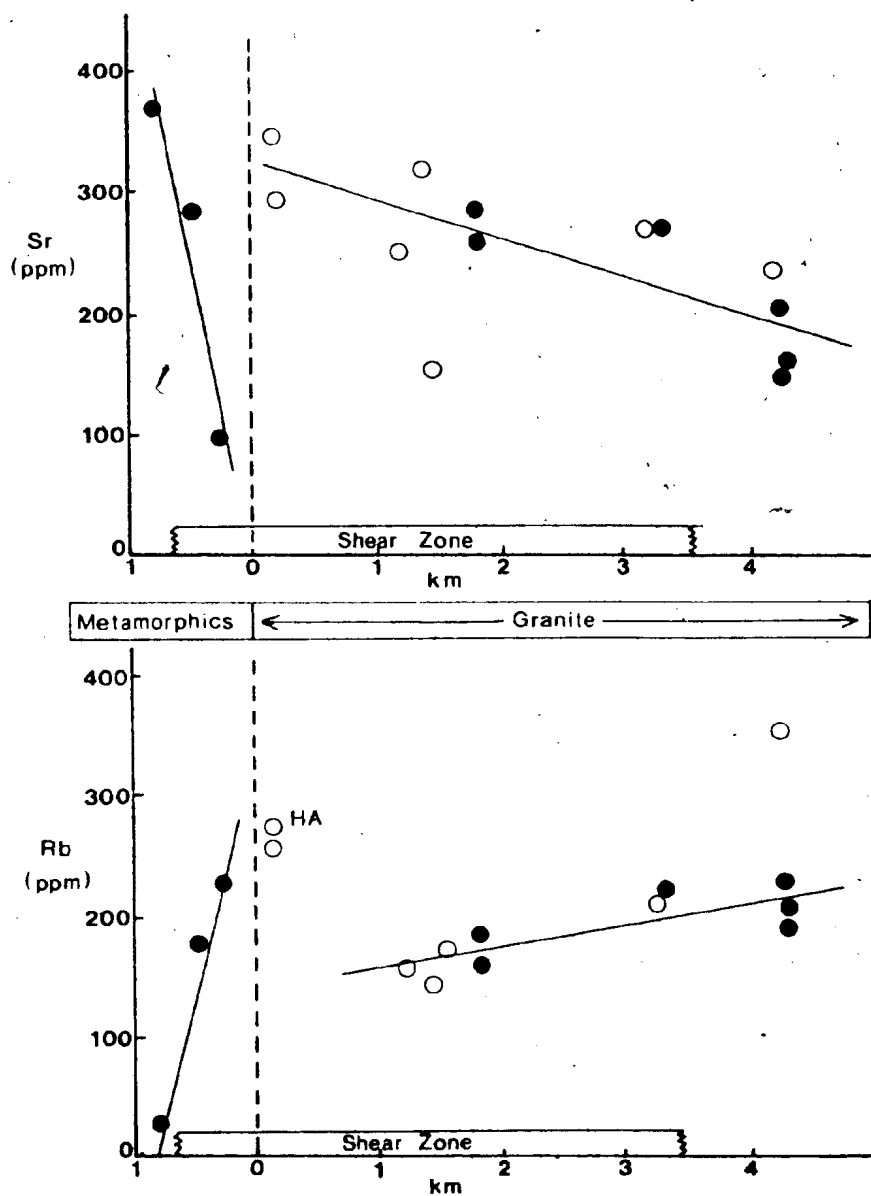
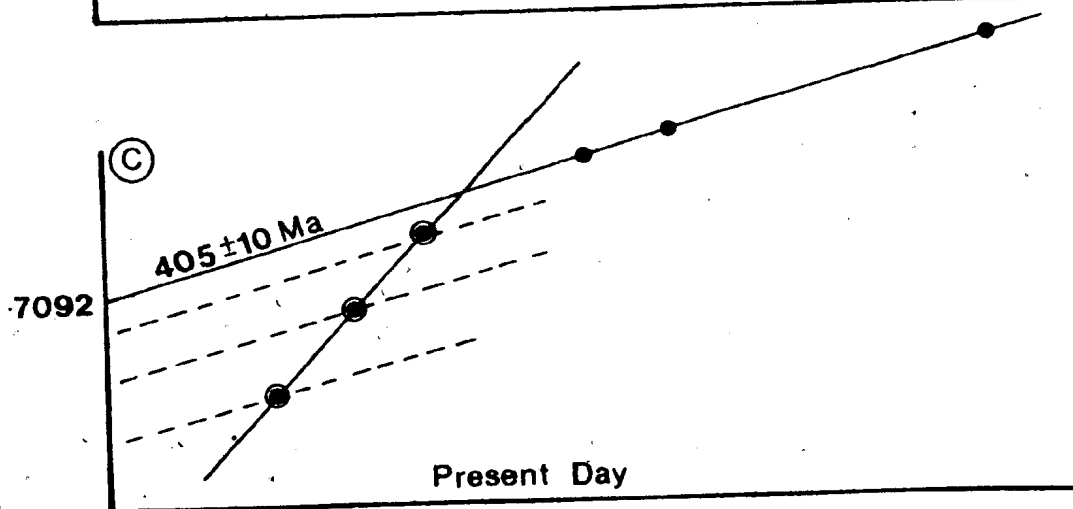
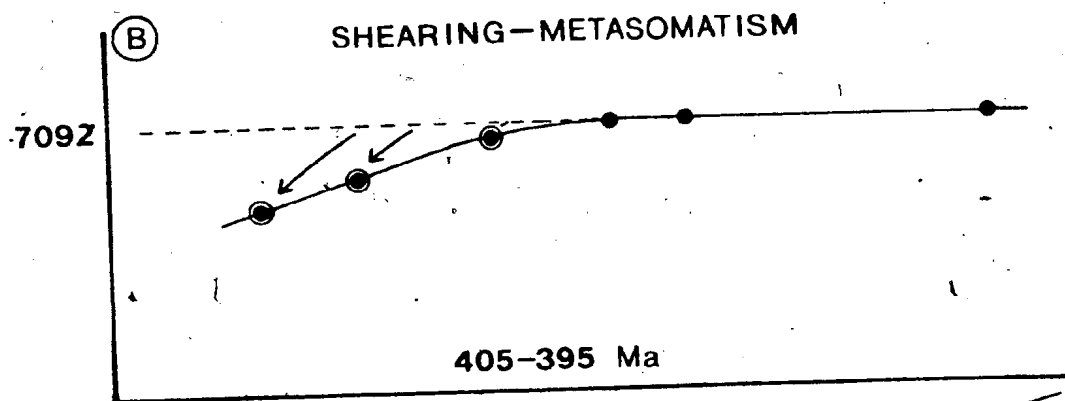
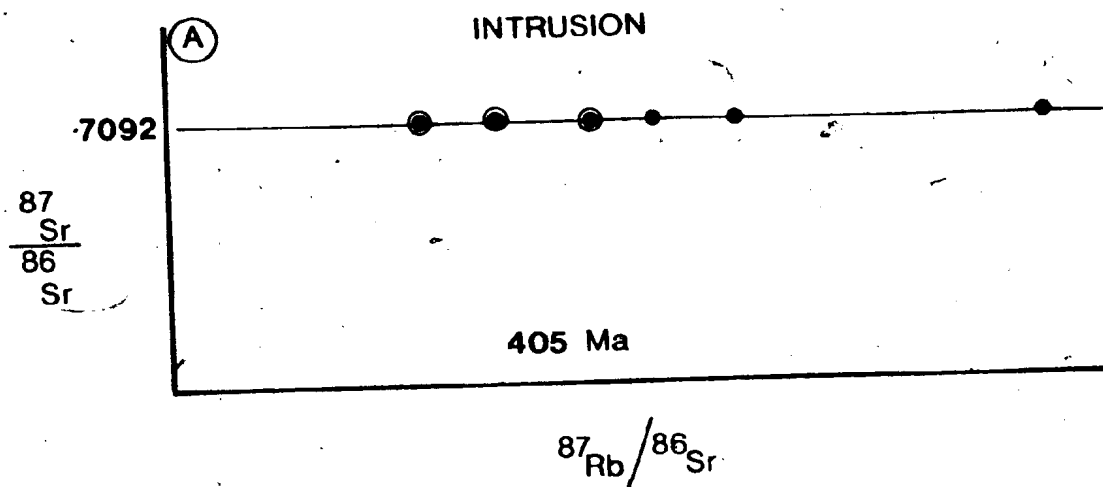


Figure 9.3 Sr and Rb variation in the Granite Cliff Shear Zone. H.A. represents hydrothermally altered samples; solid circles in granite represent whole rock isochron samples.

Figure 9.4 Open system behaviour of Sr and Rb during the emplacement of the Grey River megacrystic granite.

- 9.4A Intrusion of the megacrystic granite at 405 ± 10 Ma with an initial ratio of 0.7092 but with a range in Rb/Sr ratio.
- 9.4B Between 405 and 395 Ma the southern margin of the batholith was metasomatically altered during shearing, and Sr and Rb exchange between the metamorphic rocks and granite caused variation in the initial $^{87}\text{Sr}/^{86}\text{Sr}$ ratio in the deformed samples.
- 9.4C Present day situation: Metasomatically altered samples lie on a family of isochrons that parallel the isochron defined by the undeformed samples.



of Sr and Rb occurred during deformation in the shear zone, and that the megacrystic granite exchanged Sr with the metamorphic complex, which had a high Sr/Rb ratio.

The curvature in the Grey River Rb/Sr "isochron" may therefore be explained by changes in initial $^{87}\text{Sr}/^{86}\text{Sr}$ as a result of metasomatic exchange of Sr with the metamorphic complex, during or immediately after emplacement (Figure 9.4). Since the time differential between intrusion and shearing is small, the variably exchanged samples will fall on a family of isochrons essentially parallel to the isochron defined by the undeformed samples.

The present data suggest that the megacrystic granite was intruded at 405 ± 10 Ma, with the shearing at 395 ± 8 Ma overlapping the emplacement age for the granite. These dates represent a maximum age for the leucogranite which post-tectonically intrudes these units.

If the 405 ± 10 Ma Rb/Sr date for the granite is correct then the discordant older K/Ar age must have been caused by either potassium loss (Evernden and Kistler, 1970) or excess argon (many references in Dalrymple and Lanphere, 1969). In the Grey River situation potassium loss (without argon loss) is not indicated since the analysed biotites were either fresh or only partially chloritised (c.f. Shepherd et al., 1976). This would suggest that the discordant K/Ar ages are produced by excess argon, and this will be discussed in more detail below.

9.4 AGE RELATIONS: MINERALISATION

K-Ar age determination on muscovite separates from various stages of the mineralisation are shown in Figure 9.1. They exhibit a spread in age ranging from 386 ± 6 Ma to 329 ± 4 Ma. The various stages of mineralisation displayed in Figure 9.1 are apparently separated by age, but more importantly these subdivisions are matched by grain size variations of the mineral phases. Muscovite from the greisen stage is characteristically fine-grained, and is produced by alteration of mafic minerals in the amphibolitic gneiss wall rock; in contrast, the muscovite selvage and vein samples are coarse-grained, being precipitated directly from the hydrothermal fluid.

Grain size has a considerable effect on argon diffusion, with argon loss being greatest for fine grained minerals (Dalrymple and Lanphere, 1969; Hart, 1964). This should result in younger ages in the latter (Hart, 1964), which is the opposite to that observed at Grey River, suggesting that another factor is affecting these mineral ages, namely excess argon. This possibility is strengthened when coupled with the strong suggestion of excess argon in the granites which appear on other evidence to be related to the mineralisation.

Excess argon is a common problem in K/Ar dating (McDougall et al., 1969), and can be caused in several ways; as inherited argon (via xenolithic contamination), or environmental excess argon, occluded in minerals at the time

of formation. It is suggested (McDougall et al., 1969), that much of the latter excess argon is contained in fluid inclusions.

It has been demonstrated that many fluid inclusions from a variety of hydrothermal environments contain ^{40}Ar (Wahler, 1958; Rama et al., 1965; Lippolt and Gentner, 1963) and a correlation between ^{40}Ar and CO_2 -bearing inclusions is evident (Rama et al., 1965). Pegmatitic minerals such as beryl and feldspar are also known to contain radiogenic argon (Damon and Kulp, 1958). Funkhouser and Naughton (1968) have shown by crushing and decrepitation experiments that radiogenic argon (and helium) reside in secondary inclusions within minerals from ultramafic xenoliths in Hawaiian lavas, and account for the anomalous (old) K-Ar ages for these xenoliths (Funkhouser et al., 1966). Furthermore, these inclusions are known to contain significant quantities of CO_2 (Roedder, 1965).

These data suggest that CO_2 may act as a sink for rare gases such as ^{40}Ar (Green, 1979), and may be the cause or symptom of excess radiogenic argon found in minerals from hydrothermal and magmatic environments. Micas do not generally contain fluid inclusions (Rama et al., 1968), but if precipitated from a fluid (hydrothermal or magmatic) containing ^{40}Ar , then they might conceivably incorporate ^{40}Ar in their lattice.

Fluid inclusion and rare-earth element evidence (presented above) show that CO_2 was a dominant component of

the magmatic-hydrothermal fluid associated with the granites and the tungsten mineralisation. During early stages of the mineralisation CO_2 contents of the hydrothermal fluid were especially high, and muscovite precipitation from such fluids (greisen, muscovite-selvedged veins) might contain excess argon. If this is correct, K/Ar ages for the mineralisation would represent maximum ages.

Note also that a sample of coarse muscovite from a wolframite-bearing vein gives a much younger age at 329 ± 4 Ma (Figure 9.1). This age might represent the true age of mineralisation since fluid inclusion evidence indicates that wolframite, and probably muscovite, were deposited when CO_2 contents of the hydrothermal fluids were very low.

9.5 REGIONAL SIGNIFICANCE

A number of Newfoundland granitic bodies exhibiting a sheared fabric or a regional cataclastic texture have been dated by Rb/Sr methods (Bell et al., 1977; Bell and Blenkinsop, 1977; Blenkinsop et al., 1976). One of these, the Lockers Bay Granite (Bell and Blenkinsop, 1977) gave a very young age at $312 \text{ Ma} \pm 18 \text{ Ma}$, which the authors interpreted to represent the age of intrusion. This is at variance with field relationships (Jayasinghe, 1978) which show that the undeformed Newport granite, dated by the same authors at $344 \pm 44 \text{ Ma}$ (Bell et al., 1979), intrudes the Lockers Bay granite. This apparent conflict was resolved by Bell et al., (1979) by taking into account the overlap in the uncertainty of the age determination.

Recently however, a U/Pb zircon date of 460 ± 20 Ma (Dept of Mines and Energy Report 80-1, 1980) for the Lockers Bay granite suggests that the Rb/Sr systematics have been affected by the deformation and apparently rehomogenised on a regional scale at 312 Ma. This is constrained by the possibility that the older U/Pb age results from inherited zircons from an older crustal component in the granite. However, the evidence of the effect of shearing on the Grey River megacrystic granite would strongly suggest that the Rb-Sr whole-rock system can behave as an open system during shearing. In the Grey River situation the rehomogenisation was incomplete (localised) and strongly affected by the chemical gradient imposed by Sr-enriched metamorphic rocks in contact with the granite. Furthermore, shearing occurred during or just after emplacement, so that younger ages did not result from the metasomatic and deformational episodes.

The mineralisation at Grey River is intimately associated with a sequence of granitic rocks which appear to have been intruded over a long period of time, ranging from 405 ± 10 Ma to a possible minimum age of 330 ± 4 Ma. A prolonged magmatic history is characteristic of the Gander Zone, and in fact of the Appalachians in general, where igneous activity related to post-collisional tectonics spans the period 460 Ma to 300 Ma (Bell *et al.*, 1977; Potter *et al.*, 1979; Keppie, 1979; Cormier and Smith, 1973; Butler and Fullagar, 1978; Fullagar and Butler, 1979).

In Newfoundland, most of the granites have initial $^{87}\text{Sr}/^{86}\text{Sr}$ ratios between 0.704 and 0.710, the Grey River megacrystic granite falling at the higher end of that range (0.7092). A few granites exhibit higher ratios (St Lawrence, 0.7220, Bell *et al.*, 1977). Strong (1980) recognised a systematic variation in initial ratio as a function of age, and delineated two parallel trends of increasing $^{87}\text{Sr}/^{86}\text{Sr}$ with decreasing age. He related such increases to variation in isotopic ratio of the source rocks, and to possible input of low $^{87}\text{Sr}/^{86}\text{Sr}$ material from the upper mantle or lower crust, through crustal thickening following continental collision.

Such isotopic data are in accord with current models for the evolution of the Newfoundland Appalachians, which imply that collision between the North American and African plates had occurred by the Middle Ordovician (Williams, 1979) so that any subduction of the Iapetus oceanic plate terminated at that time (Dean, 1978). Vast amounts of granitic material were intruded after collision, their origin relating to crustal melting via crustal thickening in Silurian-Carboniferous times, and shearing and tensional processes related to Devonian-Carboniferous deformation (Strong, 1980).

9.6 METALLOGENY

The locations of the principal tungsten deposits (and selected tin and molybdenum deposits) of the Canadian Appalachians are shown in Figure 9.5 and can be divided into

four main types.

1) Scheelite-bearing skarns (with Mo, Cu, Zn) occur on Cape Breton Island (Nova Scotia), and are associated with granitic bodies of unknown age. Carbonate-rich horizons of the George River Group of late Precambrian age are host to the mineralisation (Chatterjee, 1980 a,b).

2) Folded quartz-carbonate veins with scheelite, arsenopyrite, rutile and gold occur subparallel to the bedding of the metapelites of the Ordovician Meguma Group (Miller *et al.*, 1976; Graves, 1976). These deposits (e.g. Moose River, N.S.) are demonstrably unrelated to granitic activity and were formed by hydraulic fracturing under regional greenschist metamorphism (Graves, 1976; Miller, 1974).

3) Quartz veins with wolframite (and/or Sn and Mo-bearing minerals) are associated with felsic phases of complex Devonian to Carboniferous batholiths (e.g. Square Lake, New Brunswick; Burnt Hill, New Brunswick).

4) Fracture controlled W, Mo, Bi, Sn, Cu deposits occur in volcanic rocks (porphyry affinities) associated with subvolcanic stocks of Carboniferous age (e.g. Mt Pleasant, New Brunswick).

The association of tungsten deposits with composite batholiths is best illustrated for the 3rd and 4th types outlined above. The Burnt Hill deposit, New Brunswick (Figure 9.5e) is associated with a composite pluton of adamellite having three internal phases. These range from

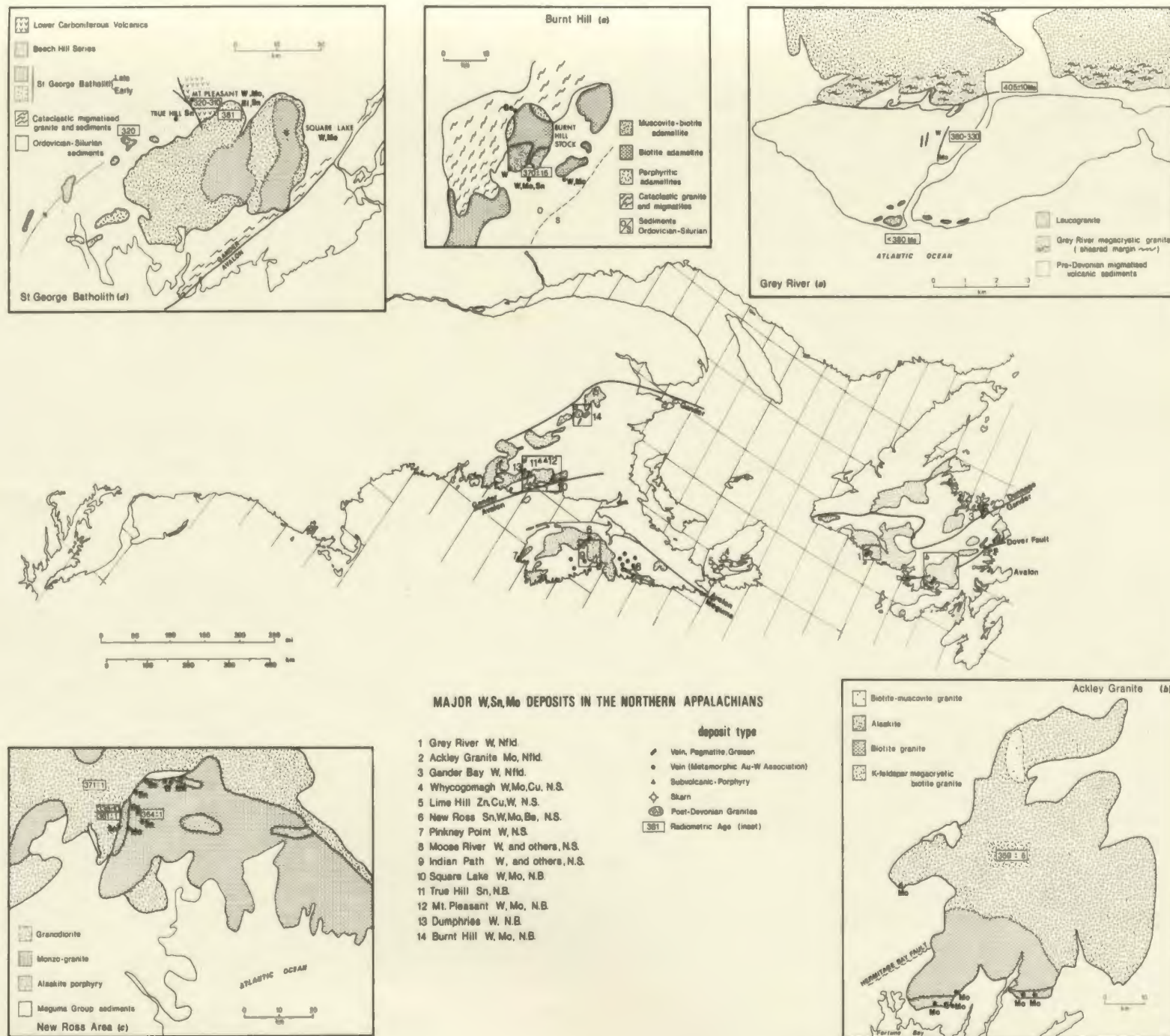


Figure 9.5

a K-feldspar megacrystic adamellite to a late muscovite-biotite adamellite with associated aplitic dykes. Several rare-metal greisen veins are associated with the youngest phases of this composite pluton (Potter, 1968).

Similar relationships hold in the New Ross area (Figure 9.5c), Nova Scotia, where Sn, W, and Mo-bearing minerals occur in greisen veins associated with the late differentiates of the composite South Mountain Batholith (Smith, 1974; Smith and Turek, 1976; MacKenzie and Clarke, 1975). Molybdenite mineralisation (Figure 9.5b) is also associated with the highly differentiated alaskitic phase of the Ackley granite in Newfoundland (Whalen, 1976). In all these areas plutonism and mineralisation span the time range 390 Ma to 340 Ma.

Perhaps the best example of tungsten mineralisation associated with prolonged magmatism is found in southern New Brunswick where the Mt Pleasant W, Mo, Bi, Sn deposit is the culmination of igneous activity stretching over 70 million years (Figure 9.5d). The St George batholith, which intrudes Ordovician/Silurian sediments, is compositionally complex, and includes early K-feldspar megacrystic granite and late aplite-porphyry phases (Ruitenberg, 1966). An age of 381 Ma is indicated for the megacrystic phase (Tupper and Hart, 1961), while the younger phase is undated, but has several associated wolframite-bearing greisen vein deposits (Ruitenberg *et al.*, 1977).

An even younger series of intrusions (320 Ma), called

the Beech Hill Series, intrudes both the St. George batholith and Lower Carboniferous volcanics, all three being geochemically related (Dagger, 1972). These high-level plutons are consanguineous with the Lower Carboniferous volcanics and give rise to the W, Mo, Bi and Sn mineralisation found at Mt Pleasant and True Hill. Thus tungsten, molybdenum and tin-bearing minerals occurrences in southern New Brunswick are deposited within, and along, the contacts of the late phase of a Middle Devonian to Lower Carboniferous granitic complexes and associated subvolcanic stocks.

Similar long-lived magmatic activity is indicated in the Grey River area with initial intrusion of K-feldspar megacrystic granite (which appears to be a ubiquitous component of most Appalachian Devonian batholiths) at 405 ± 10 Ma, followed by intrusion of a highly differentiated, highly siliceous leucogranite, which may be as young as 330 Ma. In contrast to other Appalachian tungsten deposits, evidence for a comagmatic-differentiation relationship between megacrystic granite and leucogranite is equivocal, but nonetheless suggests that the tungsten mineralisation is related genetically to the granites.

In summary, most of the major tungsten, tin, and molybdenum deposits of the Canadian Appalachians appear to be related to the youngest phases of complex granitic batholiths. These batholiths are characterised by a multiple intrusion history spanning long periods of time, with successive phases becoming more differentiated and

enriched in the ore-forming elements.

9.7 SUMMARY

Rb/Sr and K/Ar age data for the granitic rocks indicate that these rocks behaved as an open system during shear zone deformation that affected the southern margin of the Grey River megacrystic granite. Rb/Sr isotopic data from the megacrystic granite plot as a curve rather than an isochron, however a line regressed through the undeformed samples give an isotopic age of 405 ± 10 Ma, which is interpreted to represent the age of intrusion. This accords with field evidence which indicates the megacrystic granite was intruded while the region was undergoing local retrogressive metamorphism, which has been dated at 385 ± 8 Ma by K/Ar dating methods.

Large scale mobilisation of Sr (and Rb) occurred between the deformed margin of the megacrystic granite pluton and the metamorphic rocks, in response to metasomatic alteration which accompanied shear zone deformation. The Sr exchange between the metamorphic rocks and the megacrystic granite resulted in a change in initial $^{87}\text{Sr}/^{86}\text{Sr}$ ratio in the deformed margin of the pluton, which accounts for their isotopic displacement from the 405 Ma isochron defined by the undeformed samples.

K/Ar age determinations for the megacrystic granite are clearly at variance with field evidence and the Rb/Sr age determination, and suggest that the granite contained excess argon at the time of intrusion. This may also explain the

wide variation in the K/Ar ages determined for the mineralisation at Grey River which range from 385 to 330 Ma. The association of radiogenic argon with CO₂ fluids in magmatic and hydrothermal environments elsewhere, might explain the apparent presence of excess argon in the Grey River mineralisation, since fluid inclusions and geochemical studies indicate that the hydrothermal fluid evolved from the granites, and associated with the mineralisation, was CO₂-rich. Since the mineralisation was unlikely to have been formed over such a large time span the true age of the Grey River mineralisation is interpreted to be 330 Ma, the older ages being caused by excess argon.

The isotopic age data for the Grey River prospect compare with similar tungsten deposits in the Canadian Appalachians, and all appear to be associated with the youngest phases of composite batholiths intruded from Mid-Devonian to Carboniferous times.

CHAPTER 10

THE GENESIS OF THE GREY RIVER TUNGSTEN PROSPECT AND IMPLICATIONS FOR THE TRANSPORT OF TUNGSTEN IN HYDROTHERMAL FLUIDS

10.1 THE GENESIS OF THE GREY RIVER TUNGSTEN PROSPECT

The general requirements for the formation of an economic hydrothermal ore deposit have been discussed by Fyfe and Henley (1973). They include; a fluid medium capable of transporting ore-forming elements from their source to the site of deposition; a structure to focus the hydrothermal discharge, and together with a suitable chemical environment, to precipitate ore minerals at a specific locale. Finally, but not the least important, there must be an energy source available to maintain these processes over a sufficient period, to allow an economic concentration to occur. Any attempt to formulate a model for the genesis of the Grey River Tungsten Prospect must evaluate the relative importance of each of these processes.

10.1.1 Source: Ore-forming Elements

The hydrothermal veins of the Grey River Tungsten Prospect traverse the contact between a high grade metamorphic terrain and a K-feldspar megacrystic, biotite granite pluton. Furthermore the veins cut a suite of leucogranite dykes, although a few dykes contain coarse quartz centers and more rarely grade into quartz veins. Such a setting suggests a genetic relationship between the granites

(especially the leucogranites) and the mineralisation.

Biotite granite and two-mica leucogranite are typically associated with rare-metal deposits of Western Europe (Tischendorf et al., 1974; Stenprok et al., 1978; Chauris, 1978) and elsewhere (Groves, 1972; Taylor, 1979). The leucogranite occurs either as highly differentiated (aplitic) members of composite batholiths (typically K-feldspar megacrystic, biotite granite), or as individual bodies often spatially associated with biotite granite and derived from wet melting of aluminous metasediments (Chauris, 1978; Strong and Hanmer, 1980). In either case, the leucogranites are chemically specialised, being characterised by high silica and alkalis and anomalous (high) concentrations of Sn, W, F, Li, Be and B (Tischendorf, 1977; Taylor, 1979). Their high silica and alkali-rich tendency is enhanced by (auto) metasomatic alteration that precedes and accompanies Sn-W mineralisation (Baumann and Tischendorf, 1978; Burnol, 1978; Hesp and Rigby, 1974; Kozlov et al., 1974).

The Grey River granitoids exhibit similar features. The leucogranites are characterised by high silica and variable, but generally high, K_2O and Na_2O contents. Their alkali-rich nature was caused by autometasomatic alteration which occurred during their emplacement, and involved addition and redistribution of alkalis and alkaline-earth elements during development of secondary microcline and albite.

The Grey River megacrystic granite is enriched in Sn and W (42 ppm and <4-8 ppm respectively) compared to normal

crustal abundances (2.5 ppm and 1.5 ppm respectively). On the other hand the Grey River leucogranites have lower concentrations of tin compared to the megacrystic granite, while tungsten concentrations are below the detection limit (4 ppm). This reflects the lack of mafic minerals in the leucogranite (e.g. Hesp, 1971) or the partitioning of Sn and W into a vapour phase during autometasomatism.

Thus by analogy with other deposits, the granites of the Grey River area appear to have been the source of the tungsten found in the mineralisation. However, in contrast to granites of western European deposits, the granites of the Grey River area are not markedly enriched in fluorine or lithium, having concentrations close to, or marginally exceeding, normal crustal abundance (280 ppm and 45 ppm respectively). Elevated tin contents and moderate to low F and Li concentrations are common however, for granitic rocks associated with deposits containing tungsten-bearing minerals only (Tischendorf, 1970, 1973).

In the presence of a melt and aqueous fluid, the behaviour of elements such as Sn and W is dependent on their fluid-melt partition coefficients. Such coefficients may vary with the composition of the fluid phase and the crystallisation history of the melt. It has been shown that volatiles such as CO_2 , HCl, and NH_3 tend to raise the melting temperature of granites while P_2O_5 , HF, BO_3 and Li_2O lower the melting temperature (Wyllie and Tuttle, 1961; Burnham, 1967, 1979; Chorlton and Martin, 1978). The presence of elements such as Li, F and B

allows for extreme differentiation of melts (Stewart, 1978, Chorlton and Martin, 1978). However, while such elements are concentrated in late stage residual fluids it does not follow that they are partitioned into the aqueous fluid to form hydrothermal deposits. On the other hand, the raising of the granite minimum melting temperatures with the presence of CO_2 in a melt appears to oppose extreme differentiation, and unlike fluorine and lithium, its solubility in a granitic melt is low, thus favouring partitioning into a hydrothermal fluid (Burnham, 1979).

The clear evidence of the involvement of a CO_2 -rich hydrothermal fluid with tungsten mineralisation at Grey River, and elsewhere (discussed below), might imply that tungsten is readily partitioned into an aqueous fluid containing CO_2 , while tin, which shows a strong affinity for F (Hesp and Rigby, 1972), may be retained (initially) by a melt under such conditions (high P_{CO_2} , low P_{F}). Furthermore oxygen fugacity may also effect partitioning of tin between melt and fluid (Taylor, 1979), since tin can exist in a magma in both tetravalent and divalent states (Hamaguchi *et al.*, 1964).

It has been shown that granites associated with tin deposits contain ilmenite while barren granites are characterised by a magnetite-hematite \pm ilmenite assemblage, reflecting reducing and oxidising conditions respectively (Ishihara, 1977; Ishihara *et al.*, 1979). Under oxidising conditions Sn^{IV} may be retained in rock-forming minerals by substitution in

tetrahedral sites, thus accounting for the high tin contents in mineral phases such as biotite (Durasova, 1967). The presence of magnetite-hematite-ilmenite assemblages in unaltered Grey River megacrystic granite and leucogranite, implies oxidising conditions prevailed during their crystallisation. This might account for the lack of cassiterite in the hydrothermal veins since oxidising conditions would favour retention of Sn^{IV} by the melt.

10.1.2 Source: Hydrothermal Fluids

The somewhat equivocal geochemical evidence suggests that the Grey River granites were the immediate source of the ore-forming elements concentrated in the hydrothermal veins. These elements were moved via a fluid medium to their site of deposition, and an obvious source for the energy and the fluid required to accomplish this process would also be the granite.

The textural differences in the Grey River leucogranite suite, between alaskite, aplite and pegmatite, may be related to a continuing process in which the degree of volatile saturation plays a major role (e.g. Fournier, 1968; Jahns and Burnham, 1969). Crystallisation from granitic magma undersaturated in volatiles is thought to yield rocks with normal phaneritic textures (e.g. alaskite). The principal role of an aqueous fluid is to promote growth of large crystals, resulting in the formation of pegmatites (Jahns and Burnham, 1969), but if loss of a fluid from a melt after saturation is rapid, quenching of the crystallising silicate

liquid is expected and the typical product is an aplite. After disappearance of the silicate melt, the crystals and fluids may react, and result in metasomatism in adjacent country rocks or within their own system (autometasomatism). The textural and alteration features of the Grey River leucogranites thus imply the existence of an aqueous fluid phase during their emplacement.

The chemical nature of this volatile phase is indicated by REE analyses. The leucogranites show a relatively depleted light REE and enriched heavy REE pattern, and petrographic and geochemical data indicate that such a pattern is unlikely to result from any fractional crystallisation or cumulate process, implying that the REE pattern resulted from the redistribution of REE by hydrothermal fluids (Collerson and Fryer, 1978; Kerrich and Fryer, 1979; Taylor and Fryer, 1980 a,b).

The heavy REE enrichment and light REE depletion pattern suggests that a CO_2 or F-rich hydrothermal fluid interacted with the leucogranites during autometasomatic alteration. The leucogranite REE pattern is similar to those obtained from the alteration zones peripheral to the hydrothermal veins, implying that the wall rock reacted with a similar fluid. Since the leucogranite evolved an aqueous fluid phase during its emplacement, and the chemical nature of that fluid was similar to the fluid involved in the mineralisation, it is suggested that the leucogranite was the source of the hydrothermal fluid.

10.1.3 Structural Controls to Mineralisation

In hydrothermal vein systems, changes in vein strike or dip often accompany the loss or appearance of ore. In the Grey River Tungsten Prospect wall rock displacement, tension gashes in wall rock xenoliths, and slickensides on sheeted surfaces, indicate that the composite lodes were formed by repeated reopening and injection of new material into open spaces, created by the differential movement of wall rock during normal faulting. Depending on the original configuration of the fracture, normal faulting resulted in the development of thick open spaces where the fracture was steepest, while cavities developed in more shallowly dipping portions of the fracture were thinner.

Grade and structural data from composite Veins #6 and #10 reveal that there is a correlation between grade, vein width, vein attitude, and hydrothermal alteration. That is, the highest grades (1-4% WO_3) occur in the thinnest sections of the vein, which are also the most shallow dipping. Furthermore the most intense greisen alteration occurs in such sections.

These facts are consistent with the observation that internal vein movements by normal faulting controlled the distribution of ore minerals. The main structural influences were sudden changes in pressure and temperature with vein reopening (supported by fluid inclusion evidence), and decreases in the temperature of the hydrothermal fluid by increased wall rock interaction in zones of high

stress (i.e. shallow-dipping sections).

10.1.4 Physico-Chemical Controls of Mineralisation

The fluid inclusion and isotopic evidence from the hydrothermal veins indicate that the fluid involved with the mineralisation at Grey River was characterised by CO_2 and that a reduction in CO_2 contents of the fluid, as well as temperature, promoted deposition of wolframite.

The fluid inclusion types and their distribution between veins is summarised in Figure 10.1 and indicates a complex evolutionary history for the hydrothermal fluid. Since available evidence suggests derivation of the hydrothermal fluid from the leucogranite, then the initial P-T conditions of the fluid were approximately 2 kb and 600°C (as deduced from contact metamorphic features of the megacrystic granite pluton).

Falling pressure and temperature resulted in deposition of quartz-feldspar-molybdenite veins from a homogeneous supercritical $\text{CO}_2\text{-H}_2\text{O}$ fluid. During deposition of quartz-bismuthinite veins the hydrothermal solution intersected the P-T immiscibility surface for a fluid of $X_{\text{CO}_2} = 0.4$ (Figure 10.1) and separation of CO_2 -rich and water-rich fluids resulted. Fluid phase equilibria indicate that immiscibility occurred at temperatures of $390^\circ - 430^\circ$ and fluid pressures of 1000-1200 bars.

A period of hydraulic fracturing resulted in the deposition of quartz-sulphide and quartz-wolframite veins in composite lodes. Quartz-muscovite oxygen isotope fraction-

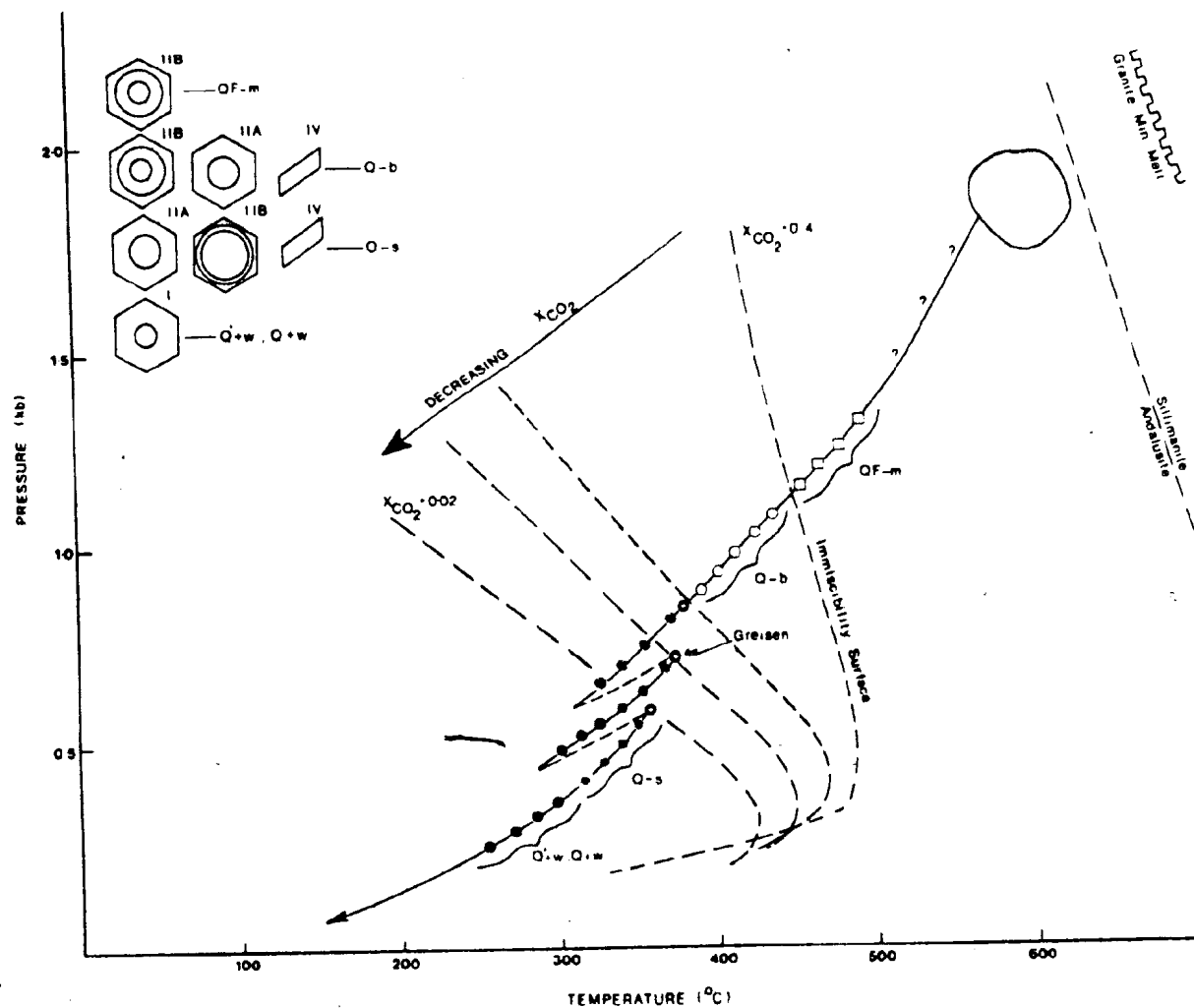


Figure 10.1 Summary of the evolution of the Grey River hydrothermal fluid. Andalusite/sillimanite equilibria from Holdaway (1971).

ation data show that the greisen envelopes to these lodes were formed at a temperature of 360-400°C. Vein movements by normal faulting during the hydraulic fracturing episode resulted in rapid decreases in fluid pressure and temperature, further depleting the hydrothermal fluid in CO₂ by promoting retrograde boiling. Deposition of wolframite occurred from a hydrothermal fluid of low salinity (0-3 equivalent wt% NaCl) and CO₂ contents (less than 10 bars), after separation of a CO₂ vapour phase by retrograde boiling.

The calculated oxygen isotopic composition of the hydrothermal fluid supports the fluid inclusion evidence of a progressive loss of CO₂ from the hydrothermal fluid with time. Early stages of mineralisation are characterised by a fluid of supposed magmatic origin while later stages of mineralisation show progressive depletion in $\delta^{18}\text{O}_{\text{H}_2\text{O}}$. This would normally be interpreted as evidence for mixing of isotopically distinct fluids, such as meteoric and magmatic waters, however available CO₂-H₂O isotopic fractionation data suggest that the loss of 40 mol% CO₂ from the hydrothermal fluid would account for the shift (depletion) in oxygen isotopic composition of the fluid.

In summary, the deposition of the veins and the paragenetic sequence of mineralisation at Grey River appear to be related to changing temperature, pressure, and compositional parameters of the hydrothermal fluid. The fluid inclusion and isotopic evidence suggests that reduction in CO₂ contents of the fluid (by immiscibility and retrograde boiling) exerts

a major control on the deposition of wolframite.

10.2 WOLFRAMITE-SCHEELITE EQUILIBRIA

Previous workers have shown that temperature, f_{O_2}/f_{S_2} , $a(Ca^{2+})/a(Fe^{2+}+Mn^{2+})$ and pH govern the transport and deposition of tungsten in hydrothermal solutions (Foster *et al.*, 1978).

Data from the Grey River Tungsten Prospect suggest that

f_{CO_2} is also important in the transport/deposition process.

The factors controlling the deposition of either wolframite

- or scheelite are the subject of much debate, the consensus being that the $a(Ca^{2+})/a(Fe^{2+}+Mn^{2+})$ and pH govern the composition of tungsten-bearing minerals (Hsu, 1976, 1977; Horner, 1979; Foster *et al.*, 1978).

At Grey River, wolframite is the primary tungsten-bearing mineral to precipitate and it is replaced by scheelite at some later time in the paragenesis. In a few localities in the vein, wolframite crystals are attached to hydrothermally altered wall rock xenoliths. This might suggest that the hydrothermal fluid leached Fe^{2+} from the wall rock to promote deposition of wolframite, but geochemical data show that both Ca^{2+} and Fe^{2+} were leached during the alteration process. Furthermore, because of multiple injection within the lodes, many of the later wolframite-bearing injections appear to be isolated from wall rock, reducing the possible effect of hydrothermal alteration.

Burt (1971, a,b; 1978) maintains that the deposition of either wolframite or scheelite is governed by the ratio of

$\mu_{F_2O_{-1}}$ to μ_{CO_2} in the ore-forming fluid. He demonstrated in a $\mu_{F_2O_{-1}} - \mu_{CO_2}$ diagram that the assemblage fluorite-ferberite, characteristic of greisen and veins, is stable only in relatively CO_2 -depleted, F_2O_{-1} -rich environments, while the assemblage calcite-scheelite, characteristic of skarns, is relatively stable in CO_2 -rich, F_2O_{-1} -depleted situations. Thus ferberite (wolframite) and calcite are incompatible and they react to form scheelite by the exchange reaction



The assemblage wolframite-fluorite is found in the greisen and hydrothermal veins at Grey River, but fluid inclusion evidence indicates that at certain times in the mineralising sequence, CO_2 was a characteristic component of the hydrothermal fluid. Carbonates are deposited immediately prior to wolframite and are found only as solid inclusions in quartz. Carbonates are notably absent from wolframite-bearing veins, although in one sample of quartz (Plate 5.5E) an unaltered wolframite crystal was observed in contact with a carbonate mineral, presumably calcite. Fluorite on the other hand is generally deposited later than quartz and wolframite (and at a lower temperature), but is not restricted to any vein type. This might imply that the F_2O_{-1} has little effect on wolframite-scheelite equilibria, except perhaps by reducing the $a(Ca^{2+})/a(Fe^{2+}+Mn^{2+})$ ratio because

* $\mu_{F_2O_{-1}}$ is equivalent to the chemical potential of HF.

of the strong affinity of F^- for Ca^{2+} (Studenikova et al., 1970). It should be noted, that in vein tungsten deposits devoid of fluorite (e.g. metamorphic vein deposits), the dominant tungsten-bearing species is scheelite (Henley et al., 1976; Graves and Zentilli, 1976; Miller et al., 1976; Fryer et al., 1979).

If wolframite was deposited in response to a drop in CO_2 content of the fluid, one would expect associated carbonates, since their solubility is dependent on P_{CO_2} (Holland, 1977). Perhaps the rarity of a carbonate-wolframite assemblage in the Grey River veins is a result of the fact that most of the wolframite is altered to scheelite. Bryzgalin (1958) notes that in alkaline solutions (at temperatures between 250° and $500^\circ C$) and in the presence of calcite, wolframite will decompose and scheelite will be deposited.

Loss of CO_2 from the fluid will affect the solution pH, thus the hydrothermal fluid coexisting with wolframite is likely to be weakly alkaline. The lack of carbonate associated with wolframite is therefore explained as a result of a reaction between wolframite and calcite to produce scheelite. The occurrence of an unaltered wolframite crystal in contact with a carbonate crystal is a fortuitous preservation induced possibly by their isolation from the cooling hydrothermal fluid. Similarly, the carbonate deposited prior to wolframite deposition is only preserved when isolated as inclusions in quartz, and therefore protected from reaction

with the cooling hydrothermal fluid.

Scheelitisation of wolframite is common in many hydrothermal vein deposits (Ramdohr, 1969), which might explain the observation of the apparent incompatibility of calcite and ferberite in such environments. Since carbonate minerals have retrograde solubility, a cooling hydrothermal fluid is likely to redissolve them, promoting a reaction with wolframite to produce scheelite.

10.3 CO₂-RICH FLUIDS AND TUNGSTEN DEPOSITS

Evidence from the Grey River Tungsten Prospect clearly illustrates that CO₂ is an important component of the hydrothermal fluid associated with a tungsten deposit formed at high fluid pressures. Fluid inclusion studies of other tungsten deposits yield similar data (Table 10.1). Ivanova (1974), summarising work on thirty East Transbaikalian and Mongolian deposits, showed that the fluids associated with tungsten deposits were dilute (less than 10 equivalent wt% NaCl) and had variable CO₂ contents (up to 27 wt%). These deposits formed at minimum fluid pressures of between 500 and 1600 bars (50-60 MPa).

Similar compositions are indicated from studies of vein Au-W deposits (Kalyuzhnyi et al., 1975) and vein Sn deposits (Koltun, 1973). On the other hand, shallow level tungsten deposits of porphyry or subvolcanic affinities, contrast markedly with higher pressure deposits when their respective fluid compositions are compared (Table 10.1). Such fluids are water-rich and are often highly saline (a

FLUID IN- CLUSION SETTING	LOCATION	MINERAL	TEMPERATURE (°C)	PRESSURE (bars)	CHEMISTRY OF DILUTED FLUID (wt %)										REFERENCES
					SiO ₂	Al ₂ O ₃	FeO	CaO	MgO	Na ₂ O	K ₂ O	SO ₄	Cl	Salinity (wt % NaCl)	
Qtz-v, pl., Gr-E	Gray River, Newfoundland	n-b n-b Q-w 700	450-480 300-400 300-350 270-300	1200-1400 1000-1200 100 850	●	●	●	●	●	●	●	●	●	5 3 1.5 0.1	Higgins, in prep.
Qtz-v, pl., Gr-P	Corruick Fell, U.K.	Q Q-w	275P 205P	500	●	●	●	●	●	●	●	●	●	8.5	Shepherd et al., 1976
Qtz-v, pl.	Takatori, Japan	Q-w	350-225	-	●	●	●	●	●	●	●	●	●	9.0-10.0	Tsutsui and Takemuchi, 1976
Qtz-v, pl.	Emamichi, Japan	s n Q	510-270 337-200 205-230	-	●	●	●	●	●	●	●	●	●	8.0 8.4 5.5-6.0	-
Qtz-v, pl.	Osami, Japan	s Q	530-270 375-225	-	●	●	●	●	●	●	●	●	●	8.5-9.0 4.4-6.0	-
Qtz-v, pl., Gr-P	Spokoyevye, USSR	Q-w	170-200	1000	●	●	●	●	●	●	●	●	●	-	Naumov and Ivanova, 1971
Qtz-v, pl., Gr-E	Nadoto, USSR	Q-w, c	200-100	1400	●	●	●	●	●	●	●	●	●	-	-
Qtz-v, pl., Gr-E	Kara Gha, USSR	Q-w	-	-	●	●	●	●	●	●	●	●	●	4.0-8.0	Ivanova et al., 1976
Qtz-v, pl.	Servilha, Portugal	Q-w	200-300P	1000	●	●	●	●	●	●	●	●	●	-	Correia, 1974
Qtz-v, pl.	Ureis, USSR	Q-w, c Q-s	300-100	-	●	●	●	●	●	●	●	●	●	-	Amfrev, et al., 1974
Qtz-v, pl.	Novoshe, Ureis, USSR	Q-s Q	270-200 205-300	300-1500	●	●	●	●	●	●	●	●	●	-	Podolskii and Purlov, 1975
Qtz-v, pl.	Yuzovskoe, USSR	Q-b, s	350-400	1000-1400	●	●	●	●	●	●	●	●	●	-	Minster et al., 1976
Qtz-v, pl., Gr-P	Korbenovo, USSR	Q-w, c, b	400-300	700	●	●	●	●	●	●	●	●	●	-	Kozlovskii et al., 1975
Qtz-v, pl.	Kanad, USSR	Q-s Q-w, b, s	300-200 275-200	900 300	●	●	●	●	●	●	●	●	●	-	Trubnikov and Frenkel, 1974
Qtz-v, pl.	Shirshak, USSR	Q-w, b, s	400-300	1500	●	●	●	●	●	●	●	●	●	-	-
Qtz-v, pl.	Tranokhaila, USSR	Q-w	400-270	1000-700	●	●	●	●	●	●	●	●	●	-	Lat'ko et al., 1976
Qtz-v, pl.	St. Michael M. Carnall, U.S.	Q-w, c Q	300-400 10	500-1000	●	●	●	●	●	●	●	●	●	10.0	Jackson and Rankin, 1976
Qtz-v, pl.	Styke, USSR	Q-w	200-300	-	●	●	●	●	●	●	●	●	●	-	Kolton, 1973
Qtz-v, pl.	Spishkovo, USSR	Q-w, s Q-s	300 400-300	-	●	●	●	●	●	●	●	●	●	-	Andrusenko and Shcherbakov, 1976
Qtz-v, volc.	Bolivia	Q-w, s	300-1200	30-500	○	●	●	●	●	●	●	●	●	4n	Kelly and Tormore, 1976
Qtz-v, volc.	Llallagua, Bolivia	Q	300-500	300	○	●	●	●	●	●	●	●	●	4-2n	Grant et al., 1977
Qtz-v, pl., Gr-E	Pinto Gordo, Peru	Q-s Q-w	400-500 175-200	70-200	○	●	●	●	●	●	●	●	●	4n 2-17	Londis and Bye, 1974

- Qtz-v = quartz vein, pl. = plutonic setting; volc = volcanic setting; Gr-E = greisen alteration - vein envelope; Gr-P = pervasive greisen alteration.
- Capitalized letter denotes mineral used in analysis; uncapitalized letter indicates associated mineral; Q = quartz, W = wulfenite, B = barite, S = scheelite, C = cassiterite, G = gold, B-b = bismuthinite, cs = copper sulphides.
- Salinity P denotes pressure correction added.
- 100 bars = 10 MPa.
- Species other than H₂O; Circles indicate relative concentration: Full circle = dominant, half-full circle = significant, empty circle = trace.
- Salinity - total dissolved salt content given in equivalent weight percent NaCl.
- A. Chemistry inferred from fluid inclusion observation of daughter minerals etc.
B. Chemical analysis of fluid inclusions.

Table 10.1 Comparison of Fluid Inclusion Data from Deep- and High-level Tungsten Deposits.

result of boiling), and have CO_2 contents of less than 10 mole% (Kelly and Turneaure, 1970; Landis and Rye, 1974; Norman et al., 1976). Thus for granite-related tungsten deposits, the proportion of CO_2 in the hydrothermal fluid appears to vary with pressure. At high pressure the hydrothermal fluid is dominated by CO_2 ; at lower pressures saline fluids predominate.

This agrees with experimental data on the composition of a fluid phase which separates from a melt, under conditions where fluid pressure exceed the confining pressure. Available partition coefficients (Wyllie and Tuttle, 1961; Burnham, 1967; Holland, 1972; Kilinc and Burnham, 1972) indicate that early formed hydrothermal fluids tend to be enriched in chloride or CO_2 . However, the relative proportions of CO_2 and Cl^- present in a fluid phase depends on their initial concentrations in the melt, and the confining pressure. Because of the low solubility of CO_2 in a granite magma (Holloway, 1976), and the "salting out" effect (Malinin, 1979), a fluid phase formed at high pressure is likely to be CO_2 -rich and halogen-poor, while a later and/or lower pressure fluid would be halogen-rich and CO_2 -poor (Burnham, 1967).

As discussed above, such a contrast in fluid chemistry might have a marked affect on the partitioning of metals between a melt and a fluid phase. Certainly Takenouchi and Imai (1975) showed that fluid inclusions in granites associated with several Japanese tungsten deposits (vein, breccia-pipe deposits), were CO_2 -rich, while granites associated with

Pb-Zn-Cu mineralisation contained highly saline inclusions.

Our present knowledge of the behaviour of tungsten in porphyry copper and molybdenum deposits (Kuck, 1978) suggests that the occurrence of tungsten minerals is strongly dependent on depositional environment. Trace amounts of wolframite can occur in copper and molybdenum-rich breccia pipes, and in quartz veins found in the centre of stocks (e.g. San Manuel Mine). Minor amounts of scheelite occur in skarn-related porphyry copper deposits such as Twin Buttes. However, Kuck (1978) has shown that part of the tungsten found in porphyry environments occurs not as wolframite or scheelite, but is incorporated in minerals such as hydrothermal rutile and magnetite found in potassic alteration zones.

There is a strong correlation between tungsten mineralisation (huebnerite) and the K-feldspar alteration zone occurring in the upper ore body of the Climax molybdenite deposit (Wallace et al., 1968; Hall et al., 1974), while in the Urad orebody the tungsten mineralisation is related to a breccia pipe body which was emplaced prior to the main molybdenite mineralisation (Wallace et al., 1978). In both deposits, minor wolframite-bearing quartz veins post date the molybdenite mineralisation (Roedder, 1971; Hall et al., 1974) and may represent remobilisation of tungsten during phyllic overprinting (Taylor and Fryer, 1980 a,b).

A vast amount of fluid inclusion data exists for porphyry copper and molybdenum deposits (Roedder, 1971; Nash, 1976; Moore and Nash, 1974; Eastoe, 1978), but few contain infor-

mation pertinent to tungsten-bearing mineralisation.

Potassic alteration zones of porphyry systems are however characterised by fluids of variable chemistry, ranging from moderate density, low salinity, CO_2 -bearing fluids to high density, high salinity fluids associated with a CO_2 vapour phase (Drake and Ypma, 1969; Roedder, 1971; Hall *et al.*, 1974; Nash, 1976; Denis, 1974). Thus apart from skarn-related deposits, primary tungsten in high level porphyry environments appears to be concentrated in early formed mineralisation, especially in potassic alteration zones where moderate concentrations of CO_2 are found (up to 10 mol%).

Carbon dioxide is a common constituent of fluids associated with tungsten mineralisation in deposits not related to granitoids. There is considerable evidence accumulating for the involvement of metamorphic fluids in hydrothermal ore deposits, especially those of the W-Au association (Fyfe and Henley, 1973; Henley *et al.*, 1976; Kerrich, 1977). This type of scheelite-bearing deposit (e.g. Dome Mine, Ontario, and Yellowknife N.W.T.) have fluid inclusions that occasionally contain liquid CO_2 (Kerrich, pers comm., 1978; Kerrich and Fryer, 1979).

Metalliferous sinters containing ore grade tungsten (3% WO_3) are found around Frying Pan Lake (Waimungu) near the Broadlands Geothermal Field (Weissberg, 1969). The geochemistry of the waters of the present day Frying Pan Lake contrast markedly with others in the Broadlands-Ohaki field, with distinctly lower Na^+ and Cl^- contents, but a greater SO_4^{2-}

concentration (Weissberg, 1969). The fluid also contained about 4 wt% CO_2 prior to boiling (Sutton and McNabb, 1977).

In summary, the association of tungsten mineralisation with CO_2 -bearing hydrothermal fluids is most marked for vein deposits formed at high fluid pressures, but the correlation is apparent in other environments, namely metamorphic, high level plutonic, and near-surface environments. In view of the control that P_{CO_2} has on transport and deposition of tungsten minerals at Grey River, and the overwhelming association of tungsten mineralisation with CO_2 -bearing fluids, it seems necessary to consider that the transport of this element in hydrothermal solutions involves carbonate or bicarbonate complexing.

10.4 TUNGSTEN TRANSPORT AS CARBONATE/BICARBONATE COMPLEXES

In most studies involving metal transport, the fluid is assumed to be a halogen-bearing brine (Holland, 1972; Henley, 1973; Foster, 1977), the assumption being based on the composition of fluid inclusions from a variety of deposits (Roedder, 1972). It has been shown by Foster (1977) that it is possible to mobilise economic concentrations of tungsten in dilute (3-7 wt% NaCl, KCl) chloride solutions. In such fluids there would be a tendency towards the association of ionic species and the formation of molecular species, with increasing temperature. However, the stability field of ionic species would increase to high temperature and pressure conditions with increasing salinity of the fluid. With these constraints, Foster et al., (1978) envisaged a possible

progression from magmatic tungsten species ($\text{WO}_3 \cdot n \text{H}_2\text{O}$), through hydrothermal molecular WCl_6 , tungstic acid (H_2WO_4) to ionic species at subcritical temperatures.

Evidence from the Grey River Tungsten Prospect indicates that the hydrothermal fluid is characterised by the presence of CO_2 and low to negligible Cl^- contents (less than 0.5 wt% NaCl). These data imply that complexes other than chloride complexes might be involved in the transport of tungsten, especially under high fluid pressures.

The association of CO_2 -rich fluids in inclusions from vein type uranium deposits has prompted workers to postulate the transport of uranium in uranyl carbonate complexes (Naumov, 1959, 1961; Poty et al., 1974; Cuney, 1978; Leroy, 1978). Naumov and Mironova (1969) noted a pronounced decrease in the CO_2 content of the hydrothermal fluid during the pitchblende stage of vein formation in the Erzgebirge. In the Limousin episyenite deposit Poty et al., (1974) demonstrated a clear relationship between the grade of uranium, and CO_2 concentration of primary inclusions. Fluid pressures of 750 bars (75 MPa) and temperatures of $340\text{--}350^\circ\text{C}$ were recorded, with small changes in temperature and pressure causing "boiling" or unmixing of the $\text{CO}_2\text{--H}_2\text{O}$ fluid, thus depleting the aqueous phase in CO_2 , destabilising the uranyl carbonate, and precipitating pitchblende.

Experimental studies on metal transport in carbonate solutions are relatively few. Boyle et al., (1975) experimenting with alkali carbonate solutions, found that gold could be

transported in such solutions under hydrothermal conditions. Baranova (1968) and Lebedev et al., (1971), from studies of thermal brines, proposed that the transport of lead was possible as various lead carbonate complexes. Langmuir (1978), in a review of uranium-mineral equilibria at low temperatures, noted that in solutions with very low CO_2 pressures of 10^{-2} atm (1 kPa), uranyl carbonates are the major species down to a pH of 5. However, with increased temperature the carbonate complexes decrease in importance relative to hydroxyl complexes. Such equilibria studies, while applicable to low temperature sedimentary uranium deposits, may not be valid for fluids of higher CO_2 concentration and temperature. In fact Legret and Poty (1977) and Legret (1978) have shown that high CO_2 partial pressures significantly increase the solubility of uranium and thorium in water at high temperatures and pressures.

Some evidence on the solubility of tungsten in carbonate solutions is available from existing metallurgical beneficiation procedures (Kornhauser and Stafford, 1978). The autoclave-soda process (Maslenitsky and Perlov, 1960; Perlov and Poprukailo, 1959; Li, 1962; Dean and Nichols, 1961) is successfully used to upgrade tungsten concentrates by dissolution of scheelite and wolframite in sodium carbonate solutions under pressure. The leachate contains a water soluble sodium tungstate, which when acidified by addition of HCl, precipitates tungstic acid. Experimental data (Churward and Bridges, 1966) on the autoclave leaching of low grade ore (4.4% WO_3 to 15.7% WO_3) by a 25 wt% Na_2CO_3 solution, indicates

that the leachate contained between 12,000 and 24,000 ppm WO_3 after one hour of leaching at a temperature of $200^{\circ}C$. These results suggest that tungsten minerals are extremely soluble in carbonate solutions.

This information, together with the obvious control by P_{CO_2} of the deposition of wolframite in the Grey River hydrothermal veins, suggests that carbonate/bicarbonate complexes might be responsible for the transport of tungsten in hydrothermal solutions. Rare-earth element analyses of altered wall rock in the Grey River deposit also support such an interpretation.

Extensive REE mobility occurred during tungsten mineralisation at Grey River, with heavy REE being enriched and light REE depleted during greisenisation. There is a strong positive correlation between HREE enrichment and tungsten concentration, suggesting that REE mobility is related to tungsten transport. Kosterin (1959) showed that the principal means of REE transport in hydrothermal solutions is in the form of REE carbonate, fluoride, or sulphate complexes. The lack of a positive correlation of fluorine with heavy REE in the alteration zone, implies that the principal means of REE (and tungsten) transport in the Grey River hydrothermal veins is by carbonate (possibly bicarbonate) complexes. Confirmation of this mode of transport awaits detailed experimental evidence on the solubility of tungsten in carbonate solutions, and stability of complexes under variable P_{CO_2} , temperature, and pH conditions.

CHAPTER 11

SUMMARY AND CONCLUSIONS

The following is a summary of the geological and geochemical features of the Grey River Tungsten Prospect.

1) Tungsten mineralisation is contained within a swarm of quartz veins and fractures that traverse the contact between a sheared K-feldspar megacrystic granite and a suite of metamorphic rocks.

2) The metamorphic rocks form part of the gneissic terrain of the Gander Zone and are lithologically dominated by polydeformed and migmatized amphibolitic gneiss. The migmatization preceded, or was concomitant with, the major D_2 folding phase, the axial plane cleavage associated with this folding phase being the dominant fabric in the area. The peak of metamorphism coincided with the D_2 deformation and reached amphibolite facies. The gneisses were retrogressed during waning stages of the D_2 deformation to greenschist facies in zones of ductile shearing, now represented by mica schists and phyllites (mylonite and ultramylonite). During this retrogressive episode a leucogranite sill was intruded into the Granite Cliff Shear Zone, the major shear zone of the area.

K-Ar ages for the amphibolite facies metamorphism and associated D_2 deformation range from 441 to 409 Ma, while the retrogressive greenschist metamorphism associated with shear zones is dated at 395 ± 8 Ma.

3) A K-feldspar megacrystic granite, part of the

Burgeo Batholith, was intruded into the metamorphic rocks during retrogressive deformation. The granite is itself intensely sheared along its southern contact which occurs within the Granite Cliff Shear Zone. The deformation however dies out towards the north. Porphyroblasts of andalusite rimmed by cordierite overgrow the mylonitic fabric of the shear zone and relate to intrusion of the megacrystic granite. These porphyroblasts were crenulated by continued deformation in the shear zone, which is evidence for the close temporal relationship between shearing and intrusion.

A Rb/Sr isochron from undeformed megacrystic granite indicates an intrusive age of 405 ± 10 Ma. However, the sheared margin of the pluton behaved as an open system during metasomatic alteration which accompanied shear zone deformation, and large scale exchange of Sr (and Rb) occurred between granite and metamorphic rock. Sr exchange resulted in a change in initial $^{87}\text{Sr}/^{86}\text{Sr}$ ratios of samples from the deformed margin of the pluton and accounts for their isotopic displacement from the 405 Ma isochron defined by the undeformed samples.

4) Following intrusion and deformation of the megacrystic granite the area was subjected to a series of post-tectonic intrusive events dominated by the emplacement of a suite of leucogranite dykes ranging from pegmatite to two-mica leucogranite and aplite. The dykes are extensively hydrothermally altered and characterised by development

of secondary microcline and albite. Textural evidence and alteration features imply the existence of a fluid phase during emplacement of the leucogranite suite. Rarely these dykes contain coarse quartz segregations and grade into quartz veins.

5) Geochemical data reveal that the Grey River granitoids are extensively altered by metasomatic processes; the megacrystic granite in a shear zone along its margin; the leucogranites by reaction with a coexisting fluid phase (autometasomatism). Metasomatism in the latter affects mainly the alkalis and alkaline earths and possibly some base metals. Any conclusive geochemical evidence for a differentiation trend between the megacrystic granite and the leucogranite is masked by their associated metasomatism.

Metallogenically the megacrystic granite is tin- and tungsten specialised, with values of 42 ppm and between < 4 and 8 ppm respectively. The leucogranites exhibit much lower concentrations (9 ppm, < 4 ppm, respectively) which may reflect the lack of mafic minerals, or leaching, or partitioning of these elements into the fluid phase during autometasomatism. Except for lithium and fluorine concentrations, the granites, especially the leucogranite, are geochemically similar to granites associated with tin and tungsten deposits of western Europe and elsewhere.

6) Available geochemical and field evidence suggests that the leucogranites are intimately associated with the mineralisation, providing both the hydrothermal fluid and

the ore-forming elements necessary for the formation of the ore deposit.

7) The tungsten-bearing hydrothermal veins range from north-striking tensional fractures and veinlets to quartz lodes, the latter formed by repeated opening and injection of mineralisation into open spaces created by differential movements of wall rock during normal faulting. These internal vein movements structurally controlled the distribution of mineralisation, with wolframite being concentrated in the shallow-dipping, thinnest sections of the veins where greisen alteration is more intense.

8) The mineralisation may be divided into four main stages; the Early Stage; the Composite Stage; the Sulphide Stage; and the Late Stage. The first two quantitatively dominate the mineralisation and are associated with the tungsten mineralisation. The Early Stage is characterised by quartz-feldspar and molybdenite-bearing tensional veins which are common in western and southwestern parts of the mineralised area. The Composite Stage is composed of five vein types, two or more of which are grouped as components of the composite lodes. In paragenetic order the vein types of this stage are, quartz-bismuthinite, quartz-wolframite, greisen, quartz-sulphide and quartz-wolframite.

The wolframites of the two quartz-wolframite vein types present in this stage of mineralisation, are compositionally distinct, the early wolframite being more iron-rich than the later one. Quartz deposition occurred early in the sequence

of mineralisation in any vein type, and when associated with wolframite, coprecipitational features are indicated.

Sulphides were deposited later than quartz (and wolframite) in any given vein type.

9) K-Ar age determinations on muscovite from various stages of the mineralisation exhibit a spread in age ranging from 386 ± 6 Ma to 329 ± 4 Ma. In view of the nature of the mineralisation, such a range in age is unreasonable and the true age of mineralisation is interpreted to be approximately 330 Ma, with the older dates being the result of excess argon.

10) A distinct temporal and spatial zonation of mineralisation is evident, both within individual veins or lodes, and between veins. Minerals with pegmatitic affinity occur in early formed veins that are more prevalent in southern or southwestern parts of the mineralised area. Higher temperature minerals such as molybdenite and bismuthinite are also concentrated in southern exposures and give way to the north to lower temperature assemblages containing galena. The latter exhibit high contents of Ag and Bi and have exsolved Ag and Bi-tellurides and sulphosalts and native bismuth by annealing. Sulphide, oxide, and tungstate phase equilibria indicate that the pH of the hydrothermal fluid increased with time and that during wolframite deposition high f_{O_2} and low f_{S_2} conditions prevailed.

11) Fluid inclusion data indicate a complex evolutionary history for the hydrothermal fluid. Initially a homo-

geneous supercritical fluid ($X_{\text{CO}_2} = 0.4$), with a density of 0.65 deposited veins containing quartz and feldspar (and later molybdenite and muscovite) at temperatures of $450^\circ - 500^\circ\text{C}$ and fluid pressures of 1200-1400 bars. With falling pressure and temperature this supercritical fluid intersected the solvus of the $\text{CO}_2 - \text{H}_2\text{O}$ system and two immiscible fluids separated, namely a CO_2 -rich fluid and water-rich fluid.

The simultaneous trapping, in quartz of the quartz-bismuthinite vein type, of CO_2 -rich and H_2O -rich fluid inclusions, as well as solid inclusions of calcite, is evidence for the existence of an immiscible heterogeneous fluid during this phase of mineralisation. A unique solution for pressure and temperature, obtained from the intersection of isochores from separate but coexisting immiscible fluids, indicates immiscibility occurred at temperatures of $390-430^\circ$ and fluid pressures of 1000-1200 bars.

A period of repeated hydraulic fracturing resulted in the deposition of quartz-sulphide and quartz-wolframite composite lodes. Using quartz-muscovite oxygen isotope fractionations, a temperature in the range $350^\circ-400^\circ\text{C}$ (depending on which fractionation equation used) is indicated for greisen mineralisation which occurs as an alteration envelope to these lodes. Vein movements by normal faulting promoted rapid decreases in fluid pressure and temperature, and when the vapour pressure exceeded the load pressure, retrograde boiling occurred, releasing a vapour phase rich

in CO_2 . The microthermometric data indicate that deposition of the quartz-sulphide veins occurred at fluid pressures of 350 bars and temperatures of $300^\circ\text{--}390^\circ\text{C}$.

Fluid inclusions in quartz from the quartz-wolframite veins suggest that the deposition of wolframite occurred at $270^\circ\text{--}330^\circ\text{C}$, and at fluid pressures less than 350 bars, from an aqueous fluid of low salinity (0-3 equivalent wt% NaCl) and CO_2 content (less than 10 bars P_{CO_2} at room temperature), after separation of a CO_2 -vapour phase by retrograde boiling. Salinities determined by clathrate melting and depression of freezing point methods indicate quite low solute concentrations during the evolution of the hydrothermal fluid. Calculations of the effect of dissolved CO_2 in the aqueous phase, on the temperature of melting of ice and CO_2 clathrate, suggest that the amount of NaCl actually dissolved in the fluid might have been quite small (less than 0.25 - 0.5 wt% NaCl).

Overall, the fluid inclusion data indicate that the fluid involved with tungsten transport at Grey River was characterised by CO_2 and that a reduction in CO_2 content of the fluid (by immiscibility and retrograde boiling), as well as temperature, promoted deposition of wolframite.

12) Oxygen isotope data suggest that the hydrothermal fluid was dominantly of magmatic origin. The calculated $\delta^{18}\text{O}_{\text{H}_2\text{O}}$ indicates a progressive depletion in isotopic composition, ranging from 7.3 ‰ to 0.5 ‰, with time. Available $\text{CO}_2\text{--CaCO}_3\text{--H}_2\text{O}$ fractionation factors show that this

shift in isotopic composition is accounted for by the loss of 40 mol% CO_2 from the hydrothermal fluid (by immiscibility and retrograde boiling) as indicated from fluid inclusion data.

13) Rare-earth element data indicate that extreme REE mobility occurred in the hydrothermal environment and resulted in heavy REE enrichment and light REE depletion. This suggests that CO_3^{-2} was the dominant anionic species in the hydrothermal fluid and implies that mobilisation of REE occurred by carbonate-complexing. Moreover a positive correlation occurs between heavy REE enrichment and high tungsten concentrations, suggesting that REE mobility is related to tungsten transport. Together with the evidence on the control on deposition of wolframite by P_{CO_2} , this suggests that the transport of tungsten in hydrothermal fluids might be due to carbonate-complexing.

14) The evolution of a CO_2 -rich fluid phase from a granitic magma appears to have a profound effect on oxidation conditions and crystallisation history of the latter, and the partitioning of ore-forming elements from melt to fluid. Evidence from the Grey River Tungsten Prospect suggests that the partitioning of tungsten is favoured by high f_{O_2} -high f_{CO_2} conditions which appear also to promote retention of tin in the magma, although the activity of fluorine may have an effect on the distribution of the latter. Furthermore the activity of fluorine may influence the type of tungsten mineral precipitated; wolframite being

favoured in the presence of F^- because of the strong affinity of the latter for Ca^{2+} (i.e. formation of fluorite).

15) The rarity of a carbonate-wolframite assemblage in the Grey River Tungsten Prospect superficially supports suggestions of previous workers of an incompatibility between these minerals in griesen and vein environments. The evidence however indicates that the two are unstable in a cooling alkaline hydrothermal fluid where they react to form scheelite. Carbonates are only preserved as inclusions in quartz where they are isolated from reaction with the cooling hydrothermal fluid.

Thus these conclusions all illustrate the previously unrecognised importance of CO_2 in the transport and deposition of tungsten in the hydrothermal environment.

REFERENCES

- ABRIKASOV, N.K. and BANKINA, V.F., 1957. The Bismuth-Tellurium system. *Zh. Neorg. Khim.*, V. 3, pp. 659-661.
- ALBUQUERQUE, C.A.R.DE., 1977. Geochemistry of the tonalitic and granitic rocks of the Nova Scotia/southern plutons. *Geochim. Cosmochim. Acta*, V. 41, pp. 1-13.
- ALBUQUERQUE, C.A.R.DE., 1978. Rare earth elements in "Younger" granites of Northern Portugal. *Lithos*, V. 1, pp. 219-229.
- ALLISON, J. and LA TOUR, T.E., 1977. Brittle deformation of hornblende in a mylonite: A direct geochemical analogue of ductile deformation by translation gliding. *Can. J. Earth Sci.*, V. 14, pp. 1953-1958.
- ANDERSON, A.L., 1948. Tungsten mineralisation at the Ima Mine Blue Wing district, Lemhi County, Idaho. *Econ. Geol.*, V. 43, pp. 181-206.
- ANDRUSENKO, N.I. and SHCHEPAT'YEV, K., 1974. Temperature conditions and stages of formation of subvolcanic gold-silver deposits of central Kamchatka. *Geochem. Int.*, V. 11, pp. 130-137.
- ANUFRIYEV, YU.N., MOSKALYUK, A.A., POKROVSKII, P.V. and PURTOV, V.K., 1974. Mineral forming solutions of hydrothermal deposits of Ural (abstract). *Int. Assoc. of the Genesis of Ore Deposits, 4th Symp.*, Varna, pp. 241-242.
- BABCOCK, R.S., 1973. Compositional models of metasomatic processes. *Lithos*, V. 6, pp. 279-90.
- BAHYRYCZ, G.S., 1957. Geology of the Grey River area, Newfoundland, with special references to the metamorphism. Unpubl. M.Sc. thesis, McGill University, 101 pp.
- BAILEY, D.K., 1974. Continental rifting and alkaline magmatism. In: *The Alkaline Rocks*, Sorensen, H. (Ed). Wiley and Sons, N.Y., pp. 148-159.
- BARABANOV, W.F., 1971. Geochemistry of Tungsten. *Int. Geol. Review*, V. 3, pp. 332-344.
- BARANOVA, N.N., 1968. Composition of lead carbonate complexes and their dissociation constants at 25°, 250° and 300°C. *Geochem. Intn.*, V. 5, pp. 13-20.

- BAKER, F., FRIEDMAN, I., HUNTER, D.R. and GLEESON, J.D., 1976. Oxygen isotopes of some trondhjemitic acid gneisses and associated mafic rocks. *Precambrian Res.*, V. 3, pp. 547-557.
- BARNES, H.L. and ERNST, W.G., 1976. Identity and ionisation in hydrothermal fluids: The system $\text{MgO-H}_2\text{O-NaOH}$. *Am. J. Sci.*, V. 261, pp. 129-150.
- BAUMANN, L. and TISCHENDORF, G., 1978. The metallogeny of tin in The Erzgebirge. In: *Metallisation associated with acid magmatism*. Stempok, M., Burnol, L. and Tischendorf, G. (Eds). *Ustredni Ustav Geologicky, Praha*, V. 3, pp. 17-28.
- BEACH, A., 1976. The interrelations of fluid transport, deformation, geochemistry, and heat flow in early Proterozoic shear zones in the Lewisian Complex. *Phil. Trans. Roy. Soc. Lond., Series A.*, V. 280, pp. 569-604.
- BEACH, A., 1979. Metamorphic Processes in shear zones (Abstract). *Proc. Intern. Conf. on Shear Zones in Rocks*. Univ. of Barcelona, abstracts, p. 73.
- BEACH, A. and FYFE, W.S., 1972. Fluid transport and shear zones at Scourie, Sutherland. Evidence of overthrusting. *Contr. Min. Petrol.*, V. 36, pp. 175-180.
- BELL, K. and BLENKINSOP, J., 1977. Geochronological evidence of Hercynian activity in Newfoundland. *Nature*, V. 265, pp. 616-617.
- BELL, K., BLENKINSOP, J. and STRONG, D.F., 1977. The geochronology of some granitic bodies from eastern Newfoundland and its bearing on Appalachian evolution. *Can. J. Earth Sci.*, V. 14, pp. 456-476.
- BELL, K., BLENKINSOP, J., BERGER, A.R. and JAYASINGHE, N.R., 1979. The Newport granite; its age, geological setting and implications for the geology of northeastern Newfoundland. *Can. J. Earth Sci.*, V. 16, pp. 264-269.
- BELL, T.H. and ETHERIDGE, M.A., 1976. The deformation and recrystallisation of quartz in a mylonitic zone, central-Australia. *Tectonophysics*, V. 32, pp. 255-268.
- BERNER, R.A., 1964. Iron sulphides formed from aqueous solution at low temperatures and atmospheric pressure. *J. Geol.*, V. 72, pp. 293-306.

- BESWICK, A.E. and SCOUCIE, G., 1978. A correction procedure for metasomatism in an Archean greenstone belt. *Precamb. Res.*, V. 6, pp. 235-248.
- BETHKE, P.M. and RYE, R.O., 1979. Environment of ore deposition in the Creede Mining district, San Juan Mountains Colorado: Part IV: Source of fluids from oxygen, hydrogen, and carbon isotope studies, *Econ. Geol.*, V. 74, pp. 1832-1851.
- BIERMAN, C., 1977. The formation of sheaf-like aggregates of hornblende in carbonschiefer from the central Scandinavian Caledonides. *Tectonophysics*, V. 39, pp. 487-499.
- BILAL, A. and TOURET, J., 1976. Fluid inclusions in catazonal xenoliths from Bournac (Massif Central, France). *Bull. Soc. Fr. Min. Crist.*, V. 99, pp. 134-139 (in french).
- BLACKWOOD, R.F., 1976. The relationship between the Gander and Avalon Zones in the Bonavista Bay region, Newfoundland. Unpubl. M.Sc. thesis, Memorial Univ. of Newfoundland, 156 pp.
- BLACKWOOD, R.F., 1977. Geology of the Hare Bay Area, north-western Bonavista Bay. In: Report of Activities, 1976. Newfoundland Min. Dev. Div. Report 77-1, pp. 7-14.
- BLACKWOOD, R.F., 1978. Northeastern Gander Zone, Newfoundland. In: Report of Activities, 1977. Newfoundland Min. Dev. Div. Report 78-1, pp. 72-79.
- BLACKWOOD, R.F. and KENNEDY, M.J., 1975. The Dover Fault: Western boundary of the Avalon Zone in Northeastern Newfoundland. *Can. J. Earth. Sci.*, V. 12, pp. 320-325.
- BLAIN, C.F. and ANDREWS, R.L., 1977. Sulphide weathering and the evaluation of gossans in mineral exploration. *Min. Sci. Engng.*, V. 9, pp. 119-150.
- BLAKE, D.H. and SMITH, J.W., 1970. Mineralogical zoning in the Herberton tin field, north Queensland, Australia. *Econ. Geol.*, V. 65, pp. 993-997.
- BLATTNER, P., 1975. Oxygen isotopic composition of fissure-grown quartz, adularia and calcite from Broadlands geothermal field, New Zealand. *Am. J. Sci.*, V. 275, pp. 785-800.

- BLENKINSOP, J., CUCMAN, P.F. and BELL, K., 1976. Age relationships along the Hermitage Bay-Dover Fault System, Newfoundland. *Nature*, V. 262, pp. 577-578.
- BLOUNT, C.W. and DICKSON, F.W., 1969. The solubility of anhydrite (CaSO_4) in $\text{NaCl-H}_2\text{O}$ from 100° to 450°C and 1 to 1000 bars. *Geoch. Cosmoch. Acta.*, V. 33, pp. 227-246.
- BOKII, G.B. and ANIKIN, I.N., 1956. The determination of the solubility of scheelite (CaWO_4) in water and in aqueous solution of NaCl and LiCl by the radio-chemical method. *Rus. J. Inorg. Chem.*, V. 1, pp. 240-243.
- BOTTINGA, Y., 1968. Calculation of fractionation factors for carbon and oxygen isotope exchange in the system calcite-carbon dioxide-water. *J. Phys. Chem.*, V. 72, pp. 800-808.
- BOTTINGA, Y. and CRAIG, H. 1969. Oxygen isotope fractionation between CO_2 and water, and the isotope composition of marine atmospheric CO_2 . *Earth Plan. Sci. Lett.*, V. 5, pp. 285-295.
- BOTTINGA, Y. and JAVOY, M., 1973. Comments on oxygen isotope thermometry. *Earth Plan. Sci. Lett.*, V. 20, pp. 250-265.
- BOWDEN, P., BENNETT, J.N., WHITLEY, J.E., and MOYES, A.B., 1979. Rare earths in Nigerian Mesozoic Granites and related rocks. In: *Origin and distribution of the elements. Physics and Chemistry of the Earth.* Ahrens, L.H., (Ed), V. 11, pp. 479-491. Pergamon Press. N.Y.
- BOYLE, R.W., 1970. Regularities in wall rock alteration phenomena associated with epigenetic deposits. In: *Intn. Union Geol. Sci. A. No. 2. Problems of Hydrothermal Ore Deposits.*, Pouba, Z. and Stemprok, M., (Eds), pp. 233-260.
- BOYLE, R.W., ALEXANDER, W.M. and ASLIN, G.E.M., 1975. Some observations on the solubility of gold. *Geol. Surv. Cana. Paper* 75-24, 6 pp.
- BOZZO, A.T., CHEN, H.S., KAS, H.R., BARDUHN, A.J., 1975. The properties of hydrates of chlorine and carbon dioxide. *Desalination*, V. 16, pp. 303-320.
- BROWN, P.A., 1975. Basement-cover relationships in southwest Newfoundland. Unpubl. PhD thesis, Memorial Univ. of Newfoundland, 260 pp.

- BROWN, P.A., 1976. Geology of the Rose Blanche map area (110/10) Newfoundland. Newfoundland Min. Dev. Div., Report 76-5, 40 pp.
- BROWNE, P.R.L., ROEDDER, E. and WODZICKI, A., 1974. Comparison of past and present geothermal water from a study of fluid inclusion, Broadlands field, New Zealand (abstract). E.O.S., V. 55, p. 456.
- BRYZGALIN, O.V., 1958. The origin of scheelite in skarn ore deposit. Geokhimiya, pp. 297-304.
- BURNHAM, C.W., 1967. Hydrothermal fluids at the magmatic stage. In Geochemistry of Hydrothermal Ore Deposits. Barnes, H.L., (Ed), pp. 34-76. Holt, Rinehart and Winston Inc., N.Y.
- BURNHAM, C.W., 1979. Magmas and Hydrothermal fluids. In: Geochemistry of hydrothermal ore deposits. 2nd Edition. Barnes, H.L., (Ed), pp. 71-136. Wiley Interscience.
- BURNHAM, C.W., HOLLOWAY, J.R. and DAVIS, N.E., 1969. The specific volume of water in the range 1000 to 8900 bars, 20° to 900°C. Am. J. Sci., V. 267-A, pp. 70-95.
- BURNOL, L., 1978. Different types of leucogranites and classification of types of mineralisation associated with acid magmatism in the northwestern part of the French Massif Central. In: Metall. Assoc. with Acid Magm., V. 3, pp. 191-205. Stempok, M., Burnol, L. and Tischendorf, G., (Eds), Ustr. Ust. Geol., Praha.
- BURT, D.M., 1971a. Mineral stabilities in the system Ca-Fe-W-O-C-F in skarns, veins and greisen (abstract). Geol. Soc. Am. Abs. with prog., V. 3 (7), p. 520.
- BURT, D.M., 1971b. The influence of fluorine on the facies of Ca-Fe-Si skarns. Carnegie Inst. Wash. Yearbook, 71 (1971-1972), pp. 447-450.
- BURT, D.M., 1978. Wolframite-scheelite equilibria involving fluorine, phosphorus, and sulfur. (abstract). Geol. Soc. Am. Abs. with prog., V. 3, p. 375.
- BUTLER, A.J. and GREEN, B.A., 1976. Silica resources of Newfoundland. Newfoundland Min. Dev. Div. Report 70-2. 68 pp.
- BUTLER, J.R. and FULLAGAR, P.D., 1978. Petrochemical and geochronological studies of plutonic rocks in southern Appalachians: III. Leucocratic adamellites of the Charlotte belt near Salisbury, North Carolina. Geol. Soc. Am., V. 89, pp. 460-466.

- CAMUS, F., 1975. Geology of the El Teniente Ore-body with emphasis on wall rock alteration. *Econ. Geol.*, V. 70, pp. 1341-1372.
- CARMICHAEL, D.M., 1979. On the mechanism of prograde metamorphic reactions in quartz-bearing pelitic rocks. *Contrib. Min. Petrol.*, V. 66, pp. 113-117.
- CARPENTER, L.G. and GARRETT, D.E., 1959. Tungsten in Searles Lake. *Mining Engineering*, V. 11, pp. 301-303.
- CASADEVALL, T. and RYE, R.O., 1980. The Tungsten Queen Deposit, Hamme district, Vance County, North Carolina: A stable isotope study of a metamorphosed Quartz-huebnerite vein. *Econ. Geol.*, V. 75 pp. 523-537.
- CHANG, L.L.Y., 1967. Solid solution of scheelite with other $R^{II}WO_4$ -type tungstates. *Am. Miner.*, V. 52, pp. 427-432.
- CHANG, L.L.Y. and BEVER, J.E., 1973. Lead sulphosalt minerals. Crystal structures, stability relations, and paragenesis. *Mineral Sci. Engng.*, V.5, pp. 181-191.
- CHAO, E.C.T. and FLEISCHER, M., 1960. Abundance of Zirconium in igneous rocks. *Rep. Int. Geol. Cong. XXI Session*, I, pp. 106-131.
- CHATTERJEE, A.K., 1980a. Lime Hill zinc-tungsten deposit. In: GAC/MAC field trip No. 6 guide book. "Mineral deposits and mineralogenic provinces of Nova Scotia", pp. 45-51.
- CHATTERJEE, A.K., 1980b. Whycocomagh tungsten-molybdenum-copper deposit. In GAC/MAC field trip No. 6 guide book. "Mineral deposits and mineralogenic provinces of Nova Scotia", pp. 52-59.
- CHAURIS, L., 1978. Compared structure, petrology and metallogeny of the two-mica granites associated with the three Variscan granitic belts in the Armorican massif (France) - First results and future projects. In: Grandclaude, P.L. and Stussi, J.M., (Eds), *Sci. de la Terre*, No. 11, pp. 23-30, May, 1978.
- CHEN, H.S., 1972. The thermodynamics and composition of carbon dioxide hydrate. Unpubl. M.S. thesis, Syracuse Univ, 67 pp.
- CHORLTON, L.G., 1978. La Poile project, southwestern Newfoundland. Report of Activities (1977), Newfoundland Dev. Div., Report 78-1, pp. 85-89.
- CHORLTON, L.B. and MARTIN, R.F., 1978. The effect of boron on the granite solidus. *Can. Mineral.*, V. 16, pp. 239-244.

- CHURCHWARD, P.E. and BRIDGES, D.W., 1966. Tungsten recovery from low-grade concentrates by amine solvent extraction. U.S. Bureau of Mines, R.I.-6845.
- CHURIKOV, V.S., 1959. Certain features of the chemical composition of wolframite. In: Materials relating to geology, petrography, mineralogy, and geochemistry of ore deposits. Izd-vo An SSSR, Moscow.
- CLARK, A.H., 1970. Manganese-iron ratios in wolframite, South Crofty mine, Cornwall: A discussion. Econ. Geol., V. 65, pp. 889-892.
- CLARK, A.H. and SILLITOE, R.H., 1970. Tungstenian wulfenites, Mina San Samuel, Cochiyuyo de Llampos, Chile. Am. Mineral., V. 55, pp. 2114-2118.
- CLARK, A.H., FARRAR, E., COELLES, J.C., HAYNES, S.J., LORTIE, R.B., MCBRIDE, S.L., QUIRT, G.S., ROBERTSON, R.C.R., ZENTILLI, M., 1976. Longitudinal variations in the metallogenic evolution of the Central Andes. A progress report. In: Metallogeny and Plate Tectonics, Strong D.F., (Ed), GAC Special Paper 14, pp. 23-58.
- CLARK, S.P. 1966. Handbook of physical constants. G.S.A. Memoir 97, 587 pp.
- CLAYTON, R.N. and MAYEDA, T., 1963. The use of bromine pentafluoride in the extraction of oxygen from oxides and silicates for isotopic analysis. Geoch. Cosmochim Acta, V. 27, pp. 43-52.
- CLAYTON, R.N., O'NEIL, J.R. and MAYEDA, T.K., 1972. Oxygen isotope exchange between quartz and water. J. Geophys. Res., V. 77, pp. 3057-3067.
- COLLERSON, K.D. and FRYER, B.J., 1978. The role of fluids in the development of the early continental crust. Contrib. Min. Petrol., V. 67, pp. 151-167.
- COLLINS, P.L.F., 1979. Gas hydrates in CO₂-bearing fluid inclusions and use of freezing data for estimation of salinity. Econ. Geol., V. 74, pp. 1435-1444.
- COLMAN-SADD, S.P., 1974. The geologic development of the Bay d'Espoir area, southeastern, Newfoundland. Unpubl. Ph.D thesis, Memorial Univ. of Newfoundland, 271 pp.
- COLMAN-SADD, S.P., 1978. Gaultois map area (IM/12), Newfoundland. Report of Activities (1977). Newfoundland Min. Dev. Div. Report 78-1, pp. 90-96.

- CORMIER, R.F. and SMITH, T.E., 1973. Radiometric ages of granitic rocks, southwestern Nova Scotia. *Can. J. Earth Sci.*, V. 10, pp. 1201-1210.
- CRAIG, J.R., 1967. Phase relations and mineral assemblages in the Ag-Bi-Pb-S system. *Mineral Deposita*, V. 1, pp. 278-306.
- CRAWFORD, M.L., FILER, J. and WOOD, C., 1979. Saline fluids associated with retrograde metamorphism. *Bull. Mineral.*, V. 102, pp. 562-568.
- CREASEY, S.O., 1959. Some phase relations in hydrothermally altered rocks of porphyry copper deposits. *Econ. Geol.* V. 54, pp. 351-373.
- CUNEY, M., 1978. Geologic environment, mineralogy, and fluid inclusions of the Bois Noirs-Limouzat uranium vein, Forez, France, *Econ. Geol.*, V. 73, pp. 1567-1610.
- CURRIE, K.L. and PAJARI, G.E., 1977. Igneous and metamorphic rocks between Rocky Bay and Ragged Harbour. N.E. Newfoundland. Report of Activities. Part A. G.S.C. paper 77-1A, pp. 341-345.
- CZAMANSKE, G.K. and HALL, W.E., 1975. The Ag-Bi-Pb-Sb-S-Se-Te mineralogy of the Darwin lead-silver-zinc deposit, southern California. *Econ. Geol.*, V. 70, pp. 1092-1110.
- DAGGER, G.W., 1972. Genesis of the Mount Pleasant W-Mo-Bi deposit, New Brunswick, Canada. *Trans. Inst. Min. Metall.*, V. 81, B73-B103.
- DALRYMPLE, G.B. and LANPHERE, M.A., 1969. Potassium-argon dating: Principles, techniques and applications to geochronology. W.H. Freeman and Company, San Francisco, 258 pp.
- DAMON, P.E. and KULP, J.L., 1958. Excess helium and argon in beryl and other minerals. *Am. Mineral.*, V. 43, pp. 433-459.
- DEAN, K.C. and NICHOLS, I.L., 1961. Froth flotation and chemical processing of Colorado ferberite ore. U.S. Bureau Mines Report of Inv. -5869, 15 pp.
- DEAN, P.L., 1978. The volcanic stratigraphy and metallogeny of Notre Dame Bay, Newfoundland. Unpubl. M.Sc. thesis, Memorial Univ. of Newfoundland, 204 pp.

- DEAN, P.L. and STRONG, D.F., 1977. Folded thrust faults in Notre Dame Bay, central Newfoundland. *Am. J. Sci.*, V. 277, pp. 97-108.
- DEICHA, G., 1955. Les lacunes des cristaux et leurs inclusion fluides; signification dans la genèse des gîtes minéraux et des roches. Paris, Masson et Cie.
- DEINES, P. and GOLD, D.P., 1969. The change in carbon and oxygen isotopic composition during contact metamorphism of Trenton limestone by the Mt Royal pluton. *Geoch. Cosmoch. Acta.*, V. 33, pp. 421-424.
- DEKATE, Y.G. 1967. Tungsten occurrences in India and their genesis. *Econ. Geol.*, V. 62, pp. 556-61.
- DENIS, M., 1964. Alteration and associated fluids in the Sierrita porphyry copper (Arizona, U.S.A.) and comparison with other deposits of the same type. Unpubl. Thesis, University of Nancy.
- DOLLINGER, G. and BLACK, J.D., 1975. Deformation mechanism in experimentally and naturally deformed amphibolites. *Earth Plan. Sci. Lett.*, V. 26, pp. 409-416.
- DRAKE, W.E. and YPMA, P.J.M. 1969. Fluid inclusion study of the Mineral Park porphyry copper deposit, Kingman, Arizona (abstract). In: *Fluid Inclusion Research*, E. Roedder (Ed), V. 2, pp. 15-16.
- DURASOVA, N.A., 1967. Some problems of the geochemistry of tin. *Geochem. Intern.*, V. 4, pp. 671-681.
- EASTOE, C.J., 1978. A fluid inclusion study of the Panguna porphyry copper deposit, Bougainville, Papua New Guinea. *Econ. Geol.*, V. 73, pp. 721-748.
- ELLIS, A.J., 1959. The solubility of carbon dioxide in water at high temperature. *Am. J. Sci.*, V. 257, pp. 217-234.
- EMMERMANN, R., DAIEVA, L. and SCHNEIDER, J., 1975. Petrologic significance of rare earth distribution in granites. *Contrib. Min. Petrol.*, V. 52, pp. 267-283.
- ENGEL, A.E.J., ENGEL, G. and HAVEN, R.G., 1965. Chemical characteristics of oceanic basalt and the upper mantle. *Geol. Soc. Am. Bull.*, V. 76, pp 719-734.

- ENJOJI, M. and TAKENOUCHI, S., 1976. Present and future researches of fluid inclusions from vein type deposits. Mining Geology Spec. Issue, No. 7, pp. 85-100.
- ERMAKOV, N.P. and PIZNYUR, A.V., 1974. Finding commercial ore by use of thermobarogeochemical indices of conditions of mineral formation (abstract). In: Fluid Inclusion Research, E. Roedder (Ed), V. 7, p 56. Univ. of Michigan Press.
- EVANS, B.W., 1965. Application of a reaction-rate method to the breakdown equilibria of muscovite and muscovite and quartz. Am. J. Sci., V. 263, pp. 647-667.
- EVERNDEN, J.F. and KISTLER, R.W., 1970. Chronology of emplacement of Mesozoic batholithic complexes in California and Western Nevada. U.S. Geol. Surv. Prof. Paper 623, 42 pp.
- FAURE, G., 1977. Principles of Isotope Geology. J. Wiley and Sons. N.Y., 464 pp.
- FIELD, C.W., JONES, M.B. and BRUCE, W.R. 1971. Sulphur isotopic composition of hydrothermal sulphides and the role of Eh-pH (abstract). Geol. Soc. Am. Abst. with Prog., V. 3, p. 118.
- FLINTER, B.H., HESP, W.R. and RIGBY, D., 1972. Selected geochemical, mineralogical and petrological features of granitoids of the New England Complex, Australia, and their relation to Sn, W, Mo and Cu mineralisation. Econ. Geol., V. 67, pp. 1241-1262.
- FLYNN, R.T. and BURNHAM, C.W., 1977. An experimental determination of rare-earth partition coefficients between a chloride containing vapour phase and a silicate melt. In: Experimental trace element geochemistry. Drake, M.J. and Holloway, J.R. (Eds), pp. 685-701. Pergamon Press, Oxford, England.
- FORD, J.H., 1978. A chemical study of alteration at the Panguna porphyry copper deposit, Bougainville, Papua New Guinea. Econ. Geol., V. 73, pp. 703-720.
- FOSTER, R.P., 1973. Some aspects of the geochemistry of tungsten. Unpubl. Ph.D. thesis, Univ. of Manchester, 242 pp.
- FOSTER, R.P., 1976. Discussion of Shepherd et al., 1976. Trans. Inst. Min. Metall., V. 85, B298-B299.

- FOSTER, R.P., 1977. Solubility of scheelite in hydrothermal chloride solutions. *Chem. Geol.*, V. 20, pp. 27-43.
- FOSTER, R.P., MANN, A.G., ARMIN, T. and BURMEISTER, B., 1978. Richardson's Kop wolframite deposit: a geochemical model for the hydrothermal behaviour of tungsten. In: *Mineralisation in metamorphic terranes*, Verwoerd, W.J. (Ed), *Geol. Soc. S. Afr.*, Spec. Publ. 4, pp. 107-128.
- FOURCADE, S. and JAVOY, M., 1973. Rapports $^{18}\text{O}/^{16}\text{O}$ dans les roches du vieux socle catazonal d'In Ouzzal (Sahara algerien). *Contrib. Min. Petrol.*, V. 42, pp. 235-244.
- FOURNIER, R.B., 1968. Mechanism of formation of alaskite, aplite, and pegmatite in a Dike swarm, Yosemite National Park, California. *Geol. Soc. Am. Memoir* 116, pp. 249-274.
- FREY, F.A., CHAPPELL, B.W. and ROY, S.D., 1978. Fractionation of rare-earth elements in the Tuolumne Intrusive series, Sierra Nevada batholith, California. *Geology*, V. 6, pp. 239-242.
- FREIDMAN, I. and O'NEIL, J.R., 1977. Compilation of stable isotope fractionation factors of geochemical interest. *U.S. Geol. Surv. Prof. Paper* 440-KK.
- FRYER, B.J., 1977. Rare earth evidence in iron formation for changing oxidation states. *Geochim. Cosmochim. Acta*, V. 41, pp. 361-367.
- FRYER, B.J., KERRICH, R., HUTCHINSON, R.W., PEIRCE, M.G. and RODGERS, D.S., 1979. Archaean precious-metal hydrothermal systems, Dome mine, Abitibi greenstone belt: I. Patterns by alteration and metal distribution. *Can. J. Earth Sci.*, V. 16, pp. 421-439.
- FULLAGAR, P.D. and BUTLER, J.R., 1979. 325 to 265 m.y. old granitic plutons in the Piedmont of the southeastern Appalachians. *Am. J. Sci.*, V. 279, pp. 161-185.
- FUNKHOUSER, J.G. and NAUGHTON, J.J., 1968. Radiogenic helium and argon in ultramafic inclusions from Hawaii. *J. Geophy. Res.*, V. 73, pp. 4601-4607.
- FUNKHOUSER, J.G., BARNES, I.L. and NAUGHTON, J.J., 1966. Problems in the dating of volcanic rocks by the potassium-argon method. *Bull. Volcanol.*, V. 29, pp. 709-720.

- FYFE, W.S., and HENLEY, R.W., 1973. Some thoughts on chemical transport processes with particular reference to gold. *Min. Sci. Engng.*, V. 5, pp. 295-303.
- GANEEV, I.G. and SECHINA, N.P., 1960. Geochemical peculiarities of wolframite. *Geochem.*, pp. 617-623.
- GARNETT, R.H.T., 1966. Relationship between tin content and structure of lodes at Geevor Mine, Cornwall. *Trans. Inst. Min. Metall. Sect. B.*, V. 75, Bi-B22.
- GLATZ, A.C., 1967. The Bi_2Te_3 - Bi_2S_3 system and the synthesis of the mineral tetradymité. *Am. Mineral.*, V. 52, pp. 161-170.
- GONCHAROV, V.I. and VORONTSOVA, L.A., 1976. Hydrothermal solution compositions for some Yakutia tin deposits. *Geochem. Int.*, V. 13, pp. 27-33.
- GRAF, J.L., 1977. Rare earth elements as hydrothermal traces during the formation of massive sulfide deposits in volcanic rocks. *Econ. Geol.*, V. 72, pp. 527-548.
- GRANT, J.N., HALLS, C., AVILA, W. and AVILA, G., 1977. Igneous geology and the evolution of hydrothermal systems in some sub-volcanic tin deposits of Bolivia. In: *Volcanic processes in ore genesis*. I. Gass (Ed). *Inst. Min. Metall./Geol. Soc. Lond.*, Special paper 7, pp. 117-126.
- GRAVES, M.C., 1976. The formation of gold-bearing quartz veins in Nova Scotia: Hydraulic fracturing under conditions of greenschist regional metamorphism during early stages of deformation. Unpubl. M.Sc. thesis, Dalhousie Univ., 80 pp.
- GRAVES, M.C. and ZENTILLI, M., 1976. Gold-bearing quartz veins formed during continental collision (abstract). *GAC/MAC prog. with abstr.*, V. 1, p. 57.
- GRAY, C.M. and COMPSTON, W., 1978. A rubidium-strontium chronology of the metamorphism and prehistory of Central Australian granulites. *Geochim. Cosmochim. Acta.*, V. 42, pp. 1735-1747.
- GRAY, I.M., 1958. The Grey River Tungsten deposit, south Newfoundland. Unpubl. M.Sc. thesis, Royal School of Mines, London, 84 pp.
- GREEN, H.W., 1979. Trace elements in the fluid phase of the earth's mantle. *Nature*, V. 277, pp. 465-467.

- GRESENS, R., 1967. Compositional-volume relationships of metasomatism. *Chemical Geology*, V. 2, pp. 47-65.
- GREENWOOD, H., 1973. Thermodynamic properties of gaseous mixtures of H₂O and CO₂ between 450°C and 800°C and 0 to 500 bars. *Am. J. Sci.*, V. 273, pp. 561-571.
- GROVES, D.I., 1972. The geochemical evolution of Tin-bearing granites in the Blue Tier batholith, Tasmania. *Econ. Geol.*, V. 67, pp. 445-457.
- GROVES, D.I. and BAKER, W.E., 1972. The regional variation in composition of wolframites from Tasmania. *Econ. Geol.*, V. 67, pp. 362-368.
- GROVES, D.I. and SOLOMON, M., 1969. Fluid inclusion studies at Mt. Bischoff, Tasmania. *Trans. Inst. Min. Metall. Sect. B*, V. 78, B1-B11.
- GROVES, D.I., SOLOMON, M. and RAFTER, T.A., 1970. Sulphur isotope fractionation and fluid inclusion studies at the Rex Hill Mine, Tasmania. *Econ. Geol.*, V. 65, pp. 459-469.
- GRUBB, P.L.C., 1967. Solid solution relationship between wolframite and scheelite. *Am. Miner.*, V. 52, pp. 418-426.
- GUNDLACH, H., 1967. Transport und Abscheidungsbedingungen von wolframerzen aus wasserigenlösungen. In: *Pegmatische Lagerstätten und ihre Wirtschaftliche Bedeutung*. Clausthal-Zellerfeld.
- GUNDLACH, H. and THORMANN, W., 1960. Versuch einer Deutung der Entstehung von Wolfram und Zinnlagerstätten. *Z. Dtsch. Geol. Ges.*, V. 112, pp. 1-35.
- HAAS, J.L., 1971. The effect of salinity on the maximum thermal gradient of a hydrothermal system at hydrostatic pressure. *Econ. Geol.*, V. 66, pp. 940-946.
- HALL, A., 1971. Greisenisation in the granite at Cligga Head, Cornwall. *Proc. Geol. Assoc.*, V. 82, pp. 209-230.
- HALL, W.E. and CZAMANSKE, G.K., 1972. Mineralogy and trace element contents of the Wood River lead-silver deposits, Blaine County, Idaho. *Econ. Geol.*, V. 67, pp. 350-361.

- HALL, W.E., FREIDMAN, I. and NASH, J.T., 1964. Fluid inclusions and light stable isotope study of the Climax molybdenum deposit, Colorado. *Econ. Geol.* V. 69, pp. 884-901.
- HAMAGUCHI, H., KURODA, R., ONUMA, N., KAWAGUCHI, K., MITSUBAYASHI, T. and HOSOHARA, K., 1964. The geochemistry of tin. *Geoch. Cosmochim. Acta.*, V. 28, pp. 1039-1053.
- HANMER, S., 1980. Major Acadian sinistral shear in Newfoundland: Geological support for paleomagnetic models (abstract). In: *GAC/MAC Prog. with Abst.*, V. 5, p. 58.
- HANSON, G.H., 1978. The application of trace elements to the petrogenesis of igneous rocks of granitic composition. *Earth Plan. Sci. Lett.*, V. 38, pp. 26-43.
- HART, S.R., 1964. The petrography and isotopic mineral age relations of a contact zone in the Front Ranges, Colorado. *J. Geol.*, V. 72, pp. 493-525.
- HASKIN, L.A., 1966. On rare earth element behaviour in igneous rocks. In: *Origin and distribution of the elements. Physics and chemistry of the earth.* Ahrens, L.H. (Ed), II, pp. 739-743. Pergamon Press, N.Y.
- HASKIN, L.A., WILDEMAN, R.T., FREY, F.A., COLLINS, K.A., KEEDY, C.R. and HASKIN, M.A., 1966. Rare earths in sediments. *J. Geophy. Res.*, V. 71, pp. 6091-6105.
- HELGESON, H.C., 1979. Mass transfer among minerals and hydrothermal solutions. In: *Geochemistry of hydrothermal ore deposits*, 2nd Edition, Barnes, H.L. (Ed). pp. 568-610. Wiley-Interscience, N.Y.
- HENLEY, R.W., 1973. Solubility of gold in hydrothermal chloride solutions. *Chem. Geol.*, V. 11, pp. 73-87.
- HENLEY, R.W. and SHEPPARD, D.S., 1977. Hydrothermal activity and hydrothermal chemistry in the metamorphic environment. In: *Geochemistry 1977*. N.Z. D.S.I.R. Bull. 218, p. 84-94.
- HENLEY, R.W., NORRIS, R.J. and PATERSON, C.J., 1976. Multi-stage ore genesis in the New Zealand geosyncline. A history of post-metamorphic lode emplacement. *Mineral Deposita*, V. 11, pp. 180-196.

- HESP, W.R., 1971. Correlation between tin content of granitic rocks and their chemical and mineralogical composition. In: *Geochemical Exploration*, Boyle, R.W. (Ed), Can. Inst. Min. Metall., Special volume II, pp. 341-353.
- HESP, W.R. and RIGBY, D., 1972. The transport of tin in acid igneous rocks. *Pacific Geology*, V. 4, pp. 135-152.
- HESP, W.R. and RIGBY, D., 1974. Some geochemical aspects of tin mineralisation in the Tasman geosyncline. *Mineral Deposita*, V. 9, pp. 49-60.
- HEWETT, D.F. and FLEISCHER, M., 1960. Deposits of the manganese oxides. *Econ. Geol.*, V. 55, pp. 1-55.
- HEWETT, D.F., FLEISCHER, M., CONKLIN, N., 1963. Deposits of the manganese oxides: Supplement. *Econ. Geol.*, V. 58, pp. 1-51.
- HICKMAN, M.E., 1980. Rb-Sr age and isotope study of two Precambrian shear belts, west Greenland (abstract). *E.O.S.*, V. 61, No. 17, p. 384.
- HIETANAN, A., 1963. Idaho batholith near Pierce and Bungalow, Clearwater County, Idaho. *U.S. Geol. Surv. Prof. Paper*, 344 D, 42 pp.
- HIGGINS, W.H. and SWANSON, E., 1956. Preliminary report. Grey River Tungsten Prospect. Coddung Mining Co., Buchans. Unpubl., 9 pp.
- HOEFFS, J. and FREY, M., 1976. The isotopic composition of carbonaceous matter in a metamorphic profile from the Swiss Alps. *Geochim. Cosmochim. Acta.*, V. 40, pp. 945-951.
- HOLDAWAY, M.J., 1971. Stability of andalusite and the aluminium silicate phase diagram. *Am. J. Sci.*, V. 271, pp. 97-131.
- HOLL, R., 1977. Early Paleozoic ore deposits of the Sb-W-Hg formation in the Eastern Alps and their genetic interpretation. In: *Time and strata-bound ore deposits*, Klemm, D.D. and Schneider, H.J. (Eds), pp. 169-198. Springer-Verlag. N.Y.
- HOLL, R., MAUCHER, A. and WESTENBERGER, H., 1972. Synsedimentary-diagenetic ore fabrics in the Strata- and Time-bound scheelite deposits of Kleinarthal and Felbertal in the Eastern Alps. *Mineral Deposita*, V. 7, pp. 217-226.

- HOLLAND, H.D., 1967. Gangue minerals in hydrothermal deposits. In: Geochemistry of hydrothermal ore deposits, Barnes, H.L. (Ed), pp. 382-436. Holt, Rinehart, Winston, IAC., N.Y.
- HOLLAND, H.D., 1972. Granites, solutions, and base metal deposits. Econ. Geol., V. 67. pp. 281-301.
- HOLLISTER, L.S. and BURRUSS, R.C., 1976. Phase equilibria in fluid inclusions from the Khtada Lake metamorphic complex. Geochim. Cosmochim. Acta., V. 40, pp. 163-175.
- HOLLOWAY, J.R., 1976. Fluids in the evolution of granitic magmas. Consequences of finite CO_2 solubility. Geol. Soc. Am. Bull., V. 87, pp. 1513-1518.
- HORNER, C., 1979. Solubility and hydrolysis of FeWO_4 and MnWO_4 in the $25^\circ - 300^\circ\text{C}$ range and the zonation of wolframite. Chem. Geol., V. 27, pp. 85-98.
- HOSKING, K.F.G., 1951. Primary ore deposits in Cornwall. Trans. Roy. Geol. Soc. Cornwall, V. 18, pp. 309-359.
- HOSKING, K.F.G. and POLKINGHORNE, J.P.R., 1954. The significance of the variable iron content of the "wolframites" of the west of England. Trans. Roy. Geol. Soc. Cornwall, V. 18, pp. 526-534.
- HSU, L.C., 1976. The stability relations of the wolframite series. Am. Miner., V. 61. pp. 944-955.
- HSU, L.C., 1977. Effects of oxygen and sulphur fugacities on the scheelite-tungstenite and powellite-molybdenite stability relations. Econ. Geol., V. 72, pp. 664-670.
- HSU, L.C. and GALLI, D.E., 1973. Origin of the scheelite-powellite series of minerals. Econ. Geol., V. 68, pp. 681-696.
- HYNDMAN, D.W., 1972. Petrology of igneous and metamorphic rocks. McGraw - Hill Book Company, N.Y., 533 pp.
- IRVINE, T.N. and BARAGAR, W.R.A., 1971. A guide to the chemical classification of the common volcanic rocks. Can. J. Earth Sci., V. 8, pp. 523-548.
- ISHIHARA, S., 1977. The magnetite-series and ilmenite-series granitic rocks. Mining. Geol., V. 27, pp. 293-305.

- ISHIHARA, S., SAWATA, H., ARPORNSUWAN, S., BUSARACOME, P. and BUNGBRAKEARTI, N., 1979. The magnetite-series and ilmenite-series granitoids and their bearing on tin mineralisation particularly of the Malay peninsula region. Geol. Soc. Malasia, Bull. 11, pp. 103-110.
- IVANOVA, G.F., 1963. Content of tin, tungsten and molybdenum in granites enclosing tin-tungsten deposits. Geochem., pp. 492-500.
- IVANOVA, G.F., 1966. Thermodynamic evaluation of the possibility of tungsten transport as halogen compounds. Geochem. Intern., V. 3, pp. 964-973.
- IVANOVA, G.F., 1969. Conditions of concentration of tungsten during greisenisation. Geochem. Intern., V. 6, pp. 12-21.
- IVANOVA, G.F., 1974. Geochemical and physico-chemical conditions of tungsten migration and deposition. In: Metallisation associated with Acid magmatism, Stempok, M. (Ed), V., pp. 267-269. Ustredni Ustav Geolog., Prague.
- IVANOVA, G.F. and BUTUZOVA Ye.G., 1968. Distribution of tungsten, tin and molybdenum in the granites of eastern Transbaikaliya. Geochem. Intern., V. 5, pp. 572-583.
- IVANOVA, G.F., KHITAROV, D.N., LEVKIN, N.I., MILOWSKIY, G.A. and BANNYKH, L.P., 1976. Gas liquid inclusion data on the composition of tungsten-bearing hydrothermal solutions. Geochem. Intern., V. 13, pp. 17-26.
- JACKSON, N.J. and RANKIN, A.H., 1976. Fluid inclusion studies at St. Michaels Mount. Proc. Ussher Soc., V. 3, pp. 430-434.
- JAHS, R.H. and BURNHAM, C.W., 1969. Experimental studies of pegmatite genesis: I. A model for the derivation and crystallisation of granitic pegmatites. Econ. Geol., V. 64, pp. 843-864.
- JARVIS, J.C., WILDEMAN, T.R. and BANKS, N.G., 1975. Rare earths in the Leadville limestone and its marble derivatives. Chem. Geol., V. 16, pp. 27-37.
- JAVOY, M., 1977. Stable isotopes and geothermometry. J1. Geol. Soc. Lond., V. 133, pp. 609-636.

- JAYASINGHE, N.R., 1976. Geology of the Wesleyville area, Newfoundland. Unpubl. M.Sc. thesis, Memorial Univ. of Newfoundland, 228 pp.
- JAYASINGHE, N.R., 1978. Devonian alkaline basalt dykes of northeastern Newfoundland: evidence of a tensional environment. Can. J. Earth Sci., V. 15, pp. 848-853.
- JAYASINGHE, N.R., 1979. Granitoids of the Wesleyville area in northeastern Newfoundland: A study of their evolution and geological setting. Unpubl. Ph.D. thesis, Memorial Univ. of Newfoundland, 350 pp.
- JAYASINGHE, N.R., and BERGER, A.R., 1976. On the plutonic evolution of the Wesleyville area, Bonavista Bay, Newfoundland. Can. J. Earth Sci., V. 13, pp. 1560-1570.
- JEFFERY, P.G., 1959. The geochemistry of tungsten with special reference to the rocks of the Uganda protectorate. Geochim. Cosmochim. Acta., V. 16, pp. 278-295.
- JENNESS, S.F., 1963. Terra Nova and Bonavista map areas, Newfoundland (2DE1/2 and 2C). Geol. Surv. Can., Memoir 327, 184 pp.
- JOHNS, W.D. and HUANG, W.H., 1967. Distribution of chlorine in terrestrial rocks. Geochim. Cosmochim. Acta., V. 31, pp. 35-50.
- JUZA, J., KMONICEK, V. and SIFNER, V., 1965. Measurement of the specific volume of CO₂ in the range 700 to 4000 bars and 50° to 475°C. Physica., V. 31. pp. 1735-1744.
- KADOWAKI, R.S., 1957. General report of the Grey River Tungsten Prospect. Buchans Mining Co., Buchans. Unpubl., 16 pp.
- KALYUZHNYI, VL. A., DAVIDENKO, N.M., ZINCHUK, I.N., SVOREN, I.M. and POSITSKIY, B.I., 1975. Role of CO₂-H₂O and CH₄-H₂O fluids in the forming of ore of gold at Chukotka (abstract). In: Fluid Inclusion Research, Roedder, E. (Ed), V. 8, p. 82. Univ. of Michigan Press.
- KARUP-MOLLER, S., 1972. New data on pavonite, gustavite and some related sulphosalt minerals. N. Jh. Min. Abh., V. 117, pp. 19-38.

- KARUP-MOLLER, S., 1973. New data on schirmerites. *Can. Mineral.*, V. 11, pp. 952-957.
- KELLY, W.C. and TURNEAURE, F.S., 1970. Mineralogy, paragenesis and geothermometry of the tin and tungsten deposits of the eastern Andes, Bolivia: *Econ. Geol.*, V. 65, pp. 609-680.
- KELLY, W.C. and RYE, R.O., 1979. Geologic, fluid inclusion, and stable isotope studies of the tin-tungsten deposits of Panasqueira. *Econ. Geol.*, V. 74, pp. 1721-1822.
- KENNEDY, G.C., 1954. Pressure-volume-temperature relations of CO₂ at elevated temperatures and pressures. *Am. M. Sci.*, V. 252, pp. 225-41.
- KENNEDY, G.C. and HOLSER, W.T., 1966. Pressure-volume-temperature and phase relations of water and CO₂. In: *Handbook of Physical Constants*, Clark, S.P. (Ed). *Geol. Soc. Am. Memoir* 97. pp 371-383.
- KENNEDY, M.J., 1975. Repetitive orogeny in the northern Newfoundland Appalachians. New plate models based on Newfoundland examples. *Tectonophysics*, V. 28, pp. 39-87.
- KENNEDY, M.J., 1976. Southeastern margin of the northeastern Appalachians. Late Precambrian orogeny on a continental margin. *Geol. Soc. Am. Bull.*, V. 87. pp. 1317-1325.
- KENNEDY, M.J. and MCGONIGAL, M.H., 1972. The Gander Lake and Davidsville Groups of northeastern Newfoundland: New data and geotectonic implications. *Can. J. Earth Sci.*, V. 9, pp. 452-459.
- KEPPIE, J.D., 1979. Geological map of the Province of Nova Scotia. 1:500,000 map. Dept. Mines and Energy, Nova Scotia.
- KERR, P.F., 1940. Tungsten-bearing manganese deposits at Golconda, Nevada. *Econ. Geol.*, V. 51, pp. 1359-1390.
- KERRICH, R., 1977. Yellowknife mineralisation: The product of metamorphic degassing (abstract). *Geol. Soc. Am.*, Abst. with prog., pp. 1048-1049.
- KERRICH, R. and FRYER, B.J., 1979. Archaean precious-metal hydrothermal systems, Dome Mine, Abitibi greenstone belt. II. REE and oxygen isotope relationships. *Can. J. Earth Sci.*, V. 16, pp. 440-458.

- KERRICH, R., BECKINSALE, R.D. and SHACKLETON, N.J., 1978. The physical and hydrothermal regime of tectonic vein systems: Evidence from stable isotope and fluid inclusion studies. N. Jb. Miner. Abh., V. 131, pp. 225-239.
- KERRICK, D.M., 1977. The genesis of zoned skarns in the Sierra Nevada, California. J. Petrol., V. 18, pp. 144-181.
- KILINC, I.A. and BURNHAM, C.W., 1972. Partitioning of chloride between a silicate melt and coexisting aqueous phase from 2 to 8 kilobars. Econ. Geol., V. 67, pp. 231-235.
- KLOMINSKY, J., REIDER, M., KIEFT, C. and MRAZ, L., 1971. Heyrovskite $Pb_{0.86}Bi_{0.08}(Ag,Cu)_{0.04}S \cdot Bi_2S_3$ from Horky, Czechoslovakia, a new mineral of genetic interest. Mineral. Deposita, V. 6, pp. 133-147.
- KOBE, L.A. and LYNN, R.E., 1953. The critical properties of elements and compounds. Chem. Reviews, V. 52, pp. 117-236.
- KOGARKO, L.N. and RYABCHIKOV, I.D., 1970. Physico-chemical aspects of the genesis of Greisen deposits. In: Problems of hydrothermal ore deposits, Poucha, Z. and Stemprok, M. (Eds). Intn. Union Geol. Sci., No. 2, pp. 331-334.
- KOIDE, H. and BHATTACHARJI, S., 1978. Geometric patterns of active strike-slip faults and their significance as indicators for areas of energy release. In: Energetics of geological processes, Saxena, S.K. and Bhattacharji, S. (Eds), pp. 47-66.
- KOLTUN, L.I., 1965. Application of mineralothermometric analysis in studies of the origin of certain gold ore deposits in Ural. In: Research on the nature of mineral-forming solutions, Yermakov, N.P. (Ed), pp. 426-457.
- KOLTUN, L.I., 1973. Some data on temperatures and solution composition during formation of the Etyka Sn deposit (abstract). In: Fluid inclusion research, Roedder, E. (Ed), V. 7, p. 107. Univ. of Michigan Press.
- KONNERUP-MADSEN, J., 1979. Fluid inclusions associated with metamorphosed molybdenite mineralisation in Vest-Agder, south Norway. Econ. Geol., V. 74, pp. 1221-1230.

- KORNHAUSER, B.A. and STAFFORD, P.T., 1978. Tungsten. U.S. Bureau of Mines, Mineral commodities profile, MCP-21, .22 pp.
- KOSALS, Ya.A. and MAZUROV, M.P., 1970. Behaviour of molybdenum, tungsten, tin, niobium and tantalum in the emplacement of the Bitu-Dzhida granite intrusion of southern Baykalia. *Geochem. Int.*, V. 7, pp. 506-517.
- KOSALS, Ya.A. and DMITRIYEVA, A.M., 1973. Sequences and temperatures in formation of the Buluktay molybdenum-tungsten deposit, southwestern Transbaykal. *Intn. Geol. Review*, V. 15, pp. 25-30.
- KOSTER VAN GROSS, A.F. and WYLLIE, P.J., 1968. Melting relationships in the system $\text{NaAlSi}_3\text{O}_8\text{-NaF-H}_2\text{O}$ to 4 kilobars pressure. *J. Geol.*, V. 76, pp. 50-70.
- KOSTERIN, A.V., 1959. The possible modes of transport of the rare earths of hydrothermal solutions. *Geochem.*, V. 4, pp. 381-387.
- KOZLOV, V.D., SHEREMET, Ye.M. and YANOVSKIY, J.M., 1974. Geochemical characterisation of the Mesozoic pluma-site leucocratic granites of the Transbaykalia tin-tungsten belt. *Geochem. Intn.*, V. 11, pp. 997-1008.
- KOZLOWSKI, A., KARWOWSKI, L. and OLSZYNSKI, W., 1975. Tungsten-tin-molybdenum mineralisation in the Markonasze massif. *Geologica Polonica*, V. 25, pp. 415-430.
- KRAUSKOPF, K.B., 1970. Tungsten (Wolfram). In: *Handbook of geochemistry*, Wedepohl, K.H. (Ed), Section 74-B - 74-0. Springer Verlag, Berlin.
- KRAYNOV, S.R., KAPRANOV, S.D. and PETROV, N.G., 1965. Main features of the geochemistry of tungsten in sub-surface and surface waters of the areas of tungsten deposits. *Geochem. Intn.*, V. 2, pp. 987-907.
- KUCK, P.H., 1978. The behaviour of molybdenum, tungsten, and titanium in the porphyry copper environment. Unpubl. Ph.D thesis, Arizona Univ., 296 pp.
- LANDIS, G.P. and RYE, R.O., 1974. Geologic, fluid inclusion and stable isotope studies of the Pasto Bueno tungsten-base metal ore deposit, northern Peru. *Econ. Geol.*, V. 69, pp. 1025-1059.
- LANGMUIR, D., 1978. Uranium solution-mineral equilibria at low temperatures with application to sedimentary ore deposits. *Geochim. Cosmochim. Acta*, V. 42, pp. 547-569.

- LARSON, S.D., 1955. Phase studies of the two-component carbon dioxide-water system involving the carbon dioxide hydrate. Unpubl. Ph.D. thesis, Univ. of Michigan, 84 pp.
- LAZ'KO, E.M., DOROSHENKO, Yu.P., KOLTUN, L.I., LYAKHOV, Yu.V., MYAS, N.I. and PIZNYUR, A.V., 1976. Processes of hydrothermal minerogenesis in the east Transbaikalian deposits from a study of gas-liquid inclusions in minerals. In: Fluid Inclusion Research, Roedder, E. (Ed), V. 8, p. 102. Univ. of Michigan Press.
- LEBEDEV, L.M., BARANOVA, N.M. and NIKITINA, I.B., 1971. On the form of occurrence of lead and zinc in the Cheleken thermal brines. *Geochem. Intn.*, V. 8, pp. 511-516.
- LEGRET, M., 1978. Solubility de ThO_2 et UO_2 en milieu aqueux à haute pression et haute température. Etude expérimentale de la solution solide $\text{UO}_2\text{-ThO}_2$. In: Rapport annual, 1977. C.R.P.G., Nancy, France, p. 49.
- LEGRET, M. and POTY, B., 1977. Solubite de ThO_2 en milieu aqueux à haute température et haute pression. *Sci. de la Terre*, 5e reunion annuelle, Paris, p. 313.
- LEROY, J., 1978. The Margnac and Fanay Uranium deposits of the La Crouzille district (Western Massif Central, France): Geologic and fluid inclusion studies. *Econ. Geol.*, V. 73, pp. 1611-1634.
- LI, K.D., 1962. Chemical processing of tungsten ores and concentrates. *J. Metals*, V. 14, pp. 413-417.
- LIPPOLT, H.J. and GENTER, W., 1963. K-Ar dating of some limestones and fluorites (examples of K-Ar ages with low Ar concentrations). In: *Radioactive Dating*, Intn. Atomic Energy Agency, Vienna, pp. 239-244.
- LOWRY, H.H. and ERICKSON, W.R., 1927. The densities of coexisting liquid and gaseous carbon dioxide and the solubility of water in liquid carbon dioxide. *J. Am. Chem. Soc.*, V. 49, pp. 2929-2934.
- LYAKHOVICH, V.V. and BALANOVA, T.T., 1969. Mean contents of W, Mo, Sn, Ta, Nb, and Zn in sphene and ilmenites from granites. *Geochem. Intn.*, V. 6, pp. 281-287.
- MCDUGALL, I., POLACH, H.A. and STIPP, J.J., 1969. Excess radiogenic argon in young subaerial basalts from the Auckland volcanic field, New Zealand. *Geochim. Cosmochim. Acta*, V. 33, pp. 1485-1520.

- MCLENNAN, S.M. and TAYLOR, S.R., 1979. Rare-earth mobility associated with uranium mineralisation. *Nature*, V. 282, pp. 247-250.
- MCLENNAN, S.M., FRYER, B.J. and YOUNG, G.M., 1979. The geochemistry of the carbonate-rich Espanola formation (Huronian) with emphasis on the rare-earth elements. *Can. J. Earth Sci.*, V. 16, pp. 230-239.
- MACDONALD, G.A. and KATSURA, T., 1964. Chemical composition of Hawaiian lavas. *J. Petrol.*, V. 5, pp. 82-133.
- MACKENZIE, G.B. and CLARKE, D.B., 1975. Petrology of the south mountain Batholith, Nova Scotia. *Can. J. Earth Sci.*, V. 12, pp. 1209-1218.
- MAGARITZ, M. and HOFMANN, A., 1978. Diffusion of Sr, Ba, and Na in obsidian. *Geochim. Cosmochim. Acta.*, V. 42, pp. 595-605.
- MALAKHOV, A.A., 1969. Bismuth and antimony in galenas as indicators of some conditions of ore formation. *Geokhimiya*, V. 11, pp. 1283-1296. (In Russian).
- MALININ, S.D., 1979. Solubility of CO₂ in aqueous solutions of electrolytes (problem of salting out). *Geochem. Intn.*, V. 15, pp. 108-119.
- MALININ, S.D. and SAVELYEVA, N.I., 1973. The solubility of CO₂ in NaCl and CaCl₂ solutions at 250, 500 and 750 under elevated CO₂ pressures. *Geochem. Intn.*, V. 10, pp. 410-418.
- MALININ, S.D. and KUROVSKAYA, N.A., 1975. Solubility of CO₂ in chloride solutions at elevated temperatures and CO₂ pressures. *Geochem. Intn.*, V. 12, pp. 199-201.
- MASLENITSKY, N.N. and PERLOV, P.M., 1960. Development of the autoclave-soda process for the treatment of tungsten concentrates. In: *International Mineral Processing Congress*, 1959. *Trans. Inst. Min. Metall. Lond.*, 1960, pp. 839-854.
- MATHIEU, G.I., 1961. Concentration tests on two samples of tungsten ore from the Grey River area, Newfoundland for ASARCO, Newfoundland. CANMET, Investigation report. IR 61-97, 28 pp.
- MATHIEU, G.I. and BRUCE, R.W., 1970. High intensity magnetic separation on a tungsten ore from the Grey River property of ASARCO. CANMET, Investigation report. IR 70-6, 5 pp.

- MAUCHER, A., 1965. Die Antimon-Wolfram-Quecksilber formation und ihre Beziehungen zu Magmatismus und Geotektonik. Freiburger Forsch., C. 186, pp. 173-180.
- MAUCHER, A., 1976. The strata-bound cinnabar-stibnite-scheelite deposits. In: Handbook of Strata-bound and stratiform ore deposits, Wolf, K.H. (Ed), V. 7, pp. 477-503.
- MEYER, C. and HEMLEY, J.J., 1967. Wall rock alteration. In: Geochemistry of hydrothermal ore deposits, Barnes, H.L. (Ed), pp. 166-235. Holt, Rinehart and Winston Inc., N.Y.
- MILLER, C.K., 1974. Scheelite mineralisation in the region of the Moose River gold district, Halifax County, Nova Scotia. Unpubl. B.Sc. Hons. thesis, Dalhousie Univ., 39 pp.
- MILLER, C.K., GRAVES, M.C. and ZENTILLI, M., 1976. Scheelite mineralisation of southwestern Nova Scotia. Report of Activities, Geol. Surv. Can., Paper 76-1, pp. 331-332.
- MINTSER, E.F., 1979. The geochemical properties of the behaviour of bismuth in hypogene processes. In: Geochemistry of bismuth, Angino, E.E. and Long, D.T. (Eds), Benchmark Papers in Geology, V. 49, pp. 268-327. Dowden, Hutchinson and Ross, Penna.
- MINTSER, E.F., NECHELYUSTOV, G.N., MANUCHARYANTS, B.O., OVCHINNIKOV, V.V. and TURSUNGAZIYEV, B.T., 1976. Bismuth ore mineralisation from Mironovskoe deposit (abstract). In: Fluid inclusion research, Roedder, E. (Ed), V. 9, p. 89. Univ. of Michigan Press.
- MITCHELL, A.H.G., 1973. Metallogenic belts and angle of dip of the Benioff Zones. Nature, V. 245, pp. 49-52.
- MITCHELL, A.H.G. and GARSON, M.S., 1972. Relationship of porphyry copper and circum-pacific tin deposits to paleo-Benioff zones. Trans. Inst. Min. Metall., V. 81, B10-B25.
- MITCHELL, A.H.G. and GARSON, M.S., 1976. Mineralisation at plate boundaries. Miner. Sci. Engng., V. 8, pp. 129-169.

- MOLLER, P., MORTEANI, G., HOFFES, J. and PAREKH, P.P., 1979. The origin of the ore-bearing solution in the Pb-Zn veins of Western Harz, Germany, as deduced from rare-earth element and isotope distribution in calcites. *Chem. Geol.*, V. 26, pp. 197-215.
- MOORE, J. McM., 1975. A mechanical interpretation of the vein and dyke system of the S.W. England ore field. *Mineral. Deposita.*, V. 10, pp. 374-388.
- MOORE, J. McM., 1977. Exploration prospects for stockwork tungsten-tin ores in southwest England. *Min. Mag. Lond.*, Feb., pp. 97-103.
- MOORE, J. McM. and JACKSON, N., 1977. Structure and mineralisation in the Cligga Head granite stock, Cornwall. *J. Geol. Soc. Lond.*, V. 133, pp. 467-480.
- MOORE, W.J. and NASH, J.T., 1974. Alteration and fluid inclusion studies of the Porphyry copper ore body at Bingham, Utah. *Econ. Geol.*, V. 69, pp. 631-645.
- MOREL, P. and IRVING, E., 1978. Tentative paleocontinental maps for the early Phanerozoic and Proterozoic. *J. Geol.*, V. 86, pp. 535-561.
- MULLINS, W.J., 1958. The geology of the Cape La Hune area, S.W. coast of Newfoundland with special reference to igneous and metamorphic petrology. Unpubl. B.Sc. thesis, Mt. Allison Univ., 56 pp.
- NASH, J.T., 1976. Fluid inclusion petrology-data from porphyry copper deposits and applications to exploration. *U.S. Geol. Surv. Prof. Paper*, 907D, 16 pp.
- NAUMOV, G.B., 1959. Transportation of uranium in hydrothermal solutions as a carbonate. *Geochem.*, V. 1, pp. 5-20.
- NAUMOV, G.B., 1961. Some physico-chemical characteristics of the behaviour of uranium in hydrothermal solution. *Geochem.*, V. 3, pp. 127-147.
- NAUMOV, G.B. and MIRONOVA, O.F., 1969. Das Verhalten der Kohlensäure in hydrothermalen Lösungen bei der Bildung der Quarz-Nasturan-Kalzit-Gänge des Erzgebirges. *Zeitschr. Angew. Geologie*, V. 15, pp. 240-241.
- NAUMOV, G.B. and IVANOVA, G.F., 1971. The pressure and temperature conditions for formation of wolframite deposits. *Geochem. Intern.*, V. 8, pp. 381-394.

- NORMAN, D.I., LANDIS, G.P. and SAWKINS, F.J., 1976. H₂S and SO₂ detected in fluid inclusions (abstract). Geol. Soc. Am. Abstr. with prog., V. 8, p. 1031.
- NORONHA, F., 1974. A study of fluid inclusions in quartz veins from the tungsten deposit at Borralha, northern Portugal (abstract). In: Fluid Inclusion Research, Roedder, E. (Ed.), V. 8, p. 135. Univ. of Michigan Press.
- ODIKADZE, G.L., 1968. Distribution of the rarer ore elements in the El'dzhurta intrusive massif Kabarda-Balkar. Geochem. Intn., V. 5, pp. 1010-1015.
- O'DRISCOLL, C.F. and HUSSEY, E.M., 1977. The Avalonian orogeny of the western Avalon Zone (abstract). Geol. Soc. Am. 12th Ann. Meeting. Binghamton, N.Y., p. 306.
- ONTOEV, D.O., NISSENBAUM, P.N. and ORGANOVA, N.I., 1960. The nature of high bismuth and silver contents in galena of the Bukulinsk deposit and some problems of isomorphism in the system PbS-Ag₂S-Bi₂S₃. Geochem., V. 5, pp. 494-510.
- O'NEIL, J.R., CLAYTON, R.N. and MAYEDA, T.K., 1969. Oxygen isotope fractionation in divalent metal carbonates. J. Chem. Phys., V. 51, pp. 5547-5558.
- ORVILLE, P.M., 1963. Alkali ion exchange between vapour and feldspar phases. Am. J. Sci., V. 261, pp. 201-237.
- PAJARI, G.E., PICKERELL, R.K. and CURRIE, K.L., 1979. The nature, origin, and significance of the Carmanville ophiolitic melange, northeastern Newfoundland. Can. J. Earth Sci., V. 16, pp. 1439-1451.
- PATERSON, C.J., BLATTNER, P., HENLEY, R.W. and NORRIS, R.J., 1975. Origin of scheelite mineralisation at Glenorchy, New Zealand in light of oxygen isotope data. Manuscript, in prep.
- PEARCE, J.A. and CANN, J.R., 1973. Tectonic setting of basic volcanic rocks determined using trace element analysis. Earth. Plan. Sci. Lett., V. 19, pp. 290-300.
- PEARCE, T.H., GORMAN, B.C. and PICKETT, T.C., 1975. The TiO₂-K₂O-P₂O₅ diagram: A method of discriminating between oceanic and non-oceanic basalts. Earth Plan. Sci. Lett., V. 24, pp. 419-426.

- PECHER, A., 1979. Composition and density of the fluid phase through a major crustal shear zone. Data on fluid inclusions in quartz from the Himalayan Main Central Thrust Zone, Central Nepal. Bull. Mineralogie, V. 102, pp. 537-554.
- PEREIRA, J. and DIXON, C.J., 1971. Mineralisation and plate tectonics. Mineral. Deposita, V. 6, pp. 404-405.
- PERLOV, P.M. and POPRUKAILO, V.M., 1959. Interaction of iron and manganese tungstates with soda solution in conditions of the autoclave-soda process. Obogash. Rud., V. 4, pp. 15-19.
- PICKERILL, R.K., PAJARI, G.E., CURRIE, K.L. and BERGER, A.R., 1978. Carmanville map area, Newfoundland, the northeastern end of the Appalachians. Report of Activities, Geol. Surv. Can. paper, 78-1A, pp. 209-216.
- PIPEROV, N.B., PENCHEV, N.P. and ZIDAROVA, B.P., 1979. The analysis of volatiles from fluid inclusions in hydrothermal fluoride. Chem. Geol. V. 27, pp. 215-232.
- POKROVSKII, P.V. and PURTOV, V.K., 1975. Gas-liquid inclusions in quartzes of veins of huebnerite deposits of the Boevsko Biktimirovskoe ore zone in the central Urals (abstract). In: Fluid Inclusion Research, Roedder, E. (Ed), V. 8, p. 144. Univ. of Michigan Press.
- POPOVA, N.N., NECHELJUSTOV, G.N. and RAZINA, I.S., 1966. The rare elements in the molybdenum-tungsten deposit of central Kazakhstan. Nauka Press, Moscow.
- POTTER, R.R., 1968. Geology of the Burnt Hill area with special reference to the ore controls in the vicinity of the Burnt Hill Tungsten Mine. Unpubl. Ph.D. thesis, Carleton Univ., 260 pp.
- POTTER, R.R., HAMILTON, J.B. and DAVIS, J.L., 1979. Geological map of New Brunswick 1:500,000. Map No. NR-1.
- POTTER, R.W., 1977. Pressure corrections for fluid inclusions homogenisation temperature based on the volumetric properties of the system NaCl-H₂O. U.S. Geol. Surv. Res., V. 5, pp. 603-608.

- POTTER, R.W. and CLYNNE, M.A., 1978. Solubility of highly soluble salts in aqueous media. Part 1, NaCl, KCl, CaCl₂, Na₂SO₄ and K₂SO₄ solubilities to 100°C. U.S. Geol. Surv., J. Res., V. 6, p. 707-711.
- POTY, B.P., LEROY, J. and CUNEY, M., 1974. Les inclusions fluides dans les minerais des gisements d'uranium intragranitiques du Limousin et du Forez (Massif Central, France). In: Formation of uranium ore deposits. I.A.E.A. Proc., Vienna, Austria, pp. 569-582.
- POTY, B.P., STALDER, H.A. and WEISBROD, A.M., 1974. Fluid inclusion studies in quartz from fissures of western and central Alps. Schweiz. Min. Petr. Mitt., V. 54, pp. 150-159.
- RAICEVIC, D. and BRUCE, R.W., 1971. Tungsten concentration from Grey River Property of ASARCO, Newfoundland. CANMET Investigation Report, IR 71-70.
- RAMA, S.N.I., HART, S.R. and ROEDDER, E., 1965. Excess radiogenic argon found in fluid inclusions. J. Geophys. Res., V. 70, pp. 509-511.
- RAMDOHR, P., 1969. The ore minerals and their intergrowths. 3rd Edition, Pergamon Press, London, 1174 pp.
- RAYMENT, B.D., DAVIS, G.R. and WILSON, J.D., 1971. Controls to mineralisation at Wheal Jane, Cornwall. Trans. Inst. Min. Metall., V. 80, B224-237.
- REEDMAN, A.J., 1967. Geological environment and genesis of the tungsten deposit of Kigezi district, south-western Uganda. Unpubl. Ph.D. thesis, Univ. of Leeds, 250 pp.
- RICHARDSON, S.W., 1968. Staurolite stability in a part of the system Fe-Al-Si-O-H. J. Petrol., V. 9, pp. 467-488.
- RICHARDSON, S.W., GILBERT, M.C. and BELL, P.M., 1969. Experimental determination of kyanite-andalusite and andalusite-sillimanite equilibria: The aluminium silicate triple point. Am. J. Sci., V. 267, pp. 259-272.
- RILEY, G.C., 1959. Burgeo-Ramea, Newfoundland. Can. Geol. Surv. Map 22-1959.
- RILEY, J.P. and CHESTER, R., 1971. Introduction to marine chemistry. Academic Press, 465 pp.

- ROBERTS, J.L., 1970. The intrusion of magma into brittle rocks. In: Mechanism of igneous intrusion, Newall, C. and Rast, N. (Eds). Geol. J. Spec. issue, V. 2, pp. 286-388.
- ROEDDER, E., 1965. Liquid CO₂ inclusions in olivine-bearing nodules and phenocrysts from basalts. Am. Miner., V. 50, pp. 1746-1782.
- ROEDDER, E., 1970. Application of an improved crushing microscope stage to studies of gases in fluid inclusions. Schweiz. Min. Petr. Mitt., V. 50, pp. 41-58.
- ROEDDER, E., 1971. Fluid inclusion studies on the porphyry-type ore deposits at Bingham, Utah, Butte, Montana and Climax, Colorado. Econ. Geol., V. 66, pp. 98-120.
- ROEDDER, E., 1972. Composition of fluid inclusions. U.S. Geol. Surv. Prof. Paper, 440-JJ, 164 pp.
- ROEDDER, E., 1976. Fluid inclusions evidence on the genesis of ores in sedimentary and volcanic rocks. In: Handbook of strata-bound and stratiform ore deposits, Wolf, K.H. (Ed), V. 2, pp. 67-110. Elsevier.
- ROEDDER, E. and BODNAR, R.J., 1980. Geologic pressure determinations from fluid inclusion studies. Ann. Rev. of Earth and Planetary Sci., V. 8, in press.
- ROEDDER, E. and COOMBS, D.S. 1967. Immiscibility in granitic melts, indicated by fluid inclusions in ejected granitic blocks from Ascension Island. J. Petrol., v. 8, pp. 415-417.
- ROSASCO, G.J., ROEDDER, E. and SIMMONS, J.H., 1975. Laser-excited Raman spectroscopy for non destructive partial analysis of individual phases in fluid inclusions in minerals. Science, V. 190, pp. 557-560.
- ROSE, A.W., 1970. Zonal relations of wall rock alteration and sulphide distribution at porphyry copper deposits. Econ. Geol., V. 65, pp. 920-936.
- ROY, S.S., 1977. Mylonite microstructures and their bearing on the development of mylonites - an example from deformed trondhjemites of the Bergen arc region, S.W. Norway. Geol. Mag., V. 114, pp. 445-458.

- RUITENBERG, A.A., 1966. Mineral deposits in granitic intrusion and related metamorphic aureoles in parts of the Welsford, Loch Alva, Musquash and Pennfield areas, New Brunswick. Dept. of Nat. Resources. Report of Investigation, No. 9, 40 pp.
- RUITENBERG, A.A., McCUTCHEON, D., VENUGOPAL, V. and PIERCE, G.A., 1977. Mineralisation related to post-Acadian tectonism in southern New Brunswick. *Geoscience Canada*, V. 4, p. 13-23.
- SALANCI, B. and MOH, G.H., 1969. Die Experimentelle Untersuchung des pseudobinaren Schnittes $PbS-Bi_2S_3$ innerhalb des $Pb-Bi-S$ system in Beziehung zu naturalischen Blei-Wismuth-Sulphosalzen. *N. Jh. Miner. Abh.*, V. 112, pp. 63-95.
- SASAKI, A., 1959. Variation of unit cell parameters in wolframite series. *Miner. J.*, V. 2, pp. 375-396.
- SAWKINS, F.J., 1966. Preliminary fluid inclusion studies of the mineralisation associated with the Hercynian granites of southwest England. *Trans. Inst. Min. Metall.*, V. 75, B109-B112.
- SCOTT, S.D., 1976. Application of the sphalerite geobarometer to regionally metamorphosed terrains. *Am. Min.*, V. 61, pp. 661-670.
- SCRUTTON, R.A., 1973. The age relationships of igneous activity and continental breakup. *Geol. Mag.*, V. 110, pp. 227-234.
- SHCHERBA, G.N., 1970a. Greisens (part 1). *Int. Geol. Rev.*, V. 12, pp. 114-150.
- SHCHERBA, G.N., 1970b. Greisens (part 2). *Int. Geol. Rev.*, V. 12, pp. 239-255.
- SHEPHERD, T.J., BECKINSALE, R.D., RUNDLE, C.C. and DURHAM, J., 1976. Genesis of Carrock Fell Tungsten deposits, Cumbria: Fluid inclusion and isotopic study. *Trans. Inst. Min. Metall.*, V. 85, B63-B73.
- SHEPPARD, S.M.F., 1977. The Cornubian Batholith, S.W. England. D/H and $^{18}O/^{16}O$ studies of kalinite and other alteration minerals. *J. geol. Soc.*, V. 133, pp. 573-592.
- SHEPPARD, S.M.F., NEILSEN, R.L. and TAYLOR, H.P., 1971. Hydrogen and oxygen isotope ratios in minerals from porphyry copper deposits. *Econ. Geol.*, V. 66, pp. 575-542.

- SHIEH, Y.N. and TAYLOR, H.P., 1969. Oxygen and carbon isotope studies of contact metamorphism of carbonate rocks. *J. Petrol.*, V. 10, pp. 307-331.
- SHIEH, Y.N. and SCHWARCZ, H.P., 1974. Oxygen isotope studies of granite and migmatite, Grenville Province of Ontario, Canada. *Geochim. Cosmochim. Acta.*, V. 38, pp. 21-45.
- SILLITOE, R.H., 1972. A plate tectonic model for the origin of porphyry copper deposits. *Econ. Geol.*, V. 67, pp. 184-197.
- SILLITOE, R.H., 1976. Andean mineralisation: A model for the metallogeny of convergent plate margins. *Geol. Assoc. Can. Special paper*, No. 14, pp. 59-100.
- SKAARUP, P., 1974. Strata-bound scheelite mineralisation in skarns and gneisses from the Bindal area, northern Norway. *Mineral. Deposita.*, V. 9, pp. 299-308.
- SMITH, F.G., 1949. Transport and deposition of the non-sulphide vein minerals. III. Phase relations at the pegmatite stage. *Econ. Geol.*, V. 43, pp. 535-546.
- SMITH, T.E., 1974. The geochemistry of the granitic rocks of Halifax County, Nova Scotia. *Can. J. Earth Sci.*, V. 11, pp. 650-657.
- SMITH, T.E. and TUREK, A., 1976. Tin bearing potential of some Devonian granitic rocks in S.W. Nova Scotia. *Mineral. Deposita.*, V. 11, pp. 234-245.
- SMYTH, W.R., 1979. Reconnaissance of the Burgeo Map area (IIP, west half), Newfoundland. Report of Activities, 1978. Newfoundland Min. Dev. Div., Report 79-1, pp. 54-57.
- SMYTH, W.R., 1980. Reconnaissance geology of the White Bear River (IIP/14) and Dolland Brook (IIP/15) map areas. In: Current Research, Newfoundland Min. Dev. Div., Report 80-1, pp. 89-92.
- SORBY, H.C., 1858. On the microscopical structure of crystals, indicating the origin of minerals and rocks. *Geol. Soc. Journal.*, V. XIV, pp. 453-500.
- SOTNIKOV, V.I. and IZYUMOVA, L.G., 1965. Tungsten in the granite massif of various ore contents, Gorny Altay (abstract). *Geochem. Intn.*, V. 2, p. 132.

- SOURIRAJAN, W. and KENNEDY, G.C., 1962. The system $H_2O-NaCl$ at elevated temperatures and pressures. *Am. J. Sci.*, V. 260, pp. 115-141.
- SPRINGER, G., 1971. The synthetic solid-solution series $Bi_2S_3-BiCuPbS_3$ (bismuthinite-alkinite). *N. Jh. Min. Monatsch.*, H. 1, pp. 19-24.
- STEMPROK, M. and SULCEK, A., 1969. Geochemical profile through an ore-bearing lithium granite. *Econ. Geol.*, V. 64, pp. 392-404.
- STEMPROK, M., BURNOL, L. and TISCHENDORF, G., 1978. Metallisation associated with acid magmatism. *Ustredni Ustav Geologicky, Praha*, V. III, 446 pp.
- STEVENS, W.E. and HALLIDAY, A.N., 1979. Compositional variation in the Galloway plutons. In: The origin of granite batholiths - geochemical evidence, Atherton, D. and Tarney, E. (Eds), pp. 9-17. Shiva Press, Orpington.
- STEWART, D.B., 1978. Petrogenesis of lithium-rich pegmatites. *Am. Mineral.*, V. 63, pp. 970-980.
- STORMER, J.C. and CARMICHAEL, I.S.I., 1971. The free energy of sodalite and the behaviour of chloride, fluoride, and sulphate in silicate magmas. *Am. Mineral.*, V. 56, pp. 292-306.
- STRONG, D.F., 1974. Plate tectonic setting of Appalachian-Caledonian mineral deposits as indicated by Newfoundland examples. *Trans. Soc. Min. Eng., A.I.M.E.*, V. 256, pp. 121-128.
- STRONG, D.F., 1975. Plateau lavas and diabase dikes of northwestern Newfoundland. *Geol. Mag.*, V. 111, p. 501-514.
- STRONG, D.F., 1977. Volcanic regimes of the Newfoundland Appalachians. *Geol. Soc. Canada, Special Paper*, No. 16, pp. 61-90.
- STRONG, D.F., 1980. Granitoid rocks and associated mineral deposits of eastern Canada and western Europe. *Geol. Assoc. Can., Special Paper in honour of J.T. Wilson. D. Strangway (Ed), in press.*
- STRONG, D.F. and DICKSON, W.L., 1978. Geochemistry of Paleozoic granitoid plutons from contrasting tectonic zones of northeast Newfoundland. *Can. J. Earth Sci.*, V. 15, p. 145-156.

- STRONG, D.F. and HANMER, S.K., 1980. The leucogranites of southern Brittany: Origin by faulting, frictional heating, fluid flux, and fractional melting. (Manuscript under review).
- STRONG, D.F., DICKSON, W.L., O'DRISCOLL, C.F. and KEAN, B.F., 1974a. Geochemistry of eastern Newfoundland granitoid rocks, Newfoundland. Dept. Mines and Energy Report, 74-3, 140 pp.
- STRONG, D.F., DICKSON, W.L., O'DRISCOLL, C.F., KEAN, B.F. and STEVENS, R.K., 1974b. Geochemical evidence for long-lived east-dipping Appalachian subduction zone in Newfoundland. *Nature*, V. 248, pp. 37-39.
- STUDENIKOVA, Z.V., IVANOVA, G.F. and BRYZGALIN, O.V., 1970. On the possible sources and transportation of tungsten in the formation of deposits of greisen type. In: Problems of Hydrothermal Ore Deposition, Pouba, Z. and Stempok, M. (Eds). *Intn. Union. Geol. Sci.*, No. 2, pp. 89-92.
- STUMPFL, E.F., 1976. Stratabound ore deposits and metamorphism, new aspects (abstract). 25th *Intn. Geol. Cong.*, V. 1, pp. 194-195.
- SUTHERLAND-BROWN, A., 1976. Porphyry deposits of the Canadian Cordillera. *Can. Inst. Min. Metall. Special Vol.*, 15, 510 pp.
- SUTTON, F.M. and McNABB, A., 1977. Boiling curves at Broadlands geothermal field, New Zealand. *N.Z.J. of Science*, V. 20, pp. 333-337.
- TAKENOUCHI, S. and KENNEDY, G.C., 1965a. The solubility of carbon dioxide in NaCl solutions at high temperatures and pressure. *Am. J. Sci.*, V. 263, p. 445-54.
- TAKENOUCHI, S. and KENNEDY, G.C., 1965b. Dissociation pressures of the phase $\text{CO}_2 \cdot 5.75\text{H}_2\text{O}$. *J. Geol.*, V. 73, pp. 383-390.
- TAKENOUCHI, S. and IMAI, H., 1975. Glass and fluid inclusions in acidic igneous rocks from some mining areas in Japan. *Econ. Geol.*, V. 70, pp. 750-769.
- TAUSON, L.V. and KOZLOV, V.D., 1973. Distribution functions and ratios of trace element concentrations as estimators of the ore-bearing potential of granites. In: *Geochemical Exploration. Inst. Min. Metall.*, pp. 37-44.

- TAYLOR, B.E. and O'NEIL, J.R., 1977. Stable isotope studies of metasomatic Ca-Fe-Al-Si skarns and associated metamorphic and igneous rocks, Osgood Mountains, Nevada. *Contrib. Min. Petrol.*, V. 63, pp. 1-50.
- TAYLOR, H.P., 1974. The application of oxygen and hydrogen isotope studies to problems of hydrothermal alteration and ore deposition. *Econ. Geol.*, V. 69, pp. 843-883.
- TAYLOR, H.P., 1978. Oxygen and hydrogen isotope studies of plutonic granitic rocks. *Earth Plan. Sci. Lett.*, V. 38, pp. 177-210.
- TAYLOR, H.P., 1979. Oxygen and hydrogen isotope relationships in hydrothermal ore deposits. In: *Geochemistry of Hydrothermal Ore Deposits*, 2nd Edition, Barnes, H.L. (Ed), pp. 236-277. Wiley Interscience.
- TAYLOR, R.G., 1979. Geology of tin deposits. *Developments in Economic Geology* 11. Elsevier Scientific Publ. Co., N.Y. 543 pp.
- TAYLOR, R.G. and HOSKING, K.F.G., 1970. Manganese-iron ratios in wolframite, South Crofty Mine, Cornwall. *Econ. Geol.* V. 65, pp. 47-53.
- TAYLOR, R.P. and FRYER, B.J., 1980a. Multiple-stage hydrothermal alteration in porphyry copper systems in northern Turkey: The temporal interplay of potassic, propylitic, and phyllic fluids. *Can. J. Earth Sci.*, V. 17, pp. 901-926.
- TAYLOR, R.P. and FRYER B.J. 1980b. Rare earth element geochemistry as an aid to interpreting hydrothermal data ore deposits: In: *Metallisation associated with acid magmatism*. Evans, A.E. (Ed), V. 4, in press. John Wiley and Sons, Chichester, England.
- TAYLOR, S.R., 1965. The application of trace element data to problems in petrology. *Physics and Chemistry of the Earth*, V. 6, pp. 133-213.
- TAYLOR S.R. and GORTON, M.P., 1977. Geochemical application of spark source mass spectrometry. III. Element sensitivity, precision and accuracy. *Geochim. Cosmochim. Acta.*, V. 41, pp. 1375-1380.
- TISCHENDORF, G., 1970. Zur geochemischen Spezialisierung der Granite des West Erzgebirgischen Teil plutons. *Geologie*, V. 19, pp. 25-40.

- TISCHENDORF, G., 1973. The metallogenic basis of tin exploration in the Erzgebirge. Trans. Inst. Min. Metall., V. 82, B9-B24.
- TISCHENDORF, G., 1977. Geochemical and petrographic characteristics of silicic magmatic rocks associated with rare-element mineralisation. In: Metallisation associated with Acid Magmatism, Stempok, M., Burnol, L. and Tischendorf, G. (Eds.), Ustredni Ustav Geolog., Praha., V. 2, pp. 41-46.
- TISCHENDORF, G., LANGE, H. and SCHUST, F., 1974. On the relation between granites and tin deposits on the Erzgebirge G.D.R. In: Metallisation associated with Acid Magmatism, Stempok, M. (Ed), Ustredni Ustav Geolog., Praha, V. 1, pp. 132-136.
- TOHEIDE, K. and FRANCK, E.U., 1963. Das Zweiphasengebeit und die Kritische Kurve in system Kohlendioxid-Wasser bis zu Drucken von 3500 bar. Z. Phys. Chem. Neufolge, V. 37, pp. 388-401.
- TOURET, J., 1971. Le Facies granulite en Norvege meridionale: 2. Les inclusion fluides. Lithos, V. 4, pp. 423-436.
- TOURET, J., 1977. The significance of fluid inclusions in metamorphic rocks. In: Thermodynamics in Geology, Fraser, D.G. (Ed), D. Reidel Publ. Co., Amsterdam, pp. 203-227.
- TUGARINOV, A.I. and NAUMOV, V.B., 1972. Physico-chemical parameters of hydrothermal mineral formation. Geochem. Intn., V.9, pp. 161-167.
- TUPPER, W.M. and HART, S.H., 1961. Minimum age of the middle Silurian in New Brunswick based on K-Ar method. Bull. Geol. Soc. Am., V. 72, pp. 1285-1287.
- TURNER, F.J., 1968. Metamorphic Petrology: Mineralogical and Field Aspects. McGraw-Hill Book Co., N.Y., 403 pp.
- TWENHOFEL, W.H., 1947. The Silurian of eastean Newfoundland with some data relating to physiography and Wisconsin glaciation of Newfoundland. Am. J. Sci., V. 245, pp. 65-122.
- TWENHOFEL, W.H. and MacCLINTOCK, A., 1940. Surface of Newfoundland. Bull. Geol. Soc. Am., V. 51, pp. 1663-1728.

- UREY, H.C., 1947. The thermodynamic properties of isotopic substances. J. Chem. Soc., pp. 562-581.
- VAN HOOK, H.J., 1960. The ternary system $\text{Ag}_2\text{S}-\text{Bi}_2\text{S}_3-\text{PbS}$. Econ. Geol., V. 55, pp. 759-788.
- VINOGRADOV, A.P., 1962. The average content of chemical elements in the main types of igneous rocks of the earth. Geochemistry, pp. 164-174.
- WAHLER, W., 1956. Über die in Kristallen Engeschlossen Flüssigkeiten und Gase. Geochim. Cosmochim. Acta., V. 9, pp. 105-135.
- WALLACE, S.R., MUNCASTER, N.K., JONSON, D.C., MACKENZIE, W.B., BOOKSTROM, A.A. and SURFACE, V.E., 1968. Multiple intrusion and mineralisation at Climax, Colorado. In: Ore deposits of the United States 1933-1967, Ridge, J. (Ed), A.I.M.E., V. 1, pp. 605-640.
- WALLACE S.R., MACKENZIE, W.B., BLAIR, R.G. and MUNCASTER, N., 1978. Geology of the Urad and Henderson molybdenite deposits, Clear Creek County, Colorado, with a section on a comparison of these deposits with those at Climax, Colorado. Econ. Geol., V. 73, pp. 325-368.
- WEISSBERG, B.G., 1969. Gold-silver ore grade precipitates from New Zealand thermal waters. Econ. Geol., V. 64, pp. 95-108.
- WHALEN, J.B., 1976. Geology and geochemistry of molybdenite showing of the Ackley City batholith, Fortune Bay, Newfoundland. Unpubl. M.Sc. thesis, Memorial Univ. of Newfoundland, 267 pp.
- WHITNEY, J.A., 1975. Vapour generation in a quartz monzonite magma: A synthetic model with applications to porphyry copper deposits. Econ. Geol., V. 70, pp. 346-358.
- WHITNEY, J.A., 1977. A synthetic model for vapour generation in tonalitic magmas and its economic ramifications. Econ. Geol., V. 72, pp. 686-690.
- WIEBE, R. and GADDY, V.L., 1939. The solubility in water of carbon dioxide at 50°, 75°, and 100°C at pressures to 700 atmospheres. Am. Chem. Soc. J., V. 61, pp. 315-318.

- WIEBE, R. and GADDY, V.L., 1940. The solubility of carbon dioxide in water at various temperatures from 12° to 40° and at pressures to 500 atmospheres. *Am. Chem. Soc. J.*, V. 62, pp. 815-817.
- WILLIAMS, H., 1964. The Appalachians in northeastern Newfoundland. A two-side symmetrical system. *Am. J. Sci.*, V. 262, pp. 1137-1158.
- WILLIAMS, H., 1971. Burgeo (east half), Newfoundland. *Geol. Surv. Can.*, Map 1280, 1:250,000 scale.
- WILLIAMS, H., 1979. Appalachian orogen in Canada. *Can. J. Earth Sci.*, V. 16, pp. 792-807.
- WILLIAMS, H. and STEVENS, R.K., 1974. The ancient continental margin of eastern North America. In: *The Geology of Continental margins*, Burk, C.A. and Drake, C.L. (Eds), pp. 781-794. Springer Verlag, N.Y.
- WYLLIE, P.J. and TUTTLE, O.F., 1961. Experimental investigation of silicate systems containing two volatile components: Part II. *Am. J. Sci.*, V. 259, pp. 128-143.
- YORK, D., 1969. Least squares fitting of a straight line with correlated errors. *Earth Plan. Sci. Lett.*, V. 5, pp. 320-324.
- YPMA, P.J.M., 1963. Rejuvenation of ore deposits as exemplified by the Belledonne metalliferous province. Thesis, Univ. of Leiden, 212 pp.

APPENDIX A

ANALYTICAL AND DETERMINATIVE METHODS

A.1 SAMPLE COLLECTION AND PREPARATION

Whenever possible, a single bulk sample (of about 1 to 2 kg) was collected from representative localities (localities marked on maps 1, 2 and 3) of the various rock types. Samples collected from drill core were on average 30 cm long, or of an appropriate shorter length to ensure homogeneity of lithology. Thinsections were cut from prospective geochemical samples to determine their eligibility (e.g. freshness, etc.) for subsequent analysis.

Samples were broken into chips with a sledge hammer and scanned with a powerful magnet to reduce iron contamination from the hammer. The sample was then coned, split and quartered. One quarter was then pulverised for about two minutes in a tungsten carbide Siebtechnik swing mill to produce a powder of -100 mesh. After grinding each sample the tungsten-carbide bowl and rings were scrubbed in hot water with an abrasive silica cleanser. Contamination between different rock types was reduced by pulverising silica sand in the mill prior to a change in rock type. The powders were stored in appropriately labelled glass jars.

Chips of those samples destined for Sn and W analysis were crushed to a powder in a porcelain plate pulverisor (Bico-type UA). Further grain size reduction (-100 mesh)

was achieved by grinding in a mechanical agate grinder.

A.2 ANALYTICAL TECHNIQUES

A.2.1 Major and Minor Element Analysis

Major and minor elements were determined using a Philips 1450 fully automated X-ray fluorescence spectrometer. The unit is equipped with spectrometer/detector, X-ray generator, PDP mini computer, teletype input/output, and a self-feeding sample tray. U.S.G.S. prepared rock powders were used as standards for the calibration. D. Press of Memorial University wrote various computer programs and did the calibrations for the X-ray spectrometry. Precision and Accuracy data are given in Table A.2.1.1.

Preparation of fused disc for X-ray spectrometry:-

One-half a gram of rock powder was accurately weighed and added to a mixture of 4.0g of flux ($\text{Li}_2\text{B}_4\text{O}_7$) and 0.5g of La_2O_3 . Additional flux was added to compensate for loss on ignition of rock sample. This mixture was transferred to a previously cleaned (Conc. HCl-distilled water-heat) platinum crucible. A small amount of ammonium nitrate was added to the mixture as an oxidising agent.

The crucible was heated and agitated on a Claisse Fluxer (six samples at one time) till the sample was melted and homogeneous. The molten sample was poured onto a platinum disc mold and allowed to cool. After cooling the sample was labelled and stored in a dessicator.

Loss on ignition (H_2O , CO_2 , SO_2) was determined by weighing an amount of sample into a porcelain crucible,

heating to 1050°C for two hours, cooling in a dessicator, and weighing to determine the percent loss of volatiles.

Table A.2.1.1

Precision and Accuracy of Replicate Determinations
(21 determinations, single pellet, BCR-1)

Element	Accepted* value	Mean	Standard Deviation	Range Low High	
SiO ₂	54.85	54.18	0.151	53.91	54.42
TiO ₂	2.2	2.14	0.007	2.13	2.15
Al ₂ O ₃	13.68	13.36	0.176	13.04	13.68
Fe ₂ O ₃ **	13.52	13.44	0.058	13.35	13.56
MnO	0.19	0.17	0.004	0.16	0.18
MgO	3.49	3.51	0.043	3.44	3.60
CaO	6.98	7.00	0.020	6.94	7.03
Na ₂ O	3.29	3.27	0.065	3.15	3.37
K ₂ O	1.68	1.66	0.012	1.64	1.68
P ₂ O ₅	0.33	0.34	0.014	0.32	0.36

* Abbey, 1975.

** Total Fe.

Several samples were reanalysed by atomic absorption spectrometry (Analyst: Mrs G. Andrews). Samples were prepared using established procedures (Langmyhr and Paus, 1968) and the major elements determined on a Perkin Elmer model 370 atomic absorption spectrometer with digital readout. Several samples required dissolution in aqua regia solution, especially those containing sulphides.

Phosphorus was determined on a Bausch and Lomb Spectronic

20 Colourimeter according to a modified method after Shapiro and Brannock (1962).

A granitic rock standard (G-1) was analysed four times in a similar manner to the samples to determine the precision of the A.A.S. method.

Table A.2.1.ii
Precision of A.A.S. analysis (n=4)

Element	Published value	\bar{X}	S	Range	
				Low	high
SiO ₂	69.11	69.70	0.57	68.20	69.96
Al ₂ O ₃	15.40	15.10	0.24	14.75	15.60
Fe ₂ O ₃	2.65	2.60	0.02	2.64	2.74
MgO	0.76	0.80	0.05	0.75	0.82
CaO	1.94	2.00	0.10	1.92	2.14
Na ₂ O	4.07	4.30	0.02	4.07	4.21
K ₂ O	4.51	4.56	0.02	4.50	4.57
TiO ₂	0.50	0.50	0.01	0.47	0.51
MnO	0.03	0.03	0.0	-	-

S = standard deviation

\bar{X} = mean

* Flanagan (1970)

A.2.2 Trace Element Analysis

Trace elements were determined by X-ray fluorescence on pressed pellet discs (except Sn, W, and REE analyses) using a Philips 1450 automatic x-ray fluorescence spectrometer.

The samples were prepared in the following manner:-

1. Approximately 10g of rock powder was thoroughly

mixed with 1-1.5g of binding (Union Carbide Phenolic Resin, material TR-16933) agent.

2. This powder was pressed into a disc in a Herzog hydraulic press at a pressure of 30 tons p.s.i., for one minute.

3. The disc was baked in the oven at 200°C for 10 minutes. After cooling the discs were labelled and stored in a moisture-controlled cabinet.

The precision and accuracy of the trace element analyses were determined by analysing standard rock samples and are shown below.

Table A.2.2.i

Precision and Accuracy
XRF : Trace Elements

	V	Cr	Ni	Cu	Zn	Ga	Rb	Sr	Y	Zr	Nb	Ba	Pb
W-1	240	92	70	117	85	20	22	189	24	98	8	171	7
S	5	6	3	4	2	2	2	6	2	2	1	12	3
N	13	13	13	13	13	13	13	13	11	13	13	13	13
P	240	120	78	110	86	16	21	190	25	105	9.5	160	8
G-2	43	13	2	17	85	24	166	477	11	292	10	1865	27
S	3	3	2	1	2	1	2	7	2	3	1	30	2
N	10	10	10	10	10	10	10	10	11	10	10	10	10
P	34	9	6	11	85	23	170	480	12	300	14	1850	29

S = standard deviation
N = number of determinations
P = published values

(Flanagan, 1973)

Lithium was determined by Atomic Absorption Spectrometry (Analyst: G. Andrews). The data are estimated to be accurate to within $\pm 5\%$.

Fluorine was determined by a specific ion electrode method using an Orion Meter. Analyses were determined by the Analysis Laboratory, Dept. of Mines and Energy, Higgins Line, St. Johns, under the supervision of H. Wagenbauer. The detection limit by this method is approximately 20 ppm. Errors are estimated to be $\pm 5\%$ above 500 ppm.

A.2.3 Rare-Earth Elements

Ten REE were analysed by a modified (Fryer, 1977) version of the thin-film X-ray fluorescence procedure of Eby (1972).

Samples were prepared by the following method:-

- 1) 1 to 2 aliquots of rock powder are weighed accurately into 100 ml Teflon beakers.
- 2) Approximately 50 μ g of Tm solution (internal yield standard) is pipetted accurately into each beaker. Discard the drop in the uplift motion from the automatic pipetter.
- 3) Add a few drops of 2N HCl to dissolve carbonates.
- 4) Treat solids with 15 ml of conc HF and 2 ml HClO_4 and evaporate to dryness (at 300°C).
- 5) Treat solids again with 15 ml of conc HF and evaporate to dryness (solids are converted to AlF complexes).
- 6) 10 ml aliquots of 2N HCl and 2N HClO_4 are added and taken to dryness.
- 7) Another 10 mls of 6N HCl are added and warmed to

dissolve residue (solution should consist of soluble chlorides).

- 8) Slowly evaporate to dryness.
 - 9) After evaporation the sample is redissolved in 15 ml liquid of less than 1 N HCl (use distilled water if possible).
 - 10) Filter sample into column - let sample go through - no solution on top of resin.
 - 11) Wash beaker with 5 ml 2 N HCl - let it go through .
 - 12) Rinse filter with 2 ml 2 N HCl - let it go through.
 - 13) Remove filter being careful not to touch tip to the side.
 - 14) Wash column with about 5 ml 2 N HCl.
 - 15) Repeat, wash with 5 ml 2 N HCl.
 - 16) Add 5 ml + 70 ml 2 N HCl - the 5 ml is for protecting the resin.
 - 17) Clean column tip and stopcock - discard eluted solution (REE in resin).
 - 18) Place clean teflon beaker under column and add 5 ml 6 N HCl to equilibrate column.
 - 19) Add 5 ml + 90 ml 6 N HCl to remove REE from resin.
 - 20) Evaporate eluted solution to dryness.
-
- 21) To clean columns - wash with 50 ml 6 N HCl.
 - 22) Remove stopcocks - clean tips into clean nalgene beakers.
 - 23) Dump with 2 ml H₂O.

24) Re-equilibrate resin with distilled water in beaker and put back into column.

25) Redissolve REE eluant with approximately 20 ml of distilled H_2O .

26) Add 2 drops of conc. H_2SO_4 and warm on hot plate for 1 hour.

27) After cooling, filter into a 50 ml pyrex beaker.

28) Evaporate solution to dryness on hot plate. H_2SO_4 must be completely removed (put in oven for 2 minutes).

29) Wash sides of beaker with 5 ml of 6 N HCl and evaporate to convert sulphates to chlorides.

30) Add 15 ml of very dilute HCl (< 0.1 N). Warm to dissolve REE chlorides and then cool.

31) Add ion-exchange paper and allow to equilibrate for 24 hours.

32) Evaporate solution to dryness using infra-red lamp.

33) Store in labelled envelope until analysis

Samples were analysed on a fully automatic Philips 1450 X-ray fluorescence spectrometer using a rhodium (3000W) tube.

The data are considered accurate to $\pm 5-10\%$ or 0.1 ppm, whichever is the greater. A comparison of analyses of the standard rock BCR-1 with analyses of Flanagan (1973) shows that they fall within the estimated analytical uncertainties.

Table A.2.3.i
Accuracy of REE Determinations

	La	Ce	Pr	Nd	Sm	Eu	Gd	Dy	Er	Yb
BCR-1*	26.2	56.4	6.86	30.5	7.27	2.03	7.33	6.43	3.76	2.82
Published values	26	53.9	7	29	6.6	1.94	6.6	6.3	3.59	3.36

* average of 4 determinations.

A.2.4 Tungsten and Tin Analysis

Specially prepared (see Appendix A.1) samples were analysed by Dr B. Kronberg (University of Western Ontario) using spark source mass spectrometry. Rock powders were mixed with an equal weight of graphite and were sparked in a Jeol Mass Spectrometer (JMS-OIBM-2). Electrodes were prepared using standard procedures (Taylor, 1965). The mass spectra were detected photographically and were interpreted semi-quantitatively (Waldron, 1959) using U.S.G.S. standards (Flanagan, 1973). The data are considered accurate to within a factor of three. Thus a reading of 10 ppm has an upper and lower limit of 30 and 3 ppm respectively.

A.2.5 Electron Microprobe Analysis

Electron microprobe analyses of opaque minerals (tungstates, sulphides etc.) were done on an automated microprobe; the JEOL JXA-50A electron probe microanalyser with Krisel control through a PDP-11 computer. Operating conditions include an accelerating voltage of 15 kV, a beam current of approximately 0.3 microamps, a beam size of approximately 1-2

microns, and a counting rate of 30,000 with a default time of 30 seconds. Counts were corrected by the Krisel Magic correction program.

A selection of pure metal and mineral standards were used to calibrate the instrument. Lack of an adequate tungstate standard (pure W standard used instead) resulted in counting errors of 1.4% (2σ limits) on W. Thus analyses of wolframite/scheelite totalling between 98% and 101% were acceptable.

A.2.6 The Determination of Wolframite Composition by X-ray Diffraction Analysis

The unit cell parameters of the wolframite minerals increase almost linearly with increasing MnO content (Berman and Campbell, 1957). Measurements of the peak separations $2\theta_{111} - 2\theta_{11\bar{1}}$ (Sasaki, 1959) and $2\theta_{110} - 2\theta_{011}$ (Foster, 1973) allows the determination of the MnWO_4 component of a wolframite crystal by comparison with the experimental curves of Sasaki (1959). Peak separation was large enough for (110) and (011) peaks to allow relatively accurate reading. For all samples a minimum of four scans were completed using a Philips diffractometer, a scanning speed of 1° in 4 minutes and a chart speed of 300 mm/hr. Analyses are estimated to be accurate to within ± 6 mol% (Foster, 1973).

The data are presented in Appendix B.4.

APPENDIX B
GEOCHEMICAL DATA

B.1 GRANITOIDS

Samples from the two igneous rock suites, K-feldspar megacrystic granite (Unit 7) and leucogranite (Unit 9), are labelled MG and LSG respectively. Locations of samples are plotted on maps 1 and 2 (in map folder).

Total Fe is recorded as Fe_2O_3 except where FeO was determined. Major elements in wt%; trace elements in ppm; n.d. - not determined.

Table B.1.i.
Geochemical Data: Granitoids

SAMPLE	MG 549	MG 550	MG 544	MG 556	MG 542
SiO ₂	64.84	62.94	63.65	69.06	63.06
TiO ₂	0.73	0.79	0.87	0.52	0.86
Al ₂ O ₃	16.27	16.60	16.06	14.80	16.09
Fe ₂ O ₃	4.28	4.82	5.17	3.35	5.23
FeO	n.d.	n.d.	n.d.	n.d.	n.d.
MnO	0.09	0.09	0.10	0.07	0.08
MgO	1.33	1.55	1.90	1.00	1.92
CaO	2.79	2.99	3.23	1.97	3.20
Na ₂ O	3.72	3.50	3.55	3.08	3.57
K ₂ O	4.70	4.74	3.61	5.29	3.96
P ₂ O ₅	0.27	0.31	0.29	0.15	0.31
L.O.I.	0.93	0.89	1.99	0.28	1.93
TOTAL	99.95	99.09	100.42	99.57	100.21
Zr	297	330	356	198	348
Sr	265	264	323	147	248
Rb	212	214	127	228	153
Zn	60	70	72	50	76
Ba	804	915	724	456	836
Nb	18	13	17	12	18
Ga	20	24	19	17	24
Pb	35	37	15	39	27
Ni	6	8	11	7	15
Cr	9	7	19	13	13
V	5	89	89	48	91
Y	31	37	42	27	47
F	n.d.	1300	n.d.	840	n.d.
Li	n.d.	14	n.d.	34	n.d.
Cu	21	21	25	11	22

Table B.1.i. continued.

SAMPLE	MG 557A	MG 571	MG 557B	MG 545	MG 555
SiO ₂	68.67	63.26	67.91	64.20	67.40
TiO ₂	0.62	0.78	0.62	0.75	0.60
Al ₂ O ₃	15.06	16.38	14.75	16.10	14.60
Fe ₂ O ₃	4.18	5.10	4.07	1.63	1.42
FeO	n.d.	n.d.	n.d.	3.02	2.19
MnO	0.08	0.10	0.08	0.08	0.08
MgO	1.25	1.54	1.36	1.88	1.22
CaO	2.43	3.19	2.41	3.19	2.38
Na ₂ O	3.20	4.01	3.43	4.49	3.18
K ₂ O	4.63	4.69	4.85	2.58	4.96
P ₂ O ₅	0.18	0.29	0.17	0.30	0.19
L.O.I.	0.46	0.50	0.46	1.40	0.56
TOTAL	100.83	99.84	100.11	99.32	98.98
Zr	230	399	230	350	225
Sr	200	278	200	251	155
Rb	200	156	200	182	187
Zn	58	76	58	70	53
Ba	706	806	706	310	538
Nb	16	11	16	18	13
Ga	21	24	21	21	18
Pb	27	28	27	16	33
Ni	9	12	9	11	9
Cr	16	2	16	16	23
V	64	84	64	93	58
Y	56	37	56	32	39
F	920	n.d.	920	n.d.	960
Li	35	n.d.	35	36	37
Cu	13	19	13	22	13

Table B.1.i. continued.

SAMPLE	MG 288	LSG 552A	LSG 492	LSG 511	LSG 547
SiO ₂	65.50	74.25	74.53	74.85	75.80
TiO ₂	0.64	0.24	0.04	0.02	0.15
Al ₂ O ₃	15.50	14.10	13.66	14.68	12.83
Fe ₂ O ₃	1.74	1.60	0.78	0.48	1.01
FeO	2.46	n.d.	n.d.	n.d.	n.d.
MnO	0.11	0.03	0.03	0.02	0.02
MgO	1.62	0.40	0.27	0.12	0.26
CaO	2.81	0.59	0.92	0.64	0.36
Na ₂ O	3.31	3.01	3.31	4.23	2.26
K ₂ O	4.24	6.11	5.35	5.19	6.69
P ₂ O ₅	0.24	0.09	0.02	0.03	0.04
L.O.I.	1.15	0.50	0.26	0.36	0.36
TOTAL	99.08	100.92	99.17	100.63	99.88
Zr	244	179	48	58	82
Sr	232	88	204	144	80
Rb	194	222	159	200	270
Zn	67	35	18	18	26
Ba	776	393	768	134	329
Nb	14	8	10	20	10
Ga	19	15	17	20	14
Pb	28	57	66	75	37
Ni	14	5	-	4	5
Cr	26	12	2	5	8
V	84	16	4	4	14
Y	56	34	12	31	9
F	725	n.d.	n.d.	20*	n.d.
Li	61	n.d.	3	6	n.d.
Cu	10	10	16	16	10

* detection limit for fluorine.

Table B.1.i. continued.

SAMPLE	LSG 591	LSG 501	LSG 593	LSG 423A	LSG 513
SiO ₂	73.71	73.57	75.05	75.00	74.65
TiO ₂	0.02	0.07	0.00	0.01	0.00
Al ₂ O ₃	14.88	14.22	14.51	13.68	14.32
Fe ₂ O ₃	0.61	1.25	0.37	0.58	0.56
FeO	n.d.	n.d.	n.d.	n.d.	n.d.
MnO	0.02	0.04	0.03	0.02	0.08
MgO	0.18	0.27	0.14	0.09	0.19
CaO	1.22	1.51	1.07	0.73	0.90
Na ₂ O	4.11	3.86	4.24	4.01	3.18
K ₂ O	5.01	4.42	4.94	5.41	5.96
P ₂ O ₅	0.02	0.03	0.05	0.02	0.04
L.O.I.	0.34	0.41	0.08	0.31	0.10
TOTAL	100.12	99.65	100.48	99.86	99.98
Zr	55	75	53	55	74
Sr	180	248	73	113	121
Rb	188	104	188	196	218
Zn	19	30	15	28	18
Ba	258	624	37	197	32
Nb	16	12	9	24	9
Ga	20	17	16	19	16
Pb	50	31	52	73	76
Ni	3	-	-	1	-
Cr	12	7	-	16	7
V	-	13	-	-	-
Y	23	n.d.	29	27	28
F	n.d.	53	n.d.	23	n.d.
Li	n.d.	11	n.d.	7	4
Cu	11	9	7	10	8

Table B.1.i. continued.

SAMPLE	LSG 497	LSG 506	LSG 494	LSG 508A	LSG 592
SiO ₂	75.28	75.65	74.73	74.44	75.95
TiO ₂	0.02	0.05	0.02	0.02	0.03
Al ₂ O ₃	14.95	13.20	14.38	14.12	14.29
Fe ₂ O ₃	0.93	0.66	0.67	0.57	0.56
FeO	n.d.	n.d.	n.d.	n.d.	n.d.
MnO	0.02	0.02	0.00	0.01	0.01
MgO	0.18	0.38	0.29	0.08	0.18
CaO	2.25	0.57	0.92	1.35	1.67
Na ₂ O	4.37	4.17	3.71	4.03	4.97
K ₂ O	2.39	4.13	5.82	4.40	2.26
P ₂ O ₅	0.01	0.02	0.01	0.02	0.01
L.O.I.	0.32	0.25	0.22	0.18	0.34
TOTAL	100.72	99.10	100.77	99.22	100.05
Zr	29	96	61	53	46
Sr	316	116	231	185	269
Rb	63	104	184	158	77
Zn	15	20	17	20	17
Ba	377	595	1318	251	181
Nb	4	9	8	11	6
Ga	14	12	14	16	17
Pb	50	30	17	74	40
Ni	-	-	-	-	-
Cr	13	5	14	7	3
V	2	1	8	-	3
Y	5	10	13	14	8
F	n.d.	n.d.	n.d.	20*	n.d.
Li	n.d.	6	n.d.	6	n.d.
Cu	9	9	10	6	9

Table B.1.i. continued.

SAMPLE	LSG 423	LSG 422	LSG 414	LSG 424	LSG 508B
SiO ₂	75.20	74.45	74.20	73.90	74.60
TiO ₂	0.02	0.01	0.00	0.00	0.03
Al ₂ O ₃	13.77	14.77	14.60	13.90	14.30
Fe ₂ O ₃	0.56	0.48	0.14	0.08	0.17
FeO	n.d.	n.d.	0.28	0.59	0.29
MnO	0.02	0.02	0.05	0.03	0.02
MgO	0.07	0.14	0.11	0.15	0.08
CaO	0.72	1.37	0.91	0.84	1.40
Na ₂ O	4.07	3.88	3.77	3.67	3.94
K ₂ O	5.26	4.42	4.64	5.25	4.28
P ₂ O ₅	0.04	0.02	0.22	0.00	0.04
L.O.I.	0.31	0.33	0.46	0.32	0.21
TOTAL	100.04	99.89	99.16	98.73	99.32
Zr	50	56	52	54	53
Sr	144	276	56	115	185
Rb	180	140	159	196	158
Zn	17	16	20	25	20
Ba	139	509	25	183	251
Nb	17	6	12	23	11
Ga	17	14	19	16	16
Pb	71	73	43	75	74
Ni	-	1	3	1	-
Cr	6	7	5	7	7
V	4	3	-	3	-
Y	26	5	12	27	14
F	n.d.	n.d.	158	23	20*
Li	2	n.d.	6	n.d.	6
Cu	8	8	8	7	6

Table B.1.i. continued.

SAMPLE	LSG 517	LSG 552B
SiO ₂	74.70	73.30
TiO ₂	0.03	0.24
Al ₂ O ₃	13.70	13.80
Fe ₂ O ₃	0.15	1.75
FeO	0.33	n.d.
MnO	0.01	0.02
MgO	0.08	0.43
CaO	1.00	0.61
Na ₂ O	3.58	2.83
K ₂ O	4.96	6.17
P ₂ O ₅	0.03	0.10
L.O.I.	0.36	0.05
TOTAL	98.90	99.30
Zr	46	179
Sr	151	88
Rb	174	222
Zn	19	35
Ba	350	393
Nb	416	8
Ga	17	15
Pb	51	57
Ni	3	5
Cr	10	12
V	8	16
Y	20	34
F	n.d.	n.d.
Li	5	n.d.
Cu	8	10

B.2 COMPOSITION OF WOLFRAMITE FROM ELECTRON MICROPROBE ANALYSIS

Table B.2.i
Wolframite Composition
(wt% and Atomic Proportions)

SAMPLE	621	621	621	621	621B	621B
WO ₃	73.08	74.56	75.35	75.11	76.63	74.49
SiO ₂	.07	.04	.04	.07	.01	.01
MgO	.27	.27	.21	.30	.29	.22
MnO	11.43	10.65	10.26	11.55	11.04	11.37
CaO	.05	.03	.04	.05	.02	.05
MoO ₃	-	.07	-	-	-	-
Nb ₂ O ₅	.06	.05	-	.06	.14	.04
FeO*	12.96	13.43	14.02	12.44	12.98	12.74
TOTAL	97.91	99.11	99.93	99.59	101.11	98.94
W	.973	.980	.984	.980	.988	.980
Si	.004	.004	.004	.004	-	-
Mg	.020	.020	.016	.023	.020	.020
Mn	.496	.457	.438	.492	.465	.488
Ca	.004	-	.004	.004	-	.004
Mo	-	-	-	-	-	-
Nb	-	-	-	-	.004	-
Fe	.555	.570	.590	.523	.539	.543
TOTAL	2.051	2.031	2.035	2.027	2.016	2.035
Mn/Fe	0.89	0.80	0.74	0.94	0.86	0.80
Vein	G	G	G	G	G	G

Table B.2.i. continued.

SAMPLE	661	255	255	255A	255A	255A
WO ₃	74.27	72.61	72.83	74.23	73.59	75.02
SiO ₂	.04	.03	.04	.07	.08	.07
MgO	.25	.18	.27	.29	.18	.27
MnO	9.66	9.72	10.82	10.59	10.10	10.38
CaO	.03	.02	.07	.04	-	-
MoO ₃	-	-	-	-	.13	-
Nb ₂ O ₅	-	.07	.05	-	.07	.18
FeO	13.94	15.50	14.05	13.63	14.69	14.01
TOTAL	98.20	98.12	98.13	98.86	98.84	99.93
W	.984	.965	.965	.977	.969	.977
Si	-	-	.004	.004	.004	.004
Mg	.020	.012	.020	.023	.016	.020
Mn	.418	.422	.469	.457	.434	.441
Ca	-	-	.004	.004	-	-
Mo	-	-	-	-	.004	-
Nb	-	-	-	-	-	.004
Fe	.598	.664	.602	.578	.625	.590
TOTAL	2.020	2.063	2.063	2.043	2.051	2.035
Mn/Fe	0.70	0.64	0.78	0.79	0.69	0.75
Vein	G	4	4	4	4	4

Table B.2.i. continued.

SAMPLE	255A	255A	255A	689	79-25	249
WO ₃	75.65	73.98	74.68	73.76	74.31	74.23
SiO ₂	.03	.05	.05	.05	.09	.05
MgO	.11	.14	.20	.17	-	.15
MnO	.59	12.01	9.82	12.11	16.20	10.50
CaO	.07	.02	-	-	.02	.02
MoO ₃	-	.01	-	-	-	-
Nb ₂ O ₅	.08	.20	.02	.07	.29	.04
FeO	12.67	12.43	14.07	12.09	7.59	13.30
TOTAL	100.20	98.83	98.84	98.25	98.48	98.34
W	.984	.977	.984	.977	.984	.984
Si	-	.004	.004	.004	.004	.004
Mg	.008	.012	.016	.012	-	.012
Mn	.492	.516	.422	.523	.699	.457
Ca	.004	-	-	-	-	-
Mo	-	-	-	-	-	-
Nb	-	.004	-	-	.008	-
Fe	.531	.527	.598	.520	.324	.570
TOTAL	2.020	2.039	2.023	2.035	2.020	2.027
Mn/Fe	0.93	0.98	0.71	0.01	2.16	0.80
Vein	4	4	4	4	17	5

Table B.2.i. continued.

SAMPLE	249	684	684	165	699	699
WO ₃	74.77	74.11	73.56	74.16	74.49	73.31
SiO ₂	.04	-	.04	.02	.02	.06
MgO	.20	.17	.16	.06	.05	.04
MnO	9.96	12.56	13.02	13.95	15.44	15.03
CaO	-	.04	.02	.02	.03	.02
MoO ₃	-	-	-	-	.06	-
Nb ₂ O ₅	.10	.30	.12	.12	.18	.09
FeO	13.32	10.67	10.68	9.58	9.04	9.41
TOTAL	98.39	97.85	97.61	98.00	99.31	97.96
W	.992	.988	.980	.988	.977	.977
Si	-	-	.004	-	-	.004
Mg	.016	.012	.012	.004	.004	.004
Mn	.434	.547	.566	.605	.664	.652
Ca	-	.004	-	-	-	-
Mo	-	-	-	-	-	-
Nb	.004	.008	.004	.004	.004	.004
Fe	.570	.457	.461	.415	.383	.402
TOTAL	2.016	2.016	2.027	2.016	2.031	2.043
Mn/Fe	0.76	1.20	1.23	1.46	1.73	1.62
Vein	5	1	1	10	10	.10

Table B.2.i. continued.

SAMPLE	651	216	216	216	625	625
WO ₃	75.31	73.48	73.74	74.76	74.32	74.02
SiO ₂	.04	.07	.04	.04	-	.02
MgO	.04	.07	.10	.08	.08	.08
MnO	16.89	14.63	14.64	14.23	15.77	15.77
CaO	.02	.02	.02	.01	.04	.01
MoO ₃	-	-	-	.09	-	.00
Nb ₂ O ₅	.04	.08	-	-	.11	.10
FeO	7.80	9.90	9.64	9.86	8.37	8.37
TOTAL	100.51	98.24	98.18	99.07	98.69	98.36
W	.980	.973	.980	.984	.980	.980
Si	.004	.004	-	-	-	-
Mg	.004	.004	.008	.008	.008	.008
Mn	.719	.633	.637	.613	.680	.684
Ca	-	-	-	-	.004	-
Mo	-	-	-	.004	-	-
Nb	-	-	-	-	.004	.004
Fe	.328	.422	.414	.418	.355	.359
TOTAL	2.035	2.035	2.039	2.027	2.031	2.035
Mn/Fe	2.19	1.50	1.54	1.47	1.92	1.91
Vein	10	10	10	10	10	10

Table B.2.i. continued.

SAMPLE	625	377C	391	391	631	631
WO ₃	74.57	73.83	73.99	74.33	75.26	75.13
SiO ₂	.07	.04	.01	-	-	-
MgO	.09	.09	.05	.06	.09	.09
MnO	15.92	14.74	15.22	15.54	14.37	14.29
CaO	.07	.02	.03	.02	.02	.02
MoO ₃	-	-	.02	-	-	-
Nb ₂ O ₅	.02	.30	-	-	.05	.12
FeO	8.19	9.20	9.20	9.25	9.32	9.30
TOTAL	98.90	98.23	98.53	99.20	99.11	98.97
W	.984	.980	.980	.977	.992	.992
Si	.004	-	-	-	-	-
Mg	.008	.008	.004	.004	.008	.008
Mn	.688	.641	.660	.668	.617	.617
Ca	-	-	-	-	-	-
Mo	-	-	-	-	-	-
Nb	-	.008	-	-	-	.004
Fe	.348	.395	.395	.391	.395	.395
TOTAL	2.031	2.031	2.039	2.039	2.012	2.016
Mn/Fe	1.98	1.62	1.67	1.71	1.56	1.56
Vein	10	10	10	10	10	10

Table B.2.i. continued.

SAMPLE	631	217A	151B	583	356	627
WO ₃	74.86	74.52	74.02	74.04	74.61	73.78
SiO ₂	.06	.04	.08	.06	.04	.03
MgO	.08	.06	.07	.06	.09	.06
MnO	13.86	15.21	13.65	15.36	14.78	14.88
CaO	.02	.02	-	-	-	.05
MoO ₃	.07	-	-	-	-	-
Nb ₂ O ₅	.21	.08	.22	-	.11	.49
FeO	9.43	8.99	10.11	8.66	8.96	9.23
TOTAL	98.59	98.92	98.16	98.18	98.59	98.52
W	.988	.984	.984	.984	.988	.977
Si	.004	-	.004	.004	-	-
Mg	.008	.004	.004	.004	.008	.004
Mn	.598	.656	.594	.688	.641	.645
Ca	-	-	-	-	-	.004
Mo	-	-	-	-	-	-
Nb	.004	-	.004	-	.004	.012
Fe	.402	.383	.434	.371	.383	.395
TOTAL	2.004	2.027	2.023	2.031	2.023	2.035
Mn/Fe	1.49	1.71	1.37	1.85	1.67	1.63
Vein	10	10	10	10	10	10

Table B.2.i. continued.

SAMPLE	707	707	671	649	671A	619
WO ₃	74.79	74.10	74.27	74.80	73.72	74.27
SiO ₂	-	.17	.02	.08	.04	.06
MgO	.24	.30	.02	.11	.25	.12
MnO	12.77	10.86	15.73	11.93	13.95	15.10
CaO	.02	.88	.02	-	.02	.04
MoO ₃	-	-	.02	.07	.04	.05
Nb ₂ O ₅	-	.03	.10	-	.18	-
FeO	10.84	11.96	8.38	12.02	10.09	8.75
TOTAL	98.66	98.20	98.56	99.02	98.29	98.39
W	.988	.980	.984	.984	.977	.984
Si	-	.004	-	.004	-	.004
Mg	.020	.023	-	.008	.020	.008
Mn	.551	.469	.680	.512	.605	.652
Ca	-	.047	-	-	-	.004
Mo	-	-	-	-	-	-
Nb	-	-	.004	-	.004	-
Fe	.461	.512	.359	.512	.430	.375
TOTAL	2.020	2.035	2.027	2.020	2.035	2.027
Mn/Fe	1.29	0.92	1.89	1.0	1.41	1.74
Vein	10	10	10	10	10	10

Table B.2.i. continued.

SAMPLE	V6B	V6B	V6B	V6B	V6B	V6B
WO ₃	76.76	75.99	73.95	74.86	75.64	75.25
SiO ₂	.04	.04	.04	.02	.08	-
MgO	.11	.09	.08	.09	.06	.08
MnO	15.95	16.18	19.82	19.12	19.45	19.09
CaO	.01	.02	.01	.02	.02	-
MoO ₃	-	-	.02	-	.12	-
Nb ₂ O ₅	.15	.05	.02	.05	.12	-
FeO	8.07	8.47	4.20	4.66	4.59	4.59
TOTAL	101.09	100.84	98.14	98.82	100.08	99.02
W	.988	.984	.980	.988	.984	.992
Si	-.04	-	.004	-	.004	-
Mg	.008	.008	.008	.008	.004	.008
Mn	.672	.684	.859	.824	.828	.824
Ca	-	-	-	-	-	-
Mo	-	-	-	-	.004	-
Nb	.004	-	-	-	.004	-
Fe	.336	.355	.180	.199	.191	.195
TOTAL	2.012	2.031	2.031	2.020	2.020	2.020
Mn/Fe	2.00	1.93	4.77	4.14	4.34	4.23
Vein	6	6	6	6	6	6

Table B.2.i. continued.

SAMPLE	V6C	222	681	681	V6A	683
WO ₃	74.84	74.16	73.70	73.87	74.29	74.83
SiO ₂	.12	.01	.09	.09	.06	.08
MgO	.07	.02	.05	.06	.05	.07
MnO	18.42	21.48	19.97	19.64	18.50	17.38
CaO	-	-	.02	.02	-	.02
MoO ₃	.05	.05	-	.07	-	-
Nb ₂ O ₅	.15	.09	-	.03	.04	.03
FeO	5.88	2.50	4.14	4.13	5.14	6.70
TOTAL	99.54	98.30	97.97	97.90	98.09	99.12
W	.977	.984	.980	.984	.988	.984
Si	.008	-	.004	.004	.004	.004
Mg	.004	-	.004	.004	.004	.008
Mn	.789	.930	.867	.855	.805	.746
Ca	-	-	-	-	-	-
Mo	-	-	-	-	-	-
Nb	.004	.004	-	-	-	-
Fe	.246	.105	.176	.176	.223	.285
TOTAL	2.027	2.023	2.031	2.023	2.023	2.027
Mn/Fe	3.21	8.86	4.93	4.86	3.61	2.62
Vein	6	6	6	6	6	6

Table B.2.i. continued.

SAMPLE	V6E	V6C	V6C	680
WO ₃	74.71	73.99	73.54	73.94
SiO ₂	.03	.09	.09	.04
MgO	.05	.07	.07	.02
MnO	19.36	19.16	19.07	19.23
CaO	.02	.02	.02	.01
MoO ₃	-	.02	.14	-
Nb ₂ O ₅	.06	-	-	-
FeO	4.67	4.93	5.02	4.62
TOTAL	98.91	98.28	97.96	97.86
W	.984	.980	.977	.984
Si	-	.004	.004	.004
Mg	.004	.004	.008	.004
Mn	.836	.832	.828	.836
Ca	-	-	-	-
Mo	-	-	.004	-
Nb	-	-	-	-
Fe	.199	.211	.215	.199
TOTAL	2.023	2.031	2.035	2.027
Mn/Fe	4.20	3.94	3.85	4.20
Vein	6	6	6	6

G = Greisen Vein #10.

1? - Possible northern extension of Vein #1.

* Total Fe determined as FeO.

B.3 COMPOSITION OF SCHEELITE FROM ELECTRON MICROPROBE

ANALYSIS

Table B.3.i
Scheelite Composition
(wt% and Atomic Proportions)

SAMPLE	377C	377C	377C	377C	377C
WO ₃	78.54	78.88	79.09	79.28	78.85
SiO ₂	.04	.05	.09	.09	.06
MgO	.02	.04	.02	.04	.02
MnO	-	.03	.04	.07	-
CaO	20.15	20.25	20.54	20.58	20.37
MoO ₃	-	.06	.04	-	.06
Nb ₂ O ₅	.02	-	.03	-	-
FeO*	.09	.05	.02	-	.02
TOTAL	98.86	99.34	99.84	100.05	99.38
W	.980	.980	.977	.980	.980
Si	.004	.004	.004	.004	.004
Mg	-	.004	-	.004	-
Mn	-	-	-	.004	-
Ca	1.043	1.043	1.051	1.051	1.047
Mo	-	-	-	-	-
Nb	-	-	-	-	-
Fe	.004	.004	-	-	-
TOTAL	2.031	2.035	2.031	2.043	2.031
Vein	10	10	10	10	10
Zoned	R	R	R	R	C

Table B.3.i. continued.

SAMPLE	377C	377C	377C	621	621
WO ₃	78.97	79.74	80.05	78.03	77.32
SiO ₂	-	.03	.04	.06	.07
MgO	.01	.02	.03	.06	.07
MnO	.01	-	-	.03	-
CaO	20.44	20.33	20.58	20.06	20.54
MoO ₃	-	-	.14	-	-
Nb ₂ O ₅	.14	.10	-	.09	-
FeO*	-	.01	.03	.05	.05
TOTAL	99.58	100.23	100.86	98.37	98.06
W	.980	.984	.980	.980	.973
Si	-	-	-	.004	.004
Mg	-	-	.004	.004	.004
Mn	-	-	-	-	-
Ca	1.051	1.039	1.043	1.043	1.066
Mo	-	-	.004	-	-
Nb	.004	.004	-	-	-
Fe	-	-	-	-	.004
TOTAL	2.035	2.027	2.031	2.031	2.051
Vein	10	10	10	G	G
Zoned	C	C	C	-	-

Table B.3.i. continued.

SAMPLE	621	391	391
WO ₃	79.41	78.81	79.04
SiO ₂	.06	.02	.04
MgO	.03	.02	.06
MnO	-	.03	.06
CaO	20.30	20.34	20.18
MoO ₃	.02	.02	-
Nb ₂ O ₅	-	-	-
FeO*	.04	.03	.04
TOTAL	99.87	99.26	99.38
W	.984	.980	.984
Si	.004	-	-
Mg	.004	-	.004
Mn	-	-	.004
Ca	1.039	1.047	1.035
Mo	-	-	-
Nb	-	-	-
Fe	-	-	-
TOTAL	2.031	2.027	2.027
Vein	G	10	10
Zoned	-	-	-

G = Greisen, R = Rim, C = Core.
 * Total Fe as FeO

B.4 X-RAY DIFFRACTION ANALYSIS OF WOLFRAMITES

Table B.4.i
X-ray Diffraction Data - Wolframite

Sample No.	Vein	$2\theta_{110} - 2\theta_{011}$	Mol% MnWO_4
217	10	0.575	53 ⁺⁶
155	10	0.575	53
373	10	0.550	65
162	10	0.575	53
376	10	0.575	53
391	10	0.575	53
377	10	0.575	53
584	10	0.575	53
165	10	0.550	65
378	10	0.550	65
208	10	0.575	53
51	10	0.575	53
467	10	0.575	53
583	10	0.550	65
453	10	0.575	53
130	6	0.525	78
127	6	0.550	65
222	6	0.525	78
223	6	0.535	73
221	6	0.525	78
V6C	6	0.525	78
244	1	0.580	50
386	1	0.600	40
255	4	0.600	40
249	5	0.600	40
249A	5	0.590	45

B.5 ALTERATION GEOCHEMICAL DATA

Location of samples are plotted on maps 2 and 3 (in map folder). Total Fe is recorded as Fe_2O_3 . Density determinations were made on rock chips using a Jolly's Spring Balance.

Table B.5.i
Alteration Geochemical Data
(wt%, ppm and g/cc)

SAMPLES	64	383	2-201	9-68	9-62	9-64
Fe ₂ O ₃	-	-	3.10	2.56	2.16	-
TiO ₂	0.91	1.00	1.08	0.96	0.93	0.42
P ₂ O ₅	0.14	0.11	0.21	0.41	0.25	0.05
SiO ₂	52.93	57.59	52.90	54.30	54.60	45.40
CaO	8.94	3.04	8.57	7.62	6.44	1.86
K ₂ O	0.59	3.32	0.50	1.11	2.40	10.27
MgO	5.22	3.31	4.75	4.36	4.65	2.16
Al ₂ O ₃	17.95	18.63	17.60	17.20	17.00	29.40
FeO	-	-	5.77	5.17	8.86	-
Na ₂ O	2.49	3.58	2.93	3.27	3.05	0.23
L.O.I.	0.95	0.93	1.66	2.15	2.48	6.07
MnO	0.17	0.11	0.18	0.16	0.23	0.05
Total Fe	9.09	8.20	9.51	8.30	11.99	2.3
TOTAL	99.38	99.82	99.25	99.35	99.99	98.21
Zr	113	196	113	146	132	25
Sr	364	281	374	467	392	17
Rb	29	177	95	135	547	1968
Zn	78	82	94	89	126	42
Cu	25	13	41	27	106	24
Ba	185	692	233	289	310	478
Nb	7	16	7	9	9	10
Pb	4	16	-	13	7	-
Ni	25	54	18	9	46	67
Li	-	-	44	48	154	679
Cr	45	95	30	27	108	23
V	196	174	212	208	217	297
Y	24	30	30	33	84	227
F	-	-	950	1090	6040	23360
Ga	21	30	24	19	24	110
W	<4	<4	n.d.	n.d.	n.d.	n.d.
Sn	25	75	n.d.	n.d.	n.d.	n.d.
Density	3.009	2.982	3.038	2.950	3.285	3.379

Table B.5.i. continued.

SAMPLES	166	360	453	436	431	434
Fe ₂ O ₃	-	-	-	-	-	-
TiO ₂	0.40	0.03	0.15	0.05	0.46	0.87
P ₂ O ₅	0.06	0.03	0.08	0.02	0.25	0.18
SiO ₂	48.4	85.26	52.10	65.49	59.20	49.10
CaO	6.71	2.41	1.88	7.18	5.09	7.07
K ₂ O	7.64	2.13	6.87	3.72	5.53	7.63
MgO	2.16	0.47	1.34	0.59	1.96	4.11
Al ₂ O ₃	21.80	6.28	19.60	10.61	16.00	18.76
FeO	-	-	-	-	-	-
Na ₂ O	0.19	0.04	0.15	0.26	0.50	0.42
L.O.I.	9.80	1.93	6.30	6.65	4.67	6.06
MnO	0.05	0.02	0.54	0.02	0.09	0.10
Total Fe	1.98	1.03	5.83	5.82	4.50	4.77
TOTAL	99.21	99.63	98.84	100.41	98.00	99.07
Zr	35	8	55	8	208	95
Sr	35	4	12	10	88	32
Rb	1499	425	1463	681	1181	1748
Zn	53	38	185	30	53	73
Cu	38	490	57	38	414	142
Ba	299	63	159	96	306	264
Nb	12	8	88	11	11	11
Pb	3	124	46	-	-	-
Ni	27	3	33	13	23	34
Li	328	64	379	108	277	496
Cr	36	19	12	16	27	39
V	127	49	135	61	109	164
Y	42	11	-	44	-	-
F	60000	18760	19160	53400	32960	40000
Ga	81	31	118	41	32	37
W	n.d.	6000	n.d.	n.d.	n.d.	n.d.
Sn	n.d.	40	n.d.	n.d.	n.d.	n.d.
Density	3.056	2.800	2.897	2.812	2.980	2.958

Table B.5.i. continued.

SAMPLES	362	363	556	542	545	549
Fe ₂ O ₃	-	-	-	-	1.63	-
TiO ₂	0.08	0.49	0.52	0.86	0.75	0.73
P ₂ O ₅	0.08	0.02	0.15	0.31	0.30	0.27
SiO ₂	50.84	32.30	69.06	63.06	64.20	64.84
CaO	8.08	17.60	1.97	3.2	3.19	2.79
K ₂ O	1.35	3.39	5.29	3.96	2.58	4.70
MgO	5.67	9.44	1.00	1.92	1.88	1.33
Al ₂ O ₃	17.65	8.26	14.80	16.09	16.10	16.27
FeO	-	-	-	-	3.02	-
Na ₂ O	2.77	-	3.08	3.57	4.49	3.72
L.O.I.	1.63	16.63	0.28	1.93	1.40	0.93
MnO	0.27	0.45	0.07	0.08	0.08	0.09
Total Fe	10.68	10.98	3.35	5.23	4.98	4.28
TOTAL	100.09	99.10	99.57	100.21	99.32	99.95
Zr	72	32	198	348	350	297
Sr	439	159	147	248	251	265
Rb	252	1206	228	153	182	212
Zn	104	361	50	76	70	60
Cu	180	137	11	22	22	21
Ba	224	103	456	836	310	804
Nb	6	4	12	18	18	18
Pb	5	-	39	27	16	35
Ni	19	349	7	15	11	6
Li	102	412	34	n.d.	36	n.d.
Cr	53	1626	13	13	16	9
V	236	190	48	91	93	5
Y	15	-	27	47	32	31
F	-	23360	840	n.d.	n.d.	n.d.
Ga	21	22	17	24	21	20
W	70	40	<4	n.d.	n.d.	n.d.
Sn	5	25	25	n.d.	n.d.	n.d.
Density	3.187	2.703	2.681	2.839	2.649	-

Table B.5.i. continued.

SAMPLES	20-192	20-196	20-194	20-198	20-199
Fe ₂ O ₃	2.06	0.44	-	-	-
TiO ₂	1.07	0.86	0.18	0.20	0.20
P ₂ O ₅	0.33	0.24	0.16	0.09	0.53
SiO ₂	61.70	64.30	71.50	73.60	73.10
CaO	2.95	3.38	2.17	4.02	3.19
K ₂ O	4.57	3.28	4.23	3.82	4.41
MgO	1.79	1.82	0.59	0.66	0.77
Al ₂ O ₃	16.56	16.00	11.90	10.70	12.50
FeO	2.83	3.62	-	-	-
Na ₂ O	4.14	4.53	0.05	0.28	0.18
L.O.I.	2.01	1.85	3.97	3.72	3.82
MnO	0.13	0.16	0.14	0.08	0.08
Total Fe	5.20	4.46	3.49	2.19	0.91
TOTAL	100.08	100.47	98.40	99.38	99.69
Zr	399	326	148	143	86
Sr	294	343	24	38	27
Rb	272	265	881	770	927
Zn	68	68	618	155	33
Cu	40	32	161	175	22
Ba	843	663	214	204	192
Nb	17	17	8	10	6
Pb	66	20	39	59	-
Ni	19	19	30	28	31
Li	58	36	144	295	134
Cr	15	13	9	2	7
V	100	86	32	35	27
Y	69	65	123	109	128
F	2640	1160	18360	31360	22660
Ga	18	19	19	18	24
W	n.d.	n.d.	n.d.	n.d.	n.d.
Sn	n.d.	n.d.	n.d.	n.d.	n.d.
Density	3.073	3.018	3.002	3.137	2.955

Sample Description for Table B.5.i

64	Amphibolitic gneiss, unaltered.
383	Mica schist, unaltered.
2-201	Amphibolitic gneiss, unaltered.
9-68	Amphibolitic gneiss, unaltered. Drill core.
9-62	Mica schist, unaltered. Drill core.
9-64	Greisen envelope. Phyllic alteration zone. Drill core.
166	Greisen envelope. Phyllic alteration zone.
360	Greisen and vein. Phyllic alteration zone.
453	Greisen envelope. Phyllic alteration zone.
436	Greisen and vein. Phyllic alteration zone.
431	Greisen envelope. Biotitic alteration zone.
434	Greisen envelope. Biotitic alteration zone.
362	Greisen envelope. Biotitic alteration zone.
363	Greisen envelope. Calcic alteration zone.
556	Megacrystic granite, undeformed, unaltered.
542	Deformed megacrystic granite, unaltered.
545	Deformed megacrystic granite, unaltered.
549	Deformed megacrystic granite, unaltered.
20-192	Deformed megacrystic granite, unaltered. Drill core.
20-196	Deformed megacrystic granite, unaltered. Drill core.
20-194	Greisen envelope. Silicic alteration. Drill core.
20-198	Greisen envelope. Silicic alteration. Drill core.
20-199	Greisen envelope. Silicic alteration. Drill core.

B.6 DESCRIPTION OF SAMPLES USED IN OXYGEN ISOTOPE ANALYSIS
AND RADIOMETRIC DATING.

- 385 Quartz feldspar-molybdenite vein. Molybdenite in vugs with muscovite.
- 685 Quartz-bismuthinite vein, Vein #1, coarsely crystalline quartz with bismuthinite and muscovite in vugs.
- 687 Quartz-bismuthinite vein, Vein #5, poorly crystalline quartz with minor pyrite.
- 684 Quartz*-wolframite vein, Vein #1, sheeted veinlet, wolframite distributed unevenly within veinlet.
- 166 Greisen, Vein #10. Assemblage, quartz, muscovite, fluorite, wolframite, scheelite and pyrite.
- 436 Greisen, Vein #10. Assemblage, quartz, muscovite, fluorite, wolframite, scheelite and pyrite.
- 720 Quartz-sulphide vein, Vein #10 adit level. Quartz, clear, well formed crystals. Pyrite, chalcopyrite in vugs.
- 626 Quartz-sulphide vein, Vein #10 adit level. Late Quartz injection. White quartz with moderate development of crystal faces. Pyrite, chalcopyrite in vugs.
- 377 Quartz-wolframite vein, Vein #10, adit level. Assemblage, quartz, scheelite (zoned), wolframite and minor sulphides. Late quartz injection.
- 652 Quartz-wolframite vein, Vein #10, adit level. Assemblage, quartz, scheelite, wolframite, fluorite and muscovite.
- 651 Quartz-wolframite vein, Vein #10, adit level. Breccia vein contains a lot of wall rock xenoliths. Assemblage, quartz, wolframite, scheelite, chalcopyrite, pyrite, sericite.
- 671 Quartz-wolframite vein, Vein #10, surface. Whitish quartz with large bladed wolframite crystals intergrown with it. Pyrite minor, wolframite altered to scheelite and tungstite.

- 165 Quartz-wolframite vein, Vein #10, adit level.
Assemblage quartz-wolframite. No sulphides. Quartz milky white.
- 627 Quartz-wolframite vein, Vein #10, adit level. Early quartz injection. Assemblage, quartz, wolframite scheelite, pyrite, and chalcopyrite.
- 648 Quartz-wolframite vein, Vein #10, adit level. Early quartz injection. Assemblage-quartz, wolframite, minor pyrite, chalcopyrite.
- 623 Quartz-wolframite vein, Vein #10, adit level. Early quartz injection. Whitish quartz - vugs with pyrite and chalcopyrite. Wolframite intergrown with quartz.
- 661 Quartz-wolframite vein, Vein #10, adit level. Vein contains abundant wall rock xenoliths. Assemblage quartz, wolframite, scheelite, minor pyrite.
- 670 Quartz-wolframite vein, Vein #10, surface. Sheeted quartz vein with sulphides and muscovite in small vugs. Wolframite intergrown with quartz.
- 610 Quartz-wolframite vein, Vein #10, adit level. Sheeted quartz vein with wolframite, pyrite and chalcopyrite.
- 678 Quartz-wolframite vein, Vein #6, surface. White coarse quartz with bladed wolframite crystals and sulphides predominantly pyrite and chalcopyrite.
- 555 Coarse-grained megacrystic granite containing quartz, K-feldspar, plagioclase, biotite, sericite, and minor epidote, chlorite, opaques, sphene, and apatite. K-feldspar megacrysts are euhedral and only slightly aligned. Minor saussuritisation of plagioclase is evident.
- 556 Coarse-grained megacrystic granite containing quartz, K-feldspar, plagioclase, biotite, opaques and minor epidote, apatite, sphene and sericite. The microperthitic, euhedral, orthoclase megacrysts are not aligned. Biotite shows minor alteration to chlorite. Plagioclase is essentially fresh.

- 557 Similar to sample 556 above.
- 545 Coarse-grained megacrystic granite with an assemblage of quartz, K-feldspar, plagioclase, biotite, sphene, sericite, chlorite, opaques, and minor apatite. Orthoclase megacrysts have reddish colour and are typically twinned. There is a strong alignment of megacrysts. Deformation by ductile shearing is evident from recrystallisation of quartz and development of K-feldspar augen. Mafic minerals wrap around the megacrysts.
- 550 Similar to sample 545 but with less evidence of shearing.
- 571 Similar to sample 545.
- 415 Post-tectonic pegmatite dyke associated with aplite and leucogranite. K-feldspar and quartz occurs in graphic texture. Coarse muscovite books occur. Plagioclase in albitic and commonly altered to sericite.
- 495 Quartz diorite gneiss containing an assemblage of quartz, plagioclase, hornblende, biotite, chlorite, epidote and opaques. Hornblende is overgrown by biotite. Quartz and feldspar show evidence of some ductile shearing (recrystallisation and kinking respectively).
- 64 Amphibolitic gneiss. Mineralogy dominated by hornblende and plagioclase but also contains minor quartz, opaques and biotite. Ductile shearing evidenced by recrystallisation of quartz and growth of biotite after hornblende.
- 71 Mica schist from shear zone containing quartz, feldspar, biotite and muscovite. Mylonite texture evident with feldspar forming porphyroclasts in a fine-grained recrystallised matrix of quartz and mica. Biotite forms after hornblende which occurs sporadically as relief grains in biotite.

- 432 Greisen. Occurs as an alteration envelope to Vein
453 #10. All samples contain assemblage of muscovite,
166 fluorite, quartz and pyrite in various proportions.
390 Wolframite and scheelite occur sporadically.
444
- 206 ' Tensional quartz veins. Muscovite occurs as 0.5 - 1.0
603 cm thick selvages to these veins which contain quartz,
568 chlorite, fluorite, bismuthinite, pyrite, scheelite,
301 and rarely beryl.
- 518 Altered rock xenolith in quartz-wolframite veinlet.
Mineralogy consists of quartz, muscovite (sericite),
and pyrite.

APPENDIX C
ORE MINERALOGY

C.1. MINERAL ASSEMBLAGES

Table C.1.i
Ore Mineral Assemblages

	Wf	Sc	Ccp	Sph	Py	Po	Bm	Gn	Td	Ss	He	Ps	Hd	Mc	Cb	Mo	Mu	Hm	Tg	Bi
21			x	x	x		x	x			x	x		x						
22			x	x	x	x								x	x					
23			x	x	x						x	x		x	x		x			x
98A					x		x	x												
118A,B	x	x			x			x							x		x			x
151B	x	x	x	x	x			x				x		x						x
152					x		x									x	x			
165	x	x	x	x	x															
214					x		x	x												x
216	x	x	x	x	x			x			x									
217	x	x	x	x	x	x									x		x			
236			x	x	x		x	x												x
314					x		x		x				x			x	x			x
353	x	x			x		x													
356	x	x	x	x	x		x	x									x			
376	x	x	x		x														x	
377	x	x	x														x			
391	x	x	x	x	x			x												x
392			x	x	x			x												x

Table C.1.i. continued.

	Wf	Sc	Ccp	Sph	Py	Po	Bm	Gn	Td	Ss	He	Ps	Hd	Mc	Cb	Mo	Mu	Hm	Tg	Bi
467	x	x	x		x		x										x			x
583	x	x	x		x			x												
610			x	x											x		x			
619	x	x	x		x			x			x	x								x
621	x	x															x			
624	x	x	x	x	x			x						x						x
625	x	x	x		x			x												x
627	x	x	x		x		x	x												
631	x	x	x	x	x									x						
644B					x		x	x			x	x	x							
649	x	x	x	x	x	x														
651	x	x	x	x	x												x			
661	x	x	x		x										x					
669	x	x															x		x	
671A	x	x	x		x															
707	x	x			x		x													
Port-1					x											x				
122								x												
V6C	x		x	x	x			x		x	x	x		x						

Table C.1.i. continued.

	Wf	Sc	Ccp	Sph	Py	Po	Bm	Gn	Td	Ss	He	Ps	Hd	Mc	Cb	Mo	Mu	Hm	Tg	Bi
V6C	x	x	x	x										x						
V6E	x	x	x	x	x			x						x						x
V6A	x	x	x		x															
675	x	x			x			x			x	x		x						x
681	x	x	x	x	x			x												x
683	x	x																	x	
680	x	x	x	x	x			x												
222	x	x	x	x	x			x		x	x	x		x						x
V6B	x	x	x	x	x			x				x		x						x
529A,B			x	x	x			x												
528A,B,C			x	x	x			x							x					
249	x	x	x																x	
687	x	x																		
689	x	x																	x	
255	x	x																	x	

Wf = wolframite, Sc = scheelite, Ccp = chalcopyrite, Sph = sphalerite, Py = pyrite, Po = pyrrhotite, Bm = bismuthinite, Gn = galena, Td = tetradymite, Ss = unknown sulphosalts, He = hessite, Ps = pilsenite, Hd = hedleyite, Mc = marcasite, Cb = carbonate, Mo = molybdenite, Mu = muscovite, Hm = hematite, Tg = tungstite, Bi = bismuth.

C.2 REFLECTED LIGHT PROPERTIES OF LEAD-, BISMUTH-,
SILVER-TELLURIDES AND SULPHOSALTS

Table C.2.1
Reflected Light Properties

Mineral	Hardness	Colour	<u>Isotropic</u> <u>Anisotropic</u>	Reflectance*	Notes
Tetradymite	low < Bi_2S_3	white: with creamy yellow tint	aniso-distinct biref-wk.	> Py ≈ 55	as inclusions in annealed bismuthinite.
Pilsenite	low-v. low	white with creamy tint	aniso-wk-dist	R-60	intergrowth with Hessite
Hedleyite	low < gn > bismuth	white with creamy tint	aniso: dist- strong blue, grey and pale brown	R-60	associated with bismuth + galena + hessite
Hessite	v. low < pilsenite	grey with bluish tint	aniso: dist- strong light-blue - light-brown colours	R-40	associated with bismuth tellurides
Native Bismuth	v. low	pale white with pinkish tint	aniso: weak scratches emphasise A	R > hedleyite ≈ .70	hard to polish, scratches common, tarnishes quickly, pinkish brown colour
Pb, Bi, Ag- Sulphosalt "B"	low ≈ galena	lighter than galena	aniso-wk	R-gn	exsolution lamellae of galena
Pb, Bi, Ag- Sulphosalt "C"	low ≈ galena	lighter than galena	aniso-dist	R-gn	exsolution lamellae of galena

* estimated.

APPENDIX D
CONSTRUCTION OF GRESENS
COMPOSITION-VOLUME DIAGRAMS

The process of chemical transfer in a rock system can be represented by the following mass-action equation:

$$aA + X = bB$$

where: a = grams of parent rock A, b = grams of product rock B, X = grams of material added or removed.

The chemical transfer (Δx_n) in grams of a component n between phase A and B can be calculated from the following equation:

$$\Delta x_n = a \left((K_v x_n^B \frac{d_B}{d_A}) - x_n^A \right) \quad - \text{ (Babcock, 1973) } \quad (D-1)$$

where: K_v = ratio between final and initial volume of the rock mass.

d_A = density of parent rock.

d_B = density of product rock.

x_n^A = the weight fraction of chemical component n in rock A.

x_n^B = the weight fraction of chemical component n in rock B.

If the weight a is arbitrarily designated as 100 grams, then Δx_n becomes grams per 100 grams or weight percent.

To construct the gain/loss diagram (Camus, 1975; Ford, 1978) one assumes $K_v = 1$, i.e. that there is no change in volume during metasomatism. The Gresens composition-volume

diagrams are constructed using the equation above and substituting different values of K_v .

APPENDIX E

FLUID INCLUSION ANALYTICAL TECHNIQUES

E.1 SPECIFICATIONS AND OPERATION OF THE CHAIXMECA HEATING/
FREEZING STAGE

The Chaixmeca apparatus consists of three components:

- 1) a heating and freezing stage which is attached to an ordinary petrographic microscope stage.
- 2) a control unit which monitors the temperature of the stage and commands the heating and cooling of the stage either manually or automatically.
- 3) a pressurised liquid nitrogen container which acts both as a reservoir and feeder of the liquid nitrogen first through the control unit and then through the stage.

The system is illustrated in Figure E.1.i and operates in the temperature range $+600^{\circ}\text{C}$ to -190°C . The body of the heating freezing stage contains a heating element and an internal ring chamber that is the conduit for the cooling liquid nitrogen. A great advantage the Chaixmeca stage has over other models is the built-in condenser system, which consists of two convergent silica lenses. This arrangement permits clear observation of very small inclusions in the size 1-5 μm .

Samples are placed in the center of the top flat surface of the condenser lens close to the temperature sensor (a platinum resistance sensor measuring 100 ohms at 0°C). The sample is isolated from the atmosphere by a metallic cover

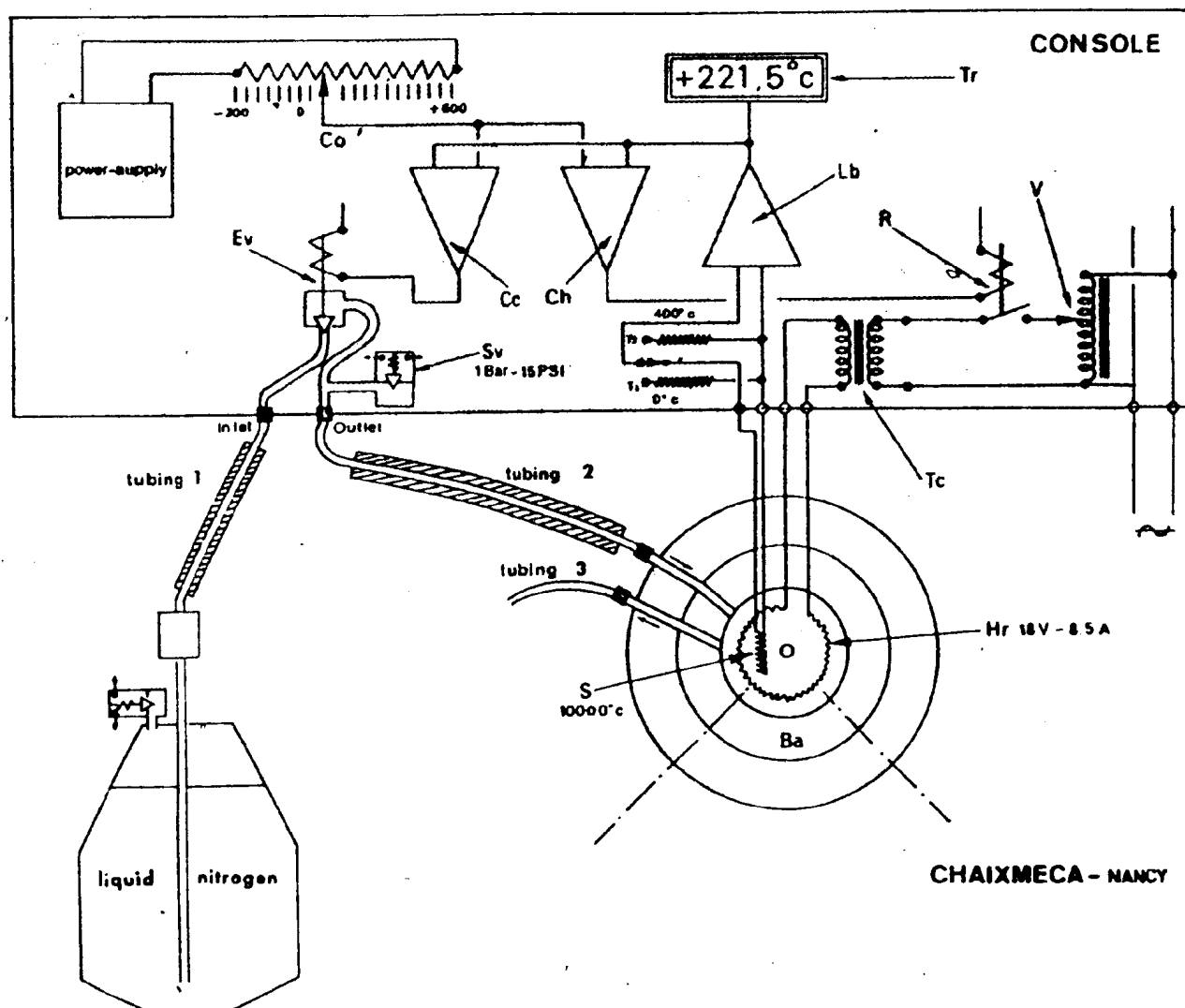


Figure E.1.i The CHAIXMECA system.

and optically polished silica window.

The electronic console commands both the heating and cooling of the stage either manually or automatically. The temperature measurements are determined by the sensor which is connected to linear bridge and a digital readout. The readout resolves the temperature to $\pm 0.1^{\circ}\text{C}$. The temperature readout is automatic but may be held at any time by activating a hold button enabling the observer to concentrate on the microscopic observation of phase changes and read the temperature later.

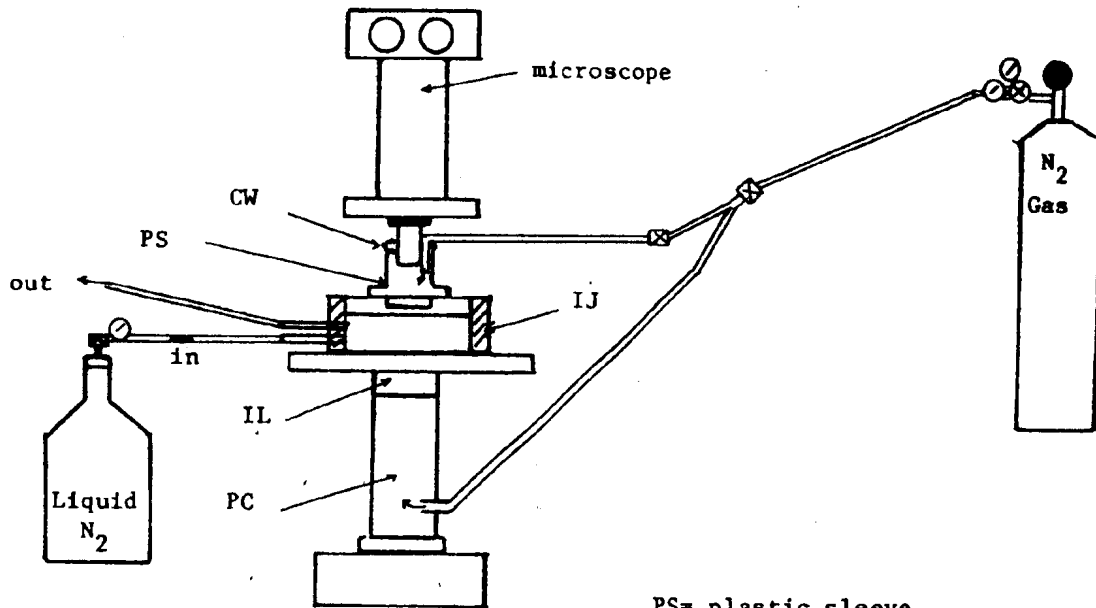
The automatic controller (C) can be used to stabilise the stage at any temperature on long duration runs but for fine temperature measurements the stage should be operated manually.

Electronic specifications for the Chaixmeca stage are given in the users manual. The control unit should be turned on 15 minutes before the operation of the stage to allow the electronics to warm up.

Operation of Stage Below 0°C

Figure E.1.ii illustrates the layout for operation of the stage below 0°C . Rapid cooling occurs by the flow of liquid nitrogen through the stage. If the exit valve of the pressurised liquid nitrogen container is open then switching on of the electronic valve in the control unit results in a flow of liquid nitrogen through the system. When there is no liquid nitrogen circulating the electronic valve must be off as it can easily be destroyed by rapid

Freezing mode.



PS= plastic sleeve
 CW= cotton wool
 IL= infrared lens
 IJ= Insulating Jacket
 PC= perspex column
 CJ= cooling jacket for lens
 SW= silica window
 H/F= heating/ freezing stage

Heating mode.

Figures not drawn to scale.

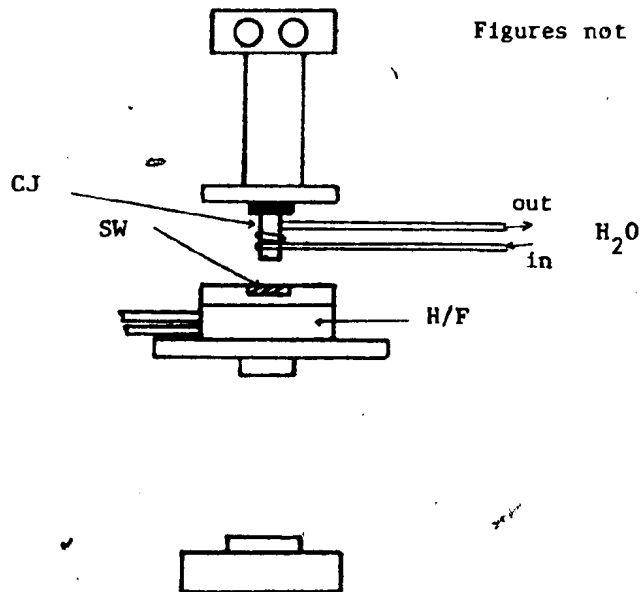


Figure E.1.ii Freezing mode/heating mode CHAIXMECA stage.

overheating.

As a result of severe ice formation on the sample, objective lens, and infra-red lens at low temperatures, some adaptations were made to the layout of the system. A flow of dry N_2 gas regulated by a needle valve was used to prevent this icing up. The gas flows into a perspex column placed beneath the infra-red lens and also into a tube which is fitted between the objective lens and the plastic sleeve. The flow of dry N_2 gas is turned on while the stage is being cooled by liquid N_2 and allows the observer to see the freezing process. When the stage is at the required temperature the liquid N_2 flow is stopped by turning off the electronic valve on the console. Warming of the stage to room temperature is achieved by equilibration with the atmosphere. The dry gas flow is continued as the stage warms up but is eventually shut off when the temperature reaches -24°C . This eliminates the extra thermal gradient induced by the gas flow when measuring the freezing point.

Operation of the Stage Above 0°C

Figure E.1.ii illustrates the layout of the stage in the heating mode. Above 30°C the plastic sleeve and the plastic tubing should be removed from the stage. The silica window is placed in position below the objective lens and a water cooled jacket is placed around the objective lens to protect it from overheating.

Heating rates especially near phase transformation points

should be quite low. A rate of less than $0.5^{\circ}\text{C}/\text{min}$ is advisable when the temperature approaches homogenisation temperature.

Clathration

Clathration was detected in type II inclusions by the following criteria:

- a) Observation of double freezing.
- b) Decrease in volume of liquid CO_2 on cooling.
(Type IIB).
- c) Motion of gas bubble on melting of gas hydrate.
- d) Irregular interface between aqueous solution and liquid or vapour CO_2 .
- e) Increase in volume or sudden reappearance of liquid CO_2 on decomposition of hydrate.

The T_m clathrate were obtained using the following procedure:

Slow heating rates of less than 0.2°C per minute were followed by rapid cooling ($2^{\circ} - 5^{\circ}$ temperature drop) near the T_m clathrate. If the clathrate is still present it will grow rapidly on cooling to deform the CO_2 gas/ H_2O fluid interface. Near the T_m clathrate the temperature is increased in steps of 0.1°C until the clathrate is melted, and a sudden drop in temperature will not nucleate it.

E.2 CALIBRATION OF CHAIXMECA STAGE

The operation of any heating/freezing stage must be done with care and with regard for possible sources of error. The greatest error is caused by thermal gradients within the

stage, especially between the sample and hot surface. Also such things as the cold microscope lens can have considerable effect on the thermal gradient characteristics of the stage.

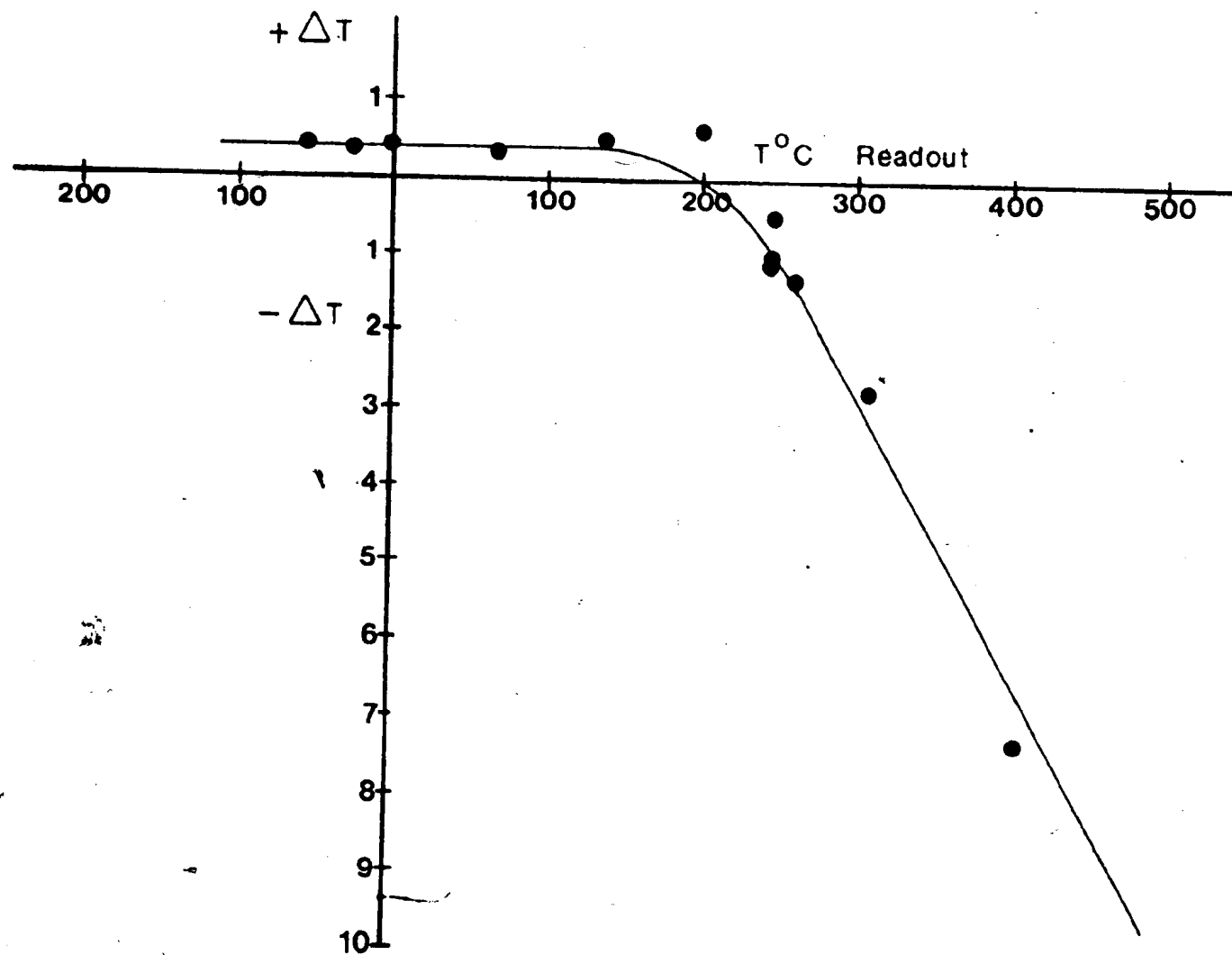
Such gradients were minimised by ensuring that during observations of phase changes (homogenisation, melting, etc.) the heating rates were less than $0.5^{\circ}\text{C}/\text{minute}$. Also centering the inclusion for each measurement ensured that steep horizontal temperature gradients within the stage were minimised. Increasing the magnification of the lens also had a similar effect on this gradient by reducing the field of view.

The Chaixmeca stage, like other instruments measuring physical or chemical quantities, must be calibrated prior to use. Ideally, during calibration runs one must be able to mimic conditions that will be operational during the running of the fluid inclusion samples. The dimension of the calibration sample should approximate the thickness of the unknown samples, and the size and shape of the inclusions.

For heating calibration crystals of organic and inorganic compounds (Tables E.2.i, E.2.ii) of known melting point were used. Chaixmeca supplies a few of these compounds but others were obtained from British Drug House (BDH), Merck Chemicals, and A.H. Thomas Co., Philadelphia, P.A.

A few crystals of the chemical standards were placed between thin glass plates (coverslip glass, thickness $150\text{ }\mu\text{m}$) of approximate $1\text{ cm} \times 1\text{ cm}$. Four thicknesses of the glass

Figure E.2.i Calibration curve for CHAIXMECA heating/freezing stage.



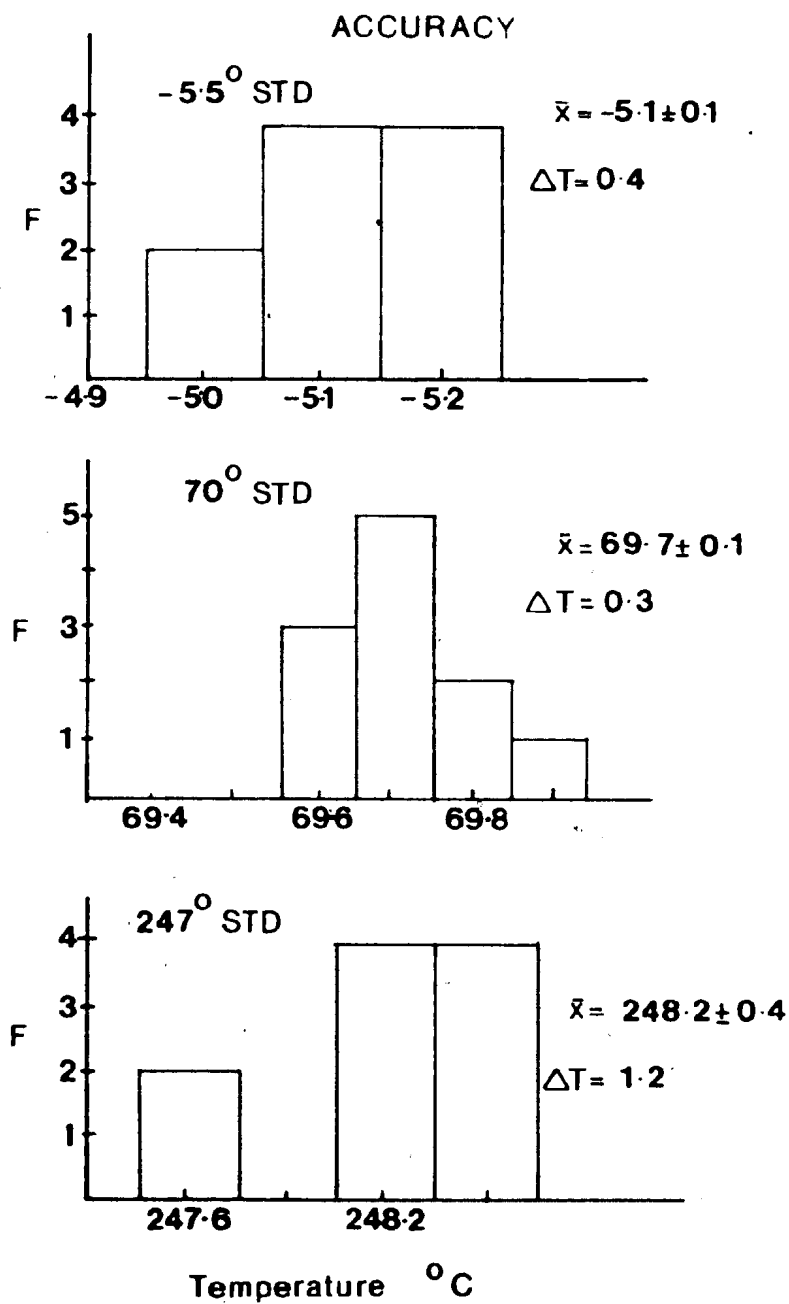


Figure E.2.ii Accuracy measurements of standard chemicals.

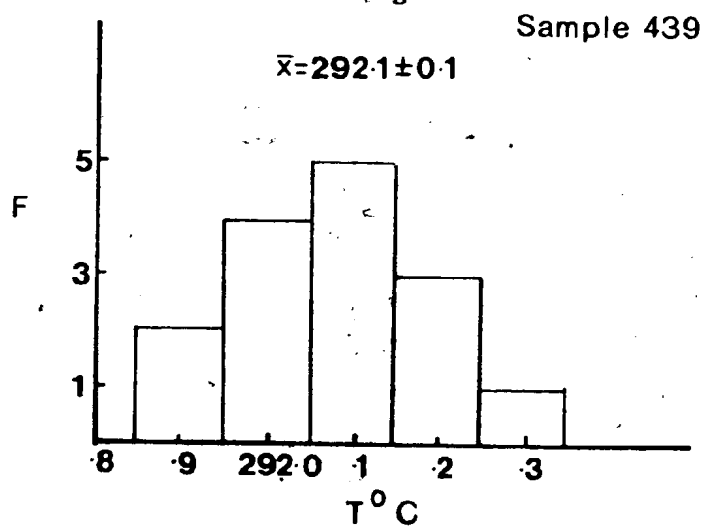


Figure E.2.iii Precision measurements on a L-V inclusion.

plates were used to obtain the approximate thickness of the unknown samples. The chemical standards were placed between the upper two plates. Because impurities lower the melting point of the chemical standards, the temperature of the last crystal to melt was used as the melting point.

Similar procedures were used to calibrate for freezing runs, the chemical standards being organic liquids (Table E.2.iii). A standard sample of quartz containing pure liquid CO_2 inclusions (supplied by Chaixmeca) was used to calibrate the stage at the temperature of -56°C , the melting point of solid CO_2 .

The combined heating and freezing calibration curve is illustrated in Figure E.2.i. Black dots mark the calibration data points, the curve being a line of best fit between them. Calibration points were checked every four months with no variation evident over that period.

Accuracy and precision measurements were made on chemical standards and a representative fluid inclusion respectively. Accuracy data for three freezing and heating standards are given in Figure E.2.ii. These data indicate that below 0°C measurements are accurate to within $\pm 0.2^\circ\text{C}$ (2 σ limits). The design of the Chaixmeca stage does not allow for control of the heating rate below -40°C thus measurements in this region are probably only accurate to $\pm 0.5^\circ\text{C}$.

Above 100°C the temperature correction curve (Figure E.2.i) was found to be a linear function of the measured

temperature. The relative uncertainty from accuracy measurements indicated an error of approximately 0.5%.

Precision measurements (Figure E.2.iii) using a L-V inclusion from sample Q-439-10 indicated a relative error of approximately $\pm 0.25^{\circ}\text{C}$ for homogenisation temperatures of 292°C .

Histogram plots of heating and freezing data (in text) used bar widths of 5°C and 0.8°C respectively, which exceeds the errors of accuracy and measurement.

E.3 PREPARATION OF FLUID INCLUSION SECTIONS

Ideally sections should be thin (0.5 - 0.2 mm) plates with both sides polished and parallel. The technique described here evolved from a series of trials with various cements, cutting and grinding procedures, and polishing techniques. By no means automated, the technique is useful, in that specimens are subjected to little thermal stress during preparation, thereby eliminating the possibility of inclusion leakage especially in low temperature minerals. The technique could be considerably automated but output in its present form is adequate running at 10-15 specimens every two days.

1. Specimen cut into 1 cm thick block measuring approximately $2\frac{1}{2}$ cm by 2 cm. Care must be taken to ensure that overheating of the specimens does not result from frictional heat produced at the cutting edge of the blade. Such overheating can decrepitate inclusions in the mineral a considerable distance from the surface. For this reason a very thin

diamond edged blade (Felker 5" OLO 5/8) and a slow cutting speed are used to minimise thermal damage.

2. The specimen block is placed on a Hillquist coarse vertical grinder and the best side is ground down 1 mm to ensure that any damage due to cutting is removed. The Hillquist grinder is water cooled but care must be taken to grind relatively slowly so as not to heat the specimen.

3. The coarsely ground side is then briefly ground by hand on the horizontal lap using 220 and 320 grits (carborundum powder). Next grind by hand on glass using 600 and 800_{µm} abrasive powders.

4. After cleaning and drying, the roughly polished side is attached to an ordinary thin section glass plate with a soluble glue - Trycolac - a liquid coverslip used as an alternative for coverslips in normal thin section preparation.

Trycolac Mk IV is distributed by Petrologic Ltd., 34 Algoma St. N., Thunder Bay, Ontario P7A 4Z3. Press the specimen firmly on the coverslip to remove any air bubbles present between specimen and glass. Allow to stand 12-24 hours to dry (do not use heat to dry!).

5. Mounted specimens are then ground on the Hillquist coarse vertical grinder till the specimen is approximately 0.6 - 0.8 mm thick (depending on the translucent properties of the mineral concerned). Grind briefly on the horizontal lap using 220 and 320 grits followed by grinding on glass with 600_{µm} and 800_{µm} powders.

6. Specimen is then polished by hand on a Unipole

U
polisher using a 1 μ m alumina powder. Polishing takes approximately 15-20 minutes/specimen for quartz.

At this stage the specimen could be used for observation of inclusions under a normal petrographic microscope. A quicker method of evaluating the suitability of specimens for later heating/freezing analysis is to omit the polishing stage (6) and use oils and a coverslip on the top surface of the specimen.

7. Those specimens deemed suitable for analysis are then placed in a Xylene solution (a covered shallow tray placed in fume cupboard is best). Leave for 5-12 hours after which time the glue should have dissolved and the specimen separated from the glass. Clean with acetone and allow to dry.

8. Remount on glass slide with Trycolac glue following step 4.

9. Briefly grind new exposed surface on horizontal lap using 220 and 320 carborundum grits followed by 600-800 μ m powders on glass.

10. Polish side, following step 6.

It is best to undertake detailed description of the fluid inclusions before removing it from the glass slide. The specimens are generally quite fragile and if removed from the glass at this stage excessive handling may result in breakage.

11. Prior to analysis on the heating/freezing stage the specimen is removed from the glass slide by immersion

in Xylene. Thoroughly clean specimen with acetone and allow to dry.

By this stage the specimen will have parallel polished sides and will be approximately 0.5 - 0.3 mm thick.

Table E.2.i

Melting Temperatures of Some Pure Organic
Compounds Suitable for Heating Stage Calibration

COMPOUND	MELTING TEMPERATURE (°C)
alpha-Napthylamine	50
Benzylidene	52
Diphenylamine	53.5
p-Dichlorobenzene	54
Phenyl benzoate	69
*Chauxmeca Std.	70
Phenylacetic acid	76
8-Hydroxyquinoline	76
Vanillin	82
m-Dinitrobenzene	89.5
Benzil	95
alpha-Napthol	96
Catechol	104
Resorcinol	112
Acetanilide	114
Benzoic acid	122
beta-Napthol	123
Urea	132
*Merck Std.	135
Phenylurea (mono)	148
Benzilic acid	150
Salicylic acid	159
Hydroquinone	170
p-Tolyurea (mono)	181
Succinic acid	185
*Merck Std.	200
3, 5 - Dinitrobenzoic acid	205
p-Nitrobenzoic acid	239
p-Chlorobenzoic acid	239
s-Diphenylurea	242
*Chauxmeca Std.	247
*BDH - Merck Std.	260
Cichonine	264
S-Di-p-tolyurea	268
s-Di-alpha-napthylurea	298
Diacetyl-p-phenylenediamine	303
*Chauxmeca Std.	306.8
NN-Diacetylbenzidine	317

* standard used in calibration

Table E.2.ii

Melting Points of Some Pure Inorganic Compounds
and Metals Suitable for Calibration of the Heating
Stage (After, Weast, 1971-1972)

COMPOUND	MELTING POINT (°C)
*Potassium dichromate (BDH Std.)	398
Lead (i) chloride	501
Barium nitrate	592
Potassium chloride	776
Sodium chloride	801
Lithium fluoride	842
Silver	960.8
Gold	1063

Table E.2.iii

Melting Temperatures of Some Pure Organic Compounds
(Liquids at Room Temperatures)
Suitable for Freezing Stage Calibration

COMPOUND	MELTING TEMPERATURE (°C)
Tetradecane	+5.86
*Water	0
*Tridecane	-5.5
N-Dodecane	-9.6
O-Xylene	-25.18
*Decane	-29.7
M-Xylene	-47.86
*Carbon dioxide	-56.6

* standard used in calibration

APPENDIX F

FLUID INCLUSION DATA

Code for Samples:

e.g. Q-439-10 (Prefix denotes mineral analysed; Q = quartz, F = fluorite, S = scheelite. First number records the sample number (locations marked on maps 2 and 3) and the second number, the vein number).

Salinity is recorded in equivalent weight% NaCl. Homogenisation is to the liquid unless otherwise stated (V = vapour, C = CO₂, H = H₂O, C.P. = critical phenomenon)

F.1 TYPE I INCLUSIONS

Table F.1.i
Microthermetric Data

SPECIMEN	Incl.#	Vol.% Vap.	Tm ice °C	Salinity%	Th °C
Q-377-10	36	15	-3.1	5.1	-
	37	20	-3.1	4.9	-
	38	15	-2.9	4.7	279
	39	22	-2.5	4.3	280
	40	25	-0.8	1.7	275
	41	15	-3.1	5.0	283
	42	15	-	-	276
	43	15	-	-	266
	44	10	-	-	220
	45	20	-	-	274
	46	15	-0.5	1.0	265
	47	15	-1.4	2.4	-
	48	18	-3.7	5.6	272

Table F.1.i continued.

SPECIMEN	Incl. #	Vol. % Vap.	Tm ice °C	Salinity ‰	Th °C
Q-377-10	49	20	-1.8	3.1	270
	50	18	-0.5	1.0	266
	51	20	-0.3	0.8	266
	52	20	-2.4	4.0	284
	53	35	0	0	312
	54	20	-2.0	3.5	285
	55	15	-2.0	3.5	259
	56	17	-2.0	3.5	277
S-377-10	57	30	-2.0	3.5	-
	58	20	-1.5	1.9	275
	59	20	-1.8	3.1	285
	60	15	-2.1	3.6	281
	61	15	-1.8	3.1	266
	62	15	-0.6	1.1	265
	63	15	-0.2	0.5	277
	64	20	-0.6	1.1	273
	65	20	-0.6	1.1	273
	66	25	-0.2	0.5	266
	67	20	-0.2	0.5	-
	68	25	-1.6	2.7	-
	69	15	-1.2	2.2	282
	70	15	-0.8	1.6	275
	71	20	-2.0	3.5	-
	72	20	-2.7	4.4	284
	73	20	-2.9	4.9	270
	74	20	-2.6	4.3	279
	75	20	-2.1	3.6	282
Q-611-10	83	15	-1.0	1.8	242
	84	10	-1.3	2.3	238
	85	10	-1.3	2.3	237
	86	10	-0.8	1.3	237

Table F.1.i continued.

SPECIMEN	Incl. #	Vol. % Vap.	Tm ice °C	Salinity ‰	Th °C
Q-611-10	87	12	-1.1	2.0	264
	88	15	-3.7	6.0	290
	89	20	-3.4	5.4	241
	90	18	-2.2	3.7	238
	91	20	-2.0	3.5	249
	92	25	-3.0	5.0	258
	93	10	-1.6	2.8	240
	94	15	-1.7	2.9	236
Q-643-10	115	20	-1.6	2.7	278
	116	20	-2.2	3.7	277
	117	22	-2.6	4.3	274
	118	15	-2.0	3.5	276
	119	12	-2.4	4.1	264
	120	20	-	-	281
	121	20	-	-	276
Q-649-10	125	20	-2.4	4.1	265
	126	15	-2.2	3.7	230
	127	20	-2.8	4.7	281
	128	5	-2.8	4.7	240
F-652-10	129	22	-3.0	5.0	245
	130	18	-3.1	5.1	260
	131	20	-3.0	5.0	250
	132	10	-2.8	4.7	210
	135	15	-2.0	3.4	263
	136	20	-2.1	3.5	266
	137	22	-2.0	3.4	272
	138	20	-1.9	3.3	271
	139	35	-2.4	4.1	265
	140	20	-	-	265
	141	25	-0.4	1.0	300

Table F.1.i continued.

SPECIMEN	Incl. #	Vol. % Vap.	Tm ice °C	Salinity ‰	Th °C
Q-652-10	142	35	-2.8	4.9	273
	143	28	-2.4	4.1	309
	144	15	-2.9	4.9	263
	145	22	-3.1	5.1	311
	146	50	-2.8	4.9	280
	147	15	-2.9	4.8	272
	148	20	-2.5	4.2	275
	149	25	-2.0	3.4	263
	150	20	-0.9	1.8	258
Q-667-10	151	10	-3.3	5.1	209
	152	5	-3.2	5.0	230
	153	10	-2.4	4.1	210
	154	7	-2.5	4.2	210
Q-669-10	165	25	-1.9	3.3	268
	166	22	-2.0	3.4	279
	167	20	-	-	270
	168	20	-	-	260
	169	22	-	-	268
Q-684-1	201	15	-	-	250
	202	10	-	-	260
	203	20	-	-	258
	204	10	-	-	256
Q-687-5	216	20	-	-	273
	217	22	-	-	275
	218	15	-3.5	5.6	264
	219	15	-3.1	5.1	263
	220	20	-	-	268
Q-244-1	237	15	-3.4	5.4	275

Table F.1.i continued.

SPECIMEN	Incl. #	Vol. % Vap.	Tm ice °C	Salinity ‰	Th °C
Q-244-1	238	15	-3.7	6.0	291
	239	25	-4.0	6.3	258
	240	15	-4.0	6.3	260
	241	10	-	-	278

F.2 TYPE IIA INCLUSIONS

Table F.2.i
Microthermetric Data

SPECIMEN	Incl. #	Vol. % Vap.	Tm ice °C	Salinity ‰	Th °C
Q-439-10	1	21	-	-	282
Q-246-1	2	25	-	-	331
	3	20	-	-	280
	4	20	-	-	284
	5	20	-	-	304
	6	20	-	-	275
	7	18	-	-	304
	8	20	-	-	308
	9	20	-	-	310
Q-709-10	10	20	-5.0	8.0	-
	11	25	-4.3	7.0	-
	12	30	-5.5	8.5	-
	13	25	-5.4	8.3	-
	14	17	-	-	314
	15	30	-	-	316
	16	25	-	-	310
	17	20	-4.4	7.0	-
	18	28	-5.8	9.0	-
	20	20	-4.5	7.1	-
	21	30	-6.5	9.5	-
	22	15	-7.2	10.7	-
	23	15	-7.0	10.4	-
	24	18	-4.9	7.7	318
	25	22	-4.5	7.1	322
	26	25	-	-	322
	27	30	-	-	300
	28	20	-	-	326
	29	30	-4.7	7.5	315

Table F.2.i continued.

SPECIMEN	Incl. #	Vol. % Vap.	Tm ice °C	Salinity%	Th °C
Q-709-10	30	70	-	-	309(G)
	32	60	-	-	315
	33	25	-5.1	7.8	303
	34	25	-6.2	9.1	304
Q-610-10	76	20	-4.8	7.4	308
	77	20	-4.7	7.2	280
	78	18	-2.9	4.8	274
	79	20	-2.8	4.7	301
	80	10	-	-	204
	81	25	-3.2	5.0	305
	82	15	-2.9	4.8	276
	95	15	-4.6	7.2	302
Q-720-10	96	15	-4.5	7.1	297
	97	5	-4.1	6.4	206
	98	15	-4.1	6.4	269
	99	5	-4.2	6.5	222
	100	7	-3.7	6.0	224
	101	8	-4.5	7.1	239
	102	15	-	-	300
	103	20	-2.9	5.0	-
	104	20	-2.9	5.0	-
	105	25	-3.9	6.3	309
	106	22	-3.9	6.3	315
	107	15	-	-	220
	108A	5	-3.7	6.0	240
	108B	50	-1.9	3.3	320
	109	15	-3.9	6.3	304
	110	20	-3.9	6.3	305
	111	15	-3.8	6.2	304
	112	25	-3.7	6.0	305
	113	28	-1.9	3.3	295
	114	10	-2.2	3.7	241

Table F.2.i continued.

SPECIMEN	Incl. #	Vol. % Vap.	Tm ice °C	Salinity ‰	Th °C
Q-720-10	122	12	-3.6	5.9	287
	123	28	-3.9	6.2	304
	124	35	-	-	316
Q-688-10	155	15	-5.4	8.3	269
	156	15	-5.2	8.0	294
	157	20	-2.4	4.1	283
	158	15	-4.4	7.0	245
	159	20	-4.9	7.6	322
	160	10	-4.1	6.4	234
	161	10	-3.7	6.0	235
	162	15	-4.1	6.4	255
	163	10	-	-	240
	164	15	-4.8	7.5	265
Q-450-10	170	30	-4.9	7.6	312
	171	20	-4.7	7.4	319
	172	20	-4.6	7.3	309
	173	25	-4.7	7.4	330
	174	20	-5.1	7.8	317
	175	30	-5.0	7.7	315
	176	20	-4.9	7.6	329
	177	20	-5.0	7.7	336
	178	35	-4.3	6.9	320
	179	25	-	-	313
	180	25	-3.5	5.6	306
	181	20	-3.9	6.2	347
	182	20	-4.4	7.0	319
	183	25	-4.0	6.3	307
	184	15	-3.4	5.3	294
	185	30	-4.2	6.4	331
	186	25	-3.9	6.2	328
	187	20	-4.0	6.3	327
	188	40	-3.9	6.2	326

Table F.2.i continued.

SPECIMEN	Incl. #	Vol. % Vap.	Tm ice °C	Salinity ‰	Th °C
Q-450-10	189	20	-3.5	5.6	311
	190	20	-4.2	6.4	303
	191	30	-4.0	6.3	300
	192	30	-4.1	6.4	324
Q-685-1	193	20	-4.9	7.6	287
	194	15	-1.9	3.3	257
	195	20	-4.4	6.9	277
	196	20	-4.4	6.9	289
	197	20	-4.7	7.5	-
	198	15	-3.5	5.6	257
	199	10	-0.5	1.0	256
	200	20	-4.9	7.6	286
	205	30	-6.0	9.2	306
	206	20	-5.9	9.1	290
Q-687-5	207	20	-6.0	9.2	289
	208	15	-	-	291
	209	10	-4.7	7.5	276
	210	15	-4.4	6.8	280
	211	20	-4.0	6.3	282
	213	20	-4.2	6.5	282
	214	20	-4.3	6.6	281
	215	15	-4.3	6.6	284
	242	7	-	-	221
	243	10	-	-	269
Q-240-1	244	7	-	-	219
	245	20	-	-	259
	246	25	-	-	266
	247	15	-	-	264

Table F.2.ii

Type IIA Inclusions - Clathrate Data

SAMPLE	Vol% Vap.	Tn °C			Tm °C			Th °C	
		CO ₂ (g)	ice	clathrate	CO ₂	ice	clathrate	Th CO ₂	Th CO ₂ +H ₂ O
Q-709-10	20	-	-48	-43	-	-4.6	+5.8	-	-
	25	-	-48	-35	-	-4.9	-	-	-
	20	-	-45	-35	-	-4.9	-	-	-
	20	-	-50	-48	-	-4.4	-	-	-
	20	-	-47	-46	-	-4.7	+6.1	-	-
	25	-	-48	-35	-	-4.9	+7.8	-	-
	30	-	-49	-35	-	-5.1	+7.6	-	-
	20	-	-52	-38	-	-5.5	+7.1	-	-
	30	-	-49	-37	-	-5.0	+7.5	-	-
Q-687-5	30	-	-	-	-	-6.0	+7.9	-	306
	25	-	-	-	-	-5.9	+7.9	-	290
	20	-	-	-	-	-6.0	-	-	289
	25	-	-	-	-	-	+7.8	-	298
	20	-	-	-	-	-4.2	-	-	282
Q-249-5	26	-	-	-	-	-	+7.6	-	272
	22	-	-	-	-	-	+7.5	-	287

F.3 TYPE IIB (AND IIB*) INCLUSIONS

Table F.3.i
Microthermetric Data

SAMPLE	Vol. % Vap. CO ₂	Tn °C			Tm °C			Th °C	
		CO ₂ (s)	ice	clathrate	CO ₂	ice	clathrate	CO ₂	CO ₂ +H ₂ O
Q-253A-3	25	-	-	-	-	-	-	+30.9	-
	15	-94	-	-	-57.0	-	+7.9	+30.4	>270*
	18	-	-	-	-	-	-	+30.3	-
	73	-100	-	-	-60.0	-	+7.1	+30.4	>275
	27	-	-	-	-	-	-	+30.9	-
	17	-103	-	-	-62.0	-	+7.2	+30.9	-
	53	-	-	-	-	-	+7.9	+30.9	-
Q-249A-5	13	-	-	-	-	-	+7.9	+31.0	-
	30	-	-	-	-	-	+7.7	-	-
	43	-	-	-	-	-	-	+30.8	-
	29	-	-	-	-	-	-	+30.8	-
	14	-	-	-	-	-	-	+30.1	-
	18	-	-	-	-	-	-	+30.9	-
	30	-	-	-	-	-	-	+30.9	-
	35	-	-	-	-	-	-	+30.1	-

Table F.3.i continued.

SAMPLE	Vol. % Vap. CO ₂	Tn °C			Tm °C			Th °C	
		CO ₂ (s)	ice	clathrate	CO ₂	ice	clathrate	CO ₂	CO ₂ +H ₂ O
Q-249B-5	18	-	-	-	-	-	-	+30.8	290 (H)
	22	-	-	-	-	-	-	+30.2	>263
	10	-	-	-	-	-	-	+30.9	>262
Q-385A	20	-	-	-	-	-	-	+30.0	-
	25	-	-	-	-	-	-	+31.0	-
	42	-	-	-	-	-	-	+31.0	-
	29	-	-	-	-	-	-	+29.6	-
	33	-	-	-	-	-	-	+30.8	-
	42	-	-	-	-	-	-	+30.5	-
	40	-	-	-	-	-	-	+30.7	-
	41	-	-	-	-	-	-	+30.7	-
Q-385B	45	-	-	-	-	-	-	+30.5	311 (CP)
	45	-	-	-	-	-	-	+30.6	>296
	40	-	-	-	-	-	-	+30.9	>296
	35	-	-	-	-	-	-	+30.8	361 (c)
	38	-	-	-	-	-	-	+30.9	>276
	45	-	-	-	-	-	-	+30.6	359 (c)
	47	-98	-	-	-60.0	-	-	+27.6	>298
	48	-100	-	-	-59.0	-	+7.1	+30.1	>284
	54	-	-	-	-	-	-	+27.6	>274

Table F.3.i continued.

SAMPLE	Vol. % Vap. CO ₂	Tn °C			Tm °C			Th °C	
		CO ₂ (s)	ice	clathrate	CO ₂	ice	clathrate	CO ₂	CO ₂ +H ₂ O
Q-385B	60	-95	-	-	-61	-	+7.0	+30.9	346 (CP)
	41	-	-	-	-	-	+7.0	+30.4	>313
	65	-	-	-	-	-	+7.6	+26.0	284 (C)
Q-385C	54	-	-	-	-	-	+7.1	+30.3	298 (C)
	48	-	-	-	-	-	+7.0	+30.4	>250
	45	-	-	-	-	-	-	+30.2	>325
	40	-	-	-	-	-	+7.2	+30.5	320 (C)
Q-385D	35	-	-	-	-	-	-	+30.8	>282
	52	-	-	-	-	-	-	+30.9	>263
	24	-	-	-	-	-	-	+30.3	>240
	54	-	-	-	-	-	-	+30.9	352 (H)
Q-385E	33	-	-	-	-	-	-	+30.3	>253
	20	-	-	-	-	-	-	+30.2	330 (H)
	21	-	-	-	-	-	-	+30.7	>323
	25	-	-	-	-	-	-	+30.7	>289
	313	-	-	-	-	-	-	+30.9	>295
Q-253A-3	20	-98	-	-	-59.2	-	-	+30.0	-
	40	-	-	-	-	-	-	+28.6	>230

Table F.3 i continued.

SAMPLE	Vol. % Vap. CO ₂	Tn °C			Tm °C			Th °C	
		CO ₂ (s)	ice	clathrate	CO ₂	ice	clathrate	CO ₂	CO ₂ +H ₂ O
Q-385F	40	-	-	-36	-	-	+7.1	+30.9	-
	45	-104	-	-33	-58.1	-	+7.5	+30.9	-
	35	-	-	-	-	-	+7.4	+30.9	-
	60	-	-	-	-	-	+7.1	+39.8	-
	35	-	-	-	-	-	+7.0	+30.8	-
Q-709-10	80	-107	-	-32	-58.2	-	+8.7	+21.5(V)	-
	80	-94	-	-30	-57.5	-	+10.0	+20.5(V)	308.6(H)
	30	-	-50	-42	-	-4.9	+9.1	+17.4(V)	-
	40	-	-	-31	-	-	+9.0	+17.9(V)	-
	50	-	-52	-30	-	-	+9.1	+17.6(V)	-

* decrepitated.

F.4 TYPE IIC INCLUSIONS (ASSOCIATED WITH TYPE IIB INCLUSIONS)

Table F.4.i
Microthermetric Data

SAMPLE	Vol% Vap.	Tm °C			Th °C	
		CO ₂	ice	clathrate	CO ₂	H ₂ O+CO ₂
Q-249-5	18	-	-	-	-	-
	26	-	-	+7.6	-	272
	22	-	-	+7.5	-	287
Q-385	20	-	-	-	-	261
Q-687-5	30	-	-6.0	+7.9	-	306
	25	-	-5.9	+7.9	-	290
	20	-	-6.0	-	-	289
	25	-	-	+7.8	-	298
	20	-	-4.2	-	-	282
Q-709-10	30	-	-	+5.4	-	-
	80	-	-	+10	-	309
	75	-	-	-	-	315
Q-249-5	20	-	-	-	-	283
	22	-	-	-	-	275
Q-246-1	20	-	-	-	-	304
Q-709-10	17	-	-	-	-	316
	20	-	-4.4	-	-	-
	30	-	-6.5	-	-	-
	18	-	-4.9	-	-	318
Q-249-5	20	-	-	-	-	290
	23	-	-	-	-	283
Q-709-10	20	-	-	-	-	323
	26	-	-	-	-	317
	20	-	-	-	-	297
	25	-	-	-	-	325

Table F.4.i continued.

SAMPLE	Vol% Vap.	Tm °C			Th °C	
		CO ₂	ice	clathrate	CO ₂	H ₂ O+CO ₂
Q-709-10	25	-	-	-	-	286
Q-385	15	-	-	-	-	215
	20	-	-	-	-	30
	20	-	-	-	-	290
	25	-	-	-	-	324
	20	-	-	-	-	302
Q-709-10	30	-	-	-	-	339
	15	-	-	-	-	294
	20	-	-	-	-	320

Table F.4.ii
Type IIC - Clathrate Data

SAMPLE	Vol% Vap.	Tn °C			Tm °C			Th °C	
		CO ₂	ice	clathrate	CO ₂	ice	clathrate	CO ₂	CO ₂ +H ₂ O
Q-709-10	30	-	-50	-30	-	-4.9	+7.1	-	-
	25	-	-47	-35	-	-4.5	+7.0	-	-
	20	-	-44	-37	-	-4.6	-	-	-
	25	-	-48	-35	-	-4.7	+7.0	-	-
	20	-	-49	-39	-	-4.8	+7.1	-	-
	20	-	-49	-37	-	-4.6	+7.0	-	-
	30	-	-47	-37	-	-4.8	-	-	-
	20	-	-50	-41	-	-4.6	+7.1	-	-
	20	-	-	-	-	-	-	-	-
	20	-	-47	-35	-	-4.8	+7.4	-	-
	30	-	-44	-38	-	-4.4	+7.1	-	-
	32	-	-49	-39	-	-4.5	+6.8	-	-
	35	-	-49	-37	-	-4.7	+7.4	-	-
	40	-	-45	-37	-	-4.9	+7.3	-	-

F.5 TYPE I, GALENA #1 VEIN

Table F.5.i
Microthermetric Data

	Vol. % Vapour	Th °C
Q-528	45	346
	22	200
	20	254
	35	255
	22	308
	35	308
	30	345
	30	307
	35	332
	35	363
	36	368
	30	323
	12	279
	15	198
	15	195
	15	196
	15	198
	15	203
	15	201

APPENDIX G

EQUILIBRIUM TEMPERATURES ($^{\circ}\text{C}$) OF $\text{NaCl-H}_2\text{O}$ SOLUTIONS (5-30 WEIGHT% NaCl) AS A FUNCTION OF FLUID DENSITY AND PRESSURE (From Rich, 1975)

NOTE: Fluid densities were calculated from the data given by Lemmlein and Klevtsov (1961) and Washburn (1926-1930).

Table G.i
P-T-Density Data

5 WEIGHT% NaCl SOLUTION P (atm)

	<u>250</u>	<u>500</u>	<u>750</u>	<u>1000</u>	<u>1250</u>	<u>1500</u>	<u>1750</u>
.95	169	189	209	229	250	269	288
.93	197	218	238	259	280	300	319
.90	222	242	263	284	305	325	345
.88	244	264	285	307	329	349	370
.85	263	284	306				
.82	282	303	325	348	370	370	392
.80	298	320	343	367	391	393	415
.77	313	336	361	386	410	414	437
Fluid p .75	326	351	377	403	428	434	459
(g/cc) .72	337	364	392	419	445	453	478
.70	349	376	406	434	462	472	498
.67	359	388	420	450	480	490	519
.64	366	398	431	465	497	511	
.62	374	408	446	482	518		
.60	381	419	459	499			
.57	387	430	474	516			
.54		443	489				
.52		458	505				

Table G.i continued.

		10 WEIGHT% NaCl SOLUTION						
		P (atm)						
		<u>250</u>	<u>500</u>	<u>750</u>	<u>1000</u>	<u>1250</u>	<u>1500</u>	<u>1750</u>
Fluid p (g/cc)	1.00	172	192	212	232	252	272	292
	.96	205	226	247	268	288	308	329
	.94	231	253	275	297	318	340	360
	.91	255	277	301	324	347	370	391
	.88	277	300	325				
	.86	296	321	346	372	386	395	419
	.83	313	339	365	392	417	421	445
	.80	329	356	383	411	437	443	468
	.78	344	373	400	428	456	464	491
	.75	358	387	416	445	475	484	511
	.72	370	401	431	462	492	503	
	.70	381	412	445	477	508	522	
	.67	390	424	458	493	525		
	.62		431	467	503			

		15 WEIGHT% NaCl SOLUTION						
		P (atm)						
		<u>250</u>	<u>500</u>	<u>750</u>	<u>1000</u>	<u>1250</u>	<u>1500</u>	<u>1750</u>
Fluid p (g/cc)	1.03	175	195	216	237	258	280	299
	1.00	209	231	253	275	296	318	339
	.97	238	261	283	306	328	350	372
	.94	266	289	312	335	359	382	403
	.92	290	314	339				
	.89	312	336	362	386	411	409	432
	.86	330	356	381	408	433	435	460
	.83	349	375	401	429	455	459	482
	.80	364	393	419	446	476	480	506
	.78	378	407	436	465	495	501	
	.75	392	423	452	480	513	522	

Table G.i continued.

20 WEIGHT% NaCl SOLUTION

		P (atm)						
		250	500	750	1000	1250	1500	1750
Fluid p (g/cc)	1.06	178	199	221	243	265	287	308
	1.04	213	235	258	280	303	325	348
	1.01	245	268	291	314	337	359	383
	.98	276	299	322	345	369	391	415
	.95	303	327	351				
	.92	328	350	375	400	423	441	445
	.89	348	372	397	422	446	446	471
	.86	368	393	413	445	469	470	515
	.83	384	410	436	464	490	495	520
	.80	398	426	453	480	509	516	

25 WEIGHT% NaCl SOLUTION

		P (atm)						
		250	500	750	1000	1250	1500	1750
Fluid p (g/cc)	1.10	181	203	226	247	269	292	312
	1.07	217	239	262	285	308	332	354
	1.04	251	275	298	321	345	368	392
	1.01	286	309	332	356	381	404	428
	.98	316	341	365				
	.95	344	368	392	418	439	438	462
	.92	365	389	413	440	465	465	492
	.89	385	410	434	462	487	489	
	.86	399	425	450	482	508	512	

30 WEIGHT% NaCl SOLUTION

		P (atm)						
		250	500	750	1000	1250	1500	1750
Fluid p (g/cc)	1.13	184	207	229	250	273	296	316
	1.10	221	244	265	290	313	336	360
	1.07	258	281	304	327	353	376	399
	1.04	296	319	342	367	392	416	441
	1.01	332	355	379				
	.98	362	386	411	436	462	454	479
	.95	382	407	431	458	483	486	511
	.92	401	427	453	479	505	509	

APPENDIX H

CALCULATED SPECIFIC VOLUMES (cc/g)

OF IDEAL CO₂-H₂O MIXTURES (x_{CO_2} = 0.100 TO 0.900)

FOR TEMPERATURES 50-500°C AND TOTAL PRESSURES 200-4000 BARS

(From Rich, 1975)

Note: Calculations were performed using the data of
Burnham et al., (1969), Juza et al., (1965),
Kennedy (1954), and Kennedy and Holser (1966).

Table H.i
 $x_{\text{CO}_2} = 0.100$

P_t (bars)

T ($^{\circ}\text{C}$)	<u>200</u>	<u>400</u>	<u>600</u>	<u>800</u>	<u>1000</u>	<u>1400</u>	<u>1500</u>	<u>2000</u>	<u>2500</u>	<u>3000</u>	<u>3500</u>	<u>4000</u>
50	1.061	1.014	.9913	.9757	.9639	.9442	.9408					
100	1.257	1.088	1.046	1.021	1.004	.9786	.9738	.9495				
150	1.502	1.191	1.116	1.080	1.055	1.022	1.014	.9859	.9631			
200	1.720	1.310	1.201	1.148	1.116	1.072	1.063	1.028	1.000	.9778		
250	1.934	1.447	1.299	1.229	1.186	1.130	1.119	1.076	1.043	1.016	.9932	
300	2.180	1.607	1.418	1.326	1.268	1.196	1.182	1.129	1.089	1.057	1.031	1.008
350	2.572	1.825	1.574	1.448	1.372	1.274	1.255	1.189	1.141	1.102	1.071	1.045
400	9.204	2.224	1.798	1.609	1.502	1.366		1.256	1.197	1.152	1.115	
450	11.49	3.650	2.203	1.848	1.671	1.482		1.334	1.260	1.206	1.162	
500	13.23	5.278	2.927	2.204	1.903	1.621						

Table H.1 continued.

$$x_{\text{CO}_2} = 0.200$$

P_t (bars)

<u>T (°C)</u>	<u>200</u>	<u>400</u>	<u>600</u>	<u>800</u>	<u>1000</u>	<u>1400</u>	<u>1500</u>	<u>2000</u>	<u>2500</u>	<u>3000</u>	<u>3500</u>	<u>4000</u>
50	1.106	1.028	.9944		.9560	.9298	.9255					
100	1.430	1.137	1.069		1.007	.9716	.9651	.9345				
150	1.830	1.286	1.163		1.069	1.022	1.012	.9754	.9470			
200	2.171	1.454	1.272		1.142	1.079	1.066	1.021	.9871	.9603		
250	2.488	1.640	1.395		1.220	1.142	1.126	1.071	1.031	.9991	.9733	
300	2.713	1.839	1.533		1.310	1.211	1.192	1.126	1.078	1.041	1.011	.9854
350	3.252	2.082	1.702		1.417	1.290	1.267	1.185	1.129	1.086	1.051	1.022
400	8.608	2.463	1.924		1.545	1.380		1.250	1.182	1.133	1.093	
450	10.53	3.659	2.288		1.703	1.489		1.322	1.241	1.184	1.137	
500	12.01	5.040	2.901		1.910	1.616						

Table H.1 continued.

$$x_{\text{CO}_2} = 0.400$$

 P_t (bars)

T ($^{\circ}\text{C}$)	<u>200</u>	<u>400</u>	<u>600</u>	<u>800</u>	<u>1000</u>	<u>1400</u>	<u>1500</u>	<u>2000</u>	<u>2500</u>	<u>3000</u>	<u>3500</u>	<u>4000</u>
50	1.171	1.050	.9986	.9673	.9444	.9088	.9032					
100	1.680	1.208	1.102	1.048	1.011	.9620	.9528	.9130				
150	2.307	1.425	1.231	1.144	1.089	1.022	1.009	.9599	.9243			
200	2.824	1.665	1.377	1.251	1.178	1.088	1.070	1.010	.9680	.9349		
250	3.291	1.919	1.533	1.270	1.159	1.136	1.064	1.014	.9750	.9437		
300	3.742	2.176	1.701	1.491	1.372	1.233	1.207	1.120	1.061	1.017	.9820	.9514
350	4.234	2.455	1.888	1.629	1.484	1.314	1.283	1.179	1.111	1.061	1.021	.9877
400	7.751	2.808	2.107	1.785	1.608	1.402		1.241	1.161	1.106	1.060	
450	9.141	3.657	2.410	1.979	1.749	1.500		1.304	1.212	1.512	1.100	
500	10.25	4.590	2.863	2.230	1.920	1.608						

Table H.1 continued.

$$x_{\text{CO}_2} = 0.600$$

P_t (bars)

T ($^{\circ}\text{C}$)	<u>200</u>	<u>400</u>	<u>600</u>	<u>800</u>	<u>1000</u>	<u>1400</u>	<u>1500</u>	<u>2000</u>	<u>2500</u>	<u>3000</u>	<u>3500</u>	<u>4000</u>
50	1.215	1.064	1.002	.9634	.9357	.8944	.8875					
100	1.853	1.257	1.126	1.057	1.014	.9554	.9444	.8985				
150	2.636	1.521	1.278	1.170	1.104	1.022	1.006	.9494	.9081			
200	3.276	1.810	1.449	1.293	1.204	1.094	1.073	1.004	.9542	.9167		
250	3.847	2.112	1.628	1.423	1.305	1.170	1.143	1.059	1.002	.9580	.9232	
300	4.377	2.408	1.816	1.558	1.414	1.248	1.217	1.117	1.050	1.001	.9619	.9289
350	4.918	2.712	2.016	1.702	1.530	1.330	1.294	1.175	1.098	1.044	1.001	.9643
400	7.156	3.047	2.234	1.856	1.656	1.416		1.234	1.146	1.087	1.038	
450	8.179	3.654	2.495	2.033	1.781	1.507		1.292	1.193	1.130	1.075	
500	9.036	4.305	2.837	2.240	1.927	1.603						

Table H.1 continued.

$$x_{\text{CO}_2} = 0.800$$

P_t (bars)

T ($^{\circ}\text{C}$)	<u>200</u>	<u>400</u>	<u>600</u>	<u>800</u>	<u>1000</u>	<u>1400</u>	<u>1500</u>	<u>2000</u>	<u>2500</u>	<u>3000</u>	<u>3500</u>	<u>4000</u>
50	1.248	1.075	1.004	.9608	.9299	.8838	.8763					
100	1.980	1.293	1.142	1.065	1.016	.9505	.9382	.8876				
150	2.878	1.591	1.312	1.189	1.114	1.022	1.004	.9415	.8967			
200	3.605	1.916	1.502	1.324	1.222	1.099	1.075	.9977	.9446	.9039		
250	4.251	2.253	1.672	1.464	1.330	1.178	1.149	1.055	.9933	.9461	.9083	
300	4.844	2.527	1.901	1.608	1.446	1.259	1.225	1.114	1.042	.9889	.9474	.9119
350	5.416	2.901	2.110	1.756	1.564	1.342	1.302	1.172	1.089	1.031	.9856	.9469
400	6.722	3.223	2.326	1.909	1.783	1.427		1.228	1.135	1.073	1.022	
450	7.475	3.654	2.556	2.072	1.805	1.513		1.282	1.178	1.113	1.056	
500	8.150	8.812	2.819	2.248	1.932	1.599						

Table H.1 continued.

$$X_{\text{CO}_2} = 0.900$$

P_t (bars)

T ($^{\circ}\text{C}$)	<u>200</u>	<u>400</u>	<u>600</u>	<u>800</u>	<u>1000</u>	<u>1400</u>	<u>1500</u>	<u>2000</u>	<u>2500</u>	<u>3000</u>	<u>3500</u>	<u>4000</u>
50	1.261	1.079	1.004	.9598	.9274	.8796	.8718					
100	2.031	1.308	1.149	1.068	1.017	.9483	.9356	.8832				
150	2.974	1.620	1.326	1.197	1.118	1.022	1.004	.9384	.8918			
200	3.739	1/960	1.523	1.336	1.230	1.101	1.076	.9956	.9407	.8986		
250	4.417	2.310	1.727	1.481	1.340	1.182	1.151	1.054	.9898	.9410	.9023	
300	5.034	2.648	1.935	1.628	1.458	1.263	1.228	1.113	1.038	.9839	.9414	.9048
350	5.618	2,977	2.148	1.778	1.577	1.347	1.306	1.171	1.086	1.026	.9792	.9400
400	6.546	3.293	2.365	1.930	1.696	1.431		1.226	1.131	1.067	1.015	
450	7.192	3.651	2.581	2.088	1.814	1.515		1.279	1.173	1.107	1.049	
500	7.786	4.017	2.812	1.150	1.934	1.598						

REFERENCES

- ABBEY, S., 1968. Analysis of rocks and minerals by atomic absorption spectroscopy. Pt. 2. Determination of Tot. Fe, Mg, Ca, Na, and K. Geol. Surv. Canada. Paper 68-20, 21 p.
- BERMAN, J. and CAMPBELL, W.J., 1957. Relationship of composition to thermal stability in the huebnerite-ferberite series of tungstates. U.S. Bureau of Mines, Rept. Investigation, 5300, 18 p.
- BURNHAM, C.W., HOLLOWAY, J.R. and DAVIS, N.F., 1969. The specific volume of water in the range 1000 to 8900 bars, 200 to 900°C. Am. J. Sci., V. 267A, pp. 70-95.
- EBY, G.N., 1972. Determination of rare-earth, yttrium and scandium abundances in rocks and minerals by an ion exchange-X-ray fluorescence procedure. Anal. Chem., V. 44, pp. 2137-2143.
- FLANAGAN, F.J., 1970. Sources of geochemical standards - II. Geochim. Cosmochim. Acta., V. 34, pp. 121-125.
- FLANAGAN, F.J., 1973. 1972 values for internal geochemical reference standards. Geochim. Cosmochim. Acta., V. 37, pp. 1189-1200.
- FOSTER, R.P., 1973. Some aspects of the geochemistry of tungsten. Unpubl. Ph.D. thesis, Univ. of Manchester, 242 p.
- FRYER, B.J., 1977. Rare earth evidence in iron formation for changing oxidation states. Geochim. Cosmochim. Acta., V. 41, pp. 361-367.
- JUZA, J., KMONICEK, V. and SIFNER, O., 1965. Measurement of the specific volume of CO₂ in the range 700 to 4000 bars and 50° to 475°. Physica, V. 31, pp. 1735-1744.
- KENNEDY, G.C., 1954. Pressure-volume-temperature relations of CO₂ at elevated temperature and pressure. Am. J. Sci., V. 252, pp. 225-241.
- KENNEDY, G.C. and HOLSER, W.T., 1966. Pressure-volume-temperature and phase relations of water and CO₂. In: Handbook of Physical Constants, Clark, S.P. (Ed), Geol. Soc. Am., Memoir 97, pp. 383.

- LEMMLEIN, G.C. and KLEVTSOV, P.V., 1961. Relations among the principal thermodynamic parameters in a part of the system $H_2O-NaCl$. *Geochem.*, V. 2, pp. 148-158.
- RICH, R.A., 1975. Fluid inclusions in metamorphosed Paleozoic rocks of eastern Vermont. Unpubl. Ph.D. thesis, Harvard University, 299 p.
- SASAKI, A., 1959. Variation in unit cell parameters in wolframite series. *Miner. J.*, V. 2, pp. 375-396.
- SHAPIRO, L. and BRANNOCK, W.W., 1962. Rapid analysis of silicate carbonate and phosphate rocks. U.S. Geol. Surv., Bull. 1144A, pp. 31A-3.
- TAYLOR, S.R., 1965. Geochemical analysis by spark source mass spectrometry. *Geochim. Cosmochim. Acta.*, V. 29, pp. 1246-1261.
- WASHBURN, E.W., 1926-1930. International critical tables of Numerical data, physics, chemistry and technology. McGraw-Hill Book Co., N.Y., 1120 p.
- WEAST, R.C., 1977-1978. Handbook of chemistry and physics. 58th Edition. The Chemical Rubber Co., Cleveland, Ohio, 642 p.



COMPOSITE LONGITUDINAL SECTION

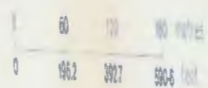
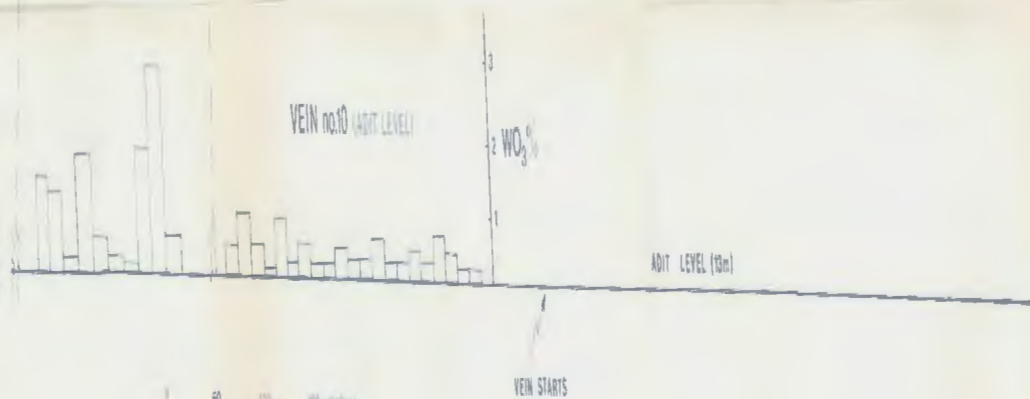
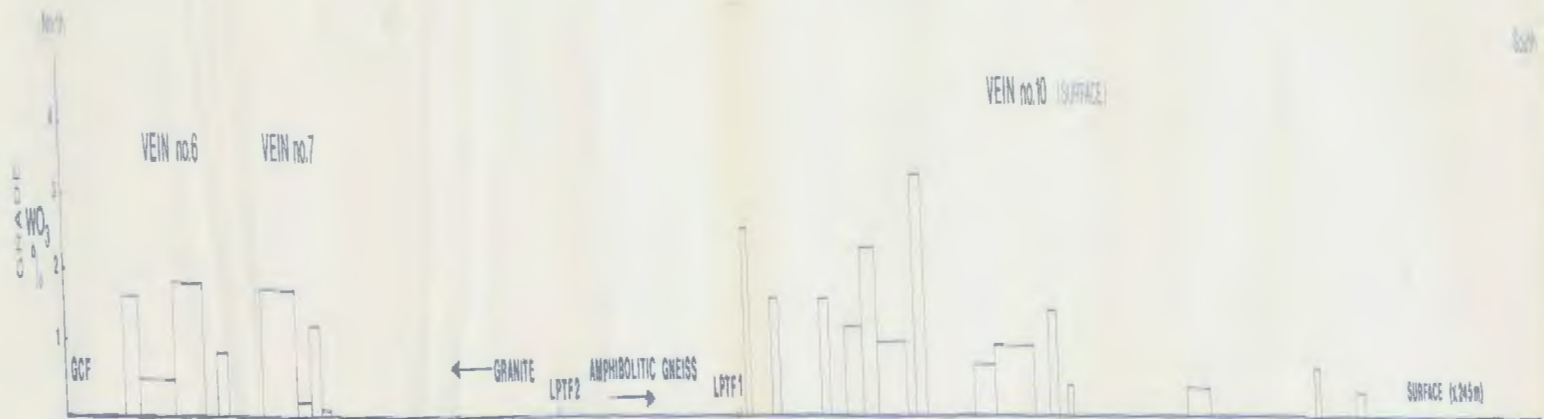


Figure 55: Comparison of wussy data (Vein 10 and 11)

The Geology Of The Grey River Area

MAP 1

Geology after Bahyrycz (1957) Modified by N.C. Higgins -1980-

Legend

Symbols

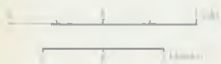
DEVONIAN-CARBONIFEROUS
POST TECTONIC

DEVONIAN
LATE TECTONIC

PRE-DEVONIAN
SYNTECTONIC

- 10 Diabase dykes
- 9 Leucogranite (aplite, pegmatite, two-mica leucogranite)
- 8 Composite dykes (pegmatite, diorite, alaskite)
- 7 K-feldspar megacrystic granite, 7a: sheared, 7b: undeformed
- 6 Mafic to intermediate dykes
- Peridotite
- 4 Leucogranite, Orthoquartzite (mylonite, ribbon mylonite)
- 7c Metaconglomerate (?) Calcareous Schist (?)
- 3c Phyllite (Ultramylonite)
- 3b Mica Schist (Mylonite)
- 2a Amphibolitic gneiss (sugen gneiss)
- 1 Quartz diorite gneiss, diorite gneiss
- 1 Tonalitic gneiss

- Geologic boundary (defined, assumed, gradational)
- Schistosity, Gneissosity, Cleavage, Foliation (inclined, vertical, unknown dip)
- Lineation
- Fault
- Vein
- Diabase dyke
- MINERAL
wolframite, scheelite
galena
molybdenite
- Adit
- LPTF Long Pond Twin Fault 1&2
- GCF Granite Cliff Fault
- Sample location
- Houses
- Lake
- Bog





COMPOSITE ADIT PLAN: VEIN NUMBER 10

Map 3

GEOLOGY BY N.C. HIGGINS 1980

Fracture (solid line) - 10'

Vein

Graben

Graben - 10'

Concentric veins - secondary joint

Amphibolite - 10' - 20'

Orthoquartzite, Foliated Schistosity

Joint strike dip (inclined vertical)

Strike dip vein (inclined vertical)

Fault dip

Average Grade 1000'

Average Thickness of Vein feet

Molybdenite

Grid System

ADIT ELEV 62